

AD_____

Award Number: W81XWH-04-1-0142

TITLE: V.I.T.A.L. (Vanguard Investigations of Therapeutic Approaches to Lung Cancer)

PRINCIPAL INVESTIGATOR: Waun Ki Hong, M.D.
Reuben Lotan, Ph.D.
David Stewart, M.D.

CONTRACTING ORGANIZATION: The University of Texas M. D. Anderson Cancer
Center
Houston, TX 77030

REPORT DATE: January 2008

TYPE OF REPORT: Annual

PREPARED FOR: U.S. Army Medical Research and Materiel Command
Fort Detrick, Maryland 21702-5012

DISTRIBUTION STATEMENT: Approved for Public Release;
Distribution Unlimited

The views, opinions and/or findings contained in this report are those of the author(s) and should not be construed as an official Department of the Army position, policy or decision unless so designated by other documentation.

REPORT DOCUMENTATION PAGE				Form Approved OMB No. 0704-0188	
Public reporting burden for this collection of information is estimated to average 1 hour per response, including the time for reviewing instructions, searching existing data sources, gathering and maintaining the data needed, and completing and reviewing this collection of information. Send comments regarding this burden estimate or any other aspect of this collection of information, including suggestions for reducing this burden to Department of Defense, Washington Headquarters Services, Directorate for Information Operations and Reports (0704-0188), 1215 Jefferson Davis Highway, Suite 1204, Arlington, VA 22202-4302. Respondents should be aware that notwithstanding any other provision of law, no person shall be subject to any penalty for failing to comply with a collection of information if it does not display a currently valid OMB control number. PLEASE DO NOT RETURN YOUR FORM TO THE ABOVE ADDRESS.					
1. REPORT DATE (DD-MM-YYYY) 01-01-2008		2. REPORT TYPE Annual		3. DATES COVERED (From - To) 15 DEC 2006 - 14 DEC 2007	
4. TITLE AND SUBTITLE V.I.T.A.L. (Vanguard Investigations of Therapeutic Approaches to Lung Cancer)				5a. CONTRACT NUMBER	
				5b. GRANT NUMBER W81XWH-04-1-0142	
				5c. PROGRAM ELEMENT NUMBER	
6. AUTHOR(S) Waun Ki Hong, M.D., Reuben Lotan, Ph.D., David Stewart, M.D. E-Mail: whon~@mdanderson.org				5d. PROJECT NUMBER	
				5e. TASK NUMBER	
				5f. WORK UNIT NUMBER	
7. PERFORMING ORGANIZATION NAME(S) AND ADDRESS(ES) The University of Texas M. D. Anderson Cancer Center Houston, TX 77030				8. PERFORMING ORGANIZATION REPORT NUMBER	
9. SPONSORING / MONITORING AGENCY NAME(S) AND ADDRESS(ES) U.S. Army Medical Research and Materiel Command Fort Detrick, Maryland 21702-5012				10. SPONSOR/MONITOR'S ACRONYM(S)	
				11. SPONSOR/MONITOR'S REPORT NUMBER(S)	
12. DISTRIBUTION / AVAILABILITY STATEMENT Approved for Public Release; Distribution Unlimited					
13. SUPPLEMENTARY NOTES					
14. ABSTRACT The VITAL Research Program will provide a better understanding of the cellular and molecular processes that drive lung tumorigenesis so that an accurate risk model for recurrence and/or the development of the secondary primary tumor can be developed, and the biologic agents most effective in reducing these events in the group of high-risk patients can be identified. We will be incorporating retrospective clinical trial specimens to develop our risk model and validating it with specimens collected from our Vanguard study. The research projects are proceeding well as proposed, producing valuable findings with cell lines, and will validate these results using the clinical samples obtained from the VITAL trials in the coming years.					
15. SUBJECT TERMS Lung cancer, risk model, cancer recurrence, clinical trials					
16. SECURITY CLASSIFICATION OF:			17. LIMITATION OF ABSTRACT	18. NUMBER OF PAGES	19a. NAME OF RESPONSIBLE PERSON
a. REPORT	b. ABSTRACT	c. THIS PAGE			USAMRMC
U	U	U	UU	258	19b. TELEPHONE NUMBER (include area code)

TABLE OF CONTENTS

INTRODUCTION	2
BODY	2
Project 1	4
Project 2	7
Project 3	24
Project 4	33
Project 5	45
Core B Biostatistics and Data Management	47
Core C Pathology and Specimen Procurement.....	49
Developmental Research Project 2	59
KEY RESEARCH ACCOMPLISHMENTS	61
REPORTABLE OUTCOMES.....	63
CONCLUSIONS	66
REFERENCES	68
APPENDICES	71
Appendix 1: (Core B) Trial Summary via Event Charts and Data Management Activities for VITAL	
Appendix 2: Publications	

INTRODUCTION

Smoking-related cancers such as lung and head and neck cancers are a major cause of cancer death in the United States. About 25% of lung cancer patients are diagnosed with stage I or II disease and undergo surgery with curative intent, but the 5-year survival for the group of patients is only 30%-70%. Patients with a strong history of smoking and prior early-stage cancer are found to be at high risk for cancer recurrence or development of second primary tumors (SPTs). An effective adjuvant therapy after surgery in this group of patients is not well established yet. The survival benefit of adjuvant chemotherapy was uncertain until recent findings reported by Winton and colleagues (Winton et al., 2005). They found that adjuvant chemotherapy (vinorelbine and cisplatin) increases the 5-year survival of surgically resected non-small cell lung cancer (NSCLC) patients, resolving the debate over the benefit of adjuvant chemotherapy. Thus, better-designed clinical trials and basic research are needed to establish the standard of care for these patients after surgery.

The program VITAL (Vanguard Trial of Investigational Therapeutics in Adjuvant Treatment of Lung Cancer) developed in 2003 was developed to gain a better understanding of the molecular events underlying the progression of NSCLC in order to develop a risk model for cancer recurrence and development of smoking-related SPT in the high-risk population, and to identify effective preventive agents for this group of patients. Specifically, our objectives are:

- To identify biologically-based treatments for prevention of cancer recurrence and development of second primary tumors in high-risk patients;
- To understand molecular events in premalignant tissues that contribute to progression or malignancy;
- To develop a risk prediction model for disease recurrence and development of second primary tumors in high-risk patients by combining clinical treatment outcomes with molecular and imaging data.

Three clinical trials were proposed, in part, to acquire the necessary correlative samples to develop this risk model. Histologic assessment was planned to determine whether malignant changes would occur during this time period. Despite substantial efforts, our patient accrual was significantly lower than expected due to a number of factors (described in detail in Project 1). Thus, a major effort for the grant year was to re-assess and develop an alternative strategy to accomplish our goals of developing this risk model which is so crucial for decision making for patients and physicians in the management of this challenging disease. An overview of the changes is provided below with additional details in each relevant project.

VITAL ReVITALization Plan

When Project 1 was proposed in 2003, the standard of care for lung cancer patients treated with surgical resection was observation. Patients could only be stratified into risk groups by surgical stage. We proposed to prospectively study high-risk patients who may have changes in their bronchial epithelium, including those with smoking histories and prior cancers. Planned assessments clinically via regularly scheduled CT scan imaging as well as histological monitoring via bronchoscopy (white light and autofluorescent) with biopsies were unique to the VITAL project. Adjuvant treatment with biological agents was also planned to see if precancerous changes in the bronchial epithelium could be slowed leading to fewer recurrences or SPTs. However, the treatment for surgically resected NSCLC has significantly changed since 2003. Several clinical trials have reported the efficacy of adjuvant chemotherapy after lung cancer resection (Arriagada 2004, Winton 2005, Kato 2004, Strauss 2004, Douillard 2005). Thus, patients are now being followed by medical oncologists and guidelines for follow-up are in the works. Further analysis into the studies revealed controversies in the treatment of resected

lung cancer in stage I (Strauss 2006, Douillard 2005). Subsets of the major studies revealed lack of benefit of chemotherapy in patients with stage I tumors. Defining who was at higher risk for recurrence or SPT development was still based on clinical stage of the cancer. Biomarkers were being tested, mostly to assess prognosis (ERCC1, HER family) and not prediction (Eberhard 2005, Lynch 2004, Paez 2004, Olaussen 2006, Tsao 2005).

Predictive markers are most useful for assessing patients risk and can be used subsequently to measure response to therapy. HER-2/neu and hormone receptor status in patients with breast cancer are successful examples of biomarkers that have been incorporated into a risk model to determine additional treatment. Trastuzumab (Herceptin) is a humanized monoclonal antibody developed to target HER2/neu receptor that is overexpressed in 25% to 30% of breast cancer. The combination of trastuzumab and chemotherapy increased response rates, time to progression, quality of life, and overall survival, and became a standard therapy for the first-line treatment of women with HER2/neu-overexpressing metastatic breast cancer, whereas patients with negative estrogen/progesterone receptors whose tumors did not overexpress HER 2/neu receptor experienced no benefit with tamoxifen (Pegram 1998; Sledge 2004).

In the past year, additional tests have been utilized in determining prognosis in patients with early stage NSCLC. Investigators have reported promising data using a metagene approach and genetic assay that may predict higher risk patients with treated early stage NSCLC (Potti 2006, Chen 2007). One significant biomarker discovered for clinical relevance for NSCLC treatment includes epidermal growth factor receptor (EGFR) mutations or amplification (Eberhard 2005, Lynch 2004, Paez 2004, Lee 1997, Pao 2004, Tsao 2005). The FDA approval of two biological agents in NSCLC (erlotinib and bevacizumab) has also spurred additional research into biomarkers to predict response to therapy (Sandler 2006, Shepherd 2005). The field of lung cancer treatment and investigation has truly evolved with a new paradigm established in the last few years. Despite all this progress, however, there is still no data on markers to predict risk nor follow-up investigations of the biology of the bronchial epithelium and the changes that may occur over time. A risk model is still a vital need for this patient population.

Because of the rationale and data outlined above, we amended the VITAL project to focus on its strengths and uniqueness including the development of the risk model and to ensure the timely completion of our major objectives:

- 1. Circumvent low accruals using surgical specimens in our tissue bank.** These specimens (about 500 samples) of resected lung cancer will be utilized for biomarker assessment and will serve as the foundation for a biomarker-based risk assessment model.
- 2. Continue enrolling patients in our Vanguard trial to accrue 50-60 patients.** This cohort will provide sufficient biospecimens for the aims proposed in the other projects of the VITAL program. Additionally, the clinical data obtained from these patients will be used to test the biomarker-based risk assessment model and the follow-up bronchoscopy specimens will provide important information for biomarker changes in the bronchial epithelium.
- 3. Close the celecoxib and erlotinib trials to focus resources on specimen analyses to develop the biomarker risk model.**

4. **Perform two additional discovery projects related to increased risk which are only now possible due to continued progress in VITAL.**
 - a. **Identify gene expression signatures in bronchial brush specimens using high-throughput genomics approach.**
 - b. **Identify genes expression signatures in epithelial cells detected by LIFE bronchoscopy that determine aggressiveness.**

These revisions will optimize the use of our resources to accomplish our main objectives of our original proposal, adapting to the current research in the field, and capitalizing on our strengths.

PROGRESS REPORT (BODY)

Project 1: Biologic Approaches for Adjuvant Treatment of Aerodigestive Tract Cancer

(PI and co-PIs: Drs. Waun Ki Hong, Edward S. Kim, Rodolfo C. Morice, David J. Stewart)

Aim 1 Assess the smoking-related disease-free survival in patients who are current or former smokers with a prior definitively-treated stage I/II lung or head and neck cancer.

The main objective for this project was to open the Vanguard study at MDACC as well as the 2 other participating sites. Enrollment was planned for a total of 300 patients with definitively treated stage I/II lung or head and neck cancer and at least a 20-pack-year smoking history. Patients undergo baseline testing including chest x-ray, CT scan, labs, bronchoscopy, and other specimen collections (i.e., sputum, saliva, serologies). Bronchoscopies and specimen collection are performed at baseline and at months 12, 24 and 36. White-light alone or white light and autofluorescence modalities is used. Abnormal areas detected by bronchoscopy are biopsied. Histologic assessment is performed to determine whether malignant changes will occur during the time period. If severe dysplasia, carcinoma *in situ* or carcinoma is discovered, patients followed the plans outlined in the clinical protocol. Once patients have completed 3-years of testing, they are followed until the study is completed.

Update

In the past year, we have continued enrolling patients in the VITAL/Vanguard trials. A total of 45 patients have been enrolled in the Vanguard trial. Patient clinical data and tissues have been and continue to be collected and will be distributed to investigators of VITAL research projects through the VITAL Pathology Core. (For details, please refer to the Pathology Core update, pg. 49-58.)

Due to a change in the standard treatment plans in which patients are followed more closely by their local medical oncologist, our patient accrual has been lower than expected even after taking several important actions in grant year 3 (2006). These changes were determined after we conducted a review of the trial in our lung NCI program project which initially had similar difficulties to learn and adopt important measures which were successful in improving patient accrual. Several small but important modifications were made to this protocol that we expected to improve accrual with higher risk patients balanced with the ability to accrue sufficient numbers of patients to obtain statistical significance with this trial. These changes included lessening the number of follow-up visits to allow patients to be seen by their local oncologist, opening the trial to include stage III patients, and decreasing the pack years required to 10 pack years. The higher risk stage III patients offset the decrease in pack years but allowed for more

patients to be eligible for these trials. In addition, we increased the study personnel, such as research nurses, entirely dedicated to just the trials in this program.

We also worked to increase the visibility for our program and clinical trials distributing patient brochures and advertising the trials on the radio and on our website (www.mdanderson.org/lung) to increase awareness nationally and internationally to improve the patient accrual. For our lung NCI program project, these measures were successful in increasing accrual and expect to see similar increases for this program. However, after monitoring the results of these measures, we concluded that we were unlikely to accrue sufficient patients for these studies to accomplish our goals. Consequently, we put together a “reVITALization” plan for this program as described above to accomplish the goals of the original program through alternative means. This plan and the associated re-budgeting of the remainder patient care funds were submitted to our Office of Research Administration, Grants and Contracts Administration, and to the DoD for approval. The plan was approved in November 2007. The Vanguard protocol is being amended to accommodate these changes.

Plan: Continue enrolling patients in our Vanguard trial to accrue 50-60 patients.

By continuing accrual to 50-60 patients, we will have the necessary prospective specimens to fulfill the goals of Projects 2-5. Other biomarker analyses in these projects may be fulfilled using retrospective specimens. This combination will maximize our analyses while reducing the time required to develop the proposed risk model using the supplemental retrospective specimens (See Aim 3 and Core C below).

Project 2. The *in vitro* studies using normal bronchial epithelial cells to test new potential chemoprevention combination of biologic agents will not be translated to patients at this time. Validation of expression in tissue specimens of potential targets or markers at base-line will not be affected because the retrospectively collected TMA specimens can be used.

Project 3. If the collection of the 10 patients with different combination of LIFE and white-light bronchoscopy abnormalities is completed with the 50-60 Vanguard patients, there will be no significant impact. Validation of expression in tissue specimens of potential targets or markers at base-line will not be affected because the retrospectively collected TMA specimens can be used.

Projects 4 and 5. These two projects did not have specific plans for fresh specimens. They counted on the base-line and follow-up FFPE specimens from the Vanguard patients to validate markers in bronchial tissues. These 2 projects will benefit from this revised proposal because they will have both tumor and adjacent epithelial specimens from a larger number of cases with more end-points (recurrence or SPTs).

Aim 2 Evaluate effects of biologic agents as adjuvant therapy on the modulation of histology and specific biomarkers in this high-risk population.

Current adjuvant chemotherapy offers some benefits in the high-risk patients, but is not a long-term preventive strategy. We plan to open several biologic adjuvant clinical trials with novel agents such as celecoxib, erlotinib, lonafarnib, and possibly others. Considerable preclinical data exist for these agents for cancer as well as normal or precancerous bronchial epithelium.

Update

Revised Aim 2. Focus has been shifted to the development of a risk model (see Aim 3 / Revised Task 3). These trials had to be abandoned due to the poor accruals from the changes in standard of care for lung cancer patients. Retrospective specimens will be used and this information will be assessed from the clinical data associated with them.

This trial is currently being in the process of being closed. By closing the celecoxib trial and not opening the proposed erlotinib trial, we will focus our efforts on the productive analysis of samples, leading to the same outcome – development of a risk model – faster.

Aim 3 Develop a lung cancer risk model to help predict the likelihood of development utilizing imaging and biologically-based information in this high-risk population.

Patients with a history of smoking and a prior surgically resected stage I/II head and neck or lung cancer are at high risk for cancer recurrence or SPTs. There are no standard interventions, which have been proven to help reduce the risk of cancer occurrence. A Gail risk model implemented in the initial management of breast cancer screening has proven useful and has helped with early detection and more stringent follow-up in the higher risk cohorts. Patients enrolled in the Vanguard trial will have aggressive post-operative follow-up with analysis including frequent serologies, bronchial specimens and CT scanning. Trends in these multiple biomarkers would be analyzed and used to develop a predictive model. Establishing a risk model will eventually help identify patients who may be at higher risk for lung cancer development and promote earlier interventions for prevention.

Update

Revised Aim 3. Develop a lung cancer risk model to help predict the likelihood of cancer recurrence and second primary tumor (SPT) development utilizing clinical, pathologic and biomarker information obtained prospectively and retrospectively from the high-risk population of patients (Years 4-5).

Dr. Ignacio Wistuba, Pathology Core Director, has identified archival tissue specimens from over 600 surgically resected lung cancers, stages I/II, available for our use in our tissue bank (period 2002-2005) which would meet the criteria in our proposed trials. These retrospective specimens are entirely from NSCLC patients, no head and neck cancer patients, and have follow-up for a minimum of 2 years. All NSCLC cases specimens with adjacent bronchial structures will be included in the study. Complete clinical and pathologic characteristics will need to be audited and incorporated into our Lung P01 database. We will thus increase our samples size from 300 to 500 for use in developing our risk model by switching from prospective to retrospective specimens. Our focus in VITAL is on epithelial changes, not changes in the tumor itself. Hence, by including only patients with adjacent bronchial epithelium, the same goal of developing a risk model can be achieved. See Core C for more detail.

Key Research Accomplishments

- Enrolled 11 more patients in the Vanguard study, for a total of 45.
- Continued to collect patient clinical data and tissues for distribution to support research projects in the VITAL grant.
- Two patients completed the 1 year mark/bronchoscopy.
- ReVITALization proposal and budget was approved and plan is being implemented.

Conclusions

The completion of the Vanguard trials is important to this grant. However, the ultimate goal is the development of a risk model for development of SPT and recurrence. This model will be developed utilizing the resources from both Vanguard and our exhaustive Lung Cancer Tissue Bank. This is a top priority for our program.

Project 2: Identification of Biomarkers of Response to Chemoprevention Agents in Lung Epithelium

(PI and co-PIs: Li Mao, M.D., Reuben Lotan, Ph.D., John Minna, M.D.)

Lung cancer continues to be the deadliest among all cancers in the United States with over 165,000 deaths annually for the last few years and an overall 5-year survival rate of less than 15% (Jemal et al., 2007). Early detection of premalignant lesions or tumors appears to be an efficient approach to reducing the morbidity and mortality from lung cancer because the survival of early stage lung cancer patients is much better than that of patients with advanced cancers. Therefore, new strategies for the early diagnosis, prevention and treatment of this dreadful disease are urgently needed (Wistuba and Gazdar 2006; Sato et al., 2007). The development of early detection tools for lung cancer requires improved molecular testing by identification and understanding of early events in the multi-step process of lung carcinogenesis, which involves the accumulation of genetic and epigenetic alterations over the long course of exposure to carcinogens such as tobacco smoke (Mao, 2002; Wistuba and Gazdar 2006; Sato et al., 2007). To date, there are no validated biomarkers for early detection. Moreover, one or a few genes may not provide sufficient specificity given the multi-factorial process of lung carcinogenesis and heterogeneous nature of lung cancer. Thus, the effort to search for more specific and sensitive biomarkers of early lung cancer is warranted. The development of high-throughput gene expression analyses, e.g., DNA-chips or microarrays, provides opportunities to define biomarkers (signatures) of risk of cancer development. During the last few years, several studies reported molecular classification of human lung carcinomas on the basis of gene expression and described numerous putative biological markers of cancer (Meyerson et al., 2004). However, only limited number of studies has attempted to identify genes that are modulated at early stages of human lung carcinogenesis such as premalignant state because of the limited availability of premalignant lung tissues suitable for RNA extraction. We hypothesized that immortalized, transformed and tumorigenic human bronchial epithelial cell (HBEC) line models will have similar abnormalities in gene expression profiles as premalignant and malignant tissues *in vivo*. Therefore, such cell models will be useful to identify markers of early disease.

We proposed to use genomic and proteomic analyses to identify changes in gene expression (including mRNA and miRNAs) and proteins which correlate/associate with cancer risk in the carcinogen damaged aerodigestive tract field and also use these signatures to monitor the response of this field to chemoprevention. We will develop and use a model HBEC system to study the effect of specific oncogenic changes and also the response of these manipulated HBECs to various carcinogenic and chemoprevention agents. Thus, we will determine modifications of these changes by chemopreventive agents in premalignant cells *in vitro* and to use probes for the modified genes and proteins to analyze tissue specimens from individuals participating in the chemoprevention clinical trials.

Aim 1 Develop immortalized human bronchial epithelial cell cultures using a subset of patient tissue specimens collected in Project 1 and characterize the expression profiles of these cells using oligonucleotide based microarrays.

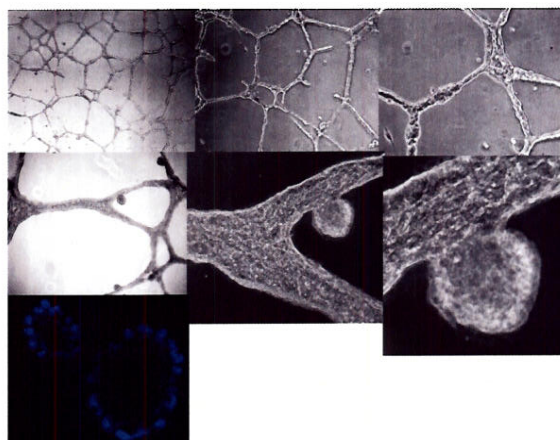
The main goal of this aim of this project is to establish these cultures from the patients entered onto the clinical trial described in Project 1 and to characterize their gene expression profiles.

Update

We continued our efforts to develop additional immortalized HBEC strains, and have made considerable progress in:

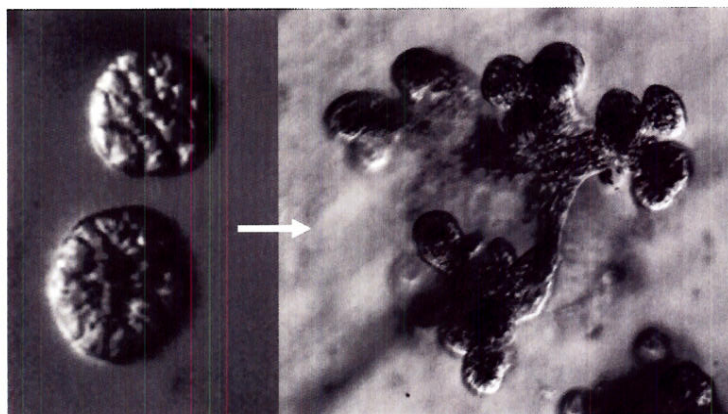
A. Generating immortalized HBECs from different individuals that were collected on various tissue procurement protocols at The University of Texas Southwestern and at M. D. Anderson Cancer Center. *Currently we have generated HBECs from over 45 different individuals.* These represent males, females, a spectrum of smoking status, as well as persons with and without lung cancer. We have also immortalized 15 of these same bronchial epithelial specimens with oncogenic HPV E6 and E7. We have also made several pairs of immortalized HBECs and lung cancer cell lines from the same patient.

Figure 1. Development of Matrigel Culture Where HBECs Recapitulate Lung Branching Morphogenesis and Sac Formation.



Phase contrast microscopic figures at different magnifications of HBECs grown in Matrigel. Note the formation of branching structures and sacs. Bottom left-hand figure shows one of sacs stained with DAPI to show nuclei. (Collaboration with O. Delgado and J. Shay at UTSW)

Figure 2. Immortalized HBECs Differentiate and Can Aggregate or Undergo Branching Morphogenesis



4-5 days on matrigel 13 days on matrigel high density

(Collaboration with O. Delgado and J. Shay at UTSW)

B. Recently, we have started several immortalized cells from peripheral small airway epithelial cells (SAECs) that are different from the prior HBECs we made from proximal (large) airway cells.

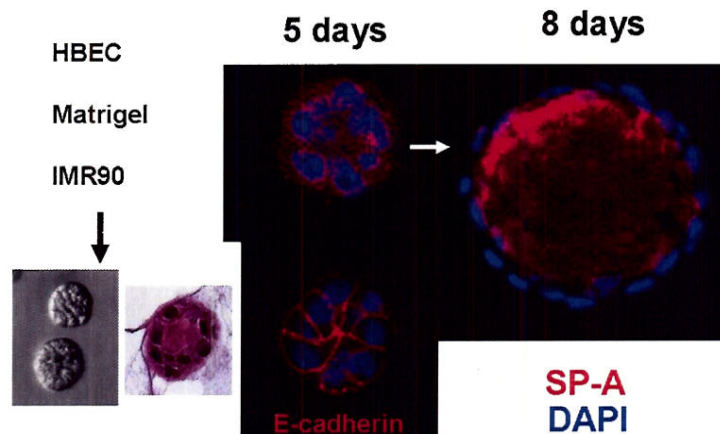
C. New methods for differentiation of HBECs into 3-dimensional tissue surrogates *in vitro*. One of the key aspects of testing oncogenic changes and the effect of chemoprevention agents on the preneoplastic HBEC series is to develop methods for allowing these cells to differentiate under controlled conditions *in vitro* and then test for the effect of oncogenic and chemoprevention changes on the patterns of

differentiation. Recently, we have developed a methods using Matrigel and have found that the HBECs form complex structures representing branching morphogenesis and SAC formation in the lung (Figures 1, 2). These differentiated HBECs begin to express the pulmonary epithelial specific marker surfactant protein A (SPA) (Figure 3).

D. Genomic analyses. We have performed Illumina and Affymetrix mRNA gene expression, and array based DNA comparative genome hybridization analyses (aCGHs) profiles on these HBECs and representative results are presented in Aim 3 below.

E. We have also participated as part of several consortiums on **genome wide aCGH analyses of lung cancers** for the detection of new amplified oncogenes in the development of lung cancer (also described in Aim 3 below).

Figure 3. HBECs in 3-D Matrigel Culture Differentiate to Express The Pulmonary Epithelial Specific Marker Surfactant Protein A (SPA).



HBECs were grown in liquid culture over Matrigel with a human lung fibroblast IMR90 feeder layer for 5 and 8 days. Panels on left show phase contrast and H and E photomicrographs of the cultures. Panels on right show staining with DAPI (blue for the nuclei) and immunostaining red (bottom left panel for E Cadherin) and on right for SP-A that is secreted into the lumen of the sphere created by the HBECs in this culture. (Collaboration with O. Delgado and J. Shay at UTSW)

Aim 2 Characterize effects of the chemopreventive agents used in Project 1 on cell proliferation and apoptosis in the immortalized human bronchial epithelial cell cultures developed in Specific Aim 1.

We will determine the potential role of different chemopreventive agents [e.g., celecoxib, N-[4-hydroxyphenyl]retinamide (4-HPR), Iressa (gefitinib), and SCH63663] alone or in combination with one another for their effects on cell proliferation and apoptosis in cell cultures established in Aim 1. We will also determine the relative sensitivity among the various cell cultures to each of the agents by determining the 50% growth inhibitory concentration (IC_{50}). Results from this Specific Aim were presented in the report last year.

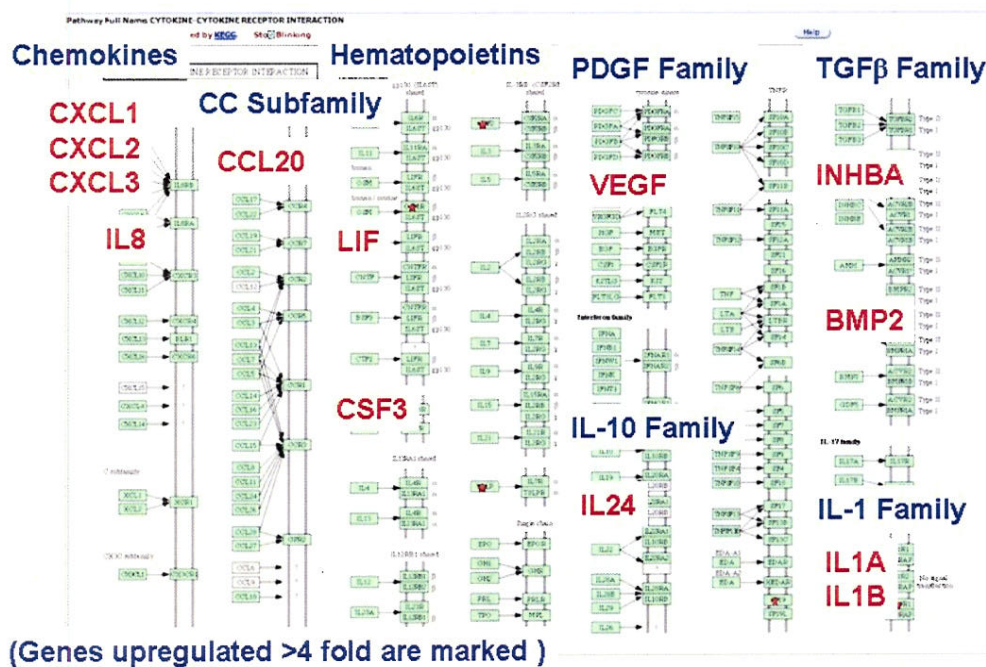
Aim 3 Identify gene expression and protein “signatures” which reflect lung tumorigenesis and sensitivity or resistance to chemopreventive regimens proposed in Project 1, and to validate the signatures and to determine their biological importance in precancer cell models of lung cancer.

Update

1) Detection of genes upregulated or downregulated by insertion of oncogenic changes into HBECs.

As described in prior reports, we have generated HBECs oncogenically manipulated to contain oncogenic KRAS^{V12}, stable knockdown (by shRNA) of p53 or the combination of these two changes. In addition, we have made multiple other oncogenic changes (e.g. mutant EGFR, CMYC, BCL2, PTEN knockdown). The expression profiles for these HBEC lines with preneoplastic changes have been determined using Illumina v2 and Affymetrix U133 2 plus arrays as well as using quantitative RT PCR for selected genes. We have identified a series of genes specifically upregulated or downregulated in these manipulated HBECs. We have focused this year on changes in expression of cytokine genes and their receptors that occur after expression of oncogenic KRASV12 into the HBECs. The expression of these soluble cytokines may provide a marker for the development of oncogenic KRAS changes in the bronchial epithelium before full fledged cancer develops and also (along with their receptors) represent chemoprevention targets. There were a series of such cytokine genes and their receptors identified in HBECs after expression of oncogenic KRASV12 (Figure 4).

Figure 4. Expression of a Specific Cytokine Program after Introduction of Oncogenic KRAS^{V12} into HBECs.



Oncogenic KRASV12 or a control vector were introduced into immortalized HBEC lines and the cells underwent mRNA expression profiling with Illumina v2 arrays without (control vector) and with oncogenic KRASV12 expression. Genes with >4 fold expression up-regulation were identified and bioinformatic pathway- functional analysis for cytokine expression and their receptors performed. These genes are indicated in red with the various gene families identified shown in blue. Results summarized from multiple arrays on several different HBEC KRASV12 transfectants. (Sato et al, In Prep).

2) Oncogenic manipulation and biologic selection for complete tumorigenic transformation of immortalized normal human bronchial epithelial cells

As reported previously, to develop an *in vitro* model system to study the multi-step pathogenesis of lung cancer, we established a series of cdk4/hTERT-immortalized HBECs which can be genetically manipulated that are able to differentiate into mature airway cells in organotypic cultures, but do not form colonies in soft agar or tumors in nude mice (Vaughan et al., 2006). We observed that combinations of p53 knockdown with mutant EGFR or with physiological levels of oncogenic KRAS^{V12} in our HBECs showed partial progression towards malignancy. These cells formed colonies in soft agar, but failed to form tumors in nude mice. The detailed findings have been published in *Cancer Research* (Sato et al., 2006). We have gone on to add other oncogenes such as c-Myc and also biologic selection for the presence of large colonies that can grow in soft agar. This identified several tumorigenic clones. Of interest, tumors from the same clone were able to differentiate into several histologies indicating the likely presence of a “tumor stem cell” or “tumor propagating cell” component (Figure 5).

3) Perform array based CGH analysis of HBECs and primary non-small cell lung cancer.

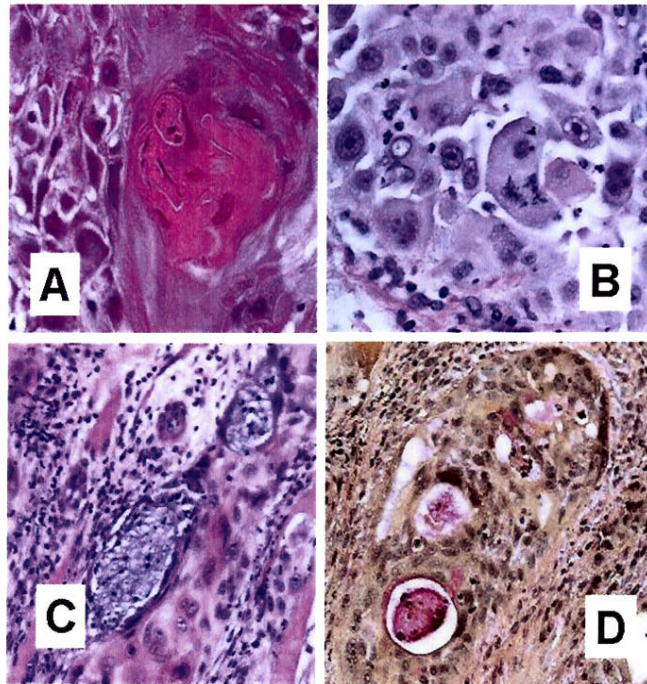
HBEC aCGH Analysis

In collaboration with the laboratory of Dr. Wan Lam at the British Columbia Cancer Agency (BCCA), we have studied copy number changes by array CGH (aCGH) in the series of HBECs with and without oncogenic manipulation. These have led to the identification of a few recurrent copy number changes in HBECs with immortalization (Figure 6, top panel). The addition of oncogenic changes, such as KRASV12 and p53 knockdown, leads to a few other consistent changes (Figure 6, bottom panel).

Non-Small Cell Lung Cancer aCGH Analysis

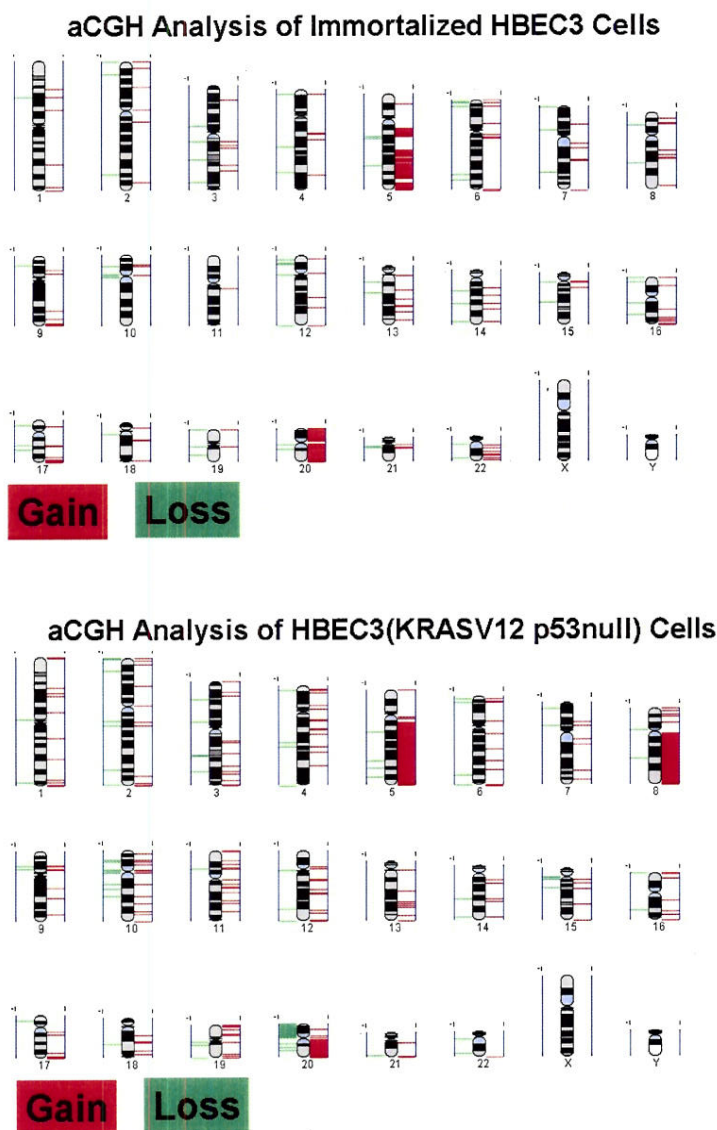
Somatic alterations in cellular DNA underlie almost all human cancers. The prospect of targeted therapies and the development of high-resolution, genome-wide approaches are now spurring systematic efforts to characterize cancer genomes. We reported a large-scale project to characterize copy-number alterations in primary lung adenocarcinomas. By analysis of a large collection of tumors (n = 371) using dense single nucleotide polymorphism arrays, we identify a

Figure 5. Five Genetic Changes Convert HBECs from One Clone into Several Different Histologic Tumor Types.



HBEC3 cells were oncogenically altered with KRASV12, p53 knockdown and c-myc in addition to cdk4 (p16 bypass) and hTERT and then were selected for soft agar large colony formation. These cells gave tumors in nude mice. The tumors had different histologies: A. Squamous cell carcinoma. B. Large cell/giant cell carcinoma. C. Adenocarcinoma with squamous features H&E D. Adenocarcinoma with squamous features mucicarmine stain. (Sato et al, In Prep).

Figure 6. Array CGH (aCGH) Analysis Identifies Areas of Amplification and Deletion Found in HBECs After Introduction of Oncogenic KRASV12 and p53 Knockdown.



aCGH (32,000 element BAC array in laboratory of Dr. Wan Lam British Columbia Cancer Agency, BCCA) was performed with comparison to normal DNA. The results for amplification (red) and deletion (green) are displayed on a cartoon karyogram for all human chromosomes. The amplification changes on chromosomes 5 and 20 are consistently seen with HBEC immortalization. In the example shown with oncogenic changes a 20p deletion and 8q amplification were found.

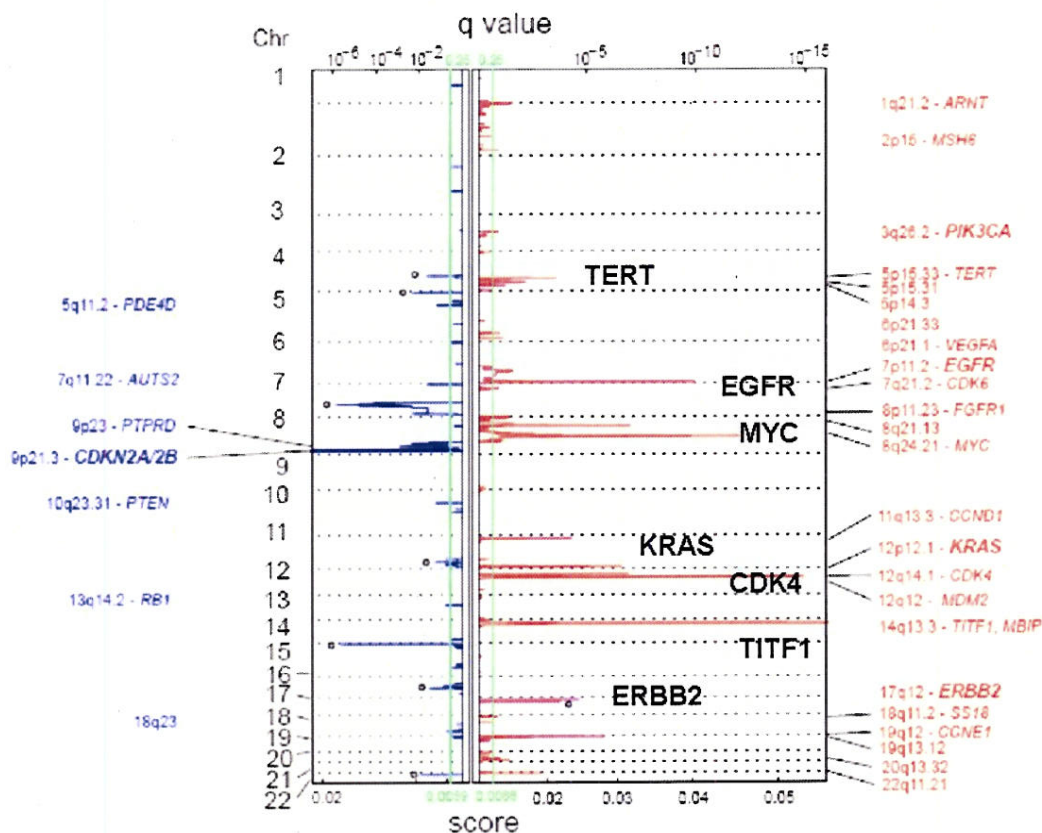
total of 57 significantly recurrent events. We find that 26 of 39 autosomal chromosome arms show consistent large-scale copy-number gain or loss, of which only a handful have been linked to a specific gene (Figure 7). We also identify 31 recurrent focal events, including 24 amplifications and 7 homozygous deletions. Only six of these focal events are currently associated with known mutations in lung carcinomas. The most common event, amplification of chromosome 14q13.3, is found in approximately 12% of samples. On the basis of genomic and functional analyses, we identify NKX2-1 (NK2 homeobox 1, also called TTF1), which lies in the minimal 14q13.3 amplification interval and encodes a lineage-specific transcription factor, as a novel candidate proto-oncogene involved in a significant fraction of lung adenocarcinomas (Figures 7, 8). More generally, our results indicate that many of the genes that are involved in lung adenocarcinoma remain to be discovered. (Weir et al, 2007.)

Aim 4 Develop techniques to assess these molecular signatures in tissue specimens and serum obtained in Project 1, and assess the relevance of these molecular signatures as *in vivo* biomarkers using baseline and post-treatment specimens.

Perform functional analysis of the role of TITF1 in HBECS and non-small cell lung cancers.

Genomic profiling of 128 lung cancer cell lines and tumors revealed frequent focal DNA amplification at cytoband 14q13.3, a locus not amplified in other tumor types. The smallest region of recurrent amplification spanned the homeobox transcription factor TITF1, previously linked to normal lung development and function (Figure 8). Since TITF1 is a known transcription factor, we were searching for genes whose expression was correlated with TITF1 expression particularly in lung cancer. We thus performed genome wide mRNA expression profiling on

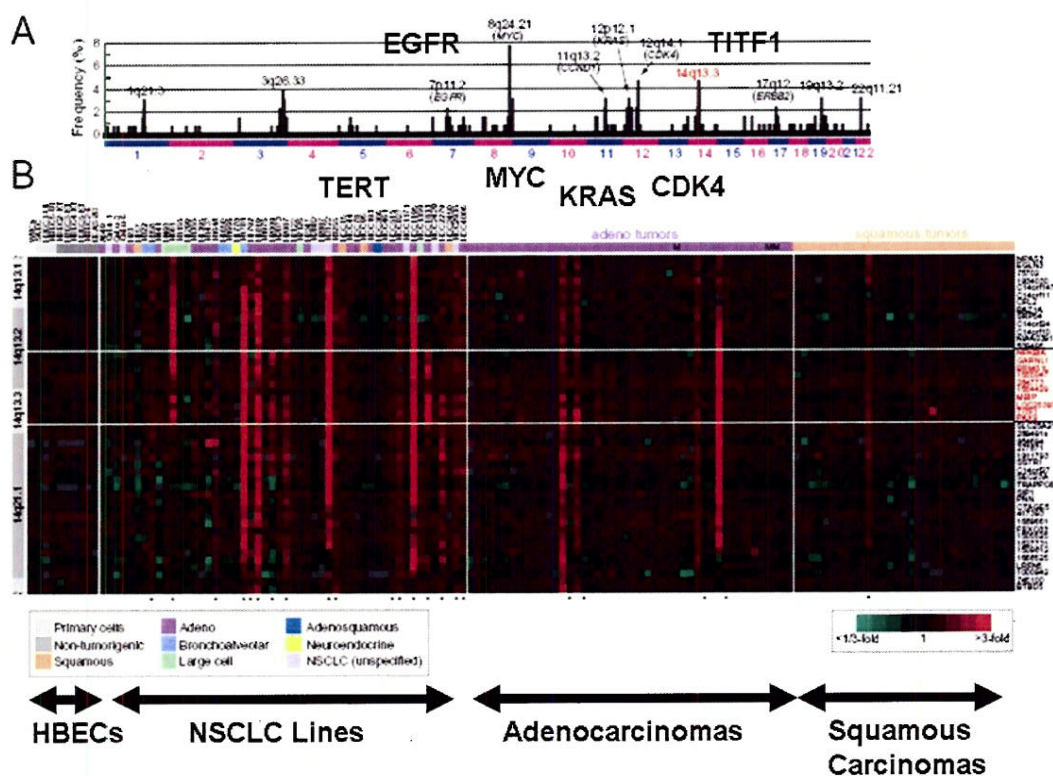
Figure 7. Genome Wide Copy Number Analysis Using High Density SNP Arrays on Primary Lung Adenocarcinomas Identifies Recurrent Areas of Oncogene and *TITF1* Amplification.



Characterizing the Cancer Genome in Lung Adenocarcinoma. Analysis of copy-number alterations in 371 primary tumor samples and 242 matched normal controls. Affymetrix 250K Sty arrays, representing over 238,000 human SNPs were used for this analysis. Statistical analysis of copy number alterations shows 31 recurrent focal events, including 24 amplifications (red bars to the right) and 7 homozygous deletions (blue bars to the left). The recurrent amplification of genes for *TERT*, *EGFR*, *C-MYC*, *KRAS*, *CDK4*, *TITF1*, and *ERBB2* (*HER2*) are identified. *TITF1* was amplified in 12% of primary lung adenocarcinomas. This work was performed as part of a consortium effort and reported in Weir et al, 2007.

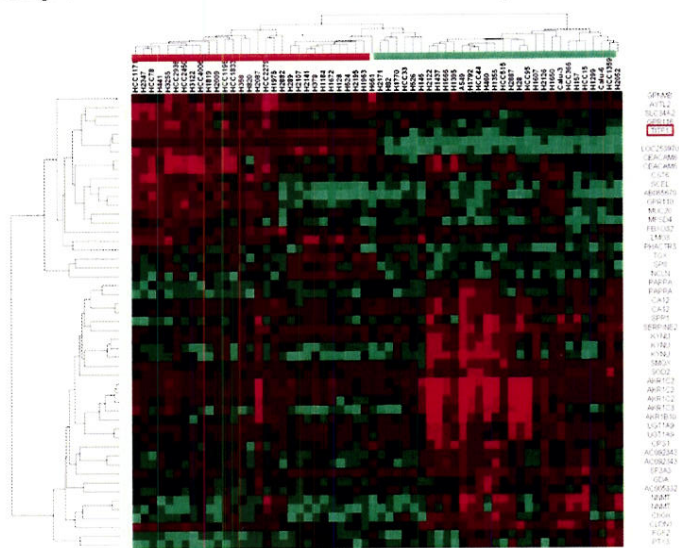
lung cancers with and without TTF1 amplification and/or expression Figure 9 shows a “HEAT” map of the genes we identified whose expression correlates (up or down) with TTF1 expression. As part of this effort, we found that the HBECS did not express TTF1. When amplified, TTF1 exhibited increased expression at both the RNA and protein level. siRNA-mediated knockdown of TTF1 in lung cancer cell lines with amplification led to reduced cell proliferation, manifested by both decreased cell-cycle progression and increased apoptosis (Figure 10). Our findings indicate that TTF1 amplification and over expression contribute to lung cancer cell proliferation rates and survival, and implicate TTF1 as a lineage-specific oncogene in lung cancer. (Kwei et al, 2008, In Press).

Figure 8. aCGH Analysis of HBECS, NSCLC Lines, and Primary Non-Small Cell Lung Cancers Identifies Recurrent Oncogene and *TTF1* Amplifications.



aCGH was performed on HBECS, NSCLC lines, and primary adenocarcinomas and squamous cell lung cancers by Jon Pollack lab at Stanford with 42,000 element cDNA arrays. Note recurrent amplification of oncogenes and *TTF1*. (A) Frequency plot of cytobands harboring high-level DNA amplification, here defined as tumor/normal aCGH ratios > 3, in NSCLC cell lines (Supplementary Table 1) and tumors. Selected cytobands with frequent amplification are indicated. (B) Genomic profiles by CGH on cDNA microarrays of NSCLC cell lines and tumors, histologies indicated (M indicates metastasis), for a segment of chromosome 14q13.1-q21.1. Genes are ordered by genome position. Red indicates positive tumor/normal aCGH ratios (scale shown), and samples called gained at 14q13.3 are marked below by closed circle. Genes and ESTs (IMAGE clone ID shown) on microarray residing within the amplicon core are highlighted by red text. Work done in collaboration with Dr. Jon Pollack at Stanford University Medical Center and reported in Kwei et al, 2007, In Press.

Figure 9. Genome Wide mRNA Expression Analysis of Lung Cancers With and Without TITF1 Expression.



Non small cell lung cancer (NSCLC) and small cell lung cancer (SCLC) lines (columns) had expression profiling with Affymetrix U133 2 plus arrays performed and also had the expression of TITF1 examined by Q RT PCR as well as by arrays. The tumor lines with TITF1 expression (red bar across the top) and without TITF1 expression (green bar across the top) were identified and genes whose expression was correlated with TITF1 expression (rows) were identified and placed into the HEAT map. Increased expression indicated by red while decreased expression of each gene indicated in green with color intensity indicating the amount of increased or decreased expression. Note there were both NSCLC and SCLCs that expressed TITF1.

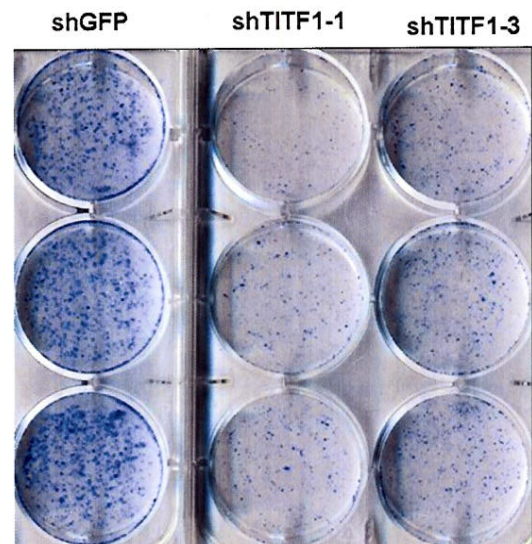


Figure 10. Knockdown of TITF1 Expression Inhibits Clonal Growth of NSCLCs Overexpressing TITF1. NCI-H2087 cells express large amounts of TITF1 without gene amplification. shRNAs targeted against TITF1 were developed (shTITF1-1 and shTITF1-3) as well as a control shRNA (shGFP) and introduced into H2087 cells with a *neo* selectable marker and colonies isolated in selection media. Note the large number of colonies formed with the control shGFP and greatly decreased colony formation with the two different TITF1 shRNAs. Similar results were seen when shRNAs were used with TITF1 amplified NSCLCs but not when tested in TITF1 non expression lung cancers. Reported in Weir et al, 2007, and Kwei et al, 2007, In Press.

Revised Aim 4. Test gene and protein signatures in prospective clinical specimens obtained from the 50-60 patients accrued (Years 4-5). Retrospective specimens will be used initially and signatures will be validated with prospective specimens.

Because of the complex system in cellular biology and cell-cell interactions in tissues, the conventional single gene-based hypothesis testing approach has been augmented by systems-based global analyses. We plan to take advantage of the availability of bronchial brush specimens from the 50-60 patients enrolled in the Vanguard study (brush specimens from up to 6 sites of each individuals are available from the 34 patients already enrolled) to perform global gene expression analyses using DNA microarrays. This approach will allow us to determine the expression status of the whole genome for each brush sample simultaneously. The gene expression profiles obtained will allow us to identify gene expression signatures and to address the following important issues in lung cancer risk assessment:

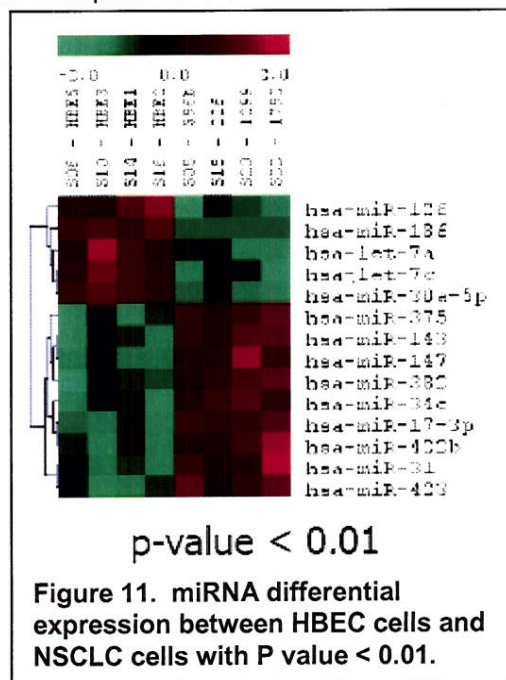
- i. Identify genes critical to lung cancer development by comparing differentially expressed genes between the bronchial epithelial cells closer to the primary tumor site and the bronchial epithelial cells at normal lobes of the lung;
- ii. Identify gene expression signatures predicting local recurrence and SPTs by comparing expression profiles between samples obtained from those who develop local recurrence or SPTs with samples from those who do not develop these events;
- iii. Identify the natural changes of gene expression patterns in the bronchial epithelial cells after surgical resection of primary lung cancer by measuring common differences between the expression profiles of the initial bronchial sampling and those of second sampling 12 month after;
- iv. Identify the potential utility of the dynamic changes in gene expression signatures measured in iii above to better predict lung cancer recurrence and SPTs compared to signatures of a single time point because a persistent or progressive nature of gene expression patterns will likely provide additional information in our risk model development.

This work has just begun as a part of the ReVITALization plan and will be a focus of the next grant year.

Aim 5. Identify gene expression signatures that characterize progression from immortalized to transformed to tumorigenic human bronchial epithelial cells based on already available high-throughput gene expression microarray data and validate these signatures using tissue microarrays (TMAs) containing normal bronchial epithelium, hyperplasia, squamous metaplasia, dysplasias, squamous cell carcinomas, atypical adenomatous hyperplasia, and adenocarcinomas (Years 4-5).

Update

miRNAs are involved in the regulation of gene expression during development and carcinogenesis. Although previous studies have compared miRNA expression profiles between NSCLC tissues and the corresponding normal lungs, the complex cellular structures of the normal lung tissues may complicate data interpretation, which may impact the accuracy of conclusions and direction of future studies. The objective of this study is to identify differentially expressed miRNAs between normal and malignant lung epithelial cells using immortalized normal bronchial epithelial cell lines and NSCLC cell lines and to determine biological roles of the differentially expressed miRNAs in lung tumorigenesis. Four immortalized HBEC lines and four NSCLC cell lines were used. HBEC cells were cultured with Keratinocyte-SFM media system whereas NSCLC cells were cultured with DMEM/low glucose supplemented and 5% fetal bovine serum. Total RNA was extracted using *mirVana*TM miRNA Isolation Kit (Ambion, Austin, TX): Microarray fabrication, hybridization, and data acquisition were performed at LC Sciences (Houston, TX USA). The expression profiles of 445 unique mature miRNAs were determined. The expression ratios between the two groups of samples were analyzed and differentially expressed miRNAs with P values < 0.01 were



considered significant. Fourteen of the 445 miRNAs were differentially expressed including 5 downregulated and 9 upregulated in NSCLC cells compared to HBEC cells (Figure 11). Interestingly, 4 of the 5 downregulated miRNAs (let-7a, let-7c, miR-126, and miR-30a-5p) have been reported downregulated in NSCLC whereas only 1 (miR-17-3p) of the 9 upregulated miRNAs has been documented to be upregulated in NSCLC previously. We revealed a panel of differentially expressed miRNAs potentially important in lung cancer initiation and progression. The low concordance of the upregulated miRNAs identified here compared to those found using tumor/normal tissues suggests a contribution of the non-epithelial components of the normal lung tissues. Further studies are needed to determine expression of the candidate miRNAs in primary bronchial epithelial cells and NSCLC and to determine the biological roles of the candidate miRNAs in lung cancer initiation and progression.

Aim 6. Identify gene expression signatures in bronchial brush specimens from the 50-60 patients enrolled in the Vanguard study using high-throughput genomics approach (Years 4-5).

Update

We have collected and processed bronchial brush specimens from patients enrolled in the Vanguard trial of Project 1. At each time point, six brush specimens are collected and processed for DNA, RNA, and protein analyses. The following table summarizes the samples currently available for analyses.

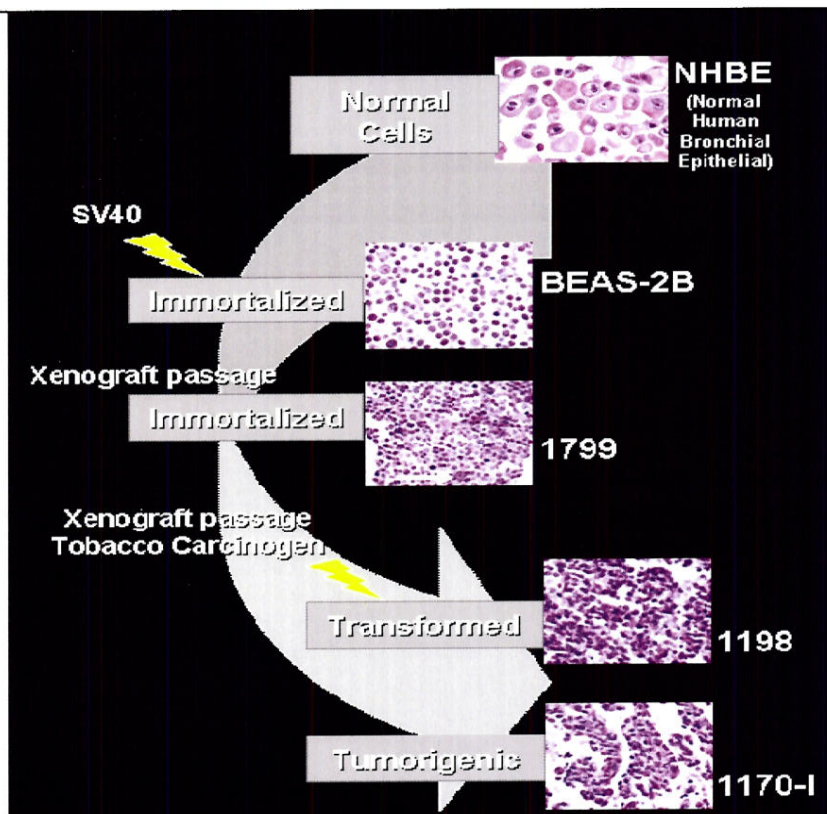
Table 1. Specimen collection.

	No. of patients	Bronchial brush sites					
		LB10	LUL	MC	RB10	RML	RUL
Baseline	38	38	38	38	38	38	38
12 months	20	20	20	20	20	20	20
24 months	9	9	9	9	9	9	9
36 months	1	1	1	1	1	1	1
Total	68						408

These samples will be used for gene and protein analysis in the next two years as proposed in our reVITALization plan. This aim will be performed in the next two years.

In the present study, we used an *in vitro* human lung carcinogenesis model consisting of normal human bronchial epithelial (NHBE) cells, BEAS-2B cells, which are NHBE immortalized with SV40 T/ Adeno12 virus (Reddel et al., 1988) and transformed (1198) and tumorigenic (1170-I) cells derived from BEAS-2B after exposure to cigarette smoke condensate *in vivo* (Klein-Szanto et al., 1992). Immortalized HBECs (1179), also derived from BEAS-2B but without exposure to cigarette smoke condensate were also used (Figure 12). These isogenic cells represent normal, immortalized, transformed and tumorigenic cells and their study offer an opportunity to identify different progressive changes in genotype or epigenetic changes.

Figure 12. *In vitro* model for the study of lung carcinogenesis. We have used a model that includes Normal human bronchial epithelial (NHBE) cell strain and cell lines that were derived from NHBE cells by immortalization with a hybrid adenovirus/SV40 large T antigen and called BEAS-2B (Reddel et al., 1988). Derivatives of the BEAS-2B cells isolated by Klein-Szanto et al., (1999) include immortalized 1799 cells, transformed non-tumorigenic 1198 cells and tumorigenic 1170-I HBE cells. In all of these cell lines SV40 T antigen binding inactivates the wild type p53. The 1198 and 1170-I cells have high levels of epidermal growth factor receptor (EGFR) and its ligand transforming growth factor alpha (TGFA) and both form colonies in soft agar yet only 1170-I cells express collagenase and are tumorigenic. In addition, we used normal small airway epithelial cells (SAEC) not shown in the schema. (Reddel et al, 1988; Klein-Szanto et al, 1992)



Comparison of gene expression in HBEC, SAEC, BEAS-2B, 1799, 1198, and 1170-I by Affymetrix oligonucleotide microarray. The expression of genes in normal (NHBE and SAEC) lung epithelial cells, immortalized BEAS-2B and 1799, transformed 1198, and tumorigenic 1170-I cells was analyzed using Affymetrix U133A chip. A subset of 1221 genes that were expressed differentially by at least 1.65 fold in immortal, transformed and tumorigenic cells relative to the normal cells included 466 down regulated and 346 upregulated genes throughout the carcinogenesis continuum as shown in Figure 13.

Functional pathway analysis of genes included in this profile using the INGENUITY software found that most of them are involved in cell cycle regulation or DNA replication and several are related to chromosomal instability (**MCM2-7, GMNN, CDC6, CDT1**, DUSP6, CAV1, FEN1, UBE2C, PTTG1, TOP2A, 14-3-3, NME1, TPX2, S100A4&8) (Figure 14).

We focused additional attention on several genes related to DNA replication, which increased in the carcinogenesis model including the minichromosome maintenance (MCM) genes MCM2, MCM3, MCM4, MCM5, MCM6, and MCM7, the essential DNA replication factor (licensing factor) CDT1, Geminin (GMNN) protein that is both an inhibitor of DNA synthesis and inducer of differentiation and CDC6, an essential regulator of DNA replication in eukaryotic cells involved in the assembly of pre-replicative complexes at origins of replication during the G1 phase of the cell division cycle and also in the activation and maintenance of the checkpoint mechanisms that coordinate S-phase and mitosis. MCM2-7, CDC6, CDT1 and GMNN all function together. The MCM2-7 proteins form a heterohexamer, function as DNA helicases and have been implicated at the initiation step of DNA synthesis. The assembly of functional MCM2-7 complexes on chromatin requires a sequential binding of CDC6 to origin recognition complex (ORC) to form a functional ORC-CDC6 ATPase, while CDT1 may link this ATPase to the MCM2-7 complex, which permits the recruitment of replication factors through a multistep

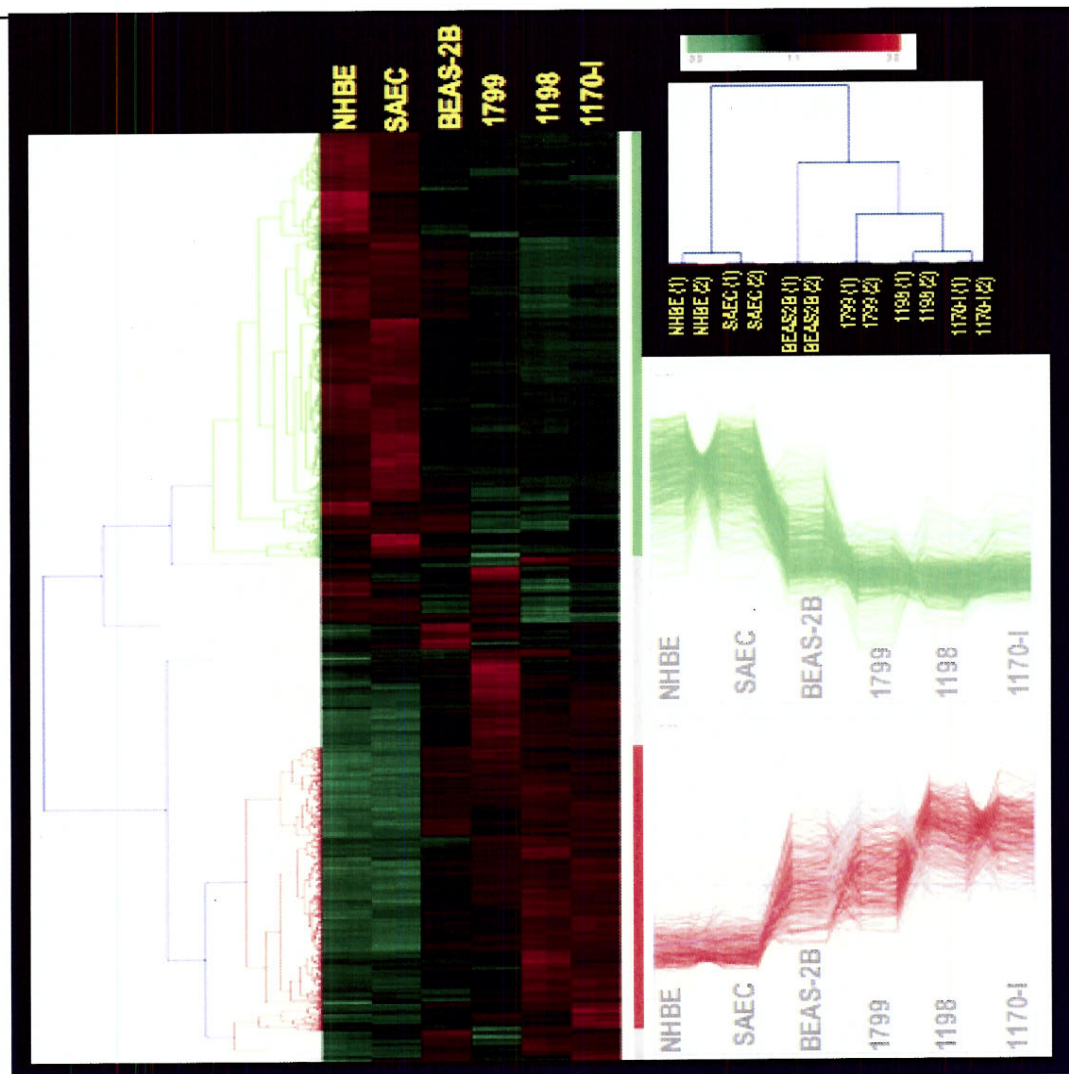


Figure 13. Differential expression of 812 genes in normal small airway epithelial cells (SAEC), BEAS-2B, 1799, 1198, and 1170 compared to NHBE cells. Unsupervised hierarchical clustering of the 1221 genes selected as differentially expressed (>1.65 fold change) based on Pearson Correlation with average linkage. The color scale (red to green) indicates the expression normalized by genes obtained with the microarray chip. They were further selected by SOM analysis of the Affymetrix data. Colored matrix (red high expression, green low expression) show different genes (each row is one gene) and the columns are mean of duplicate samples of RNA analyzed from the cell lines indicated at the top of the left panel. The panels on the right show graphic presentation of gradual changes (up or down) in expression level from normal lung epithelial cells to tumorigenic cells.

reaction leading to formation of replication forks, the functional units of DNA synthesis. In multicellular organisms, loading of MCM2–7 is also regulated by the geminin (GMNN) protein, which binds to CDT1 and stabilizing it in G2/M phases and also binding to Cdt1 - MCM2–7 complex and enhancing MCM2–7 recruitment onto chromatin after pre-RC formation (Mairoano et al., 2006). Our finding that all of these genes are unregulated supports the conclusion that they are important for the replication of immortalized, transformed and tumorigenic cells.

Expression of MCM2 in NSCLC cell lines is higher than in normal NHBE cells. To further determine whether MCM2 is increased in human NSCLC cell lines isolated from human tumors not generated artificially as in the BEAS-2B system, we employed

Genes in the network	Score	No. focus Gene	Top categories
↓ANKA4* , ↑AURKA* , ↑CCNA2 , ↑CCNB1 , ↑CCNB2 , ↑CDC2* , ↑CDC6* , ↑CDC7 , ↑CDC20 , ↑CDC25B , ↑CDC25C , ↑CDC45L , ↑CDT1 , ↑CKS1B , ↓CSTA , ↓FOS , ↑FOXM1 , ↑GMNN , ↑HMMR* , ↓LAMP2* , ↓LTBP2 , ↑MCM2 , ↑MCM3 , ↑MCM4* , ↑MCM5 , ↑MCM6 , ↑MCM7* , ↓MMP10 , ↑PTTG1 , ↓RBP1 , ↑RUVBL2 , ↓SERPINB7 , ↓TGFB1 , ↑TPX2 , ↑UBE2C	47	35	DNA Replication, Recombination, and Repair, Cell Cycle, Cellular Assembly and Organization
↑BUB1* , ↑BUB1B , ↓CD44* , ↑CENPE , ↑CENPF , ↑CSE1L* , ↓CSPG2* , ↓CTSB* , ↑DKK1 , ↑EIF5A* , ↓F3 , ↑FBLN1* , ↓FLNB , ↑FLOT1* , ↓FN1* , ↓GJB3* , ↓ITGB6 , ↑KPNA2 , ↑KPNB1* , ↓LTBP1 , ↑NXF1 , ↑PLEKHC1 , ↓PTHLH* , ↑RAE1 , ↑RANBP1 , ↑RCC1 (includes EG:1104), ↓S100A10 , ↓S100A11* , ↑TFPI , ↑TGM1 , ↓THBS1* , ↑THY1* , ↓TNC , ↓TXNIP* , ↑XPO1	47	35	Cancer, Cell-To-Cell Signaling and Interaction, Cellular Compromise
↓APLP2* , ↓APOE , ↓APP , ↑ATAD2 , ↓BIK , ↑CCT2* , ↑CCT5 , ↓CD59* , ↑CDKN2A* , ↑DHFR* , ↑DONSON , ↓FABP5 , ↑FEN1* , ↑G1P2 , ↓GLUL* , ↑HLA-C , ↓IER3 , ↓IFI16 , ↑IFITM2 , ↓ITM2B , ↑KIAA0101 , ↑MAP1B , ↓MCL1* , ↑MELK , ↑MSH6 , ↑PCNA , ↓RAB38 , ↑RFC4 , ↓S100A7 , ↓SNCA , ↑TCP1 , ↑TMEM97* , ↓TNFAIP3* , ↑TNFSF10* , ↑UCHL1	47	35	DNA Replication, Recombination, and Repair, Cell Death, Neurological Disease
↑AURKB , ↑BIRC5* , ↑BRRN1 , CDCA8 , ↑CENPA* , ↑CNAP1 , DES , ↑DNAJA1* , ↓FSCN1 , ↑HCAP-D3 , ↑HCAP-G , ↑HCAP-H2 , ↑HSP90AA1 , ↑HSPA8* , INCENP , ↑KIF23 , ↑KIF4A , ↓LINA1 , ↓LMNB1 , ↑LUZP5 , ↑NASP* , ↑PRC1 , ↓PRNP , PTGES3 , RACGAP1 , SMC2L1 , ↑SMC4L1* , ↑SOD1 , ↑STIP1* , ↑TLN1 , ↑TOP2A* , ↑TWIST1 , ↑UPP1 , ↑VIM , ↓YWHAZ*	27	26	Cell Cycle, Cellular Assembly and Organization, DNA Replication, Recombination, and

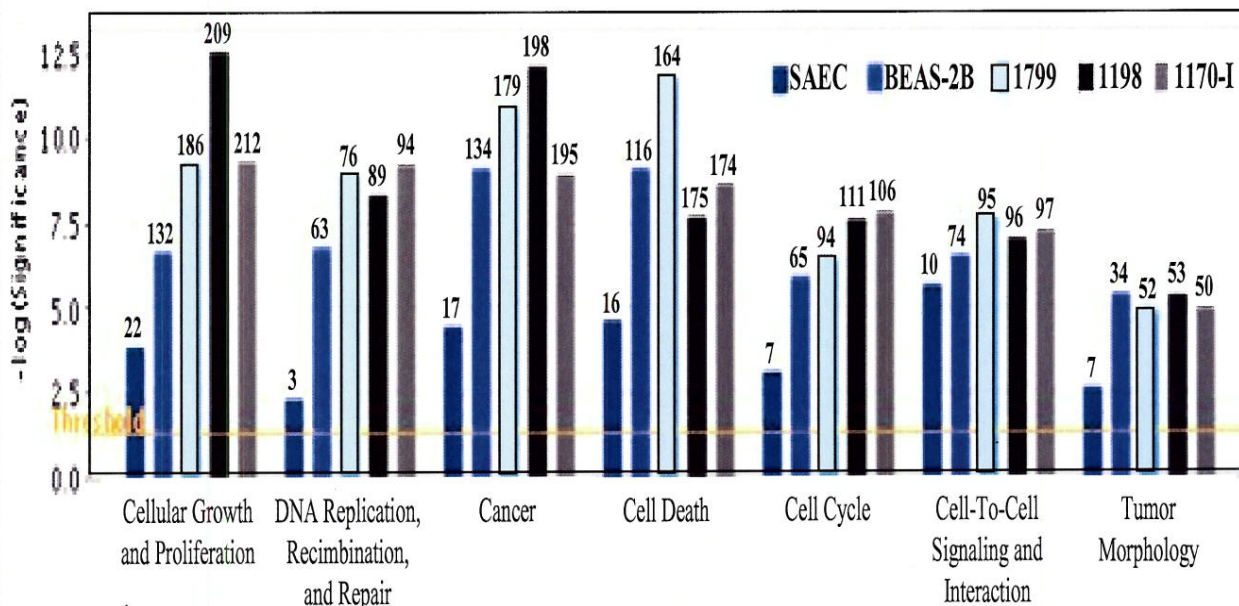


Figure 14. Examples of the genes modulated in the *in vitro* lung carcinogenesis model grouped in the main networks generated from Ingenuity Pathway Analysis (IPA) software after comparison of each cell line to NHBE cell transcriptome. Data in the table correspond to tumorigenic cell line 1170-I compare to NHBE. Genes in bold fonts displayed > 2-fold change. The Arrow indicates increase or decrease of gene expression in 1170-I compared with NHBE. The score is the negative log of P and indicates the likelihood of focus genes in a network being found together due to chance. No. of focus gene refers to the genes differentially regulated in the *in vitro* model, within an IPA network composed with a maximum number of 35 genes. The lower panel shows numbers of genes in different categories in the different cell lines.

quantitative RT-PCR method and analyzed 25 NSCLC cell lines compared to normal NHBE and SAEC cells (Figure 15, upper panel bar graph). All NSCLC expressed a higher level of MCM2 mRNA than the two normal cell strains. We then analyzed the different cells constituting the *in vitro* carcinogenesis model as well as several NSCLC cell lines using western immunoblotting and found that MCM2 protein increased from very low levels in the two normal cell strains SAEC and NHBE to higher levels in immortalized BEAS-2b and 1799 and even higher levels in transformed 1198 and tumorigenic 1170-I cells (Figure 15, lower panel). Finally, in collaboration with I. Wistuba (Core C), we analyzed the expression of MCM2 mRNA by quantitative RT-PCR using RNA isolated from surgical specimens from 20 adenocarcinomas and 17 squamous cell carcinomas (SCCs) and their paired corresponding normal tissues and found that with the exception of two SCCs all other tumors showed higher expression than their paired normal tissues (Figure 16; upper panel). These findings demonstrate that the findings from *in vitro* model apply to human tumors *in vivo*. Recently, also in collaboration with I. Wistuba, we have started to examine the expression of MCM2 in pathology specimens of normal, premalignant and malignant lung tissues and found higher expression of MCM2 protein in metaplasia, dysplasia and SCC compared to normal tissue (Figure 17).

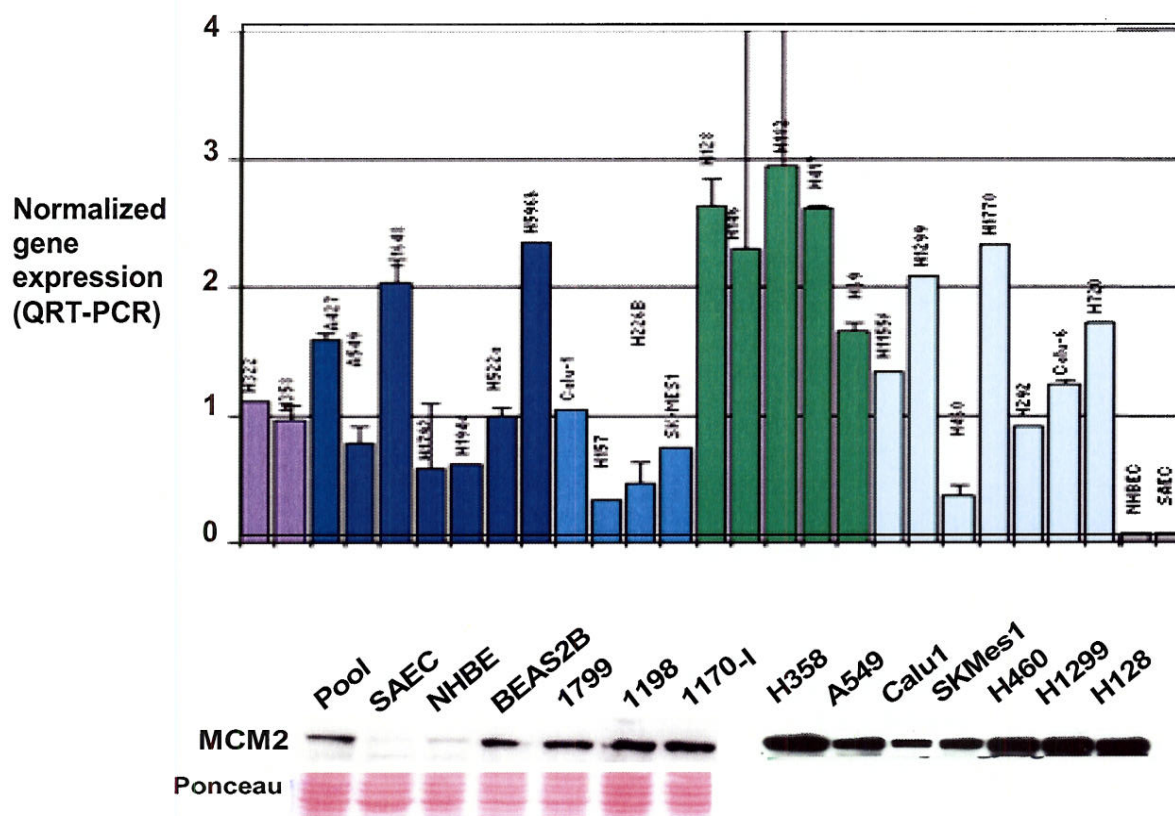


Figure 15. Expression of mini-chromosome maintenance 2 (MCM2) in the BEAS-2B carcinogenesis model and in different NSCLC cancer cell lines. The cell lines indicated above each bar were harvested and used for preparation of RNA samples. The samples were treated with DNase and 1 mg of RNA was reverse transcribed after control of quality and used for quantitative real-time PCR with primers for MCM2 (upper panels). Note that the normal cells are the two last bars on the right. Select cell lines were used to extract proteins. Protein samples were used for western immunoblotting with anti-MCM2 antibodies with Ponceau S staining of the proteins on the membrane as a control for loading in the different lanes (lower

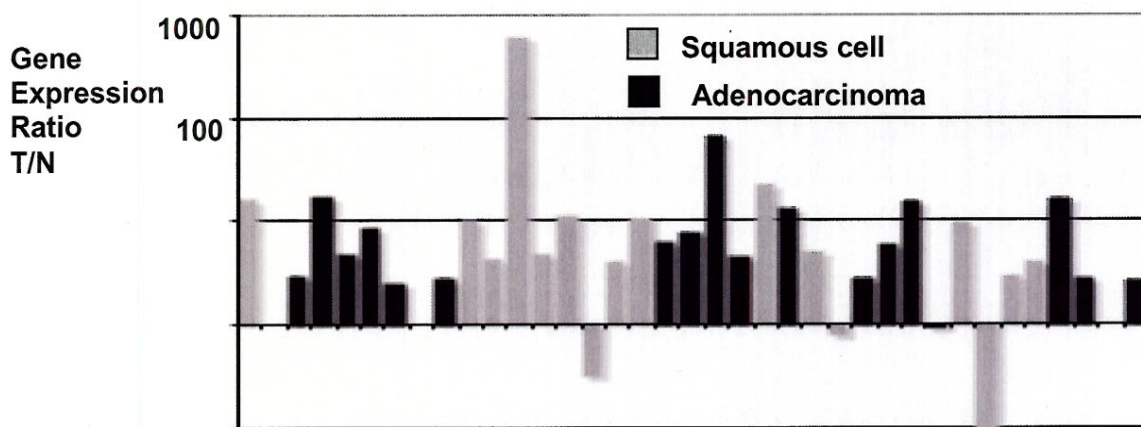


Figure 16. The expression levels of MCM2 gene measured by quantitative real-time PCR using RNA extracted from the surgical specimens from human NSCLC (20 adenocarcinomas and 17 SCC) and their non-tumoral counterparts. The bars represent the ratio of expression in paired tumor and normal tissue RNAs.

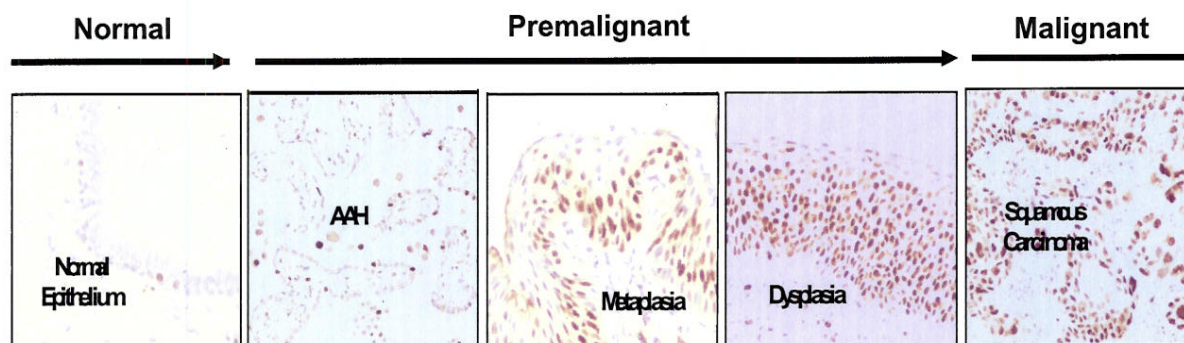


Figure 17. The expression levels of MCM2 assessed by immunohistochemistry in normal, preneoplastic, and neoplastic human lung tissues. Formalin-fixed paraffin-embedded tissues were sectioned into 5µm thick sections, which were then deparaffinized and processed for immunohistochemical analysis using anti-MCM-2 antibodies.

In the coming year, we will perform similar studies with several other biomarkers based on identification of clusters of genes that populate prominent pathways. MCM2 and some of the new potential markers will be analyzed in lung tissue microarrays and their expression or suppression in early lesions will be related to prognosis and possible early diagnosis.

Key Research Accomplishments:

- Established additional immortalized HBEC strains from multiple donors.
- Developed new methods for differentiating HBECs into complex epithelium using Matrigel and found that the HBECs have the cellular program intact to form branching morphogenesis and SACs and to expression pulmonary epithelial specific proteins such as SPA.
- Genetically manipulated the HBECs to derive isogenic strains that expressed oncogenic KRAS, mutant EGFR, and/or loss of p53 expression as well as HBECs with various EGFR tyrosine kinase domain mutations alone or with p53 knockout, and characterized their biologic and gene expression behavior showing they had partial progression towards malignancy
- Identified gene expression signatures associated with the introduction of oncogenic changes into the HBEC cells especially changes in expression of a set of cytokine genes and their receptors that are targets for early detection and chemoprevention of KRASV12 mediated lung cancer.
- Demonstrated progression of oncogenically manipulated HBECs to full malignancy after biologic selection in soft agar and identified the ability of such clones to differentiate into several histologic types of lung cancer.
- Performed genomic wide expression profiling and array CGH analysis for copy number changes in HBECs and in primary lung cancers. These have led to the identification of several amplified areas that will provide excellent probes for the early detection of preneoplastic changes in smoking damaged lung epithelium as well as biomarkers for chemoprevention studies.
- One of the key new genes identified as amplified in lung cancer pathogenesis is the lineage specific transcription factor TTF1. Functional studies of this gene indicate that it is essential for the continued growth of lung cancers. It is thus an excellent target for both early detection and for chemoprevention and potentially lung cancer therapeutics.
- Identified miRNA expression signatures differentially expressed between non-cancerous and cancerous bronchial epithelial cells.
- Identified novel miRNAs that are potentially important in the initiation and progression of lung cancer.
- Continued to collect and process bronchial brush specimens which now total 408.
- Identified 346 upregulated genes and 466 downregulated genes that displayed expression level variation from NHBE and normal small airway epithelial cells (SAEC) to the tumorigenic cell line (1170-I)
- Discovered that functional pathway analysis of the gene array data revealed modulation of expression of many genes involved in DNA replication, cell cycle, cell adhesion, and enzymatic pathways
- Confirmed the differential expression of one putative biomarker, - MCM2, at the mRNA and protein levels in the premalignant cell line model, as well as in cell lines derived from human lung cancers, by Western blotting and quantitative real-time PCR, and immunohistochemical analyses.
- The findings support the conclusion that MCM2-7, GMNN, CDC6, and CTD1 are all important for the replication of immortalized, transformed and tumorigenic cells.

Conclusions

We have developed new methods to study the differentiation of human bronchial epithelial cells with and without oncogenic changes *in vitro* including the study of branching morphogenesis, SAC formation, and the expression of lung specific proteins. We have found that oncogenically manipulated HBECs are capable of forming tumors of several histologies. We have defined a new series of amplified genes in lung cancer pathogenesis and especially highlighted the key role of TITF1 expression in the pathogenesis of lung cancer. Our results indicate that the use of the *in vitro* human lung carcinogenesis model for oligonucleotide microarray hybridization provides a powerful approach to identify molecules that may be involved in early or late events in human lung carcinogenesis. In addition, we have been successful in identifying potentially important players in tumor initiation and progression using miRNA arrays.

Future investigations are expected to allow us to identify valuable biomarkers, such as MCM2 that will be validated in large collection of lung cancers and lung premalignancies and to determine the biological role of the identified mRNAs in lung cancer tumorigenesis. These systems and genes will be tested for their expression and alteration in preneoplastic samples from VITAL obtained biospecimens in other portions of this grant. We are specifically trying to overexpress TITF1 in HBECs to see if it can drive these cells towards malignancy.

Project 3: Premalignant Bronchial Epithelia: Molecular and Cellular Characterization of Lung Tumorigenesis

(PI and co-PIs: Walter Hittelman, Ph.D., Ja Seok Koo, Ph.D., Rodolfo C. Morice, M.D.)

Aim 1 Identify and characterize differentially expressed genes in the LIFE bronchoscopy-identified abnormal areas of the bronchial epithelia of enrolled subjects in VITAL trials.

Previous studies have shown that bronchial regions that appear abnormal by LIFE bronchoscopy show increased genetic changes when compared to normal appearing sites, even if there are no differences in histological appearance. Since LIFE-positive lesions are at increased risk for cancer development, especially when they contain particular genetic alterations, we hypothesize that these LIFE-positive sites represent lesions at an early stage of tumorigenesis and may differentially express genes important for driving tumorigenesis. Thus, comparative gene expression analyses between LIFE-positive and LIFE-negative sites within the same individual may provide a filter for identifying genes whose levels of expression are important for driving tumorigenesis.

Update

1. LIFE Bronchoscopy and Sample Collection

Since the autofluorescence bronchoscopy system became available on Aug 16, 2005, we have collected 48 cases of Vanguard samples guided by light-induced fluorescence endoscopy (LIFE) technology. Among them, 17 cases matched our criteria and the samples of both biopsy and bronchial brushing from each of them were obtained.

The biopsies collected were cultured to isolate the primary tracheobronchial epithelial cells; all 17 cases were successfully cultured. A portion of these cells were used for studies described in Specific Aim 2.

The cells from the brushes were used to extract RNA for further microarray analysis. We have isolated total RNA from 15 cases and submitted for microarray analysis. RNA from 2 cases did not pass the quality control for array assay (87% success rate). Among them, transcriptome data from 11 cases were available for further evaluation.

Currently, these 11 microarray data sets are being analyzed by our biostatistic and bioinformatic team to identify differentially expressed genes in LIFE abnormal bronchial epithelial cells.

2. Molecular characterization of premalignant bronchial epithelial cells

Preliminary microarray analysis using RNA from a couple of brush specimens in LIFE abnormal lesions indicated that the expression of the proinflammatory cytokine interleukin (IL)-1 β and several angiogenic CXC chemokine genes were upregulated in the LIFE abnormal cells comparing with the LIFE normal cells. As IL-1 β has been shown to be involved in angiogenesis, we investigated whether LIFE abnormal cells have proangiogenic property via IL-1 β induced CXCL chemokines. Since the cells isolated from biopsies are limited, we initially used an NSCLC cell line, A549, and normal human tracheobronchial epithelium (NHTBE) cells.

We found that IL-1 β upregulated an array of proangiogenic CXCL chemokine genes in A549 and NHTBE cells, as determined by microarray analysis (Table 2). Further analysis revealed that IL-1 β induced much higher protein levels of CXCL chemokines in A549 cells than in NHTBE cells. Conditioned medium from IL-1 β treated A549 cells markedly increased endothelial cell migration, which was suppressed by neutralizing antibodies against CXCL5 and CXCR2 (Figure 18). This result suggests that IL-1 β -induced CXCL5 plays an important role in IL-1 β induced angiogenesis. We also found that IL-1 β -induced CXCL chemokine gene overexpression was dramatically abrogated in A549 cells with the knockdown of NF- κ B or cyclic adenosine monophosphate response element-binding protein (CREB) (Figure 19). Moreover, the expression of both the CXCL chemokine genes and CREB was greatly increased in the tumorigenic NSCLC cell line compared with normal and premalignant *in vitro* lung cancer model cell lines. A small molecule inhibitor of CREB activity [naphthol phosphate] inhibited IL-1 β -induced CXCL chemokine gene expression and angiogenic activity in NSCLC (Figure 20). This result suggests that LIFE abnormal bronchial epithelial cells may have an angiogenic property. Further studies are underway to confirm this finding. A manuscript summarized these findings is submitted to Cancer Prevention Research and a manuscript summarized the findings of the role of CREB in the growth and survival of NSCLC is accepted for publication in Cancer Research.

In conjunction with our previous results demonstrating that targeting the CREB signaling pathway suppresses the growth and survival of NSCLC (Cancer Research, 2008, In Press) and that overexpression of CREB is associated with a negative prognosis in NSCLC patients (Cancer Research, 2008, In Review), these results strongly indicate that CREB may serve as a preventive and/or therapeutic target for NSCLC.

Table 2. Analysis of IL-1 β induction of CXC chemokine gene expression in NHTBE and A549 cells using microarray and real-time PCR analysis.

Gene Name	Systematic Name	Gene Description	NHTBE (fold change)		A549 (fold change)	
			microarray	PCR	microarray	PCR
CXCL1	NM_001511	Homo sapiens chemokine (C-X-C motif) ligand 1	18.6	11.9	32.5	26.9
CXCL2	NM_002089	Homo sapiens chemokine (C-X-C motif) ligand 2	18.6	12.9	23.3	14.9
CXCL3	NM_002090	Homo sapiens chemokine (C-X-C motif) ligand 3	18.2	29.9	19.2	11.7
CXCL5	NM_002994	Homo sapiens chemokine (C-X-C motif) ligand 5	173.3	95.9	12.0	8.2
CXCL6	NM_002993	Homo sapiens chemokine (C-X-C motif) ligand 6	31.3	80.6	13.9	28.8
CXCL8	NM_000584	Homo sapiens chemokine (C-X-C motif) ligand 8	11.9	17.6	40.8	32.4
VEGF	NM_001025366	Homo sapiens vascular endothelial growth factor	2.49	1.93	3.2	2.14

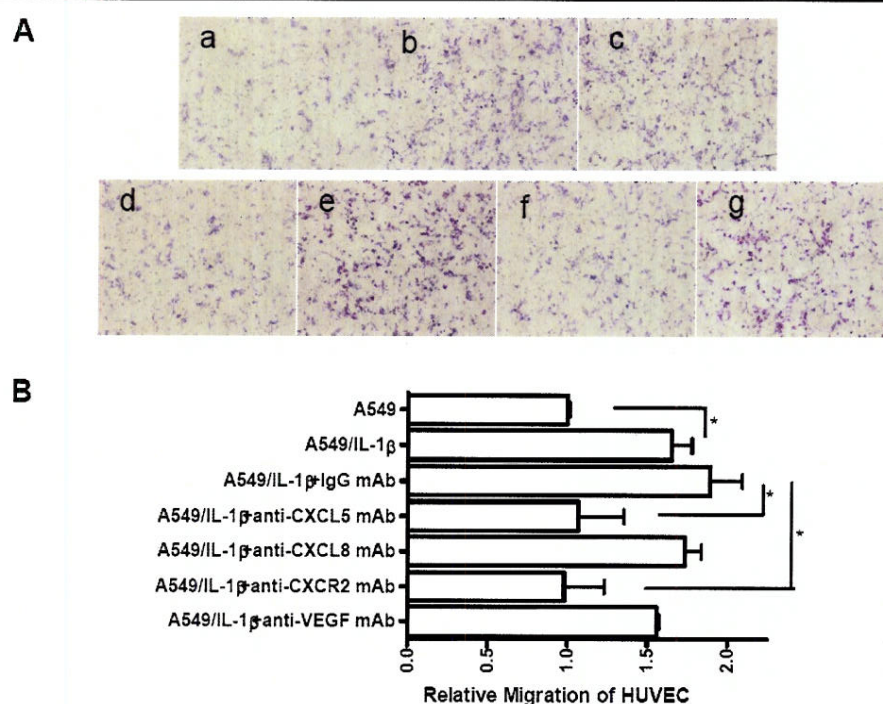
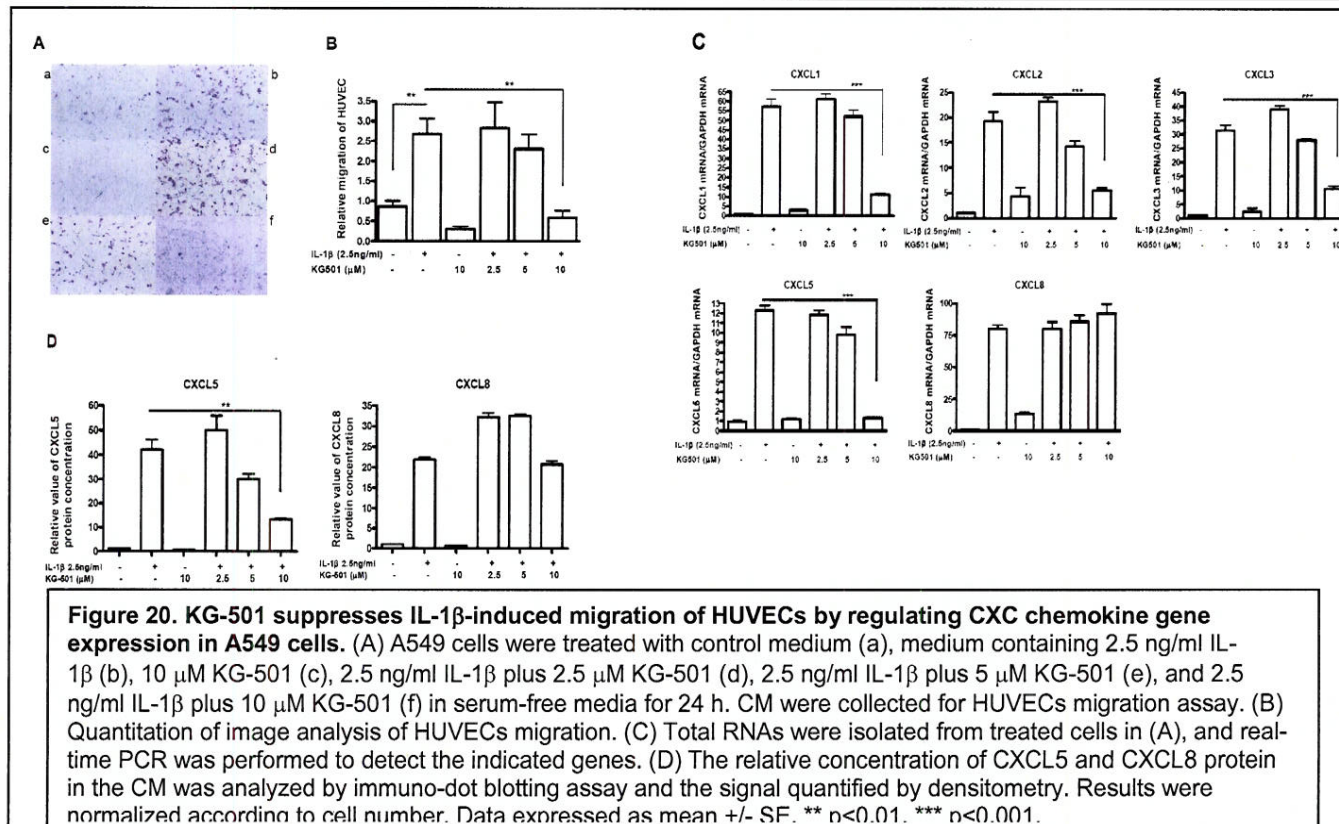
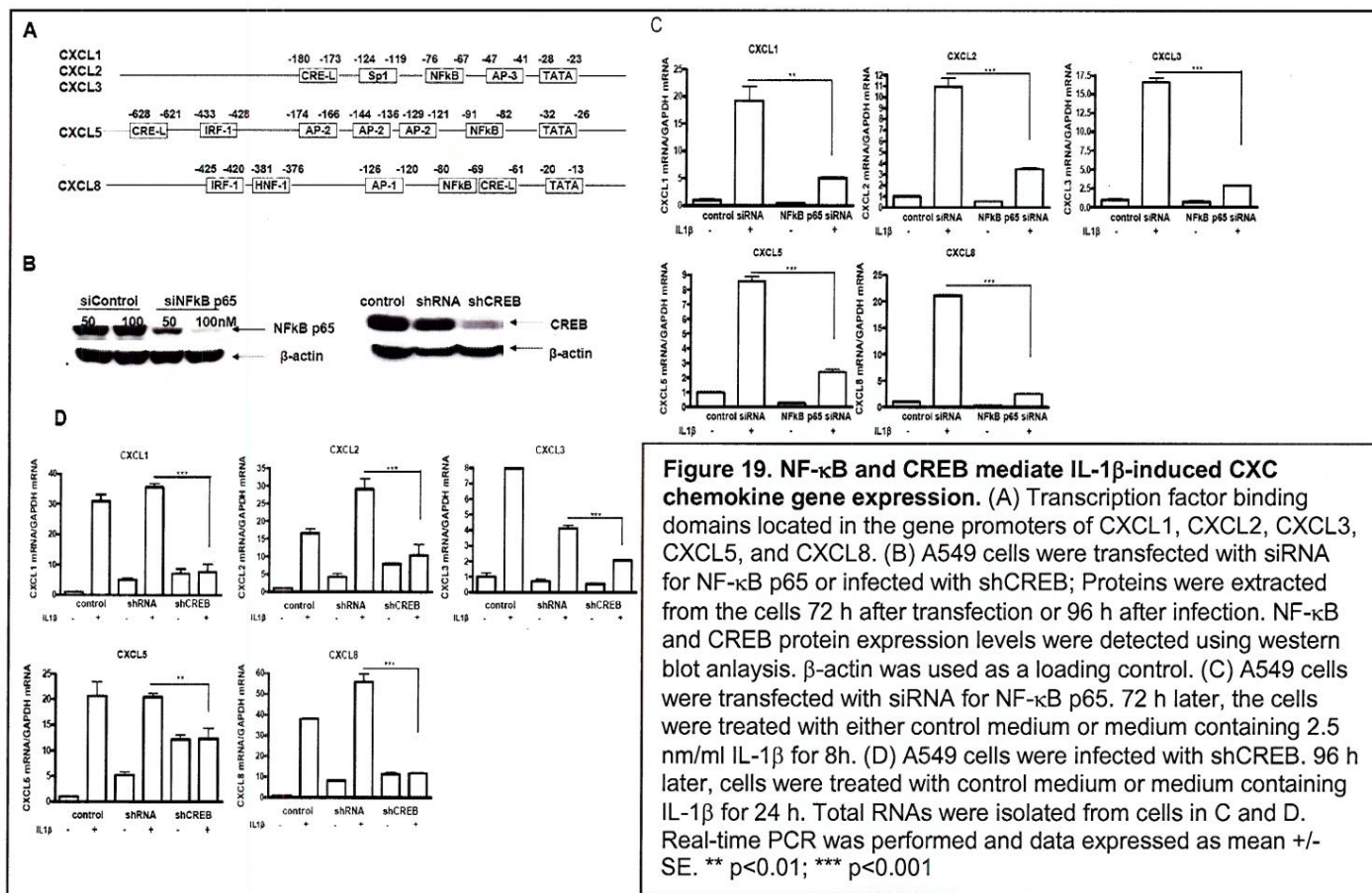


Figure 18. IL-1 β significantly augments the angiogenic activity of NSCLC by inducing the expression of angiogenic CXC chemokine genes. (A) Culture media (CM) were collected from A549 cells treated with either control medium (a) or medium containing 2.5 ng/ml IL-1 β (b) in serum-free medium for 24 h and from IL-1 β treated A549 cells preincubated with 10 μ g/ml of murine IgG (c), and an anti-CXCL5 monoclonal antibody (mAb) (d), an anti-CXCL8 mAb (e), an anti-CXCR2 mAb (f), or an anti-VEGF mAb (g) at 37°C for 1 hr. HUVECs migration assay was performed in response to the indicated CM. Cells were photographed after 16 h of incubation at 37°C. (B) Image analysis of HUVECs migration was quantified using the ImageJ software program. Data were expressed as the mean \pm SE. * ($p < 0.05$).



Aim 2 Establish an organotypic model system that mimics *in vivo* interactions between normal, premalignant, and malignant bronchial epithelial cells in the lung using cells derived from bronchial biopsies and immortalized bronchial cells.

Our prior studies using chromosome *in situ* hybridization to visualize genetic changes in the bronchial epithelium of current and former smokers suggested that, over years of tobacco smoke exposure, the combination of accumulating genetic damage, ongoing tissue damage, and wound healing results in a mosaic of evolving clonal outgrowths throughout the bronchial epithelium. To better understand the molecular basis of preferential outgrowth of more advanced bronchial epithelial clones, we proposed to utilize a cell culture model whereby normal and abnormal bronchial epithelial cells are grown on collagen or stromal cell-coated, suspended filters and exposed to an air-liquid interface. This organotypic culture environment mimics lung stratified epithelium, complete with basal cells, ciliated columnar cells, and mucus-producing goblet cells. Our group has extended this model system by tagging cell populations with fluorescent probes (e.g., green fluorescence protein) that allows us to carry out live cell imaging of mixed clonal populations. This model system permits characterization of the ability of more advanced bronchial epithelial cell populations to expand on the growth surface at the expense of less advanced bronchial epithelial cell populations.

Update

Our long-term plan associated for this Specific Aim was to obtain biopsy specimens from individuals participating in the clinical trial of Project 1 and to compare the differential growth properties in organotypic cultures of bronchial epithelial cells derived from LIFE bronchoscopy positive regions with those from negative regions. While awaiting initiation of fluorescence bronchoscopy in the clinic and the development of paired bronchial epithelial outgrowths from biopsy sites (one from fluorescence normal and one from fluorescence abnormal), we focused our *in vitro*, organotypic studies on already established bronchial epithelial cell types, including commercially available normal bronchial epithelial cells, cells from bronchial biopsies that have been immortalized (HCC-BE cells) with transfection of cyclin dependent kinase 4 (cdk4) and telomerase (h-TERT) by our colleagues in Dallas (Jerry Shay, John Minna), as well as cells that were derived from Ad12/SV40-transfected bronchial epithelial cells (BEAS 2B) and subsequently immortalized *in vivo* (1799), transformed with carcinogens (1198), and then selected for a tumorigenic phenotype (1170).

In studies reported in prior Progress Reports, we showed that the relative ability of these different cell populations to compete for the three dimensional growth plane in the organotypic cultures by marking the different cell populations with distinct fluorescent living color probes (e.g., GFP, RFP, and CFP), plating the cells in distinct colonies in the same culture model, and then monitoring their relative capability to expand at the expense of other marked cell populations. We used live cell fluorescence microscopy to examine the populational interactions over time (generating digital movies of the time course of the interactions), and we used laser scanning confocal microscopy to examine the three-dimensional aspects of competing cell populations. We found that more neoplastically-advanced bronchial epithelial cell populations showed increased ability to expand their colony borders at the expense of more normal bronchial epithelial cell populations, however, retention of E-cadherin was important for maintaining this preferential ability to take over the growth plane. Among the cdk4/h-TERT-immortalized cell populations, we found that the HCC-BE2 cells were most capable of preferential colony outgrowth (HCC-BE2 > HCC-BE3 > HCC-BE1 > NHBE cells). These results need repeating for confirmation. It will be interesting to examine the gene expression array results from the other projects in VITAL to identify the signaling pathways associated with preferential clonal expansion.

One challenge that we will face when we carry out the proposed studies with fresh bronchial cell outgrowths (obtained from biopsies from different lung sites from the same individual and initiated by Dr. Koo's laboratory) is that the cells will not contain living color markers. Since these bronchial epithelial cells will not have been immortalized *ex vivo* and have a limited number of culture passages, it would be difficult to transfect these cells and then select for cells that have been stably transfected using antibiotic selection. Also, fresh normal cells are known to have low transfection frequencies. We therefore decided to utilize lentiviral infection technologies to generate bronchial epithelial populations containing living color genes. Lentiviral infection strategies have the advantage of high infection rates and the expression of the genes does not require that the cell populations be rapidly proliferating. We initiated the generation of lentiviral vectors that will allow us to label these bronchial epithelial cells either GFP, YFP, monoRFP, or CFP in these freshly generated cultures. We also initiated the generation of lentiviral vectors that will allow us to infect cells with color-tagged genes or siRNAs of interest to better characterize the molecular underpinnings of preferential clonal outgrowth.

We are making advances on two aspects of the project that will facilitate future work. First, we have initiated the development of image analysis strategies that will allow us to better automate the quantitative description of interacting clonal bronchial epithelial populations. This involves mixing labeled and unlabeled bronchial epithelial cells from the same population in order to automatically record the location of individual cells over time. Interestingly, while the population of cells as a whole may appear to be moving in a particular direction, individual cells are found to move in several directions (some even in the opposite direction). Second, we have acquired a spectral imaging camera that can be attached to our live cell imaging microscope. This camera acquires whole spectral characteristics for each picture element in the image. With the accompanying software, this permits one to examine and distinguish multiple colors at once. This imaging system, along with new multi-labeling technologies recently described in the literature (Livet et al, 2007), will enable us to better examine the clonal interactions both from a population perspective as well as from a single cell perspective.

Aim 3 Determine the mechanisms of genetic instability and elucidate the signaling pathways associated with clonal outgrowth of premalignant and malignant bronchial epithelial cells using the organotypic model system.

Our prior studies using chromosome *in situ* hybridization to visualize genetic changes in the bronchial epithelium of current and former smokers suggested that current tobacco exposure was associated with increased levels of ongoing genetic instability (i.e., chromosome polysomy). Upon smoking cessation, while the initiated clonal outgrowths appeared to be maintained over tens of years, the levels of ongoing genetic instability appeared to decrease gradually during the first year following smoking cessation. However, in some cases, we observed evidence for ongoing genetic instability in the bronchial epithelial cells even 10-20 years following smoking cessation. Since nearly half of the newly diagnosed lung cancer cases occur in former smokers, we felt that this finding suggested that there might exist an ongoing intrinsic process of genetic instability in the lungs of some former smokers that drives continued genetic evolution toward lung cancer even after cessation of extrinsic carcinogenic exposure.

Our working hypothesis is that years of tobacco exposure induces a chronic damage and wound healing cycle that results both in the accumulation of genetic alterations in the epithelial cells that influences both chromosome stability mechanisms (e.g., loss of cell cycle checkpoint and cell loss mechanisms through loss of p16 expression, p53 mutations, cyclin D1 overexpression, etc) and creates a poor growth environment (e.g., altered stromal signals). The goal of this

specific aim was to utilize the lung organotypic model to address this hypothesis *in vitro* utilizing bronchial epithelial cells derived from LIFE bronchoscopically identified “abnormal” and “normal” regions of the lung of current and former smokers participating in the clinical trial of Project 1.

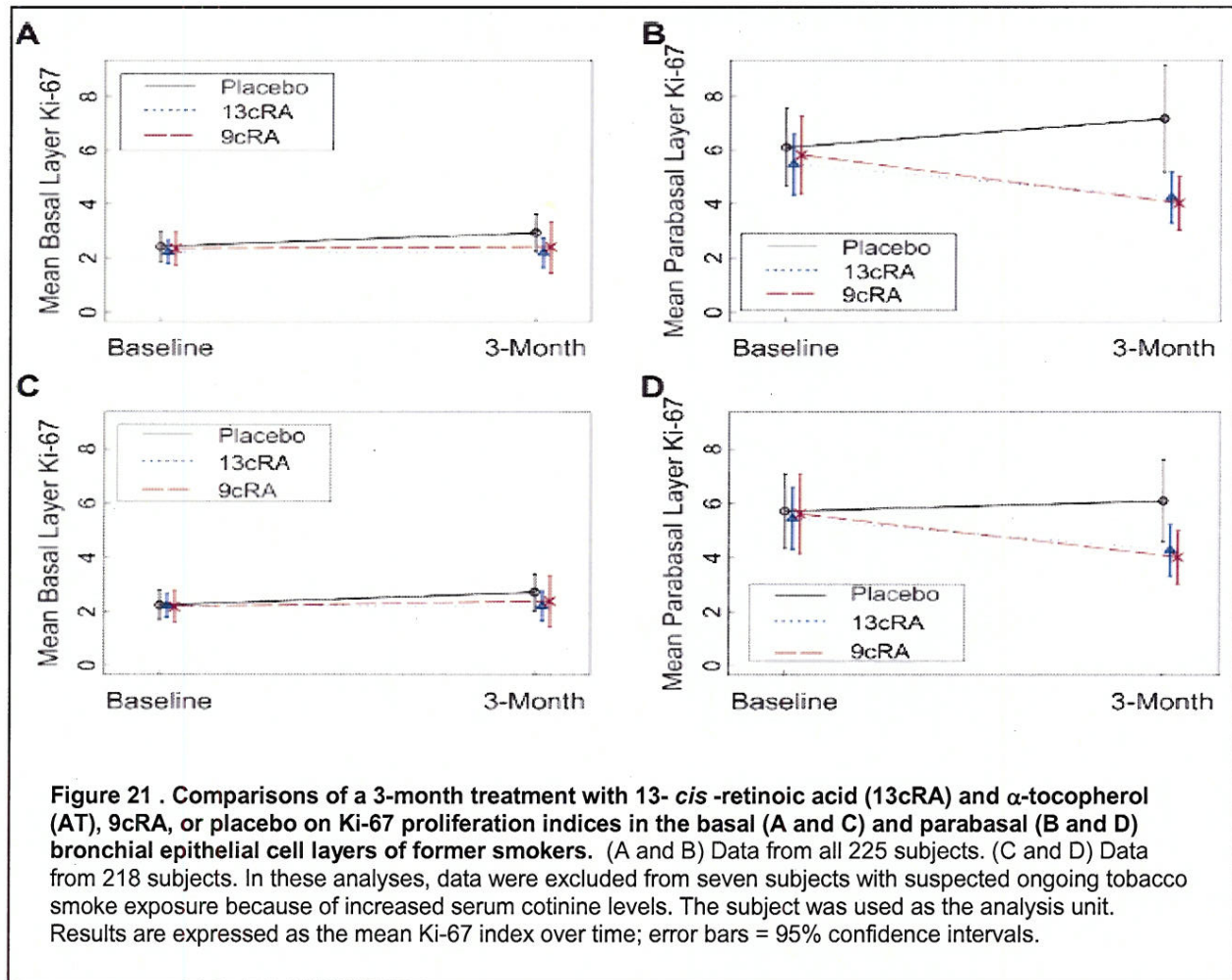
Update

We previously provided data that suggested that ongoing genetic instability could be detected in these bronchial epithelial cells and led to the development of subclonal outgrowths. When grown in the three dimensional, lung organotypic culture model, we found that spatial dysregulation of proliferation was associated with increased genetic instability as measured by examining the fidelity of mitosis. NHBE cells were found to preferentially proliferate and divide at the basal layer, and this was associated with genetic fidelity at anaphase. In contrast, more neoplastically-advanced cells were found to also proliferate away from the basal layer, and this was associated with increased levels of mitotic error (i.e., chromosome bridges, lagging chromosomes, and multipolar spindles). While the cdk4/hTERT immortalized normal bronchial epithelial cells derived from subjects with a tobacco history predominantly divided at the basal layer, they do show cells proliferating away from the basal layer and these cells show increased levels of mitotic error. We also observed increased levels of stress response (i.e., phospho-Histone H2AX staining) in the parabasal and superficial layers of the cultures in these more advanced cell populations, suggestive either of altered DNA replication control or response to DNA damage downstream of mitotic error. Our *in vitro* studies with premalignant oral epithelial cells have demonstrated that overexpression of cyclin D1 can lead to dysregulated cell cycle control and mitotic errors very similar to that seen in these bronchial epithelial organotypic cultures. We therefore hypothesize that, since the cyclin D1 partner for kinase activity is cdk4, and since these bronchial epithelial cells have been immortalized with cdk4, similar genetic instability mechanisms may be at play.

We recently reported in JNCI (Hittelman et al, 2007) that treatment of former smokers with either 13-cis-retinoic acid or 9-cis-retinoic acid is associated with decreased levels of proliferation (Ki-67 labeling) in the parabasal layers of the bronchial epithelium of former smokers (Figure 21). Therefore, we are hopeful that regulating proliferation in the bronchial epithelium may result in decreased genetic instability and perhaps ultimately delay cancer onset in individuals at increased lung cancer risk. Our findings in this organotypic culture model may therefore provide a testing ground for potential preventive strategies.

Aim 4 Characterize the impact of chemopreventive and/or chemotherapeutic agents on early lung tumorigenesis events in reconstructed bronchial epithelium and in the bronchial biopsies of subjects entered onto the clinical trials in Project 1.

The goals of the first three specific aims of this project are essentially to develop and utilize the lung organotypic culture model to identify the factors that control ongoing clonal expansion and genetic instability in the lungs of current and former smokers. The idea behind this fourth specific aim is to integrate the information garnered from the first three specific aims to identify targeted strategies to slow preferential outgrowth of more advanced bronchial epithelial cells and to decrease the levels of ongoing genetic instability. We also proposed to determine whether treatment of these organotypic cultures with the chemopreventive agents used in the clinical trial of Project 1 would slow these aberrant properties *in vitro* and whether results obtained in the organotypic culture model reflected that seen in the lungs of the participants in the clinical trial.



Update

This aspect of the project has been delayed until the necessary lentiviral vectors are completed so that we may visualize clonal interactions and genetic instability directly in living primary bronchial epithelial cells derived from bronchial biopsies taken from fluorescence normal and abnormal regions. Dr. Koo has already established more than 14 such pairs of primary cultures and they remain in the frozen state ready to move forward when the lentiviral vectors are completed.

Aim 5. Identify gene expression signatures in epithelial cells detected by LIFE bronchoscopy that determine aggressiveness.

- Determine genes involved in the migration and invasion character of LIFE normal and LIFE abnormal cells.
- Determine the genes involved in the angiogenic character of LIFE normal and LIFE abnormal cells.
- Determine if the genes identified in Tasks 6.1-6.2 are altered in our retrospective samples using TMAs.

This new aim under the ReVITALization plan will be performed in conjunction with Dr. Wistuba, Core C Director. Our preliminary results from our research in VITAL have shown that epithelial cells isolated from bronchial biopsies of LIFE abnormal mucosa can be characterized as more aggressive (invasive and migratory) than those of LIFE normal mucosa. Microarray analysis suggested that several CXCL-chemokine signaling pathways are mainly deregulated in LIFE abnormal cells. Moreover, we identified that pro-angiogenic ELR+ (glutamic acid, lysine and arginine motif) chemokines were strongly upregulated by inflammatory cytokines in lung cancer cells.

Based on these studies, we hypothesize that LIFE abnormal cells acquire aggressive behaviors via abnormal expression of genes in CXCL-chemokine pathways. To test the hypothesis, we set following specific goals:

- i. **To determine genes involved in the migration and invasion character of LIFE normal and LIFE abnormal cells.** In this aim, we will confirm the migration and invasion tendency of LIFE normal and LIFE abnormal cells using organotypically cultured bronchial epithelial cells reconstituted from LIFE normal and abnormal biopsies from 10 different patients. We will further characterize the differentially regulated genes in the chemokine pathways. Expression level of genes involved in this process, particularly CXCL chemokines, will be determined by real-time PCR and ELISA methods. Critical CXCLs involved in migration and invasion of LIFE abnormal cells will be identified by measuring effective blocking of migration and invasion after treatment with blocking antibody or siRNA targeting specific CXCLs.
 - ii. **To determine the genes involved in the angiogenic character of LIFE normal and LIFE abnormal cells.** In this aim, we will measure whether the CXCLs identified play a crucial role in induction of neoangiogenesis of vascular cells to LIFE abnormal cells. We will co-culture LIFE normal/LIFE abnormal cells with HUVEC to compare the angiogenesis and tube formation of HUVEC (human vascular endothelial cells) induced by LIFE normal and LIFE abnormal cells. We will also use animal model-LIFE abnormal cells mixed in the Matrigel plug- to test angiogenic factors produced from LIFE abnormal cells.
- As seen above in Aim 1, we have already identified several using our cytokine arrays. Research will continue this next year to further elucidate these genes and their roles in tumor initiation and progression.
- iii. **To determine if the genes identified in Aims 1A and 1B are altered in our retrospective samples using TMAs.** Critical proteins newly identified in the work above will be examined and verified by IHC analysis in TMA using the archived tissues in collaboration with Dr. Wistuba.

Upon completion of these studies, we will be able to clearly define the main characteristics of LIFE abnormal cells with definitive targets for the premalignant epithelial cells.

Key Research Accomplishments

- Determined that the proangiogenic chemokine CXCL5 is strongly upregulated by IL-1 β cytokine in premalignant and malignant lung cancer cell lines. CREB is required for the upregulation of the proangiogenic chemokine gene.
- Determined that targeting the CREB signaling pathway using chemical or genetic methods suppresses the growth and survival of NSCLC.

- Discovered that CREB is gradually overexpressed during lung cancer progression and overexpression of CREB is associated with negative prognosis in NSCLC patients.
- Determined that treatment of former smokers with either 13-cis-retinoic acid or 9-cis-retinoic acid is associated with decreased levels of proliferation (Ki-67 labeling) in the parabasal layers of the bronchial epithelium of former smokers.
- Further developed our imaging technologies and quantitative analytical algorithms for the future analyses of these studies.

Conclusions

We conclude that CREB may play an important role in driving tumorigenesis of lung cancer by modulating the proangiogenic chemokines of premalignant and malignant cells in response to the proinflammatory cytokine IL-1 β .

We have continued to develop new strains of bronchial epithelial cells from individuals participating in our lung chemoprevention and long-term follow up trials. We have continued to develop and characterize the growth and competitive capabilities of bronchial epithelial cells with regard to their preferential ability to take over the growth surface from other bronchial epithelial cells. Moreover, we have initiated studies to better understand the molecular mechanisms underlying the preferential takeover advantage of one cell strain over another. We have also improved our ability to monitor and quantify the growth interactions between cell populations using digital imaging and live cell microscopy.

In the coming year, we will complete the analysis of microarray data and identify/characterize differentially expressed genes in premalignant bronchial epithelial cells. As we obtain bronchial epithelial cells derived from subjects showing abnormal autofluorescence patterns in their bronchial lining, we will inoculate these cells into the organotypic cultures and examine their degree of ongoing genetic instability and preferential clonal outgrowth. We will also examine the effect of chemopreventive agents on preferential clonal outgrowth and genetic instability.

Project 4: Modulation of Death Receptor-Mediated Apoptosis for Chemoprevention

(Project Leader and co-leader: Shi-Yong Sun, Ph.D.; Fadlo R. Khuri, M.D.)

The objective of Project 4 is to understand the role of death receptor (DR)-mediated apoptotic pathways in lung carcinogenesis, cancer prevention, and therapy in order to develop mechanism-driven combination regimens by modulating DR-mediated apoptosis for chemoprevention and therapy of lung cancer. Following is a summary of our research progress:

Aim 1 To determine whether decoy receptor (DcR) and tumor necrosis factor-related apoptosis-inducing ligand (TRAIL) expression are reduced or lost while DR remains largely expressed and whether procaspase-8 and FLIP expression and Akt activity are increased during lung carcinogenesis.

Update

We finished IHC detection of DR5 and caspase-8 in tissue array slides, which were purchased from Imgenex (IMH-358; San Diego, CA) and consist of 50 cases of human lung cancers (48 NSCLCs and 2 SCLCs) and 9 cases of normal lung (adjacent to cancer) tissues. Among lung cancer cases, there are 10 cases of lymph, bone or soft tissue metastatic tissues. In general, most of the cases of normal tissues do not express either DR5 or caspase-8 while the majority of lung cancer tissues, including

metastatic ones, express both DR5 and caspase-8. We detected no caspase-8 expression in two cases of SCLCs and DR5 expression in one of two NSCLCs. These results are consistent with published results in the literature indicating that some key components in the extrinsic apoptotic pathway are frequently inactivated, likely by gene methylation, in SCLCs (Shivapurkar et al. 2002; Hopkins-Donaldson et al. 2003).

We will continue to determine c-FLIP, DR4 and TRAIL expression in the final program grant year.

Aim 2 To establish TRAIL-resistant cell lines from a TRAIL-sensitive lung cancer cell line and determine whether levels of DcRs, DRs, procaspase-8, TRAIL and FLIPs and Akt activity are altered and are associated with cell resistance to TRAIL and DR-inducing agents.

Update

The nuclear p68 RNA helicase is a prototypical DEAD box family of RNA helicase. The p68 RNA helicase plays a very important role in cell proliferation and early organ development and maturation. Its expression levels were shown to correlate with tumor progression and transformation. In collaboration with Dr. Zhi-Ren Liu at Georgia State University (Atlanta, GA), we have shown that phosphorylation of the p68 RNA helicase is dramatically increased in TRAIL-resistant cell lines, which was established in our lab through the VITAL program. We have demonstrated that the double tyrosine phosphorylation of p68 RNA helicase confers resistance to TRAIL-induced apoptosis, most likely through upregulation of XAF-1, a newly discovered cellular factor that facilitates cell apoptosis by binding and changing subcellular localization of XIAP (Figure 22).

Because cross-resistance to some DR-inducing agents was not found in TRAIL-resistant lung cancer cell lines, we have focused on addressing the question whether these agents modulate the death receptor-mediated apoptotic pathways and, if yes, whether the modulation impacts apoptosis by these DR-inducing agents. Following are our findings in this regard:

- a. Modulation of DR5 and c-FLIP expression and enhancement of TRAIL-induced apoptosis by the celecoxib derivative dimethyl-celecoxib (DMC) which lacks COX-2-inhibitory activity.

Celecoxib exhibits anticancer activity in both preclinical studies and clinical practice. However, celecoxib has relatively weak apoptosis-inducing activity and modest cancer therapeutic efficacy. Therefore, efforts have been made to develop derivatives of celecoxib with superior anticancer activity. 2,5-dimethyl-celecoxib (DMC) is a derivative of celecoxib that lacks COX-2-inhibitory activity. Several preclinical studies have demonstrated that DMC has better apoptosis-inducing activity than celecoxib, albeit with undefined mechanisms, and exhibits anticancer activity in animal models. In this study, we primarily investigated DMC's cooperative effect with TRAIL on induction of apoptosis and the underlying mechanisms in human NSCLC cells. We found that DMC was more potent than celecoxib in decreasing the survival and inducing apoptosis of NSCLC cells. When combined with TRAIL, DMC exerted enhanced or synergistic effects on induction of apoptosis, indicating that DMC cooperates with TRAIL to augment induction of apoptosis (Figure 23). Exploring the underlying mechanism of the synergy between DMC and TRAIL, we have demonstrated that DMC induces a CHOP-dependent expression of DR5, a major TRAIL receptor, and reduces the levels of c-FLIP (both FLIP_L and FLIP_S), key inhibitors of death receptor-mediated apoptosis, by facilitating c-FLIP degradation through a ubiquitin/proteasome-dependent mechanism. Importantly, enforced expression of c-FLIP or silencing of DR5 expression contribute to cooperative induction of apoptosis by the combination of DMC and TRAIL (Figures 24, 25). Collectively, we conclude that DMC sensitizes human NSCLC cells to TRAIL-induced

apoptosis via induction of DR5 and downregulation of c-FLIP. This work was published in *Molecular Pharmacology* (Chen et al. 2007).

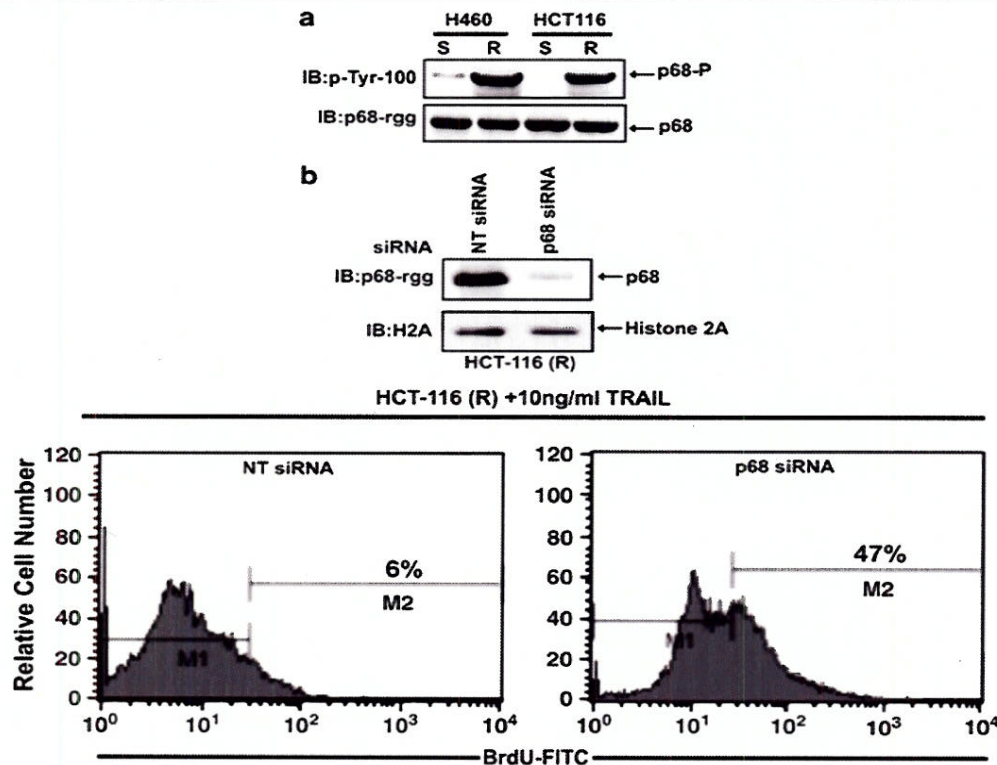
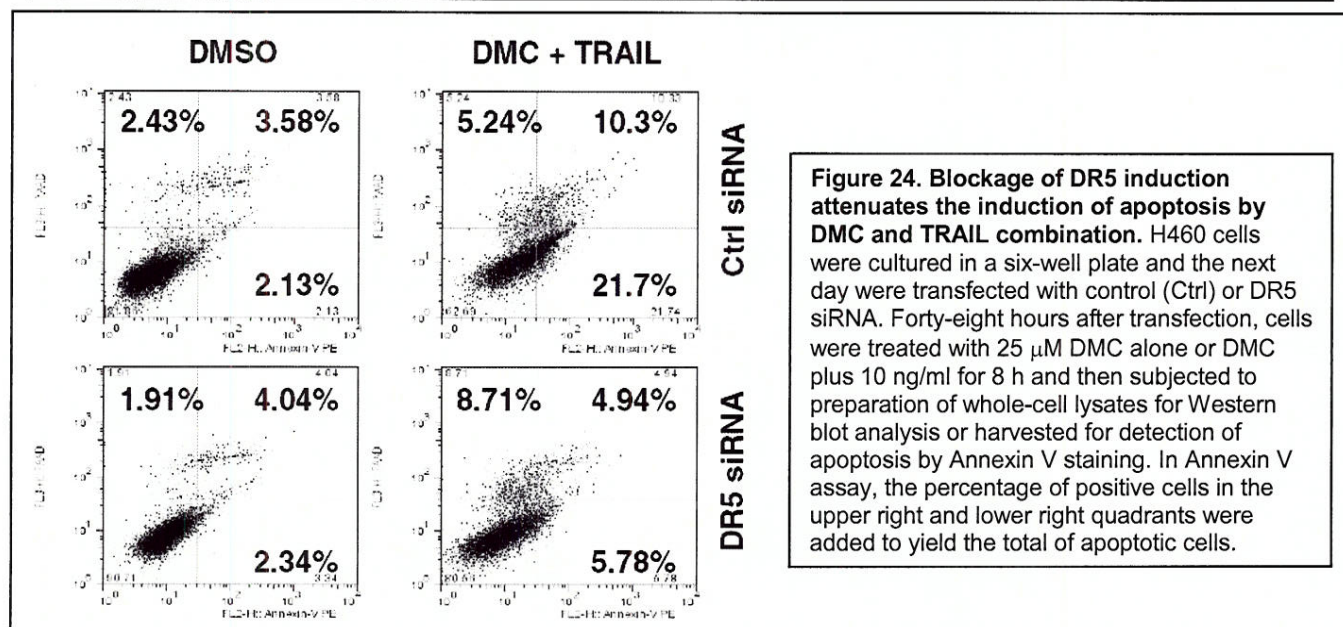
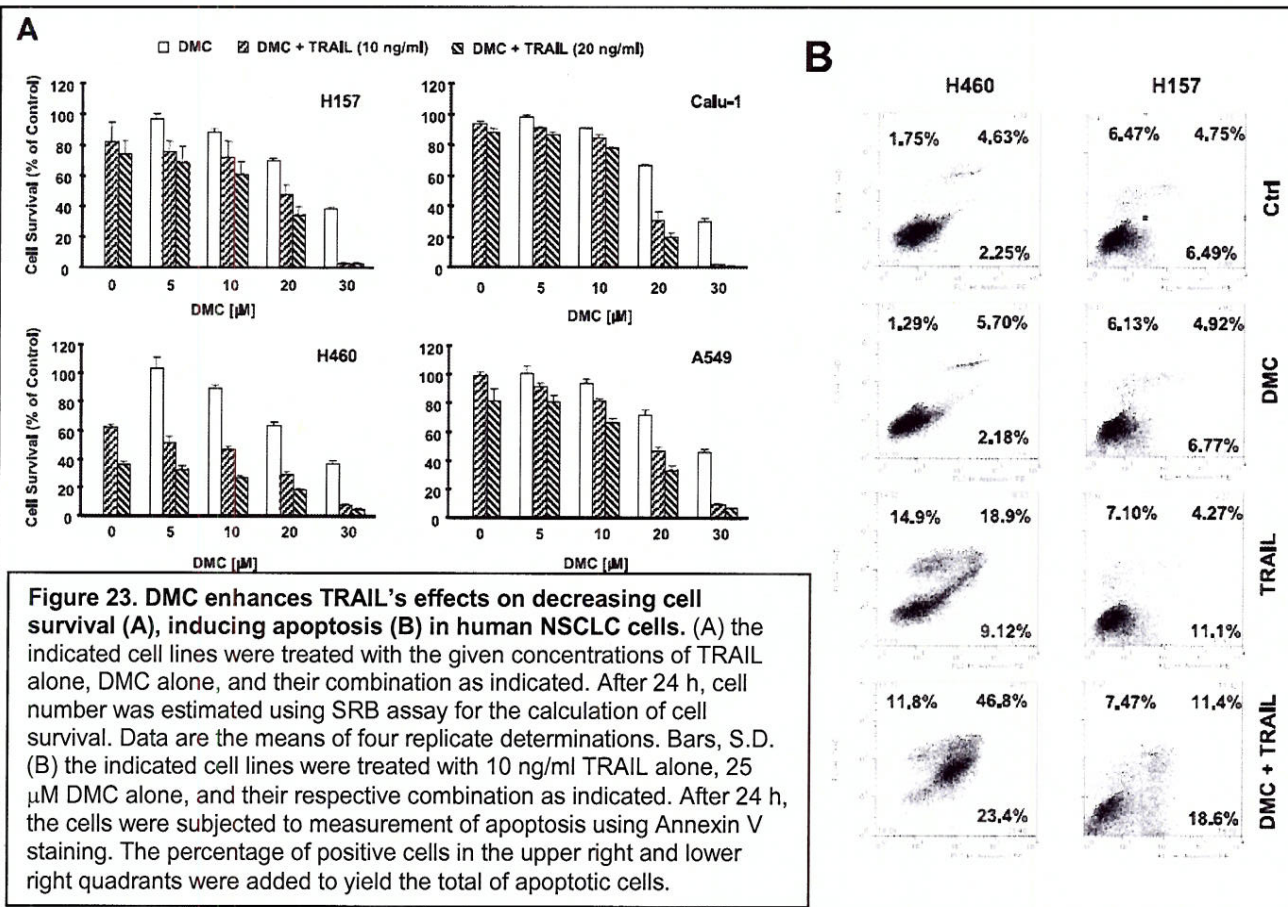


Figure 22. P68 is phosphorylated and is required for TRAIL resistance. (a) Tyrosine phosphorylation of p68 RNA helicase in two TRAIL sensitive (S) H460 and HCT116 cell lines and two engineered TRAIL-resistant (R) H460 and HCT116 cell lines. P68 was immuno-precipitated (IP:PAbp68) from nuclear extracts and followed by IB with appropriate antibody (indicated). The IB:p68-rgg is a loading control. (b) P68 is required for TRAIL resistance of HCT-116R cells. Upper panel, the p68 expression in HCT-116R cells that were treated by siRNA against p68 (p68) or NT was examined by IB with antibody p68-rgg. IB:H2A is a loading control. Lower panel, the 'TdT-mediated dUTP nick end labeling' (TUNEL) assay of the apoptosis of HCT-116R cells under the treatment of 10 ng/ml of TRAIL. P68 was knocked down by siRNA against p68 (p68 siRNA) or cells were treated with NT siRNA. The number on the right is the percentage of apoptotic cells and the number on the left is the percentage of surviving cells.

- b. The proteasome inhibitor PS-341 (Bortezomib) upregulates death receptor 5 expression leading to induction of apoptosis and enhancement of TRAIL-induced apoptosis despite increase of c-FLIP and survivin in human lung cancer cells.

The proteasome inhibitor PS-341 (Bortezomib or Velcade), an approved drug for treatment of patients with multiple myeloma, is currently being tested in clinical trials against various malignancies including lung cancer. Preclinical studies have demonstrated that PS-341 induces apoptosis and enhances TRAIL-induced apoptosis in human cancer cells with undefined mechanisms. In the present study, we show that PS-341 induced caspase-8-dependent apoptosis, cooperated with TRAIL to induce apoptosis, and upregulated death receptor 5 (DR5) expression in human NSCLC cells. DR5 induction correlated with PS-341's ability to induce apoptosis. Blockage of PS-341-induced DR5 upregulation using DR5 small interference RNA rendered cells less sensitive to apoptosis induced by either PS-341 or its combination with TRAIL, indicating that DR5 upregulation mediates PS-341-induced apoptosis and enhancement of TRAIL-induced apoptosis in human NSCLC cells. We exclude the involvement of c-FLIP and survivin in mediating these events because c-FLIP and survivin protein levels were actually

elevated upon exposure to PS-341. Reduction of c-FLIP with c-FLIP siRNA sensitized cells to PS-341-induced apoptosis, suggesting that c-FLIP elevation protects cells from PS-341-induced apoptosis (Figure 26). Thus, the present study highlights the important role of DR5 upregulation in PS-341-induced apoptosis and enhancement of TRAIL-induced apoptosis in human NSCLC cells. This part of work has been published in Cancer Research (Liu et al, 2007).



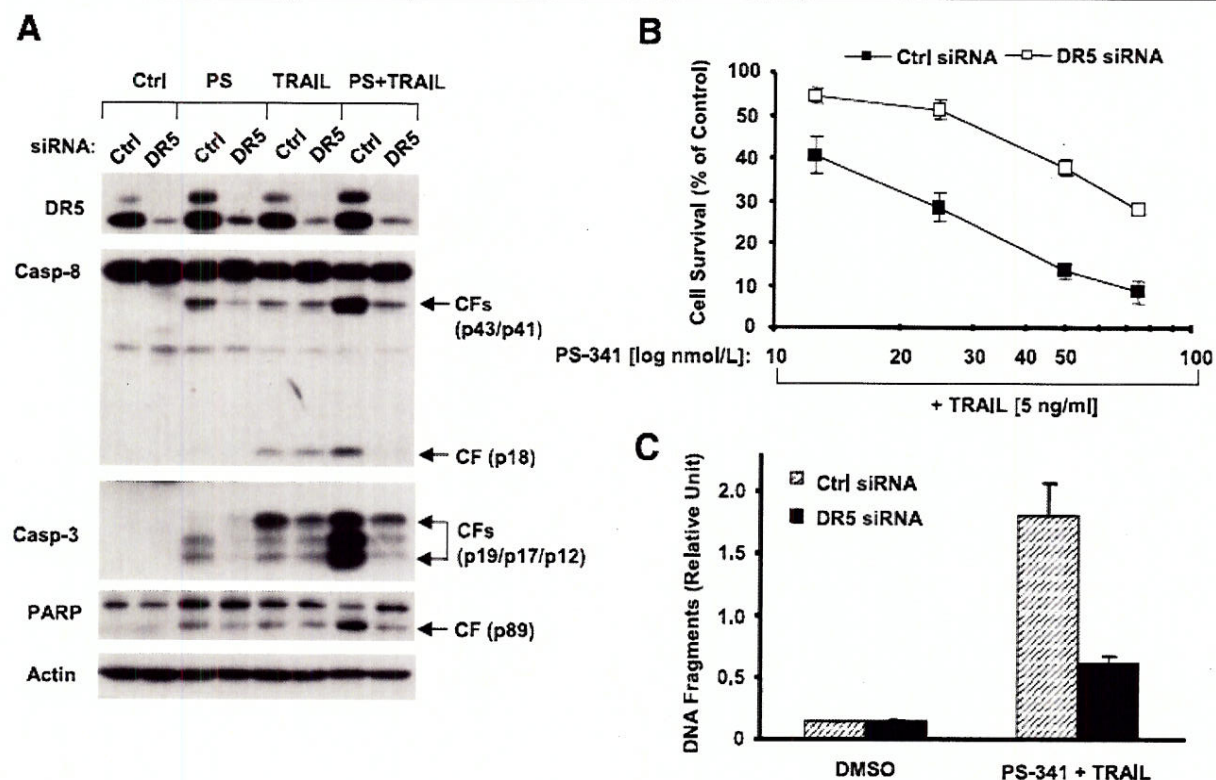
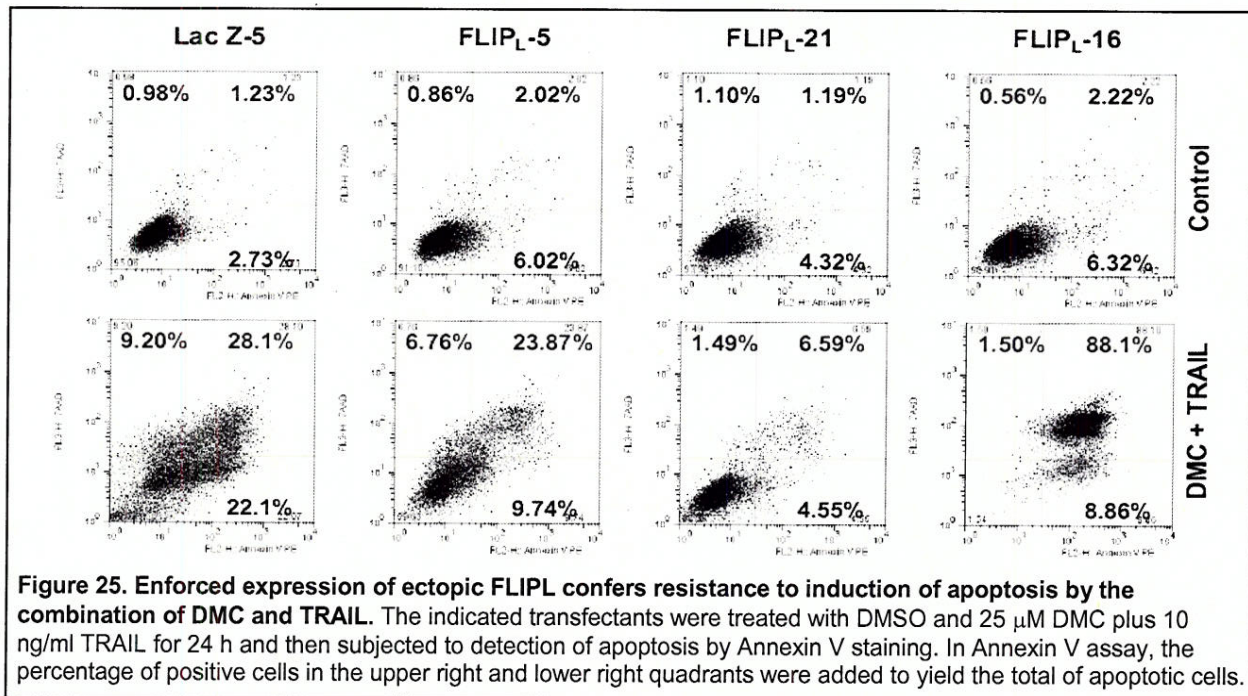
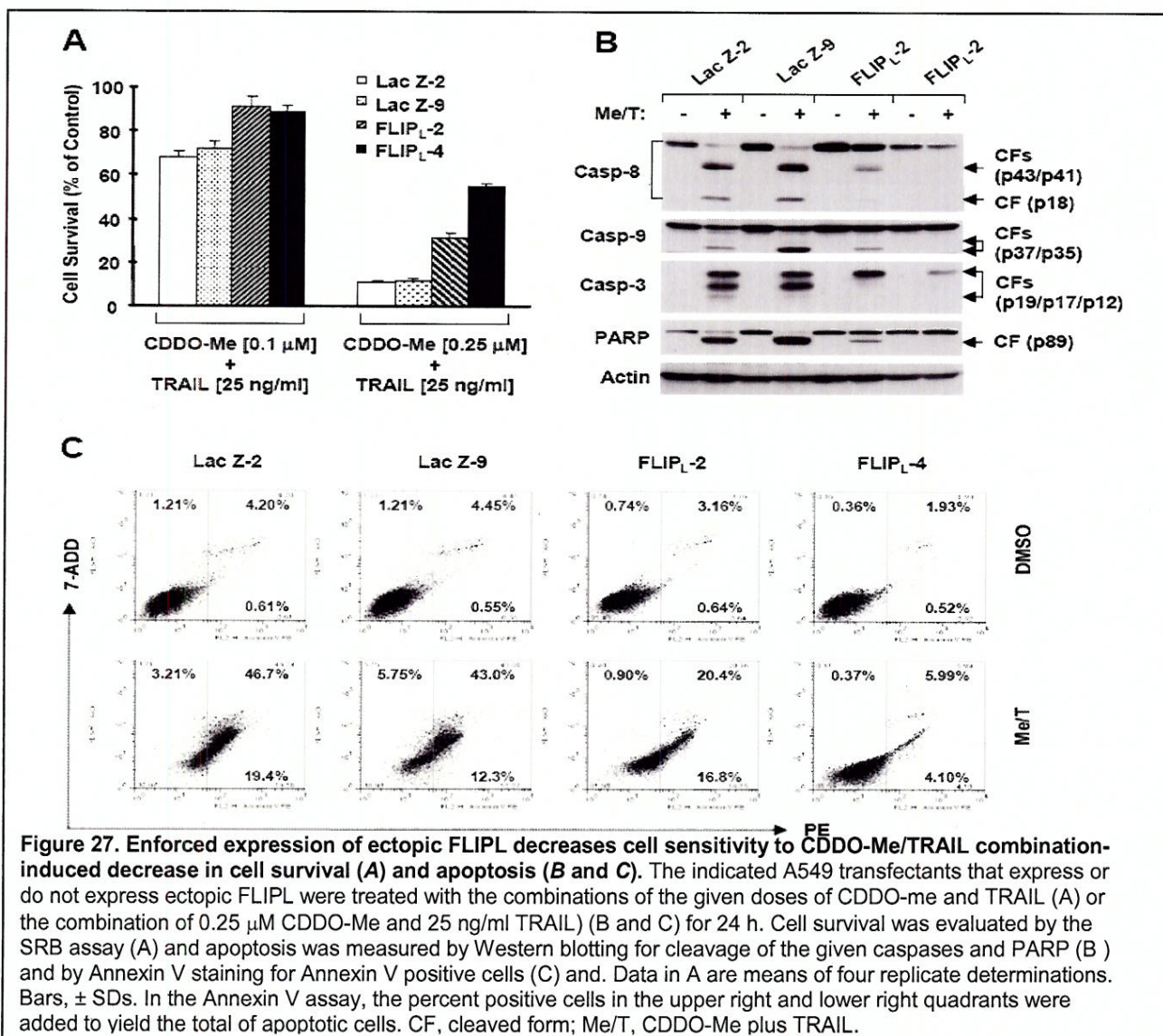


Figure 26. Silencing of DR5 expression attenuates the ability of PS-341 to cooperate with TRAIL to activate caspases. (A), decrease cell survival (B), and increase DNA fragmentation (C). H157 cells were cultured in a 24-well plate and on the 2nd day transfected with control or DR5 siRNA. Twenty-four hours after the transfection, cells were reseeded in a 6-well plate (A) or 96-well plates (B and C) and treated with 50 nmol/L PS-341 (PS), 5 ng/mL TRAIL or PS-341, and TRAIL combination (PS+TRAIL; A), with 5 ng/mL TRAIL in combination with the indicated concentrations of PS-341, respectively (B), or with the solvent control DMSO or the combination of 50 nmol/L PS-341 and 10 ng/mL TRAIL (C) on the 2nd day after reseeding. After 24 h (A and B) or 12-h (C) treatment, the cells were either harvested for preparation of whole-cell protein lysates and subsequent Western blot analysis (A) or subjected to estimation of cell number by SRB assay (B) or measurement of DNA fragmentation using the Cell Death Detection ELISAPlus kit (C). Points are columns, mean of triplicate (B and C) determinations; bars, SD.

- c. c-Jun N-terminal kinase (JNK)-independent c-FLIP downregulation contributes to induction of apoptosis by the novel synthetic triterpenoid methyl-2-cyano-3, 12-dioxooleana-1, 9-dien-28-oate (CDDO-Me) in human lung cancer cells.

The novel synthetic triterpenoid methyl-2-cyano-3, 12-dioxooleana-1, 9-dien-28-oate (CDDO-Me) induces apoptosis of cancer cells, enhances TRAIL-induced apoptosis, and exhibits potent anticancer activity in animal models with a favorable pharmacokinetic profile. Thus, CDDO-Me is being tested in Phase I clinical trials. In an effort to understand the mechanism by which CDDO-Me induces apoptosis, particularly in human lung cancer cells, we previously demonstrated that CDDO-Me induces apoptosis involving c-Jun N-terminal kinase (JNK)-dependent upregulation of DR5 expression. In the current work, we determined the modulatory effects of CDDO-Me on the levels of c-FLIP, a major inhibitor of death receptor-mediated caspase-8 activation, and its impact on CDDO-Me-induced apoptosis and enhancement of TRAIL-induced apoptosis in human lung cancer cells. CDDO-Me rapidly and potently decreased c-FLIP levels including both long (FLIP_L) and short (FLIP_S) forms of c-FLIP in multiple human lung cancer cell lines. The presence of the proteasome inhibitor MG132, but not the JNK inhibitor SP600125, prevented CDDO-Me-induced c-FLIP reduction. Moreover, CDDO-Me increased ubiquitination of c-FLIP. Thus, CDDO-Me induces ubiquitin/proteasome-dependent c-FLIP degradation independently of JNK activation. Importantly, overexpression of c-FLIP (e.g., FLIP_L) protected cells not



only from CDDO-Me-induced apoptosis, but also from induction of apoptosis by the combination of CDDO-Me and TRAIL. Accordingly, silencing of c-FLIP with c-FLIP siRNA sensitized cancer cells to CDDO-Me. Collectively, these results indicate that c-FLIP downregulation contributes to CDDO-Me-initiated apoptosis and also to enhancement of TRAIL-induced apoptosis by CDDO-Me (Figure 27). This part of the work has been published in *Cancer Biology and Therapy* (Zou et al. 2007).

- d. CHOP-dependent death receptor 5 induction is a major component of SHetA2-induced apoptosis in lung cancer cells.

The flexible heteroarotinoids (Flex-Hets) represent a novel type of synthetic retinoids without activity in binding and transactivating retinoid receptors. Preclinical studies have demonstrated that Flex-Hets induce apoptosis of cancer cells while sparing normal cells and exhibit anticancer activity *in vivo* with improved therapeutic ratios over conventional retinoid receptor agonists. Flex-Hets have been shown to induce apoptosis through activation of the intrinsic apoptotic pathway. The present study has revealed a novel mechanism underlying Flex-Het-induced apoptosis involving induction of DR5. The representative Flex-Het SHetA2 effectively inhibited the growth of human lung cancer cells in cell culture and in mice. SHetA2 induced apoptosis, which could be abrogated by silencing caspase-8 expression, indicating that SHetA2 triggers a caspase-8-dependent apoptosis. Accordingly, SHetA2

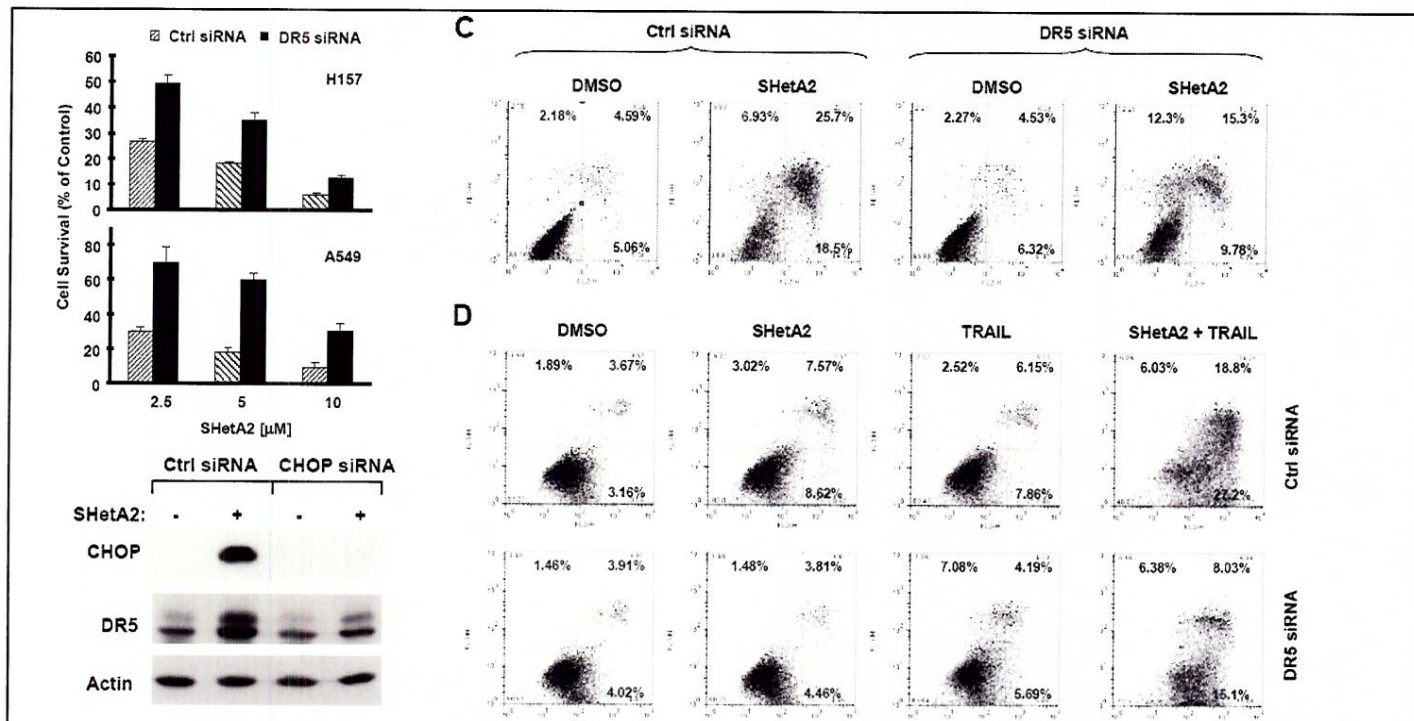
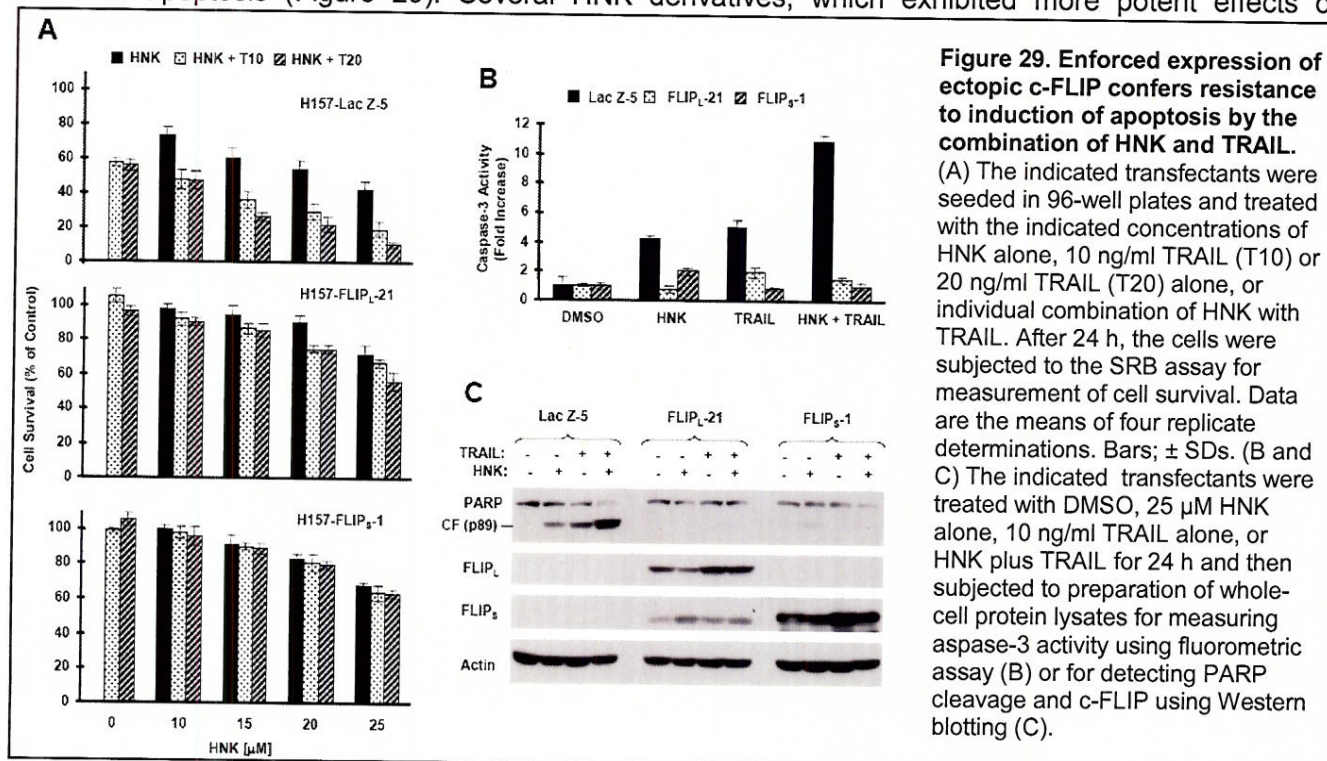


Figure 28. Blockage of DR5 induction attenuates SHetA2's ability to decrease cell survival (A), induce apoptosis (C) and augment TRAIL-induced apoptosis (D) in human NSCLC cells. SHetA induces CHOP expression which is responsible for DR5 up-regulation by SHetA2 (B). (A) The indicated cell lines were cultured in 6-well plates and next day transfected with control (Ctrl) or DR5 siRNA. 24 h after the transfection, cells were reseeded in 96-well plates and treated with the indicated concentrations of SHetA2. After 48 h, the cells were subjected to the SRB assay for calculation of cell survival. Data are the mean of four replicate determinations. Bars, \pm SDs. (B) A549 cells were transfected with control (Ctrl) or CHOP siRNA. After 48 h, the cells were treated with 10 μ M SHetA2 for 12 h and then subjected to preparation of whole-cell protein lysates and subsequent Western blot analysis. (C and D), H157 (C) or A549 (D) cells were cultured in 6-well plates and the next day transfected with control (Ctrl) or DR5 siRNA. 48 h after the transfection, the cells were exposed to DMSO or 10 μ M SHetA2 for 48 h (C) or treated with DMSO control, 10 μ M SHetA2 alone, 20 ng/ml TRAIL alone or SHetA2 combined with TRAIL for 24 h (D). The cells were then harvested for Annexin V assay to detect apoptosis. The percent positive cells in the upper right and lower right quadrants were added to yield the total of apoptotic cells.

Upregulated DR5 expression including cell surface levels of DR5 and augmented TRAIL-induced apoptosis. Importantly, small interference RNA (siRNA)-mediated blockade of DR5 induction conferred cell resistance to SHetA2-induced apoptosis as well as SHetA2/TRAIL-induced apoptosis. These results demonstrate that DR5 induction is a key component of apoptosis induced by SHetA2 or by SHetA2 combined with TRAIL. SHetA2 exerted CHOP-dependent transactivation of the DR5 promoter. Consistently, SHetA2 induced CHOP expression, which paralleled DR5 upregulation, whereas siRNA-mediated blockade of CHOP induction prevented DR5 upregulation, indicating CHOP-dependent DR5 upregulation by SHetA2. Collectively, we conclude that SHetA2 induces CHOP-dependent DR5 upregulation, leading to caspase-8 activation and subsequent apoptosis (Figure 28). This part of the work has been submitted to Cancer Research for publication.

- e. The natural product Honokiol preferentially inhibits c-FLIP and augments death receptor-induced apoptosis.

Targeting death receptor-mediated apoptosis has emerged as an effective strategy for cancer therapy. However, certain types of cancer cells are intrinsically resistant to death receptor-mediated apoptosis. In an effort to identify agents that can sensitize cancer cells to death receptor-induced apoptosis, we have identified Honokiol (HNK), a natural product with anticancer activity, as demonstrated in various preclinical studies, as an effective sensitizer of death receptor-mediated apoptosis. HNK alone moderately inhibited the growth of human lung cancer cells; however, when combined with TRAIL, greater effects on decreasing cell survival and inducing apoptosis than TRAIL alone were observed, indicating that HNK cooperates with TRAIL to enhance apoptosis. This was also true to Fas-induced apoptosis when combined with Fas ligand or an agonistic anti-Fas antibody. Among several apoptosis-associated proteins tested, c-FLIP was the only one that was rapidly downregulated by Honokiol in all of the tested cell lines. The downregulation of c-FLIP by HNK could be prevented by the proteasome inhibitor MG132. Moreover, HNK increased c-FLIP ubiquitination. These results indicate that HNK downregulates c-FLIP by facilitating its degradation through a ubiquitin/proteasome-mediated mechanism. Enforced expression of ectopic c-FLIP abolished Honokiol's ability to enhance TRAIL-induced apoptosis (Figure 29). Several HNK derivatives, which exhibited more potent effects on



downregulation of c-FLIP than HNK, showed better efficacies than Honokiol in inhibiting the growth and enhancing TRAIL-induced apoptosis as well. Collectively, we conclude that c-FLIP downregulation is a key event for HNK to modulate the death receptor-induced apoptosis. This part of the work has been submitted to Molecular Cancer Therapeutics for publication (The manuscript is attached).

In summary, we have identified small molecules that indeed modulate the death receptor-mediated apoptosis, which even participated in apoptosis-induced by these molecules. However, cells resistant to TRAIL are still sensitive to these small molecules. Collectively, our results suggest that DR-inducing agents induce apoptosis involving mechanisms in addition to modulation of the death receptor-mediated apoptotic pathway.

Aim 3 To determine whether suppression of PI3K/Akt activity sensitizes premalignant and/or malignant airway epithelial cells to apoptosis induced by DR-induced agents via enhancement of TRAIL/DR-mediated mechanism.

Update

- a. CHOP/GADD153-dependent upregulation of death receptor 5 expression and farnesyltransferase inhibitor (FTI)-induced apoptosis in human lung cancer cells.

In an effort to reveal their mechanisms of action, we have determined that the FTIs, SCH66336 and R115777, induce DR5 expression, including cell surface DR5 levels in human lung cancer cells, which contribute to FTI-induced apoptosis. Moreover, SCH66336 induces CHOP/GADD153 expression, leading to an increase in DR5 transactivation and expression. Therefore, we conclude that FTIs induce DR5 expression through a CHOP/GADD153-dependent mechanism, contributing to induction of apoptosis in human lung cancer cells. In addition, the combination of an FTI with TRAIL exerts synergistic effects on induction of apoptosis in human lung cancer cells. Our new findings reveal a novel mechanism by which FTIs induce apoptosis and suggest a novel therapeutic strategy for enhancing efficacy of the FTIs by combining with TRAIL. In addition, we recommend monitoring the modulation of CHOP/GADD153 and DR5 expression in FTI-based lung cancer therapy. These data have been published in Journal of Biological Chemistry (JBC) (Sun et al, 2007) and Cancer Research (Qiu et al. 2007), respectively.

- b. The alkylphospholipid perifosine inhibits Akt and enhances activation of the extrinsic apoptotic pathway.

The Akt inhibitor, perifosine, is an alkylphospholipid exhibiting antitumor properties and is currently in Phase II clinical trials for various types of cancer. The mechanisms by which perifosine exerts its antitumor effects including induction of apoptosis are not well understood. The current study focused on the effects of perifosine on induction of apoptosis and underlying mechanisms in human NSCLC cells. Perifosine at clinically achievable concentration ranges of 10-15 μ M effectively inhibited the growth and induced apoptosis of NSCLC cells. Perifosine inhibited Akt phosphorylation and reduced the levels of total Akt. Importantly, enforced activation of Akt attenuated perifosine-induced apoptosis. These results indicate that Akt inhibition is necessary for perifosine-induced apoptosis. Despite activation of both caspase-8 and caspase-9, perifosine strikingly induced the expression of the TRAIL receptor, DR5, and downregulated c-FLIP, an endogenous inhibitor of the extrinsic apoptotic pathway, with limited modulatory effects on the expression of other genes including Bcl-2, Bcl-X_L, PUMA and survivin. Silencing of either caspase-8 or DR5 attenuated perifosine-induced apoptosis. Consistently, further downregulation of c-FLIP expression with c-FLIP siRNA sensitized cells to perifosine-induced apoptosis, whereas enforced overexpression of ectopic c-FLIP conferred resistance to perifosine. Collectively, these data indicate that activation of the extrinsic apoptotic pathway plays a critical role in

perifosine-induced apoptosis (Figure 30). Moreover, perifosine cooperates with TRAIL to enhance induction of apoptosis in human NSCLC cells, thus warranting future *in vivo* and clinical evaluation of perifosine in combination with TRAIL in treatment of NSCLC. This part of the work has been published in Molecular Cancer Therapeutics (Elrod et al, 2007).

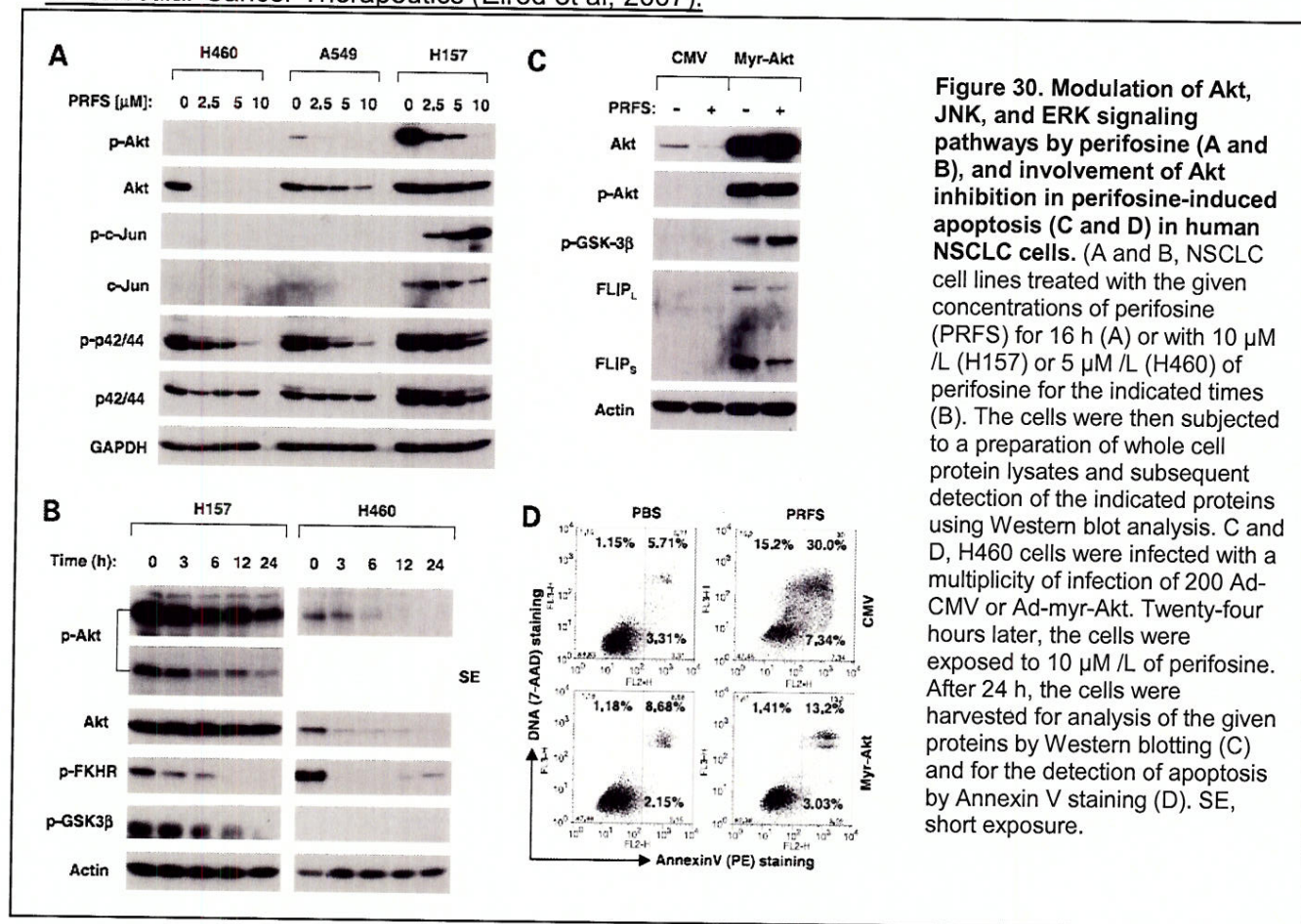


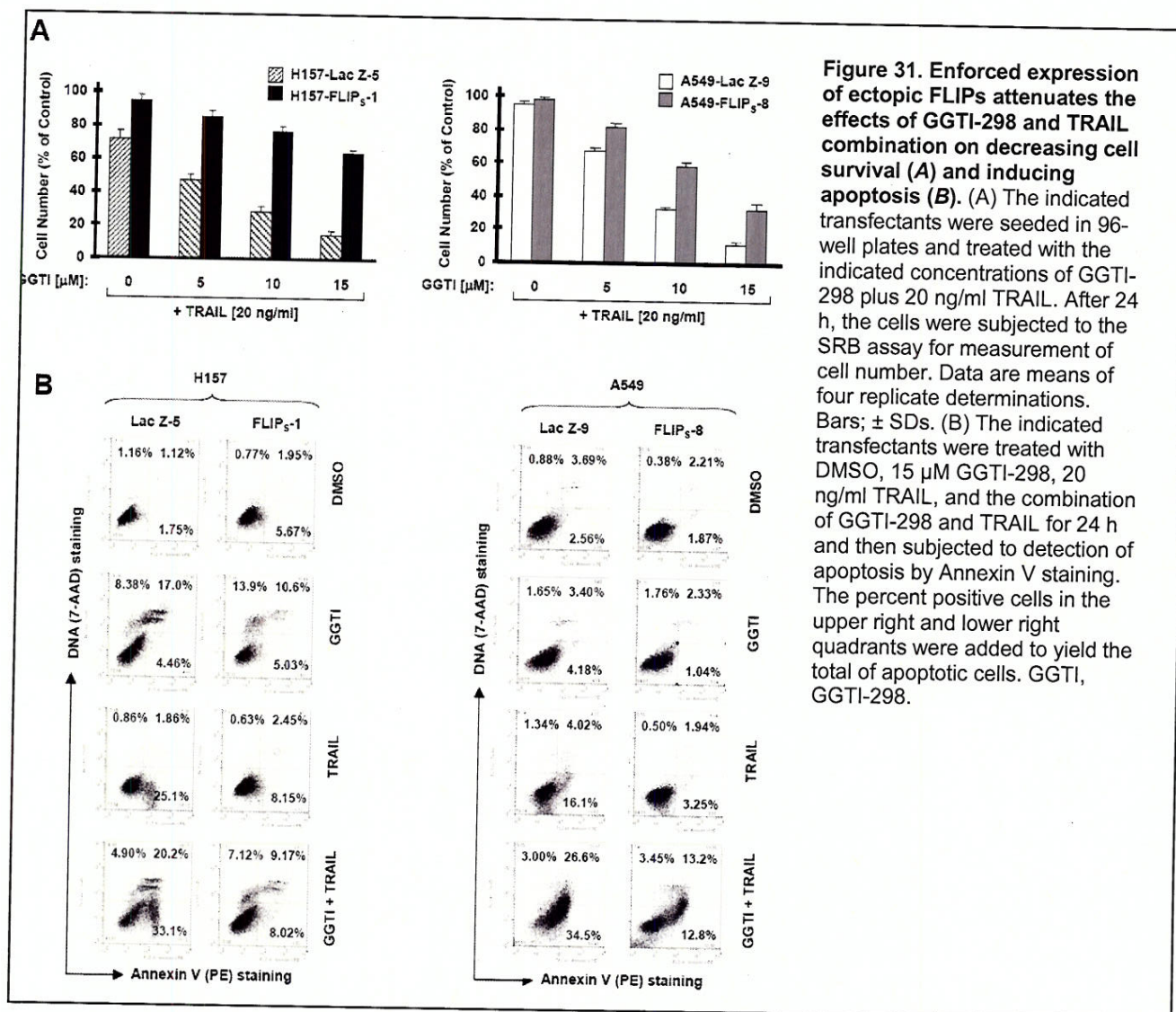
Figure 30. Modulation of Akt, JNK, and ERK signaling pathways by perifosine (A and B), and involvement of Akt inhibition in perifosine-induced apoptosis (C and D) in human NSCLC cells. (A and B, NSCLC cell lines treated with the given concentrations of perifosine (PRFS) for 16 h (A) or with 10 μ M /L (H157) or 5 μ M /L (H460) of perifosine for the indicated times (B). The cells were then subjected to a preparation of whole cell protein lysates and subsequent detection of the indicated proteins using Western blot analysis. C and D, H460 cells were infected with a multiplicity of infection of 200 Ad-CMV or Ad-myr-Akt. Twenty-four hours later, the cells were exposed to 10 μ M /L of perifosine. After 24 h, the cells were harvested for analysis of the given proteins by Western blotting (C) and for the detection of apoptosis by Annexin V staining (D). SE, short exposure.

c. Celecoxib antagonizes perifosine's anticancer activity through inhibition of COX-2 activation.

Given that celecoxib increases phosphorylation in some NSCLC cell lines as we mentioned in our previous progress report, we hypothesized that inhibition of Akt phosphorylation with perifosine, an Akt inhibitor, would enhance celecoxib's anticancer efficacy. Surprisingly, we found that the two drug combination did not show any better effects on inhibiting the growth of human NSCLC cells; rather, the combination exhibited antagonistic effects in multiple cell lines. We have demonstrated that this antagonism also occurs in lung cancer xenograft models in mice. By understanding the mechanism underlying the antagonism, we have revealed that perifosine induces COX-2 expression and increase COX-2 activity, while the presence of celecoxib attenuates perifosine's ability to increase COX-2 expression and activity. Moreover, blockage of COX-2 induction by both antisense and siRNA approaches decreased cell sensitivity to perifosine. Collectively, these data indicate that the activation of COX-2 contributes to perifosine's anticancer activity including apoptosis induction and growth arrest. These data are clinically relevant as they suggest that patients who are administered perifosine should not also take COX-2 inhibitors such as celecoxib, so as to avoid potential drug contradiction. For detail, please see attached full text of our manuscript, which is ready for submission. We will continue to investigate how perifosine induces COX-2 expression and how COX-2 activation contributes to induction of apoptosis as well as growth arrest.

d. Inhibition of geranylgeranyltransferase I downregulates c-FLIP levels, induces DR5 expression, and augments tumor necrosis factor-related apoptosis-inducing ligand-induced apoptosis.

Geranylgeranyltransferase I (GGTase I) has emerged as a cancer therapeutic target. Accordingly, small molecules that inhibit GGTase I have been developed and exhibit encouraging anticancer activity both *in vitro* and *in vivo* in preclinical studies. However, the underlying anticancer mechanisms of GGTase I inhibitors remain unclear. We previously demonstrated that FTIs increase Akt phosphorylation while inducing DR5 expression and enhancing TRAIL-induced apoptosis. Here we investigated whether GGTase I inhibitors exert similar effects. We found that inhibition of GGTase I by GGTI-298 induced apoptosis and augmented TRAIL-induced apoptosis in human lung cancer cells. GGTI-298 induced DR5 expression and reduced the levels of c-FLIP, particularly the short form of c-FLIP (FLIP_S); these effects were associated with GGTI-298's ability to induce apoptosis and augment TRAIL-induced apoptosis. Consistently, another highly selective GGTase I inhibitor, GGTI-DU40, but not its inactive analog SN-



DU40, exerted similar effects. Enforced expression of c-FLIP or knockdown of DR5 expression protected cells from induction of apoptosis by the combination of GGTI-298 and TRAIL, indicating that induction of DR5 and downregulation of c-FLIP mediate augmentation of TRAIL-induced apoptosis by GGTase I inhibition. Moreover, enforced reduction of endogenous c-FLIP levels by siRNA in GGTI-298-resistant cells sensitized the cells to GGTI-298-induced apoptosis, whereas enforced ectopic c-FLIP expression protected cells from GGTI-298-induced apoptosis (Figure 31). These results suggest that activation of the extrinsic apoptotic pathway also contributes to GGTI-298-induced apoptosis. Thus, our findings reveal a novel mechanism underlying GGTase I inhibition-induced apoptosis and also suggest a novel cancer therapeutic strategy by combining a GGTase I inhibitor with TRAIL. In terms of Akt phosphorylation, GGTase inhibitors clearly increased Akt phosphorylation in one cell line while decreasing Akt phosphorylation in another cell lines, showing cell line-dependent effects on Akt phosphorylation. This part of the work has been submitted to JBC for publication.

In summary, it seems common that some anticancer agents increase Akt phosphorylation while inducing DR5 expression or activating the extrinsic apoptotic pathway. Increase in Akt phosphorylation does not necessarily attenuate the anticancer efficacy of these anticancer drugs. Thus, it appears that drug-activated apoptotic signal can override the drug-induced survival signal, leading to cell death.

Aim 4 To determine whether DRs, DcRs, c-FLIP, and procaspase-8 serve as biomarkers for lung cancer chemoprevention and therapy.

Update

These studies will begin as soon as tissue slides from clinical trials are received.

Key Research Accomplishments

- Determined that several groups of the compounds with cancer therapeutic potential including celecoxib and its derivative, FTIs, GGTase inhibitors, proteasome inhibitors, triterpenoids, the natural product honokiol, the synthetic retinoid SHetA2 and PPAR γ ligands modulate DR5 expression and/or c-FLIP levels (mostly by downregulation), which contribute to induction of apoptosis and/or enhancement of TRAIL-induced apoptosis.
- Discovered that CHOP/GAD153 mediates DR5 expression induced by certain anticancer agents (e.g. SCH66336; DMC and SHetA2).
- Identified a positive role of COX-2 activation in mediating perfosine-mediated anticancer activity.

Conclusions

Appropriate modulation of the extrinsic death receptor-mediated apoptotic pathway such as upregulation of DR5 and or reduction of c-FLIP levels by small molecules (e.g., celecoxib, lonafarnib, bortezomib) may eliminate premalignant or malignant lung epithelial cells via promoting apoptotic cell death to achieve cancer chemopreventive and therapeutic goals. Moreover, the potential of the modulation of DR5 and c-FLIP as predictive biomarkers for certain drugs in the clinic warrants further investigation.

Project 5: Molecular Strategies Targeting the AKT Signaling Pathway for Lung Cancer Chemoprevention and Therapy

(PI and co-PI: Ho-Young Lee, Ph.D., Edward S. Kim, M.D.)

Our goal is to find novel chemopreventive/therapeutic agents that can prevent lung carcinogenesis effectively. Results from our work and others' have demonstrated that Akt, which has a clear role in cellular survival and transformation, is constitutively active in premalignant and malignant HBEs and in NSCLC cell lines. These findings suggest an importance of PI3K/Akt signaling pathway in lung carcinogenesis. The purpose of our studies is to determine whether activation of Akt induces malignant transformation of HBE cells and to develop novel agents inhibiting Akt activity as a strategy of preventing lung carcinogenesis.

In the past 4 years, we focused our efforts on Aims 2 and 3.

Aim 1 Develop a retroviral vector expressing constitutively active Akt and characterize the *in vitro* and *in vivo* effects of Akt activation on the malignant transformation of HBE cells.

Update

As previously reported, we finished constructing retroviral vectors expressing constitutively active or dominant negative Akt1, 2, or 3. The Akt constructs were confirmed by sequencing and western blot analysis. Viral titers have been determined by colony formation assay. To analyze the roles of Akt 1, 2 or 3 in the survival of HBE cells, BEAS2B cells were stably transfected with retroviral vectors expressing constitutively active Akt 1, 2, or 3. We have been analyzing the survival of the cells in the stress conditions (UV, growth factor withdrawal, cigarette carcinogens).

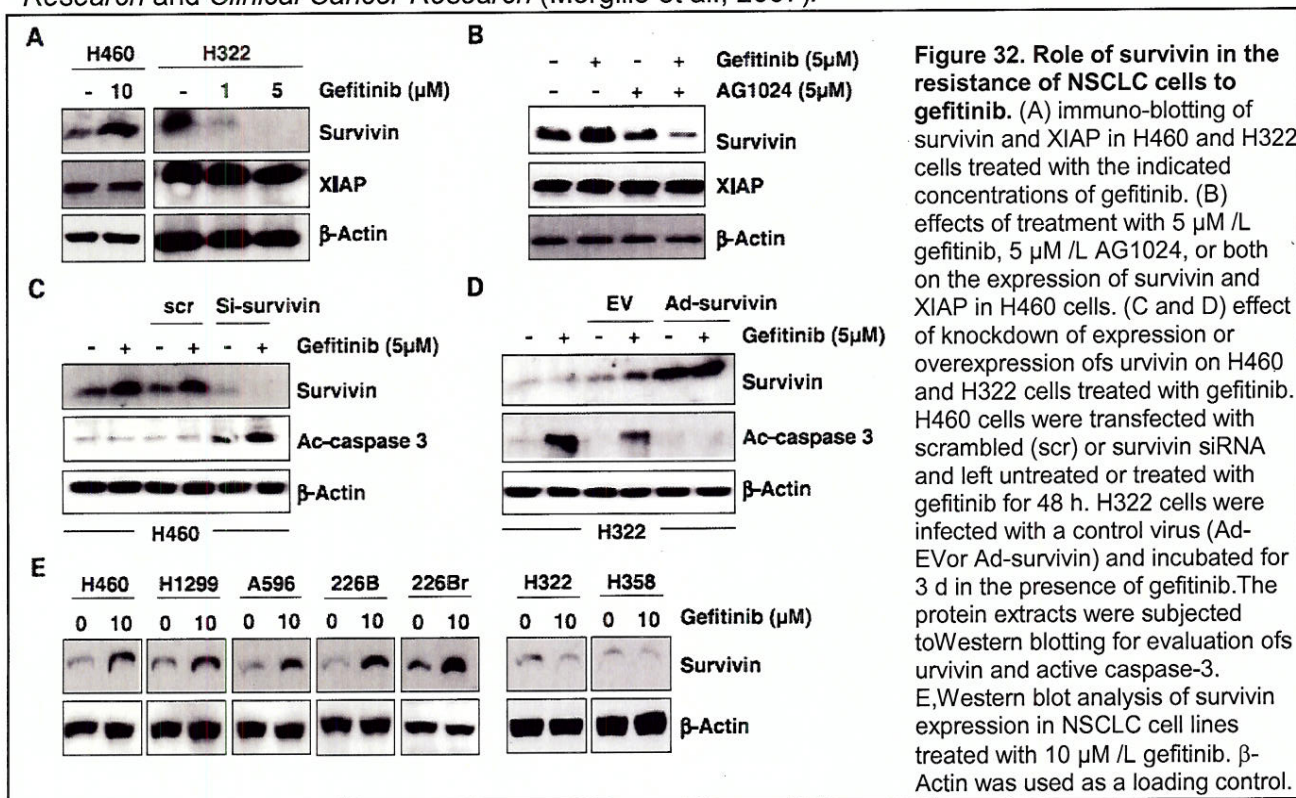
Aim 2 Evaluate the ability of chemopreventive agents used in VITAL trials (gefitinib, erlotinib, SCH66336, and celecoxib, alone and in combination) to inhibit Akt activity and induce apoptosis in transformed HBE and NSCLC cell lines.

Update

We have previously demonstrated the potential of insulin growth factor 1 receptor (IGF-1R)/Akt pathway as a target for lung chemopreventive and therapeutic strategies in NSCLC by using IGFBP-3, a major IGF-binding protein inducing apoptosis, FTI SCH66336 (Lee et al., JNCI 2004), retinoids (Han J-Y et al., CCR 2005; Lee H-Y et al., *J Clin Onc* 2005), and the natural product deguelin (Lee et al., JNCI 2005). Last year, we reported that IGFBP-3 mediates antitumor activities of SCH66336 in HNSCC by inhibiting angiogenesis (Oh et al., CCR 2006), suggesting that IGFBP-3 could be a primary target for antitumor activities of FTIs and that IGFBP-3 may be an effective therapeutic approach against angiogenesis in HNSCC. We also reported the therapeutic activities and action mechanism of erlotinib on NSCLC cells. We found that treatment with erlotinib-induced association between EGFR and IGF-1R, leading to activation of IGF-1R/PI3K/Akt/ mammalian target of rapamycin (mTOR)-mediated *de novo* protein synthesis of survivin and, thus, protected NSCLC cells from the EGFR-tyrosine kinase inhibitor (TKI)-mediated apoptosis (Figure 32) (Morgillo et al., Cancer Res 2007).

This year, we have further confirmed the therapeutic activities and action mechanism of gefitinib on NSCLC cells. Similar to erlotinib, treatment with gefitinib stimulated the IGF-1R signaling

pathway through the EGFR:IGF-1R heterodimer and induced survivin expression, neutralizing the antitumor action of the drug. These findings indicated that suppression of the IGF-1R signaling pathways may prevent or delay development of resistance to EGFR TKIS, including erlotinib and gefitinib, in NSCLC cells. Detailed findings have been published in *Cancer Research and Clinical Cancer Research* (Morgillo et al., 2007).



Aim 3 Determine whether Akt is activated in bronchial specimens from enrolled patients in VITAL trials and whether treatment with chemopreventive agents suppresses Akt level or activity in these patients.

Update

Previous findings have shown that tobacco carcinogens activate Akt. This year, we have assessed the downstream mediators of Akt pathway for the tobacco carcinogen-induced lung carcinogenesis. To this end, we investigated the role of survivin, an inhibitor of apoptotic protein, in the tobacco carcinogen-induced malignant transformation of HBE cells. We found that survivin mRNA expression was detected in 41% (7 of 17) of bronchial brush specimens from heavy smokers (at least 20 pack/year). Tobacco components nicotine and its related carcinogen 4-(methylnitrosamino)-1-(3-pyridyl)-1-butanone (NNK) increased survivin mRNA and protein expression levels in primary cultured normal HBE cells and immortalized HBE cells. Bronchial epithelium in mice administered with NNK also showed increased expression of survivin. Nicotine and NNK stimulated the Akt/mTOR pathway in normal HBE cells, leading to increased *de novo* synthesis of survivin protein. Induced survivin expression increased the survival potential of the cells, which was blocked by transfection with survivin-specific siRNA. siRNA-induced downregulation of survivin expression also suppressed the tumorigenic potential of premalignant and malignant HBE cells exposed to the tobacco components. These findings suggest that NNK and nicotine induce survivin protein synthesis in normal HBE cells by activating the Akt/mTOR pathway and thus blockade of the pathway effectively inhibits the tobacco-induced malignant transformation of HBE cells.

Project 1 is continuing to accrue patients and collecting samples through Core C. When additional tissue and serum samples are available, we will complete the correlative studies proposed in this Aim.

Key Research Accomplishments

- Established the immortalized HBE cell lines stably transfected with retroviral vectors expressing constitutively active Akt1, 2, or 3. The effects of overactivation of Akt on cell viability under variable stress conditions have been characterized.
- Determined that the EGFR TKI Gefitinib induced association between EGFR and IGF-1R, activated IGF-1R/PI3K/Akt/mTOR-mediated *de novo* protein synthesis of survivin in NSCLC cells. Inhibition of IGF-1R signaling pathways or knock-down of survivin expression abolished resistance to the gefitinib and induced apoptosis in NSCLC cells.
- Determined that NNK and nicotine induce survivin protein synthesis in normal HBE cells by activating the Akt/mTOR pathway
- Determined that survivin expression is induced as an early event in lung carcinogenesis.

Conclusions

We have determined that suppression of the IGF-1R signaling pathways may prevent or delay development of resistance to gefitinib in NSCLC cells and that blockade of the IGF-1R/PI3K/Akt pathway effectively inhibits the tobacco-induced malignant transformation of HBE cells.

Core B: Biostatistics & Data Management Core

(Core Director: J. Jack Lee, Ph.D.)

Core Goals:

1. To provide statistical design, sample size/power calculations, and integrated, comprehensive analysis for each basic science, pre-clinical, and clinical study.
2. To develop a data management system that provides tracking, quality control, and integration of clinical, pathological, and basic science data.
3. To provide statistical and data management support for genomic and imaging studies including microarray, proteomics, protein antibody array, and spiral CT.
4. To develop and adapt innovative statistical methods pertinent to biomarker-integrated translational lung cancer studies.
5. To generate statistical reports for all projects.
6. To collaborate and assist all project investigators in the publication of scientific results.

As a part of the ReVITALization plan approved this past year, we have significantly revised and added to our second goal above to further support the development of the risk model.

Revised Goal 2. *Develop a data management system that provides tracking, quality control, and integration of clinical, pathological, and basic science data. New database modules will be developed and integrated to the existing VITAL web-based database and with the clinical database from the Department of Thoracic/Head and Neck Medical Oncology.*

Update

The Biostatistics and Data Management Core has continued to work actively with all the VITAL Projects in their research efforts, especially in the area of biostatistical support and consulting in the clinical trial design, implementation, conduct, and analysis of experimental results.

Our major effort in the fourth year is in the area of providing statistical/data management support for the “ReVITALization” of Project 1. Due to the slow accrual for the Vanguard trial, we have proposed to circumvent the problem by incorporating a historical cohort recruited at M. D. Anderson from 2002 to 2005. Biostatistical Core was involved in the revision process. We have interacted with study PI, IRB, and regulatory agencies to address critiques and provide revisions. In the meantime, the celecoxib trial and the erlotinib trial have been closed.

We have developed and continue to provide enhancement of a web-enabled database system to facilitate the conduct of the Vanguard Trial. For the ReVITALization effort, we have revamped the data dictionary to incorporate retrospectively collected tissue specimens and data. The goal is to have an integrated database which can be used to store data from both the prospective trial and the retrospective cohort. New database modules are being developed and integrated to the existing VITAL web-based database and with the clinical database from the Department of Thoracic/Head and Neck Medical Oncology. The modules to be developed include:

1. A comprehensive clinical data module which include the medical history, treatment, and detailed follow-up information.
2. A tissue specimen tracking and inventory module which track the types of amount of tissues collected over time.
3. TMA module which will be integrated with the existing VITAL web-based data management system for biomarker data already established by Core B to include the experimental data obtained from the tumor tissue and adjacent bronchial epithelial sites for TMA analyses.

The database allows remote data capture from any computer with a web browser. It is secure, password protected, and is within our institutional firewall. The database also allows the research nurse to schedule patient visits and will print out labels for tissue acquisition. It can track the tissue distribution in both sending and receiving. The integrated reporting system provides real-time inventory reports based on the most upto-date data. We have added the function to collect the 18-month blood biomarkers. Selected screen shots are provided in the Appendix 1. Major efforts are underway to support the revitalization effort. The database is fully functional and has captured 38 patients registered in the trial as of November 2007.

In addition, we have continued to work on statistical methods for evaluating interaction for combination therapy to determine whether the effect is synergistic, additive, or antagonistic. One manuscript has been published and two of them were in press. The related S-PLUS codes are available for download from <http://biostatistics.mdanderson.org/SoftwareDownload/>.

Key Research Accomplishments

- Provided statistical insight during the development of the ReVITALization of Project 1.
- Expanded the core web-enabled database system to incorporate retrospective tissue data.
- Developed an interactive index and model for multiple drug interaction assessment.

Conclusions

The Biostatistics and Data Management Core continues to provide active biostatistical support for the ReVITALization of Project 1 and all other VITAL projects. The Core will continue to enhance the web-enabled database system to include both prospective and retrospective sample data, as well as new biomarkers and targeting strategies. The development of a predictive risk model is the ultimate goal of this core in conjunction with other VITAL projects.

Core C: Pathology and Specimen Procurement Core

(Core Director: Ignacio Wistuba, M.D.)

Aim 1. Develop and maintain a repository of tissue and other biologic specimens from patients enrolled on the clinical trials in Project 1.

Update

Using the procedures and system established for sample collection, processing, banking and distribution, we have acquired, processed and banked a total of 740 specimens from patients enrolled in the Vanguard clinical trial (Project 1). Of these, 401 tissue samples obtained from baseline and follow-up bronchoscopies have been obtained, processed and banked in the Core tissue bank (Table 3). In addition, resected specimens from the majority of lung cancer and head/neck tumors have been reviewed and banked.

Table 3. Summary of specimens collected and banked in the Pathology Core

Type of Specimen	Number
Sputum	37
Buccal Brush	37
Bronchial Brush	227
Bronchial Wash	38
Tissue Specimens	401
Total	740

Aim 2. Maintain a comprehensive database of tissue and specimen characteristics from patients enrolled in the clinical trials of Project 1, including pathologic characteristics of each specimen, inventory and distribution

Update

The Biostatistics Core has developed a web-based database which has been used to catalogue all the specimens obtained and banked in the Pathology Core, and to report pathology diagnosis. From the Vanguard patients, 339 cytological specimens and 401 bronchial biopsies have been tracked and inventoried using the web-site database. As LIFE bronchoscopy biopsies have been performed in all these patients, LIFE abnormalities have been banked in a database to be correlated with histopathological features.

Aim 3. Provide comprehensive pathologic characterization of all tissues and other biologic specimens and assist in preparation and evaluation of studies involving these tissues

Update

Using the comprehensive list of histology diagnosis for bronchoscopy biopsies prepared at the beginning of this project, we have processed and histopathologically diagnosed 401 tissue specimens from bronchoscopies in a timely fashion (Table 4). Two H&E-stained tissue sections have been examined per bronchial biopsy. Although normal bronchial epithelium has been detected in at least one site examined in most subjects, a number histopathological changes have been detected. The most frequent abnormality detected were goblet cell metaplasia (9.48%) and basal cell hyperplasia (13.22%). Of interest, squamous metaplasia (2.74%) and dysplasia (0.75%) were infrequently detected. No severe dysplasia, carcinoma *in situ* and invasive carcinoma has been detected. Histopathological analysis of the resected lung and head/neck cancer samples has been also been performed. Tissue blocks from all these samples are available for future biomarker analysis.

Table 4. Summary of histopathology diagnosis of bronchial biopsies obtained from clinical trial (Project 1).

Diagnosis	N	%
No Tissue/Denuded Epithelium	8	2.00
Normal Epithelium	315	78.55
Goblet Cell Metaplasia (GCM)	38	9.48
Basal Cell Hyperplasia (BCH)	53	13.22
Combined GCM/BCH	6	1.50
Squamous Metaplasia	11	2.74
Mild Dysplasia	3	0.75

Aim 4. Provide centralized immunohistochemistry and laser capture microdissection services, nucleic acid extractions and assistance with construction and evaluation of tissue arrays.

Update

A centralized immunohistochemistry (IHC) laboratory is in place as part of the Pathology Core with manual and automated IHC techniques and *in situ* tissue-based methodologies, such as fluorescent *in situ* hybridization (FISH) and laser capture microdissection. As reported previously, tissue microarray (TMA) construction is also in place, and a complete set of lung cancer specimens (N = 400, TMA set I) is available. The samples obtained from the Clinical Trial (Project 1) have not been processed and distributed yet, because the relatively small number of specimens obtained so far. To circumvent the lack of specimens from the Clinical Trial, the Pathology Core has developed the following strategy to make specimens available for biomarkers validation to VITAL research projects:

1. Tumor (NSCLC) TMAs, set II. We have reviewed 500 stages I to IIIA lung cancer surgically resected specimens in our Institution from January 1/2003 to December 31/2005 and obtained archival formalin-fixed paraffin embedded specimens to identify tumor and adjacent normal or preneoplastic bronchial and bronchiolar epithelia. Of these, 150 cases have been fully reviewed and characterized pathologically and TMAs construction is in progress. We expect to finalize set II TMA construction by May 2008. Detailed demographic and clinical information is being obtained in all these cases, including follow up for recurrence, secondary tumor development and survival.

2. Preneoplasia TMA. As reported previously, from a subset of early lung cancer surgically resected in our Institution from 1997 to 2002, we have identified and selected 504 histologically normal and abnormal bronchial, bronchiolar and alveolar epithelium specimens to be examined

for molecular marker expression using IHC. All these specimens have been placed in TMAs and in collaboration with VITAL research projects' PIs and others, we have examined 26 IHC markers (Table 5), most of them related to potential targets for targeted-chemoprevention strategies.

Table 5. Summary of immunohistochemistry (IHC) markers examined in respiratory epithelium specimens placed in TMAs.

Immunohistochemistry Markers Examined in Respiratory Epithelium	
E-Cadherin (VITAL Project 2)	FGFR2 (VITAL Project 2)
Caspase-8 (VITAL Project 2)	Syndecan-1 (VITAL Project 2)
STAT-5 (VITAL Project 2)	Survivin (VITAL Project 4)
P70S6K (VITAL Project 2)	SCC-1 (VITAL Project 3)
NF- κ B	SCC-2 (VITAL Project 3)
IRAK-1 (VITAL Project 2)	pCREB (VITAL Project 3)
IGF (VITAL Project 4)	CREB (VITAL Project 3)
IGFR1 (VITAL Project 4)	PTTG
EGFR (VITAL Project 4)	Integrin- β 6
Caveolin-1	N-cadherin
FUS-1	Vimentin
bFGF (VITAL Project 2)	β -catenin
FGFR1 (VITAL Project 2)	MMP-9

Using both tumor and preneoplasia TMAs, we have examined the role of the expression of several pathways and multiple markers in the early pathogenesis of lung cancer, including survivin, SCC-1/2, CREB/pCREB, bFGF/FGFR, estrogen and progesterone receptors, epithelial-mesenchyma transition (EMT) markers, STAT-1, TITF-1 and Fus-1 (3p21.3) tumor suppressor gene. Brief descriptions of the data obtained in those analyses are the following:

a. Expression of Survivin in the early pathogenesis of lung cancer

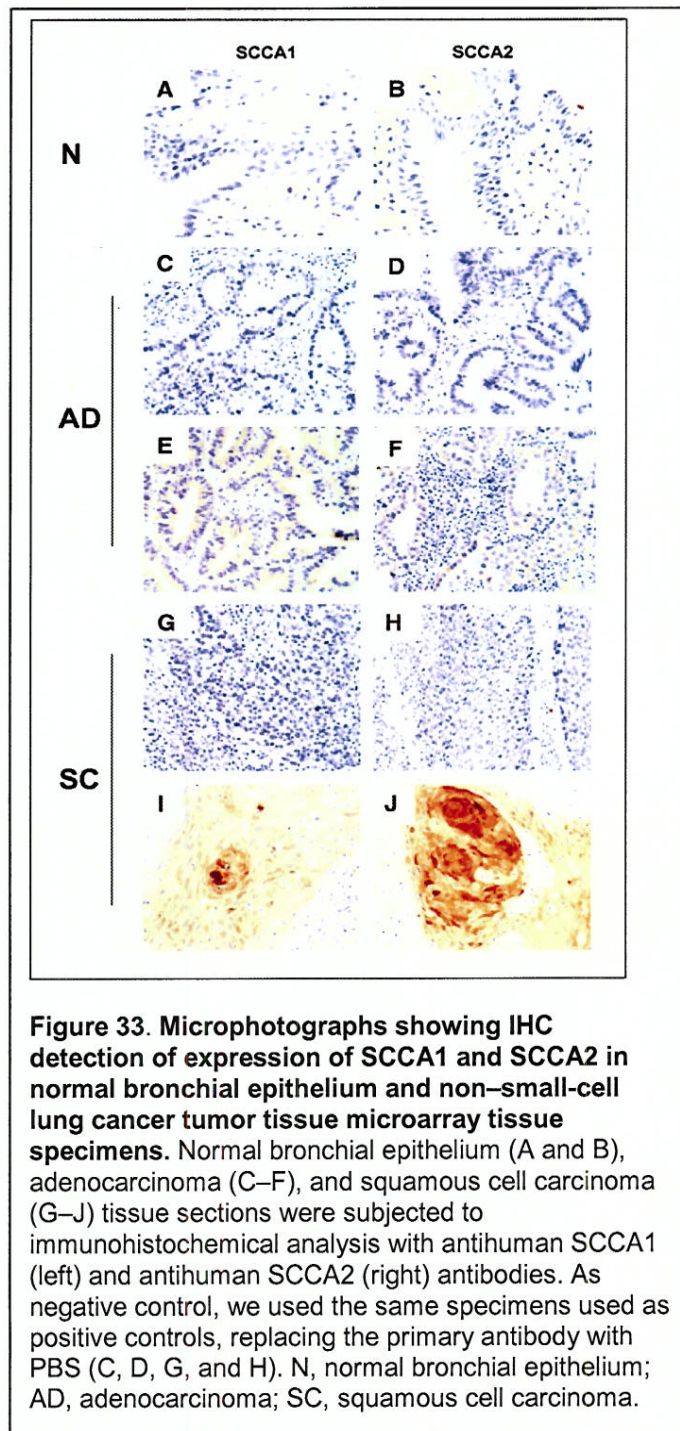
The aim of this study was to assess the difference in the Survivin expression among different lesion bronchial epithelium histologies obtained from lung cancer patients. Survivin expression levels were presented in the form of cytoplasm scores and nuclei scores as determined by IHC analysis. Survivin expression was examined in normal tissue, atypical adenomatous hyperplasia (AAH) lesion, basal cell hyperplasia (BCH), squamous metaplasia (SQM), low and high-grade (including carcinoma *in situ*) dysplasia lesions. A total of 379 lesions were obtained out of 94 lung cancer patients. Because cytosolic survivin plays an essential role in protecting cells from apoptotic stimuli and promoting tumorigenesis, we analyzed the cytosolic survivin expression in these tissue specimens. Surprisingly, cytosolic survivin expression was detected in normal specimens (47.3%). It was also detected in the specimens of epithelial hyperplasia (57.3%), squamous metaplasia (63.6%), low-grade squamous dysplasia (83.3%), high-grade squamous dysplasia (79.2%), and atypical adenomatous hyperplasia (35.5%). The mean cytosolic survivin score was significantly higher for the high-grade squamous dysplasia specimens than for the specimens of normal tissue ($P < 0.001$), epithelial hyperplasia ($P < 0.001$), and squamous metaplasia ($P = 0.01$). The mean cytosolic survivin score for the low-grade squamous dysplasia specimens was significantly higher than those for the specimens of normal tissue ($P = 0.014$) and epithelial hyperplasia ($P = 0.004$; Fig. 1D). These data suggest that survivin expression was induced early during lung carcinogenesis. These data are part of a publication in collaboration with Dr. Ho-Young Lee's lab (Project 4), M. D. Anderson Cancer Center, in Cancer Research on December 2007 (Jin et al 2007).

b. SCCA1 and SCCA2 expression levels in normal and malignant lung tissue specimens.

As part of Project 3, Dr. Koo's lab analyzed protein expression patterns in the apical surface fluid (ASF) from aberrantly differentiated squamous metaplastic normal human tracheobronchial epithelial (NHTBE) and mucous NHTBE cells. Comparative two-dimensional PAGE analysis revealed 174 unique proteins in the ASF of squamous NHTBE cells compared with normal mucociliary differentiated NHTBE cells. Among them, 64 well-separated protein spots were identified by liquid chromatography-tandem mass spectrometry, revealing 22 different proteins in the ASF from squamous NHTBE cells. Expression of six of these proteins [SCC antigen 1

(SCCA1), SCC antigen 2 (SCCA2), S100A8, S100A9, Annexin I, and Annexin II] in the squamous NHTBE cells was further confirmed with immunoblot analysis. Notably, SCCA1 and SCCA2 were verified as being expressed in squamous metaplastic NHTBE cells but not in normal mucous NHTBE or normal bronchial epithelium. Moreover, SCCA1 and SCCA2 expression increased in *in vitro* lung carcinogenesis model cell lines with increasing malignancy.

To determine whether SCCA1 and SCCA2 expression is elevated in NSCLC tissue specimens and the specificity of these proteins expression in adenocarcinoma and squamous cell carcinoma histologies, we performed IHC analysis using tumor TMA samples. SCCA1 and SCCA2 immunostaining levels were detected in the cytoplasm of tumor cells in both tumor histology specimens (Figure 33). However, the protein expression frequency was obviously higher in squamous cell carcinoma [positive, SCCA1 42.4% (n = 45) and SCCA2 65.7% (n = 69); negative, SCCA1 57.6% (n = 61) and SCCA2 34.3% (n = 36)] compared with adenocarcinoma [positive, SCCA1 33.3% (n = 58) and SCCA2 39.8% (n = 70); negative, SCCA1 66.7% (n = 116) and SCCA2 60.2% (n = 106)] histology, especially for SCCA2. In contrast, the expression of the two proteins was undetectable in normal bronchial epithelia adjacent to tumors from each histology site (Figure 33). These results indicate that SCCA1 and SCCA2 are not expressed in normal bronchial epithelium and they are highly expressed in squamous cell carcinoma of the lung. Somewhat surprisingly,



approximately one third of adenocarcinomas showed SSICA1 and SSICA2 expression by IHC. These data are in collaboration with Dr. Peter Koo's lab (Project 3), M. D. Anderson Cancer Center.

c. CREB and p-CREB IHC overexpression in NSCLC.

Based on the identification of the transcription factor CREB as an important regulator of growth of several types of cancers and our recent findings of its importance in normal differentiation of bronchial epithelial cells, we hypothesized that CREB plays an important pathobiologic role in lung carcinogenesis. IHC analysis of CREB and p-CREB expression in the 45 whole paraffin-embedded NSCLC specimens and adjacent normal bronchial and bronchiolar epithelial tissue specimens showed stronger nuclear staining for CREB and p-CREB in both adenocarcinoma and squamous cell carcinoma tissue than in normal tissue. Statistical analysis showed significantly higher immunostaining scores for both CREB (1.37 versus 0.73; $P = 0.013$) and p-CREB (1.96 versus 1.05; $P = 0.0002$) in tumor tissue than in normal tissue. Then, we performed IHC analysis of CREB and p-CREB expression in the 310 NSCLC TMAs to assess potential associations of CREB and p-CREB overexpression with the patients' demographic and clinicopathologic characteristics and histologic subtypes of NSCLC. According to the Wilcoxon rank sum test, the CREB and p-CREB immunostaining scores were significantly higher in the squamous cell carcinoma specimens than in the adenocarcinoma and bronchioloalveolar carcinoma specimens (CREB: 0.61 versus 0.43, $P = 0.002$; p-CREB: 0.32 versus 0.25, $P = 0.008$). These are the first reported results illustrating the potential of CREB as a molecular target for the prevention and treatment of NSCLC, especially in never-smokers. These data are part of a publication in collaboration with Dr. Peter Koo's lab (Project 3), M. D. Anderson Cancer Center, recently accepted for publication in Cancer Research (Seo et al, In Press).

d. Expression of basic fibroblast growth factor and fibroblast growth factor receptors 1 and 2 in the pathogenesis of lung cancer.

To identify the patterns of protein expression of basic fibroblast growth factor (bFGF), fibroblast growth factor receptor (FGFR) 1, and FGFR2 in non-small cell lung carcinoma (NSCLC) and their role in the early pathogenesis of squamous cell carcinoma of the lung, we examined archived material from surgically resected NSCLC specimens ($n = 321$) and adjacent bronchial epithelial specimens ($n = 426$) for the expression of bFGF, FGFR1, and FGFR2 as determined by IHC analysis and correlated our findings with clinicopathologic features of patients with NSCLC. Overall, NSCLC tumors demonstrated high bFGF, FGFR1, and FGFR2 expression. In both histologic types of NSCLC (adenocarcinoma and squamous cell carcinoma), cytoplasmic expression scores for the three markers were significantly higher than in histologically normal epithelia. The pattern of expression in NSCLC varied according to histologic type and cellular localization for the three markers. Nuclear bFGF ($P = 0.03$) and FGFR1 ($P = 0.02$) levels were significantly higher in women than in men. Although cytoplasmic FGFR1 expression was significantly higher ($P = 0.002$) in ever smokers than in never smokers, nuclear FGFR1 ($P = 0.0001$) and FGFR2 ($P = 0.003$) expression was significantly higher in never smokers. Different prognostic patterns for the expression of these markers were detected for both histologic types. We detected relatively low levels of expression of all markers in normal and mildly abnormal epithelia, including bronchial squamous metaplasia. However, in dysplastic stages, we detected significantly higher expression of all markers. bFGF, FGFR1, and FGFR2 are frequently overexpressed in NSCLC, and different expression patterns can be detected in its two major types. bFGF signaling pathway activation may be an early phenomenon in the pathogenesis of squamous cell carcinoma and thus an attractive novel target for lung cancer chemopreventive

and therapeutic strategies. These data are part of a manuscript in preparation in collaboration with Dr. Reuben Lotan's lab (Project 2), M. D. Anderson Cancer Center.

- e. Expression of estrogen and progesterone receptors identifies a subset of NSCLC and correlates with EGFR mutations.

Estrogen (ER) α and β and progesterone (PR) receptors are transcription factors that regulate the expression of multiple genes and have been involved in the pathogenesis of NSCLC. There are conflicting results reported on the expression of ER receptors in NSCLC tissue specimens using different commercially available antibodies (Abs) and IHC detection methods. Correlation between ER expression and EGFR mutation status has been reported in lung cancer cell lines. Our aims were to compare the expression pattern as determined using IHC analysis in tumor tissues of six commercially available ER antibodies (four α and two β) in a large set (N=317) of NSCLCs TMAs containing 201 adenocarcinomas and 116 squamous cell carcinomas; and correlate the expression of ER and PR with patient clinico-pathologic characteristics, and in adenocarcinomas with EGFR mutation status. The Abs used were: a) ER α : clone 6F11 (2 Abs), clone HC-20, and clone 1D5N; b) ER β : clone H-150 and 14C8; and, c) PR: polyclonal. While all Abs against ER α expressed in the nucleus (5%, 7%, 34% and 36% of cases) and two in the cytoplasm (18% and 42%) of tumor cells, both ER β Abs stained in both tumor cell locations (nucleus 42% and 44%; cytoplasm 98% and 20%). PR expressed only at nuclear level (63%). All ER α Abs stained significantly higher in the nucleus of adenocarcinomas (vs. squamous; $P=0.0048-0.0001$), three Abs stained higher in females (vs. males; $P=0.037-0.0067$), especially older than 50 years of age ($P=0.021-0.0043$), and never smokers (vs. smokers; $P=0.0227-0.0009$). One Ab, raised against the ER α N-terminus protein (clone 1D5N, Lab Vision Co, Fremont, CA) significantly correlated with all those variables when stained in the nucleus and with worse recurrence free survival (HR 1.77, 95% CI 1.11, 2.81; $P=0.015$) when stained in the cytoplasm. An ER β Ab and the PR antibody stained significantly ($P=0.0069$ and $P=0.05$, respectively) higher in adenocarcinomas. Higher nuclear and cytoplasm expressions of two ER α Abs and higher nuclear expression of an ER β Ab correlated with the presence of EGFR mutation in adenocarcinomas ($P=0.0029$ to <0.00001). Based on these findings, we selected one Ab for each receptor to study the expression in the early pathogenesis of lung cancer. We found that cytoplasmic ER β and nuclear PR were expressed in the normal small bronchial and bronchiolar epithelium, but not alveolar cells, adjacent to lung adenocarcinomas as a field effect phenomenon. Our findings indicate that both ERs and PR express in NSCLC. We identified Abs against ERs that distinguish a subset of NSCLC having defined clinico-pathologic features, including EGFR mutation in lung adenocarcinoma histology, and those patients may benefit from hormonal receptor antagonist therapy. An abstract reporting these data has been submitted to the 2008 AACR Annual Meeting.

- f. Epithelial-mesenchymal transition (EMT) expression in the pathogenesis of lung cancer.

Epithelial to mesenchymal transition (EMT) has been implicated in the development and progression of epithelial tumors. In lung cancer, individual EMT markers' expression has been studied and correlated with prognosis. To better define the role of the EMT phenotype of lung cancer pathogenesis and progression, we studied the expression of 6 proteins, E-Cadherin, N-Cadherin, β -Catenin, MMP9, Integrin- α v β 6 (Int- β 6) and Vimentin in 209 adenocarcinomas (ADC) and 116 squamous cell carcinomas (SCC) using IHC analysis. EMT expression was correlated with EGFR and p-EGFR IHC and EGFR mutational status. Female gender associated with higher E-Cadherin intensity and lower N-Cadherin cytoplasmic score. ADC correlated with higher E-Cadherin class and intensity and with N-Cadherin membrane and

cytoplasmic intensities. Smoking correlated with lower E-Cadherin intensity and higher N-Cadherin membrane class and cytoplasmic score. Never smokers showed higher E-Cadherin and Int- β 6 intensities, and former smokers had significant higher N-Cadherin membrane class and cytoplasmic score. EGFR class correlated positively with β -Catenin membrane class, but negatively with N-Cadherin membrane and cytoplasmic intensities. p-EGFR class correlated with N-Cadherin membrane and cytoplasmic intensities, but associated negatively with higher Vimentin staining. Higher Int- β 6 levels showed worse overall survival (HR=4.4). No correlations were seen between markers' expression and EGFR mutations. Our findings indicate that in lung cancer EMT is a frequent phenomenon in NSCLC and correlates with tumor histology, smoking history and survival.

Next, we examined the expression of a subset of EMT-related markers using IHC analysis: E-Cadherin, Integrin- α β 6, N-Cadherin, Vimentin and MMP9, in 328 normal and preneoplastic lesions from 105 patients with lung cancer. High expression of E-Cadherin was seen in 52.4% of normal epithelia, 74.4% hyperplastic epithelia, 86.7% in squamous metaplasias and 54.4% of dysplastic-carcinoma (DYS-CIS) *in situ* lesions. Integrin expression showed progressive increase from normal epithelia (21.2%) to DYS-CIS (41.9%). N-Cadherin had both membrane and cytoplasmic expression with normal epithelia showing high membranous signal in 21.1%, hyperplasias in 4%, squamous metaplasias in 11.8%, and DYS-CIS in 3.7%. Squamous metaplasias showed the higher N-Cadherin cytoplasmic expression with a mean score of 11.8 and DYS-CIS showed the lowest with a mean score of 4.8%. Vimentin showed an irregular pattern of expression with normal epithelia with a mean score of 17.4, hyperplasias 30.2, squamous metaplasias 23.5, and DYS-CIS 18.5. MMP9 did not show great variations in expression with mean scores of 63 for normal epithelia and 60.7 on the other end of the histological spectrum (DYS-CIS). Although EMT is not overtly manifested in lung preneoplastic lesions, however, there is a clear tendency mostly noted in E-Cadherin and Integrin that suggest that this phenomenon may play an important role in lung cancer development.

g. STAT1 expression in NSCLC.

Despite recent advances, the prognosis of NSCLC is still dismal. The recurrence rate of early-stage NSCLC is ~40% within five years after a potentially curative treatment. Because of the limited prognostic power of the current pathologic and clinical criteria, providing accurate molecular prediction of the clinical outcome is currently needed. Recently, using cDNA microarray and RT-PCR methods it has been reported that the expression of genes HER3, LCK (lymphocyte-specific protein tyrosine kinase), DUSP6 (dual-specificity phosphatase 6), and STAT1 (signal transducer and activator transduction 1) closely associate with recurrence-free and overall survival among NSCLC patients (Chen et al, New Eng J Med 2007: 356:11-20). The overexpression of HER3 and LCK were risk factors and DUSP6 and STAT1 protective factors for outcome. As only HER3 protein expression has been previously reported in lung cancer, we investigated the expression of those four proteins in a large set of NSCLC TMA specimens (N=306; 194 adenocarcinomas and 112 squamous cell carcinomas) using IHC detection, and correlated their expression with clinico-pathologic features, including prognosis. Protein expression was examined semi-quantitatively using both intensity and extension of staining, and a final score was calculated for each marker. HER3 and DUSP6 proteins were expressed only in the cytoplasm of tumor cells, STAT-1 expressed in both tumor and stromal cell compartments, and LCK expressed only in inflammatory stromal cells. HER3 was detected in 38% of NSCLCs in malignant cells and LCK in 85% of tumors in inflammatory stromal cells. DUSP6 and STAT1 proteins were not detected in 12% and 45% of tumors, respectively. None of the markers expression correlated with patients' recurrence-free and overall survival. STAT1 expression was significantly lower in patients with squamous cell carcinoma compared to

adenocarcinoma ($P=0.01$), non-smoking history ($P=0.0015$), and higher TNM stages ($P=0.015$). Our findings point out the difficulties of validating gene expression data using protein expression analysis and tissue-based *in situ* methodologies are important to identify the type of cells expressing specific molecular markers. We have confirmed at the protein level that STAT1 is frequently lost in NSCLC tumor tissues and the pattern of immunostaining in tumor cells is compatible with tumor suppressor gene activity. We also report for the first time that DUSP6 protein is lost in a subset of NSCLC and along with STAT1 may represent a novel tumor suppressor gene for this neoplasm. We plan to study the molecular mechanisms of STAT1 loss of expression in NSCLC and its role in the early pathogenesis of lung cancer. An abstract reporting these data has been submitted to the 2008 AACR Annual Meeting.

- h. *TTF1* gene amplification and protein expression identify a subset of NSCLC with worse prognosis.

TTF1 a lineage-specific transcription factor frequently overexpressed in lung adenocarcinoma. In collaboration, we have recently reported gene amplification in a subset of these tumors (Weir et al, 2007). To better characterize *TTF1* copy number in NSCLC and correlate it with protein expression, we studied both gene copy number and protein expression using FISH and IHC assays in a large series ($N=324$) of surgical resected NSCLCs placed in TMAs, including 205 adenocarcinomas and 119 squamous cell carcinomas. We correlated our findings with patients' clinico-pathologic characteristics, and in a subset of adenocarcinomas with tumor *EGFR* (exons 19-21) and *KRAS* (exons 1 and 2) mutation status. *TTF1* amplification (clustered gene signals) was detected in 19% (51 out of 269) of tumors, without differences by histology (18% of squamous cell carcinoma and 19% of adenocarcinoma). TTF1 protein high expression (semiquantitative score ≥ 200 , range 0-300) was detected exclusively in adenocarcinomas (48%), and in this tumor type correlated with gene amplification ($P=0.005$). No correlation between TTF1 abnormalities and patients' smoking status was detected. In adenocarcinomas, protein overexpression using the semiquantitative IHC score, but not gene amplification, correlated with *EGFR* and *KRAS* mutations: TTF1 high level of expression was more frequently found in *EGFR* (16/21, 76% vs. 59/172, 34% of wild-type, $P<0.001$) and *KRAS* (8/11, 72% vs. 26/75, 34%, $P=0.016$) mutant compared with wild-types tumors. Survival analysis shows that for adenocarcinoma *TTF1* amplification correlated with worse recurrence-free survival ($P=0.001$), while protein high level of expression correlated with better recurrence-free survival ($P=0.036$). Our findings indicate that *TTF1* amplification occurs in a subset of NSCLCs, including both major tumor histologies: adenocarcinoma and squamous cell carcinoma. The association of TTF1 expression with *EGFR* and *KRAS* mutation in lung adenocarcinomas may correlate with the peripheral airway origin of these tumors. Both *TTF1* gene amplification and protein expression correlate with NSCLC patients' prognosis. An abstract containing these data has been submitted to the 2008 AACR Annual Meeting.

- i) Loss and reduction of Fus1 protein expression is a frequent phenomenon in the pathogenesis of lung cancer.

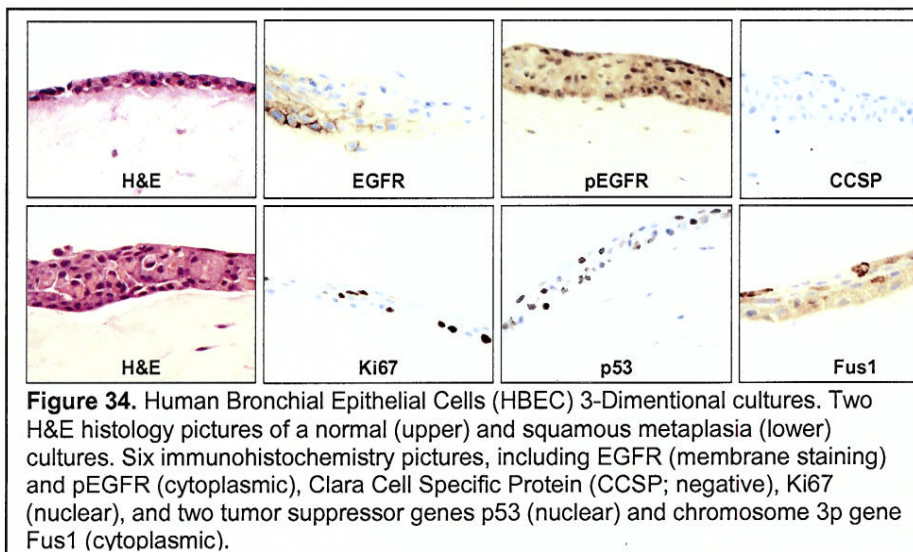
FUS1, a novel tumor-suppressor gene located in the chromosome 3p21.3 region, may play an important role in lung cancer development. Loss or reduction of Fus1 protein has not been examined in large series of lung cancers and their sequential preneoplastic lesions. Using TMAs, we examined Fus1 expression in 22 SCLC and 281 NSCLC (172 adenocarcinomas and 109 squamous cell carcinomas) tissue specimens using IHC detection and correlated those findings with the clinicopathological features of the cases. To investigate the role of Fus1 abnormal expression in the sequential pathogenesis of NSCLC, we studied Fus1 expression in 68 histologically normal bronchial epithelia, 120 basal cell hyperplasias, 23 squamous metaplasias,

62 squamous dysplasias, and 56 specimens of atypical adenomatous hyperplasia (AAH) obtained from lung cancer patients. Loss and reduction of expression was detected in 100% of SCLCs and 82% of NSCLCs, without significant differences between adenocarcinoma and squamous cell carcinoma histologies. In NSCLCs, loss of Fus1 expression was associated with significantly worse overall survival. Squamous metaplasia and dysplasia expressed significantly lower levels of Fus1 than did normal ($p = 0.014$ and 0.047 , respectively) and hyperplastic ($p = 0.013$ and 0.028) bronchial epithelia. In conclusion, our findings show a high frequency of Fus1 protein loss and reduction of expression in lung cancer and suggest that reduction of this protein may play an important role in the early pathogenesis of lung squamous cell carcinoma. All these findings support the concept that *FUS1* gene and Fus1 protein abnormalities could be used to develop new strategies for molecular cancer chemoprevention and therapy for a significant subset of lung tumors. These data are part of a publication in d. Inhibition of geranylgeranyltransferase I downregulates c-FLIP levels, induces DR5 expression, and augments tumor necrosis factor-related apoptosis-inducing ligand-induced apoptosis.

GGTase I has emerged as a cancer therapeutic target. Accordingly, small molecules that inhibit GGTase I have been developed and exhibit encouraging anticancer activity both *in vitro* and *in vivo* in preclinical studies. However, the underlying anticancer mechanisms of GGTase I inhibitors remain unclear. We previously demonstrated that FTIs increase Akt phosphorylation while inducing DR5 expression and enhancing TRAIL-induced apoptosis. Here we investigated whether GGTase I inhibitors exert similar effects. We found that inhibition of GGTase I by GGTI-298 induced apoptosis and augmented TRAIL-induced apoptosis in human lung cancer cells. GGTI-298 induced DR5 expression and reduced the levels of c-FLIP, particularly the short form of c-FLIP (FLIP_S); these effects were associated with GGTI-298's ability to induce apoptosis and augment TRAIL-induced apoptosis. Consistently, another highly selective GGTase I inhibitor, GGTI-DU40, but not its inactive analog SN-DU40, exerted similar effects. Enforced expression of c-FLIP or knockdown of DR5 expression protected cells from induction of apoptosis by the combination of GGTI-298 and TRAIL, indicating that induction of DR5 and downregulation of c-FLIP mediate augmentation of TRAIL-induced apoptosis by collaboration with Project 3 accepted for publication in Clinical Cancer Research (Prudkin et al, In Press).

In addition, we processed three-dimensional (3-D) organotypic culture of human bronchial epithelial cells (HBEC) in collaboration with Dr. John Minna, Project 2. To evaluate the phenotypic characteristics of the HBEC cultures and to test the effect of oncogenic manipulation in HBECs on their ability to differentiate and to invade, we have prepared three-dimensional organotypic culture.

HBEC cells only expressing hTERT and Cdk4 cells formed a confluent layer of cells on the upper surface of a fibroblast and collagen gel under layer and developed both ciliated and mucous-producing cell types. A repository of archival paraffin blocks (N=230) and histology sections



(N=470) from 12 3-D cultures has been developed in Dr. Wistuba's Lab and they are available for investigators. Detailed histologic characterization of those 3-D cultures, as well as IHC analysis of those specimens, have been performed in Dr. Wistuba's lab.

Our plan is to expand our repository of 3-D HBECs cultures and develop 3-D cultures using the potentially developed immortalized normal alveolar cells. Core C will prepare paraffin-embedded 3-D cultures for histopathologic, histochemical, immunohistochemical (Figure 34), FISH and microdissection methodologies, as well as TMA construction.

As a part of our ReVITALization plan, Core C has added 2 additional aims:

- Aim 5.** Identify ~600 surgically resected tissue specimens from stages I/II NSCLC (tumor, normal and abnormal adjacent bronchial epithelium specimens) and their complete clinical and pathologic information.
- Aim 6.** Examine over 40 biomarkers in those specimens by immunohistochemical (IHC) and tissue microarrays (TMAs).

We have already identified the tissue specimens for our retrospective studies and worked with Core B on the database development. We will also have additional collaborations on new aims with other projects in this program as a result of the plan (Project 2 -Tasks 5 -6 and Project 3 - Task 6).

Key Research Accomplishments

- Created a centralized immunohistochemistry (IHC) laboratory with manual and automated IHC techniques and *in situ* tissue-based methodologies.
- Developed a repository of archival samples from 3-D HBEC cultures for future use.
- Supported the various VITAL projects by processing tissue and culture samples, and providing pathological and histological characterization of those specimens, and maintaining samples repositories.

Conclusions

We have acquired and banked 740 specimens from bronchoscopies and resected specimens from lung cancer and head/neck tumor patients and used the web-enabled database developed by the Biostatistics Core to track and inventory bronchoscopy specimens and report histopathological features of 401 bronchial mucosa tissue specimens. We have selected, prepared and examined by immunohistochemistry a number of molecular markers in a large series (N=504) of respiratory epithelium specimens which have been used to examine several IHC markers related to VITAL-related projects. We will continue to select and process retrospective tissue samples for the ReVITALization Project 1 as well as consult with the Biostatistics Core in enhancing the database to include these samples. Support for all VITAL projects will continue with regard to histology, pathology, and cytology assessments, specimen procurement and processing, and biomarker analysis.

Developmental Research Project (DRP) 2: Biomarkers for Aggressive Lung Carcinomas in African American Men

(PI: Sharon Lobert, Ph.D., University of Mississippi, Jackson, MS)

Biological factors, in addition to health care access, are likely to contribute to the disparity in survival for Caucasian men and African American men diagnosed with lung cancer. Lung tumors are classified into two major categories: small cell lung cancer (SCLC and NSCLC. The heterogeneity of NSCLCs complicates efforts to determine prognosis and select appropriate treatment regimens. β class III tubulin has been identified as a marker of neuroendocrine differentiation in lung cancer and as a potentially important biomarker for aggressive tumors (SCLC, neuroendocrine type large cell carcinomas, and some adenocarcinomas). Our proposed research focuses on two hypotheses: 1) β class III tubulin levels are higher in NSCLCs from African American men compared to white men; and 2) the expression of proteins that alter microtubule dynamics is increased in NSCLCs from African American men compared to white men. Higher levels of these proteins would reduce the effectiveness of antimitotic agents used in the treatment of NSCLC that stabilize (paclitaxel) or destabilize (vinorelbine) mitotic spindles. Stages IA, IB and IV NSCLCs ($n = 80$) will be obtained from the NCI Cooperative Human Tissue Network and quantitative real-time RT-PCR will be used to measure tubulin isotype, stathmin and MAP4 mRNA levels. Equal numbers of samples from white and African American males will be examined. Western blotting will be used to verify protein levels.

Update

Year Three Goal: Complete the comparison of β -tubulin isotypes, stathmin, and MAP4 by quantitative and semiquantitative Western blotting.

Our goal was to determine whether β -tubulin mRNA levels could be useful as biomarkers. Using quantitative real-time RT-PCR, we measured the levels of seven classes of β -tubulin isotypes, stathmin, and MAP4 in 64 NSCLC and 12 normal lung tissue specimens (see Table 6). We found significantly higher fractions of β -tubulin classes II and V mRNA compared to other isotypes in all tumor samples ($p < 0.05$) (Figure 35). In addition, the ratio of β -tubulin classes II/V mRNA was significantly higher in NSCLCs compared to normal tissues ($p < 0.001$) (Figure 35c). The data suggest that the ratio of β -tubulin classes II and V mRNA could be useful as a biomarker for NSCLCs, tumor differentiation and/or aggressiveness. Furthermore, the ratio of MAP4 to stathmin mRNA was found to be higher in diseased tissues compared to normal lung tissues suggesting this ratio might also be used as a clinically relevant biomarker (Figure 35d). This project was completed this year and a manuscript was submitted to Tumor Biology.

Key Research Accomplishments

- Determined that the ratio of β -tubulin classes II/V mRNA was significantly higher in NSCLCs compared to normal and correlated with level of differentiation.
- Determined that ratio of MAP4 to stathmin mRNA was also found to be higher in tumor than normal lung tissue.

Conclusions

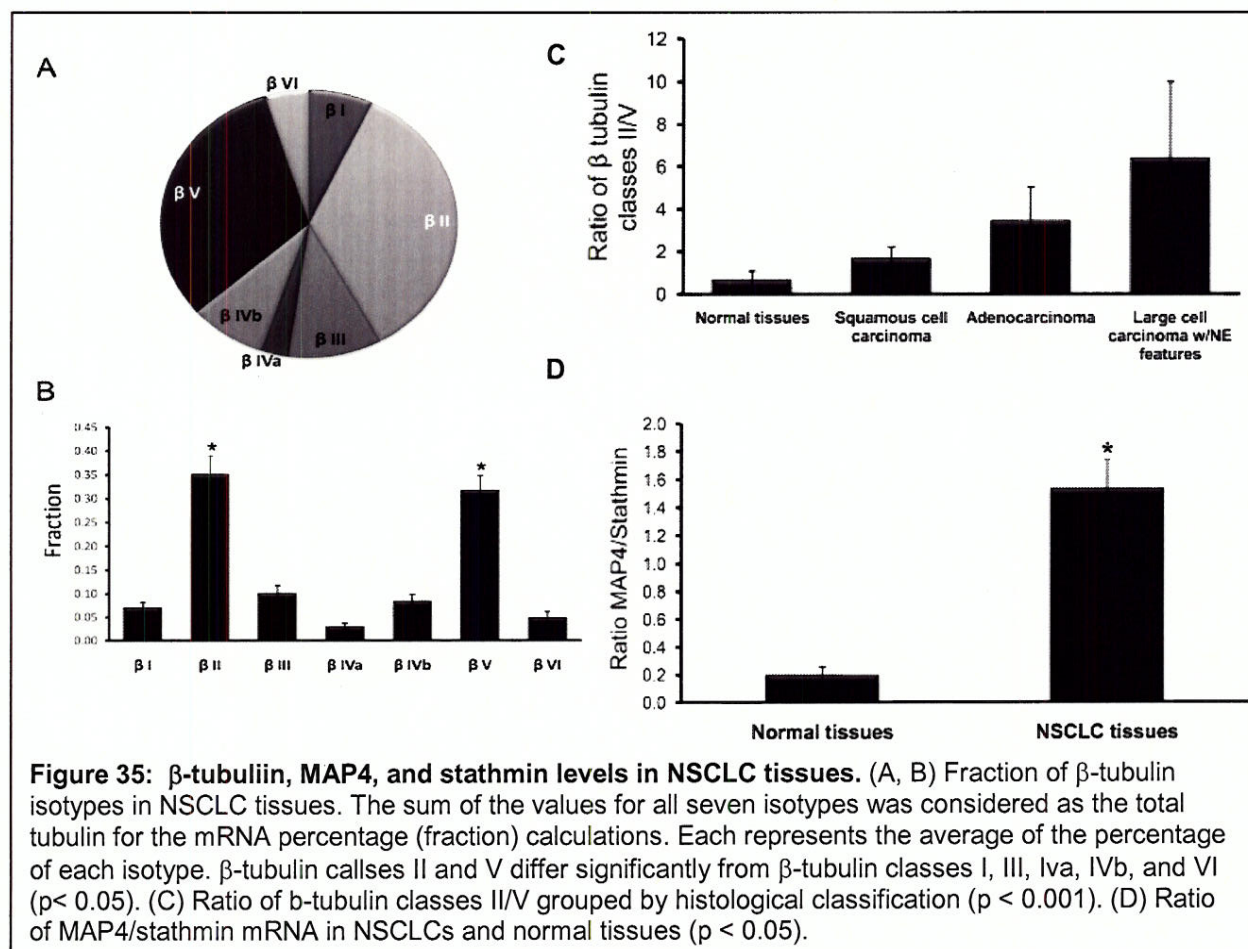
Ratios of β -tubulin classes II/V and of MAP4/stathmin mRNA were found to correlate with the level of differentiation in lung tissue. These changes are likely due to dysregulation of microtubule dynamics in the disease state, essential for cell division and proliferation, but these mechanisms need to be further explored.

Table 6. NSCLC and normal lung tissue samples.

NSCLC samples		Race	
		*BM	WM
Number of samples		20	44
Age range		43-71	40-85
Tissue differentiation			
	Poorly differentiated	9	19
	Moderately differentiated	4	15
	Well differentiated	3	4
	Not determined	5	5
Histological classification			
	Squamous cell carcinoma	8	18
	Adenocarcinoma	6	10
	Large cell carcinoma with neuroendocrine features	1	3
	Various	5	13

Normal tissues		Race	
		*BM	WM
Number of samples		2	10
Age range		75-76	40-82

* BM-African American males; WM-White males.



KEY RESEARCH ACCOMPLISHMENTS

Project 1: Biologic Approaches for Adjuvant Treatment of Aerodigestive Tract Cancer

- Enrolled 11 more patients enrolled in the Vanguard study, for a total of 45.
- Continued to collect patient clinical data and tissues for distribution to support research projects in the VITAL grant.
- Two patients completed the 1 year mark/bronchoscopy.
- ReVITALization proposal and budget was approved and plan is being implemented.

Project 2: Identification of Biomarkers of Response to Chemoprevention Agents in Lung Epithelium

- Established additional immortalized HBEC strains from multiple donors.
- Developed new methods for differentiating HBECs into complex epithelium using Matrigel and found that the HBECs have the cellular program intact to form branching morphogenesis and SACs and to expression pulmonary epithelial specific proteins such as SPA.
- Genetically manipulated the HBECs to derive isogenic strains that expressed oncogenic KRAS, mutant EGFR, and/or loss of p53 expression as well as HBECs with various EGFR tyrosine kinase domain mutations alone or with p53 knockout, and characterized their biologic and gene expression behavior showing they had partial progression towards malignancy
- Identified gene expression signatures associated with the introduction of oncogenic changes into the HBEC cells especially changes in expression of a set of cytokine genes and their receptors that are targets for early detection and chemoprevention of KRASV12 mediated lung cancer.
- Demonstrated progression of oncogenically manipulated HBECs to full malignancy after biologic selection in soft agar and identified the ability of such clones to differentiate into several histologic types of lung cancer.
- Performed genomic wide expression profiling and array CGH analysis for copy number changes in HBECs and in primary lung cancers. These have led to the identification of several amplified areas that will provide excellent probes for the early detection of preneoplastic changes in smoking damaged lung epithelium as well as biomarkers for chemoprevention studies.
- One of the key new genes identified as amplified in lung cancer pathogenesis is the lineage specific transcription factor TTF1. Functional studies of this gene indicate that it is essential for the continued growth of lung cancers. It is thus an excellent target for both early detection and for chemoprevention and potentially lung cancer therapeutics.
- We have identified miRNA expression signatures differentially expressed between non-cancerous and cancerous bronchial epithelial cells.
- Identified novel miRNAs that are potentially important in the initiation and progression of lung cancer.
- Continued to collect and process bronchial brush specimens which now total 408.
- Identified 346 upregulated genes and 466 downregulated genes that displayed expression level variation from NHBE and normal small airway epithelial cells (SAEC) to the tumorigenic cell line (1170-I)

- Discovered that functional pathway analysis of the gene array data revealed modulation of expression of many genes involved in DNA replication, cell cycle, cell adhesion, and enzymatic pathways
- Confirmed the differential expression of one putative biomarker,- MCM2, at the mRNA and protein levels in the premalignant cell line model, as well as in cell lines derived from human lung cancers, by Western blotting and quantitative real-time PCR, and immunohistochemical analyses.
- The findings support the conclusion that MCM2-7, GMNN, CDC6, and CTD1 are all important for the replication of immortalized, transformed and tumorigenic cells.

Project 3: Premalignant Bronchial Epithelia: Molecular and Cellular Characterization of Lung Tumorigenesis

- Determined that the proangiogenic chemokine CXCL5 is strongly upregulated by IL-1 β cytokine in premalignant and malignant lung cancer cell lines. CREB is required for the upregulation of the proangiogenic chemokine gene.
- Determined that targeting the CREB signaling pathway using chemical or genetic methods suppresses the growth and survival of NSCLC.
- Discovered that CREB is gradually overexpressed during lung cancer progression and overexpression of CREB is associated with negative prognosis in NSCLC patients.
- Further developed our imaging technologies and quantitative analytical algorithms for the future analyses of these studies.

Project 4: Modulation of Death Receptor-Mediated Apoptosis for Chemoprevention

- Determined that several groups of the compounds with cancer therapeutic potential including celecoxib and its derivative, FTIs, GGTase inhibitors, proteasome inhibitors, triterpenoids, the natural product honokiol, the synthetic retinoid SHetA2 and PPAR γ ligands modulate DR5 expression and/or c-FLIP levels (mostly by downregulation), which contribute to induction of apoptosis and/or enhancement of TRAIL-induced apoptosis.
- Discovered that CHOP/GAD153 mediates DR5 expression induced by certain anticancer agents (e.g. SCH66336; DMC and SHetA2).
- Identified a positive role of COX-2 activation in mediating perifosine-mediated anticancer activity.

Project 5: Molecular Strategies Targeting the AKT Signaling Pathway for Lung Cancer Chemoprevention and Therapy

- Established the immortalized HBE cell lines stably transfected with retroviral vectors expressing constitutively active Akt1, 2, or 3. The effects of overactivation of Akt on cell viability under variable stress conditions have been characterized.
- Determined that the EGFR TKI Gefitinib induced association between EGFR and IGF-1R, activated IGF-1R/PI3K/Akt/mTOR-mediated *de novo* protein synthesis of survivin in NSCLC cells. Inhibition of IGF-1R signaling pathways or knock-down of survivin expression abolished resistance to the gefitinib and induced apoptosis in NSCLC cells.
- Determined that NNK and nicotine induce survivin protein synthesis in normal HBE cells by activating the Akt/mTOR pathway
- Determined that survivin expression is induced as an early event in lung carcinogenesis.

Core B: Biostatistics & Data Management Core

- Provided statistical insight during the development of the ReVITALization of Project 1.
- Expanded the core web-enabled database system to incorporate retrospective tissue data.
- Developed an interactive index and model for multiple drug interaction assessment.

Core C: Pathology and Specimen Procurement Core

- Created a centralized immunohistochemistry (IHC) laboratory with manual and automated IHC techniques and *in situ* tissue-based methodologies.
- Developed a repository of archival samples from 3-D HBEC cultures for future use.
- Supported the various VITAL projects by processing tissue and culture samples, and providing pathological and histological characterization of those specimens, and maintaining samples repositories.

Developmental Research Project (DRP) 2: Biomarkers for Aggressive Lung Carcinomas in African American Men

- Determined that the ratio of β -tubulin classes II/V mRNA was significantly higher in NSCLCs compared to normal and correlated with level of differentiation.
- Determined that ratio of MAP4 to stathmin mRNA was also found to be higher in tumor than normal lung tissue.

REPORTABLE OUTCOMES

Publications:

Articles (attached in Appendix 2)

1. Chen S, Liu XG, Yue P, Schonthal AH, Khuri FR, Sun S-Y. CCAAT/enhancer binding protein homologous protein-dependent death receptor 5 induction and ubiquitin/proteasome-mediated cellular FLICE-inhibitory protein downregulation contribute to enhancement of tumor necrosis factor-related apoptosis-inducing ligand-induced apoptosis by dimethyl-celecoxib in human non small-cell lung cancer cells. *Mol Pharmacol* 72:1269-79, 2007.
2. Elrod HA, Lin Y-D, Yue P, Wang X, Lonail S, Khuri FR, Sun S-Y. The alkylphospholipid perifosine induces apoptosis of human lung cancer cells requiring inhibition of Akt and activation of the extrinsic apoptotic pathway. *Mol Cancer Ther* 6:2029-38, 2007.
3. Elrod HA, Sun S-Y. Modulation of death receptors by cancer therapeutic agents. *Cancer Biol Ther* 7(2), 2007. [Epub ahead of print].
4. Lee JJ, Kong M, Ayers GD, Lotan R. Interaction index and different methods for determining drug interaction in combination therapy. *J Biopharm Statistics* 17:461-80, 2007.
5. Liu XG, Yue P, Chen S, Hu L, Lonail S, Fadlo FR, Sun S-Y. The proteasome inhibitor PS-341 upregulates death receptor 5 expression leading to induction of apoptosis and enhancement of TRAIL-induced apoptosis despite upregulation of c-FLIP and survivin in human lung cancer cells. *Cancer Res* 67:4981-8, 2007.

6. Morgillo F, Kim W-Y, Kim ES, Ciardiello F, Hong WK, Lee HY. Implication of the insulin-like growth factor-IR pathway in the resistance of non-small cell lung cancer cells to treatment with gefitinib. *Cancer Research and Clinical Cancer Research* 13(9):2795-2803, 2007.
7. Qiu Y, Liu X, Yue P, Lonial S, Khuri FR, Sun S-Y. The farnesyltransferase inhibitor R115777 upregulates DR5 expression and enhances TRAIL-induced apoptosis in human lung cancer cells. *Cancer Res* 67:4973-80, 2007.
8. Sun S-Y, Liu X, Yue P, Zhou Z, Zou W, Marcus AI, Khuri FR. The farnesyltransferase inhibitor lonafarnib induces CCAAT/enhancer-binding protein homologous protein-dependent expression of death receptor 5, leading to induction of apoptosis in human cancer cells. *J Biol Chem* 282:18800-9, 2007.
9. Weerasinghe P, Garcia GE, Zhu Q, Yuan P, Feng L, Mao L, Jing N. Inhibition of Stat3 activation and tumor growth suppression of non-small cell lung cancer by G-quartet oligonucleotides. *Int J Oncol* 31(1):129-36, 2007.
10. Weir BA, Woo MS, Getz G, Perner S, Ding L, Beroukhi R, et al. Characterizing the cancer genome in lung adenocarcinoma. *Nature* 450(7171):893-8, 2007.
11. Wistuba I. Genetics of Preneoplasia: Lessons from Lung Cancer. Genetics of preneoplasia: lessons from lung cancer. *Curr Mol Med* 7(1):3-14, 2007.
12. Zou W, Chen S, Liu XG, Yue P, Sporn MB, Khuri FR, Sun S-Y. c-FLIP downregulation contributes to induction of apoptosis and enhancement of TRAIL-induced apoptosis by the novel synthetic triterpenoid methyl-2-cyano-3, 12-dioxooleana-1, 9-dien-28-oate (CDDO-Me) in human lung cancer cells. *Cancer Biol Ther* 6(10), 2007. [Epub ahead of print].
13. Zou W, Liu X, Yue P, Khuri FR, Sun SY. PPAR γ ligands enhance TRAIL-induced apoptosis through DR5 upregulation and c-FLIP downregulation in human lung cancer cells. *Cancer Biol Ther* 6:99-106, 2007.

Manuscripts submitted, in revision, or in review

1. Aggarwal S, Kim SW, Ryu SH, Chung WC, Koo JS. Suppression of the Growth and Survival of Non-Small Cell Lung Cancer Cells by Targeting CREB Signaling Pathway. *Cancer Research* (In Press).
2. Chen S, Raja SM, Yue P, Peterson YK, Khuri FR, Sun SY. Inhibition of geranylgeranyltransferase I downregulates c-FLIP levels, induces DR5 expression, and augments Tumor necrosis factor-related apoptosis-inducing ligand-induced apoptosis. *J Biol Chem* (Submitted).
3. Cucchiarelli V, Hiser L, Smith H, Frankfurter A, Spano A, Correia JJ, Lobert S. b-Tubulin isotype classes II and V expression patterns in nonsmall cell lung carcinomas. *Tumor Biology* (Submitted).
4. Elrod HA, Yue P, Khuri FR, Sun S-Y. Activation of cyclooxygenase-2 mediates growth arrest and apoptosis induced by perifosine in human lung cancer cells. In preparation.
5. Jin Q, Menter DG, Mao L, Hong WK, Lee HY. Survivin expression in normal human bronchial epithelial cells: an early and critical step in tumorigenesis induced by tobacco exposure. *Carcinogenesis* (In Press).
6. Kong M, Lee JJ. A semiparametric response surface model for assessing drug interaction. *Biometrics* (In Press).
7. Kwei KA, Kim YH, Girard L, et al. Genomic profiling identifies TITF1 as a lineage-specific oncogene amplified in lung cancer. *Oncogene* (In Press).
8. Lee JJ, Kong M. Confidence Interval of Interaction Index for Assessing Multiple Drug Interaction. *Statistics in Biopharmaceutical Research* (In Press).
9. Lin YD, Chen S, Yue P, Zou W, Bendrook DM, Liu S, Le TC, Berlin KD, Khuri FR, Sun SY. CHOP-dependent death receptor 5 induction is a major component of SHetA2-induced apoptosis in lung cancer cells. *Cancer Res* (Submitted).
10. Lockwood WW, Chari R, Coe BP, et al. DNA Amplification is a Ubiquitous Mechanism of Oncogene Activation in Lung and Other Cancers. (Submitted).

11. Prudkin L, Behrens C, Liu DD, Zhou X, Ozburn N, Bekele BN, et al. Loss and reduction of Fus1 protein expression is a frequent phenomenon in the pathogenesis of lung cancer. *Clin Cancer Res* (In Press).
12. Raja SM, Chen S, Yue P, Acker TM, Lefkove B, Arbiser J, Khuri FR, Sun SY. The Natural product honokiol preferentially inhibits c-FLIP and augments death receptor-induced apoptosis. *Mol Cancer Ther* (Submitted).
13. Seo HS, Liu DD, Bekele BN, Kim MK, Pisters K, Lippman SM, Wistuba II, Koo JS. CREB Overexpression: A Feature Associated with Negative Prognosis in Never-Smokers with NSCLC. *Cancer Research* (In Review).
14. Sun HX, Chung WC, Ryu SH, Ju Z, Kim E, Kurie JM, and Koo JS. CREB Regulation of CXCL Chemokine Gene Expression in Lung Carcinogenesis. *Cancer Research* (In Review).

Abstracts (attached in Appendix 2)

1. Lacroix L, Tahara E, Behrens C, Kadara H, Lotan D, Wistuba II, Lotan R. Identification of biomarkers for human lung carcinogenesis by analysis of transcriptomes of cell lines representing different stages of lung carcinogenesis. American Association for Cancer Research Annual Meeting 2007, Los Angeles, California, April 2007, Abstract # 2956.
2. Tang X, Ozburn N, Hong WK, Wistuba II. Caveolin-1 gene methylation as a field effect phenomenon in lung cancer patients. AACR Annual Meeting 2007, Los Angeles, California, April 2007.

Abstracts submitted

1. Li X, Tang X, Behrens C, Dong W, Ozburn N, Woods DM, Yin G, Hong WK, Moran C, Wistuba I. STAT1 is Expressed in Non-Small Cell Lung Carcinoma., AACR Annual Meeting 2008, submitted.
2. Raso MG, Behrens C, Liu S, Prudkin L, Woods DM, Ozburn N, Moran C, Lee JJ, Wistuba I. Immunohistochemical Expression of Estrogen and Progesterone Receptors Identifies a Subset of Non-small Cell Lung Cancers and Correlates with *EGFR* Mutations . AACR Annual Meeting 2008, submitted.
3. Saintigny P, Ren H, Zhou X, Mao L. microRNA (miRNA) species differentially expressed between immortalized normal bronchial epithelial cells and non-small cell lung cancer (NSCLC) cells. AACR Annual Meeting 2008, submitted.
4. Tang X, Sun M, Behrens C, Prudkin L, Ozburn N, Gazdar AF, Moran C, Varella-Garcia M, Wistuba II. *TTF-1* Gene Amplification and Protein Expression Pattern Identify Adenocarcinoma of Lung with Worse Prognosis. AACR Annual Meeting 2008, submitted.

Resources:

- 1) Based on our findings in human lung cancer cells, we have successfully applied similar concepts in receiving the recently funded head and neck cancer SPORE (project 2; SY Sun and FR Khuri as Project Co-Leaders), which focuses on investigating the role of dysregulation of the death receptor-apoptotic pathway in the metastasis of head and neck cancer and targeting this pathway for treatment of head and neck cancer. (Project 4, Drs. Sun and Khuri)
- 2) Establishment of multiple NSCLC cell lines that stably express c-FLIP (FLIP_L and FLIP_S, respectively). (Project 4, Drs. Sun and Khuri)

CONCLUSIONS

Project 1: The completion of the Vanguard trials is important to this grant. However, the ultimate goal is the development of a risk model for development of SPT and recurrence. This model will be developed utilizing the resources from both Vanguard and our exhaustive Lung Cancer Tissue Bank. This is a top priority for our program.

Project 2: We have developed new methods to study the differentiation of human bronchial epithelial cells with and without oncogenic changes *in vitro* including the study of branching morphogenesis, SAC formation, and the expression of lung specific proteins. We have found that oncogenically manipulated HBECs are capable of forming tumors of several histologies. We have defined a new series of amplified genes in lung cancer pathogenesis and especially highlighted the key role of TITF1 expression in the pathogenesis of lung cancer. Our results indicate that the use of the *in vitro* human lung carcinogenesis model for oligonucleotide microarray hybridization provides a powerful approach to identify molecules that may be involved in early or late events in human lung carcinogenesis. In addition, we have been successful in identifying potentially important players in tumor initiation and progression using miRNA arrays.

Future investigations are expected to allow us to identify valuable biomarkers, such as MCM2 that will be validated in large collection of lung cancers and lung premalignancies and to determine the biological role of the identified mRNAs in lung cancer tumorigenesis. These systems and genes will be tested for their expression and alteration in preneoplastic samples from VITAL obtained biospecimens in other portions of this grant. We are specifically trying to overexpress TITF1 in HBECs to see if it can drive these cells towards malignancy.

Project 3: We conclude that CREB may play an important role in driving tumorigenesis of lung cancer by modulating the proangiogenic chemokines of premalignant and malignant cells in response to the proinflammatory cytokine IL-1 β .

We have continued to develop new strains of bronchial epithelial cells from individuals participating in our lung chemoprevention and long-term follow up trials. We have continued to develop and characterize the growth and competitive capabilities of bronchial epithelial cells with regard to their preferential ability to take over the growth surface from other bronchial epithelial cells. Moreover, we have initiated studies to better understand the molecular mechanisms underlying the preferential takeover advantage of one cell strain over another. We have also improved our ability to monitor and quantify the growth interactions between cell populations using digital imaging and live cell microscopy.

In the coming year, we will complete the analysis of microarray data and identify/characterize differentially expressed genes in premalignant bronchial epithelial cells. As we obtain bronchial epithelial cells derived from subjects showing abnormal autofluorescence patterns in their bronchial lining, we will inoculate these cells into the organotypic cultures and examine their degree of ongoing genetic instability and preferential clonal outgrowth. We will also examine the effect of chemopreventive agents on preferential clonal outgrowth and genetic instability.

Project 4: Appropriate modulation of the extrinsic death receptor-mediated apoptotic pathway such as upregulation of DR5 and or reduction of c-FLIP levels by small molecules (e.g., celecoxib, lonafarnib, bortezomib) may eliminate premalignant or malignant lung epithelial cells via promoting apoptotic cell death to achieve cancer chemopreventive and therapeutic goals.

Moreover, the potential of the modulation of DR5 and c-FLIP as predictive biomarkers for certain drugs in the clinic warrants further investigation.

Project 5: 1) Suppression of the IGF-1R signaling pathways may prevent or delay development of resistance to gefitinib in NSCLC cells. 2) Blockade of the IGF-1R/PI3K/Akt pathway effectively inhibits the tobacco-induced malignant transformation of HBE cells.

Core B: The Biostatistics and Data Management Core continues to provide active biostatistical support for the ReVITALization of Project 1 and all other VITAL projects. The Core will continue to enhance the web-enabled database system to include both prospective and retrospective sample data, as well as new biomarkers and targeting strategies. The development of a predictive risk model is the ultimate goal of this core in conjunction with other VITAL projects.

Core C: We have acquired and banked 740 specimens from bronchoscopies and resected specimens from lung cancer and head/neck tumor patients and used the web-enabled database developed by the Biostatistics Core to track and inventory bronchoscopy specimens and report histopathological features of 401 bronchial mucosa tissue specimens. We have selected, prepared and examined by immunohistochemistry a number of molecular markers in a large series (N=504) of respiratory epithelium specimens which have been used to examine several IHC markers related to VITAL-related projects. We will continue to select and process retrospective tissue samples for the ReVITALization Project 1 as well as consult with the Biostatistics Core in enhancing the database to include these samples. Support for all VITAL projects will continue with regard to histology, pathology, and cytology assessments, specimen procurement and processing, and biomarker analysis.

DRP2: Ratios of β -tubulin classes II/V and of MAP4/stathmin mRNA were found to correlate with the level of differentiation in lung tissue. These changes are likely due to dysregulation of microtubule dynamics in the disease state, essential for cell division and proliferation, but these mechanisms need to be further explored.

References

Arriagada R, Bergman B, Dunant A, et al: Cisplatin-based adjuvant chemotherapy in patients with completely resected non-small-cell lung cancer. *N Engl J Med* 350(4):351-60, 2004.

Chen HY, Yu SL, Chen CH, et al: A five-gene signature and clinical outcome in non-small-cell lung cancer. *N Engl J Med* 356(1):11-20, 2007.

Douillard J, Rosell R, Delena M, et al: ANITA: Phase III adjuvant vinorelbine (N) and cisplatin (P) versus observation (OBS) in completely resected (stage I-III) non-small-cell lung cancer (NSCLC) patients (pts): Final results after 70-month median follow-up. On behalf of the Adjuvant Navelbine International Trialist Association. *Journal of Clinical Oncology*, 2005 ASCO Annual Meeting Proceedings. Vol 23, No. 16S, Part I of II (June 1 Supplement), 2005: 7013.

Eberhard DA, Johnson BE, Amler LC, et al. Mutations in the epidermal growth factor receptor and in KRAS are predictive and prognostic indicators in patients with non-small-cell lung cancer treated with chemotherapy alone and in combination with erlotinib. *J Clin Oncol* 23:5900-5309, 2005.

Hopkins-Donaldson S, Ziegler A, Kurtz S, Bigosch C, Kandioler D, Ludwig C, Zangemeister-Wittke U, Stahel R. Silencing of death receptor and caspase-8 expression in small cell lung carcinoma cell lines and tumors by DNA methylation. *Cell Death Differ* 10:356-64, 2003.

Howell A, Cuzick J, Baum M, et al: Results of the ATAC (Arimidex, Tamoxifen, Alone or in Combination) trial after completion of 5 years' adjuvant treatment for breast cancer. *Lancet* 365(9453):60-2, 2005.

Jemal A, Siegel R, Ward E, Murray T, Xu J, Thun MJ. Cancer statistics, 2007. *CA: a cancer journal for clinicians* 57(1):43-66. 2007.

Hittelman, W. N., Liu, D. D., Kurie, J. M., Lotan, R., Lee, J. S., Khuri, F., Ibarguen, H., Morice, R. C., Walsh, G., Roth, J. A., Minna, J., Ro, J. Y., Broxson, A., Hong, W. K., and Lee, J. J. Proliferative changes in the bronchial epithelium of former smokers treated with retinoids. *J Natl Cancer Inst* 99:1603-1612, 2007.

Kato H, Ichinose Y, Ohta M, et al: A randomized trial of adjuvant chemotherapy with uracil-tegafur for adenocarcinoma of the lung. *N Engl J Med* 350(17):1713-21, 2004.

Klein-Szanto AJ, Iizasa T, Momiki S, Garcia-Palazzo I, Caamano J, Metcalf R, Welsh J, Harris CC. A tobacco specific N-nitrosamine or cigarette smoke condensate causes neoplastic transformation of xenotransplanted human bronchial epithelial cells. *Proc Natl Acad Sci USA* 89:6693-7, 1992.

Lee JY, Kim JH, Lee YH, et al. Correlation between K-ras gene mutation and prognosis of patients with nonsmall cell lung carcinoma. *Cancer* 79:462-467, 1997.

Livet J, Weissman TA, Kang H, Draft RW, Lu J, Bennis RA, Sanes JR, Lichtman JW. Transgenic strategies for combinatorial expression of fluorescent proteins in the nervous system. *Nature* 450:56-62, 2007.

Lynch TJ, Bell DW, Sordella R, et al. Activating mutations in the epidermal growth factor receptor underlying responsiveness of non-small-cell lung cancer to gefitinib. *N Engl J Med* 350:2129-2139, 2004.

Mao L. Recent advances in the molecular diagnosis of lung cancer. *Oncogene* 21:6960-9, 2002.

Meyerson M, Franklin WA, Kelley MJ. Molecular classification and molecular genetics of human lung cancers. *Semin Oncol* 31(1 Suppl 1):4-19, 2004.

Olaussen KA, Dunant A, Fouret P, et al: DNA repair by ERCC1 in non-small-cell lung cancer and cisplatin-based adjuvant chemotherapy. *N Engl J Med* 355(10):983-91, 2006.

Paez JG, Janne PA, Lee JC, et al. EGFR mutations in lung cancer: correlation with clinical response to gefitinib therapy. *Science* 304:1497-1500, 2004.

Pao W, Miller V, Zakowski M, et al. EGF receptor gene mutations are common in lung cancers from “never smokers” and are associated with sensitivity of tumors to gefitinib and erlotinib. *Proc Natl Acad Sci U S A* 101:13306-13311, 2004.

Pegram MD, Lipton A, Hayes DF, et al: Phase II study of receptor-enhanced chemosensitivity using recombinant humanized anti-p185HER2/neu monoclonal antibody plus cisplatin in patients with HER2/neu-overexpressing metastatic breast cancer refractory to chemotherapy treatment. *J Clin Oncol* 16(8):2659-71, 1998.

Potti A, Mukherjee S, Petersen R, et al: A genomic strategy to refine prognosis in early-stage non-small-cell lung cancer. *N Engl J Med* 355(6):570-80, 2006.

Reddel RR, Ke Y, Gerwin BI, McMenamin MG, Lechner JF, Su RT, Brash DE, Park JB, Rhim JS, Harris CC. Transformation of human bronchial epithelial cells by infection with SV40 or adenovirus-12 SV40 hybrid virus, or transfection via strontium phosphate coprecipitation with a plasmid containing SV40 early region genes. *Cancer Res* 48:1904-9, 1988.

Sandler A, Gray R, Perry MC, et al: Paclitaxel-carboplatin alone or with bevacizumab for non-small-cell lung cancer. *N Engl J Med* 355(24):2542-50, 2006.

Sato M, Shames DS, Gazdar AF, Minna JD. A translational view of the molecular pathogenesis of lung cancer. *J Thorac Oncol* 2(4):327-43, 2007.

Shepherd FA, Rodrigues Pereira J, Ciuleanu T, et al: Erlotinib in previously treated non-small-cell lung cancer. *N Engl J Med* 353(2):123-32, 2005.

Shivapurkar N, Toyooka S, Eby MT, Huang CX, Sathyanarayana UG, Cunningham HT, Reddy JL, Brambilla E, Takahashi T, Minna JD, Chaudhary PM, Gazdar AF. Differential inactivation of caspase-8 in lung cancers. *Cancer Biol Ther* 1:65-9, 2002.

Sledge GW Jr. HRe-2 stay: the continuing importance of translational research in breast cancer. *J Natl Cancer Inst* 96(10):725-7, 2006.

Strauss GM, Herndon J, Maddaus MA, et al: Randomized clinical trial of adjuvant chemotherapy with paclitaxel and carboplatin following resection in Stage IB non-small cell lung cancer

(NSCLC): Report of Cancer and Leukemia Group B (CALGB) Protocol 9633. PASCO 2004 Abstract 7019.

Strauss GM, Herndon JE, Maddaus MA, et al: Adjuvant chemotherapy in stage IB non-small cell lung cancer (NSCLC): Update of Cancer and Leukemia Group B (CALGB) protocol 9633. *Journal of Clinical Oncology*, 2006 ASCO Annual Meeting Proceedings Part I. Vol 24, No. 18S (June 20 Supplement), 2006: 7007.

Tsao MS, Sakurada A, Cutz JC, et al: Erlotinib in lung cancer - molecular and clinical predictors of outcome. *N Engl J Med* 353(2):133-44, 2005.

Vaughan MB, Ramirez RD, Wright WE, Minna JD, Shay JW. A three-dimensional model of differentiation of immortalized human bronchial epithelial cells. *Differentiation* 74(4):141-8, 2006.

Winton T, Livingston R, et al. Vinorelbine plus cisplatin vs observation in resected non-small cell lung cancer. National cancer Institute of Canada Clinical Trials Group; National Cancer institute of the United States Intergroup JBR.10 Trial Investigators. *N Engl J Med* 352(25):2589-97, 2005.

Wistuba II, Gazdar A. Lung cancer preneoplasia. *Annu Rev Pathol* 1:331-48, 2006.

APPENDICES

APENDIX 1

Appendix 1 gives the trial summary via event charts and the data management activities for the VITAL study.

(I) Trial Summary by Event Charts:

Event charts provide a graphical summary on the trial conduct at the individual patient level. A calendar event chart shows each event on the calendar date scale while an interval event chart shows the events on the time since registration scale. The reference and the figure legend are given below.

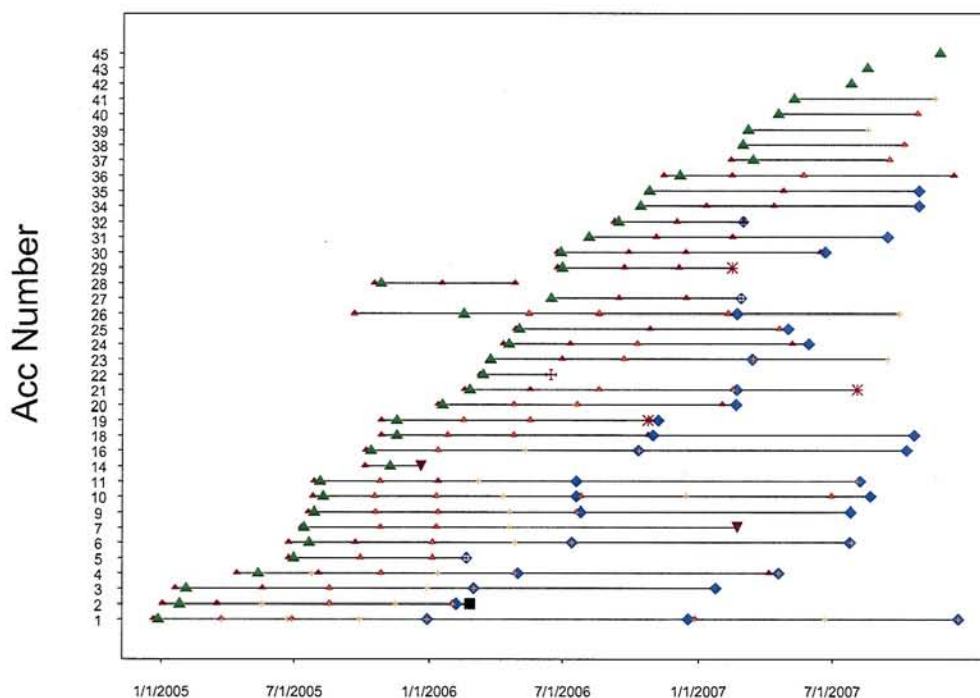
Reference:

Lee JJ, Hess KR, Dubin JA. Extensions and applications of event charts. *American Statistician* 54:63-70, 2000.

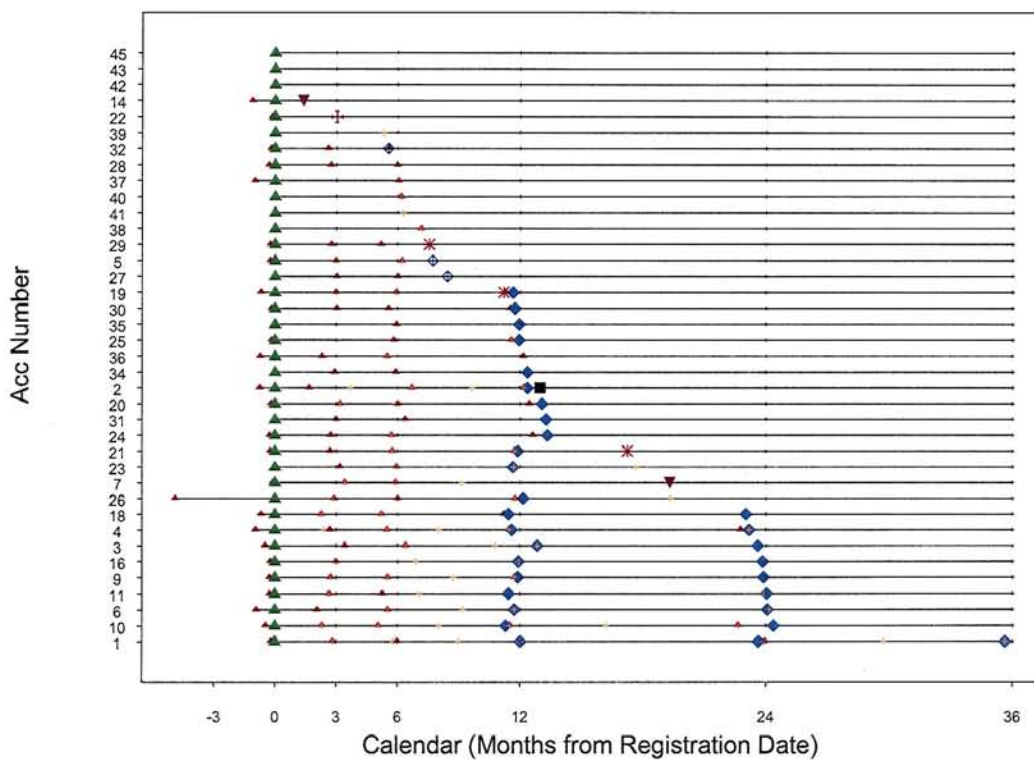
Legend

▲	Registration	⊕	Recurrence Date
▲	Blood Date	⊕	Metastasis Date
◆	Bronchoscopy Date	✱	SPT Date
+	Clinic Visit Date	■	Death Date
		▼	Off Drug/Off Study Date

Calendar Event Chart for VITAL Study

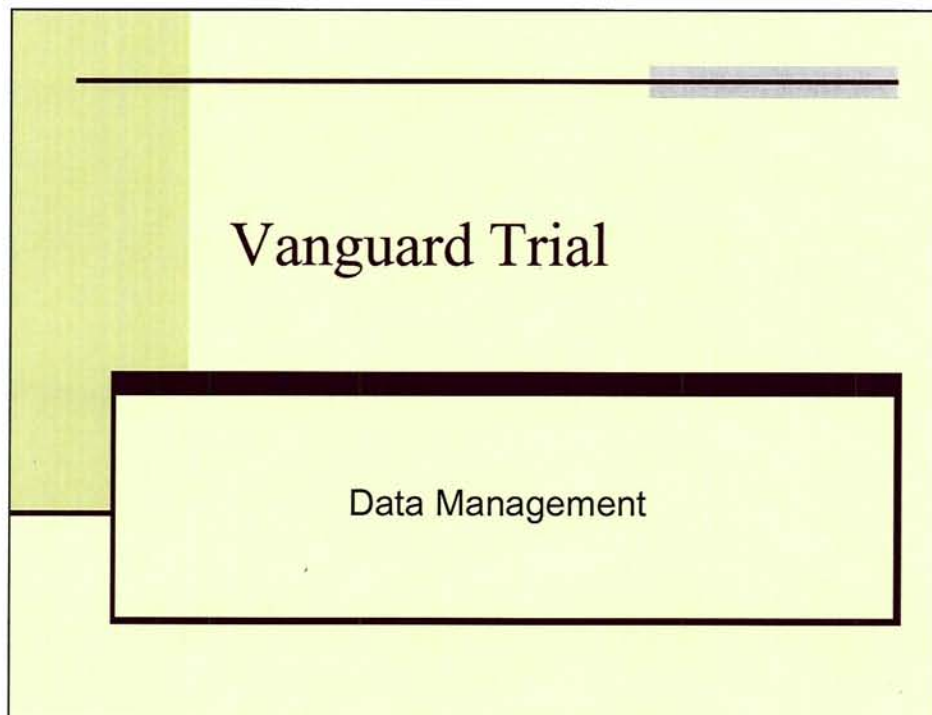


Interval Event Chart for VITAL Study

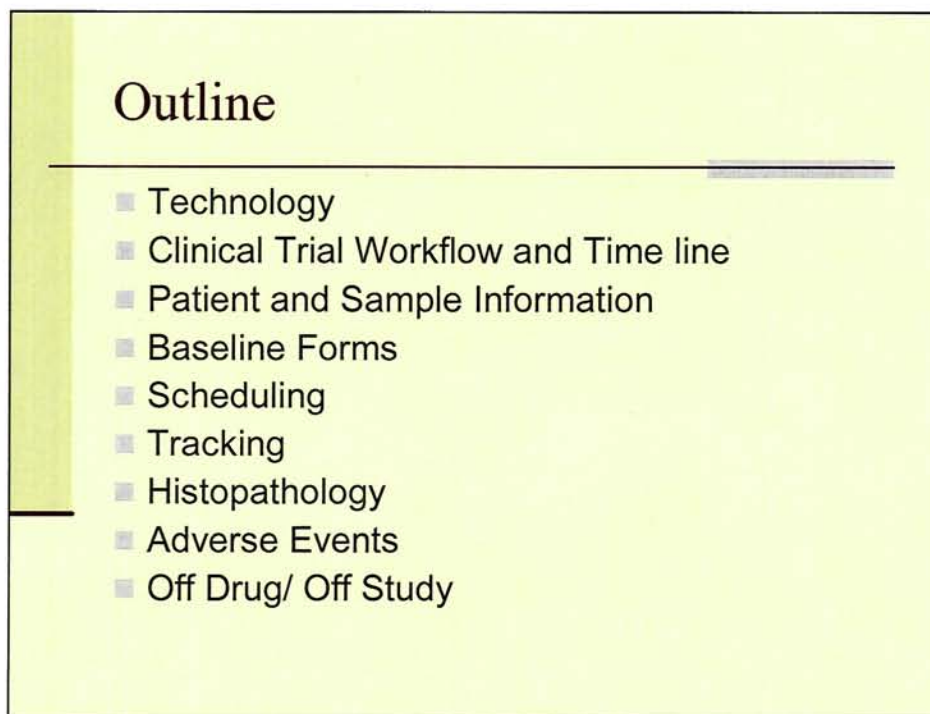


(II) Data Management Activities

Slide 1



Slide 2



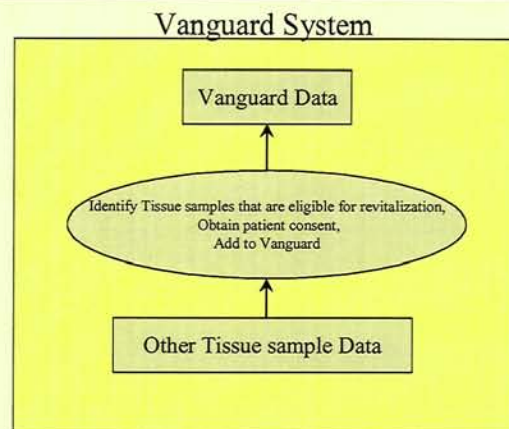
Slide 3

Revitalization

- Additional Data is being captured to support the revitalization effort.
- Previously collected tissue is evaluated for eligibility for the revitalization effort.
- Once eligible, we will be able to quickly include it into Vital.
- [This phase is currently in development]

Slide 4

Revitalization



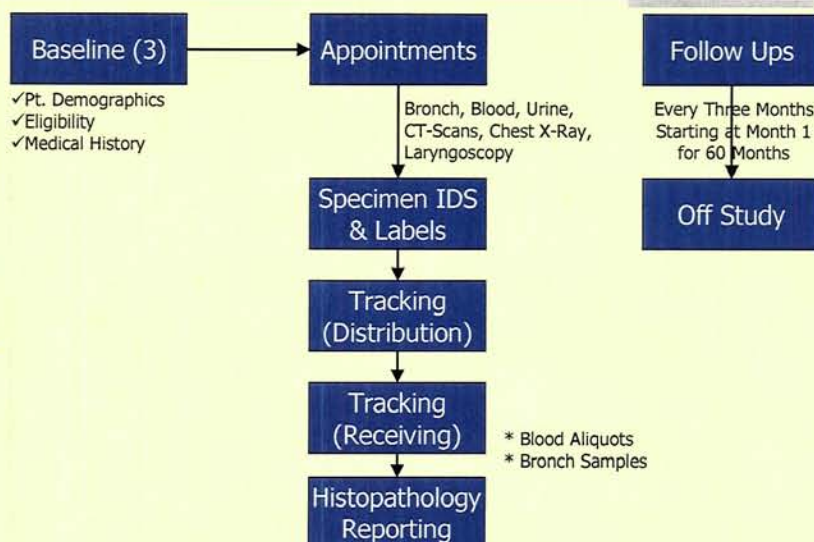
Slide 5

Technology

- ASP.Net (VB.Net)
- Web Based Software (Internet Explorer)
- SQL Server 2000 (SP3a)
- Windows 2003 Server (Operating System)
- SQL Server 2K Reporting Services
- Secure Socket Layer (SSL)

Slide 6

Clinical Trial Workflow



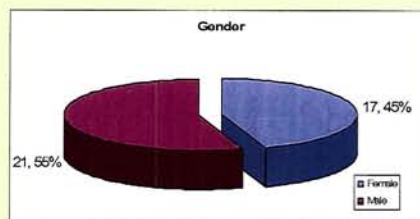
Slide 7

Forms Summary	
Baseline Forms	
A1	
A2	
B1	
Scheduling	
Schedules	
	Bronchoscopy
	Serology
	Chest Xray
	CT Chest
	Laryngoscopy
Tracking	
Specimen Labels	
Tracking	
	Not Yet Delivered
	Delivered, Not Received
	Delivered and Received
	Future Visits
	All of the above
Pathology Processing	
Pathology Processing	
	Pathology Slice/Cut Entry
	Histopathology Report
Other Patient Related Forms	
Monthly Follow Up	
	3 through 60 months
Off Drug / Off Study	
MRN Accession	
Adverse Events	
Reporting	
Reporting	
	Complete Timeline of Events
	Snapshot Summary

Slide 8

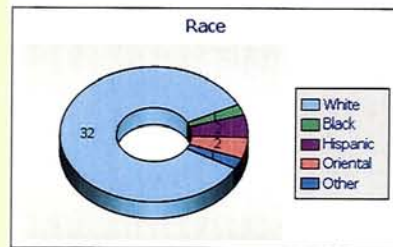
Patient Information

Patients	38
Dropouts	10
Active Patients	28



Slide 9

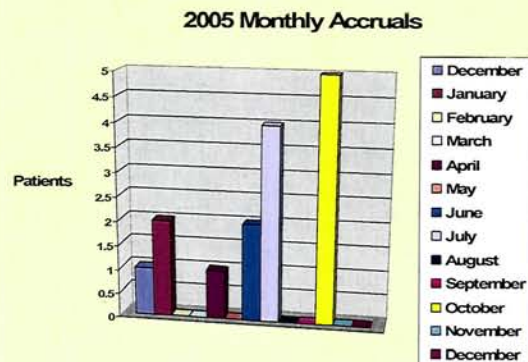
Patient Information



Race	Subtotal	Percentage
White	32	84.2%
Black	1	2.6%
Hispanic	2	5.3%
Oriental	2	5.3%
Other	1	2.6%
Total	38	

Slide 10

Patient Information

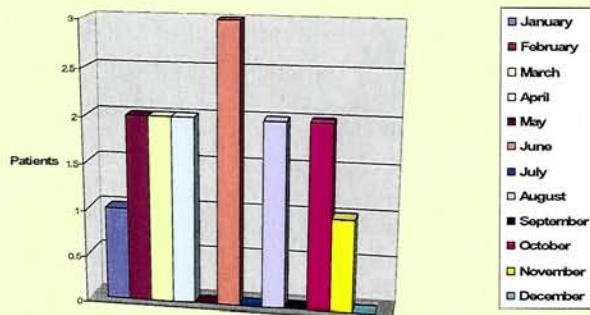


Monthly Accruals		
2004	December	1
2005	January	2
	February	0
	March	0
	April	1
	May	0
	June	2
	July	4
	August	0
	September	0
	October	5
	November	0
	December	0
		15

Slide 11

Patient Information

2006 Monthly Accruals

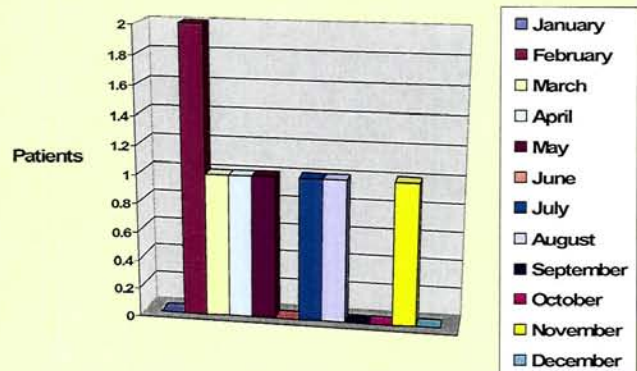


Monthly Accruals		
2006	January	1
	February	2
	March	2
	April	2
	May	0
	June	3
	July	0
	August	2
	September	0
	October	2
	November	1
	December	0
		15

Slide 12

Patient Information

2007 Monthly Accruals

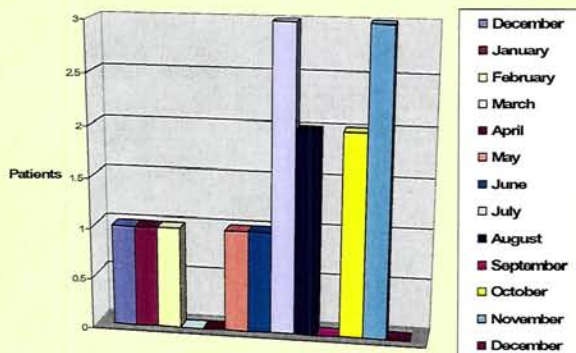


Monthly Accruals		
2007	January	0
	February	2
	March	1
	April	1
	May	1
	June	0
	July	1
	August	1
	September	0
	October	0
	November	1
	December	0
		8

Slide 13

Patient Information

2005 Baseline Bronch Visits

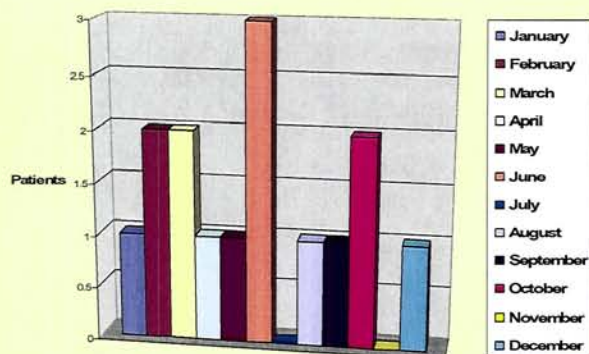


Baseline Bronch Visits		
2004	December	1
2005	January	1
	February	1
	March	0
	April	0
	May	1
	June	1
	July	3
	August	2
	September	0
	October	2
	November	3
	December	0
		15

Slide 14

Patient Information

2006 Baseline Bronch Visits

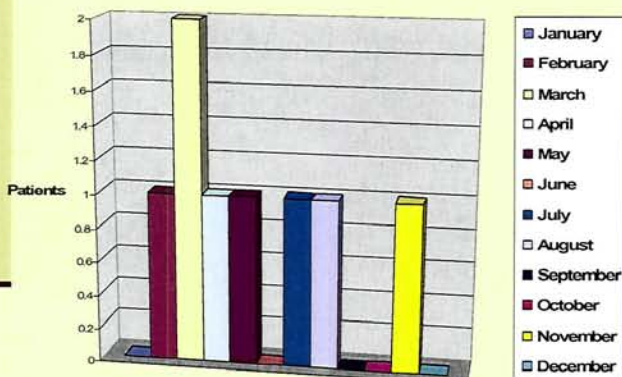


Baseline Bronch Visits		
2006	January	1
	February	2
	March	2
	April	1
	May	1
	June	3
	July	0
	August	1
	September	1
	October	2
	November	0
	December	1
		15

Slide 15

Patient Information

2007 Baseline Bronch Visits

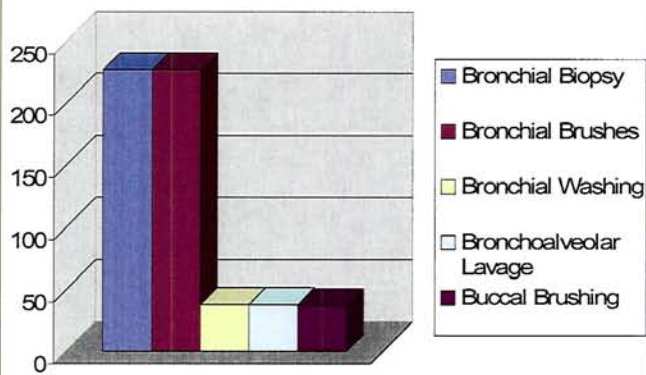


Baseline Bronch Visits		
2007	January	0
	February	1
	March	2
	April	1
	May	1
	June	0
	July	1
	August	1
	September	0
	October	0
	November	1
	December	0
		8

Slide 16

Sample Information

Baseline Bronchoscopy Samples Collected

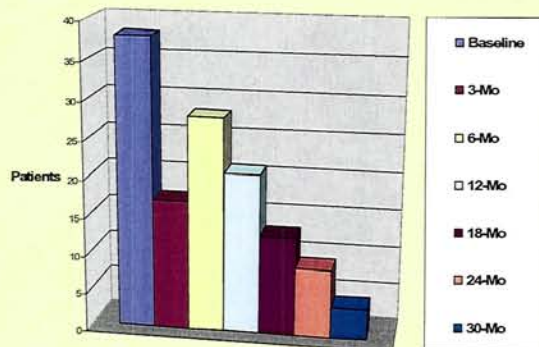


	Count
Bronchial Biopsy	227
Bronchial Brushes	227
Bronchial Washing	38
Bronchoalveolar Lavage	38
Buccal Brushing	37
Total	567

Slide 17

Sample Information

Blood Samples by Visits

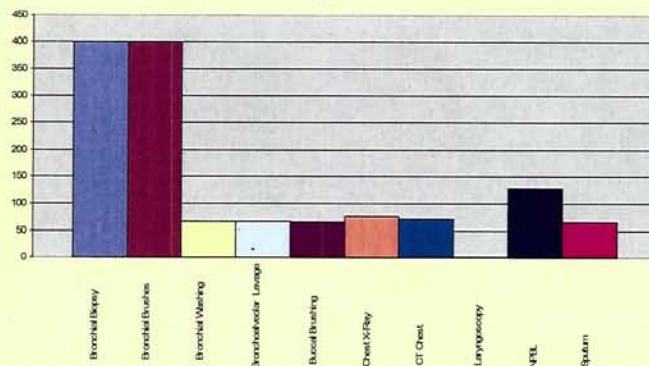


Blood Samples by Visits	
Baseline	38
3-Mo	17
6-Mo	28
12-Mo	21
18-Mo	13
24-Mo	9
30-Mo	4
	130

Slide 18

Sample Information

Samples Collected



Blood Samples by Visits	
Bronchial Biopsy	401
Bronchial Brushes	401
Bronchial Washing	67
Bronchoalveolar Lavage	67
Buccal Brushing	66
Chest X-Ray	76
CT Chest	72
Laryngoscopy	1
NPBL	130
Sputum	66
	1347

Slide 19

Complete Timeline of Events

MD Anderson Cancer
Vanguard: Complete Time Line of Events

Site #	Initial Visit Date	Date informed consent	Blood					Bronchoscopy				Monthly Follow Ups				Off Study
			Baseline	Month 3	Month 6	Month 12	Month 24	Month 36	Registration/Baseline	Month 12	Month 24	Month 36	Month 3	Month 6	Month 9	
19	10/27/2005	10/27/2005	10/27/2005						11/17/2005							
18	10/19/2005	10/19/2005	10/27/2005						11/17/2005							
17	10/13/2005	10/13/2005	10/13/2005													
16	10/06/2005	10/06/2005	10/06/2005	01/12/2006					10/13/2005							
15	10/06/2005	10/06/2005	10/06/2005													
14	10/05/2005	10/05/2005	10/05/2005						11/08/2005							
13	09/20/2005	09/20/2005	09/20/2005						09/26/2005							
12	08/03/2005	08/03/2005	08/03/2005													
11	07/28/2005	07/28/2005	07/28/2005	10/25/2005					08/05/2005				10/25/2005			08/08/2005
10	07/26/2005	07/26/2005	07/26/2005	10/18/2005					08/06/2005				10/18/2005			
9	07/26/2005	07/26/2005	07/26/2005	10/19/2005					07/26/2005				10/19/2005			
8	07/12/2005	07/12/2005	07/12/2005						07/26/2005							07/14/2005
7	07/11/2005	07/11/2005	07/11/2005	10/26/2005					07/14/2005				10/26/2005			
6	06/23/2005	06/23/2005	06/23/2005						07/21/2005							
5	06/23/2005	06/23/2005	06/23/2005	08/28/2005					06/06/2005				08/28/2005			
4	04/27/2005	04/27/2005	04/27/2005	08/03/2005	10/27/2005				05/13/2005				07/25/2005	10/27/2005		
3	01/25/2005	01/25/2005	01/25/2005	05/19/2005	08/18/2005				02/04/2005				05/18/2005	08/18/2005		
2	01/23/2005	01/23/2005	01/23/2005	03/19/2005	08/19/2005				01/26/2005				05/18/2005	08/18/2005		
1	12/16/2004	12/16/2004	12/22/2004	03/24/2005	06/28/2005	12/27/2005			12/28/2004	12/29/2005			02/04/2005			

Slide 20

Baseline Forms A1, A2, and B1

- Collect Patient Information
- Eligibility Criteria
- Medical History (Medications, allergies, etc)
- ETOH & Smoking Status

Slide 21

MRN, Accession

MDAH, Accession #, Randomization And C1D1 Date (Mdah,Acc,C1D1,Ran Page)			
A-C	D-F	G-I	J-L
M-O	P-R	S-U	V-X
Y-Z			
Edit	Participant	MDAH	Acc. #
+	Doe, John	12345	9
/	Doe, Lenny	23456	10
/	Doe, Kim	34567	7

Slide 22

Baseline Forms – A1

Admin Projects Histo-Pathology Lab Logout

Select a participant Status: In-Entry

*1. Patient Information: A1 (Screening A1)

Last Middle First Screening Date DOB Age (Must be 18-74 years)

Address City State Zip Code Home (Work) (Cellular)

2. How Did You Hear About The Study?

*3. Smoking History

*3.1 Are you currently smoking? Yes No

*If no, date quit smoking Age Quit Smoking N/A

*3.2 Age started smoking regularly Overall Smoking Years

*3.3 Average number of cigarettes smoked per day Actual Smoking Years

*3.4 If there was a quit-smoking period, total time during the smoking years. yrs. mos. Pack Years

4. Further Contact

4.1 Is the participant interested in the study? Yes No

4.2 If no, specify the reason

4.3 Is the patient interested in future studies? Yes No

General Comments

Slide 23

Baseline Form – A2 (Part 1 of 3)

Admin Projects Histo-Pathology Lab Logout

Select a participant Status: Ready

***1. Medical History A2**

***1.1 Gastrointestinal problems?** Yes (specify below) No

***1.1.1 Ulcers requiring medical treatment with H2 blockers** Yes No
(essential if 1.1 answered "Yes")

Other:

***1.2 Respiratory problems?** Yes (specify below) No

☐ Chronic obstructive pulmonary disease (COPD) ☐ History of pulmonary emphysema

☐ Asthma (current or within previous 5 years)

Other:

***1.3 Cardiovascular problems?** Yes (specify below) No

☐ Myocardial infarction (heart attack) ☐ Angina

☐ Chronic heart failure ☐ Congestive heart failure

☐ Coronary artery disease ☐ Coronary artery surgery

☐ Stroke ☐ Ischemic stroke: Attack (TIA)

☐ Deep vein thrombosis (DVT)

Other:

Slide 24

Baseline Form – A2 (Part 2 of 3)

***1.4 Clotting problems?** Yes (specify below) No

☐ Family history of previous stroke or clots ☐ Known factor of bleeding (aspirin)

☐ Currently taking blood thinners (e.g., warfarin)

Other:

***1.5 History of diabetes?** Yes No

***1.6 History of Systemic Lupus Erythematosus?** Yes No

***1.7 Family history of premature coronary artery disease defined as:** Yes (specify below) No

☐ Father with MI prior to age 55 ☐ Mother with MI prior to age 65

1.8 Other Medical Problems

***2. Allergies**

Allergies:

***3. Steroids, NSAIDs, And H2 Blockers**

***3.1 Are you taking any steroids?** Yes No

If yes, describe the name and dose below.

Steroid's Name Dose

***3.2 Are you taking any NSAIDs?** Yes No

If yes, describe the name and dose below.

NSAID's Name Dose

***3.3 Are you taking any H2 blockers?** Yes No

If yes, describe the name and dose below.

H2 Blocker's Name Dose

Slide 25

Baseline Form – A2 (Part 3 of 3)

*4. Surgeries / Hospitalization					
Date	Surgery / Hospitalization Type				
*4.1 Has the patient had a surgery within the past four(4) weeks? Yes No					
*5. Cancer History					
*5.1 Any previous Cancer? Yes No					
If yes, please complete the table below for all cancers.					
Cancer Type	Stage	Treatment	Diagnosis Date	Last Treatment Date	Smoking Related?
*5.2 Is patient free of cancer for at least six (6) months? Yes No					
*6. Eligibility					
*6.1 Is the participant eligible? Yes No					

Slide 26

Baseline Form – B1

1. Patient Information For The Initial Visit (Baseline B1 Page)				
Visit Date	Gender	Height	cm.	Performance Status
MDAH	Race	Weight	kg.	
*2. Medication				
3. Family History Of Cancer Information				
*4. Alcohol Status (ETOH)				
4.1 Have you ever consumed alcohol? Yes No (* if not, skip section)				
4.2 Age started consuming alcohol?				
4.3. Are you currently consuming alcohol regularly? Yes No				
If not, date quit drinking				
Age stopped drinking				
Years drinking				
4.4 Amount				
Beer (12 oz)	cans	None	Daily	Weekly
Wine (4 oz)	glasses	None	Daily	Weekly
Straight Liquor	shots	None	Daily	Weekly
Mixed Drinks (8 oz)	glasses	None	Daily	Weekly
5. Patient Consents				
Date "Informed Consent" Signed				
Optional Procedures Consented? Yes No				
Optional EPI questionnaire consented? Yes No				
EPI questionnaire given? Yes No				

Slide 27

Scheduling

- Database Driven:
 - Visit Types (Bronchoscope)
 - Sample Types (Biopsy)
 - Collection Time Points (Baseline, 1-Month)
 - Scheduler Matrix (Integrates above definitions)
 - Detail (Defines specimen label and collection)
- Specimens' Label Printing

Slide 28

Scheduling Form

Scheduler (Patient Schedules Page)

Select Patient: Doc. ID#

Visit/Time	Baseline	3 Mo	6 Mo	12 Mo	18 Mo	24 Mo	30 Mo	36 Mo
Bronchoscopy	1/25/2005							
Serology	1/3/2005	3/18/2005	6/18/2005					
Chest_XRay	1/3/2005	5/16/2005	8/16/2005					
CT_Chest	1/3/2005							
Laryngoscopy	2/14/2005							

Specimen ID# Generation

Dr. Mao

Bronchial Biopsies

☒ VBRB-05-10004-LB10 ☒ VBRB-05-10004-LBL ☒ VBRB-05-10004-MC ☒ VBRB-05-10004-RB10 ☒ VBRB-05-10004-RML

☒ VBRB-05-10004-RUL

Dr. Wistuba

Bronchial Biopsy

☒ VBY-05-10004-LB10 ☒ VBY-05-10004-LBL ☒ VBY-05-10004-MC ☒ VBY-05-10004-RB10 ☒ VBY-05-10004-RML

☒ VBY-05-10004-RUL

Bronchial Washings

☒ VBRWA-05-10004

Bronchoalveolar Lavage

☒ VBRAL-05-10004-RML

Bronchial Biopsies

☒ VBRB-05-10004-LCX

Resectons

☒ VSPB-05-10004

Slide 29

Specimen Labels

20030424	09/05/2006	20030424	09/05/2006	20030424	09/05/2006	20030424	09/05/2006
FRF	6-Mo	FRF	6-Mo	FRF	6-Mo	FRF	6-Mo
649999	10/06/1949	649999	10/06/1949	649999	10/06/1949	649999	10/06/1949
VBL-06-10996-BM		VBL-06-10996-BM		VBL-06-10996-BM		VBL-06-10996-BM	
20030424	09/05/2006	20030424	09/05/2006				
FRF	6-Mo	FRF	6-Mo				
649999	10/06/1949	649999	10/06/1949				
VBL-06-10996-BM		VBL-06-10996-BM					

Slide 30

Tracking

- Five display modes: All, NYD, NYR, DAR, & Future Visits
- Print Tracking Forms

Slide 31

Tracking Screen (Not Yet Delivered)

Vanguard Tracking System
(Tracking E1 Page)

User: Biostatistics /jewis

Display Mode: Not Yet Delivered
Laboratory: All Laboratories
Date: 11/21/2005

Filter by Year: 2005

Deliver
Collected
Add

Tracking #	Patient	Collection Date	Destination Lab	Visit Type	Delivered Date	Collected		
<input type="checkbox"/>	72 Doe, John	11/8/2005	Dr. Wistuba	Bronchoscopy				
<input type="checkbox"/>	73 Smith, Jane	11/8/2005	Dr. Mao	Bronchoscopy				
<input type="checkbox"/>	81 Doe, John	7/20/2005	Dr. Wistuba	Serology				
<input type="checkbox"/>	82 Smith, Jane	11/17/2005	Dr. Wistuba	Bronchoscopy				
<input type="checkbox"/>	83 Doe, John	11/17/2005	Dr. Mao	Bronchoscopy				
<input type="checkbox"/>	84 Smith, Jane	10/27/2005	Dr. Wistuba	Serology				
<input type="checkbox"/>	85 Doe, John	10/19/2005	Dr. Wistuba	Serology				
<input type="checkbox"/>	86 Smith, Jane	7/28/2005	Dr. Wistuba	Serology				
<input type="checkbox"/>	87 Doe, John	10/27/2005	Dr. Wistuba	Serology				
<input type="checkbox"/>	90 Smith, Jane	10/27/2005	Dr. Wistuba	Serology				
<input type="checkbox"/>	91 Doe, John	10/13/2005	Dr. Wistuba	Serology				
<input type="checkbox"/>	92 Smith, Jane	9/29/2005	Dr. Wistuba	Serology				
<input type="checkbox"/>	93 Doe, John	5/19/2005	Dr. Wistuba	Serology				
<input type="checkbox"/>	94 Smith, Jane	8/18/2005	Dr. Wistuba	Serology				
<input type="checkbox"/>	96 Doe, John	10/26/2005	Dr. Mao	Bronchoscopy				
<input type="checkbox"/>	97 Smith, Jane	11/17/2005	Dr. Wistuba	Bronchoscopy				
<input type="checkbox"/>	98 Doe, John	11/17/2005	Dr. Mao	Bronchoscopy				

Page 1 of 1
Page 1

Slide 32

Histopathology

- Track Biopsies
- Paraffin Embedding Process
- Cutting Process
- Histopathology Reporting

Pathology Processing

Pathologies

Select Patient: **Doe, John**

Pathology No.	Block	Scheduled Date	Time Line	LL	ML CA	UL	Side	Cut	Ship	Report
VBV-05-10070	A	8/9/2005	Baseline	<input type="checkbox"/>	<input type="checkbox"/>	<input type="checkbox"/>	R	<input type="checkbox"/>	<input type="checkbox"/>	<input type="checkbox"/>
VBV-05-10070	B	8/9/2005	Baseline	<input type="checkbox"/>	<input type="checkbox"/>	<input type="checkbox"/>	L	<input type="checkbox"/>	<input type="checkbox"/>	<input type="checkbox"/>

Pathology No: **VBV-05-10070** Block: **A** Total Cuts: **2**

☐ ☐ ☐ ☐ Status: Ready

Cutting Date: **11/21/2005** Number of Cuts:


Cut No.	Bad Cut	H & E	H & E Not Read	Comments	Date Cut
1	<input type="checkbox"/>	<input type="checkbox"/>	<input type="checkbox"/>		8/10/2005
2	<input type="checkbox"/>	<input type="checkbox"/>	<input type="checkbox"/>		8/10/2005

Histopathology Report

Histopathology Reports:: Pathology #:														
Cut #1														
Site	NT	DE	NA	NORM	CCM	BCH	BHG	ISQM	SQM	DYS1	DYS2	DYS3	ASQD	CIS
A1 (RLI)	<input type="checkbox"/>	<input type="checkbox"/>	<input type="checkbox"/>	<input checked="" type="checkbox"/>	<input type="checkbox"/>	<input type="checkbox"/>	<input type="checkbox"/>	<input type="checkbox"/>	<input type="checkbox"/>	<input type="checkbox"/>	<input type="checkbox"/>	<input type="checkbox"/>	<input type="checkbox"/>	<input type="checkbox"/>
A2 (RML)	<input type="checkbox"/>	<input type="checkbox"/>	<input type="checkbox"/>	<input checked="" type="checkbox"/>	<input type="checkbox"/>	<input type="checkbox"/>	<input type="checkbox"/>	<input type="checkbox"/>	<input type="checkbox"/>	<input type="checkbox"/>	<input type="checkbox"/>	<input type="checkbox"/>	<input type="checkbox"/>	<input type="checkbox"/>
A3 (RUL)	<input type="checkbox"/>	<input type="checkbox"/>	<input type="checkbox"/>	<input checked="" type="checkbox"/>	<input type="checkbox"/>	<input type="checkbox"/>	<input type="checkbox"/>	<input type="checkbox"/>	<input type="checkbox"/>	<input type="checkbox"/>	<input type="checkbox"/>	<input type="checkbox"/>	<input type="checkbox"/>	<input type="checkbox"/>
B4 (LLL)	<input type="checkbox"/>	<input type="checkbox"/>	<input type="checkbox"/>	<input type="checkbox"/>	<input checked="" type="checkbox"/>	<input type="checkbox"/>	<input type="checkbox"/>	<input type="checkbox"/>	<input type="checkbox"/>	<input type="checkbox"/>	<input type="checkbox"/>	<input type="checkbox"/>	<input type="checkbox"/>	<input type="checkbox"/>
B5 (LUL)	<input type="checkbox"/>	<input type="checkbox"/>	<input type="checkbox"/>	<input checked="" type="checkbox"/>	<input type="checkbox"/>	<input type="checkbox"/>	<input type="checkbox"/>	<input type="checkbox"/>	<input type="checkbox"/>	<input type="checkbox"/>	<input type="checkbox"/>	<input type="checkbox"/>	<input type="checkbox"/>	<input type="checkbox"/>
B6 (CAR)	<input type="checkbox"/>	<input type="checkbox"/>	<input type="checkbox"/>	<input checked="" type="checkbox"/>	<input checked="" type="checkbox"/>	<input type="checkbox"/>	<input type="checkbox"/>	<input type="checkbox"/>	<input type="checkbox"/>	<input type="checkbox"/>	<input type="checkbox"/>	<input type="checkbox"/>	<input type="checkbox"/>	<input type="checkbox"/>
Cut #2														
Site	NT	DE	NA	NORM	CCM	BCH	BHG	ISQM	SQM	DYS1	DYS2	DYS3	ASQD	CIS
A1 (RLI)	<input type="checkbox"/>	<input type="checkbox"/>	<input type="checkbox"/>	<input checked="" type="checkbox"/>	<input type="checkbox"/>	<input type="checkbox"/>	<input type="checkbox"/>	<input type="checkbox"/>	<input type="checkbox"/>	<input type="checkbox"/>	<input type="checkbox"/>	<input type="checkbox"/>	<input type="checkbox"/>	<input type="checkbox"/>
A2 (RML)	<input type="checkbox"/>	<input type="checkbox"/>	<input type="checkbox"/>	<input checked="" type="checkbox"/>	<input type="checkbox"/>	<input type="checkbox"/>	<input type="checkbox"/>	<input type="checkbox"/>	<input type="checkbox"/>	<input type="checkbox"/>	<input type="checkbox"/>	<input type="checkbox"/>	<input type="checkbox"/>	<input type="checkbox"/>
A3 (RUL)	<input type="checkbox"/>	<input type="checkbox"/>	<input type="checkbox"/>	<input checked="" type="checkbox"/>	<input type="checkbox"/>	<input type="checkbox"/>	<input type="checkbox"/>	<input type="checkbox"/>	<input type="checkbox"/>	<input type="checkbox"/>	<input type="checkbox"/>	<input type="checkbox"/>	<input type="checkbox"/>	<input type="checkbox"/>
B4 (LLL)	<input type="checkbox"/>	<input type="checkbox"/>	<input type="checkbox"/>	<input type="checkbox"/>	<input checked="" type="checkbox"/>	<input type="checkbox"/>	<input type="checkbox"/>	<input type="checkbox"/>	<input type="checkbox"/>	<input type="checkbox"/>	<input type="checkbox"/>	<input type="checkbox"/>	<input type="checkbox"/>	<input type="checkbox"/>
B5 (LUL)	<input type="checkbox"/>	<input type="checkbox"/>	<input type="checkbox"/>	<input checked="" type="checkbox"/>	<input type="checkbox"/>	<input type="checkbox"/>	<input type="checkbox"/>	<input type="checkbox"/>	<input type="checkbox"/>	<input type="checkbox"/>	<input type="checkbox"/>	<input type="checkbox"/>	<input type="checkbox"/>	<input type="checkbox"/>
B6 (CAR)	<input type="checkbox"/>	<input type="checkbox"/>	<input type="checkbox"/>	<input checked="" type="checkbox"/>	<input checked="" type="checkbox"/>	<input type="checkbox"/>	<input type="checkbox"/>	<input type="checkbox"/>	<input type="checkbox"/>	<input type="checkbox"/>	<input type="checkbox"/>	<input type="checkbox"/>	<input type="checkbox"/>	<input type="checkbox"/>
Site / Dx	Metaplasia			Dysplasia			Comments							
Right (A)	0/6 = 0.00%			<input type="checkbox"/>										
Left (B)	0/6 = 0.00%			<input type="checkbox"/>										
Overall	0/12 = 0.00%													

Slide 35

Histopathology Report

Send Email:  EMail Address:

Vanguard

BRONCHIAL METAPLASIA/DYSPLASIA PATHOLOGY REPORT

Path #: *VBV-06-06205* Pt. Name: *Eds, Rose* MDACC: *111111*

Surgeon: Biopsy Date: *8/4/2006* Slides Sent: *___/___/___*

Pathologist: Path Report Date: *___/___/___*

Site	Diagnosis
A1 (RLL)	Denuded epithelium
A2 (RML)	Normal or hyperplastic epithelium
A3 (RUL)	Normal or hyperplastic epithelium
B4 (LLL)	Normal or hyperplastic epithelium
B5 (LUL)	Normal or hyperplastic epithelium
B6 (CAR)	Normal or hyperplastic epithelium

Site	Metaplasia	Dysplasia	Comments
Right (A)	<i>0/6 = 0.00%</i>	<i>No</i>	
Left (B)	<i>0/6 = 0.00%</i>	<i>No</i>	
Overall	<i>0/12 = 0.00%</i>		

Overall Comments

Slide 36

Other Forms

- Monthly Follow Ups
- Adverse Events Form
- Off Drug/ Off Study Form

Slide 37

Monthly Follow Up

3 Months
6 Months
9 Months
12 Months
18 Months
24 Months
30 Months
36 Months
42 Months
48 Months

Select a participant
Status: Ready...no patient Selected

1. Monthly Follow Up For Month
Follow Up Date: Check here if patient missed this follow up ☐

*2. Smoking Status
Pattern Changed? ☐ Yes ☐ No
Start Date Since Last Visit
Quit Date Since Last Visit
Cigarettes a Day

*3. Alcohol Status (ETOH)
Pattern Changed? ☐ Yes ☐ No
Start Date Since Last Visit
Quit Date Since Last Visit
Amounts
Beer (12 oz.) cans ☐ None ☐ Daily ☐ Weekly ☐ Monthly ☐ Yearly
Wine (4 oz.) glasses ☐ None ☐ Daily ☐ Weekly ☐ Monthly ☐ Yearly
Straight Liquor (1 oz.) shots ☐ None ☐ Daily ☐ Weekly ☐ Monthly ☐ Yearly
Mixed Drinks (8 oz.) glasses ☐ None ☐ Daily ☐ Weekly ☐ Monthly ☐ Yearly
Reproductive Status (If female or childbearing potential)
LMP: Contraception:
Comments:

Slide 38

Adverse Events

Adverse Events

Select Patient Doe, John

Delete	Adverse Event	Start Date	Recorded By	Stop Date	Recorded By	Comments
	RASH	06/18/2005	M Quillian	08/17/2005	M Quillian	Grade 1
	FATIGUE	06/15/2005	MQUILLIAN	08/17/2005	MQUILLIAN	GRADE 1
	PAIN	06/18/2005	m QUILLIAN	08/10/2005	mQUILLIAN	GRADE 1 JOINT PAIN
	Fatigue	06/15/2005	P Cole			Baseline/Gr 1
	PVD	06/15/2003	P Cole			Baseline/Gr 2
	CAD	06/15/1989	P Cole			baseline/gr 2
	HTN	06/15/1989	P Cole			Baseline/gr 2

Slide 39

Off Drug / Off Study

1. Off Drug

Off drug date

1.1 Select one of the reasons below:

Drug-related per protocol (completed 8 months therapy)

Per physician decision:

Per patient decision:

1.1.1 If per physician decision select one of the following:

Progress:

Toxicity:

Complete:

Other:

1.1.2 If per patient decision select one of the following:

Recovery:

Other:

(Off Drug/ Study F1 Page)

2. Off Study

Off study date

Select one of the reasons below:

Per protocol (completed 8 months therapy)

Refused follow up/ unnecessary,

Physician decision,

Lost to follow up,

Slide 40

Off Drug / Off Study

Distance / travel constraint

Time constraint

Completed 3 Years of follow up

Death

Other

If other, enter reason:

If lost of follow up, date

Status: disease-free

☐ yes

☐ unknown

Developed End Points	
	Location
recurrence	<input type="text"/>
metastasis	<input type="text"/>
second primary tumor	<input type="text"/>

If deceased, date of death

Cause of death

Comments

APENDIX 2

CCAAT/Enhancer Binding Protein Homologous Protein-Dependent Death Receptor 5 Induction and Ubiquitin/Proteasome-Mediated Cellular FLICE-Inhibitory Protein Down-Regulation Contribute to Enhancement of Tumor Necrosis Factor-Related Apoptosis-Inducing Ligand-Induced Apoptosis by Dimethyl-Celecoxib in Human Non-Small-Cell Lung Cancer Cells^S

Shuzhen Chen, Xiangguo Liu, Ping Yue, Axel H. Schönthal, Fadlo R. Khuri, and Shi-Yong Sun

Winship Cancer Institute, Emory University School of Medicine, Atlanta, Georgia (S.C., X.L., P.Y., F.R.K., S.Y.S.); and University of Southern California, Los Angeles, California (A.H.S.)

Received April 25, 2007; accepted August 7, 2007

ABSTRACT

2,5-Dimethyl-celecoxib (DMC) is a derivative of celecoxib, a cyclooxygenase-2 (COX-2) inhibitor with anticancer activity in both preclinical studies and clinical practice, and lacks COX-2-inhibitory activity. Several preclinical studies have demonstrated that DMC has better apoptosis-inducing activity than celecoxib, albeit with undefined mechanisms, and exhibits anticancer activity in animal models. In this study, we primarily investigated DMC's cooperative effect with tumor necrosis factor-related apoptosis-inducing ligand (TRAIL) on the induction of apoptosis and the underlying mechanisms in human non-small-cell lung cancer (NSCLC) cells. We found that DMC was more potent than celecoxib in decreasing the survival and inducing apoptosis of NSCLC cells. When combined with TRAIL, DMC exerted enhanced or synergistic effects on the induction of apoptosis, indicating that DMC cooperates with TRAIL to augment the induction of apoptosis. To determine the

underlying mechanism of the synergy between DMC and TRAIL, we have demonstrated that DMC induces a CCAAT/enhancer binding protein homologous protein-dependent expression of DR5, a major TRAIL receptor, and reduces the levels of cellular FLICE-inhibitory protein (c-FLIP) (both the long and short forms), key inhibitors of death receptor-mediated apoptosis, by facilitating c-FLIP degradation through a ubiquitin/proteasome-dependent mechanism. It is noteworthy that enforced expression of c-FLIP or silencing of DR5 expression using DR5 small interfering RNA abrogated the enhanced effects on induction of apoptosis by the combination of DMC and TRAIL, indicating that both DR5 up-regulation and c-FLIP reduction contribute to cooperative induction of apoptosis by the combination of DMC and TRAIL. Together, we conclude that DMC sensitizes human NSCLC cells to TRAIL-induced apoptosis via induction of DR5 and down-regulation of c-FLIP.

This study was supported by Georgia Cancer Coalition Distinguished Cancer Scholar award (to S.-Y.S.) and Department of Defense VITAL grant W81XWH-04-1-0142 (to S.-Y.S. for Project 4). F.R.K. and S.-Y.S. are Georgia Cancer Coalition Distinguished Cancer Scholars.

Article, publication date, and citation information can be found at <http://molpharm.aspetjournals.org>.

doi:10.1124/mol.107.037465.

^S The online version of this article (available at <http://molpharm.aspetjournals.org>) contains supplemental material.

Celecoxib (Celebrex, Pfizer Inc., New York, NY) is an approved drug for adjuvant treatment of patients with familial adenomatous polyposis. In addition, celecoxib is being tested in various clinical trials for its chemopreventive and therapeutic efficacy against a broad spectrum of epithelial malignancies, including lung cancers, either as a single agent or in combination with other agents (Koki and Masferrer, 2002;

ABBREVIATIONS: COX-2, cyclooxygenase-2; DMC, 2,5-dimethyl-celecoxib; TRAIL, tumor necrosis factor-related apoptosis-inducing ligand; NSCLC, non-small-cell lung cancer; c-FLIP, cellular FLICE-inhibitory protein; c-FLIP_L, long form of cellular FLICE-inhibitory protein; c-FLIP_S, short form of cellular FLICE-inhibitory protein; DR, death receptor; CHOP, CCAAT/enhancer binding protein homologous protein; siRNA, small interfering RNA; JNK, c-Jun N-terminal kinase; p-c-Jun, phospho-c-Jun; ER, endoplasmic reticulum; DMSO, dimethyl sulfoxide; PARP, poly(ADP-ribose) polymerase; HA, hemagglutinin; ChIP, chromatin immunoprecipitation; SRB, sulforhodamine B; SP600125, anthra(1,9-cd)pyrazol-6(2H)-one 1,9-pyrazoloanthrone; MG132, *N*-benzoyloxycarbonyl (Z)-Leu-Leu-leucinal.

Grösch et al., 2006). Although celecoxib is a cyclooxygenase 2 (COX-2) inhibitor, it also exerts antitumor activity in tumor cells and tissues that lack the COX-2 enzyme (Grösch et al., 2006). Therefore, celecoxib seems to be able to inhibit tumor growth independently of its COX-2-inhibitory activity.

The major concern for celecoxib as a cancer therapeutic agent is that it induces apoptosis only at high concentrations ($>50 \mu\text{M}$) in cell culture systems, which exceed clinically achievable plasma levels ($<10 \mu\text{M}$) (Davies et al., 2000). In addition, a more practical issue is the potential cardiovascular side effects of celecoxib, which probably are associated with its COX-2-inhibitory activity (Dogné et al., 2006; Marwali and Mehta, 2006). Given that celecoxib has been developed and marketed mainly for the treatment of arthritis and pain but not primarily for anticancer purposes, it is conceivable that this drug might be suboptimal for inclusion in the treatment of advanced cancers, such as non-small-cell lung cancer (NSCLC). To this end, efforts have been made recently to synthesize celecoxib derivatives optimized for anticancer applications, and novel non-COX-2 inhibitory celecoxib derivatives have been identified that show better activity than celecoxib in inducing apoptosis and inhibiting the growth of tumors (Zhu et al., 2002, 2004; Kardosh et al., 2005; Pyrko et al., 2006).

Among these derivatives, 2,5-dimethyl-celecoxib (DMC) mimicked celecoxib's numerous antitumor effects, including the induction of apoptosis, the reduction of neovascularization, and the inhibition of experimental tumor growth in some *in vivo* tumor models with increased efficacy (Schönthal, 2006). Thus, this compound exhibits cancer therapeutic potential in the absence of COX-2 inhibitory activity. Recently, it has been shown that DMC down-regulates survivin expression in human cancer cells; this effect seems to correlate with DMC's ability to induce apoptosis (Pyrko et al., 2006).

There are two major apoptotic signaling pathways: the intrinsic mitochondria-mediated pathway, and the extrinsic death receptor-induced pathway, and cross-talk between these pathways is mediated by the truncation of the proapoptotic protein Bid (Hengartner, 2000). It is well known that the extrinsic apoptotic pathway is negatively regulated by the cellular FLICE-inhibitory protein (c-FLIP), including both long (FLIP_L) and short (FLIP_S) forms, through inhibition of caspase-8 activation (Krueger et al., 2001). The tumor necrosis factor-related apoptosis-inducing ligand (TRAIL) binds to its receptors: death receptor 4 (DR4, also called TRAIL-R1), and death receptor 5 (DR5, also named Apo2, TRAIL-R2, or Killer/DR5) to activate the extrinsic apoptotic pathway (Kelley and Ashkenazi, 2004). Recently, TRAIL has received much attention because it preferentially induces apoptosis in transformed or malignant cells, demonstrating potential as a tumor-selective apoptosis-inducing cytokine for cancer treatment (Kelley and Ashkenazi, 2004). Currently, TRAIL is being tested in phase I clinical trials. It is noteworthy that certain cancer therapeutic agents including celecoxib sensitize various types of cancer cells to TRAIL-induced apoptosis (Wang and El-Deiry, 2003; Kelley and Ashkenazi, 2004; Liu et al., 2004b). Thus, these agents are useful in combination with TRAIL to overcome TRAIL resistance as demonstrated in some types of cancer cells (Wang and El-Deiry, 2003).

We have shown previously that celecoxib increases DR5

expression, down-regulates c-FLIP levels, and hence enhances TRAIL-induced apoptosis in human NSCLC cells (Liu et al., 2004b, 2006). The present study determined whether DMC exerted similar effects on induction of apoptosis, modulation of DR5 and c-FLIP, and sensitization of TRAIL-induced apoptosis in human NSCLC cells. We show that DMC potently stimulates the expression of DR5, which is dependent on the transcription factor CCAAT/enhancer binding protein homologous protein (CHOP)/growth arrest and DNA damage gene 153. Furthermore, the drug stimulates ubiquitin/proteasome-mediated degradation of c-FLIP, and both of these events contribute to DMC-mediated enhancement of TRAIL-induced apoptosis.

Materials and Methods

Reagents. DMC was synthesized as described previously (Kardosh et al., 2005). Celecoxib was purchased from LKT Laboratories (St. Paul, MN). Both drugs were dissolved in DMSO at the concentration of 100 mM, and aliquots were stored at -80°C . Stock solutions were diluted to the appropriate concentrations with growth medium immediately before use. The soluble recombinant human TRAIL was purchased from PeproTech, Inc. (Rocky Hill, NJ). The specific JNK inhibitor SP600125 was purchased from BIOMOL Research Laboratories (Plymouth Meeting, PA). The proteasome inhibitor MG132 was purchased from Sigma Chemical Co. (St. Louis, MO). Rabbit polyclonal anti-DR5 antibody was purchased from ProSci Inc. (Poway, CA). Mouse monoclonal anti-DR4 antibody (B-N28) was purchased from Diaclone (Stamford, CT). Mouse monoclonal anti-FLIP antibody (NF6) was purchased from Alexis Biochemicals (San Diego, CA). Mouse monoclonal anti-CHOP antibody (B-3) was purchased from Santa Cruz Biotechnology (Santa Cruz, CA). Mouse monoclonal anticaspase-3 antibody was purchased from Imgenex (San Diego, CA). Rabbit polyclonal anticaspase-8, anticaspase-9, and anti-PARP antibodies were purchased from Cell Signaling Technology, Inc. (Danvers, MA). Rabbit polyclonal anti- β -actin antibody was purchased from Sigma Chemical Co.

Cell Lines and Cell Culture. Human NSCLC cell lines used in this study were purchased from the American Type Culture Collection (Manassas, VA). The stable H157-FLIP_L-5 and H157-FLIP_L-21 transfectants that express ectopic FLIP_L, and H157-FLIP_L-16 transfectant that were infected with lentiviral FLIP_L but did not express ectopic FLIP_L, were established as described previously (Liu et al., 2006). Both H157-lac Z-5 (Liu et al., 2006) and H157-FLIP_L-16 transfectants were used as control cell lines. These cell lines were cultured in RPMI 1640 medium containing 5% fetal bovine serum at 37°C in a humidified atmosphere of 5% CO_2 /95% air.

Cell Survival Assay. Cells were seeded in 96-well cell culture plates and were treated the next day with the agents indicated. The viable cell number was determined using the sulforhodamine B assay as described previously (Sun et al., 1997).

Detection of Apoptosis. Apoptosis was evaluated by Annexin V staining using Annexin V-PE apoptosis detection kit purchased from BD Biosciences (San Jose, CA) following the manufacturer's instructions. We also detected caspase activation by Western blotting (as described below) as an additional indicator of apoptosis.

Western Blot Analysis. Whole-cell protein lysates were prepared and analyzed by Western blotting as described previously (Sun et al., 1999; Liu et al., 2004b).

Immunoprecipitation for Detection of Ubiquitinated c-FLIP. H157-FLIP_L-21 cells, which stably express FLIP_L, were transfected with HA-ubiquitin plasmid using the FuGENE 6 transfection reagent (Roche Diagnostics, Indianapolis, IN) following the manufacturer's instructions. After 24 h, the cells were treated with DMC or MG132 plus DMC for 4 h and then were lysed for immunoprecipitation of Flag-FLIP_L using Flag M2 monoclonal antibody

(Sigma) as described previously (Chen et al., 2005) followed by the detection of ubiquitinated FLIP_L with Western blotting using anti-HA antibody (Abgent, San Diego, CA).

Silencing of DR5 Expression Using Small Interfering RNA. The nonsilencing control small interfering RNA (siRNA) and DR5 siRNA duplexes were described previously (Liu et al., 2004b). Transfection of these siRNA duplexes was conducted in six-well plates using the HiPerFect transfection reagent (QIAGEN, Valencia, CA) following the manufacturer's manual. Gene-silencing effect was evaluated by Western blot analysis.

Transient Transfection and Luciferase Activity Assay. pGL3-DR5(-552) containing a wild-type CHOP binding site and pGL3-DR5(-552)CHOPm, in which the CHOP binding site was mutated, were generously provided by H. G. Wang (University of South Florida College of Medicine, Tampa, FL) (Yamaguchi and Wang, 2004). To examine the effects of DMC on DR5 promoter activity, cells were cotransfected with 0.35 μ g of reporter plasmids and 0.25 μ g of β -galactosidase expression plasmid (Pharmacia Biotech, Piscataway, NJ) using FuGENE 6 transfection reagent (Roche Molecular Biochemicals, Indianapolis, IN) following the manufacturer's protocol. Twenty-four hours later, the cells were treated with DMC. After 12 h, the cells were lysed and subjected to luciferase activity assay using Luciferase Assay System (Promega, Madison, WI) in a luminometer. Relative luciferase activity was normalized to β -galactosidase activity, which was measured as described previously (Pfahl et al., 1990).

Chromatin Immunoprecipitation Assay. Chromatin immunoprecipitation (ChIP) assay was conducted using the ChIP assay kit purchased from Upstate Biotechnology (Charlottesville, VA) following the manufacturer's instruction and was described previously (Liu et al., 2004a). CHOP antibody for immunoprecipitation in this assay was the same used in the Western blot analysis. Mouse IgG_{2a} isotype antibody was purchased from EMD Bioscience, Inc. (La Jolla, CA). Polymerase chain reaction amplification of a 111-bp fragment of DR5 promoter containing a CHOP binding site on immunoprecipitated chromatin was conducted using the primers 5'-AGGTTAGTCCG-GTCCCTTC-3' (forward) and 5'-CAACTGCAAATCCACCACA-3' (reverse) as described previously (Abdelrahim et al., 2006).

Results

DMC Was More Potent than Celecoxib in Inhibiting the Growth and Inducing Apoptosis of Human NSCLC Cells. We first compared the effects of DMC with celecoxib on the growth of a panel of human NSCLC cell lines. In this experiment, six NSCLC cell lines including H157, H460, H1792, A549, Calu-1, and H226 were treated with increasing concentrations of DMC or celecoxib for 3 days, and then cell growth inhibition was determined. As presented in Fig. 1, A and B, both compounds inhibited the growth of the tested cell lines in a dose-dependent manner. DMC inhibited cell growth with IC₅₀ values ranging from 10 to 20 μ M, whereas celecoxib did so with IC₅₀ values ranging between 20 and 35 μ M, indicating that DMC is more effective than celecoxib in inhibiting the growth of NSCLC cells. Second, we examined the effects of DMC and celecoxib on the induction of apoptosis in four NSCLC cell lines. At the concentration of 50 μ M, DMC induced more than 60% apoptosis in all of the cell lines tested, whereas celecoxib caused only up to 35% apoptosis (Fig. 1C). Together, these results indicate that DMC is more potent than celecoxib in inhibiting cell growth and inducing apoptosis in human NSCLC cells.

DMC Cooperated with TRAIL to Augment the Induction of Apoptosis in Human NSCLC Cells. Our previous work has shown that celecoxib enhances TRAIL-induced apoptosis in NSCLC cells (Liu et al., 2004b). Therefore, we

determined whether DMC also augmented TRAIL-induced apoptosis in human NSCLC cells. To this end, we treated four NSCLC cell lines (i.e., H157, Calu-1, H460, and A549) with TRAIL alone, DMC alone, or both drugs combined and then assessed cell survival and apoptosis. As presented in Fig. 2A, the combination of DMC at concentrations of 10 to 30 μ M with either dose of TRAIL (10 or 20 nM) was much more effective in decreasing tumor cell survival than either single agent alone. For example, in Calu-1 cells, DMC alone at 20

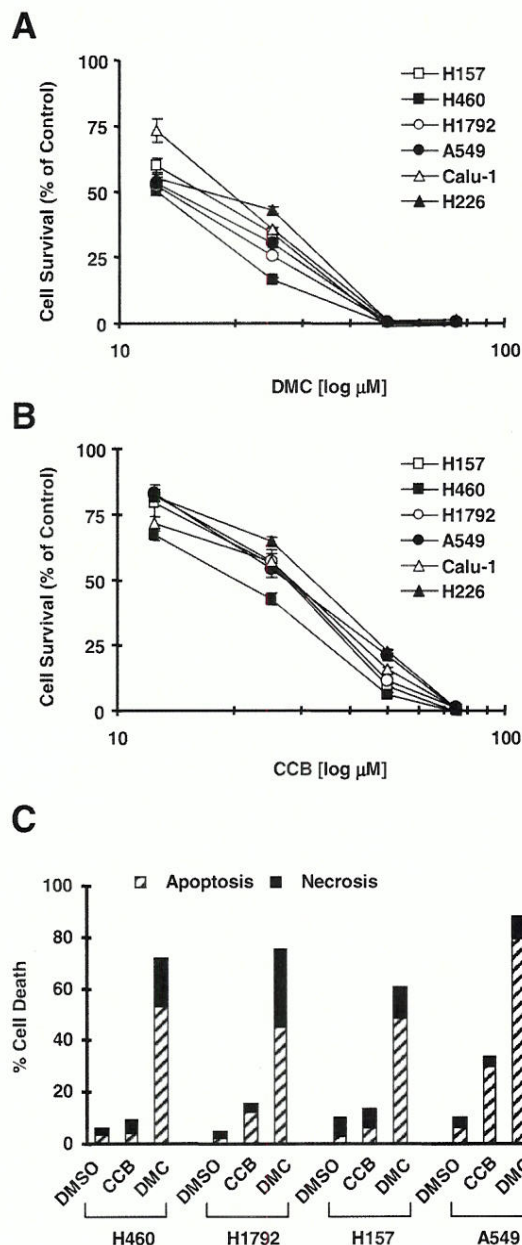


Fig. 1. DMC exhibits more potent efficacy than celecoxib in decreasing the survival (A and B) and inducing apoptosis (C) of human NSCLC cells. A and B, the indicated NSCLC cell lines were seeded in 96-well cell culture plates and were treated the next day with the given concentrations of DMC (A) or celecoxib (CCB) (B). After 3 days, cell number was estimated using the SRB assay. Cell survival was expressed as the percentage of control (DMSO-treated) cells. Data are the means of four replicate determinations; bars, \pm S.D. C, the indicated NSCLC cell lines were treated with DMSO, 50 μ M DMC, or 50 μ M celecoxib for 24 h. Cell death, including apoptosis and necrosis from these cell lines, was then determined by Annexin V staining.

μM decreased cell survival by 33%, and TRAIL (10 ng/ml) alone decreased cell survival by 10%, but the combination of the two agents reduced cell survival by almost 70%, which is greater than the sum of the effects of each agent alone. Moreover, we detected apoptosis in two NSCLC cell lines (H157 and H460) exposed to the combination of DMC and TRAIL. During a 24-h treatment, DMC at 25 μM did not increase apoptosis in either cell line, and 10 ng/ml TRAIL alone induced only 24 (H460) and 15% (H157) apoptosis.

However, the combination of DMC and TRAIL caused 63 and 30% of cells to undergo apoptosis (Fig. 2B). In addition, the combination of DMC and TRAIL was much more potent than each single agent alone in inducing cleavage of caspase-8, caspase-9, caspase-3, and PARP (Fig. 2C). Together, these results clearly indicate that DMC cooperates with TRAIL to augment the induction of apoptosis in human NSCLC cells.

DMC Induced CHOP-Dependent DR5 Expression. DR5 induction is one mechanism accounting for the sensi-

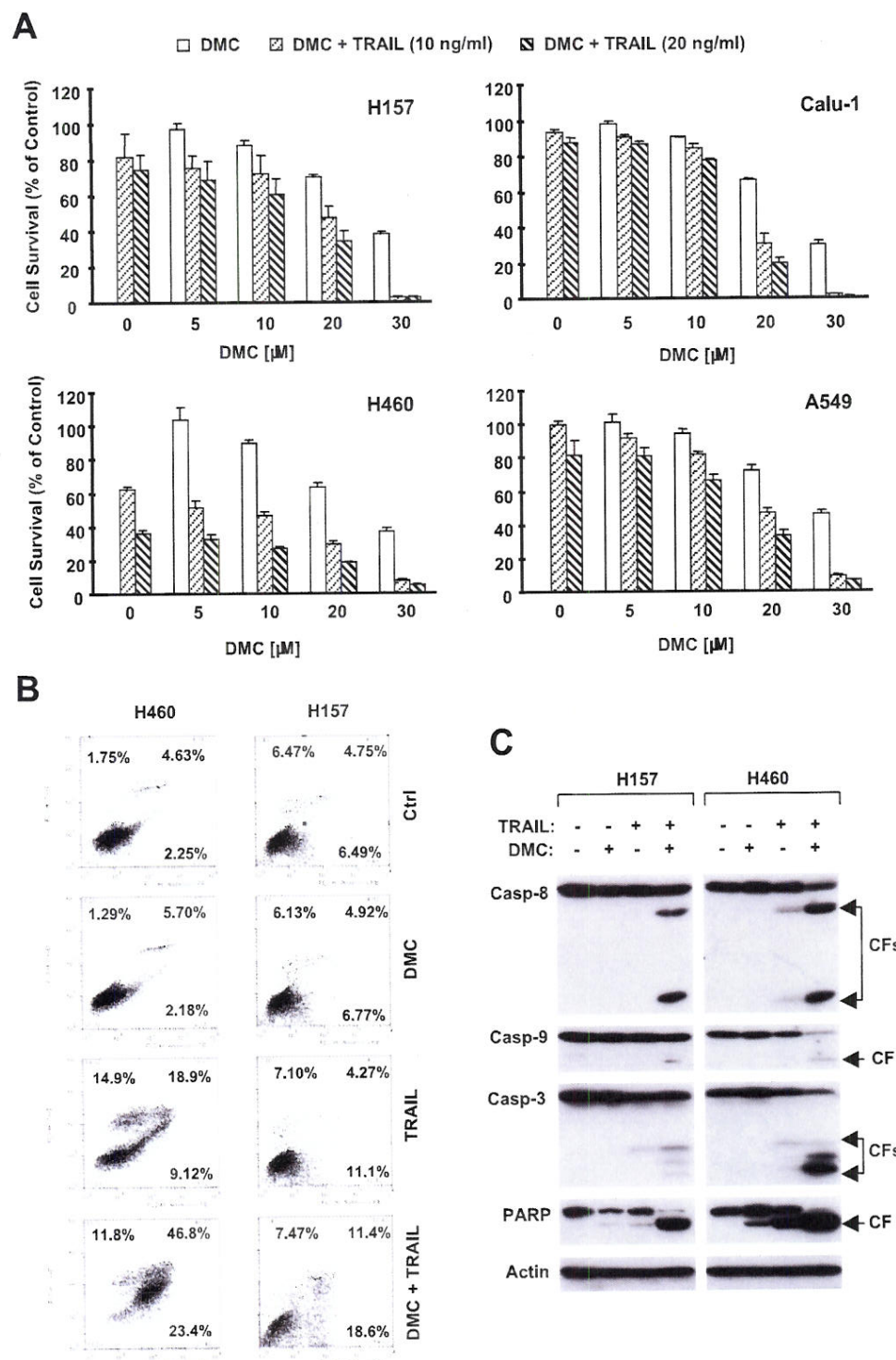


Fig. 2. DMC enhances TRAIL's effects on decreasing cell survival (A), inducing apoptosis (B), and activating caspases (C) in human NSCLC cells. A, the indicated cell lines were treated with the given concentrations of TRAIL alone, DMC alone, and their combination as indicated. After 24 h, cell number was estimated using SRB assay for the calculation of cell survival. Data are the means of four replicate determinations. Bars, S.D. B, the indicated cell lines were treated with 10 ng/ml TRAIL alone, 25 μM DMC alone, and their respective combination as indicated. After 24 h, the cells were subjected to measurement of apoptosis using Annexin V staining. The percentage of positive cells in the upper right and lower right quadrants were added to yield the total of apoptotic cells. C, the indicated cell lines were treated with 25 μM DMC alone, 10 ng/ml TRAIL alone, and their combination. After 8 h, the cells were harvested for the preparation of whole-cell protein lysates and subsequent Western blot analysis for detecting cleavage of caspases and their substrates. Casp, caspase; CF, cleaved fragment.

zation of TRAIL-induced apoptosis by some small-molecule drugs, including celecoxib (Liu et al., 2004b; Sun, 2005). Thus, we next determined whether DMC modulated DR5 expression in human NSCLC cells. By Western blot analysis, we detected a time-dependent induction of DR5 expression in both H157 and H460 cell lines exposed to DMC, which occurred early at 4 h and was sustained for at least 16 h (Fig. 3A). In addition, we found that DMC at a concentration as low as 10 μ M was able to increase DR5 expression in both H157 and H460 cell lines (data not shown). Because DR4 is another TRAIL death receptor, we also examined DR4 expression in cells exposed to DMC and found that DMC increased DR4 levels in H157 cells but not in H460 cells (Fig. 3A). Thus, we focused on DR5 in the subsequent studies.

To understand the mechanism by which DMC induces DR5 expression, we analyzed the expression of CHOP, a transcriptional factor that is known to regulate DR5 expression via binding to its promoter region (Yamaguchi and Wang, 2004; Yoshida et al., 2005; Abdelrahim et al., 2006). As shown in Fig. 3A, DMC increased CHOP levels in both H157 and H460 cell lines, and the kinetics of induction were similar to those of DR5. To determine whether CHOP mediates DMC-in-

duced DR5 expression, we compared the effects of DMC on transactivation of DR5 promoters with and without the wild-type CHOP binding site. As shown in Fig. 3B, DMC significantly increased the luciferase activity in cells transfected with pGL3-DR5(-552) carrying the wild-type promoter, but this effect was completely inhibited in cells transfected with the mutant construct pGL3-DR5(-552)CHOPm, in which the CHOP binding site was inactivated. Moreover, DMC facilitated CHOP binding to DR5 promoter evaluated by ChIP assay (Fig. 3C). Together, these results indicate that the CHOP binding site is essential for DMC-mediated transactivation of the DR5 promoter. To firmly prove that DMC-induced DR5 expression is CHOP-dependent, we knocked down CHOP expression using CHOP siRNA and then examined its impact on DMC-induced DR5 expression. As presented in Fig. 3D, DMC increased levels of CHOP in control siRNA-transfected H460 cells but not in CHOP siRNA-transfected cells, indicating the successful blockage of CHOP induction by DMC. Therefore, DMC failed to increase DR5 expression in cells transfected with CHOP siRNA compared with cells transfected with control siRNA, indicating that DR5 induction by DMC is CHOP-dependent. Together, we

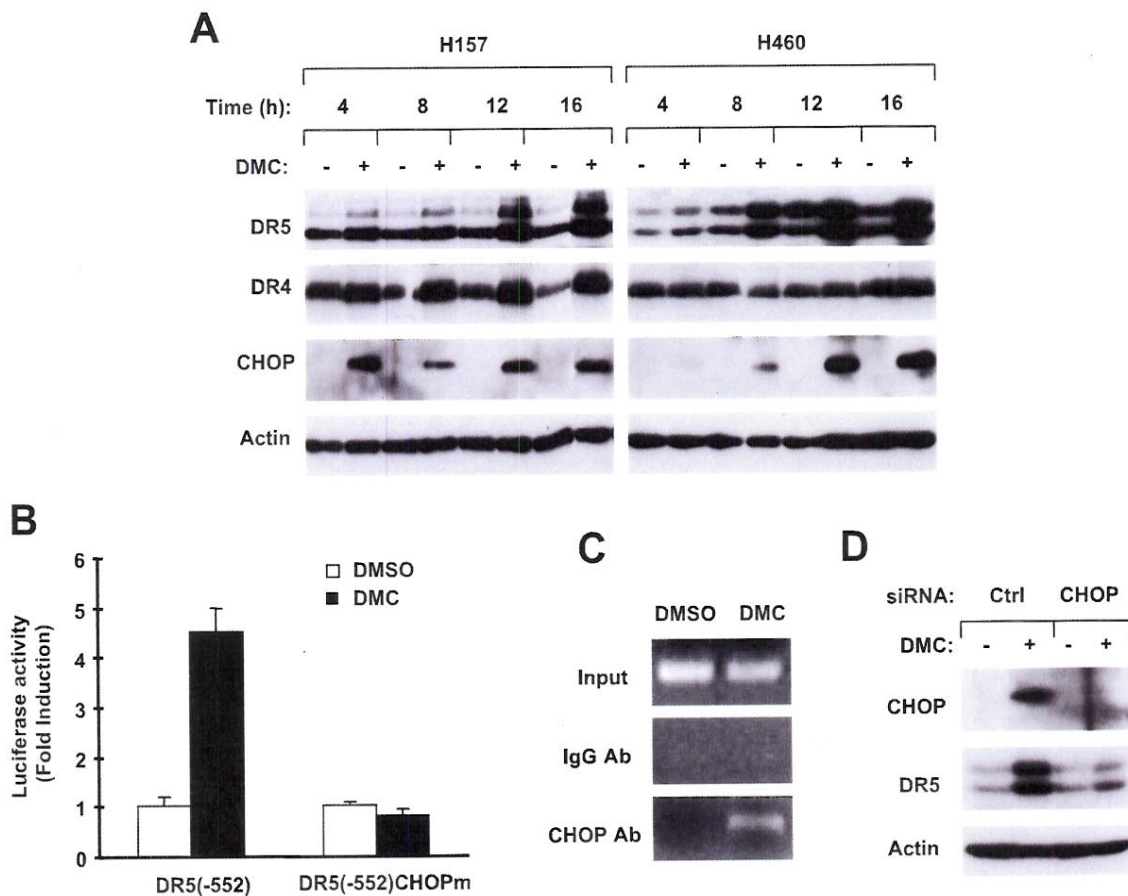


Fig. 3. DMC induces DR5 expression (A) through a CHOP-mediated mechanism (B–D). A, time-dependent modulatory effects of DMC on the expression of DR5, DR4, and CHOP. The given cell lines were treated with 25 μ M DMC for various times from 4 to 16 h as indicated and then subjected to the preparation of whole-cell protein lysates and subsequent Western blot analysis for the given proteins. B, effects of DMC on the transactivation of DR5 promoters with and without wild-type CHOP binding sites. The given reporter constructs were cotransfected with pCH110 plasmid into H460 cells. After 24 h, the cells were treated with DMSO or 25 μ M DMC for 12 h and then subjected to luciferase assay. Data are means of triplicate determinations. Bars, \pm S.D. C, DMC facilitates CHOP binding to DR5 promoter. H460 cells were treated with 25 μ M DMC for 8 h and then subjected to ChIP assay for detecting CHOP binding in the DR5 promoter. The amplified DNA fragment by polymerase chain reaction was 111 bp. Ab, antibody. D, effect of CHOP knockdown on DMC-induced DR5 expression. H460 cells were transfected with control (Ctrl) or CHOP siRNA. After 48 h, the cells were treated with 25 μ M DMC for 12 h and then subjected to the preparation of whole-cell protein lysates and subsequent Western blot analysis.

conclude that DMC induces CHOP-dependent DR5 expression in human NSCLC cells.

DMC Down-Regulated c-FLIP Levels through Ubiquitin/Proteasome-Mediated Degradation. In addition to DR5 induction, c-FLIP down-regulation is another important mechanism underlying enhancement of TRAIL-induced apoptosis by some anticancer drugs, including celecoxib (Liu et al., 2006; Zou et al., 2007). Therefore, we further determined whether DMC also down-regulates c-FLIP levels. DMC decreased the levels of both FLIP_L and FLIP_S in H157 and H460 cells at 4 h after treatment. It is interesting that prolonged treatment with DMC generated cell line-dependent results on c-FLIP modulation. The decrease of c-FLIP (FLIP_L and FLIP_S) by DMC was maintained for up to 16 h in H157 cells. However, FLIP_L was actually increased by DMC at late times (e.g., 12 and 16 h) in H460 cells, although FLIP_S was still decreased at up to 16 h (Fig. 4A). For a fixed 16-h treatment experiment, we found that DMC at concentrations ranging from 10 to 30 μ M decreased levels of FLIP_L and FLIP_S in H157 cells; however, it increased levels of FLIP_L while still reducing the levels of FLIP_S in H460 cells (Fig. 3B).

Because c-FLIP proteins are known to be regulated by ubiquitin/proteasome-mediated degradation (Kim et al.,

2002; Chang et al., 2006), we investigated whether the observed down-regulation of c-FLIP by DMC would be mediated via this process. To this end, we found that DMC-induced down-regulation of c-FLIP was abrogated by the presence of the proteasome inhibitor MG132 (Fig. 4C), indicating that DMC-induced c-FLIP reduction is proteasome-dependent. By immunoprecipitation/Western blotting, we detected the highest levels of ubiquitinated FLIP_L in cells treated with DMC plus MG132 compared with cells exposed to DMC alone or MG132 alone (Fig. 4D), indicating that DMC increases c-FLIP ubiquitination. Taken together, we conclude that DMC facilitates ubiquitin/proteasome-mediated c-FLIP degradation, leading to down-regulation of c-FLIP in human NSCLC cells.

DMC Exerted Minimal Modulatory Effects on the Expression of Bax, Bcl-X_L, Bcl-2, Bad, and Survivin. Bcl-2 family members such as Bax, Bcl-2, and Bcl-X_L and inhibitor of apoptosis proteins such as survivin are known to be involved in the regulation of the intrinsic apoptotic pathway (Hengartner, 2000; Harada and Grant, 2003). To further understand the molecular mechanism underlying DMC enhancement of TRAIL-induced apoptosis, we also analyzed the modulatory effects of DMC on Bax, Bcl-X_L, Bcl-2, Bad, and survivin in H157 and H460 NSCLC cell lines. Our results

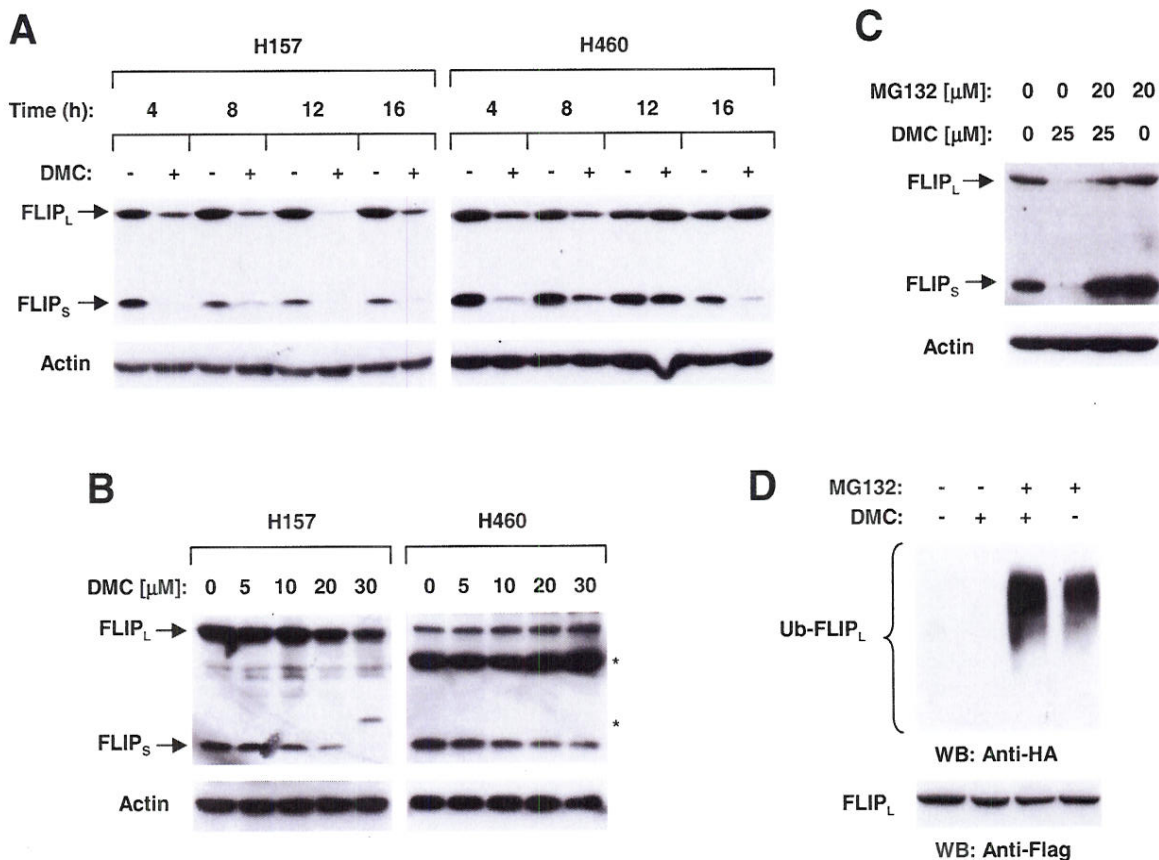


Fig. 4. DMC down-regulates c-FLIP levels (A and B) through ubiquitin/proteasome-mediated protein degradation (C and D). A and B, the given cell lines were treated with 25 μ M DMC for the indicated times (A) or with the indicated concentrations of DMC for 16 h (B). The cell lines were then subjected to preparation of whole-cell protein lysates and subsequent Western blot analysis. C, H157 cells were pretreated with 20 μ M MG132 for 30 min and then cotreated with 25 μ M DMC for another 8 h. The cells were then harvested for preparation of whole-cell protein lysates and subsequent Western blot analysis. D, H157-FLIP_L-21 cells that stably express ectopic flag-FLIP_L were transfected with HA-ubiquitin plasmid using FuGENE 6 transfection reagent for 24 h. The cells were then pretreated with 20 μ M MG132 for 30 min and then cotreated with 25 μ M DMC for 4 h. Whole-cell protein lysates were then prepared for immunoprecipitation using anti-Flag antibody followed by Western blotting (WB) using anti-HA antibody for the detection of ubiquitinated FLIP_L (Ub-FLIP_L) and anti-Flag antibody for the detection of ectopic FLIP_L.

showed that DMC only decreased the levels of survivin but had minimal effects on the expression of Bax, Bcl-X_L, Bcl-2, and Bad (see Supplemental Fig. S1). The down-regulation of survivin by DMC in human NSCLC cells is in agreement with the finding by Pyrko et al. (2006) in other types of cancer cell lines. However, we found that DMC reduced the levels of survivin in H460 cells only starting at 8 h, indicating that survivin modulation is not as early an event as the modulation of DR5 and c-FLIP in DMC-treated cells.

DMC Modulated DR5 Expression and c-FLIP Levels Independently of JNK Activation. Several studies have demonstrated that JNK activation regulates DR5 expression (Higuchi et al., 2004; Zou et al., 2004). Recently, JNK has also been demonstrated to be responsible for tumor necrosis factor-induced, ubiquitin/proteasome-mediated FLIP_L degradation (Chang et al., 2006). Therefore, we wanted to determine whether DMC induces JNK activation in human NSCLC cells and, if so, whether JNK activation is responsible for DR5 induction and c-FLIP down-regulation by DMC. By Western blot analysis, we detected that DMC increased levels of phosphorylated c-Jun (p-c-Jun), a well known substrate and indicator of JNK activation, in a time- and dose-dependent manner in H157 cells. In parallel, a comparatively smaller and later increase of total c-Jun protein levels was noted as well. However, such an increase in p-c-Jun and c-Jun was not detected in H460 cells (Fig. 5, A and B), primarily because of the absence of basal level c-Jun expression. The stimulation of c-Jun phosphorylation in H157 cells occurred early at 2 h and was sustained for up to 16 h after

DMC treatment (Fig. 5A). Moreover, p-c-Jun levels were increased even by 5 μ M DMC (Fig. 5B).

To further address the involvement of JNK activation in the modulation of DR5 and c-FLIP by DMC, we examined the effects of DMC on DR5 and c-FLIP expression in the presence of the JNK-specific inhibitor SP600125 in H157 cells. SP600125 at the concentrations of 10 to 20 μ M inhibited the phosphorylation of c-Jun (Fig. 5C), confirming that SP600125 worked as expected in our cell system. However, SP600125 did not block DMC-induced DR5 up-regulation and did not prevent the down-regulation of c-FLIP by DMC (Fig. 5C). Together, our results suggest that JNK does not play a significant role in DMC-mediated modulation of either DR5 or c-FLIP in human NSCLC cells.

DMC Enhanced TRAIL-Induced Apoptosis through DR5 Induction and c-FLIP Down-Regulation. It is well known that both DR5 and c-FLIP are key components in the TRAIL/death receptor-mediated apoptotic pathway (Wang and El-Deiry, 2003; Kelley and Ashkenazi, 2004). We wanted to know whether DR5 induction and c-FLIP down-regulation were required for DMC-mediated enhancement of TRAIL-induced apoptosis. To demonstrate the involvement of DR5 induction in cooperative augmentation of apoptosis by the combination of DMC and TRAIL, we used DR5 siRNA to block DMC-induced DR5 up-regulation and then examined its impact on the induction of apoptosis by the combination of DMC and TRAIL. In control siRNA-transfected H460 cells, we detected basal levels of DR5, which were increased by DMC treatment as expected. In contrast, in DR5 siRNA-

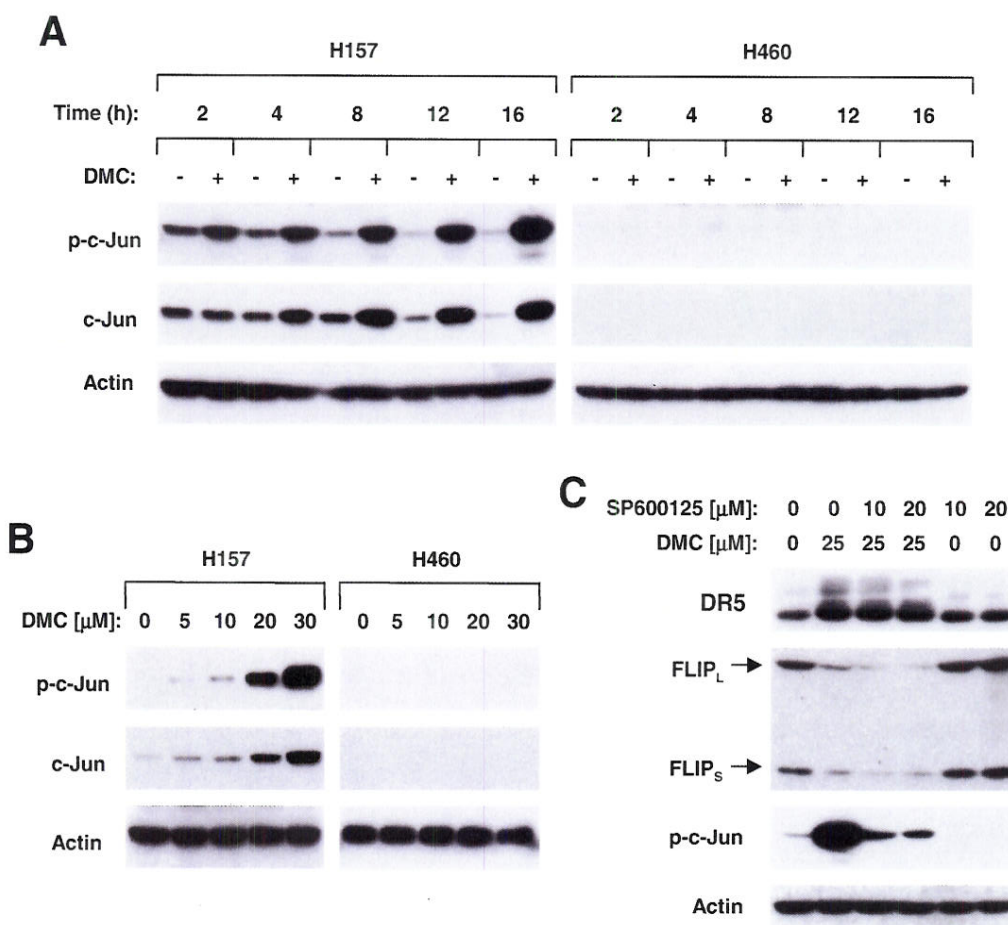


Fig. 5. Effects of DMC on JNK activation (A and B) by DMC in human NSCLC cells and the impact of JNK activation on DMC-induced DR5 expression and c-FLIP down-regulation (C). A and B, the indicated cell lines were treated with 25 μ M DMC for the given times (A) or the indicated concentrations of DMC for 16 h (B). C, H157 cells were treated with 25 μ M DMC alone, DMC plus the indicated concentrations of SP600125, and SP600125 alone for 8 h (B). Whole-cell protein lysates were then prepared from the aforementioned treatments for detection of the indicated proteins by Western blot analysis.

transfected cells, the basal levels of DR5 were substantially reduced and were not induced upon treatment with DMC (Fig. 6A). These results clearly indicate the successful knock-down of DR5 expression and blockade of DR5 induction. As a result, we detected cooperative induction of apoptosis by the combination of DMC and TRAIL in control siRNA-transfected cells but not in DR5 siRNA-transfected cells (Fig. 6B), indicating that DR5 up-regulation is required for the enhancement of TRAIL-induced apoptosis by DMC.

To determine the involvement of c-FLIP down-regulation in the induction of apoptosis by the DMC and TRAIL combination, we used a lentiviral expression system to enforce c-FLIP overexpression in NSCLC cells and then analyzed its effect on induction of apoptosis by the DMC and TRAIL combination. Taking advantage of a lentiviral expression system that achieves stable gene expression, we established H157 cell lines that stably expressed high levels of ectopic FLIP_L (i.e., H157-FLIP_L-5 and H157-FLIP_L-21). As controls, we also used H157-Lac Z-5, which expressed irrelevant Lac Z protein and H157-FLIP_L-16, which did not express ectopic FLIP_L albeit being infected with lentiviral FLIP_L (Fig. 7A). Treatment of H157-Lac Z-5 and H157-FLIP_L-16 with TRAIL, a death ligand known to activate the extrinsic death receptor-mediated apoptotic pathway, induced substantial cleavage of caspase-8, caspase-3, and PARP; however, these effects

were only minimally observed in H157-FLIP_L-5 and H157-FLIP_L-21 cells (Fig. 7A). Thus, enforced expression of ectopic FLIP_L indeed confers cell resistance to TRAIL-induced apoptosis.

By measuring cell survival, we found that the combination of DMC and TRAIL very effectively decreased cell survival in H157-Lac Z-5 and H157-FLIP_L-16 cell lines but had only a weak effect in H157-FLIP_L-5 and H157-FLIP_L-21 cells (Fig. 7B), indicating that enforced overexpression of ectopic FLIP_L confers cell resistance to the combination of DMC and TRAIL. By directly measuring apoptosis using annexin V staining after combination drug treatment, we detected much less apoptotic cell death in H157-FLIP_L-5 or H157-FLIP_L-21 cell lines than in H157-Lac Z-5 and H157-FLIP_L-16 control cell lines. Specifically, the combination of DMC and TRAIL caused 50% apoptosis in H157-Lac Z-5 cells and 97% apoptosis in H157-FLIP_L-16 control cells but only 34% apoptosis in H157-FLIP_L-5 and 11% apoptosis in H157-FLIP_L-21 cells (Fig. 7C). Thus, these results collectively show that down-regulation of c-FLIP contributes to DMC-mediated enhancement of TRAIL-induced apoptosis.

Discussion

In the present study, we demonstrated that DMC is more active than its parental compound celecoxib in decreasing the survival and inducing apoptosis of human NSCLC cells and that DMC sensitizes human NSCLC cells to TRAIL-induced apoptosis. Given that TRAIL is a potential cancer therapeutic protein and is being tested in phase I clinical trials, our finding on the enhancement of TRAIL-induced apoptosis by DMC is of clinical significance in terms of its potential application in combination with TRAIL in cancer treatment. Our previous work has shown that celecoxib enhances TRAIL-induced apoptosis in human NSCLC cells (Liu et al., 2004b). Thus, our current finding implies that DMC, which lacks COX-2 inhibitory activity, retains celecoxib's ability to enhance TRAIL-induced apoptosis and thereby indicates that the inhibition of COX-2 is not involved in these processes.

It is generally recognized that both the death receptor-mediated extrinsic and the mitochondrial intrinsic apoptotic pathways, respectively, are regulated by multiple proteins; the former involves proteins like DR5, DR4, and c-FLIP, and the latter includes Bcl-2 family members such as Bax, Bcl-2, Bcl-X_L, and inhibitor of apoptosis proteins such as survivin (Hengartner, 2000; Harada and Grant, 2003). Our results showed that DMC only decreased the levels of survivin but had minimal effect on the expression of Bax, Bcl-X_L, Bcl-2, and Bad (Supplemental Fig. S1). We noted that DMC also induced DR4 expression; however, this effect is cell line-dependent because DMC induced DR4 in H157 cells but not in H460 cells. Given the important roles of DR5 and c-FLIP in the regulation of the TRAIL-mediated extrinsic apoptotic pathway, and considering that both proteins are quickly and strongly modulated by DMC in all tested NSCLC cell lines, we believe that DR5 induction and c-FLIP down-regulation are two major key events that mediate cooperative induction of apoptosis by the combination of DMC and TRAIL. This view is further supported by our findings that blockade of DR5 induction by knocking down DR5 expression using DR5 siRNA or enforced overexpression of ectopic c-FLIP confers cell resistance to induction of apoptosis by the combination of

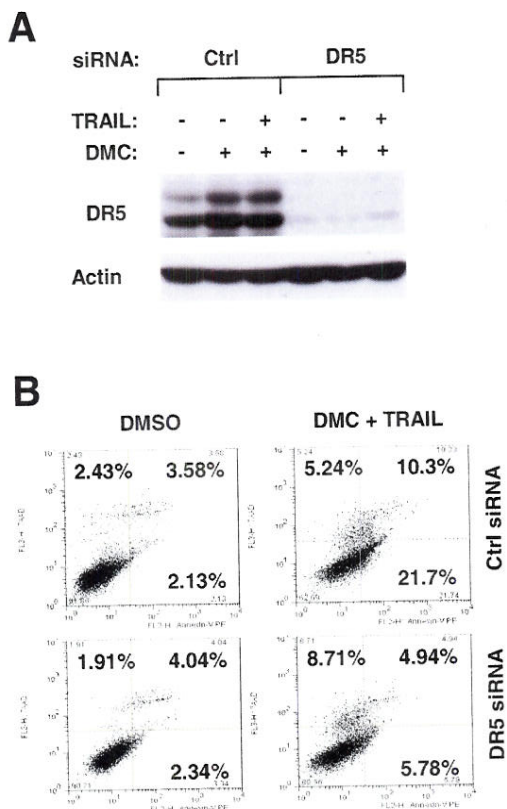


Fig. 6. Blockage of DR5 induction (A) attenuates the induction of apoptosis by DMC and TRAIL combination (B). H460 cells were cultured in a six-well plate and the next day were transfected with control (Ctrl) or DR5 siRNA. Forty-eight hours after transfection, cells were treated with 25 μ M DMC alone or DMC plus 10 ng/ml for 8 h and then subjected to preparation of whole-cell lysates for Western blot analysis (A) or harvested for detection of apoptosis by Annexin V staining (B). In Annexin V assay, the percentage of positive cells in the upper right and lower right quadrants were added to yield the total of apoptotic cells.

DMC and TRAIL. In this study, we do not exclude the possibility that DR4 and survivin modulation also contribute to DMC-mediated enhancement of TRAIL-induced apoptosis in certain cell lines (e.g., H157).

Our study further demonstrates that DMC down-regulates c-FLIP levels by facilitating ubiquitin/proteasome-mediated degradation of c-FLIP. This is evidenced by the prevention of

DMC-induced c-FLIP reduction using the proteasome inhibitor MG132 and by increased levels of ubiquitinated c-FLIP, which are detected in cells cotreated with MG132 and DMC using immunoprecipitation/Western blotting (Fig. 4). This mechanism is consistent with the one by which celecoxib decreases c-FLIP levels, as we have demonstrated previously (Liu et al., 2006), furthering the notion that DMC retains

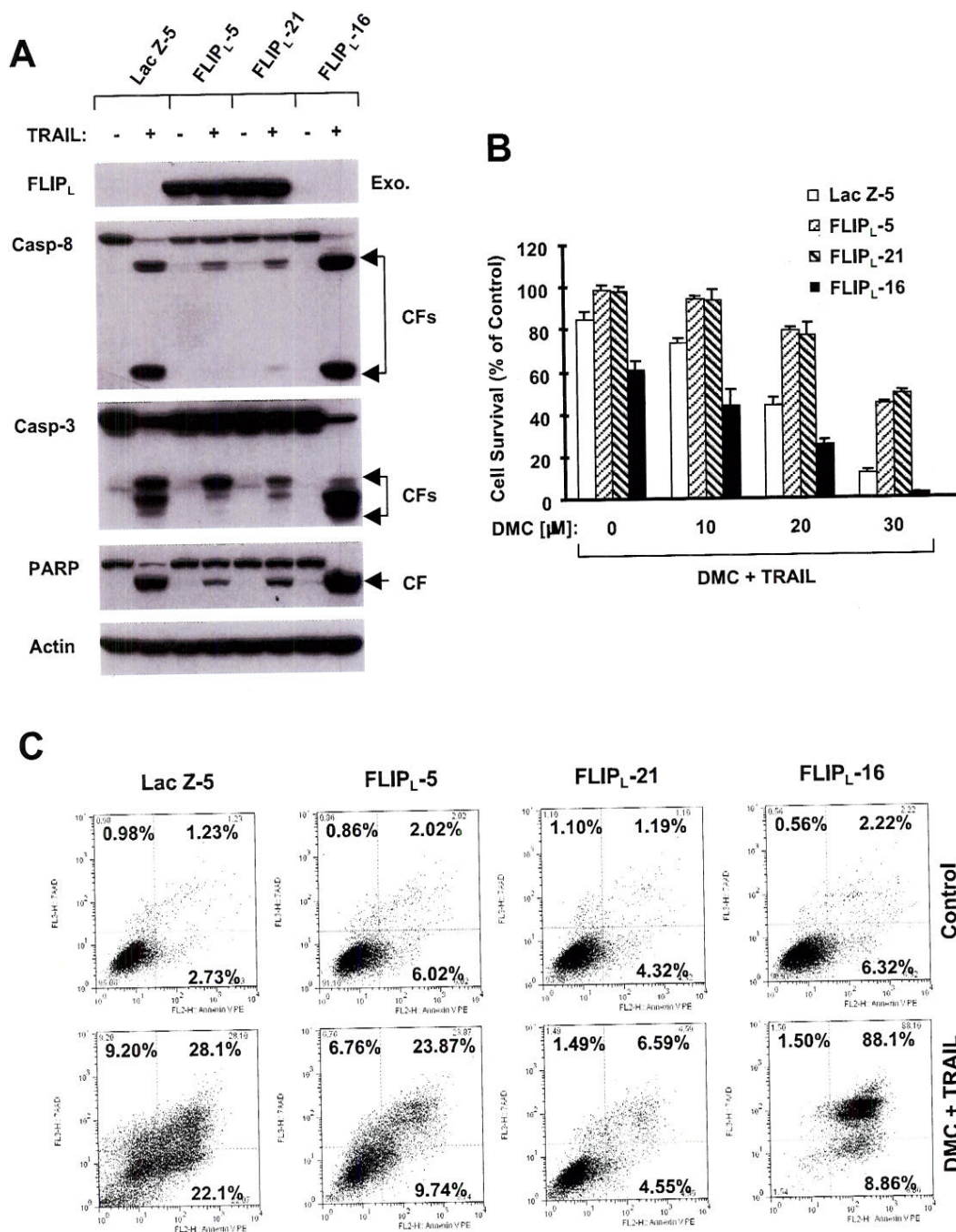


Fig. 7. Enforced expression of ectopic FLIP_L confers resistance to induction of apoptosis by TRAIL (A) or the combination of DMC and TRAIL (B and C). A, the indicated transfectants were exposed to 20 ng/ml TRAIL. After 4 h, the cells were harvested and subjected to preparation of whole-cell lysates for the detection of exogenous (Exo.) FLIP_L and caspase cleavage by Western blot analysis. B, the indicated transfectants were seeded in 96-well plates and treated with the indicated concentrations of DMC combined with 10 ng/ml TRAIL. After 24 h, the cells were subjected to the SRB assay for measurement of cell survival. Data are means of four replicate determinations. Bars, \pm S.D. C, the indicated transfectants were treated with DMSO and 25 μM DMC plus 10 ng/ml TRAIL for 24 h and then subjected to detection of apoptosis by Annexin V staining. In Annexin V assay, the percentage of positive cells in the upper right and lower right quadrants were added to yield the total of apoptotic cells.

some major biological activities similar to celecoxib, even at molecular levels. A recent study has shown that JNK activation is involved in regulating ubiquitin/proteasome-dependent degradation of FLIP_L (Chang et al., 2006). In our study, however, we did not detect a role of JNK in mediating DMC-induced c-FLIP degradation, and this conclusion is based on the following observations. First, DMC decreases both forms of c-FLIP (i.e., FLIP_L and FLIP_S), whereas JNK regulates the degradation of only FLIP_L (Chang et al., 2006). Second, DMC increases JNK activation in one cell line (i.e., H157) but not in another cell line (i.e., H460), in which c-FLIP was still down-regulated. Third, the JNK inhibitor SP600125 inhibited DMC-induced JNK activation but at the same time failed to prevent DMC-induced down-regulation of c-FLIP. It therefore seems that JNK does not play a major role in these DMC-induced processes.

We noted that FLIP_L levels were decreased by DMC at early times (e.g., 4 and 8 h) and then increased after prolonged treatment (e.g., 12 and 16 h), whereas FLIP_S levels were still reduced in H460 cells (Fig. 4A). The mechanism and biological significance of DMC-induced later increase in FLIP_L are currently unclear. It is possible that the later increase in FLIP_L may represent a survival mechanism for cells trying to escape DMC-induced cell death. Although DR5 can be induced through a JNK-dependent mechanism, as demonstrated in some studies (Higuchi et al., 2004; Zou et al., 2004), our results demonstrate that DMC induces DR5 expression in NSCLC cells independently of JNK activation because DMC did not induce JNK activation in H460 cells in which DR5 was induced and DMC could still induce DR5 expression in the presence of the JNK inhibitor SP600125 in H157 cells in which JNK was activated (Fig. 5).

DR5 is known to be regulated by p53 (Wu et al., 1997), nuclear factor- κ B (Shetty et al., 2005), and CHOP (Yamaguchi and Wang, 2004; Yoshida et al., 2005). Because DMC induced DR5 expression in H157 cells carrying mutant p53, it is likely that DMC induced a p53-independent DR5 expression. In an effort to reveal the mechanism by which DMC induces DR5 expression, we found that CHOP was induced by DMC and accompanied with DR5 up-regulation. By analyzing the DR5 promoter, we found that the presence of the CHOP binding site is required for transactivation of the DR5 promoter by DMC. ChIP assay demonstrated that DMC also enhanced the binding of CHOP to DR5 promoter. Moreover, blockade of CHOP induction by silencing CHOP expression with CHOP siRNA abolished DMC's ability to induce DR5 expression. Thus, we conclude that DMC induces a CHOP-dependent DR5 up-regulation. Because CHOP is a typical protein associated with endoplasmic reticulum (ER) stress-induced apoptosis (Oyadomari and Mori, 2004), it is possible that DMC-induced up-regulation of CHOP and DR5 is caused by ER stress. Indeed, a recent study has demonstrated that DMC indeed induces ER stress of cancer cells in both cell culture and xenograft models in vivo, including CHOP up-regulation (Pyrko et al., 2007). Future studies need to demonstrate how DMC increases CHOP expression and whether nuclear factor- κ B is activated and involved in DMC-induced DR5 expression.

It has been documented in the literature that activation of the TRAIL apoptotic pathway such as up-regulation of DR5 contributes to the induction of apoptosis by certain anticancer agents, including celecoxib (Huang et al., 2001; LaVallee

et al., 2003; Wagner et al., 2003; Liu et al., 2004b; Kabore et al., 2006). The current work does not address whether DR5 up-regulation participated in the induction of apoptosis by DMC only, although we assume that it may contribute to DMC-induced apoptosis because celecoxib induces apoptosis requiring DR5 up-regulation. The ongoing work is to test whether DR5 induction is indeed involved in DMC-induced apoptosis.

In summary, the present study has shown for the first time that DMC, a celecoxib derivative lacking COX-2 inhibitory activity, induces CHOP-mediated DR5 up-regulation and ubiquitin/proteasome-mediated down-regulation of c-FLIP, leading to the enhancement of TRAIL-induced apoptosis in human NSCLC cells. Our results clearly indicate that DMC possesses more potent anticancer activity than celecoxib, although the underlying mechanisms seem to be quite similar. Given the concern over cardiovascular side effects of celecoxib, which is associated with its anti-COX-2 activity and is also noted with other COX-2 inhibitors (Dogné et al., 2006; Marwali and Mehta, 2006), DMC might be a better candidate or alternative to celecoxib for cancer chemoprevention and therapy.

Acknowledgments

We are grateful to H.-G. Wang (University of South Florida College of Medicine, Tampa, FL) for providing DR5 reporter constructs with a wild-type and mutant CHOP binding site, respectively, and H. A. Elrod in our lab for editing of the manuscript.

References

- Abdelrahim M, Newman K, Vanderlaag K, Samudio I, and Safe S (2006) 3,3'-Diindolylmethane (DIM) and its derivatives induce apoptosis in pancreatic cancer cells through endoplasmic reticulum stress-dependent upregulation of DR5. *Carcinogenesis* 27:717-728.
- Chang L, Kamata H, Solinas G, Luo JL, Maeda S, Venuprasad K, Liu YC, and Karin M (2006) The E3 ubiquitin ligase itch couples JNK activation to TNF α -induced cell death by inducing c-FLIP(L) turnover. *Cell* 124:601-613.
- Chen C, Sun X, Ran Q, Wilkinson KD, Murphy TJ, Simons JW, and Dong JT (2005) Ubiquitin-proteasome degradation of KLF5 transcription factor in cancer and untransformed epithelial cells. *Oncogene* 24:3319-3327.
- Davies NM, McLachlan AJ, Day RO, and Williams KM (2000) Clinical pharmacokinetics and pharmacodynamics of celecoxib: a selective cyclo-oxygenase-2 inhibitor. *Clin Pharmacokinet* 38:225-242.
- Dogné JM, Hanson J, Supuran C, and Pratico D (2006) Coxibs and cardiovascular side-effects: from light to shadow. *Curr Pharm Des* 12:971-975.
- Grösch S, Maier TJ, Schiffmann S, and Geisslinger G (2006) Cyclooxygenase-2 (COX-2)-independent anticarcinogenic effects of selective COX-2 inhibitors. *J Natl Cancer Inst* 98:736-747.
- Harada H and Grant S (2003) Apoptosis regulators. *Rev Clin Exp Hematol* 7:117-138.
- Hengartner MO (2000) The biochemistry of apoptosis. *Nature* 407:770-776.
- Higuchi H, Grambihler A, Canbay A, Bronk SF, and Gores GJ (2004) Bile acids up-regulate death receptor 5/TRAIL-receptor 2 expression via a c-Jun N-terminal kinase-dependent pathway involving Sp1. *J Biol Chem* 279:51-60.
- Huang Y, He Q, Hillman MJ, Rong R, and Sheikh MS (2001) Sulindac sulfide-induced apoptosis involves death receptor 5 and the caspase 8-dependent pathway in human colon and prostate cancer cells. *Cancer Res* 61:6918-6924.
- Kabore AF, Sun J, Hu X, McCreary K, Johnston JB, and Gibson SB (2006) The TRAIL apoptotic pathway mediates proteasome inhibitor induced apoptosis in primary chronic lymphocytic leukemia cells. *Apoptosis* 11:1175-1193.
- Kardosh A, Wang W, Uddin J, Petasis NA, Hofman FM, Chen TC, and Schönthal AH (2005) Dimethyl-celecoxib (DMC), a derivative of celecoxib that lacks cyclooxygenase-2-inhibitory function, potentially mimics the anti-tumor effects of celecoxib on Burkitt's lymphoma in vitro and in vivo. *Cancer Biol Ther* 4:571-582.
- Kelley SK and Ashkenazi A (2004) Targeting death receptors in cancer with Apo2L/TRAIL. *Curr Opin Pharmacol* 4:333-339.
- Kim Y, Suh N, Sporn M, and Reed JC (2002) An inducible pathway for degradation of FLIP protein sensitizes tumor cells to TRAIL-induced apoptosis. *J Biol Chem* 277:22320-22329.
- Koki AT and Masferrer JL (2002) Celecoxib: a specific COX-2 inhibitor with anticancer properties. *Cancer Control* 9 (2 Suppl):28-35.
- Krueger A, Baumann S, Krammer PH, and Kirchhoff S (2001) FLICE-inhibitory proteins: regulators of death receptor-mediated apoptosis. *Mol Cell Biol* 21:8247-8254.
- LaVallee TM, Zhan XH, Johnson MS, Herbst C, Swartz G, Williams MS, Hembrugh WA, Green SJ, and Pribluda VS (2003) 2-Methoxyestradiol up-regulates

- death receptor 5 and induces apoptosis through activation of the extrinsic pathway. *Cancer Res* **63**:468–475.
- Liu X, Yue P, Khuri FR, and Sun SY (2004a) p53 upregulates death receptor 4 expression through an intronic p53 binding site. *Cancer Res* **64**:5078–5083.
- Liu X, Yue P, Schönthal AH, Khuri FR, and Sun SY (2006) Cellular FLICE-inhibitory protein down-regulation contributes to celecoxib-induced apoptosis in human lung cancer cells. *Cancer Res* **66**:11115–11119.
- Liu X, Yue P, Zhou Z, Khuri FR, and Sun SY (2004b) Death receptor regulation and celecoxib-induced apoptosis in human lung cancer cells. *J Natl Cancer Inst* **96**:1769–1780.
- Marwali MR and Mehta JL (2006) COX-2 inhibitors and cardiovascular risk. Inferences based on biology and clinical studies. *Thromb Haemost* **96**:401–406.
- Oyadomari S and Mori M (2004) Roles of CHOP/GADD153 in endoplasmic reticulum stress. *Cell Death Differ* **11**:381–389.
- Pfahl M, Tzukerman M, Zhang XK, Lehmann JM, Hermann T, Wills KN, and Graupner G (1990) Nuclear retinoic acid receptors: cloning, analysis, and function. *Methods Enzymol* **189**:256–270.
- Pyrko P, Kardosh A, Liu YT, Soriano N, Xiong W, Chow RH, Uddin J, Petasis NA, Mircheff AK, Farley RA, et al. (2007) Calcium-activated endoplasmic reticulum stress as a major component of tumor cell death induced by 2,5-dimethyl-celecoxib, a non-coxib analogue of celecoxib. *Mol Cancer Ther* **6**:1262–1275.
- Pyrko P, Soriano N, Kardosh A, Liu YT, Uddin J, Petasis NA, Hofman FM, Chen CS, Chen TC, and Schönthal AH (2006) Downregulation of survivin expression and concomitant induction of apoptosis by celecoxib and its non-cyclooxygenase-2-inhibitory analog, dimethyl-celecoxib (DMC), in tumor cells in vitro and in vivo. *Mol Cancer* **5**:19.
- Schönthal AH (2006) Antitumor properties of dimethyl-celecoxib, a derivative of celecoxib that does not inhibit cyclooxygenase-2: implications for glioma therapy. *Neurosurg Focus* **20**:E21.
- Shetty S, Graham BA, Brown JG, Hu X, Vegh-Yarema N, Harding G, Paul JT, and Gibson SB (2005) Transcription factor NF-kappaB differentially regulates death receptor 5 expression involving histone deacetylase 1. *Mol Cell Biol* **25**:5404–5416.
- Sun SY (2005) Chemopreventive agent-induced modulation of death receptors. *Apoptosis* **10**:1203–1210.
- Sun SY, Yue P, Dawson MI, Shroot B, Michel S, Lamph WW, Heyman RA, Teng M, Chandraratna RA, Shudo K, et al. (1997) Differential effects of synthetic nuclear retinoid receptor-selective retinoids on the growth of human non-small cell lung carcinoma cells. *Cancer Res* **57**:4931–4939.
- Sun SY, Yue P, Wu GS, El-Deiry WS, Shroot B, Hong WK, and Lotan R (1999) Mechanisms of apoptosis induced by the synthetic retinoid CD437 in human non-small cell lung carcinoma cells. *Oncogene* **18**:2357–2365.
- Wagner KW, King F, Nomoto K, Knee DA, Hampton G, Nasoff M, and Devereaux QL (2003) Activation and suppression of the TRAIL death-receptor pathway in chemotherapy sensitive and resistant follicular lymphoma cells. *Cancer Biol Ther* **2**:534–540.
- Wang S and El-Deiry WS (2003) TRAIL and apoptosis induction by TNF-family death receptors. *Oncogene* **22**:8628–8633.
- Wu GS, Burns TF, McDonald ER 3rd, Jiang W, Meng R, Krantz ID, Kao G, Gan DD, Zhou JY, Muschel R, et al. (1997) KILLER/DR5 is a DNA damage-inducible p53-regulated death receptor gene. *Nat Genet* **17**:141–143.
- Yamaguchi H and Wang HG (2004) CHOP is involved in endoplasmic reticulum stress-induced apoptosis by enhancing DR5 expression in human carcinoma cells. *J Biol Chem* **279**:45495–45502.
- Yoshida T, Shiraishi T, Nakata S, Horinaka M, Wakada M, Mizutani Y, Miki T, and Sakai T (2005) Proteasome inhibitor MG132 induces death receptor 5 through CCAAT/enhancer-binding protein homologous protein. *Cancer Res* **65**:5662–5667.
- Zhu J, Huang JW, Tseng PH, Yang YT, Fowble J, Shiau CW, Shaw YJ, Kulp SK, and Chen CS (2004) From the cyclooxygenase-2 inhibitor celecoxib to a novel class of 3-phosphoinositide-dependent protein kinase-1 inhibitors. *Cancer Res* **64**:4309–4318.
- Zhu J, Song X, Lin HP, Young DC, Yan S, Marquez VE, and Chen CS (2002) Using cyclooxygenase-2 inhibitors as molecular platforms to develop a new class of apoptosis-inducing agents. *J Natl Cancer Inst* **94**:1745–1757.
- Zou W, Liu X, Yue P, Khuri FR, and Sun SY (2007) PPARgamma ligands enhance TRAIL-induced apoptosis through DR5 upregulation and c-FLIP down-regulation in human lung cancer cells. *Cancer Biol Ther* **6**:99–106.
- Zou W, Liu X, Yue P, Zhou Z, Sporn MB, Lotan R, Khuri FR, and Sun SY (2004) c-Jun NH2-terminal kinase-mediated up-regulation of death receptor 5 contributes to induction of apoptosis by the novel synthetic triterpenoid methyl-2-cyano-3,12-dioxoleana-1,9-dien-28-oate in human lung cancer cells. *Cancer Res* **64**:7570–7578.

Address correspondence to: Dr. Shi-Yong Sun, Winship Cancer Institute, Emory University School of Medicine, 1365-C Clifton Road, Clinical Building C, Suite C3088, Atlanta, GA 30322. E-mail: shi-yong.sun@emoryhealthcare.org

The alkylphospholipid perifosine induces apoptosis of human lung cancer cells requiring inhibition of Akt and activation of the extrinsic apoptotic pathway

Heath A. Elrod, Yi-Dan Lin, Ping Yue, Xuerong Wang, Sagar Lonial, Fadlo R. Khuri, and Shi-Yong Sun

Department of Hematology and Oncology, Winship Cancer Institute, Emory University School of Medicine, Atlanta, Georgia

Abstract

The Akt inhibitor, perifosine, is an alkylphospholipid exhibiting antitumor properties and is currently in phase II clinical trials for various types of cancer. The mechanisms by which perifosine exerts its antitumor effects, including the induction of apoptosis, are not well understood. The current study focused on the effects of perifosine on the induction of apoptosis and its underlying mechanisms in human non-small cell lung cancer (NSCLC) cells. Perifosine, at clinically achievable concentration ranges of 10 to 15 $\mu\text{mol/L}$, effectively inhibited the growth and induced apoptosis of NSCLC cells. Perifosine inhibited Akt phosphorylation and reduced the levels of total Akt. Importantly, enforced activation of Akt attenuated perifosine-induced apoptosis. These results indicate that Akt inhibition is necessary for perifosine-induced apoptosis. Despite the activation of both caspase-8 and caspase-9, perifosine strikingly induced the expression of the tumor necrosis factor-related apoptosis-inducing ligand (TRAIL) receptor, death receptor 5, and down-regulated cellular FLICE-inhibitory protein (c-FLIP), an endogenous inhibitor of the extrinsic apoptotic pathway, with limited modulatory effects on the expression of other genes including Bcl-2, Bcl-X_L, PUMA, and survivin. Silencing of either caspase-8 or death receptor 5 attenu-

ated perifosine-induced apoptosis. Consistently, further down-regulation of c-FLIP expression with c-FLIP small interfering RNA sensitized cells to perifosine-induced apoptosis, whereas enforced overexpression of ectopic c-FLIP conferred resistance to perifosine. Collectively, these data indicate that activation of the extrinsic apoptotic pathway plays a critical role in perifosine-induced apoptosis. Moreover, perifosine cooperates with TRAIL to enhance the induction of apoptosis in human NSCLC cells, thus warranting future *in vivo* and clinical evaluation of perifosine in combination with TRAIL in the treatment of NSCLC. [Mol Cancer Ther 2007;6(7):2029–38]

Introduction

Alkylphospholipids are a class of antitumor agents which target the cell membrane and induce apoptosis (1, 2). Perifosine, the first orally bioavailable alkylphospholipid, has shown antitumor activity in preclinical models and is currently in phase II clinical trials (1, 3). The mechanisms by which perifosine exerts its antitumor effect remain unclear, although it seems to inhibit Akt (2, 4) and mitogen-activated protein kinase activation (5), whereas inducing c-Jun-NH₂-kinase (JNK) activation (5). Perifosine has also been shown to induce p21 expression leading to cell cycle arrest (6). In addition, perifosine, in combination with other antitumor agents such as the PDK1 inhibitor, UCN-01 (7), histone deacetylase inhibitors (8), and the chemotherapeutic agent etoposide (9), show synergistic antitumor effects.

It is well known that there are two major apoptotic pathways used by mammalian cells to undergo apoptosis. One pathway involves signals transduced through death receptors known as the extrinsic apoptotic pathway; the second pathway relies on signals from the mitochondria called the intrinsic apoptotic pathway. Both pathways involve the activation of a set of caspases, which in turn, cleave cellular substrates and result in the characteristic morphologic and biochemical changes constituting the process of apoptosis (10, 11). The extrinsic pathway is characterized by the oligomerization of cell surface death receptors and activation of caspase-8, whereas the intrinsic pathway involves in the disruption of mitochondrial membranes, the release of cytochrome *c*, and the activation of caspase-9. Through caspase-8-mediated cleavage or truncation of Bid, the extrinsic death receptor apoptotic pathway is linked to the intrinsic mitochondrial apoptotic pathway (10, 11).

Molecules that can block the extrinsic apoptotic pathway include cellular FLICE-inhibitory protein (c-FLIP). c-FLIP prevents caspase-8 activation by death receptors. There are two major isoforms of c-FLIP: FLIP_L consists of two

Received 1/4/07; revised 5/2/07; accepted 5/25/07.

Grant support: The Georgia Cancer Coalition Distinguished Cancer Scholar award (S.-Y. Sun), Department of Defense grants W81XWH-04-1-0142-VITAL (S.-Y. Sun for Project 4), DAMD17-01-1-0689-BESCT (F.R. Khuri), and an American Cancer Society Fellowship award (H.A. Elrod).

The costs of publication of this article were defrayed in part by the payment of page charges. This article must therefore be hereby marked *advertisement* in accordance with 18 U.S.C. Section 1734 solely to indicate this fact.

Note: H.A. Elrod and Y.-D. Lin contributed equally to this work and share equal first authorship. F.R. Khuri and S.-Y. Sun are Georgia Cancer Coalition Distinguished Cancer Scholars. H.A. Elrod is a recipient of an American Cancer Society Fellowship.

Requests for reprints: Shi-Yong Sun, Winship Cancer Institute, Emory University School of Medicine, 1365-C Clifton Road Northeast, C3088, Atlanta, GA 30322. Phone: 404-778-2170; Fax: 404-778-5520. E-mail: shi-yong.sun@emoryhealthcare.org

Copyright © 2007 American Association for Cancer Research.

doi:10.1158/1535-7163.MCT-07-0004

NH₂-terminal death effector domains and a COOH-terminal caspase homology domain devoid of enzymatic activity, whereas FLIP_S is only composed of the NH₂-terminal death effector domains and a short COOH-terminal stretch of amino acids not found in FLIP_L. It has been shown that c-FLIP expression correlates with resistance against death receptor-induced apoptosis in a variety of cancer cells, and c-FLIP-transfected tumor cell lines develop more aggressive tumors *in vivo* (12, 13). In addition, many studies have shown that down-regulation of c-FLIP is sufficient to confer sensitivity against death receptor-induced apoptosis, whereas c-FLIP expression is associated with chemoresistance and down-regulation of c-FLIP using antisense oligonucleotides or small interfering RNAs (siRNA) sensitizes cells to chemotherapeutic agent-induced apoptosis (12–14).

Akt is known to be critical for tumor cell survival. One of the ways that Akt promotes cell survival is to inhibit apoptosis through its ability to phosphorylate several proapoptotic proteins such as Bad, which are involved in the regulation of the intrinsic apoptotic pathway (15). Moreover, Akt also inhibits the extrinsic death receptor-mediated apoptotic pathway through up-regulation of c-FLIP expression (16, 17). Thus, Akt negatively regulates apoptosis by suppressing both the mitochondria- and death receptor-mediated pathways.

The induction of apoptosis by perifosine has been observed in several cancer cell lines (3, 8, 9, 18). However, this effect has not been determined in non-small cell lung cancer (NSCLC) cells. Moreover, the mechanisms by which perifosine induces apoptosis is generally unknown. In this study, we examined the effects of perifosine on apoptosis in human NSCLC cells and its modulation on different apoptotic molecules in an attempt to understand its mechanisms of action. Our data show that perifosine induces apoptosis, inhibits Akt activation, up-regulates death receptor 5 (DR5) expression, and reduces c-FLIP levels in NSCLC cells. In addition, perifosine in combination with tumor necrosis factor-related apoptosis-inducing ligand (TRAIL) augments the induction of apoptosis.

Materials and Methods

Reagents

Perifosine was supplied by Keryx Biopharmaceuticals, Inc. This agent was dissolved in PBS and stored at –20°C. Stock solution was diluted to the appropriate concentrations with growth medium immediately before use. Human recombinant TRAIL was purchased from Pepro-Tech, Inc.

Cell Lines and Cell Culture

The human NSCLC cell lines used in this study were described previously (19). H157 cell lines that stably express ectopic Lac Z (Lac Z-5) and FLIP_L (FLIP_L-6), respectively, and A549 cell lines that stably express ectopic Lac Z (Lac Z-9) and FLIP_L (FLIP_L-2), respectively, were described previously (20, 21). These cell lines were grown in a monolayer culture in RPMI 1640 supplemented with

glutamine and 5% fetal bovine serum at 37°C in a humidified atmosphere consisting of 5% CO₂ and 95% air.

Cell Growth Assay

Cells were cultured in 96-well cell culture plates and treated the next day with the agents indicated. Viable cell number was estimated using the sulforhodamine B assay, as previously described (19).

Western Blot Analysis

Preparation of whole cell protein lysates and Western blot analysis were described previously (22, 23). Mouse anti-caspase-3 monoclonal antibody was purchased from Imgenex. Rabbit polyclonal antibodies against PTEN, Akt, phospho (p)-Akt (Ser⁴⁷³), phospho (p)-FKHR (Ser²⁵⁶), phospho (p)-GSK3β (Ser⁹), c-Jun, phospho (p)-c-Jun (Ser⁶³), p44/42, phospho (p)-p44/42 (Thr²⁰²/Tyr²⁰⁴), survivin, caspase-8, caspase-9, poly(ADP-ribose) polymerase (PARP) were purchased from Cell Signaling Technology. Rabbit polyclonal anti-DR5 antibody was purchased from ProSci, Inc. Mouse monoclonal anti-FLIP antibody (NF6) was purchased from Alexis Biochemicals. Rabbit anti-G3PDH polyclonal antibody and mouse anti-Bax monoclonal antibody were purchased from Trevigen. Rabbit anti-Puma polyclonal antibody was purchased from EMD Biosciences, Inc. Mouse anti-Bcl-2 and rabbit anti-Bcl-X_L antibodies were purchased from Santa Cruz Biotechnology, Inc. Rabbit anti-β-actin polyclonal antibody was purchased from Sigma Chemicals. Secondary antibodies, goat anti-mouse and goat anti-rabbit horseradish peroxidase conjugates, were purchased from Bio-Rad.

Adenoviral Infection

Adenovirus harboring an empty vector (Ad-CMV) or a constitutively activated form of Akt (myristoylated Akt; Ad-myr-Akt) were provided by Lily Yang (Department of Surgery, Emory University School of Medicine, Atlanta, GA). The procedure for adenoviral infection of cancer cells was described previously (24).

Gene Silencing Using siRNA

Silencing of caspase-8, DR5, c-FLIP, and PTEN were achieved by transfecting siRNA using RNAifect transfection reagent (Qiagen) following the instructions of the manufacturer. Control, caspase-8, and DR5 siRNAs were described previously (22). These siRNAs and c-FLIP siRNA targeting the sequence 5'-AATTCTCCGAACGTGTCACGT-3' (14) were all synthesized from Qiagen. PTEN siRNA was purchased from Cell Signaling. Cells were plated in 6- or 24-well cell culture plates and transfected with the given siRNAs the next day. After 24 h, the cells were trypsinized and replated in new plates, and on the second day, treated with perifosine as indicated. Gene silencing effects were evaluated by Western blot as described above after the indicated times of treatment.

Apoptosis Assays

Apoptosis was detected either by analysis of caspase activation using Western blot analysis as described above or by Annexin V staining using Annexin V-PE apoptosis detection kit (BD Bioscience) following the instructions of the manufacturer, and analyzed by flow cytometry using FACSscan (Becton Dickinson). In addition, we measured

the amounts of cytoplasmic histone-associated DNA fragments (mononucleosome and oligonucleosomes) formed during apoptosis using a Cell Death Detection ELISA^{Plus} kit (Roche Molecular Biochemicals) according to the instructions of the manufacturer.

Results

Effects of Perifosine on Cell Survival and Apoptosis in NSCLC Cells

The effects of perifosine on cell survival were examined in a panel of NSCLC cell lines (Fig. 1A). For the majority of the cell lines tested, there was a dose-dependent decrease in cell survival. The H460 cell line was the most sensitive to perifosine, showing an IC_{50} value of $\sim 1 \mu\text{mol/L}$. The H226 cell line was the most resistant to perifosine, in which perifosine at $20 \mu\text{mol/L}$ decreased cell survival by $<20\%$. Most of the tested cell lines exhibited moderate response to perifosine with IC_{50} s ranging from 8 to $15 \mu\text{mol/L}$ (Fig. 1A), which are within the clinically achievable and safe peak plasma concentrations of 12 to $15 \mu\text{mol/L}$ (25, 26). The *p53* and *PTEN* mutation status in the NSCLC cell lines tested did not correlate with sensitivity to perifosine, suggesting that perifosine inhibits cell growth independently of *p53* and *PTEN* mutation status (Fig. 1A). In addition, we examined the protein expression levels of *PTEN*, total Akt,

and p-Akt in the cell lines tested. It seemed that those cell lines (e.g., H460 and H358) with low levels of p-Akt and high levels of *PTEN* were the most sensitive to perifosine (Fig. 1B).

We further examined the effects of perifosine on apoptosis in NSCLC cell lines. As shown in Fig. 2A, perifosine induced apoptosis in H460 and A549 cells as indicated by Annexin V-positive staining. At concentrations of $10 \mu\text{mol/L}$, perifosine induced cell death in $\sim 50\%$ of H460 cells, whereas apoptosis was induced in 23% and 33% of the A549 cells after treatment with 10 and $15 \mu\text{mol/L}$ of perifosine, respectively, suggesting that the H460 cells were more sensitive to perifosine-induced apoptosis. The H157 cells were the least sensitive to perifosine-induced apoptosis with only 10% of H157 cells undergoing apoptosis after treatment with $15 \mu\text{mol/L}$ of perifosine. We found that perifosine at concentrations ranging from 2.5 to $10 \mu\text{mol/L}$ induced cleavage of caspase-8, caspase-9, caspase-3, and PARP in H460 cells, whereas it induced partial cleavage of the caspases and PARP only at $10 \mu\text{mol/L}$ in A549 cells (Fig. 2B). In H157 cells treated with perifosine (up to $10 \mu\text{mol/L}$), we failed to detect cleaved bands of the caspases and PARP (Fig. 2B). Because perifosine is effective in decreasing cell number in H157 cells (Fig. 1), we further examined cell cycle alteration in H157 cells after exposure to perifosine and detected 17.9%, 35.8%, and 42.4% G₂-M cells in cells treated with PBS, $10 \mu\text{mol/L}$ of perifosine, and $15 \mu\text{mol/L}$ of perifosine, respectively, after a 48 h treatment, indicating that perifosine primarily decreases cell numbers in H157 cells via induction of cell cycle arrest. In the following studies, we focused on revealing the mechanisms underlying perifosine-induced apoptosis.

Effects of Perifosine on the Phosphorylation of Akt, JNK, and ERK

Perifosine has been shown to modulate Akt as well as other signaling pathways (6, 18, 27). We therefore examined whether perifosine modulated similar signal transduction pathways in human NSCLC cells. In examining Akt phosphorylation, we observed that both H460 and A549 cells have very low basal levels of p-Akt, whereas H157 cells have much higher basal levels of p-Akt. When comparing the apoptosis results presented in Fig. 2A, it seems that low basal levels of p-Akt correlated with high sensitivity to perifosine-induced apoptosis. These cell lines exhibited a concentration-dependent decrease in p-Akt levels when exposed to perifosine (p-Akt levels were only detectable in H460 cells after a very long exposure). Interestingly, perifosine also decreased the levels of total Akt in the tested cell lines (Fig. 3A) and the degree of Akt down-regulation also seemed to correlate with cell sensitivity to perifosine-induced apoptosis. In H460 cells, decreases in both Akt and p-Akt levels occurred at 3 h after treatment with perifosine (Fig. 3B), indicating that Akt down-regulation is an early event. In H157 cells, Akt levels were only slightly decreased, whereas p-Akt levels were substantially (by $2.5 \mu\text{mol/L}$ of perifosine) and rapidly (3 h posttreatment) reduced upon perifosine treatment

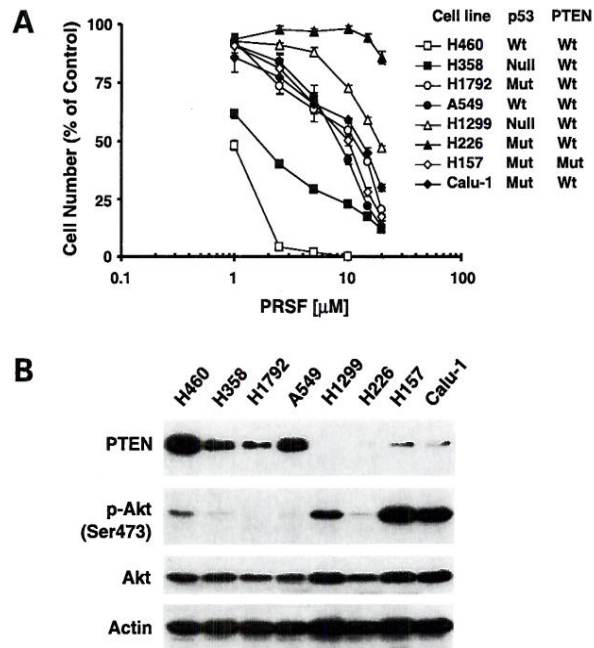


Figure 1. Effects of perifosine on the survival of NSCLC cells (A) and their association with basal levels of p-Akt (B). A, cell lines treated with different concentrations of perifosine (PRSF) ranging from 1 to $20 \mu\text{mol/L}$. After 3 d, the cells were subjected to sulforhodamine B assay for estimating the viable cells. In addition, the *p53* status and *PTEN* status of the cell lines were also indicated. Points, means of four replicate determinations; bars, SD. B, cell lines with similar cell densities were harvested for the preparation of whole cell protein lysates. The indicated proteins were analyzed by Western blot analysis.

(Fig. 3A and B). These results suggest that the perifosine-mediated decrease in p-Akt levels could be due to either Akt protein down-regulation or upstream signaling suppression, depending on the cell lines used. To our knowledge, this is the first demonstration that perifosine down-regulates the levels of total Akt in human cancer cells. We also detected a decrease in the levels of p-FKHR and p-GSK3 β , two well-known substrates of Akt (Fig. 3B), furthering the notion that perifosine inhibits Akt signaling in NSCLC cells.

In examining other signal transduction pathways, we observed the basal levels of p-c-Jun were very low in the tested NSCLC cells and were only slightly increased by perifosine in H157 cells, indicating that perifosine-induced JNK activation was a cell line-dependent event. Perifosine did not alter the levels of p42/44, but did decrease the levels of p-p42/44 in all three cell lines tested (Fig. 3A). These data indicate that perifosine down-regulates the ERK (or p42/44) signaling pathway in NSCLC cells.

Enforced Akt Activation Attenuates Perifosine-Induced Apoptosis

To decipher the role of Akt inhibition in perifosine-induced apoptosis, we artificially activated Akt in H460 cells by infecting the cells with adenoviruses carrying a

myr-Akt gene that codes a constitutively activated form of Akt, and then examined the response of these cells to perifosine treatment. Using Western blot analysis, we detected high levels of myr-Akt, p-Akt, and p-GSK3 β in cells infected with Ad-myr-Akt (Fig. 3C). In addition, infection of cells with Ad-myr-Akt also elevated the levels of c-FLIP, which has been shown to be regulated by Akt. (refs. 16, 17; Fig. 3C). In Ad-CMV-infected control cells, treatment with perifosine caused 37% apoptotic cell death (9% in PBS-treated cells) plus 15.2% necrotic cell death. However, we detected only 16% apoptosis (~12% in PBS-treated cells) and <2% necrosis in cells infected with Ad-myr-Akt after treatment with perifosine (Fig. 3D). These results clearly show that enforced Akt activation restores cell resistance to perifosine-induced apoptosis, thus indicating that Akt inhibition is necessary in mediating perifosine-induced apoptosis.

Given that there is an inverse relationship between PTEN expression and p-Akt levels (Fig. 1B), we further determined whether down-regulation of PTEN affects p-Akt levels and cell sensitivity to perifosine. Knockdown of PTEN using PTEN siRNA in H460 cells, which is the most sensitive cell line to perifosine and have the highest levels of PTEN (Fig. 1), increased basal levels of p-Akt. However,

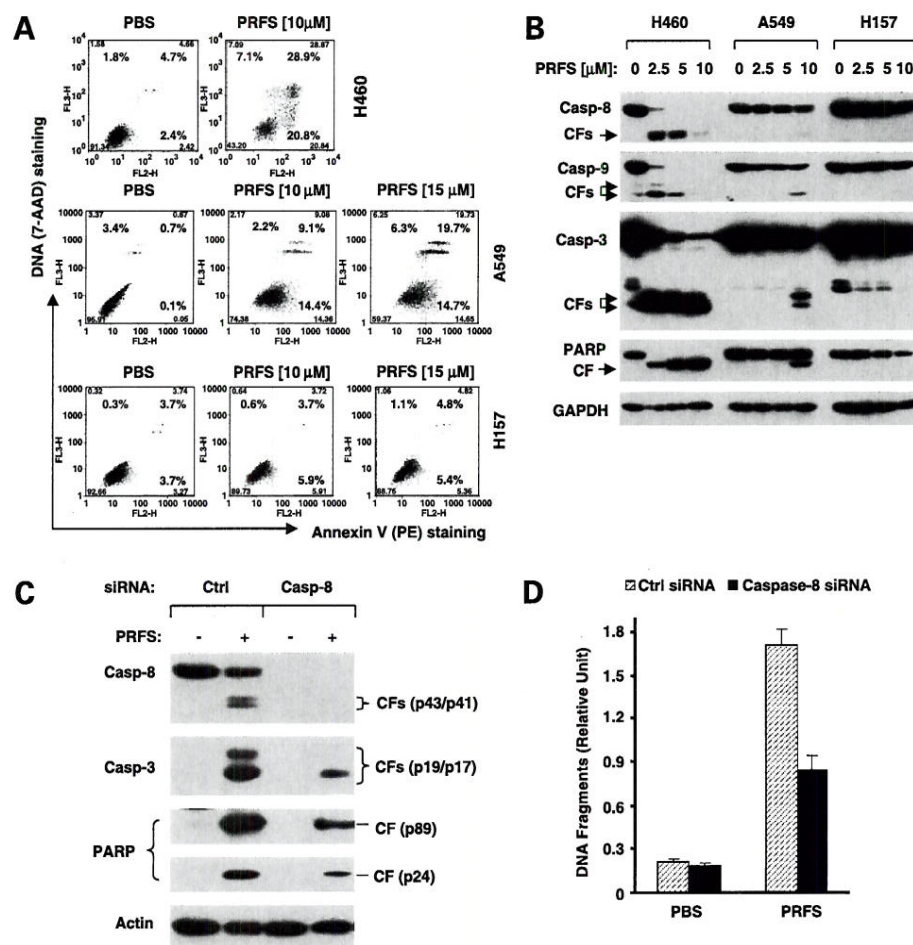
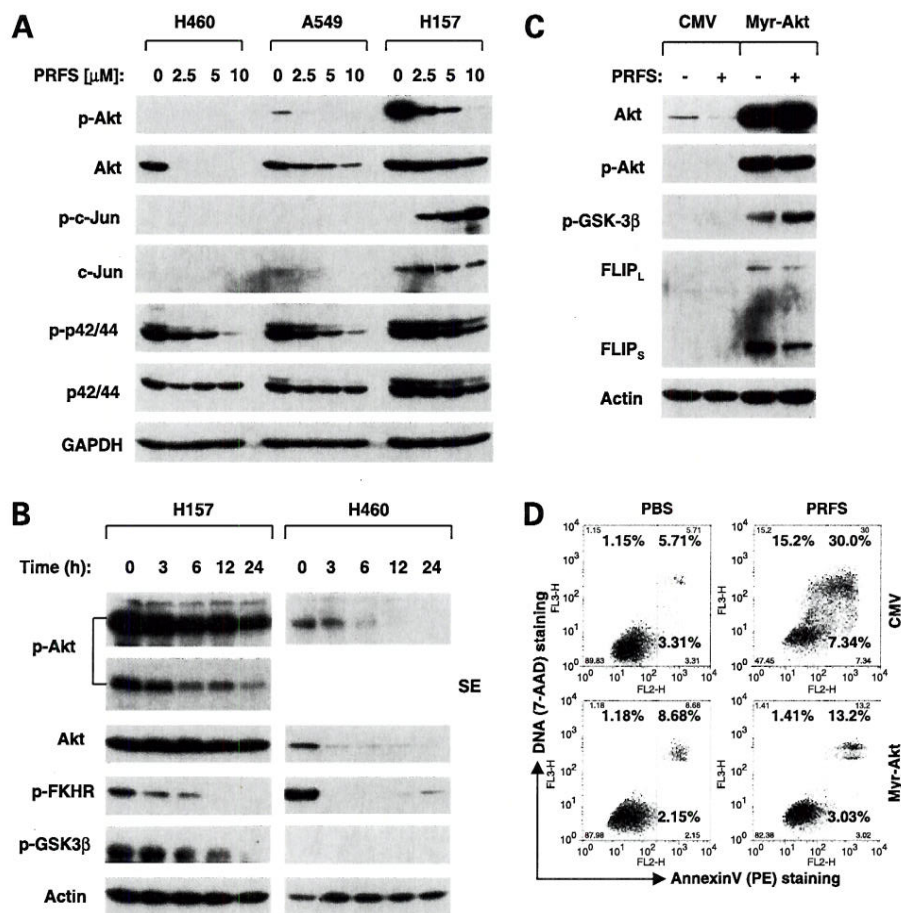


Figure 2. Effects of perifosine on apoptosis induction (A) and caspase activation (B), and involvement of caspase-8 activation in perifosine-induced apoptosis (C and D) in NSCLC cells. **A**, cell lines treated with the given concentrations of perifosine (PRFS) for 24 h and harvested for the estimation of apoptosis by Annexin V staining. Early apoptotic (bottom right), late apoptotic (top right), and necrotic (top left) cells. **B**, the indicated cell lines were treated with the given concentrations of perifosine for 16 h and harvested for the detection of caspase cleavage by Western analysis. **C** and **D**, H460 cells were seeded in 24-well plates and transfected with control (Ctrl) or caspase-8 siRNA the next day. After ~24 h, the cells were trypsinized and replated in new 6-well (C) or 96-well (D) plates. On the second day, the cells were treated with PBS or 5 μ M/L of perifosine. After 16 h, the cells were subjected to Western blot analysis for the indicated proteins (C) or ELISA for measurement of DNA fragments (D). CF, cleaved form. Columns, means of triplicate determinations; bars, SD.

Figure 3. Modulation of Akt, JNK, and ERK signaling pathways by perifosine (**A** and **B**), and involvement of Akt inhibition in perifosine-induced apoptosis (**C** and **D**) in human NSCLC cells. **A** and **B**, NSCLC cell lines treated with the given concentrations of perifosine (PRFS) for 16 h (**A**) or with 10 $\mu\text{mol/L}$ (H157) or 5 $\mu\text{mol/L}$ (H460) of perifosine for the indicated times (**B**). The cells were then subjected to a preparation of whole cell protein lysates and subsequent detection of the indicated proteins using Western blot analysis. **C** and **D**, H460 cells were infected with a multiplicity of infection of 200 Ad-CMV or Ad-myr-Akt. Twenty-four hours later, the cells were exposed to 10 $\mu\text{mol/L}$ of perifosine. After 24 h, the cells were harvested for analysis of the given proteins by Western blotting (**C**) and for the detection of apoptosis by Annexin V staining (**D**). SE, short exposure.



the p-Akt increase caused by PTEN knockdown could be abrogated by perifosine treatment. Surprisingly, perifosine decreased PTEN levels, which itself did not result in an increase of p-Akt levels, probably because perifosine also inhibits Akt phosphorylation (see Supplemental Fig. S1A).¹ As a result, down-regulation of PTEN by siRNA did not alter cell sensitivity to perifosine as shown by measuring cell number change (Supplemental Fig. S1B),¹ caspase activation (Supplemental Fig. S1A),¹ and apoptotic cells (Supplemental Fig. S1C).¹

Effects of Perifosine on the Expression of Key Molecules Involved in the Regulation of Apoptosis

To further explore how perifosine induces apoptosis, we next examined the effects of perifosine on the expression of several key genes involved in either the extrinsic apoptotic pathway (e.g., DR5 and c-FLIP) or the intrinsic apoptotic pathway (e.g., Bax, Bcl-2, Bcl-X_L, PUMA, and survivin). Perifosine increased the levels of DR5, particularly in H460 cells (Fig. 4). It seems that DR5 induction is associated with increased sensitivity of cell lines to perifosine. c-FLIP is another key protein that

inhibits the extrinsic apoptotic pathway by blocking caspase-8 activation (12). The H460 cells, which are the most sensitive to perifosine, had very low basal levels of c-FLIP, particularly FLIP_L, which were further down-regulated by perifosine, whereas the less sensitive A549 and H157 cells have high basal levels of c-FLIP, particularly FLIP_L, which were only weakly decreased by perifosine. Perifosine also decreased FLIP_S levels in these cell lines (Fig. 4). It seems that low levels of c-FLIP and their further down-regulation by perifosine were associated with high sensitivity to perifosine-induced apoptosis. Collectively, these results suggest that activation of the DR5-mediated extrinsic apoptotic pathway is important in perifosine-induced apoptosis.

In examining the signaling molecules involved in the intrinsic apoptotic pathway, we found that perifosine did not significantly alter the levels of Bcl-2 in NSCLC cells (Fig. 4). Surprisingly, perifosine decreased Bax levels in all the tested NSCLC cell lines. Perifosine decreased Bcl-X_L levels in H460 cells that were very sensitive to perifosine, but not in A549 and H157 cells that were less sensitive to perifosine (Fig. 4). These data suggest that Bcl-X_L down-regulation may affect cell sensitivity to undergo perifosine-induced apoptosis. H460 cells had low basal levels of survivin, which were further decreased by perifosine,

¹ Supplementary material for this article is available at Molecular Cancer Therapeutics Online (<http://mct.aacrjournals.org/>).

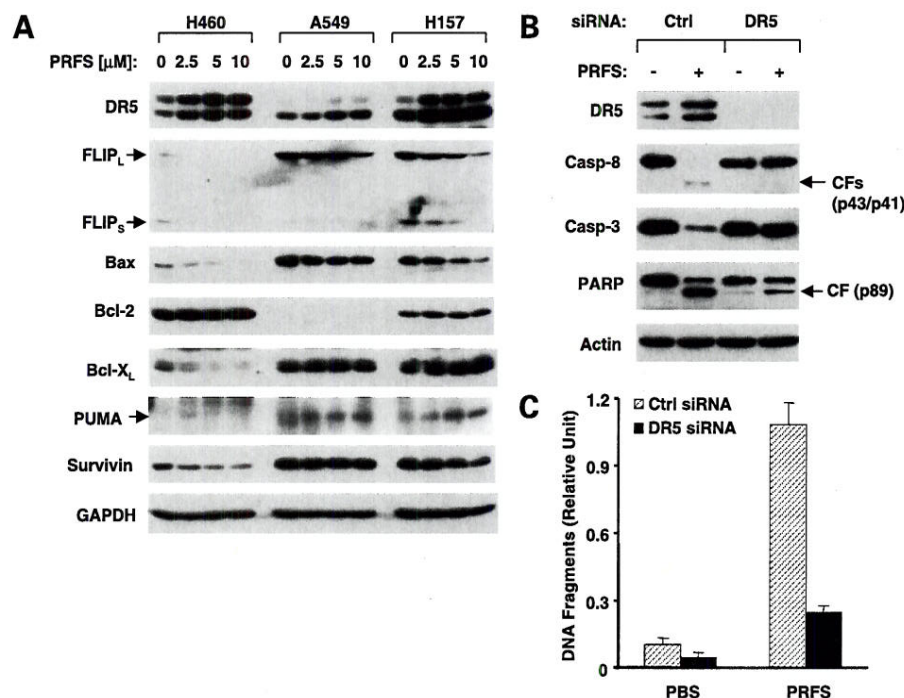


Figure 4. Modulation of apoptosis-related gene expression by perifosine (**A**) and demonstration of the role of DR5 induction in perifosine-induced apoptosis (**B** and **C**) in human NSCLC cells. **A**, NSCLC cell lines treated with the given concentrations of perifosine (PRFS) for 16 h. The cells were then subjected to a preparation of whole cell protein lysates and subsequent detection of the indicated proteins using Western blot analysis. **B** and **C**, H460 cells were seeded in six-well plates and transfected with control (Ctrl) or DR5 siRNA the next day. After ~20 h, the cells were trypsinized and replated in new 6-well (**B**) or 96-well (**C**) plates. On the second day, the cells were treated with PBS or 7.5 μ M/L of perifosine. After 16 h, the cells were subjected to Western blot analysis for the detection of the indicated proteins (**B**) or ELISA for the measurement of DNA fragments (**C**). Columns, means of triplicate determinations; bars, SD; CF, cleaved form.

whereas H157 and A549 cells had high levels of survivin, which were apparently not altered by perifosine (Fig. 4). Thus, it seems that low basal levels of survivin and its further down-regulation with perifosine are also associated with increased cell sensitivity to perifosine-induced apoptosis. PUMA was slightly increased in A549 and H157 cells, but not in H460 cells, suggesting that PUMA was not important in perifosine-induced apoptosis.

Perifosine Cooperates with TRAIL to Enhance the Induction of Apoptosis

Because perifosine induces DR5 expression and down-regulates c-FLIP levels, we hypothesized that perifosine would cooperate with TRAIL, a DR5 ligand, to enhance the induction of apoptosis. Thus, we examined the effects of perifosine in combination with TRAIL on apoptosis induction in NSCLC cells. As shown in Fig. 5A, perifosine in combination with TRAIL induced higher levels of DNA fragments than did each single agent alone. Moreover, increased amounts of cleaved caspase-8, caspase-9, caspase-3, and PARP were detected in cells treated with the perifosine and TRAIL combination, but were only minimally detected in cells treated with either perifosine or TRAIL alone (Fig. 5B). Thus, we conclude that perifosine cooperates with TRAIL to enhance the induction of apoptosis.

Perifosine Induces Apoptosis Requiring Caspase-8 Activation and DR5 Up-regulation

The data presented above strongly suggest a role for the activation of the extrinsic apoptotic pathway in perifosine-induced apoptosis. Thus, we determined whether perifosine induces apoptosis requiring activation of caspase-8 and up-regulation of DR5. To this end, we silenced the

expression of caspase-8 and DR5 using caspase-8 and DR5 siRNAs, respectively, and then examined cell sensitivity to perifosine. By Western blotting, we detected substantially reduced levels of caspase-8 levels including cleaved forms in H460 cells transfected with caspase-8 siRNA compared with those in control siRNA-transfected cells (Fig. 2C), indicating successful caspase-8 knockdown or inhibition of caspase-8 activation. Accordingly, cleavage of caspase-3 and PARP and an increase in DNA fragmentation were also attenuated in caspase-8 siRNA-transfected cells in comparison with control siRNA-transfected cells (Fig. 2C and D). These results indicate that perifosine induces a caspase-8-dependent apoptosis. Similarly, silencing of DR5 expression using DR5 siRNA abrogated DR5 induction (Fig. 4B) and impaired the ability of perifosine to induce cleavage of caspase-8, caspase-3, and PARP (Fig. 4B). In addition, an increase in DNA fragmentation in DR5 siRNA-transfected cells was also reduced compared with control siRNA-transfected cells (Fig. 4C). These data show that DR5 up-regulation is also involved in perifosine-induced apoptosis.

Manipulation of c-FLIP Levels Regulates Cell Sensitivity to Perifosine-Induced Apoptosis and Enhancement of TRAIL-Induced Apoptosis

To further show that the activation of the extrinsic apoptotic pathway participates in perifosine-induced apoptosis, we examined the sensitivity of cell lines that express ectopic FLIP_L to perifosine-induced apoptosis. As presented in Fig. 6A, perifosine increased DNA fragmentation in a dose-dependent fashion in H157-Lac Z-5 cells, but only minimally in H157-FLIP_L-6 cells. As a positive control treatment, TRAIL-induced increase in DNA fragmentation

was abolished in H157-FLIP_L-6 cells. Similarly, perifosine-induced increase in DNA fragmentation was also abrogated in A549-FLIP_L-2 cells in comparison with A549-Lac Z-9 cells (Fig. 6B). Together, these results clearly show that overexpression of ectopic c-FLIP protects cells from perifosine-induced apoptosis.

Because c-FLIP down-regulation was often associated with the enhancement of TRAIL-induced apoptosis (20, 21, 28), we further compared apoptosis induction by the combination of perifosine and TRAIL between A549-Lac Z-9 and A549-FLIP_L-2 cell lines. In agreement with the results presented in Fig. 5, the combination of perifosine and TRAIL was much more potent than either perifosine or TRAIL alone in increasing DNA fragmentation in A549-Lac Z-9 cells. However, not only perifosine and TRAIL alone but also their combination exhibited minimal effects on increasing DNA fragmentation in A549-FLIP_L-2 cells (Fig. 6B). These results clearly show that overexpression of ectopic c-FLIP confers cell resistance to the combination of perifosine and TRAIL, indicating that c-FLIP down-regulation contributes to perifosine-mediated enhancement of TRAIL-induced apoptosis.

Because the cell lines, A549 and H157, with high basal levels of c-FLIP were relatively less sensitive than H460

cells which have low basal levels of c-FLIP to perifosine-induced apoptosis, we wanted to determine whether down-regulation of c-FLIP sensitized cells to perifosine-induced apoptosis. To this end, we silenced the expression of c-FLIP (both FLIP_L and FLIP_S) using siRNA in A549 cells, and then examined their response to perifosine-induced apoptosis. As presented in Fig. 6C, transfection of c-FLIP siRNA reduced the levels of both FLIP_L and FLIP_S, which were further reduced after treatment with perifosine. Those cells whose expression of c-FLIP had been reduced with siRNA were more sensitive to caspase-8, caspase-3, and PARP cleavage after perifosine treatment compared with control cells, indicating that c-FLIP levels indeed affect cell sensitivity to perifosine-induced apoptosis.

Discussion

In this study, we have shown that perifosine exerts its growth-inhibitory effects in a panel of NSCLC cell lines, primarily through the induction of apoptosis and/or cell cycle arrest. Importantly, perifosine inhibited the growth of most of the tested NSCLC cell lines with IC₅₀s ranging between 8 and 15 μ mol/L (Fig. 1A), which are within the

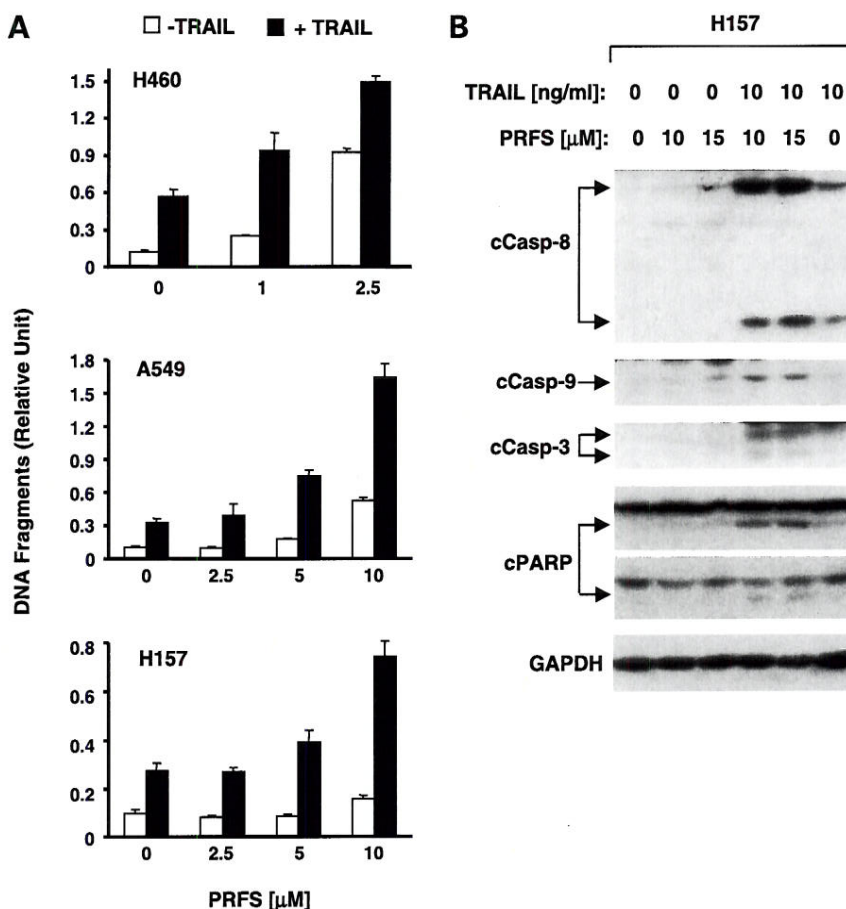


Figure 5. Perifosine cooperates with TRAIL to enhance DNA fragmentation (**A**) and caspase activation (**B**) in human NSCLC cells. **A**, cell lines plated in 96-well plates and treated with the given doses of perifosine (PRFS) alone, 20 ng/mL TRAIL alone, or TRAIL plus perifosine on the second day. After 24 h, the cells were subjected to DNA fragmentation using the Cell Death Detection ELISA kit. Columns, means of triplicate determinations; bars, SD. **B**, H157 cells were treated with perifosine alone, TRAIL alone, and their combinations. After 16 h, the cells were subjected to a preparation of whole cell protein lysates and subsequent detection of the indicated proteins by Western blot analysis. c, cleaved.

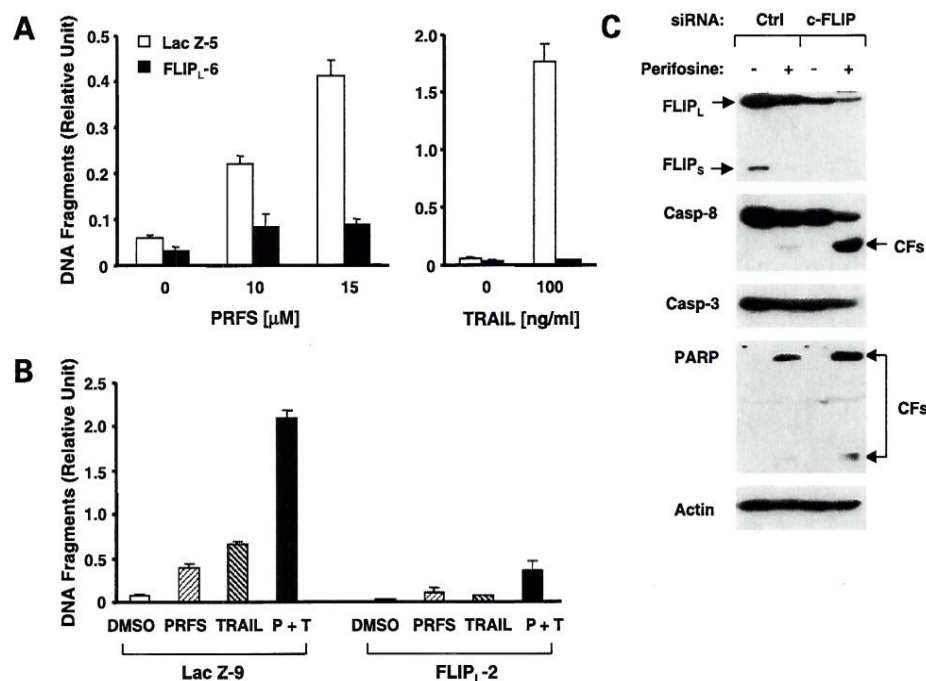


Figure 6. Overexpression of ectopic c-FLIP (A and B) and silencing of c-FLIP expression (C) modulate cell sensitivity to perifosine-induced apoptosis. **A**, H157 cell lines that stably express Lac Z and FLIP_L, respectively, were treated with the indicated concentrations of perifosine (PRFS) or TRAIL. **B**, A549 cell lines that stably express Lac Z and FLIP_L, respectively, were exposed to 10 μ mol/L of perifosine, 20 ng/mL of TRAIL, and the combination of perifosine and TRAIL (P + T). Twenty-four hours later, after the aforementioned treatment, the cells were subjected to estimation of DNA fragmentation using the Cell Death Detection ELISA kit. Columns, mean of triplicate determinations; bars, SD. **C**, A549 cells plated in 24-well plates were transfected with control (Ctrl) or c-FLIP siRNA. Twenty-four hours later, the cells were exposed to 10 μ mol/L of perifosine (PRFS). After 24 h, the cells were subjected to a preparation of whole cell protein lysates and subsequent detection of the indicated proteins using Western blot analysis. CFs, cleaved fragments.

clinically achievable and safe peak plasma concentration ranges (i.e., 10–15 μ mol/L; refs. 25, 26), suggesting the potential of perifosine in the treatment of NSCLCs.

Modulation of Akt, JNK, and ERK signaling pathways and their involvement in perifosine-induced apoptosis has been studied in other types of cancer cells (4, 18, 27). Despite the proapoptotic role of JNK activation in perifosine-induced apoptosis in multiple myeloma (18), we found that perifosine increased p-c-Jun only in one (i.e., H157 cells) of three cell lines tested (Fig. 3A). Given that H157 cells were relatively insensitive to perifosine-induced apoptosis (Fig. 2), we suggest that JNK activation is unlikely to account for the perifosine-induced apoptosis in human NSCLC cells. Perifosine was reported to either decrease or increase ERK phosphorylation depending on cancer cell type (5, 18, 27). In our study, perifosine decreased ERK phosphorylation in all of the three tested cell lines tested, regardless of cell sensitivity to TRAIL-induced apoptosis. Thus, we suggest that ERK inhibition is also unlikely to be critical for perifosine-induced apoptosis in human NSCLC cells.

Although perifosine inhibits Akt activation in different types of cancer cells including the NSCLC cells shown in the current study, enforced activation of Akt through overexpression of the constitutively activated form of Akt, myr-Akt, protects cells from perifosine-induced cell death in one type of cancer cell line (e.g., PC-3 prostate cancer cells; ref. 4) but not in another type of cancer cell (e.g., MM.1S multiple myeloma cells; ref. 18). In our study, we found that the low basal levels of p-Akt (e.g., H460 < A549 < H157) and its further down-regulation were associated with high sensitivity to perifosine-

induced apoptosis (H460 > A549 > H157; Figs. 1 and 2). Moreover, overexpression of myr-Akt in H460 cells led to increased levels of p-Akt and resistance to perifosine-induced apoptosis (Fig. 3). Collectively, we conclude that Akt inhibition plays an important role in mediating perifosine-induced apoptosis in human lung cancer cells. We noted that perifosine decreased the levels of total Akt in some NSCLC cells (e.g., H460 and A549), the potency of which is associated with cell sensitivity to perifosine-induced apoptosis, in addition to decreasing Akt phosphorylation. To the best of our knowledge, this is the first demonstration that perifosine decreases the total levels of Akt. Given that Akt reduction is an early event, which occurred at 3 h post-perifosine treatment (Fig. 3B), it is unlikely that Akt reduction occurs secondary to perifosine-induced apoptosis (e.g., cleavage by caspase activation). Nevertheless, ongoing studies are attempting to reveal how perifosine decreases the levels of total Akt.

Perifosine activated both caspase-8 and caspase-9 in human NSCLC cells (Fig. 2B), suggesting that perifosine can induce apoptosis through the extrinsic and/or intrinsic apoptotic pathways. In examining several key proteins involved in the regulation of the extrinsic or intrinsic apoptotic pathways, we found that perifosine strikingly induced DR5 expression and decreased the levels of c-FLIP in all the cells lines tested, whereas having limited or no modulatory effects on the levels of Bcl-2, Bcl-X_L, PUMA, and survivin (Fig. 4A). Importantly, the low basal levels of c-FLIP (e.g., FLIP_L) and its further down-regulation are associated with increased sensitivity to undergo perifosine-induced apoptosis (e.g., H460 cells). We noted that Bax

levels were lower and Bcl-2 levels were higher in the sensitive H460 cells than in less sensitive A549 and H157 cells (Fig. 4A). Moreover, we found that Bax levels were actually decreased in cells treated with perifosine, although the underlying mechanisms and its effects on perifosine-induced apoptosis are unclear. In fact, our preliminary data show that Bax or PUMA deficiency does not alter cell sensitivity to perifosine-induced apoptosis.² Together, we suggest that the activation of the extrinsic apoptotic pathway is important in mediating perifosine-induced apoptosis. This observation is supported by our findings that silencing of caspase-8 or DR5, or overexpression of ectopic c-FLIP protects cells from perifosine-induced apoptosis (Figs. 2, 4, and 6), whereas down-regulation of endogenous c-FLIP using c-FLIP siRNA sensitizes cells to perifosine-induced apoptosis (Fig. 6). In agreement with our findings, a recent study has shown that perifosine induces apoptosis through activation of the Fas-mediated extrinsic apoptotic pathway in human leukemia cells (29). To the best of our knowledge, this is the first study showing that perifosine modulates the expression of DR5 and c-FLIP in human cancer cells.

Some studies have shown that Akt also inhibits the extrinsic apoptotic pathway through the up-regulation of c-FLIP expression (16, 17). In this study, we have shown that perifosine inhibits Akt and reduces c-FLIP levels, both of which are involved in perifosine-induced apoptosis. Indeed, we detected increased levels of c-FLIP in cells infected with Ad-myr-Akt (Fig. 3C), suggesting that Akt activation indeed increases c-FLIP levels in the tested cells. Thus, it is possible that Akt exerts its inhibitory effect on perifosine-induced apoptosis through the up-regulation of c-FLIP. On other hand, perifosine may down-regulate c-FLIP levels through inhibition of Akt; this needs to be investigated in detail in the future.

It is known that TRAIL functions as the DR5 ligand and rapidly induces apoptosis in a wide variety of transformed cells but is not cytotoxic in normal cells *in vitro* and *in vivo* (10, 16, 17). Therefore, TRAIL is considered to be a tumor-selective, apoptosis-inducing cytokine with promising potential for cancer treatment and is currently being tested in phase I clinical trials. In our study, we showed that the combination of perifosine and TRAIL exhibited augmented induction of apoptosis in human NSCLC cells (Fig. 5), which is likely due to the ability of perifosine to induce DR5 expression and down-regulate c-FLIP levels. This finding warrants future *in vivo* animal studies and clinical evaluation of the efficacy of perifosine in combination with TRAIL for the treatment of NSCLC.

Acknowledgments

We are grateful to Zhongmei Zhou for her excellent technical assistance, Dr. Xiangguo Liu for establishment of stable cell lines that overexpress c-FLIP, and Dr. Lily Yang for providing us with Ad-CMV and Ad-myr-Akt.

References

- Hilgard P, Klenner T, Stekar J, et al. D-21266, a new heterocyclic alkylphospholipid with antitumor activity. *Eur J Cancer* 1997;33:442–6.
- Ruiter GA, Verheij M, Zerp SF, van Blitterswijk WJ. Alkyl-lysophospholipids as anticancer agents and enhancers of radiation-induced apoptosis. *Int J Radiat Oncol Biol Phys* 2001;49:415–9.
- Vink SR, Schellens JH, van Blitterswijk WJ, Verheij M. Tumor and normal tissue pharmacokinetics of perifosine, an oral anti-cancer alkylphospholipid. *Invest New Drugs* 2005;23:279–86.
- Kondapaka SB, Singh SS, Dasmahapatra GP, Sausville EA, Roy KK. Perifosine, a novel alkylphospholipid, inhibits protein kinase B activation. *Mol Cancer Ther* 2003;2:1093–103.
- Li X, Luwor R, Lu Y, Liang K, Fan Z. Enhancement of antitumor activity of the anti-EGF receptor monoclonal antibody cetuximab/C225 by perifosine in PTEN-deficient cancer cells. *Oncogene* 2006;25:525–35.
- Patel V, Lahusen T, Sy T, et al. Perifosine, a novel alkylphospholipid, induces p21(WAF1) expression in squamous carcinoma cells through a p53-independent pathway, leading to loss in cyclin-dependent kinase activity and cell cycle arrest. *Cancer Res* 2002;62:1401–9.
- Dasmahapatra GP, Didolkar P, Alley MC, et al. *In vitro* combination treatment with perifosine and UCN-01 demonstrates synergism against prostate (PC-3) and lung (A549) epithelial adenocarcinoma cell lines. *Clin Cancer Res* 2004;10:5242–52.
- Rahmani M, Reese E, Dai Y, et al. Coadministration of histone deacetylase inhibitors and perifosine synergistically induces apoptosis in human leukemia cells through Akt and ERK1/2 inactivation and the generation of ceramide and reactive oxygen species. *Cancer Res* 2005;65:2422–32.
- Nyakern M, Cappellini A, Mantovani I, Martelli AM. Synergistic induction of apoptosis in human leukemia T cells by the Akt inhibitor perifosine and etoposide through activation of intrinsic and Fas-mediated extrinsic cell death pathways. *Mol Cancer Ther* 2006;5:1559–70.
- Ashkenazi A, Dixit VM. Death receptors: signaling and modulation. *Science* 1998;281:1305–8.
- Hengartner MO. The biochemistry of apoptosis. *Nature* 2000;407:770–6.
- Kataoka T. The caspase-8 modulator c-FLIP. *Crit Rev Immunol* 2005;25:31–58.
- Wajant H. Targeting the FLICE inhibitory protein (FLIP) in cancer therapy. *Mol Interv* 2003;3:124–7.
- Longley DB, Wilson TR, McEwan M, et al. c-FLIP inhibits chemotherapy-induced colorectal cancer cell death. *Oncogene* 2006;25:838–48.
- Cheng JQ, Lindsley CW, Cheng GZ, Yang H, Nicosia SV. The Akt/PKB pathway: molecular target for cancer drug discovery. *Oncogene* 2005;24:7482–92.
- Panka DJ, Mano T, Sahara T, Walsh K, Mier JW. Phosphatidylinositol 3-kinase/Akt activity regulates c-FLIP expression in tumor cells. *J Biol Chem* 2001;276:6893–6.
- Nam SY, Jung GA, Hur GC, et al. Upregulation of FLIP(S) by Akt, a possible inhibition mechanism of TRAIL-induced apoptosis in human gastric cancers. *Cancer Sci* 2003;94:1066–73.
- Richardson PG, Mitsiades C, Hideshima T, Anderson KC. Bortezomib: proteasome inhibition as an effective anticancer therapy. *Annu Rev Med* 2006;57:33–47.
- Sun SY, Yue P, Dawson MI, et al. Differential effects of synthetic nuclear retinoid receptor-selective retinoids on the growth of human non-small cell lung carcinoma cells. *Cancer Res* 1997;57:4931–9.
- Liu X, Yue P, Schonthal AH, Khuri FR, Sun SY. Cellular FLICE-inhibitory protein down-regulation contributes to celecoxib-induced apoptosis in human lung cancer cells. *Cancer Res* 2006;66:11115–9.
- Zou W, Liu X, Yue P, Khuri FR, Sun SY. PPAR γ ligands enhance TRAIL-induced apoptosis through DR5 upregulation and c-FLIP down-regulation in human lung cancer cells. *Cancer Biol Ther* 2007;6:99–106.
- Liu X, Yue P, Zhou Z, Khuri FR, Sun SY. Death receptor regulation and celecoxib-induced apoptosis in human lung cancer cells. *J Natl Cancer Inst* 2004;96:1769–80.
- Sun SY, Yue P, Wu GS, et al. Mechanisms of apoptosis induced by the synthetic retinoid CD437 in human non-small cell lung carcinoma cells. *Oncogene* 1999;18:2357–65.

² Unpublished data.

24. Jin F, Liu X, Zhou Z, et al. Activation of nuclear factor- κ B contributes to induction of death receptors and apoptosis by the synthetic retinoid CD437 in DU145 human prostate cancer cells. *Cancer Res* 2005;65: 6354–63.
25. Crul M, Rosing H, de Klerk GJ, et al. Phase I and pharmacological study of daily oral administration of perifosine (D-21266) in patients with advanced solid tumours. *Eur J Cancer* 2002;38:1615–21.
26. Van Ummersen L, Binger K, Volkman J, et al. A phase I trial of perifosine (NSC 639966) on a loading dose/maintenance dose schedule in patients with advanced cancer. *Clin Cancer Res* 2004;10:7450–6.
27. Momota H, Nerio E, Holland EC. Perifosine inhibits multiple signaling pathways in glial progenitors and cooperates with temozolomide to arrest cell proliferation in gliomas *in vivo*. *Cancer Res* 2005;65: 7429–35.
28. Zhang S, Shen HM, Ong CN. Down-regulation of c-FLIP contributes to the sensitization effect of 3,3'-diindolylmethane on TRAIL-induced apoptosis in cancer cells. *Mol Cancer Ther* 2005;4:1972–81.
29. Gajate C, Mollinedo F. Edelfosine and perifosine induce selective apoptosis in multiple myeloma by recruitment of death receptors and downstream signaling molecules into lipid rafts. *Blood* 2007;109:711–9.

Modulation of Death receptors by cancer therapeutic agents

Heath A. Elrod and Shi-Yong Sun

Department of Hematology and Oncology, Winship Cancer Institute, Emory University School of Medicine, Atlanta, GA.

Key words: Death receptors, apoptosis, cancer therapy

Correspondence to: Shi-Yong Sun, Ph.D., Winship Cancer Institute, Emory University School of Medicine, 1365-C Clifton Road, C3088, Atlanta, GA 30322, USA. Phone: (404) 778-2170; Fax: (404) 778-5520; E-mail: shi-yong.sun@emoryhealthcare.org.

Abstract

Death receptors are important modulators of the extrinsic apoptotic pathway. Activating certain death receptors such as death receptors for tumor necrosis factor-related apoptosis-inducing factor (TRAIL) (i.e., DR4 and DR5) selectively kills cancer cells via induction of apoptosis while sparing normal cells. Thus, soluble recombinant TRAIL and agonistic antibodies to DR4 or DR5 have progressed to phase I and phase II clinical trials. Many cancer therapeutic drugs including chemotherapeutic agents have been shown to induce the expression or redistribution at the cell surface of death receptors including TRAIL death receptors. In addition, chemotherapeutic agents have also been shown to enhance induction of apoptosis by TRAIL or agonistic antibodies or overcome cell resistance to TRAIL or agonistic antibodies. Targeted induction of apoptosis by activation of the death receptor-mediated extrinsic apoptotic pathway should be an ideal therapeutic strategy to eliminate cancer cells. Therefore, death receptors, particularly TRAIL death receptors, have emerged as an important cancer therapeutic target. This article will focus on reviewing and discussing the modulation of death receptors by cancer therapeutic agents and its implications in cancer therapy.

Introduction

Apoptosis or programmed cell death is a tightly controlled process essential for embryonic development as well as normal tissue homeostasis and the regulation of cell number after an immune response. Apoptosis is regulated by signals such as growth factors, cell damage and hormones¹. Aberrant regulation of apoptosis can lead to cancer. Tumor cells often acquire resistance to normal apoptotic signals allowing for uncontrolled cell growth. The process of targeting the apoptotic pathway in tumor cells while sparing normal cells is of interest in cancer therapy. Such targeted therapy to induce apoptosis in cancer cells has emerged as a strategy to more effectively treat cancer patients and reduce toxicity.

Death receptors are key components in the extrinsic apoptotic pathway². Their activation due to ligand binding or receptor clustering and aggregation triggers an extrinsic apoptotic signaling pathway leading to apoptosis. Therefore, the death receptor ligands or agonistic antibodies against the death receptors are potent inducers of apoptosis and thereby have therapeutic potential in the treatment of cancer. One example is tumor necrosis factor (TNF)-related apoptosis-inducing ligand (TRAIL), which is the ligand for death receptor 4 (DR4) and death receptor 5 (DR5) and induces apoptosis upon ligation with DR4 or DR5. TRAIL has attracted attention recently because it preferentially induces apoptosis of transformed or malignant cells, when administered systemically, with limited inflammatory response and liver damage, which are major side effects or toxicity of other death receptor ligands such as the cytokines TNF α and Fas². Therefore, TRAIL is considered to be a tumor-selective apoptosis-inducing cytokine and a promising new candidate for cancer treatment³. There is a concern about TRAIL's potential hepatotoxicity⁴, but this can be avoided by appropriate preparation of recombinant human TRAIL^{5,6}. Currently, TRAIL is being tested in phase I clinical trials⁷. In addition to TRAIL ligand, agonistic antibodies

against DR4 and DR5, respectively, have also been developed. These antibodies mimic TRAIL's function to activate death receptor-mediated apoptosis with potential as cancer therapeutic agents and have progressed to phase I or phase II trials in treatment of multiple types of cancers ⁷.

The expression of death receptors is induced by many small molecules including some cancer therapeutic drugs. Conventional chemotherapy or radiotherapy damages proliferating cells and induces cell death usually by engaging the intrinsic mitochondrial apoptotic pathway through p53 activation ⁸. Recent studies have shown that certain small molecules can also induce apoptosis by engaging the extrinsic apoptotic pathway through the activation of death receptors. Therefore, death receptors have emerged as an important cancer therapeutic target ^{9,10}.

There are many elegant review articles on cancer therapeutic potentials of the death ligands such as TRAIL and agonistic antibodies to death receptors such as DR4 and DR5 ^{7,10-12}. This article will primarily review the recent studies on the modulation and activation of death receptors by small molecules with cancer therapeutic activity and discuss possible underlying mechanisms and their clinical implications.

Death receptor-mediated extrinsic apoptotic pathway

Apoptosis can occur through two distinct pathways: the intrinsic apoptotic pathway and the extrinsic apoptotic pathway. The intrinsic pathway results in signals from the mitochondria whereas the extrinsic pathway is characterized by activation of death receptors ¹³. Both pathways engage a family of cysteine proteases, the caspases, whose cleavage of cellular substrates leads to apoptosis. The death receptors involved in the extrinsic apoptotic pathway belong to the TNF receptor superfamily that include Fas (CD95 or Apo1), TNFR1, DR3, DR4 (TRAIL-R1), DR5 (TRAIL-R2) and DR6 ². These receptors are characterized by a cysteine-rich cytoplasmic domain

and an intracellular death domain. The death domain enables transmission of death signals after ligand binding or trimerization ². There are also decoy receptors (e.g., DcR1 and DcR2) that contain no death domain or a truncated death domain and can bind ligand but cannot signal ¹⁴. Therefore, these decoy receptors function as antagonists to inhibit death ligand/death receptor-induced apoptosis.

The death receptors, Fas, DR4 or DR5, bind to their respective ligands (i.e., FasL or TRAIL) and trimerization of the receptor occurs at the cell surface inducing apoptosis through the recruitment of adaptor proteins such as the Fas-associated death domain (FADD). The recruitment of FADD forms the death inducing signaling complex (DISC), which results in the recruitment of pro-caspase-8 to the DISC. This results in activation of caspase-8, which leads to the activation of effector caspases such as caspase-3. Death receptors can also indirectly activate effector caspases by caspase-8 cleaving Bid, which leads to activation of Bax resulting in pore formation in the mitochondrial membrane and release of cytochrome c leading to activation of caspase-9 (Fig. 1).^{2, 15} Therefore, death receptors activate the intrinsic mitochondrial apoptotic pathway in certain types of cells as well.

In contrast to Fas, DR4 and DR5, the biological function of TNF receptor 1 (TNFR1) is more complex. This complexity is reflected in the increased variety of proteins that are present in the TNFR1 complex. TNFR1 first recruits another adaptor protein, TNF-associated death domain (TRADD), which in turn not only recruits FADD, but also recruits TNFR-associated factor 2 (TRAF2) and the kinase receptor-interacting protein (RIP). TRAF2 is essential for c-Jun N-terminal kinase (JNK) activation, whereas RIP is instrumental for the activation of the NF- κ B pathway. TNF-mediated JNK activation favors its apoptosis-inducing activity, whereas NF- κ B

activation by TNF α signals inflammation and cell survival by inhibiting TNF α -induced apoptosis^{2, 16}.

Death receptors and cancer

Fas, DR4 and DR5 are generally expressed in both normal and malignant cells. However, the abnormal modulation of death receptors has been observed in several different cancers possibly as a mechanism for tumor cells to escape immunosurveillance. The Fas gene has been shown to be mutated in both hematopoietic malignancies (0-65%) and solid tumors (0-28%)¹⁷. Among the hematopoietic malignancies, high frequencies of Fas mutations occur in thyroid lymphoma (65.4%), cutaneous T-cell lymphoma (59%), and nasal NK/T cell lymphoma (50%). Among solid tumors, Fas mutations occurs frequently in bladder transitional cell carcinoma (28%) and burn scar-related squamous cell carcinoma (14.3%)¹⁷. Compared to Fas, the frequencies of DR4 and DR5 mutations detected in cancers including lung, head and neck, breast, bladder gastric and hepatocellular carcinomas, non-Hodgkin's lymphoma and chronic myelogenous leukemia are very low (0-10.6%)¹⁸⁻²⁰.

Downregulation of expression of death receptors has also been observed in cancer. In cervical cancer, the expression of Fas decreases with more progressive cervical intraepithelial neoplasia (CIN)²¹. In urothelial cancer, decreased Fas expression was significantly associated with a higher pathological grade, a more advanced stage and poorer prognosis²². In ovarian cancer, loss or downregulation of DR4 expression was observed in 10.3% and 8.8% of patients, respectively, which was associated with methylation of the DR4 gene promoter²³. As well, in small cell lung cancer a 40% reduction in Fas and DR4 expression was observed as a result of DNA methylation²⁴. A study in acute myelogenous leukemia (AML) has shown that relapse-free

survival was significantly prolonged in patients with CD95-positive AML cells compared with patients with CD95-negative AML cells ²⁵. However, in non-small cell lung cancer, poorly differentiated tumors showed increased expression of DR4, DR5 and TRAIL and the expression of DR5 was associated with increased risk of death ²⁶. Similarly, in colon cancer, the expression of DR4 and DR5 is stronger in neoplastic tissues than in normal tissues and is accompanied by a higher degree of apoptosis ²⁷. Another study in stage III colon cancer patients treated with adjuvant chemotherapy has shown that the majority of tumors showed high expression of TRAIL (83%), DR4 (92%), and DR5 (87%) and high DR4 expression was associated with worse disease-free and overall survival in these patients ²⁸. Although both DR4 and DR5 were detected in the majority of colorectal tumors, a recent study failed to demonstrate that they are associated with survival; instead, overexpression of FLIP_L, a major inhibitor of death receptor-mediated apoptosis, provides stage-independent prognostic information ²⁹. In breast cancer, DR5 expression is stronger in malignant specimens than in normal breast epithelium, and expression correlated strongly with lymph node involvement, and was independently associated with decreased survival; however, DR4 expression was not associated with survival ³⁰. These data indicate that the expression of death receptors and the correlation with tumor progression seem to be tumor type specific.

Fas-associated death domain (FADD) is the main adaptor for transmitting death signal from activation of death receptors. It has been shown that low or absent expression of the FADD protein in leukemic cells at diagnosis is a poor independent prognostic factor that can predict worse clinical outcome even for patients with standard- or good-risk AML ³¹. However, in lung adenocarcinomas, increased FADD expression is detected in aggressive tumors and is significantly associated with poor survival ³². It seems that the impact of FADD expression on cancer patient survival is also tumor-type specific.

The abnormal expression of the decoy receptors has also been observed in cancer; however, the expression of the decoy receptors and DR4 or DR5 does not always correlate with sensitivity to apoptosis³³. Tumor cells can overexpress decoy receptors, which can compete with death receptors for ligand binding. The gene coding for DcR3, a secreted protein that binds FasL, is amplified in about 50% of lung and colon cancers³⁴. Frequent gene amplification and overexpression of DcR3 were also observed in glioblastoma³⁵. In addition, DcR3 is overexpressed in carcinomas of the stomach, esophagus, rectum and liver independently of gene amplification^{36, 37}. Cells that overexpress DcR3 presumably have a survival advantage because of their ability to resist FasL-mediated attack by cytotoxic lymphocytes, although the role of DcR3 in tumorigenesis remains unclarified. In contrast to DcR3, DcR1 and DcR2 are generally downregulated in many types of cancer, largely due to gene methylation^{38, 39}. It is possible that DcR overexpressing tumors may gain a selective growth advantage by escaping from death ligand/death receptor-induced apoptosis. Given the frequent downregulation or loss of DcR1 and DcR2 expression in multiple cancers, which still express DR4 and/or DR5 or exhibit increased DR4 and DR5 expression, there may be an opportunity to treat these cancers with TRAIL or agonistic DR4 or DR5 antibodies via targeted induction of TRAIL/death receptor-mediated apoptosis of cancer cells.

General mechanisms underlying modulation of death receptors

The expression of death receptors appears to be induced by some anticancer agents. In general, modulation of death receptors involves p53-dependent and p53-independent mechanisms.

The tumor suppressor gene p53 plays a critical role in regulating apoptosis and cell cycle arrest after cells undergo cellular stress such as induction of DNA damage or hypoxia⁴⁰. p53 is

one of the most common genes mutated in cancer and can regulate many downstream target genes including death receptors. Activation of p53 can contribute to increased surface expression of Fas and apoptosis⁴¹. Fas is the first death receptor demonstrated to be directly regulated by p53 through a p53-responsive element in the first intron of the Fas gene and putative elements in the promoter⁴². Subsequently, DR5 was demonstrated to be induced by DNA-damaging agents in a p53-dependent fashion⁴³ and its transcription is directly transactivated by p53 through an intronic sequence-specific p53 DNA-binding site⁴⁴. We recently have shown that DR4 expression can also be induced by DNA damaging agents in a p53-dependent manner⁴⁵ and p53 directly regulates the transcription of DR4 through a p53 binding site located in the first intron of the DR4 gene, in a similar fashion as demonstrated in the DR5 gene⁴⁶.

Death receptors can also be regulated by p53 independent mechanisms. The Fas gene contains consensus sequences for AP-1, Sp-1, NF- κ B and NFAT in its promoter⁴⁷ and Fas transcription has been shown to be directly regulated by NF- κ B⁴⁸. Moreover, transcriptional regulation of Fas expression by AP-1 was also reported⁴⁹. There have been only a few studies dealing with p53-independent regulation of DR4 or DR5. Sheikh et al⁵⁰ reported that TNF- α , a NF- κ B activator, induced DR5 expression in a number of cancer cell lines independently of p53. Ravi et al⁵¹ reported that NF- κ B induced expression of DR4 and DR5. Shetty et al⁵² recently demonstrate that a putative NF- κ B binding site in the first intron of the DR5 gene in cooperation with the p53 binding site in this region is responsible for DR5 upregulation by etoposide or histone deacetylase (HDAC) inhibitors. We found that phorbol 12-myristate 13-acetate (TPA), a potent AP-1 activator, increased AP-1 binding to the DR4 promoter and induced DR4 expression in cancer cell lines with mutant p53⁵³, suggesting a possible role for AP-1 in DR4 regulation. We have demonstrated that this effect is mediated by an AP-1 site in the 5'-flanking region of the DR4

gene⁵³. Recently, it has been shown that DR5 can be regulated by CCAAT/enhancer-binding protein homologous (CHOP) protein through the CHOP-binding site in the 5'-flanking region of the DR5 gene^{54, 55}. In addition to these positive regulations, DR5 can also be negatively regulated through a putative binding site for the transcription repressor Yin Yang 1 (YY1) in the DR5 promoter region^{56, 57}.

Modulation of death receptor expression by cancer therapeutic agents

It is generally thought that small molecules such as chemotherapeutic agents induce apoptosis through the intrinsic apoptotic pathway. However, many small molecules with anticancer activity including chemopreventive agents modulate the expression and/or activation of death receptors, which plays a critical role in mediating drug-induced apoptosis. The modulation of death receptor expression by chemopreventive agents was discussed by us previously⁵⁸. The current review will focus on modulation of death receptors by cancer therapeutic agents and possible underlying mechanisms.

DNA damaging agents. Many studies have shown that DNA damaging chemotherapeutic agents can modulate death receptor expression and render cells more sensitive to death receptor-induced apoptosis. Cisplatin (CDDP), mitomycin, methotrexate, mitoxantrone, doxorubicin, and bleomycin induced Fas expression in human cancer cells, primarily through a p53-dependent mechanism⁴². Similarly, DR5 was demonstrated to be a DNA damaging-inducible and p53-regulated gene^{43, 44}. Following these findings, we demonstrated that DR4 is also a DNA damaging-inducible and p53-regulated gene^{45, 46}. In the literature, doxorubicin, etoposide, Ara-C, cisplatin and camptosar (CPT-11) were shown to induce the expression of both DR4 and DR5 or

only DR5 expression, through either p53-dependent, or p53-independent mechanisms^{43, 50, 59-62 45}. For example, etoposide increased the expression of both DR4 and DR5 and enhanced TRAIL-induced apoptosis in breast cancer⁵⁹ and osteogenic sarcoma cells⁶². Etoposide was also shown to induce DR5 expression in glioma cells⁶⁰, human acute leukemia cells⁶¹, and breast cancer cells⁶³. Our work showed that etoposide increased DR4 expression in lung cancer cells⁴⁵.

Currently, it is not clear whether upregulation of death receptors plays any role in DNA damaging agent-induced apoptosis. It was shown that addition of a soluble DR4 fusion protein (DR4:Fc) to cell cultures reduced the amount of etoposide-induced apoptosis in a dose-dependent manner⁵⁹. In colon cancer cells, it was recently shown that chemotherapy downregulated FLIP expression, whereas overexpression of FLIP_L potentially inhibited apoptosis induced by chemotherapy⁶⁴. Of note, a recent clinical study has shown that absence or low expression of fas-associated protein with death domain (FADD) in acute myeloid leukemia cells predicts resistance to chemotherapy and poor outcome³¹. These results suggest that the activation of the extrinsic death receptor-mediated apoptotic pathway may play a role in chemotherapy-induced apoptosis.

HDAC inhibitors. HDAC inhibitors represent a group of novel cancer therapeutic agents⁶⁵. These agents induce apoptosis and enhance TRAIL-induced apoptosis in a variety of cancer cells. Suberoylanilide hydroxamic acid (SAHA) and trichostatin A (TSA) were shown to increase the levels of cell surface DR4 and DR5 in human multiple myeloma cell lines⁶⁶. LAQ824 (a cinnamic acid hydroxamate), SAHA, MS-275, m-carboxycinnamic acid bishydroxamide (CBHA), and TSA increased the expression of DR5 and/or DR4, reduced the levels of c-FLIP, and enhanced TRAIL-induced apoptosis in human acute leukemia cells⁶⁷⁻⁷⁰. One study showed that blockage of DR5 activation using DR5 siRNA in the breast cancer cell line MCF-7 decreased HDAC inhibitor-

induced apoptosis⁵², suggesting an important role of DR5 activation in apoptosis induced by HDAC inhibitors. Two recent elegant studies have shown that HDAC inhibitors upregulate not only DR5 and Fas expression but also the expression of their ligands TRAIL and FasL in the leukemic cells. Importantly, such findings were not observed in normal hematopoietic progenitors. Moreover, they further demonstrated that HDAC inhibitors induce apoptosis of leukemia cells through activation of a specific death pathway (i.g., TRAIL/DR5)^{71, 72}.

Currently, it is not clear how HDAC inhibitors upregulate the expression of death receptors. One study has suggested that HDAC inhibitors upregulate DR5 expression through cooperative activation of NF- κ B and p53⁵². Another study has demonstrated that sodium butyrate-induced expression of DR5 involves the putative Sp1 site within the DR5 promoter region (located at -195 bp relative to the transcription start site)⁷³.

Proteasome inhibitors. Inhibition of the proteasome has been considered to be an effective strategy for cancer therapy. Thereby, novel anticancer drugs with proteasome-inhibitory activity have been developed⁷⁴. The proteasome inhibitor MG132 upregulated DR5 expression and effectively cooperated with Apo2L/TRAIL to induce apoptosis in human colon cancer cells⁷⁵. A similar finding was also demonstrated in human prostate cancer cells and primary chronic lymphocytic leukemia (CLL) cells^{55 76}. It has been demonstrated that MG132 induces DR5 at the transcriptional level involving upregulation of CHOP protein⁵⁵. Another clinically-used proteasome inhibitor, PS-341, does not affect the levels of Bax, Bak, caspase-3 and -8, c-FLIP or FADD, but elevates levels of DR4 and DR5 in human prostate and bladder cancer cells. This increase in receptor protein levels is associated with the ubiquitination of the DR5 protein⁷⁷. We also showed that PS-341 increases DR5 expression and cell surface levels and enhances TRAIL-

induced apoptosis in human lung cancer cells⁷⁸. Interestingly, MG-132 also increases apoptosis and DR5 expression in normal B-cells. However, when it is combined with TRAIL or TRAIL receptor activating antibodies the amount of apoptosis is increased in CLL cells but not in normal B cells⁷⁶.

Cyclooxygenase-2 (COX-2) inhibitors. Since COX-2 is overexpressed in malignant tissues, the COX-2 mediated signaling pathway has been recognized as a potential target for therapeutic intervention of cancer⁷⁹. Sulindac sulfide; a COX-2 inhibitor, is one of the major metabolites of sulindac that is believed to mediate its antitumorigenic effects by inducing apoptosis. Sulindac sulfide specifically upregulates DR5 and activates caspase-8 in various colon and prostate cancer cell lines. Overexpression of a dominant-negative FADD (FADD-DN) suppresses sulindac sulfide-induced apoptosis and combination of sulindac sulfide with TRAIL exhibits an enhanced apoptosis-inducing effect, suggesting the involvement of DR5 in sulindac sulfide-induced apoptosis⁸⁰. Induction of DR5 by sulindac sulfide in gastric cancer cells has also been reported. In this study, DR4 expression was also induced by sulindac sulfide⁸¹. Moreover, we found that celecoxib increased the expression of DR4 and particularly DR5 at both mRNA and protein levels in human lung cancer cells. Both overexpression of FADD-DN and silencing of DR5 expression using siRNA attenuated celecoxib-induced apoptosis. Moreover, celecoxib cooperated with TRAIL to augment the induction of apoptosis. These results indicate that the expression of death receptors, particularly DR5, contributes to celecoxib-induced apoptosis⁸². Similarly, we further showed that the celecoxib analog, dimethyl-celecoxib, which lacks COX-2-inhibitory activity, exerts similar effects on upregulation of DR5 and enhancement of TRAIL-induced apoptosis⁸³. Thus, it appears that celecoxib regulates DR5 expression independent of its COX-2 inhibitory

activity. Both celecoxib and dimethyl-celecoxib induce DR5 expression through a CHOP-dependent mechanism⁸⁴.

Retinoid-related molecules. Retinoids, which include both synthetic and naturally occurring Vitamin A (retinal) metabolites and analogs, have long been considered to have cancer chemopreventive and therapeutic potential⁸⁵. Some novel synthetic retinoids potentially induce apoptosis in cancer cells independent of retinoic acid receptors (RARs) and thus are named retinoid-related molecules (RRMs)⁸⁶. One such compound called 6-[3-(1-adamantyl-4-hydroxyphenyl)-2-naphthalene carboxylic acid (CD437 or AHPC) can induce Fas, DR4 and DR5 expression in lung cancer cells in a p53-dependent manner⁸⁷⁻⁸⁹. Importantly, CD437 does not induce the expression of Fas, DR4, and DR5, and apoptosis in normal human bronchial epithelial cells and small airway epithelial cells⁹⁰. CD437 can also induce the expression of these death receptors independent of p53 in human prostate and head and neck cancer cells^{91, 92}. The CD437 analogue 4-[3-Cl-(1-adamantyl)-4-hydroxyphenyl]-3-chlorocinnamic acid (3-Cl-AHPC) also induces the expression of Fas, DR4 and DR5 in human prostate and breast cancer cells as well⁹³. Another RRM, ST1926, in cooperation with epidermal growth factor receptor inhibitor ZD1839 also upregulates DR5 levels⁹⁴. We and others have demonstrated that CD437 and 3-Cl-AHPC activate NF- κ B, which contributes to upregulation of DR4 and DR5 by CD437 or 3-Cl-AHPC in prostate cancer cells^{95, 93}.

N-(4-hydroxyphenyl) retinamide (4HPR) is another synthetic retinoid widely tested in many cancer clinical trials. It was shown to enhance TRAIL-mediated apoptosis through enhancement of a mitochondrial-dependent amplification loop in ovarian cancer cell lines⁹⁶. However, a recent study has shown that 4-HPR up-regulates DR5 expression via the induction of the transcription

factor CHOP, which sensitizes colon cancer cells to TRAIL-induced apoptosis⁹⁷. Several studies have shown that 4HPR and its analog induce CHOP expression in different types of cancer cells, which plays a role in 4HPR-induced apoptosis⁹⁸⁻¹⁰³. Therefore, these data suggest that 4HPR induces CHOP-dependent DR5 expression.

Triterpenoids. Triterpenoids are another group of natural and synthetic compounds with cancer therapeutic potential. The natural triterpenoids betulinic acid (Fig. 2) and boswellic acid were reported to induce DR5 expression in melanoma, glioblastoma, and leukemia cells^{104, 105}. Our recent study has shown that the synthetic triterpenoid methyl-2-cyano-3,12-dioxooleana-1,9-dien-28-oate (CDDO-Me) increased the expression of DR4 and particularly DR5, and enhanced TRAIL-induced apoptosis in human lung cancer cells. Silencing of DR5 expression using siRNA inhibited both CDDO-Me-induced apoptosis and CDDO-Me-mediated enhancement of TRAIL-induced apoptosis, indicating the involvement of DR5 in both activities¹⁰⁶. Upregulation of cell surface DR4 and DR5 by CDDO-Me analogues CDDO and CDDO-Im in breast cancer cells was also reported¹⁰⁷. In addition, it has been shown that induction of DR5 by betulinic acid and CDDO-Me is independent of p53^{104, 106}. We found that CDDO-Me rapidly activated c-Jun NH₂-terminal kinase (JNK) before DR5 up-regulation. Moreover, application of the JNK-specific inhibitor SP600125 blocked CDDO-Me-induced DR5 upregulation. These results indicate that CDDO-Me induces a JNK-dependent DR5 upregulation¹⁰⁶.

Cytokines. Certain cytokines including interferons have anticancer activity. TNF α is the first cytokine demonstrated to induce the expression of DR5 in a number of cancer cell lines. The induction of DR5 by TNF α occurs at transcriptional levels irrespective of p53 status⁵⁰.

Subsequently, interferon- γ was shown to induce DR5 expression in cancer cell lines independent of p53¹⁰⁴. Interferon- α was also reported to increase DR5 expression in human hepatoma cells; this increased expression is associated with its ability to enhance TRAIL-induced apoptosis¹⁰⁸. In addition to regulation of death receptors, interferons regulate the expression of death ligands. For example, interferon γ increases TRAIL expression in colon cancer cells, which mediates interferon γ -induced apoptosis¹⁰⁹. Moreover, interferon α increased expression of TRAIL, DR4 and DR5, which were involved in interferon α -induced apoptosis in Daudi B lymphoma cells¹¹⁰. Interestingly, TRAIL itself increases the expression of DR5 in human embryonic kidney (HEK) 293, MCF-7 and MDA MB 231 epithelial cell lines while DR4 expression remains unchanged. This effect is mediated by NF- κ B activation⁶³.

Natural products. Natural products have been the most significant source of drugs and drug leads in history. Their dominant role in cancer chemotherapeutics is clear with about 74% of anticancer compounds being either natural products, or natural product-derived¹¹¹. Curcumin (Fig. 2), a plant product containing the phenolic phytochemical with apoptosis-inducing activity, has been demonstrated to increase Fas expression and induce Fas clustering in human melanoma cells, leading to the induction of apoptosis¹¹². Curcumin also increased cell surface DR4 or DR5 and augmented TRAIL-induced apoptosis in prostate cancer¹¹³ and renal cancer cells¹¹⁴. Although curcumin induced the expression of CHOP, suppression of CHOP expression by siRNA did not abrogate DR5 induction by curcumin and cell death induced by curcumin plus TRAIL, demonstrating that CHOP is not involved in curcumin-induced DR5 upregulation¹¹⁵. Sulforaphane (Fig. 2) is a naturally occurring isothiocyanate with potent anticancer activity. This agent has been demonstrated to upregulate DR5 expression and subsequently to enhance TRAIL-induced

apoptosis in hepatoma ¹¹⁶ and osteosarcoma ¹¹⁷ cells. Importantly, sulforaphane neither induces DR5 protein expression nor enhances TRAIL-induced apoptosis in normal human peripheral blood mononuclear cells ¹¹⁷. Luteolin (Fig. 2), a naturally occurring flavonoid, induces apoptosis in various cancer cells. A recent study has shown that luteolin upregulates DR5 expression in human cancer cell lines ¹¹⁸. Suppression of DR5 expression with siRNA efficiently reduced luteolin-induced caspase activation and apoptosis. Human recombinant DR5/Fc also inhibited luteolin-induced apoptosis ¹¹⁸. These results suggest that DR5 induced by luteolin plays a role in luteolin-induced apoptosis. Dihydroflavonol BB-1 (Fig. 2), an extract of the natural plant *Blumea balsamifera*, increases DR5 gene promoter activity and surface DR5 expression in a p53-independent manner in leukemia cells ¹¹⁹. Silibinin (Fig. 2), a flavonoid isolated from *Silybum marianum*, can sensitize glioma cells to TRAIL-induced apoptosis, partially due to CHOP-dependent upregulation of DR5 ¹²⁰.

Others. The synthetic glucocorticoid dexamethasone elevated DR5 expression and induced apoptosis in several types of cancer cell lines including glioblastoma, ovarian cancer, and colon cancer cell lines with mutant p53, and this induction was inhibited by the transcriptional inhibitor actinomycin D ¹⁰⁴. 2-methoxyestradiol (2ME (Fig. 2)), a natural metabolite of estradiol, is a potent antitumor and antiangiogenic agent and is currently being tested in several Phase I and Phase II clinical trials under the name Panzem. It has been recently shown that 2ME results in up-regulation of DR5 protein expression in several cancer cell lines including breast cancer cells *in vitro* and *in vivo* and renders cells more sensitive to TRAIL-induced apoptosis. Blockage of death receptor signaling by expression of dominant-negative FADD severely attenuates the ability of 2ME to induce apoptosis, suggesting that 2ME induces apoptosis through activation of the DR5-mediated

extrinsic pathway¹²¹. However, another study failed to demonstrate upregulation of DR5 by 2ME and synergism between 2ME and TRAIL in glioma cells¹²². Induction of DR5 by 2ME was also not demonstrated in another CAL51 breast cancer cell line although 2ME synergized with TRAIL to induce apoptosis¹²³. Thapsigargin (TG), an agent known to cause endoplasmic reticulum (ER) stress due to perturbations in intracellular Ca^{2+} homeostasis and induce apoptosis, upregulates DR5 expression as well as TRAIL expression^{54, 124, 125}. The induction of DR5 occurs as a consequence of TG-induced ER Ca^{2+} pool depletion¹²⁴ involving CHOP-mediated transactivation of the DR5 gene⁵⁴. Tunicamycin (Fig. 2), a naturally occurring antibiotic, upregulates DR5 expression through a CHOP-dependent mechanism and enhances TRAIL-induced apoptosis in human prostate cancer cells¹²⁶. Of note, tunicamycin-mediated induction of CHOP and DR5 protein expression was not observed in normal human peripheral blood mononuclear cells¹²⁶. Arsenic trioxide, a drug for treatment of leukemia, increases cell surface expression of DR5 and sensitizes leukaemic cells to TRAIL-induced apoptosis¹²⁷. The semisynthetic analogue of vitamin E, α -tocopheryl succinate, increases the expression of both DR4 and DR5 in human malignant mesothelioma cells in a p53-dependent manner; this increased expression is associated with its ability to enhance TRAIL-induced apoptosis^{128, 129}. As well, the alkylphospholipid perifosine increases DR5 expression in human lung cancer cells as we recently demonstrated¹³⁰.

Induction of death receptor redistribution and clustering by anticancer agents

The majority of anticancer therapeutic agents upregulate the expression of death receptors. However, some agents are able to activate the death receptors in a ligand-dependent (autocrine) or -independent way, leading to activation of the extrinsic apoptotic pathway without apparently altering the expression levels of the death receptors. Since receptor trimerization is an essential

step for activation of the death receptor-mediated extrinsic apoptosis, induction of death receptor aggregation or clustering, even in the absence of a specific death ligand, should be sufficient to trigger apoptosis. Current studies have shown that several cancer therapeutic agents activate the death receptor-mediated apoptotic pathway through lipid raft-mediated death receptor aggregation or clustering, which concentrates and activates death receptors. Induction of death receptor redistribution and clustering in lipid rafts is also an important mechanism for certain agents to sensitize cancer cells to TRAIL-induced apoptosis.

Lipid rafts are microdomains of plasma membranes enriched in sphingolipids and cholesterol¹³¹. Recently, lipid rafts have been demonstrated to be involved in control of apoptosis, particularly death receptor-mediated apoptosis^{132, 133}. Aplidine (Fig. 2) is a promising antitumor agent derived from the Mediterranean tunicate *Aplidium albicans*. This agent induces apoptosis of leukemia cells involving activation of the Fas-mediated extrinsic apoptotic pathway¹³⁴. It has been shown that Fas, TNFR1, and DR5 are clustered into lipid rafts in leukemic Jurkat cells following aplidin treatment¹³⁵. Aplidine is rapidly incorporated into membrane rafts and induces Fas clustering and apoptosis, whereas disruption of lipid rafts inhibits uptake of aplidine and prevents Fas clustering. Thus, Aplidine-induced apoptosis involves Fas activation in both a FasL-independent manner and an autocrine manner through the concentration of Fas, membrane-bound FasL, and signaling molecules in membrane rafts¹³⁵. The anticancer drug ET-18-OCH(3) (Edelfosine) does not promote the expression of Fas or FasL. However, it induces Fas-dependent apoptosis in leukemia cells independent of FasL¹³⁶. Further study has shown that ET-18-OCH(3) similar to aplidin induces apoptosis by inducing formation of lipid rafts in tumor cells, followed by its co-aggregation with Fas and recruitment of apoptotic molecules into Fas-enriched rafts^{137, 138}. A

similar mechanism was also observed in multiple myeloma cells undergoing edelfosine- or perifosine-induced apoptosis ¹³⁹.

Cisplatin, a known DNA-damaging agent, also induces clustering of Fas at the surface of human colon cancer cells. It has been demonstrated that cisplatin activates acid sphingomyelinase (aSMase) and induces ceramide production, which triggers the redistribution of Fas into the plasma membrane rafts. Such redistribution contributes to cisplatin-induced cell death and sensitizes tumor cells to Fas-mediated apoptosis ¹⁴².

Resveratrol (Fig. 2), a polyphenol found in grape skin and various other food products, exhibits both cancer chemopreventive and therapeutic activity. In contrast to other agents, studies in human colon cancer cells have shown that resveratrol does not modulate the expression of Fas, DR4, and DR5 at the surface of cancer cells; However, resveratrol induces the clustering of these death receptors and their redistribution in cholesterol and lipid rafts together with FADD and procaspase-8. These redistributions are associated with the formation of a DISC and contribute to the induction of apoptosis and sensitization of cells to death ligand- or death receptor activation-mediated apoptosis ^{140, 141}. Similarly, the flavonoid quercetin (Fig. 2) enhances TRAIL-induced apoptosis by causing the redistribution of DR4 and DR5 into lipid rafts in colon cancer cells ¹⁴³.

The COX-2 inhibitor DuP-697 does not modulate the levels of DR5 and DR4 although it enhances TRAIL-induced apoptosis in cancer cells. Instead, it sensitizes cells to TRAIL-induced apoptosis by inducing clustering of DR5 at the cell surface and the redistribution of the death-inducing signaling complex components (DR5, FADD, and procaspase-8) into cholesterol-rich and ceramide-rich domains known as lipid rafts or caveolae ¹⁴⁴. Similarly, the HDAC inhibitor depsipeptide (FR901228) also increases levels of DR4 and DR5 in membrane lipid rafts, leading to enhancement of TRAIL-induced apoptosis ¹⁴⁵.

Implications of death receptor modulation in cancer therapy

Activation of death receptors with either ligand binding or receptor aggregation triggers the extrinsic apoptotic pathway. Therefore, the death ligands (e.g., TRAIL) or agonistic death receptor antibodies (e.g., antibody against DR4 or DR5) induce apoptosis of cancer cells with cancer therapeutic potential. Currently, both TRAIL and agonistic DR4 and DR5 antibodies are being tested in clinical trials for their anticancer activities⁷. The drugs that upregulate the expression of DR4 and/or DR5, or induce redistribution of DR4 and/or DR5 at the cell surface, preferentially in malignant cancer cells, are assumed to sensitize cancer cells to treatment with either TRAIL or agonistic DR4 or DR5 antibodies. This sensitization has been documented in many preclinical studies both *in vitro* and *in vivo*⁷. The good news is that many clinically used cancer therapeutic agents including chemotherapeutic drugs upregulate the expression of DR4 and/or DR5. Therefore, it should be easy to test the combination therapy of these drugs with TRAIL or an agonistic antibodies in the clinic to enhance cancer therapy.

Some agents have been demonstrated to induce the expression of death ligands such as TRAIL. Examples of these agents are retinoic acid^{146, 147}, interferons^{147, 148}, and PI3 kinase inhibitors¹⁴⁹. Therefore, it is plausible to speculate that the combination of a death receptor-inducing drug with a death ligand-inducing agent may enhance the killing or elimination of malignant cancer cells via death ligand/death receptor-mediated apoptosis. Studying the effect of this kind of combination may develop an effective combination regimen for cancer therapy.

Apoptosis induced by the interaction between death ligand (from NK cells or T cells) and death receptors (from target cells) is the primary mechanism underlying tumor immunosurveillance^{10, 150, 151}. In death ligand-expressing cancer cells, the binding of death ligands

such as Fas ligand (FasL) and TRAIL to an increased number of death receptors due to treatment with cancer therapeutic agents may trigger the apoptotic signal leading to the death of cancer cells (autocrine mechanism). Moreover, upregulation of death receptors in cancer cells may cause these cells to become more susceptible targets for immune cells (i.e., NK and T cells) that express and secrete death ligands such as TRAIL. Therefore, cancer therapeutic agents with death receptor-inducing activity can sensitize cancer cells to death receptor-mediated immune clearance or surveillance. Similarly these agents can also enhance death receptor-based cancer immunotherapy

152-154

Summary and perspectives

Extensive studies have shown that many cancer therapeutic agents increase the expression of death receptors or activate death receptors. The question is whether modulation of death receptors plays any role in drug-induced apoptosis because it is generally thought that small molecules induce apoptosis through activation of the intrinsic apoptotic pathway. Some studies indeed suggest that certain drugs induce apoptosis via ligand-dependent or -independent activation of the death receptor-mediated extrinsic apoptotic pathway. To robustly demonstrate the role of death receptor activation in drug-induced apoptosis, establishment of cancer cell lines deficient with one (e.g., DR5), two (e.g., DR4 and DR5), or even three (e.g., DR4, DR5 and Fas) death receptors will be very helpful. These cell lines would also be valuable for screening cancer therapeutic agents that induce apoptosis through the death receptor-mediated extrinsic apoptotic pathway. The current technology of homologous recombination¹⁵⁵ makes possible such kind of studies.

Given that TRAIL and agonistic antibodies to DR4 and DR5 exhibit cancer therapeutic potential and their efficacies can be enhanced by small molecules, it will be important to develop

small molecules that upregulate the expression of DR4 and/or DR5 and potentiate TRAIL-induced apoptosis, preferentially in human cancer cells independent of p53. To this end, DR4 or DR5 should be a good target for discovery of anticancer drugs. Some clinically-used drugs such as sulindac and celecoxib, which potently increase the expression of TRAIL death receptors and enhance TRAIL-induced apoptosis, have simple chemical structures and could be considered as lead compounds for further modification. In addition, an important step is to develop assays for screening agents that upregulate TRAIL death receptors. To do so, we need a better understanding of general mechanisms by which TRAIL death receptors are induced.

Certain cancer therapeutic agents themselves are weak inducers of apoptosis in cell culture, but potently upregulate the expression of death receptors and cooperative with exogenous TRAIL to induce apoptosis. Therefore, it is important to consider the *in vivo* situation where stromal cells may impact the growth of tumors and the response of tumor cells to therapeutic drugs. We may speculate that these death receptor-inducing agents can effectively inhibit the growth of tumors by inducing apoptosis through promotion of the interaction between death receptors (in tumor cells) and endogenous death ligands (from stromal cells or immune cells) *in vivo*. If this is true, these agents should not be very effective to treat tumors (i.e., murine tumors) developed from death ligand (e.g., TRAIL)-null animals. Therefore, it is important to demonstrate this issue *in vivo*. Currently TRAIL-null¹⁵⁶ and or FasL-null¹⁵⁷ mice are available and thus make these studies possible.

In the field of death receptor research, some discrepancies in the literature among different studies may be caused by antibodies from different sources, some of which are not specific (e.g., DR4) based on our experimnce. Therefore, it is important to carefully characterize some antibodies

(e.g., through siRNA and recombinant proteins), particularly those for staining of clinical specimens. In this way, we will avoid or minimize artifacts or confusion.

In conclusion, as we further our understanding of the modulation of death receptors by cancer therapeutic agents, we will be able to more effectively and selectively target cancer cells sensitive to death receptor-mediated apoptosis.

Acknowledgements

Works in author's laboratory were supported by the Georgia Cancer Coalition Distinguished Cancer Scholar award, the Department of Defense VITAL grant W81XWH-04-1-0142 (Project 4 to S-Y Sun), and the National Cancer Center head and neck cancer SPORE grant P50 CA128613-01 (Project 2 to S-Y Sun).

S-Y Sun is a Georgia Cancer Coalition Distinguished Cancer Scholar.

References

1. Schulze-Bergkamen H, Krammer PH. Apoptosis in cancer--implications for therapy. *Semin Oncol* 2004;31: 90-119.
2. Ashkenazi A, Dixit VM. Death receptors: signaling and modulation. *Science* 1998;281: 1305-8.
3. Almasan A, Ashkenazi A. Apo2L/TRAIL: apoptosis signaling, biology, and potential for cancer therapy. *Cytokine Growth Factor Rev* 2003;14: 337-48.
4. Jo M, Kim TH, Seol DW, Esplen JE, Dorko K, Billiar TR, Strom SC. Apoptosis induced in normal human hepatocytes by tumor necrosis factor-related apoptosis-inducing ligand. *Nat Med* 2000;6: 564-7.
5. Lawrence D, Shahrokh Z, Marsters S, Achilles K, Shih D, Mounho B, Hillan K, Totpal K, DeForge L, Schow P, Hooley J, Sherwood S, Pai R, Leung S, Khan L, Gliniak B, Bussiere J, Smith CA, Strom SS, Kelley S, Fox JA, Thomas D, Ashkenazi A. Differential hepatocyte toxicity of recombinant Apo2L/TRAIL versions. *Nat Med* 2001;7: 383-5.
6. Ashkenazi A. Targeting death and decoy receptors of the tumour-necrosis factor superfamily. *Nat Rev Cancer* 2002;2: 420-30.
7. Rowinsky EK. Targeted induction of apoptosis in cancer management: the emerging role of tumor necrosis factor-related apoptosis-inducing ligand receptor activating agents. *J Clin Oncol* 2005;23: 9394-407.
8. Petak I, Houghton JA. Shared pathways: death receptors and cytotoxic drugs in cancer therapy. *Pathol Oncol Res* 2001;7: 95-106.
9. Sheikh MS, Huang Y. Death receptors as targets of cancer therapeutics. *Curr Cancer Drug Targets* 2004;4: 97-104.
10. Yagita H, Takeda K, Hayakawa Y, Smyth MJ, Okumura K. TRAIL and its receptors as targets for cancer therapy. *Cancer Sci* 2004;95: 777-83.
11. Fesik SW. Promoting apoptosis as a strategy for cancer drug discovery. *Nat Rev Cancer* 2005;5: 876-85.
12. Wajant H, Gerspach J, Pfizenmaier K. Tumor therapeutics by design: targeting and activation of death receptors. *Cytokine Growth Factor Rev* 2005;16: 55-76.
13. Zimmermann KC, Green DR. How cells die: apoptosis pathways. *J Allergy Clin Immunol* 2001;108: S99-103.
14. Ashkenazi A, Dixit VM. Apoptosis control by death and decoy receptors. *Curr Opin Cell Biol* 1999;11: 255-60.
15. Lavrik I, Golks A, Krammer PH. Death receptor signaling. *J Cell Sci* 2005;118: 265-7.
16. Wajant H. Death receptors. *Essays Biochem* 2003;39: 53-71.
17. Timmer T, de Vries EG, de Jong S. Fas receptor-mediated apoptosis: a clinical application? *J Pathol* 2002;196: 125-34.
18. Ozoren N, El-Deiry WS. Cell surface Death Receptor signaling in normal and cancer cells. *Semin Cancer Biol* 2003;13: 135-47.
19. Liu LG, Tanaka H, Ito K, Ito T, Sultana TA, Kyo T, Kimura A. Absence of gene mutation in TRAIL receptor 1 (TRAIL-R1) and TRAIL receptor 2 (TRAIL-R2) in chronic myelogenous leukemia and myelodysplastic syndrome, and analysis of mRNA Expressions of TRAIL and TRAIL-related genes in chronic myelogenous leukemia. *Acta Haematol* 2005;113: 113-23.

20. Adams J, Cuthbert-Heavens D, Bass S, Knowles MA. Infrequent mutation of TRAIL receptor 2 (TRAIL-R2/DR5) in transitional cell carcinoma of the bladder with 8p21 loss of heterozygosity. *Cancer Lett* 2005;220: 137-44.
21. Reesink-Peters N, Hougardy BM, van den Heuvel FA, Ten Hoor KA, Hollema H, Boezen HM, de Vries EG, de Jong S, van der Zee AG. Death receptors and ligands in cervical carcinogenesis: an immunohistochemical study. *Gynecol Oncol* 2005;96: 705-13.
22. Yamana K, Bilim V, Hara N, Kasahara T, Itoi T, Maruyama R, Nishiyama T, Takahashi K, Tomita Y. Prognostic impact of FAS/CD95/APO-1 in urothelial cancers: decreased expression of Fas is associated with disease progression. *Br J Cancer* 2005;93: 544-51.
23. Horak P, Pils D, Haller G, Pribill I, Roessler M, Tomek S, Horvat R, Zeillinger R, Zielinski C, Krainer M. Contribution of epigenetic silencing of tumor necrosis factor-related apoptosis inducing ligand receptor 1 (DR4) to TRAIL resistance and ovarian cancer. *Mol Cancer Res* 2005;3: 335-43.
24. Hopkins-Donaldson S, Ziegler A, Kurtz S, Bigosch C, Kandioler D, Ludwig C, Zangemeister-Wittke U, Stahel R. Silencing of death receptor and caspase-8 expression in small cell lung carcinoma cell lines and tumors by DNA methylation. *Cell Death Differ* 2003;10: 356-64.
25. Min YJ, Lee JH, Choi SJ, Chi HS, Lee JS, Kim WK, Lee KH. Prognostic significance of Fas (CD95) and TRAIL receptors (DR4/DR5) expression in acute myelogenous leukemia. *Leukemia research* 2004;28: 359-65.
26. Spierings DC, de Vries EG, Timens W, Groen HJ, Boezen HM, de Jong S. Expression of TRAIL and TRAIL death receptors in stage III non-small cell lung cancer tumors. *Clin Cancer Res* 2003;9: 3397-405.
27. Koornstra JJ, Kleibeuker JH, van Geelen CM, Rijcken FE, Hollema H, de Vries EG, de Jong S. Expression of TRAIL (TNF-related apoptosis-inducing ligand) and its receptors in normal colonic mucosa, adenomas, and carcinomas. *J Pathol* 2003;200: 327-35.
28. van Geelen CM, Westra JL, de Vries EG, Boersma-van Ek W, Zwart N, Hollema H, Boezen HM, Mulder NH, Plukker JT, de Jong S, Kleibeuker JH, Koornstra JJ. Prognostic significance of tumor necrosis factor-related apoptosis-inducing ligand and its receptors in adjuvantly treated stage III colon cancer patients. *J Clin Oncol* 2006;24: 4998-5004.
29. Ullenhag GJ, Mukherjee A, Watson NF, Al-Attar AH, Scholefield JH, Durrant LG. Overexpression of FLIPL is an independent marker of poor prognosis in colorectal cancer patients. *Clin Cancer Res* 2007;13: 5070-5.
30. McCarthy MM, Sznol M, DiVito KA, Camp RL, Rimm DL, Kluger HM. Evaluating the expression and prognostic value of TRAIL-R1 and TRAIL-R2 in breast cancer. *Clin Cancer Res* 2005;11: 5188-94.
31. Tournear L, Delluc S, Levy V, Valensi F, Radford-Weiss I, Legrand O, Vargaftig J, Boix C, Macintyre EA, Varet B, Chiocchia G, Buzyn A. Absence or low expression of fas-associated protein with death domain in acute myeloid leukemia cells predicts resistance to chemotherapy and poor outcome. *Cancer Res* 2004;64: 8101-8.
32. Chen G, Bhojani MS, Heaford AC, Chang DC, Laxman B, Thomas DG, Griffin LB, Yu J, Coppola JM, Giordano TJ, Lin L, Adams D, Orringer MB, Ross BD, Beer DG, Rehemtulla A. Phosphorylated FADD induces NF-kappaB, perturbs cell cycle, and is associated with poor outcome in lung adenocarcinomas. *Proc Natl Acad Sci U S A* 2005;102: 12507-12.
33. Debatin KM, Krammer PH. Death receptors in chemotherapy and cancer. *Oncogene* 2004;23: 2950-66.

34. Pitti RM, Marsters SA, Lawrence DA, Roy M, Kischkel FC, Dowd P, Huang A, Donahue CJ, Sherwood SW, Baldwin DT, Godowski PJ, Wood WI, Gurney AL, Hillan KJ, Cohen RL, Goddard AD, Botstein D, Ashkenazi A. Genomic amplification of a decoy receptor for Fas ligand in lung and colon cancer. *Nature* 1998;396: 699-703.
35. Arakawa Y, Tachibana O, Hasegawa M, Miyamori T, Yamashita J, Hayashi Y. Frequent gene amplification and overexpression of decoy receptor 3 in glioblastoma. *Acta Neuropathol (Berl)* 2005;109: 294-8.
36. Shen HW, Gao SL, Wu YL, Peng SY. Overexpression of decoy receptor 3 in hepatocellular carcinoma and its association with resistance to Fas ligand-mediated apoptosis. *World J Gastroenterol* 2005;11: 5926-30.
37. Li H, Zhang L, Lou H, Ding I, Kim S, Wang L, Huang J, Di Sant'Agnese PA, Lei JY. Overexpression of decoy receptor 3 in precancerous lesions and adenocarcinoma of the esophagus. *Am J Clin Pathol* 2005;124: 282-7.
38. van Noesel MM, van Bezouw S, Salomons GS, Voute PA, Pieters R, Baylin SB, Herman JG, Versteeg R. Tumor-specific down-regulation of the tumor necrosis factor-related apoptosis-inducing ligand decoy receptors DcR1 and DcR2 is associated with dense promoter hypermethylation. *Cancer Res* 2002;62: 2157-61.
39. Shivapurkar N, Toyooka S, Toyooka KO, Reddy J, Miyajima K, Suzuki M, Shigematsu H, Takahashi T, Parikh G, Pass HI, Chaudhary PM, Gazdar AF. Aberrant methylation of trail decoy receptor genes is frequent in multiple tumor types. *Int J Cancer* 2004;109: 786-92.
40. Levine AJ. p53, the cellular gatekeeper for growth and division. *Cell* 1997;88: 323-31.
41. Bennett M, Macdonald K, Chan SW, Luzio JP, Simari R, Weissberg P. Cell surface trafficking of Fas: a rapid mechanism of p53-mediated apoptosis. *Science* 1998;282: 290-3.
42. Muller M, Wilder S, Bannasch D, Israeli D, Lehlbach K, Li-Weber M, Friedman SL, Galle PR, Stremmel W, Oren M, Krammer PH. p53 activates the CD95 (APO-1/Fas) gene in response to DNA damage by anticancer drugs. *J Exp Med* 1998;188: 2033-45.
43. Wu GS, Burns TF, McDonald ER, 3rd, Jiang W, Meng R, Krantz ID, Kao G, Gan DD, Zhou JY, Muschel R, Hamilton SR, Spinner NB, Markowitz S, Wu G, el-Deiry WS. KILLER/DR5 is a DNA damage-inducible p53-regulated death receptor gene. *Nat Genet* 1997;17: 141-3.
44. Takimoto R, El-Deiry WS. Wild-type p53 transactivates the KILLER/DR5 gene through an intronic sequence-specific DNA-binding site. *Oncogene* 2000;19: 1735-43.
45. Guan B, Yue P, Clayman GL, Sun SY. Evidence that the death receptor DR4 is a DNA damage-inducible, p53-regulated gene. *J Cell Physiol* 2001;188: 98-105.
46. Liu X, Yue P, Khuri FR, Sun SY. p53 upregulates death receptor 4 expression through an intronic p53 binding site. *Cancer Res* 2004;64: 5078-83.
47. Cheng J, Liu C, Koopman WJ, Mountz JD. Characterization of human Fas gene. Exon/intron organization and promoter region. *J Immunol* 1995;154: 1239-45.
48. Chan H, Bartos DP, Owen-Schaub LB. Activation-dependent transcriptional regulation of the human Fas promoter requires NF-kappaB p50-p65 recruitment. *Mol Cell Biol* 1999;19: 2098-108.
49. Li XR, Chong AS, Wu J, Roebuck KA, Kumar A, Parrillo JE, Rapp UR, Kimberly RP, Williams JW, Xu X. Transcriptional regulation of Fas gene expression by GA-binding protein and AP-1 in T cell antigen receptor.CD3 complex-stimulated T cells. *J Biol Chem* 1999;274: 35203-10.
50. Sheikh MS, Burns TF, Huang Y, Wu GS, Amundson S, Brooks KS, Fornace AJ, Jr., el-Deiry WS. p53-dependent and -independent regulation of the death receptor KILLER/DR5 gene

- expression in response to genotoxic stress and tumor necrosis factor alpha. *Cancer Res* 1998;58: 1593-8.
51. Ravi R, Bedi GC, Engstrom LW, Zeng Q, Mookerjee B, Gelinas C, Fuchs EJ, Bedi A. Regulation of death receptor expression and TRAIL/Apo2L-induced apoptosis by NF-kappaB. *Nat Cell Biol* 2001;3: 409-16.
 52. Shetty S, Graham BA, Brown JG, Hu X, Vegh-Yarema N, Harding G, Paul JT, Gibson SB. Transcription factor NF-kappaB differentially regulates death receptor 5 expression involving histone deacetylase 1. *Mol Cell Biol* 2005;25: 5404-16.
 53. Guan B, Yue P, Lotan R, Sun SY. Evidence that the human death receptor 4 is regulated by activator protein 1. *Oncogene* 2002;21: 3121-9.
 54. Yamaguchi H, Wang HG. CHOP is involved in endoplasmic reticulum stress-induced apoptosis by enhancing DR5 expression in human carcinoma cells. *J Biol Chem* 2004;279: 45495-502.
 55. Yoshida T, Shiraishi T, Nakata S, Horinaka M, Wakada M, Mizutani Y, Miki T, Sakai T. Proteasome inhibitor MG132 induces death receptor 5 through CCAAT/enhancer-binding protein homologous protein. *Cancer Res* 2005;65: 5662-7.
 56. Baritaki S, Katsman A, Chatterjee D, Yeung KC, Spandidos DA, Bonavida B. Regulation of tumor cell sensitivity to TRAIL-induced apoptosis by the metastatic suppressor Raf kinase inhibitor protein via Yin Yang 1 inhibition and death receptor 5 up-regulation. *J Immunol* 2007;179: 5441-53.
 57. Baritaki S, Huerta-Yepez S, Sakai T, Spandidos DA, Bonavida B. Chemotherapeutic drugs sensitize cancer cells to TRAIL-mediated apoptosis: up-regulation of DR5 and inhibition of Yin Yang 1. *Mol Cancer Ther* 2007;6: 1387-99.
 58. Sun SY. Chemopreventive agent-induced modulation of death receptors. *Apoptosis* 2005;10: 1203-10.
 59. Gibson SB, Oyer R, Spalding AC, Anderson SM, Johnson GL. Increased expression of death receptors 4 and 5 synergizes the apoptosis response to combined treatment with etoposide and TRAIL. *Mol Cell Biol* 2000;20: 205-12.
 60. Nagane M, Pan G, Weddle JJ, Dixit VM, Cavenee WK, Huang HJ. Increased death receptor 5 expression by chemotherapeutic agents in human gliomas causes synergistic cytotoxicity with tumor necrosis factor-related apoptosis-inducing ligand in vitro and in vivo. *Cancer Res* 2000;60: 847-53.
 61. Wen J, Ramadevi N, Nguyen D, Perkins C, Worthington E, Bhalla K. Antileukemic drugs increase death receptor 5 levels and enhance Apo-2L-induced apoptosis of human acute leukemia cells. *Blood* 2000;96: 3900-6.
 62. Evdokiou A, Bouralexis S, Atkins GJ, Chai F, Hay S, Clayer M, Findlay DM. Chemotherapeutic agents sensitize osteogenic sarcoma cells, but not normal human bone cells, to Apo2L/TRAIL-induced apoptosis. *Int J Cancer* 2002;99: 491-504.
 63. Shetty S, Gladden JB, Henson ES, Hu X, Villanueva J, Haney N, Gibson SB. Tumor necrosis factor-related apoptosis inducing ligand (TRAIL) up-regulates death receptor 5 (DR5) mediated by NFkappaB activation in epithelial derived cell lines. *Apoptosis* 2002;7: 413-20.
 64. Longley DB, Wilson TR, McEwan M, Allen WL, McDermott U, Galligan L, Johnston PG. c-FLIP inhibits chemotherapy-induced colorectal cancer cell death. *Oncogene* 2006;25: 838-48.
 65. Kristeleit R, Fong P, Aherne GW, de Bono J. Histone deacetylase inhibitors: emerging anticancer therapeutic agents? *Clin Lung Cancer* 2005;7 Suppl 1: S19-30.

66. Fandy TE, Shankar S, Ross DD, Sausville E, Srivastava RK. Interactive effects of HDAC inhibitors and TRAIL on apoptosis are associated with changes in mitochondrial functions and expressions of cell cycle regulatory genes in multiple myeloma. *Neoplasia* 2005;7: 646-57.
67. Guo F, Sigua C, Tao J, Bali P, George P, Li Y, Wittmann S, Moscinski L, Atadja P, Bhalla K. Cotreatment with histone deacetylase inhibitor LAQ824 enhances Apo-2L/tumor necrosis factor-related apoptosis inducing ligand-induced death inducing signaling complex activity and apoptosis of human acute leukemia cells. *Cancer Res* 2004;64: 2580-9.
68. Shankar S, Singh TR, Fandy TE, Luetrakul T, Ross DD, Srivastava RK. Interactive effects of histone deacetylase inhibitors and TRAIL on apoptosis in human leukemia cells: involvement of both death receptor and mitochondrial pathways. *Int J Mol Med* 2005;16: 1125-38.
69. Nakata S, Yoshida T, Horinaka M, Shiraishi T, Wakada M, Sakai T. Histone deacetylase inhibitors upregulate death receptor 5/TRAIL-R2 and sensitize apoptosis induced by TRAIL/APO2-L in human malignant tumor cells. *Oncogene* 2004;23: 6261-71.
70. Butler LM, Liapis V, Bouralexis S, Welldon K, Hay S, Thai le M, Labrinidis A, Tilley WD, Findlay DM, Evdokiou A. The histone deacetylase inhibitor, suberoylanilide hydroxamic acid, overcomes resistance of human breast cancer cells to Apo2L/TRAIL. *Int J Cancer* 2006;119: 944-54.
71. Insinga A, Monestiroli S, Ronzoni S, Gelmetti V, Marchesi F, Viale A, Altucci L, Nervi C, Minucci S, Pelicci PG. Inhibitors of histone deacetylases induce tumor-selective apoptosis through activation of the death receptor pathway. *Nat Med* 2005;11: 71-6.
72. Nebbioso A, Clarke N, Voltz E, Germain E, Ambrosino C, Bontempo P, Alvarez R, Schiavone EM, Ferrara F, Bresciani F, Weisz A, de Lera AR, Gronemeyer H, Altucci L. Tumor-selective action of HDAC inhibitors involves TRAIL induction in acute myeloid leukemia cells. *Nat Med* 2005;11: 77-84.
73. Kim YH, Park JW, Lee JY, Kwon TK. Sodium butyrate sensitizes TRAIL-mediated apoptosis by induction of transcription from the DR5 gene promoter through Sp1 sites in colon cancer cells. *Carcinogenesis* 2004;25: 1813-20.
74. Rajkumar SV, Richardson PG, Hideshima T, Anderson KC. Proteasome inhibition as a novel therapeutic target in human cancer. *J Clin Oncol* 2005;23: 630-9.
75. He Q, Huang Y, Sheikh MS. Proteasome inhibitor MG132 upregulates death receptor 5 and cooperates with Apo2L/TRAIL to induce apoptosis in Bax-proficient and -deficient cells. *Oncogene* 2004;23: 2554-8.
76. Kabore AF, Sun J, Hu X, McCrea K, Johnston JB, Gibson SB. The TRAIL apoptotic pathway mediates proteasome inhibitor induced apoptosis in primary chronic lymphocytic leukemia cells. *Apoptosis* 2006.
77. Johnson TR, Stone K, Nikrad M, Yeh T, Zong WX, Thompson CB, Nesterov A, Kraft AS. The proteasome inhibitor PS-341 overcomes TRAIL resistance in Bax and caspase 9-negative or Bcl-xL overexpressing cells. *Oncogene* 2003;22: 4953-63.
78. Liu X, Yue P, Chen S, Hu L, Lonial S, Khuri FR, Sun SY. The proteasome inhibitor PS-341 (bortezomib) up-regulates DR5 expression leading to induction of apoptosis and enhancement of TRAIL-induced apoptosis despite up-regulation of c-FLIP and survivin expression in human NSCLC cells. *Cancer Res* 2007;67: 4981-8.
79. Meric JB, Rottey S, Olaussen K, Soria JC, Khayat D, Rixe O, Spano JP. Cyclooxygenase-2 as a target for anticancer drug development. *Crit Rev Oncol Hematol* 2006.

80. Huang Y, He Q, Hillman MJ, Rong R, Sheikh MS. Sulindac sulfide-induced apoptosis involves death receptor 5 and the caspase 8-dependent pathway in human colon and prostate cancer cells. *Cancer Res* 2001;61: 6918-24.
81. Jang TJ, Kang HJ, Kim JR, Yang CH. Non-steroidal anti-inflammatory drug activated gene (NAG-1) expression is closely related to death receptor-4 and -5 induction, which may explain sulindac sulfide induced gastric cancer cell apoptosis. *Carcinogenesis* 2004;25: 1853-8.
82. Liu X, Yue P, Zhou Z, Khuri FR, Sun SY. Death receptor regulation and celecoxib-induced apoptosis in human lung cancer cells. *J Natl Cancer Inst* 2004;96: 1769-80.
83. Chen S, Liu X, Yue P, Schonthal AH, Khuri FR, Sun SY. CHOP-dependent DR5 induction and ubiquitin/proteasome-mediated c-FLIP downregulation contribute to enhancement of TRAIL-induced apoptosis by dimethyl-celecoxib in human non-small cell lung cancer cells. *Mol Pharmacol* 2007;72: 1269-79.
84. He Q, Luo X, Jin W, Huang Y, Reddy MV, Reddy EP, Sheikh MS. Celecoxib and a novel COX-2 inhibitor ON09310 upregulate death receptor 5 expression via GADD153/CHOP. *Oncogene* 2007.
85. Sun SY, Lotan R. Retinoids and their receptors in cancer development and chemoprevention. *Crit Rev Oncol Hematol* 2002;41: 41-55.
86. Garattini E, Gianni M, Terao M. Retinoid related molecules an emerging class of apoptotic agents with promising therapeutic potential in oncology: pharmacological activity and mechanisms of action. *Curr Pharm Des* 2004;10: 433-48.
87. Sun SY, Yue P, Wu GS, El-Deiry WS, Shroot B, Hong WK, Lotan R. Mechanisms of apoptosis induced by the synthetic retinoid CD437 in human non-small cell lung carcinoma cells. *Oncogene* 1999;18: 2357-65.
88. Sun SY, Yue P, Wu GS, El-Deiry WS, Shroot B, Hong WK, Lotan R. Implication of p53 in growth arrest and apoptosis induced by the synthetic retinoid CD437 in human lung cancer cells. *Cancer Res* 1999;59: 2829-33.
89. Sun SY, Yue P, Hong WK, Lotan R. Induction of Fas expression and augmentation of Fas/Fas ligand-mediated apoptosis by the synthetic retinoid CD437 in human lung cancer cells. *Cancer Res* 2000;60: 6537-43.
90. Sun SY, Yue P, Chen X, Hong WK, Lotan R. The synthetic retinoid CD437 selectively induces apoptosis in human lung cancer cells while sparing normal human lung epithelial cells. *Cancer Res* 2002;62: 2430-6.
91. Sun SY, Yue P, Lotan R. Implication of multiple mechanisms in apoptosis induced by the synthetic retinoid CD437 in human prostate carcinoma cells. *Oncogene* 2000;19: 4513-22.
92. Sun SY, Yue P, Mao L, Dawson MI, Shroot B, Lamph WW, Heyman RA, Chandraratna RA, Shudo K, Hong WK, Lotan R. Identification of receptor-selective retinoids that are potent inhibitors of the growth of human head and neck squamous cell carcinoma cells. *Clin Cancer Res* 2000;6: 1563-73.
93. Farhana L, Dawson MI, Fontana JA. Apoptosis induction by a novel retinoid-related molecule requires nuclear factor-kappaB activation. *Cancer Res* 2005;65: 4909-17.
94. Zanchi C, Zuco V, Lanzi C, Supino R, Zunino F. Modulation of survival signaling pathways and persistence of the genotoxic stress as a basis for the synergistic interaction between the atypical retinoid ST1926 and the epidermal growth factor receptor inhibitor ZD1839. *Cancer Res* 2005;65: 2364-72.

95. Jin F, Liu X, Zhou Z, Yue P, Lotan R, Khuri FR, Chung LW, Sun SY. Activation of nuclear factor-kappaB contributes to induction of death receptors and apoptosis by the synthetic retinoid CD437 in DU145 human prostate cancer cells. *Cancer Res* 2005;65: 6354-63.
96. Cuello M, Coats AO, Darko I, Ettenberg SA, Gardner GJ, Nau MM, Liu JR, Birrer MJ, Lipkowitz S. N-(4-hydroxyphenyl) retinamide (4HPR) enhances TRAIL-mediated apoptosis through enhancement of a mitochondrial-dependent amplification loop in ovarian cancer cell lines. *Cell Death Differ* 2004;11: 527-41.
97. Kouhara J, Yoshida T, Nakata S, Horinaka M, Wakada M, Ueda Y, Yamagishi H, Sakai T. Fenretinide up-regulates DR5/TRAIL-R2 expression via the induction of the transcription factor CHOP and combined treatment with fenretinide and TRAIL induces synergistic apoptosis in colon cancer cell lines. *Int J Oncol* 2007;30: 679-87.
98. Xia Y, Wong NS, Fong WF, Tideman H. Upregulation of GADD153 expression in the apoptotic signaling of N-(4-hydroxyphenyl)retinamide (4HPR). *Int J Cancer* 2002;102: 7-14.
99. Kim DG, You KR, Liu MJ, Choi YK, Won YS. GADD153-mediated anticancer effects of N-(4-hydroxyphenyl)retinamide on human hepatoma cells. *J Biol Chem* 2002;277: 38930-8.
100. Samuel W, Kutty RK, Nagineni S, Vijayasathy C, Chandraratna RA, Wiggert B. N-(4-hydroxyphenyl)retinamide induces apoptosis in human retinal pigment epithelial cells: retinoic acid receptors regulate apoptosis, reactive oxygen species generation, and the expression of heme oxygenase-1 and Gadd153. *J Cell Physiol* 2006;209: 854-65.
101. Lovat PE, Oliverio S, Ranalli M, Corazzari M, Rodolfo C, Bernassola F, Aughton K, Maccarrone M, Hewson QD, Pearson AD, Melino G, Piacentini M, Redfern CP. GADD153 and 12-lipoxygenase mediate fenretinide-induced apoptosis of neuroblastoma. *Cancer Res* 2002;62: 5158-67.
102. Corazzari M, Lovat PE, Oliverio S, Pearson AD, Piacentini M, Redfern CP. Growth and DNA damage-inducible transcription factor 153 mediates apoptosis in response to fenretinide but not synergy between fenretinide and chemotherapeutic drugs in neuroblastoma. *Mol Pharmacol* 2003;64: 1370-8.
103. Anding AL, Chapman JS, Barnett DW, Curley RW, Jr., Clagett-Dame M. The unhydrolyzable fenretinide analogue 4-hydroxybenzylretinone induces the proapoptotic genes GADD153 (CHOP) and Bcl-2-binding component 3 (PUMA) and apoptosis that is caspase- dependent and independent of the retinoic acid receptor. *Cancer Res* 2007;67: 6270-7.
104. Meng RD, El-Deiry WS. p53-independent upregulation of KILLER/DR5 TRAIL receptor expression by glucocorticoids and interferon-gamma. *Exp Cell Res* 2001;262: 154-69.
105. Xia L, Chen D, Han R, Fang Q, Waxman S, Jing Y. Boswellic acid acetate induces apoptosis through caspase-mediated pathways in myeloid leukemia cells. *Mol Cancer Ther* 2005;4: 381-8.
106. Zou W, Liu X, Yue P, Zhou Z, Sporn MB, Lotan R, Khuri FR, Sun SY. c-Jun NH2-terminal kinase-mediated up-regulation of death receptor 5 contributes to induction of apoptosis by the novel synthetic triterpenoid methyl-2-cyano-3,12-dioxooleana-1, 9-dien-28-oate in human lung cancer cells. *Cancer Res* 2004;64: 7570-8.
107. Hyer ML, Croxton R, Krajewska M, Krajewski S, Kress CL, Lu M, Suh N, Sporn MB, Cryns VL, Zapata JM, Reed JC. Synthetic triterpenoids cooperate with tumor necrosis factor-related apoptosis-inducing ligand to induce apoptosis of breast cancer cells. *Cancer Res* 2005;65: 4799-808.

108. Shigeno M, Nakao K, Ichikawa T, Suzuki K, Kawakami A, Abiru S, Miyazoe S, Nakagawa Y, Ishikawa H, Hamasaki K, Nakata K, Ishii N, Eguchi K. Interferon-alpha sensitizes human hepatoma cells to TRAIL-induced apoptosis through DR5 upregulation and NF-kappa B inactivation. *Oncogene* 2003;22: 1653-62.
109. van Geelen CM, de Vries EG, Le TK, van Weeghel RP, de Jong S. Differential modulation of the TRAIL receptors and the CD95 receptor in colon carcinoma cell lines. *Br J Cancer* 2003;89: 363-73.
110. Oshima K, Yanase N, Ibukiyama C, Yamashina A, Kayagaki N, Yagita H, Mizuguchi J. Involvement of TRAIL/TRAIL-R interaction in IFN-alpha-induced apoptosis of Daudi B lymphoma cells. *Cytokine* 2001;14: 193-201.
111. Tan G, Gyllenhaal C, Soejarto DD. Biodiversity as a source of anticancer drugs. *Curr Drug Targets* 2006;7: 265-77.
112. Bush JA, Cheung KJ, Jr., Li G. Curcumin induces apoptosis in human melanoma cells through a Fas receptor/caspase-8 pathway independent of p53. *Exp Cell Res* 2001;271: 305-14.
113. Deeb D, Jiang H, Gao X, Hafner MS, Wong H, Divine G, Chapman RA, Dulchavsky SA, Gautam SC. Curcumin sensitizes prostate cancer cells to tumor necrosis factor-related apoptosis-inducing ligand/Apo2L by inhibiting nuclear factor-kappaB through suppression of IkappaBalpha phosphorylation. *Mol Cancer Ther* 2004;3: 803-12.
114. Jung EM, Lim JH, Lee TJ, Park JW, Choi KS, Kwon TK. Curcumin sensitizes tumor necrosis factor-related apoptosis-inducing ligand (TRAIL)-induced apoptosis through reactive oxygen species-mediated upregulation of death receptor 5 (DR5). *Carcinogenesis* 2005;26: 1905-13.
115. Jung EM, Park JW, Choi KS, Lee HI, Lee KS, Kwon TK. Curcumin sensitizes tumor necrosis factor-related apoptosis-inducing ligand (TRAIL)-mediated apoptosis through CHOP-independent DR5 upregulation. *Carcinogenesis* 2006.
116. Kim H, Kim EH, Eom YW, Kim WH, Kwon TK, Lee SJ, Choi KS. Sulforaphane sensitizes tumor necrosis factor-related apoptosis-inducing ligand (TRAIL)-resistant hepatoma cells to TRAIL-induced apoptosis through reactive oxygen species-mediated up-regulation of DR5. *Cancer Res* 2006;66: 1740-50.
117. Matsui TA, Sowa Y, Yoshida T, Murata H, Horinaka M, Wakada M, Nakanishi R, Sakabe T, Kubo T, Sakai T. Sulforaphane enhances TRAIL-induced apoptosis through the induction of DR5 expression in human osteosarcoma cells. *Carcinogenesis* 2006.
118. Horinaka M, Yoshida T, Shiraishi T, Nakata S, Wakada M, Nakanishi R, Nishino H, Matsui H, Sakai T. Luteolin induces apoptosis via death receptor 5 upregulation in human malignant tumor cells. *Oncogene* 2005;24: 7180-9.
119. Hasegawa H, Yamada Y, Komiyama K, Hayashi M, Ishibashi M, Yoshida T, Sakai T, Koyano T, Kam TS, Murata K, Sugahara K, Tsuruda K, Akamatsu N, Tsukasaki K, Masuda M, Takasu N, Kamihira S. Dihydroflavonol BB-1, an extract of natural plant *Blumea balsamifera*, abrogates TRAIL resistance in leukemia cells. *Blood* 2006;107: 679-88.
120. Son YG, Kim EH, Kim JY, Kim SU, Kwon TK, Yoon AR, Yun CO, Choi KS. Silibinin sensitizes human glioma cells to TRAIL-mediated apoptosis via DR5 up-regulation and down-regulation of c-FLIP and survivin. *Cancer Res* 2007;67: 8274-84.
121. LaVallee TM, Zhan XH, Johnson MS, Herbstritt CJ, Swartz G, Williams MS, Hembrough WA, Green SJ, Pribluda VS. 2-methoxyestradiol up-regulates death receptor 5 and induces apoptosis through activation of the extrinsic pathway. *Cancer Res* 2003;63: 468-75.

122. Braeuninger S, Chamaon K, Kropf S, Mawrin C, Wiedemann FR, Hartig R, Schoeler S, Dietzmann K, Kirches E. Short incubation with 2-methoxyestradiol kills malignant glioma cells independent of death receptor 5 upregulation. *Clin Neuropathol* 2005;24: 175-83.
123. Wood L, Leese MP, Mouzakiti A, Purohit A, Potter BV, Reed MJ, Packham G. 2-MeOE2bisMATE induces caspase-dependent apoptosis in CAL51 breast cancer cells and overcomes resistance to TRAIL via cooperative activation of caspases. *Apoptosis* 2004;9: 323-32.
124. He Q, Lee DI, Rong R, Yu M, Luo X, Klein M, El-Deiry WS, Huang Y, Hussain A, Sheikh MS. Endoplasmic reticulum calcium pool depletion-induced apoptosis is coupled with activation of the death receptor 5 pathway. *Oncogene* 2002;21: 2623-33.
125. Huang L, Xu J, Li K, Zheng MH, Kumta SM. Thapsigargin potentiates TRAIL-induced apoptosis in giant cell tumor of bone. *Bone* 2004;34: 971-81.
126. Shiraishi T, Yoshida T, Nakata S, Horinaka M, Wakada M, Mizutani Y, Miki T, Sakai T. Tunicamycin enhances tumor necrosis factor-related apoptosis-inducing ligand-induced apoptosis in human prostate cancer cells. *Cancer Res* 2005;65: 6364-70.
127. Szegezdi E, Cahill S, Meyer M, O'Dwyer M, Samali A. TRAIL sensitisation by arsenic trioxide is caspase-8 dependent and involves modulation of death receptor components and Akt. *Br J Cancer* 2006;94: 398-406.
128. Tomasetti M, Andera L, Alleva R, Borghi B, Neuzil J, Procopio A. Alpha-tocopheryl succinate induces DR4 and DR5 expression by a p53-dependent route: implication for sensitisation of resistant cancer cells to TRAIL apoptosis. *FEBS Lett* 2006;580: 1925-31.
129. Tomasetti M, Rippo MR, Alleva R, Moretti S, Andera L, Neuzil J, Procopio A. Alpha-tocopheryl succinate and TRAIL selectively synergise in induction of apoptosis in human malignant mesothelioma cells. *Br J Cancer* 2004;90: 1644-53.
130. Elrod HA, Lin YD, Yue P, Wang X, Lonial S, Khuri FR, Sun SY. The alkylphospholipid perifosine induces apoptosis of human lung cancer cells requiring inhibition of Akt and activation of the extrinsic apoptotic pathway. *Mol Cancer Ther* 2007;6: 2029-38.
131. Rajendran L, Simons K. Lipid rafts and membrane dynamics. *J Cell Sci* 2005;118: 1099-102.
132. Garcia A, Cayla X, Fleischer A, Guergnon J, Alvarez-Franco Canas F, Rebollo MP, Roncal F, Rebollo A. Rafts: a simple way to control apoptosis by subcellular redistribution. *Biochimie* 2003;85: 727-31.
133. Dimanche-Boitrel MT, Meurette O, Rebillard A, Lacour S. Role of early plasma membrane events in chemotherapy-induced cell death. *Drug Resist Updat* 2005;8: 5-14.
134. Gajate C, An F, Mollinedo F. Rapid and selective apoptosis in human leukemic cells induced by Aplidine through a Fas/CD95- and mitochondrial-mediated mechanism. *Clin Cancer Res* 2003;9: 1535-45.
135. Gajate C, Mollinedo F. Cytoskeleton-mediated death receptor and ligand concentration in lipid rafts forms apoptosis-promoting clusters in cancer chemotherapy. *J Biol Chem* 2005;280: 11641-7.
136. Gajate C, Fonteriz RI, Cabaner C, Alvarez-Noves G, Alvarez-Rodriguez Y, Modolell M, Mollinedo F. Intracellular triggering of Fas, independently of FasL, as a new mechanism of antitumor ether lipid-induced apoptosis. *Int J Cancer* 2000;85: 674-82.
137. Gajate C, Mollinedo F. The antitumor ether lipid ET-18-OCH(3) induces apoptosis through translocation and capping of Fas/CD95 into membrane rafts in human leukemic cells. *Blood* 2001;98: 3860-3.

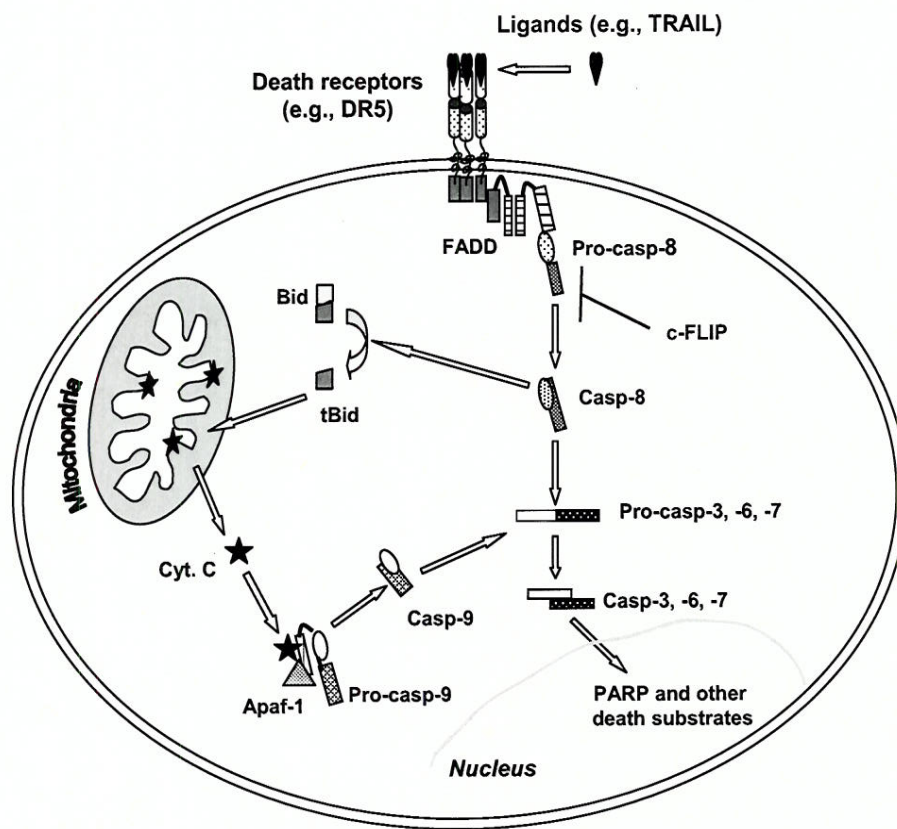
138. Gajate C, Del Canto-Jancz E, Acuna AU, Amat-Guerri F, Geijo E, Santos-Beneit AM, Veldman RJ, Mollinedo F. Intracellular triggering of Fas aggregation and recruitment of apoptotic molecules into Fas-enriched rafts in selective tumor cell apoptosis. *J Exp Med* 2004;200: 353-65.
139. Gajate C, Mollinedo F. Edelfosine and perifosine induce selective apoptosis in multiple myeloma by recruitment of death receptors and downstream signaling molecules into lipid rafts. *Blood* 2007;109: 711-9.
140. Delmas D, Rebe C, Lacour S, Filomenko R, Athias A, Gambert P, Cherkaoui-Malki M, Jannin B, Dubrez-Daloz L, Latruffe N, Solary E. Resveratrol-induced apoptosis is associated with Fas redistribution in the rafts and the formation of a death-inducing signaling complex in colon cancer cells. *J Biol Chem* 2003;278: 41482-90.
141. Delmas D, Rebe C, Micheau O, Athias A, Gambert P, Grazide S, Laurent G, Latruffe N, Solary E. Redistribution of CD95, DR4 and DR5 in rafts accounts for the synergistic toxicity of resveratrol and death receptor ligands in colon carcinoma cells. *Oncogene* 2004;23: 8979-86.
142. Lacour S, Hammann A, Grazide S, Lagadic-Gossmann D, Athias A, Sergent O, Laurent G, Gambert P, Solary E, Dimanche-Boitrel MT. Cisplatin-induced CD95 redistribution into membrane lipid rafts of HT29 human colon cancer cells. *Cancer Res* 2004;64: 3593-8.
143. Psahoulia FH, Drosopoulos KG, Doubravskia L, Andera L, Pintzas A. Quercetin enhances TRAIL-mediated apoptosis in colon cancer cells by inducing the accumulation of death receptors in lipid rafts. *Mol Cancer Ther* 2007;6: 2591-9.
144. Martin S, Phillips DC, Szekely-Szucs K, Elghazi L, Desmots F, Houghton JA. Cyclooxygenase-2 inhibition sensitizes human colon carcinoma cells to TRAIL-induced apoptosis through clustering of DR5 and concentrating death-inducing signaling complex components into ceramide-enriched caveolae. *Cancer Res* 2005;65: 11447-58.
145. Vanoosten RL, Moore JM, Ludwig AT, Griffith TS. Depsipeptide (FR901228) enhances the cytotoxic activity of TRAIL by redistributing TRAIL receptor to membrane lipid rafts. *Mol Ther* 2005;11: 542-52.
146. Altucci L, Rossin A, Raffelsberger W, Reitmair A, Chomienne C, Gronemeyer H. Retinoic acid-induced apoptosis in leukemia cells is mediated by paracrine action of tumor-selective death ligand TRAIL. *Nat Med* 2001;7: 680-6.
147. Clarke N, Jimenez-Lara AM, Voltz E, Gronemeyer H. Tumor suppressor IRF-1 mediates retinoid and interferon anticancer signaling to death ligand TRAIL. *Embo J* 2004;23: 3051-60.
148. Wang Q, Ji Y, Wang X, Evers BM. Isolation and molecular characterization of the 5'-upstream region of the human TRAIL gene. *Biochem Biophys Res Commun* 2000;276: 466-71.
149. Wang Q, Wang X, Hernandez A, Hellmich MR, Gatalica Z, Evers BM. Regulation of TRAIL expression by the phosphatidylinositol 3-kinase/Akt/GSK-3 pathway in human colon cancer cells. *J Biol Chem* 2002;277: 36602-10.
150. Wajant H, Pfizenmaier K, Scheurich P. TNF-related apoptosis inducing ligand (TRAIL) and its receptors in tumor surveillance and cancer therapy. *Apoptosis* 2002;7: 449-59.
151. Wajant H. CD95L/FasL and TRAIL in tumour surveillance and cancer therapy. *Cancer Treat Res* 2006;130: 141-65.
152. Takeda K, Stagg J, Yagita H, Okumura K, Smyth MJ. Targeting death-inducing receptors in cancer therapy. *Oncogene* 2007;26: 3745-57.

153. Simons MP, Nauseef WM, Griffith TS. Neutrophils and TRAIL: insights into BCG immunotherapy for bladder cancer. *Immunologic research* 2007;39: 79-93.
154. Shanker A, Sayers T. Sensitizing tumor cells to immune-mediated cytotoxicity. *Adv Exp Med Biol* 2007;601: 163-71.
155. Bunz F. Human cell knockouts. *Curr Opin Oncol* 2002;14: 73-8.
156. Cretny E, Takeda K, Yagita H, Glaccum M, Peschon JJ, Smyth MJ. Increased susceptibility to tumor initiation and metastasis in TNF-related apoptosis-inducing ligand-deficient mice. *J Immunol* 2002;168: 1356-61.
157. Embree-Ku M, Boeckelheide K. FasL deficiency enhances the development of tumors in p53^{+/-} mice. *Toxicol Pathol* 2002;30: 705-13.

Figure Legend

Fig. 1. Schema for extrinsic death receptor-mediated apoptotic signaling pathway. Ligation of death ligands (e.g. TRAIL) with their receptors (e.g. DR4 and DR5) results in activation of caspase-8 (Casp-8) through a death adaptor protein FADD in the death-inducing signaling complex (DISC). Activated caspase-8 can directly activate downstream caspase-3 (Casp-3), caspase-6 (Casp-6) and caspase-7 (Casp-7) leading to cleavages of their target proteins such as PARP, DFF45 and lamins. Moreover, activated caspase-8 can cleave Bid, generating truncated Bid (tBid), which can facilitate insertion of BAX into mitochondrial membrane leading to cytochrome C (Cyt. C) release. Thus, caspase-8 can also activate intrinsic mitochondria-mediated apoptotic pathway, which involves cytochrome C (Cyt. C) release from mitochondria into cytosol and subsequent caspase-9 (Casp-9) activation.

Fig. 2. Chemical structures of natural products with death receptor-modulating activity.



Elrod and Sun. Fig. 1

INTERACTION INDEX AND DIFFERENT METHODS FOR DETERMINING DRUG INTERACTION IN COMBINATION THERAPY

J. J. Lee

*Department of Biostatistics, University of Texas, M. D. Anderson
Cancer Center, Houston, Texas, USA*

M. Kong

*Department of Biostatistics and Bioinformatics, University of Louisville,
Kentucky, USA*

G. D. Ayers

*Department of Biostatistics, Vanderbilt University Medical Center,
Nashville, Tennessee, USA*

R. Lotan

*Division of Cancer Medicine, University of Texas, M. D. Anderson
Cancer Center, Houston, Texas, USA*

Studying and understanding the joint effect of combined treatments is important in pharmacology and in the development of combination therapies. The Loewe additivity model is one of the best general reference models for evaluating drug interactions. Based on this model, synergy occurs when the interaction index is less than one, while antagonism occurs when interaction index is greater than one. We expound the meaning of the interaction index, and propose a procedure to calculate the interaction index and its associated confidence interval under the assumption that the dose-effect curve for a single agent follows Chou and Talalay's median effect equation. In addition, we review four response surface models based on the Loewe additivity model using a single parameter to determine drug interactions. We describe each of these models in the context of Loewe additivity model and discuss their relative advantages and disadvantages. We also provide S-PLUS/R code for each approach to facilitate the implementation of these commonly used methods.

Key Words: Antagonism; Drug interaction; Loewe additivity model; Response surface model; Synergy.

1. INTRODUCTION

Studying and understanding the combined effects of multiple concurrent treatments has a venerable history among basic scientists, clinicians, and statisticians

Received April 19, 2006; Accepted December 30, 2006

Address correspondence to J. J. Lee, Department of Biostatistics, University of Texas, M. D. Anderson Cancer Center, Houston, Texas, USA; Fax: 713-563-4242; E-mail: jjlee@mdanderson.org

with the goal to develop better treatment regimens with increased efficacy and reduced toxicity. Many such successful studies can be found in the literature including, for example, a study of the cocktail approach to control AIDS with nucleoside reverse transcriptase inhibitors, non-nucleoside reverse transcriptase inhibitors, and protease inhibitors (Sharma et al., 2004); studies of platinum-based doublets that include a taxane, vinorelbine, or gemcitabine (Evans, 2004) or the use of chemoradiation therapy (Curran, 2003) for non-small-cell lung cancer. Advents in molecular target-based treatments for cancer have rekindled an interest in studying combinations of targeting agents, chemotherapy, and/or radiation therapy (Herbst, 2005; Niyazi and Belka, 2006). In addition, examining adverse effects following the simultaneous administration of multiple drugs is important in toxicology studies to ensure that combination therapy can be given safely. Recent advancements in systems biology also point to a promising direction in developing and quantifying effective combination therapy (Fitzgerald et al., 2006).

Data from *in vitro* and *in vivo* assays are useful for screening out inefficacious and/or toxic combination regimens while selecting the promising ones for further development. Although it is generally recognized that *in vitro* data cannot be extrapolated directly to *in vivo* or clinical settings, there are many successful examples in which *in vitro* data predict *in vivo* drug interactions (Bachmann and Ghosh, 2001). Failure of accurate predictions may be caused by the methodology used, inappropriate model selection, errant scale-up factors, biological differences, etc.

A drug-induced effect may be expressed on a continuous scale or on a binary scale. For example, in cell line studies, percent cell survival or percent cell killed is commonly applied to measure the drug effect. In animal studies, when a binary response status is recorded, the response rate, i.e., the number of responses divided by the total number assigned to a dose, can be constructed as a measurement of treatment effect (Finney, 1971; Morgan, 1992).

To characterize drug interaction, we first need to define an appropriate reference model for additive effects of drug combinations. When the effect of a combination dose is greater (less) than that predicted by the additivity model, the combination dose is synergistic (antagonistic). Historically, three additivity reference models are commonly used (Berenbaum, 1989; Greco et al., 1995): 1) effect addition, 2) Bliss independence, and 3) Loewe additivity. Excellent and comprehensive reviews on drug interaction can be found in Berenbaum (1989), Greco et al. (1995), and Tallarida (2000). The effect addition model has a simple form: $E(d_1, d_2) = E(d_1) + E(d_2)$, where $E(d_1, d_2)$ is the effect at (d_1, d_2) , and $E(d_i)$ is the effect of drug i alone at dose d_i with $i = 1, 2$. However, this model is not generally correct. For example, when $E(d_1) = E(d_2) = 70\%$, clearly $E(d_1, d_2)$ can not be 140% when the effect is measured as a proportion of cells killed. The Bliss independence model (Bliss, 1939; Greco et al., 1995; Webb, 1963) is also called effect multiplication or the fractional product, which has the form $f_{12} = f_1 f_2$. Here f_1 , f_2 , and f_{12} are the effects expressed as the fractions of the maximal effects for drug 1, drug 2, and the combination, and the maximal effect of a drug or combination is defined as the effect observed with an infinite amount of the drug or combination. For example, the Bliss independence model for percentage cell survival is $E(d_1, d_2) = E(d_1)E(d_2)$. Combination doses with effects less than predicted are

synergistic, and conversely, antagonistic. The Loewe additivity model to characterize drug interaction can be defined as:

$$\frac{d_1}{D_{y,1}} + \frac{d_2}{D_{y,2}} \begin{cases} =1, & \text{Additivity;} \\ <1, & \text{Synergy;} \\ >1, & \text{Antagonism,} \end{cases} \quad (1)$$

where d_1 , d_2 are doses of drug 1 and drug 2 in mixture, which produces an effect y , while $D_{y,1}$ and $D_{y,2}$ are the doses of drug 1 and drug 2 that produce the same effect y when given alone. The term $\frac{d_1}{D_{y,1}} + \frac{d_2}{D_{y,2}}$ is also called the interaction index at the combination dose (d_1, d_2) . If the interaction index at (d_1, d_2) is equal to, less than, or greater than 1, the combination dose (d_1, d_2) is claimed to be additive, synergistic, or antagonistic, respectively.

The Bliss independence and Loewe additivity models are the two most cited reference models for defining drug interactions (Fitzgerald et al., 2006; Greco et al., 1995; Jonker et al., 2005). The literature indicates that the Loewe additivity model works in the settings of mutually exclusive drugs while the Bliss independence model works in the settings of mutually nonexclusive drugs. However, the mechanism of drug interactions is often unknown. Debate continues over which is the better reference model for defining drug interaction. So far, there is no generally accepted agreement as to which of the two models is more appropriate. Both models were recommended by the so-called Saariselkaa agreement (Greco et al., 1992). Dreblor et al. (1999) developed *CombiTool*, software to assess drug interactions based on both of the reference models. Berenbaum (1989) showed that the two reference models are the same if the dose-effect curves are in simple exponential family, i.e., $E(d) = \exp(-\beta d)$. The Bliss independence was originally derived from probability theory, and the effect scale can only be applied to fractional effects $0 < E < 1$. Although the Bliss independence has extensive mechanistic and probabilistic support, the underlying independence assumption may be difficult to verify. On the other hand, the Loewe additivity model was defined based on the dose scale no matter the measurements of the effects. Berenbaum (1989) used a "sham combination" (i.e., a drug is combined with itself or its diluted form) thought experiment to advocate the Loewe additivity model. Although supporters of the Bliss independence model question the validity of applying the "sham combination" to general drug combination because the "sham" treatments involve the same treatment and are not independent of each other, the Loewe additivity model gives an intuitively clear and reasonable explanation for experiments beyond the "sham combination". For example, when two non-interactive and equally potent drugs are applied together, we expect that the combination dose (d_1, d_2) will have the same effect as drug 1 alone or drug 2 alone at dose level $d_1 + d_2$. Drug additivity is substantiated under the Loewe additivity model but not the Bliss independence model. The Loewe additivity model is also consistent with the graphical isobologram approach (Martinez-Irujo et al., 1998). Hence, we conclude that the Loewe additivity model is one of the best general reference models for evaluating drug interactions.

In this paper, we intend to clarify the meaning of the interaction index and compare several commonly used methods on assessing drug interaction based

on the Loewe additivity model. In Section 2, we illustrate the meaning of the interaction index, and show that the interaction index can be used to characterize the magnitude of non-additive effects. In Section 3, we derive the interaction index and demonstrate how to construct its confidence interval under the assumption that the median-effect equation holds for both agents. In addition, we review the commonly applied approach to assess drug interactions by Chou and Talalay (1984). Based on the Loewe additivity model, response surface models (RSMs) can be constructed to describe the three dimensional dose-response surface in two drug combinations and can include all of the information present in the full dose-effect data set for two drugs. In addition, the RSM can be used to quantify the amount of drug interactions and to determine the optimal combination therapy. The RSM's of Finney (1971), Greco et al. (1990), Machado and Robinson (1994), Plummer and Short (1990), and Carter et al. (1988), use a single parameter to quantify synergy, additivity, or antagonism, and have been successfully applied in many reported case studies. We review those approaches in Section 4, taking the median-effect equation as the dose-effect model for each single agent except for the model by Carter et al. (1988), which uses a logistic model. We give an example of the combination of two agents to elicit cell death in a cancer cell line study in Section 5. The results of analysis using these methods are given in Section 6 to compare and contrast the properties of various methods. In addition, we supply S-PLUS/R code to provide investigators useful tools for studying drug interactions. In Section 7, we discuss our findings and make suggestions on future research areas.

2. INTERACTION INDEX AND ITS INTERPRETATION

Suppose that the combination dose (d_1, d_2) elicits the same effect y as drug 1 alone at dose $D_{y,1}$, and drug 2 alone at dose $D_{y,2}$, then $\frac{d_1}{D_{y,1}} + \frac{d_2}{D_{y,2}}$, the interaction index at dose (d_1, d_2) , denoted by τ , measures additivity, synergy, or antagonism according to the relation shown in Eq. (1).

What does the interaction index τ mean? Note that $\frac{d_1}{D_{y,1}} + \frac{d_2}{D_{y,2}} = \tau$ can be rewritten as

$$d_1 + d_2 \frac{D_{y,1}}{D_{y,2}} = \tau D_{y,1}. \quad (2)$$

The ratio $\frac{D_{y,1}}{D_{y,2}}$ is defined as relative potency of drug 2 versus drug 1 (Morgan, 1992). Suppose the relative potency is a constant ρ at any level of effect, then one unit of drug 2 produces the same effect as ρ units of drug 1. Thus the total combined dose (d_1, d_2) will be $d_1 + \rho d_2$ in terms of drug 1 dose. Particularly, $\tau = 1$ implies $d_1 + \rho d_2 = D_{y,1}$, i.e., the total dose of the two drugs elicits the same effect as drug 1 is used alone at $D_{y,1}$, indicating additivity of the combination dose (d_1, d_2) . $\tau < 1$ implies $d_1 + \rho d_2 = \tau D_{y,1} < D_{y,1}$, i.e., the total dose is less than that when drug 1 is used alone, indicating synergy of the combination dose (d_1, d_2) ; while $\tau > 1$ implies $d_1 + \rho d_2 = \tau D_{y,1} > D_{y,1}$, i.e., the total dose is more than that when drug 1 is used alone, indicating antagonism of the combination dose (d_1, d_2) . Obviously, the smaller the τ is, the smaller is the total amount dose $d_1 + \rho d_2$, which produces the same effect as drug 1 alone at dose $D_{y,1}$. Therefore, the interaction

index, τ , is a quantitative measure capturing the mode and magnitude of drug interaction.

Geometrically, the drug interaction can be illustrated by constructing an isobole. An isobole corresponding to an effect y consists of all the combination doses (d_1, d_2) that elicit the effect y . In Fig. 1, suppose P is the point $(D_{y,1}, 0)$, Q is the point $(0, D_{y,2})$, and U is the point (d_1, d_2) ; all these points yield an effect y . Then, the relative potency $\rho = \frac{\text{length}(\overline{OP})}{\text{length}(\overline{OQ})}$, and the interaction index can be expressed as

$$\tau = \frac{d_1 + \rho d_2}{D_{y,1}} = \frac{\text{length}(\overline{OR})}{\text{length}(\overline{OP})} = \frac{\text{length}(\overline{OU})}{\text{length}(\overline{OV})} \quad \text{Fig. 1, Panel A}$$

The line \overline{RS} is parallel to the line \overline{PQ} (Fig. 1, Panel A), V is the intersection of \overline{OU} and \overline{PQ} . So when U is on the straight line \overline{PQ} , the interaction index will be 1; when U is on the south-west side of the straight line \overline{PQ} , the interaction index will be less than 1; when U is on the north-east side of the straight line \overline{PQ} , the interaction index will be greater than 1. If the isobole is a straight line \overline{PQ} (Fig. 1, Panel B), then any combination dose (d_1, d_2) on this line will have an interaction index at 1, indicating that the combination dose (d_1, d_2) is additive. If an isobole is concave down similar to the solid curve \widehat{PNQ} , then any combination dose (d_1, d_2) on this curve will have an interaction index less than 1, except at P and Q , indicating that these combination doses are synergistic. If an isobole is concave up similar to the solid curve \widehat{PMQ} , then any combination dose (d_1, d_2) on this curve will have an interaction index greater than 1, except at P and Q , indicating antagonism. However, the interaction indices for different combination doses on an isobole may

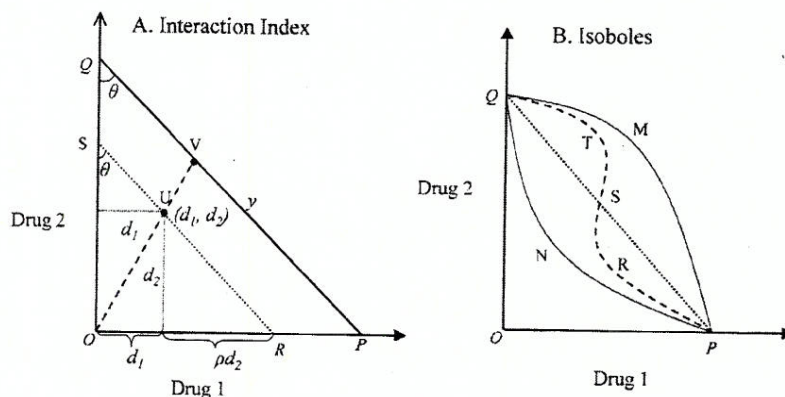


Figure 1 Geometric interpretation of the interaction index (Panel A) and examples of isoboles (Panel B). In both panels, $P = (D_{y,1}, 0)$ and $Q = (0, D_{y,2})$ showing the doses resulting effect y using single agent of drug 1 and drug 2. In Panel A, $U = (d_1, d_2)$, the effect $E(d_1, d_2) = y$, $\rho = \text{tangent}(\theta)$, and the interaction index $\tau = \frac{d_1 + \rho d_2}{D_{y,1}} = \frac{\text{length}(\overline{OR})}{\text{length}(\overline{OP})} = \frac{\text{length}(\overline{OU})}{\text{length}(\overline{OV})}$. In Panel B, the dotted straight line \overline{PQ} is a representation of a theoretical additive isobole. The solid curve \widehat{PNQ} is a representation of an isobole with synergy, \widehat{PMQ} is a representation of an isobole with antagonism, and the dashed curve \widehat{PRSTQ} is a representation of an isobole with both synergy and antagonism.

be different. For example, the interaction index for the combination dose close to points P and Q on \widehat{PNQ} will be less than 1 but close to 1, and the interaction index possibly has a minimum at point N , which means that the combination dose (d_1, d_2) at N is most synergistic among all the combination doses on \widehat{PNQ} . Similarly, the combination dose (d_1, d_2) at M may be most antagonistic among the combination doses on \widehat{PMQ} . An isobole may cross the additive isobole \widehat{PQ} , e.g. the curve \widehat{PRSTQ} . In that case, the combination doses on the segment \widehat{PRS} are synergistic, while the combination doses on the segment \widehat{STQ} are antagonistic.

3. DERIVING INTERACTION INDEX AND CONSTRUCTING ITS CONFIDENCE INTERVAL

Generally, given the dose-effect curve for each single drug, the interaction index is determined by the combination dose (d_1, d_2) and its corresponding effect y . For example, if the effect at the combination dose (d_1, d_2) is y , and the dose-effect curve is $f_1(D_1)$ for drug 1, and $f_2(D_2)$ for drug 2, then $D_{y,1} = f_1^{-1}(y)$, and $D_{y,2} = f_2^{-1}(y)$, where f_i^{-1} ($i = 1, 2$) is the inverse function of f_i . Thus we can estimate the value of the interaction index without specifying a joint model, $f(d_1, d_2)$, for the combination dose (d_1, d_2) .

In the literature, there are different models to describe dose-effect curve, such as the probit model (Finney, 1971) and the logistic model (Morgan, 1992) for a binary response variable, and the E_{\max} model, also known as Hill equation (Greco et al., 1995; Hill, 1910; Holford and Sheiner, 1981), for a continuous response variable. The E_{\max} model has the following form:

$$E = \frac{E_{\max} \left(\frac{d}{D_m}\right)^m}{1 + \left(\frac{d}{D_m}\right)^m}, \quad (3)$$

where d is the dose of drug, D_m is the median effective dose of a drug, E_{\max} is the maximal effect of the associated drug, and m is a slope parameter, also called the Hill coefficient, depicting the shape of the curve. When $E_{\max} = 1$, model ((3)) becomes Chou and Talalay's median effect equation (Chou and Talalay, 1984):

$$E = \frac{\left(\frac{d}{D_m}\right)^m}{1 + \left(\frac{d}{D_m}\right)^m}, \quad (4)$$

In our cell line study, we found the median effect Eq. (4) gave a reasonable estimation of the dose-effect curve. When m is negative, the measurements of effects described by Eqs. (3) and (4) decrease with increasing drug concentration; when m is positive, the curves rise with increasing drug concentration.

Equation (4) can be rewritten as

$$\log \frac{E}{1-E} = m(\log d - \log D_m) = \beta_0 + \beta_1 \log d, \quad (5)$$

where $\beta_0 = -m \log D_m$ and $\beta_1 = m$. The dose producing effect E can be written as

$$d = D_m \left(\frac{E}{1-E} \right)^{\frac{1}{m}}, \quad (6)$$

$$\text{or } d = \exp \left(-\frac{\beta_0}{\beta_1} \right) \left(\frac{E}{1-E} \right)^{\frac{1}{\beta_1}}. \quad (7)$$

Suppose model (5) has the form $\log \frac{E}{1-E} = \beta_0 + \beta_1 \log d + \epsilon$ with ϵ following $N(0, \sigma^2)$, we may regress $\log \frac{E}{1-E}$ on $\log d$ to get the marginal dose-effect curves $\log \frac{E}{1-E} = \hat{\beta}_{0,1} + \hat{\beta}_{1,1} \log d$ for drug 1 and $\log \frac{E}{1-E} = \hat{\beta}_{0,2} + \hat{\beta}_{1,2} \log d$ for drug 2. If the observed mean effect is y at a combination dose (d_1, d_2) , then the associated interaction index can be estimated by

$$\hat{\tau} = \frac{d_1}{\hat{D}_{y,1}} + \frac{d_2}{\hat{D}_{y,2}} = \frac{d_1}{\exp(-\frac{\hat{\beta}_{0,1}}{\hat{\beta}_{1,1}}) \left(\frac{y}{1-y} \right)^{\frac{1}{\hat{\beta}_{1,1}}}} + \frac{d_2}{\exp(-\frac{\hat{\beta}_{0,2}}{\hat{\beta}_{1,2}}) \left(\frac{y}{1-y} \right)^{\frac{1}{\hat{\beta}_{1,2}}}} \quad (8)$$

Extensive simulations (Lee and Kong, 2006) indicate that $\log(\hat{\tau})$ is approximately normal distributed, even when $\hat{\tau}$ deviates from normal distribution for large σ 's. A $(1 - \alpha) \times 100\%$ confidence interval for $\log(\tau)$ can be constructed based on the delta method (Bickel and Doksum, 2001):

$$\left[\log(\hat{\tau}) - z_{\frac{\alpha}{2}} \sqrt{\text{Var}(\log(\hat{\tau}))}, \log(\hat{\tau}) + z_{\frac{\alpha}{2}} \sqrt{\text{Var}(\log(\hat{\tau}))} \right],$$

and, thus, a $(1 - \alpha) \times 100\%$ confidence interval for τ can be formed as:

$$\left[\hat{\tau} \exp(-z_{\frac{\alpha}{2}} \sqrt{\text{Var}(\log(\hat{\tau}))}), \hat{\tau} \exp(z_{\frac{\alpha}{2}} \sqrt{\text{Var}(\log(\hat{\tau}))}) \right], \quad (9)$$

where $z_{\frac{\alpha}{2}}$ is the $1 - \frac{\alpha}{2}$ percentile of the standard normal distribution, and $\text{Var}(\log(\hat{\tau})) \simeq \frac{1}{\hat{\tau}^2} \text{Var}(\hat{\tau})$ with

$$\begin{aligned} \text{Var}(\hat{\tau}) &\simeq \sum_{i=1}^2 \left(\frac{d_i}{\hat{D}_{y,i}} \right)^2 \\ &\times \left(\frac{\text{var}(\hat{\beta}_{0,i})}{\hat{\beta}_{1,i}^2} + \frac{2\text{cov}(\hat{\beta}_{0,i}, \hat{\beta}_{1,i})(\log \frac{y}{1-y} - \hat{\beta}_{0,i})}{\hat{\beta}_{1,i}^3} + \frac{\text{var}(\hat{\beta}_{1,i})(\log \frac{y}{1-y} - \hat{\beta}_{0,i})^2}{\hat{\beta}_{1,i}^4} \right) \\ &+ \left(\frac{1}{\hat{\beta}_{1,1}} \frac{d_1}{\hat{D}_{y,1}} + \frac{1}{\hat{\beta}_{1,2}} \frac{d_2}{\hat{D}_{y,2}} \right)^2 \left(\frac{1}{y(1-y)} \right)^2 \text{var}(y). \end{aligned} \quad (10)$$

Details of the derivation of the variance in Eq. (10) can be found in Lee and Kong (2006). We can estimate $\text{var}(y)$ in Eq. (10) in two ways. When there are replicates at the combination dose (d_1, d_2) , we estimate $\text{var}(y)$ by the sample variance at (d_1, d_2) . Otherwise, we may borrow the information from estimating the dose-effect curves. Note that $\text{var}(\log \frac{y}{1-y}) \simeq \left(\frac{1}{y(1-y)} \right)^2 \text{var}(y)$ thus, we may simply substitute

$(\frac{1}{y(1-y)})^2 \text{var}(y)$ by the average of the squared residuals obtained from estimating the two dose-effect curves (Lee and Kong, 2006).

Chou and Talalay (1984) proposed to plot the interaction indices versus effects for combination doses at a fixed ratio. Their idea was to regress $\log \frac{E}{1-E}$ on $\log(d_1 + d_2)$ for the combination doses (d_1, d_2) with $\frac{d_1}{d_2} = \omega$, say, $\log \frac{E}{1-E} = \beta_{0,12} + \beta_{1,12} \log D_{12}$. Then for each fixed effect y , one may estimate the interaction index by

$$\hat{\eta} = \frac{\hat{D}_{y,12} \frac{\omega}{1+\omega}}{\hat{D}_{y,1}} + \frac{\hat{D}_{y,12} \frac{1}{1+\omega}}{\hat{D}_{y,2}}, \quad (11)$$

where $\hat{D}_{y,1} = \exp(-\frac{\hat{\beta}_{0,1}}{\hat{\beta}_{1,1}})(\frac{y}{1-y})^{\frac{1}{\hat{\beta}_{1,1}}}$, $\hat{D}_{y,2} = \exp(-\frac{\hat{\beta}_{0,2}}{\hat{\beta}_{1,2}})(\frac{y}{1-y})^{\frac{1}{\hat{\beta}_{1,2}}}$, and $\hat{D}_{y,12} = \exp(-\frac{\hat{\beta}_{0,12}}{\hat{\beta}_{1,12}})(\frac{y}{1-y})^{\frac{1}{\hat{\beta}_{1,12}}}$. A commercial software *CalcuSyn* (<http://www.biosoft.com/w/calculusyn.htm>) is available for estimating the interaction index and its confidence interval. However, the confidence interval for interaction index in Eq. (11) are constructed based on Monte Carlo techniques and the normal assumption on the parameters. We constructed the confidence interval for interaction index at observed data point based on the delta method and normal assumption on error in model (5). Extensive calculations involved in Monte Carlo techniques seem unnecessary. In a given experiment with varying doses of single agent and their combinations, we may calculate the interaction indices from Eq. (8) and their confidence intervals from Eq. (9) for the observed combination doses at the fixed ratio, and then plot the resulting interaction indices and their confidence intervals to Chou and Talalay's plot of interaction indices versus effects. Thus, the drug interactions for combination doses at the fixed ratio can be characterized.

4. COMPARISON OF FOUR APPROACHES TO DETECT DRUG INTERACTIONS

In this section, we review four response surface models. For comparison purposes we assume that the dose-effect curves follow median-effect Eq. (4) for the first three RSMs. When all the combination doses are synergistic or antagonistic, these approaches use a single synergy-antagonism parameter to summarize synergy or antagonism. In Section 5, we presented a data set from cancer cell line study (Chun et al., 2003). In Section 6, we give the results of data analysis using the method in Section 3 and the RSMs presented in this section, and illustrate the limitation of those methods, i.e., those RSMs are not adequate to capture different patterns of drug interactions when synergy, additivity, and antagonism intersperse.

4.1. Model of Greco et al. (1990)

Assume the dose-effect curves for both drugs follow the median effect Eq. (4), the model proposed by Greco et al. (1990) has the following form:

$$1 = \frac{d_1}{D_{m,1}(\frac{y}{1-y})^{\frac{1}{m_1}}} + \frac{d_2}{D_{m,2}(\frac{y}{1-y})^{\frac{1}{m_2}}} + \frac{\alpha d_1 d_2}{D_{m,1} D_{m,2} (\frac{y}{1-y})^{\frac{1}{m_1}} (\frac{y}{1-y})^{\frac{1}{m_2}}}. \quad (12)$$

Here, m_1, m_2 are the slopes of the dose-effect curves (4) for drug 1 and drug 2, respectively, and $D_{m,1}$ and $D_{m,2}$ are the median effect doses for drug 1 and drug 2, respectively. The parameter α captures the degree of synergism, additivity, or antagonism.

The dose level for each single drug producing effect y can be expressed as the right-hand side of Eq. (6), i.e., $D_{y,1} = D_{m,1} \left(\frac{y}{1-y} \right)^{\frac{1}{m_1}}$ and $D_{y,2} = D_{m,2} \left(\frac{y}{1-y} \right)^{\frac{1}{m_2}}$. The first two terms on the right-hand side of Eq. (12) are exactly the interaction index written as $\frac{d_1}{D_{y,1}} \frac{d_2}{D_{y,2}}$. So we can rewrite (12) as

$$\frac{d_1}{D_{y,1}} + \frac{d_2}{D_{y,2}} = 1 - \frac{\alpha d_1 d_2}{D_{m,1}^{\frac{1}{m_1}} D_{m,2}^{\frac{1}{m_2}} D_{y,1}^{\frac{1}{m_1}} D_{y,2}^{\frac{1}{m_2}}}$$

When $\alpha > 0$, the interaction index is less than one, synergism is detected. The larger α is, the smaller is the interaction index, therefore, the stronger is the synergy. When $\alpha < 0$, antagonism is detected; when $\alpha = 0$, additivity is detected. When we say $\alpha > 0$, or $\alpha < 0$, the inference should be made in the statistical point of view. For example, we claim $\alpha > 0$ only when the lower limit of the confidence interval for α is positive. We can estimate all five parameters ($m_1, m_2, D_{m,1}, D_{m,2}, \alpha$) by the least-squares method.

4.2. Model of Machado and Robinson

Of the several models investigated, Machado and Robinson (1994) recommended the following model which was originally derived by Plackett and Hewlett (1952):

$$\left(\frac{d_1}{D_{y,1}} \right)^\eta + \left(\frac{d_2}{D_{y,2}} \right)^\eta = 1, \quad (13)$$

Similar to the parameter α in the model of Greco et al. (1990), the parameter η captures synergism, additivity, or antagonism: when $0 < \eta < 1$, the combinations of the two drugs are synergistic; when $\eta = 1$, the combinations are additive; and when $1 < \eta < \infty$, the combinations are antagonistic. The smaller the value of η with $0 < \eta < 1$ is, the more synergistic are the combination doses. Again we should view these equalities or inequalities from the statistical point of view.

If one adopts the median effect Eq. (4) as the appropriate model of the dose-effect curve for each drug, then one can fit Machado and Robinson's model of the following form with five parameters ($m_1, m_2, D_{m,1}, D_{m,2}$, and η):

$$\left(\frac{d_1}{D_{m,1} \left(\frac{y}{1-y} \right)^{\frac{1}{m_1}}} \right)^\eta + \left(\frac{d_2}{D_{m,2} \left(\frac{y}{1-y} \right)^{\frac{1}{m_2}}} \right)^\eta = 1 \quad (14)$$

One can use the least-squares method to estimate the five parameters.

Remark 1. Note that for each fixed η , when re-scaled to pass through (1, 0) and (0, 1), all isoboles from a response surface are identical. Therefore, the model is very restrictive.

4.3. Model of Plummer and Short

Plummer and Short (1990) proposed a model of the form

$$Y = \beta_0 + \beta_1 \log(d_1 + \rho \cdot d_2 + \beta_4(d_1 \cdot \rho \cdot d_2)^{\frac{1}{2}}) \quad (15)$$

to identify and quantify departures from additivity. This model was originally proposed by Finney (1971) with a fixed relative potency ρ , and was generalized by Plummer and Short to allow relative potency ρ to vary. Here, Y is the transformed effect, d_1 is the amount of drug 1 and d_2 is the amount of drug 2 in a combination, and ρ is a relative potency of drug 2 versus drug 1 given by $\log(\rho) = \beta_2 + \beta_3 \log D_2$, in which D_2 is the solution to $d_2 + \rho^{-1}d_1 = D_2$. To use this model, the plots of Y versus the $\log(d)$ for both drugs should be linear but need not be parallel. If we adopt the median effect Eq. (4) as the dose-effect relationship for each single drug, then Y as $\log \frac{E}{1-E}$ will have a linear relationship with $\log(d)$, so model (15) is applicable. When we take $Y = \log \frac{E}{1-E}$ model (15) contains five parameters ($\beta_0, \beta_1, \beta_2, \beta_3$, and β_4). One can use the least-squares method to estimate them. The parameter β_4 captures synergism ($\beta_4 > 0$), additivity ($\beta_4 = 0$), or antagonism ($\beta_4 < 0$). Again we should make significance inferences about these relations using confidence intervals, not point estimates.

Let us explore why β_4 can capture synergy and antagonism. If we set $d_2 = 0$ for Plummer and Short's model (15), we will get

$$D_{y,1} = \exp\left(\frac{Y - \beta_0}{\beta_1}\right).$$

which is the dose of drug 1 eliciting the effect Y . If we set $d_1 = 0$ we will get

$$D_{y,2} = \frac{\exp\left(\frac{Y - \beta_0}{\beta_1}\right)}{\rho}$$

which is the dose of drug 2 eliciting the effect of Y . From model (15) we can get

$$\frac{d_1}{\exp\left(\frac{Y - \beta_0}{\beta_1}\right)} + \frac{d_2 \cdot \rho}{\exp\left(\frac{Y - \beta_0}{\beta_1}\right)} + \beta_4 \frac{(d_1 \cdot \rho \cdot d_2)^{\frac{1}{2}}}{\exp\left(\frac{Y - \beta_0}{\beta_1}\right)} = 1,$$

that is,

$$\frac{d_1}{D_{y,1}} + \frac{d_2}{D_{y,2}} = 1 - \beta_4 \frac{(d_1 \cdot d_2)^{\frac{1}{2}}}{(D_{y,1} D_{y,2})^{\frac{1}{2}}} \quad (16)$$

Therefore β_4 captures synergy, additivity, or antagonism, coincident with the Loewe additivity model. Note that Eq. (16) is one of the models mentioned by Machado and Robinson (1994) and has the shortcoming, which we pointed out in Remark 1.

4.4. Model of Carter et al. (1988)

The model proposed by Carter et al. (1988) implies that the dose-effect for a single drug follows a logistic model. The model has the following form,

$$\log \left(\frac{E}{1-E} \right) = \beta_0 + \beta_1 d_1 + \beta_2 d_2 + \beta_{12} d_1 d_2 \quad (17)$$

By setting $d_2 = 0$ we can estimate the dose of drug 1 eliciting a fixed effect y

$$D_{y,1} = \frac{\log \left(\frac{y}{1-y} \right) - \beta_0}{\beta_1}$$

By setting $d_1 = 0$ we can estimate the dose of drug 2 eliciting the fixed effect y

$$D_{y,2} = \frac{\log \left(\frac{y}{1-y} \right) - \beta_0}{\beta_2}$$

From Carter's model (17) we can obtain the interaction index

$$\frac{d_1}{D_{y,1}} + \frac{d_2}{D_{y,2}} = \frac{\beta_1 d_1}{\log \left(\frac{y}{1-y} \right) - \beta_0} + \frac{\beta_2 d_2}{\log \left(\frac{y}{1-y} \right) - \beta_0} = 1 - \frac{\beta_{12} d_1 d_2}{\log \left(\frac{y}{1-y} \right) - \beta_0} \quad (18)$$

Under the model, with a prerequisite that $\log \left(\frac{y}{1-y} \right) - \beta_0 > 0$, β_{12} captures synergy ($\beta_{12} > 0$), additivity ($\beta_{12} = 0$), or antagonism ($\beta_{12} < 0$).

5. DATA SET

A principal focus of chemoprevention research at M.D. Anderson Cancer Center is to identify efficient combinations of chemotherapeutic and biologic agents that eliminate precancerous cells or slow the carcinogenic processes in patients at high-risk for the development of cancer. Combinations of drugs acting synergistically have the primary benefits of improving therapeutic activity with lower toxicity. This is particularly important in the prevention setting because preventive regimen must elicit low toxicity profiles before they can be administered to relatively healthy subjects. For example, an experiment was conducted at M.D. Anderson Cancer Center (by Reuben Lotan) to evaluate the efficacy of two such novel agents, SCH66336 and 4-HPR, in squamous cell carcinoma cell lines (Chun et al., 2003). SCH66336, a tricyclic peptidomimetic compound, has extensive activity in preclinical studies in head and neck squamous cell carcinoma and in non-small-cell lung cancer cell lines. 4-HPR is a potent retinoid that induces apoptosis (cell death) in various malignant cells.

Cell lines of human squamous cell carcinoma were treated with SCH66336 and 4-HPR separately and in combination. After 72h, the fractions of surviving cells at each single dose and combination dose levels were calculated. Table 1 shows the fractions of surviving cells from a human squamous cell carcinoma cell line (UMSCC22B) after treatment with SCH66336 (doses ranged from 0 to 4 μ M) and 4-HPR (doses ranged from 0 to 2 μ M) alone and in combination.

Table 1 Fractions of squamous cell carcinoma cells (UMSCC22B) surviving after 72h of treatment by single and combination doses of SCH66336 and 4-HPR*

SCH66336 Dose (μM)	4-HPR Dose (μM)				
	0	0.1	0.5	1	2
0	1	0.7666	0.5833	0.5706	0.4934
0.1	0.6701	0.6539	0.4767	0.5171	0.3923
0.5	0.6289	0.6005	0.4919	0.4625	0.3402
1	0.5577	0.5102	0.4541	0.3551	0.2851
2	0.4550	0.4203	0.3441	0.3082	0.2341
4	0.3755	0.3196	0.2978	0.2502	0.1578

*The same data table was also shown in Kong and Lee (2006a), Table 2.

6. DATA ANALYSIS

We illustrate the methods described in Sections 3 and 4 to identify synergism, additivity, or antagonism by analyzing the data set in Table 1. The percentages of surviving cells ranged from 67% at 0.1 μM to only 38% at 4 μM by treating with SCH66336 alone. 4-HPR was slightly less effective as a single agent eliciting 77% surviving cells at 0.1 μM and 49% surviving cells at 2 μM . Equidose effects of the combination of the two agents ranged from 65% at 0.1 μM (total dose = $d_1 + d_2 = 0.2 \mu\text{M}$) to 23% at 2 μM (total dose = $4 \mu\text{M}$). The data suggest some supra-additive effects by the combination. For example, a total dose of 2 μM of the combination dose with $d_1 = 1 \mu\text{M}$ and $d_2 = 1 \mu\text{M}$ elicited 36% surviving cells whereas the single agent effect at this dose was 46% and 49% for SCH66336 and 4-HPR, respectively. We treat the effect, i.e., fraction of surviving cells as a continuous variable and assume the stochastic error is linear in $\log \frac{E}{1-E}$. The least squares method was applied in solving the parameters for all methods described below.

The median effect plot can be obtained by a linear regression of $\log \frac{E}{1-E}$ on $\log d$ based on the data in Table 1. Recall that $\log \frac{E}{1-E} = m(\log d - \log D_m) = \beta_0 + \beta_1 \log d$. The estimates of β_0 , $\beta_1 (=m)$, D_m , and r for drug 1, drug 2, and the mixture of the drugs with equal concentrations are summarized in Table 2.

Figure 2A shows the transformed data $\log \frac{E}{1-E}$ versus $\log d$ and the median effect plots for SCH66336 (open circles and a dashed line), 4-HPR (open triangles and a dotted line), and the mixture of the two drugs at the fixed ratio of 1:1 (filled circles and a solid line). Figure 2C shows the corresponding observed data and the fitted dose-effect curves for SCH66336, 4-HPR, and the mixture of the two drugs.

Table 2 Estimates based on Chou's median effect model

	i	$\beta_{0,i}$	Slope $\beta_{1,i} (=m_i)$	D_{mi}	r_i
SCH66336	1	0.094	-0.335	1.326	0.946
4-HPR	2	0.217	-0.398	1.726	0.979
Mixture of the two drugs with equal concentrations	12	-0.225	-0.596	0.686	0.982

The median effect equation constrains the effect to be 1 at dose zero for $m < 0$. In fact only five observations were used to calculate the median effect model for SCH66336 alone, four observations for 4-HPR alone, and four observations for the mixture. The remaining 16 data points at other combination doses were not used, indicating that the method is not very efficient. The median effect plots in Fig. 2A and r values (correlation coefficients) in Table 2 indicate that the data follow the median effect Eq. (4) reasonably well. We plotted the interaction index versus the effect E for the combinations at the fixed ratio 1:1. From the fitted dose-effect curves for SCH66336 and 4-HPR, the four estimated interaction indices based on Eq. (8) at the four combination doses (0.1, 0.1), (0.5, 0.5), (1, 1), and (2, 2) were 0.791, 0.609, 0.256, and 0.103, respectively, and their corresponding 95% confidence intervals based on Eq. (9) were [0.341, 1.833], [0.283, 1.312], [0.101, 0.647], and [0.031, 0.335], respectively. The four pairs of interaction indices versus the effects

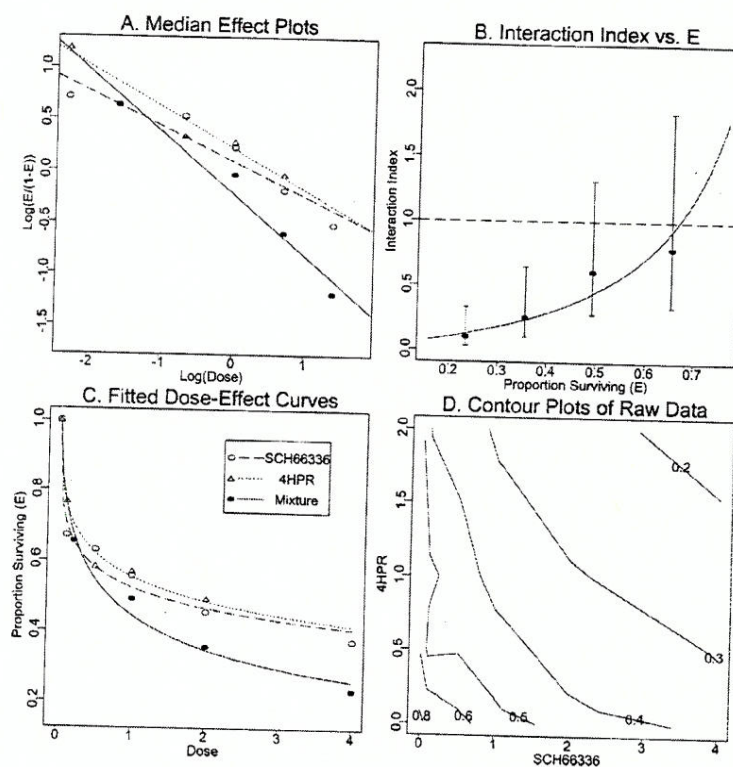


Figure 2 Results from fitting median effect equation models (Panels A and C), calculating interaction index and its confidence interval (Panel B), and the selected contour plot of the raw data (Panel D). Panel A shows the transformed observations $\log \frac{E}{1-E}$ versus $\log d$ and the median-effect plots for drug SCH66336, drug 4-HPR, and the mixture of the two drugs at the fixed ratio of 1:1. Panel B shows the curve of interaction index versus the effect E based on the three estimated median effect equations plotted in Panel A, the estimated interaction indices (in dots) along with their 95% confidence intervals (in vertical bars) at the four observations with the drug combinations at the fixed ratio of 1:1. Panel C shows the original observations effect versus dose level and the fitted dose-response curves using the median-effect equation. Panel D shows the contour plot of the raw data.

along with their 95% confidence intervals are shown in Fig. 2B. The 95% confidence intervals of the interaction indices at the combination doses (0.1, 0.1) and (0.5, 0.5) contain 1, indicating that the two combination doses are additive, while the 95% confidence intervals of the interaction indices at the combination doses (1, 1) and (2, 2) are below 1, indicating that the two combination doses are synergistic. Table 3 provides summaries of the estimated synergy-antagonism parameter, its 95% confidence interval, and the conclusion using each of the models described in Sections 3 and 4. We also assessed drug interactions for the combination doses at the fixed ratio 1:1 using the software CalcuSyn under the mutually exclusive assumption (Chou and Talalay, 1984) and concluded that the combination doses with effects less than 0.45 are synergistic, while the combination doses with effects greater than 0.45 are additive. The conclusions based on CalcuSyn are consistent with our findings based on the procedure in Section 3.

Since the data for each drug used alone follow the median effect equation reasonably well, we can use the median effect equation as dose-effect curve for the models described in Sections 4.1 to 4.3. The parameters estimated in the median effect plot could be used as the initial values for parameter estimation. We fitted each of the models mentioned in Sections 4.1 to Section 4.4, and plotted the observed values and the fitted dose-effect curves for SCH66336, 4-HPR, and the mixture of the drugs at the fixed ratio of 1:1 (Figures 3A, 3C, 4A, and 4C), where the fitted dose-response curves were obtained from the corresponding response surface models. Selected contours of each fitted response surface are shown in Figs. 3B, 3D, 4B, and 4D. Comparing these fitted curves with the raw data and comparing the contour plot of each fitted response surface with the contour plot of the raw data (Fig. 2D) provide a crude visual assessment of whether the fit is good or not. The residual sum of squares (RSS) is another useful measure of the goodness of fit.

For Greco's model, the initial values for m_1 , m_2 , D_{m1} , D_{m2} , are given in Table 2, and the initial value for α was set as 0. The two-component plot is shown in

Table 3 Summary statistics of the five methods for detecting drug interactions in the combined therapy of SCH66336 and 4-HPR on the UMSCC22B cell line

Model	Drug Syn.	Interaction Add.	Parameter Ant.	Estimated value	95% confidence interval	RSS	Conclusion
Direct Calculation	$II < 1$	$II = 1$	$II > 1$				
		$d_1 = 0.1, d_2 = 0.1$		0.791	[0.341, 1.833]	NA	Add.
		$d_1 = 0.5, d_2 = 0.5$		0.609	[0.283, 1.312]	NA	Add.
		$d_2 = 1.0, d_2 = 1.0$		0.256	[0.101, 0.647]	NA	Syn.
		$d_1 = 2.0, d_2 = 2.0$		0.103	[0.031, 0.335]	NA	Syn.
Greco's	$\alpha > 0$	$\alpha = 0$	$\alpha < 0$	5.622	[-0.464, 11.708]	0.618	Add.
Machado's	$0 < \eta < 1$	$\eta = 1$	$\eta > 1$	0.507	[0.327, 0.687]	1.232	Syn.
Plummer's	$\beta_4 > 0$	$\beta_4 = 0$	$\beta_4 < 0$	2.146	[-0.014, 4.305]	1.238	Add.
Carter's	$\beta_{12} > 0$	$\beta_{12} = 0$	$\beta_{12} < 0$	-0.003	[-0.087, 0.081]	1.399	Add.*

Note: II signifies the directly calculated Interaction Index; NA signifies not applicable; Syn. indicates synergy; Add. indicates additivity; Ant. indicates antagonism. RSS indicates residual sum of squares; Add.* indicates that Carter's model did not provide adequate fit to the data although the drug interaction parameter and its confidence interval show that the drug combinations are additive.

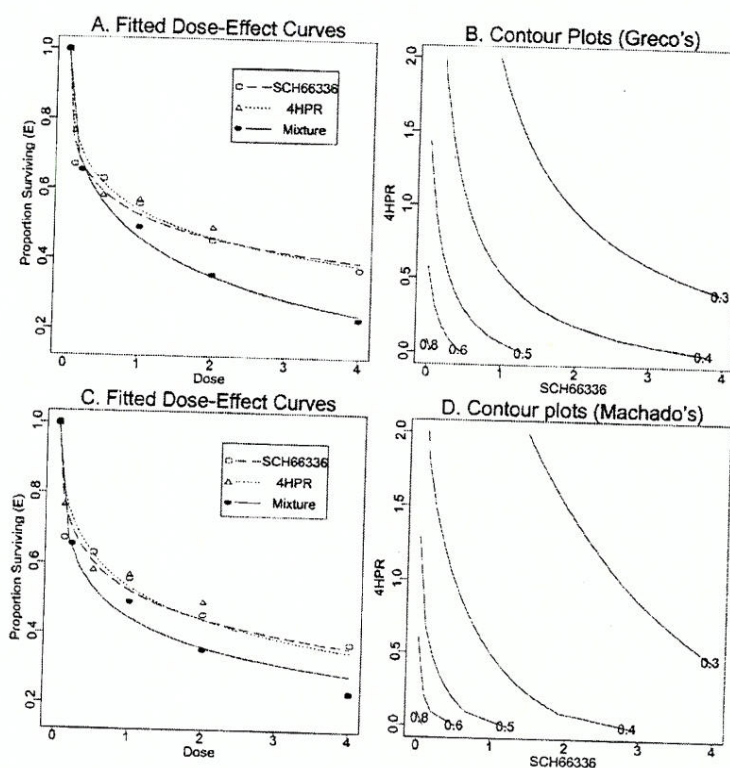


Figure 3 Results from Greco's model (Panels A and B) and Machado's model (Panel C and D): Panels A and C show the observations of effect E versus dose and the fitted dose effect curves for drug SCH66336, drug 4-HPR, and the mixture of the two drugs at the fixed ratio of 1:1. Panels B and D are the contour plots of the fitted response surfaces.

Fig. 3 (Panels A and B) and $RSS = 0.618$. The fitted parameters are $m_1 = -0.383$, $m_2 = -0.449$, $D_{m1} = 1.316$, $D_{m2} = 1.430$, and the estimated synergy-antagonism parameter $\alpha = 5.622$ with standard error 3.105. The 95% confidence interval for α is $[-0.464, 11.708]$. The confidence interval, which includes 0, precludes a statement of statistical significance for α being different from 0, and thus synergy. However, the confidence interval of α expands mostly in the positive range, suggesting that the combinations of the two drugs may have some synergistic effect instead of pure additive effect.

For Machado and Robinson's model, the initial values for m_1 , m_2 , D_{m1} , and D_{m2} were also taken from Table 2 with $\eta = 0.7$. The two plots are shown in Fig. 3 (Panels C and D) and $RSS = 1.232$. The fitted parameters are $m_1 = -0.471$, $m_2 = -0.538$, $D_{m1} = 1.220$, $D_{m2} = 1.282$, and the estimated synergy-antagonism parameter $\eta = 0.507$ with standard error 0.092, so the 95% confidence interval for η is $[0.327, 0.687]$, which does not contain 1 and indicates synergy for the combinations of the two drugs.

For Plummer and Short's model, the initial values for β_0 , β_1 could be taken as $\beta_{0,1}$ and slope m_1 in Table 2. The initial values for β_2 and β_3 were set at $\frac{\beta_{0,2} - \beta_{0,1}}{m_1}$ and

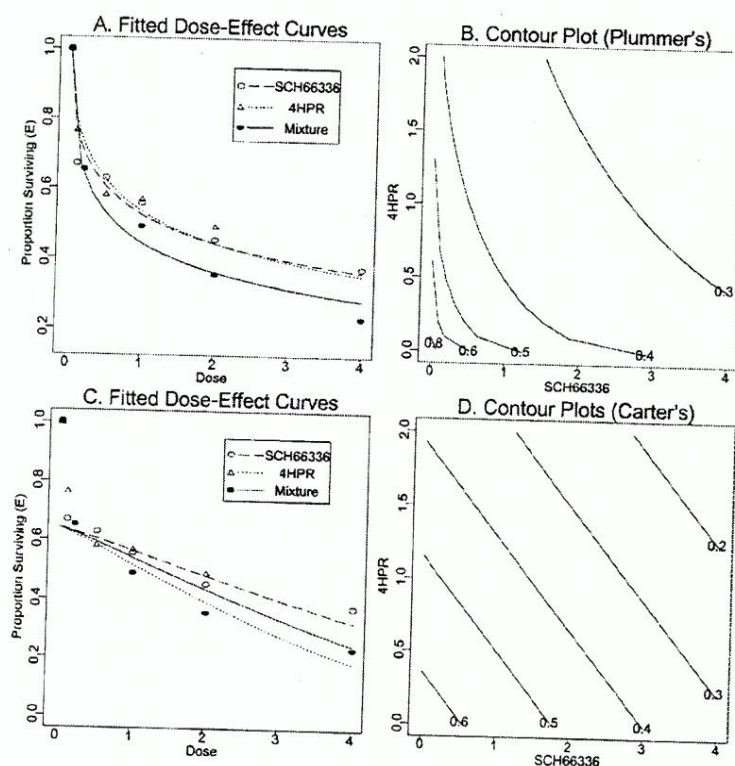


Figure 4 Results from Plummer's model (Panels A and B) and Carter's model (Panels C and D): Panels A and C show the observations of effect E versus dose and the fitted dose effect curves for drug SCH66336, drug 4-HPR, and the mixture of the two drugs at the fixed ratio of 1:1. Panels B and D are the contour plots of the fitted response surfaces.

$\frac{m_2 - m_1}{m_1}$, respectively. We used the Newton-Raphson method to solve D_2 in Plummer and Short's model. The convergence of the algorithm is sensitive to the initial value of β_4 . One should try different initial values for β_4 to see whether the solutions are obtainable and converge to the same value. In this example, we took 2.5 as the initial value for β_4 . The corresponding two plots are shown in Fig. 4 (Panels A and B) and $RSS = 1.238$. The fitted parameters are $\beta_0 = 0.099$, $\beta_1 = -0.473$, $\beta_2 = -0.083$, $\beta_3 = 0.120$, and the estimated synergy-antagonism parameter $\beta_4 = 2.146$ with standard error 1.102, so the 95% confidence interval for β_4 is $[-0.014, 4.305]$. Similar to Greco's model, the confidence interval includes 0, but just barely. The conclusion is that these combinations of the two drugs are additive.

For Carter's model (17), the initial values can be obtained using logistic regression for each single drug. The two plots are shown in Fig. 4 (Panels C and D). The fitted parameters were $\beta_0 = 0.590$, $\beta_1 = -0.331$, and $\beta_2 = -0.516$. The estimated synergy-antagonism parameter $\beta_{12} = -0.003$ with standard error 0.043, thus the 95% confidence interval for β_{12} , $[-0.087, 0.081]$, contains zero, indicating the combinations are additive. From the plots in Fig. 4 (Panels C and D), we can see that the fit is not good either for a single drug or for the mixture of the two

drugs, and the contour plot of the fitted surface is far away from the contour of the raw data. These figures show that Carter's model does not provide a good fit for our data. Table 3 also shows that Carter's model yields the largest RSS(=1.399).

In conclusion, we have fitted five models to the data in Table 1 with summary statistics shown in Table 3. We compared the fitted dose-effect curves with raw data given in Figs. 2C, 3A, 3C, 4A, and 4C. In addition, the fitted contour plots in Figs. 3B, 3D, 4B, and 4D were compared to the raw data contour plot in Fig. 2D. The correlation coefficients in Table 2 and standard regression diagnostics indicated that the Chou and Talalay model fits the data well. Data analysis by the Machado and Robinson's model led us to the conclusion that the combinations of the two drugs are synergistic on the UMSCC22B cell line (Table 3). The directly calculated interaction indices and their confidence intervals based on the procedure in Section 3 indicate that the combination doses at moderate to high dose level are synergistic but the combination doses at low level are additive. The coexistence of synergy and additivity of the two agents probably explains why the confidence intervals for Greco's α and Plummer and Short's β_4 barely include zero but tend to be positive. These findings also indicate that the RSM using a single parameter to capture drug interactions is not adequate when synergy, additivity, and antagonism intersperse.

We developed S-PLUS/R programs to provide estimates for each of the five methods described. The S-PLUS/R code and the data example are available in *synergy* which can be downloaded from <http://biostatistics.mdanderson.org/SoftwareDownload/>.

7. DISCUSSION AND FUTURE RESEARCH

Based on the directly calculated interaction indices and their confidence intervals in Section 3, one can only assess drug interactions for selected combination doses. More general approaches for estimating interaction indices and their associated confidence intervals should be derived to provide an efficient way to assess drug interaction in the situation when synergy, additivity, and antagonism intersperse. Furthermore, if the dose-effect curve for a single drug does not follow the median effect equation, alternative models with a better fit should be considered to provide a more accurate assessment of drug interaction.

Response surface models provide a reasonable overall picture of dose response relationships. However, our case study in Section 6 illustrates that these response surface models are not adequate to describe the pattern when some combination doses are synergistic while other combination doses are additive or antagonistic, e.g., in the case that a response surface has a similar contour as \widehat{PRSTQ} (Fig. 1, Panel B). Generally speaking, such limitation exists for all response surface models using a single synergy-antagonism parameter. New methods are needed to identify and quantify departures from additivity when synergism and antagonism are inconsistent over all combination doses within the same data. Kong and Lee (2006a) extend Plummer and Short's approach and use a function of the two doses d_1 and d_2 instead of the single parameter β_4 to capture drug interactions. Kong and Lee (2006b) propose a two-component semiparametric model to capture the mixed patterns of drug interactions. These extended approaches can detect different patterns of synergy and antagonism among combination doses of two drugs.

For our data set, we had only a single outcome measure, i.e., fraction of surviving cells, at each combination dose. We used the least-squares method to estimate the parameters in the models as mentioned above. The results will be the same as the maximum likelihood estimate for normally distributed errors. If we have multiple observations for each drug combination, we can detect whether the variance is constant, and, if not, use the weighted least-squares method to improve the fit. Although we applied the above five methods to *in vitro* study data, these methods can be applied to *in vivo* studies as well. For example, if we know the total number of subjects (n) and the number of subjects (r) who respond to the treatment at each drug combination, we can assume that r follows a binomial distribution with parameter n and E , where E is the expected probability of response (i.e., the expected response rate) at the combination. Then we may use the maximum likelihood method to estimate the parameters in each model. Further statistical inferences can be made accordingly.

One of the important issues in studying drug synergy is to devise the most proper and efficient experimental design. Tan et al. (2003) proposed an optimal experimental design in the sense that it reduces the variability in modeling synergy while allocating the doses to minimize the sample size and to extract maximum information on the joint action of the drugs. Straetmans et al. (2005) gave a ray design for 96-well experiment and used a three-parameter log-logistic model to assess synergy. As the interest in combination therapy continues to increase, methodology development and experimental design for studying drug interaction deserve more attention.

ACKNOWLEDGMENTS

The research was supported in part by grants from the National Cancer Institute CA16672, CA97007, CA91844, and Department of Defense W81XWH-04-1-0142 and W81XWH-05-2-0027. The authors are thankful to Dr. Gary Rosner for his helpful comments, to John Boik for providing analysis results using *CalcuSyn*, and to Lee Ann Chastain for editorial assistance.

REFERENCES

- Bachmann, K. A., Ghosh, R. (2001). The use of *in vitro* methods to predict *in vivo* pharmacokinetics and drug interactions. *Current Drug Metabolism* 2:299–314.
- Berenbaum, M. C. (1989). What is synergy? *Pharmacological Reviews* 41:93–141.
- Bickel, P. J., Doksum, K. A. (2001). *Mathematical Statistics: Basic Ideas and Selected Topics*. Vol. 1. Prentice Hall: New Jersey.
- Bliss, C. I. (1939). The toxicity of poisons applied jointly. *Annals of Applied Biology* 26:585–615.
- Carter, W. H. Jr., Gennings, C., Staniswalis, J. G., Cambell, E. D., White, K. L. Jr. (1988). A statistical approach to the construction and analysis of isobolograms. *Journal of American College Toxicology* 7:963–973.
- Chou, T. C., Talalay, P. (1984). Quantitative analysis of dose-effect relationships: the combined effects of multiple drugs or enzyme inhibitors. *Advances in Enzyme Regulation* 22:27–55.
- Chun, K. H., Lee, J. J., Ayers, G. D., Lotan, R. (2003). Synergistic induction of apoptosis in human head and neck squamous cell carcinoma (HNSCC) cell lines by the

- combination of the synthetic retinoid 4HPR and the farnesyltransferase inhibitor SCH66336. Proceedings of American Association for Cancer Research 44.
- Curran, W. J. Jr. (2003). Evolving chemoradiation treatment strategies for locally advanced non-small-cell lung cancer. *Oncology (Huntingt)* 17(12 Suppl 13):7-14.
- Drebler, V., Muller, G., Suhnel, J. (1999). CombiTool-A new computer program for analyzing combination experiments with biologically active agents. *Computers and Biomedical Research* 32:145-160.
- Evans, T. L. (2004). Highlights from the tenth world conference on lung cancer. *Oncologist* 9(2):232-238.
- Finney, D. J. (1971). *Probit Analysis*. Cambridge: Cambridge University Press.
- Fitzgerald, J. B., Schoeberl, B., Nielsen, U. B., Sorger, P. (2006). Systems biology and combination therapy in the quest for clinical efficacy. *Nature Chemical Biology* 2(9):458-466.
- Greco, W. R., Park, H. S., Rustum, Y. M. (1990). Application of a new approach for the quantitation of drug synergism to the combination of cis-diamminedichloroplatinum and 1- β -D-arabinofuranosylcytosine. *Cancer Research* 50:5318-5327.
- Greco, W. R., Bravo, G., Parsons, J. C. (1995). The search of synergy: a critical review from a response surface perspective. *Pharmacological Reviews* 47(2):331-385.
- Greco, W. R., Unkelbach, H. D., Poch, G., Suhnel, J., Kundi, M., Bodeker, W. (1992). Consensus on concepts and terminology for combined-action assessment: the Saariselka Agreement. *Arch. Complex Environ. Stud.* 4:65-69.
- Herbst, R. S. (2005). Role of novel targeted therapies in the clinic. *British Journal of Cancer* 92(Suppl 1):S21-27.
- Hill, A. V. (1910). The possible effects of the aggregation of the molecules of haemoglobin on its dissociation curves. *The Journal of Physiology* 40:iv-vii.
- Holford, N. H. G., Sheiner, L. B. (1981). Understanding the dose-effect relationship: clinical application of pharmacokinetic-Pharmacodynamic models. *Clinical Pharmacokinetics* 6:429-453.
- Jonker, D. M., Visser, S. A. G., van der Graaf, P. H., Voskuyl, R. A., Danhof, M. (2005). Towards a mechanism-based analysis of pharmacodynamic drug-drug interactions in vivo. *Pharmacology and Therapeutics* 106:1-18.
- Kong, M., Lee, J. J. (2006a). A general response surface model with varying relative potency for assessing drug interactions. *Biometrics* 62:986-995.
- Kong, M., Lee, J. J. (2006b). A semiparametric response surface model for assessing drug interactions. (Submitted).
- Lee, J. J., Kong, M. (2006). A confidence interval for interaction index for assessing multiple drug interaction. (Submitted).
- Machado, S. G., Robinson, G. A. (1994). A direct, general approach based on isobolograms for assessing the joint action of drugs in pre-clinical experiments. *Statistics in Medicine* 13:2289-2309.
- Martinez-Irujo, J. J., Villahermosa, M. L., Mercapide, J., Cabodevilla, J. F., Santiago, E. (1998). Analysis of the combined effect of two linear inhibitors on a single enzyme. *Biochemical Journal* 329:689-698.
- Morgan, B. J. T. (1992). *Analysis of Quantal Response Data*. Chapman and Hall.
- Niyazi, M., Belka, C. (2006). Isobologram analysis of triple therapies. *Radiation Oncology* Oct 17:1-39.
- Plackett, R. L., Hewlett, P. S. (1952). Quantal responses to mixtures of poisons. *Journal of the Royal Statistical Society B* 14:141-163.
- Plummer, J. L., Short, T. G. (1990). Statistical modeling of the effects of drug combinations. *Journal of Pharmacological Methods* 23:297-309.

- Sharma, P. L., Nurpeisov, V., Hernandez-Santiago, B., Beltran, T., Schinazi, R. F. (2004). Nucleoside inhibitors of human immunodeficiency virus type 1 reverse transcriptase. *Current Topics in Medicinal Chemistry* 4(9):895-919.
- Straetmans, R., O'Brien, T., Wouters, L., Dun, J. V., Janicot, M., Bijmens, L., Burzykowski, T., Aerts, M. (2005). Design and analysis of drug combination experiments. *Biometrical Journal* 47(3):299-308.
- Tallarida, R. J. (2000). *Drug Synergism and Dose-Effect Data Analysis*. New York: Chapman and Hall.
- Tan, M., Fang, H., Tian, G., Houghton, P. J. (2003). Experimental design and sample size determination for testing synergism in drug combination studies based on uniform measures. *Statistics in Medicine* 22:2091-2100.
- Webb, J. L. (1963). *Enzyme and Metabolic Inhibitors*. New York: Academic Press.

The Proteasome Inhibitor PS-341 (Bortezomib) Up-Regulates DR5 Expression Leading to Induction of Apoptosis and Enhancement of TRAIL-Induced Apoptosis Despite Up-Regulation of c-FLIP and Survivin Expression in Human NSCLC Cells

Xiangguo Liu, Ping Yue, Shuzhen Chen, Liping Hu, Sagar Lonial, Fadlo R. Khuri, and Shi-Yong Sun

Department of Hematology and Oncology, Winship Cancer Institute, Emory University School of Medicine, Atlanta, Georgia

Abstract

The proteasome inhibitor PS-341 (bortezomib or Velcade), an approved drug for treatment of patients with multiple myeloma, is currently being tested in clinical trials against various malignancies, including lung cancer. Preclinical studies have shown that PS-341 induces apoptosis and enhances tumor necrosis factor-related apoptosis-inducing ligand (TRAIL)-induced apoptosis in human cancer cells with undefined mechanisms. In the present study, we show that PS-341 induced caspase-8-dependent apoptosis, cooperated with TRAIL to induce apoptosis, and up-regulated death receptor 5 (DR5) expression in human non-small cell lung cancer (NSCLC) cells. DR5 induction correlated with the ability of PS-341 to induce apoptosis. Blockage of PS-341-induced DR5 up-regulation using DR5 small interfering RNA (siRNA) rendered cells less sensitive to apoptosis induced by either PS-341 or its combination with TRAIL, indicating that DR5 up-regulation mediates PS-341-induced apoptosis and enhancement of TRAIL-induced apoptosis in human NSCLC cells. We exclude the involvement of c-FLIP and survivin in mediating these events because c-FLIP (i.e., FLIP_s) and survivin protein levels were actually elevated on exposure to PS-341. Reduction of c-FLIP with c-FLIP siRNA sensitized cells to PS-341-induced apoptosis, suggesting that c-FLIP elevation protects cells from PS-341-induced apoptosis. Thus, the present study highlights the important role of DR5 up-regulation in PS-341-induced apoptosis and enhancement of TRAIL-induced apoptosis in human NSCLC cells. [Cancer Res 2007;67(10):4981-8]

Introduction

The tumor necrosis factor (TNF)-related apoptosis-inducing ligand (TRAIL) receptor death receptor 4 (DR4; also called TRAIL-R1) and death receptor 5 (DR5; also named Apo2, TRAIL-R2, TRICK2, or Killer/DR5) belong to the TNF receptor gene superfamily, all of which share a similar, cysteine-rich extracellular domain and additional cytoplasmic death domain (1). Both DR4 and DR5, located at the cell surface, become activated or trimerized on binding to their ligand TRAIL or overexpression

and then signal apoptosis through caspase-8-mediated activation of caspase cascades (1). Recently, these death receptors have attracted much more attention because their ligand TRAIL preferentially induces apoptosis in transformed or malignant cells, showing potential as a tumor-selective apoptosis-inducing cytokine for cancer treatment. The expression of DR4 and DR5 is inducible by certain stimuli, including some cancer therapeutic agents (2, 3). It has been documented that induction of DR4 and/or DR5 accounts for induction of apoptosis and/or enhancement of TRAIL-induced apoptosis by certain cancer therapeutic agents (4-9).

Caspase-8 activation is a critical step in initiating death receptor-induced apoptosis (1). c-FLIP is the major protein that prevents caspase-8 from activation by death receptors. Although more than 10 isoforms of c-FLIP mRNA have been described, only 2 of them, FLIP_s and FLIP_L, have been significantly studied at the protein level (10). Both proteins can be recruited to the death-inducing signaling complex (DISC) to inhibit caspase-8 activation (10, 11). There are an increasing number of studies showing that modulation of c-FLIP levels affects cell sensitivity to death receptor-mediated apoptosis (10, 11).

It is well known that the extrinsic death receptor-mediated pathway can activate the intrinsic mitochondria-mediated pathway, through caspase-8-mediated cleavage or truncation of Bid protein, leading to induction of apoptosis (12). Survivin, a family member of the inhibitor of apoptosis proteins, acts downstream of mitochondria to prevent processing of initiator caspase-9 from the apoptosome, leading to inhibition of the activity of the effector caspases. Thus, survivin modulates both the extrinsic and the intrinsic apoptotic pathways (13). Many studies have shown that induction of survivin expression causes cellular resistance to drug-induced apoptosis, whereas down-regulation of survivin using various means, such as small interfering RNA (siRNA), either induces apoptosis or sensitizes cells to undergo drug- or death ligand/receptor-induced apoptosis (13).

PS-341 (also called bortezomib or Velcade) is an approved drug for treatment of patients with relapsed multiple myeloma. Currently, there are many ongoing clinical trials that test the anticancer efficacy of PS-341 or its combinations with other agents in different types of cancers, including lung cancer (14, 15). Many preclinical studies documented that PS-341 alone or in combination with other cancer therapeutic agents, including TRAIL, induces apoptosis in a variety of human cancer cells *in vitro*, including both hematologic and solid tumor malignancies, and inhibits the growth of tumor xenografts *in vivo* (16, 17). However, the molecular mechanisms underlying PS-341-induced apoptosis and enhancement of apoptosis when combined with other agents, including TRAIL, particularly in human lung cancer

Note: Supplementary data for this article are available at Cancer Research Online (<http://cancerres.aacrjournals.org/>).

F.R. Khuri and S-Y. Sun are Georgia Cancer Coalition Distinguished Cancer Scholars.

Requests for reprints: Shi-Yong Sun, Winship Cancer Institute, Emory University School of Medicine, 1365-C Clifton Road Northeast, C3088, Atlanta, GA 30322. Phone: 404-778-2170; Fax: 404-778-5520; E-mail: shi-yong.sun@emoryhealthcare.org.

©2007 American Association for Cancer Research.

doi:10.1158/0008-5472.CAN-06-4274

cells, remain largely uncharacterized, although it seems to be associated with nuclear factor- κ B inhibition (14, 18, 19), c-Jun NH₂-terminal kinase (JNK) activation (19–21), or Bik and Bim accumulation (22, 23) shown in certain types of cancer cells.

PS-341 has been shown to sensitize cells to TRAIL-induced apoptosis in certain types of cancer cells; this effect seems to be associated with Bik accumulation or c-FLIP down-regulation (22–24). Other proteasome inhibitors, such as MG132, increase DR5 expression, which mediates induction of apoptosis and enhances TRAIL-induced apoptosis by these inhibitors (25–27). To show the mechanism by which PS-341 induces apoptosis in human non-small cell lung cancer (NSCLC) cells, we studied the effects of PS-341 on the expression of DR4, DR5, c-FLIP, and survivin and their effect on PS-341-induced apoptosis and enhancement of TRAIL-induced apoptosis. Our results show that DR5 up-regulation plays an important role in PS-341-induced apoptosis and enhancement of TRAIL-induced apoptosis in human NSCLC cells.

Materials and Methods

Reagents. The powder of pure PS-341 was provided by Millennium Pharmaceuticals. It was dissolved in DMSO at a concentration of 1 mmol/L, and aliquots were stored at -80°C . Stock solutions were diluted to the desired final concentrations with growth medium just before use. MG132 and epoxomicin, two additional proteasome inhibitors, were purchased from Sigma Chemical Co. and Calbiochem, respectively. Human recombinant TRAIL was purchased from Biomol or PeptoTech, Inc. Rabbit polyclonal anti-DR5 antibody was purchased from ProSci, Inc. Mouse monoclonal anti-DR4 antibody (B-N28) was purchased from Diaclone. Mouse monoclonal anti-FLIP antibody (NF6) was purchased from Alexis Biochemicals. Mouse monoclonal anti-caspase-3 was purchased from Imgenex. Rabbit anti-caspase-8, anti-caspase-9, anti-caspase-6, anti-lamin A/C, and anti-poly(ADP-

ribose) polymerase (PARP) antibodies and mouse monoclonal anti-survivin antibody were purchased from Cell Signaling Technology, Inc. Rabbit polyclonal anti- β -actin antibody was purchased from Sigma Chemical.

Cell culture. The human NSCLC cell lines used in this study were purchased from the American Type Culture Collection. They were grown in monolayer culture in RPMI 1640 with glutamine (Sigma Chemical) supplemented with 5% fetal bovine serum at 37°C in a humidified atmosphere consisting of 5% CO_2 and 95% air. The immortalized normal human bronchial epithelial cell lines BEAS-2B (28) and HBEC3KT (29) were provided by Dr. R. Lotan (M. D. Anderson Cancer Center, Houston, TX) and J.D. Minna (The University of Texas Southwestern Medical Center, Dallas, TX) and cultured as described previously (28, 29).

Cell survival assay. Cell survival was estimated by sulforhodamine B (SRB) assay as described previously (30).

Western blot analysis. Preparation of whole-cell protein lysates and the procedures for the Western blotting were described previously (4).

Detection of apoptosis. The amounts of cytoplasmic histone-associated DNA fragments (mononucleosome and oligonucleosomes) formed during apoptosis were measured using a Cell Death Detection ELISA^{plus} kit (Roche Molecular Biochemicals) according to the manufacturer's instructions. The sub-G₁ population was analyzed using flow cytometry as described previously (31). In addition, caspase activation and their substrate cleavage were also detected by Western blot analysis as described above as another indicator of apoptosis.

Detection of cell surface death receptors. The procedure for direct antibody staining and subsequent flow cytometric analysis of cell surface protein was described previously (32). The mean fluorescence intensity (MFI) that represents antigenic density on a per cell basis was used to represent DR5 expression level. Phycoerythrin-conjugated mouse anti-human DR5 (DJR2-4) and anti-human DR4 (DJR1) monoclonal antibodies and phycoerythrin mouse IgG1 isotype control (MOPC-21/P3) were purchased from eBioscience.

Gene silencing using siRNA. The siRNA duplexes for control, *caspase-8*, *DR4*, and *DR5* genes were described previously (4, 5). c-FLIP siRNA duplex

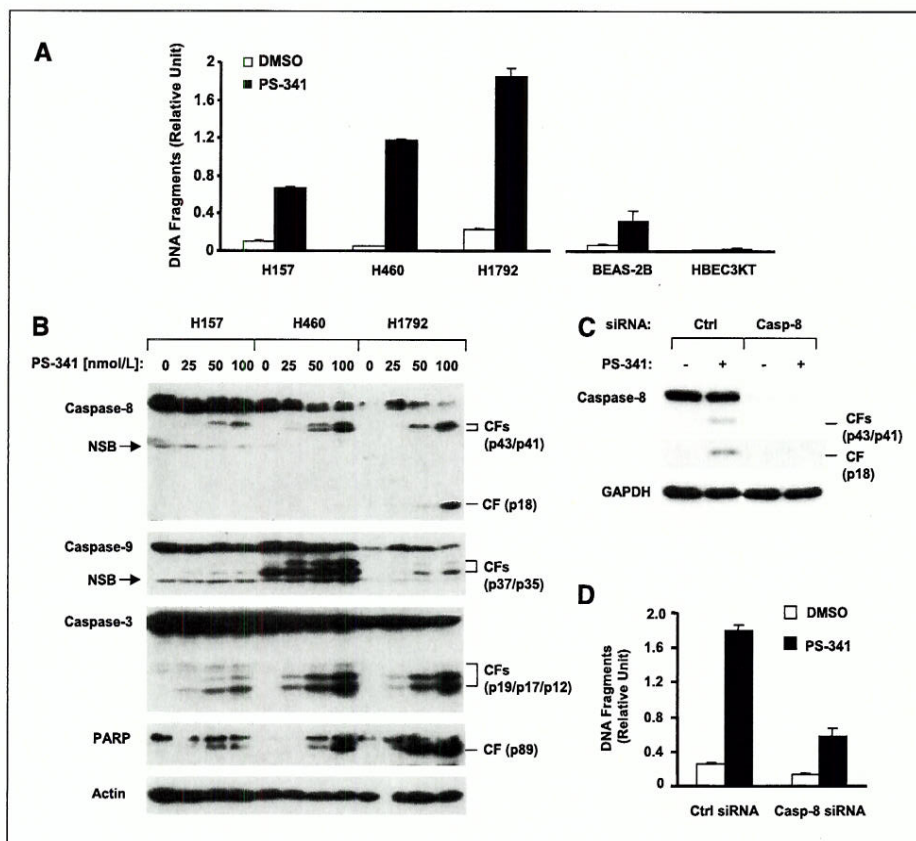
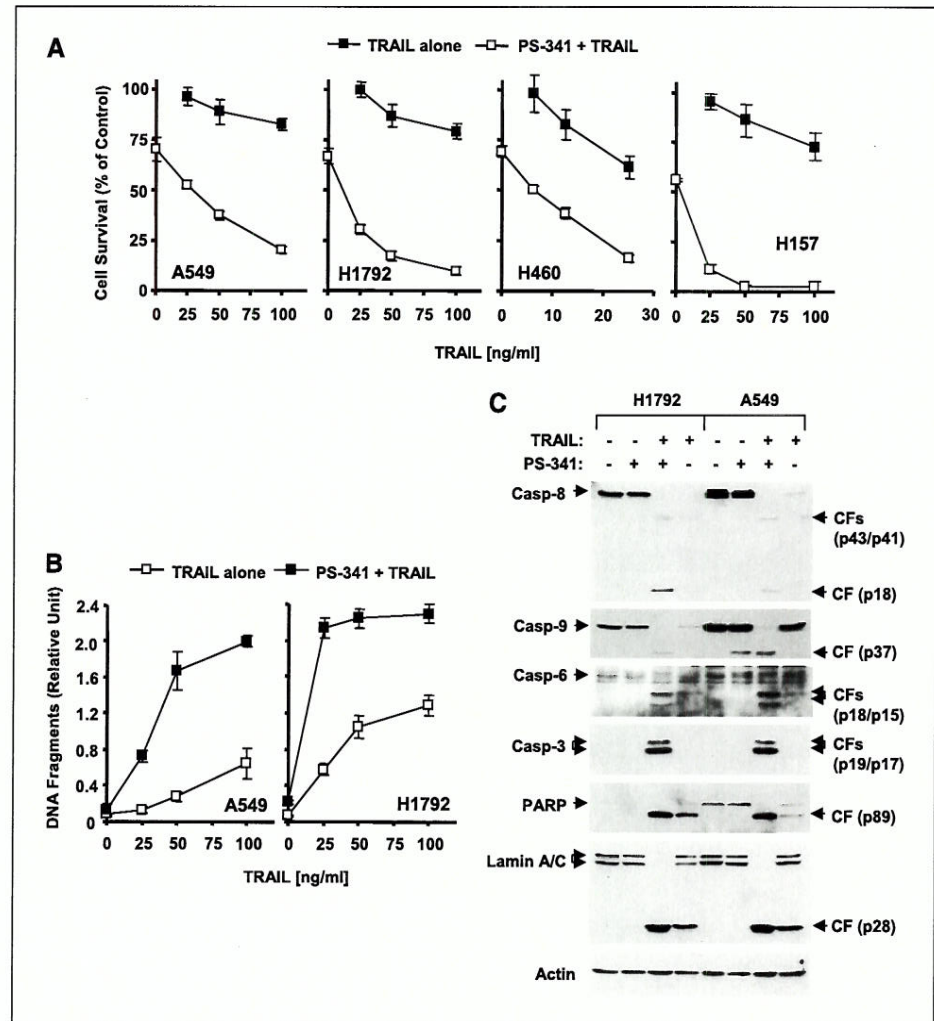


Figure 1. PS-341 induces DNA fragmentation (A), caspase activation (B), and caspase-8-dependent apoptosis (C and D). A, the indicated cell lines were treated with 50 nmol/L PS-341 for 24 h and then subjected to evaluation of DNA fragmentation. B, the indicated cell lines were treated with the given concentrations of PS-341 for 24 h and then subjected to preparation of whole-cell protein lysates and subsequent Western blot analysis. C and D, H157 cells were cultured in a 24-well plate and on the 2nd day transfected twice with control (Ctrl) or caspase-8 (*Casp-8*) siRNA with a 48-h interval between transfections. Forty hours after the second transfection, cells were treated with 50 nmol/L PS-341. The cells were either harvested for preparation of whole-cell protein lysates and subsequent Western blot analysis after an 8-h treatment (C) or subjected to estimation of DNA fragmentation using the Cell Death Detection ELISA^{plus} kit after a 24-h treatment (D). Columns, mean of triplicate determinations; bars, SD. CF, cleaved fragment. NSB, nonspecific band.

Figure 2. Combination of PS-341 and TRAIL exerts augmented effects on decreasing cell survival (A), increasing DNA fragmentation (B), and activating caspases (C). A, the indicated cell lines were treated with the given concentrations of TRAIL alone, 50 nmol/L PS-341 alone, and their respective combinations as indicated. After 24 h, cell number was estimated using the SRB assay for calculation of cell survival. Points, mean of four replicate determinations; bars, SD. B, the indicated cell lines were treated with the indicated concentrations of TRAIL alone, 50 nmol/L PS-341 alone, and their respective combinations as indicated. After 18 h, the cells were subjected to measurement of DNA fragmentation using the Cell Death Detection ELISA^{Plus} kit. Points, mean of triplicate determinations; bars, SD. C, the indicated cell lines were treated with 50 nmol/L PS-341 alone, 50 ng/mL TRAIL alone, and their combination. After 15 h, the cells were harvested for preparation of whole-cell protein lysates and subsequent Western blot analysis for detecting cleavage of caspases and their substrates.



targeting the sequence 5'-AATTCTCCGAACGTGTCACGT-3' of *c-FLIP* gene (+514 to +534) was described previously (33). Transfection of these siRNA duplexes was conducted in 24-well or 96-well plates using the HiPerFect transfection reagent (Qiagen) following the manufacturer's manual. Gene silencing effects and caspase activation were evaluated by Western blot analysis, whereas DNA fragmentation and cell survival were measured by a Cell Death Detection ELISA^{Plus} kit and the SRB assay, respectively, as described above.

Results

PS-341 induces caspase-8-dependent apoptosis. To understand the mechanism by which PS-341 induces apoptosis in human NSCLC cells, we first determined the effects of PS-341 on induction of apoptosis by measuring DNA fragmentation in several NSCLC cell lines. As shown in Fig. 1A, PS-341 increased DNA fragmentation in H157, H460, and H1792 cell lines, indicating that these cell lines undergo apoptosis on PS-341 treatment. The sensitivities to undergo apoptosis of these cell lines are H1792 > H460 > H157. We also determined the effects of PS-341 on induction of apoptosis in BEAS-2B and HBEC3KT immortalized normal human bronchial epithelial cells. Compared with NSCLC cell lines, these normal cell lines were much less sensitive to PS-341-induced apoptosis (Fig. 1A).

We next determined the effects of PS-341 on activation of different caspases in the above human NSCLC cell lines. PS-341 at the tested

concentration range (25–100 nmol/L) effectively induced cleavage of caspase-8, caspase-9, caspase-3, and PARP as indicated by appearance of the cleaved forms of these proteins in H157, H460, and H1792 cells treated with PS-341, showing that PS-341 activates these caspases (Fig. 1B). Moreover, it seemed that the degree of caspase-8 activation, but not caspase-9 activation, by PS-341 was associated with cell sensitivities to undergo cleavage of caspase-3 and PARP and DNA fragmentation (Fig. 1B), suggesting that caspase-8 activation may be important in PS-341-induced apoptosis. Thus, we further determined whether caspase-8 activation is required for PS-341-induced apoptosis. To this end, we used caspase-8 siRNA to block caspase-8 activation. As presented in Fig. 1C, the levels of uncleaved caspase-8 in caspase-8 siRNA-transfected cells were substantially decreased compared with those in cells transfected with control siRNA. Accordingly, we detected cleaved forms of caspase-8 in control siRNA-transfected cells, but not in cells transfected with caspase-8 siRNA, on PS-341 treatment, indicating a successful inhibition of caspase-8 activation induced by PS-341. Under these conditions, PS-341 efficiently increased levels of DNA fragments in control siRNA-transfected cells but only weakly in caspase-8 siRNA-transfected cells (Fig. 1D). These results indicate that caspase-8 activation is required for PS-341-induced apoptosis in human NSCLC cells.

PS-341 cooperates with TRAIL to enhance apoptosis. Sensitization of TRAIL-induced apoptosis by PS-341 has been

documented in other types of cancer cells but not in lung cancer cells. Thus, we examined the effects of PS-341 in combination with TRAIL on cell survival and apoptosis in several human NSCLC cell lines, including A549, which is relatively resistant to TRAIL-induced apoptosis (34). TRAIL at concentrations ranging from 25 to 100 ng/mL decreased cell survival by $\leq 25\%$ in A549, H1792, and H157 cells, whereas PS-341 at 50 nmol/L alone decreased cell survival by $<30\%$ in A549 and H1792 cells and by $<50\%$ in H157 cells. However, the combination of PS-341 and TRAIL achieved 50% to 80% decreases in cell survival in A549 and H1792 cells and $>90\%$ in H157 cells (Fig. 2A). Similar result was also observed in TRAIL-sensitive H460 cells (Fig. 2A).

By specifically measuring DNA fragmentation, a hallmark of apoptosis, we detected enhanced DNA fragmentation in both H1792 and A549 cell lines treated with the combination of PS-341 and TRAIL (Fig. 2B). For example, TRAIL at 50 ng/mL alone and PS-341 at 50 nmol/L alone exerted limited effects on increasing DNA fragmentation (0.280 and 0.133 arbitrary units, respectively) in A549 cells. However, their combination increased DNA fragmentation up to 1.67 arbitrary unit (Fig. 2B). Collectively, these results clearly indicate that the combination of PS-341 and TRAIL exhibits a more than additive (synergistic) effect on induction of apoptosis in human NSCLC cells. Moreover, we also examined the effects of the combination on caspase activation in these cell lines. As presented in Fig. 2C, the combination of PS-341 and TRAIL was obviously more potent than each single agent in inducing cleavage of caspase-8, caspase-9, caspase-6, and caspase-3 and their substrates PARP and lamin A/C, evidenced by increased amounts of cleaved bands in cells treated with the combination in comparison with those in cells treated with either PS-341 or TRAIL alone. These data further support that the combination of PS-341 and TRAIL enhances apoptosis in human NSCLC cells.

PS-341 up-regulates the expression of DR5, FLIP_s, and survivin. Because both caspase-8 activation and enhancement of

TRAIL-induced apoptosis involve TRAIL death receptors and c-FLIP, we next examined the effects of PS-341 on the expression of DR4, DR5, and c-FLIP in these NSCLC cell lines. By Western blot analysis, we detected increased and dose-dependent DR5 expression in the three NSCLC cell lines after exposure to PS-341. The degrees of DR5 induction in these cell lines were H1792 $>$ H460 $>$ H157 cells (Fig. 3A), which correlate with cell sensitivity to undergo apoptosis and caspase-8 activation as described above (Fig. 1A and B). PS-341 increased DR4 levels in H1792 cells but not in H157 and H460 cells (Fig. 3A). In agreement, cell surface DR5 levels were increased in the three cell lines treated with PS-341, whereas cell surface DR4 levels were substantially increased only in H1792 cells (Fig. 3B). PS-341 did not apparently alter FLIP_L levels; instead, it increased FLIP_s levels in the three cell lines, particularly in H157 and H460 cells (Fig. 3A), which were less sensitive to PS-341-induced apoptosis compared with H1792 cells (Fig. 1A). We noted that the basal levels of c-FLIP in H157 and H460 cells were much higher than in H1792 cells (Fig. 3A). These results suggest that c-FLIP up-regulation may protect cells from PS-341-induced apoptosis. Together, these results suggest that DR5 up-regulation, rather than c-FLIP modulation, plays an important role in PS-341-mediated apoptosis and enhancement of TRAIL-induced apoptosis in human NSCLC cells.

It is well known that survivin, Bcl-2, and Bcl-X_L are other important proteins involved in regulating apoptosis or enhancing TRAIL-induced apoptosis (13, 35, 36). Therefore, we also measured the levels of these proteins in cells exposed to PS-341. PS-341 did not alter the expression of either Bcl-2 or Bcl-X_L in human NSCLC cells even at concentrations up to 1 μ mol/L (see Supplementary Fig. S1). In a similar fashion to FLIP_s modulation, we found that PS-341 also increased the levels of survivin in the tested NSCLC cell lines, particularly in H460 and H1792 cells (Fig. 3A).

We also examined the effects of two other proteasome inhibitors, MG132 and epoxomicin, on the expression levels of DR5, c-FLIP, and

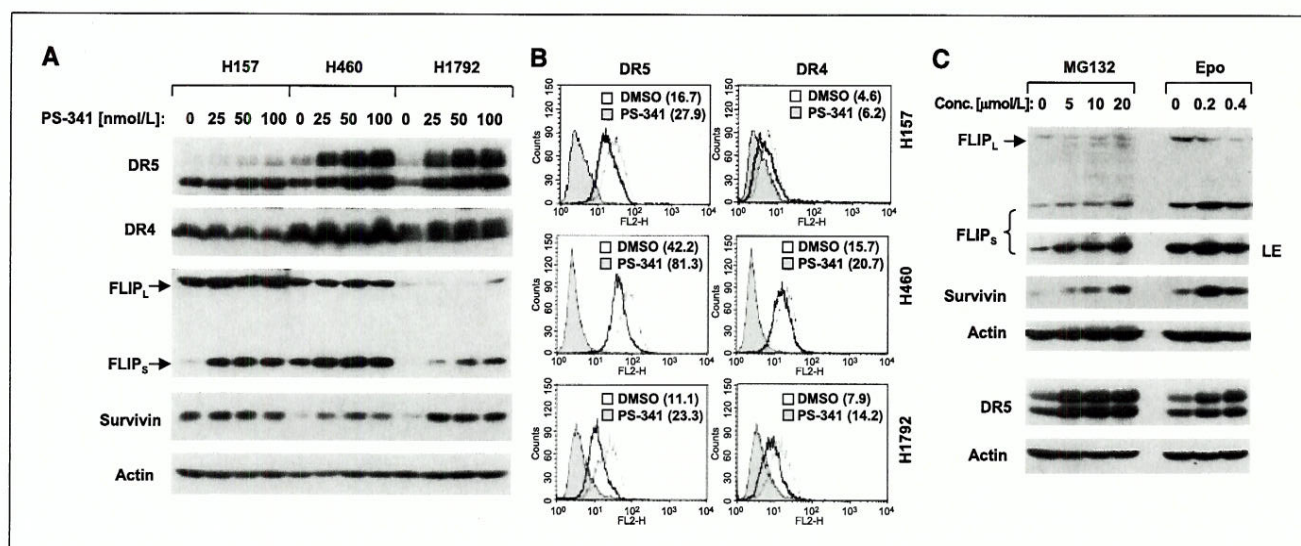
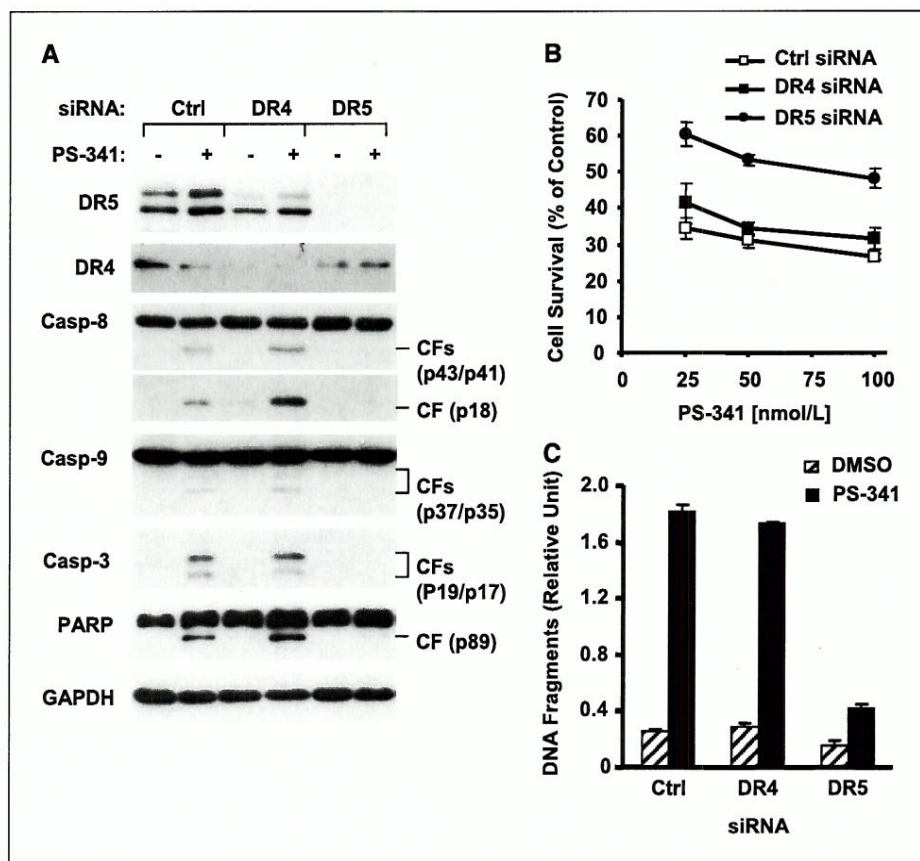


Figure 3. Effects of PS-341 as well as other proteasome inhibitors on the expression of DR5, DR4, c-FLIP, and survivin (A and C) and cell surface distributions of death receptors (B) in human NSCLC cell lines. A, the indicated cell lines were treated with the given concentrations of PS-341 for 8 h and then subjected to preparation of whole-cell protein lysates. The given proteins were detected using Western blot analysis. B, the indicated cell lines were treated with 50 nmol/L PS-341 for 12 h and then harvested for analysis of cell surface DR5 and DR4 by immunofluorescent staining and subsequent flow cytometry. Filled gray peaks, cells stained with a matched control phycoerythrin-conjugated IgG isotype antibody; open peaks, cells stained with phycoerythrin-conjugated anti-DR5 or DR4 antibody. The number in each parenthesis is the MFI. C, H460 cells were treated with the indicated concentrations of MG132 or epoxomicin (Epo) for 8 h and then subjected to preparation of whole-cell protein lysates. The given proteins were detected using Western blot analysis. LE, longer exposure.

Figure 4. Silencing of DR5 expression protects cells from PS-341-induced activation of caspases (A), decrease in cell survival (B), and increase in DNA fragmentation (C) in H157 human NSCLC cells. H157 cells were cultured in a 24-well plate and on the 2nd day transfected twice with control, DR4, or DR5 siRNA with a 48-h interval between transfections. Forty hours after the second transfection, cells were treated with 50 nmol/L PS-341 (A), the indicated concentrations of PS-341 (B), or 25 nmol/L PS-341 (C). The cells were either harvested for preparation of whole-cell protein lysates and subsequent Western blot analysis after an 8-h treatment (A) or subjected to estimation of cell number by SRB assay (B) or measurement of DNA fragmentation using the Cell Death Detection ELISA^{Plus} kit (C) after a 24-h treatment. Points and columns, mean of four replicate (B) or triplicate (C) determinations; bars, SD.



survivin. As presented in Fig. 3C, FLIP_S, but not FLIP_L, was elevated in cells treated with either MG132 or epoxomicin. Similarly, we also detected increases in survivin levels in cells exposed to either MG132 or epoxomicin. In addition, we also found that both MG132 and epoxomicin induced DR5 expression. Collectively, these results suggest that elevation of FLIP_S and survivin by PS-341 is likely to be a consequence of proteasome inhibition.

DR5 up-regulation contributes to PS-341-induced apoptosis. To determine whether DR5 up-regulation is involved in PS-341-induced apoptosis in human NSCLC cells, we used DR5 siRNA to block PS-341-induced DR5 up-regulation and then determined its effect on PS-341-induced apoptosis. As presented in Fig. 4A, transfection of DR5 siRNA into H157 cells effectively decreased the basal levels of DR5 expression and PS-341-induced DR5 up-regulation. In this experiment, we also included DR4 silencing as a control, transfection of which into H157 cells substantially reduces the basal levels of DR4 expression. These results indicate successful knockdown of either DR5 or DR4. Under these conditions, DR5 siRNA protected cells from PS-341-induced decrease in cell survival, whereas DR4 siRNA did not have such an effect (Fig. 4B). By measuring caspase activation using Western blot analysis, we found that PS-341 induced cleavage of caspase-8, caspase-9, caspase-3, and PARP in cells transfected with control or DR4 siRNA but not in DR5 siRNA-transfected cells (Fig. 4A). Accordingly, PS-341 increased DNA fragmentation in cells transfected with control or DR4 siRNA, but this effect was drastically inhibited in DR5 siRNA-transfected cells (Fig. 4C). In agreement, we observed that PS-341 also induced less amounts of cleaved forms of caspase-8, caspase-3, and PARP and DNA fragments in DR5 siRNA-transfected H460 cells than in control siRNA-trans-

fected H460 cells (see Supplementary Fig. S2). Together, these results indicate that DR5 up-regulation plays a critical role in mediating PS-341-induced apoptosis in human NSCLC cells.

DR5 up-regulation contributes to PS-341-mediated enhancement of TRAIL-induced apoptosis. Because PS-341 increases FLIP_S levels, we also determined whether PS-341 enhances TRAIL-induced apoptosis via up-regulation of DR5. The combination of PS-341 and TRAIL exhibited enhanced effects on cleavage of caspase-8, caspase-3, and PARP, as indicated by the levels of the cleaved bands by Western blotting, in control siRNA-transfected cells but not in cells transfected with DR5 siRNA (Fig. 5A). Accordingly, the combination of PS-341 and TRAIL was significantly less active in decreasing cell survival (Fig. 5B) and in increasing DNA fragmentation (Fig. 5C) in DR5 siRNA-transfected cells than in cells transfected with control siRNA. Together, these results indicate that PS-341 up-regulates DR5 expression, leading to enhancement of TRAIL-induced apoptosis.

PS-341 induces apoptosis independently of TRAIL ligand. The preceding data clearly indicate that PS-341 induces apoptosis in human NSCLC cells through a DR5-mediated mechanism, whereas others have shown that PS-341 increased TRAIL expression, which contributes to PS-341-induced apoptosis in primary chronic lymphocytic leukemia cells (37). Thus, we further determined if PS-341-induced DR5-dependent apoptosis involves the TRAIL ligand. By Western blot analysis, we observed that H157 cells expressed very low levels of TRAIL, which were not further increased by PS-341 (see Supplementary Fig. S3A). The presence of soluble recombinant DR5Fc, which neutralizes TRAIL, abolished TRAIL-induced decrease in cell survival and increase in DNA fragmentation but failed to protect cells from PS-341-induced cell death (see Supplementary

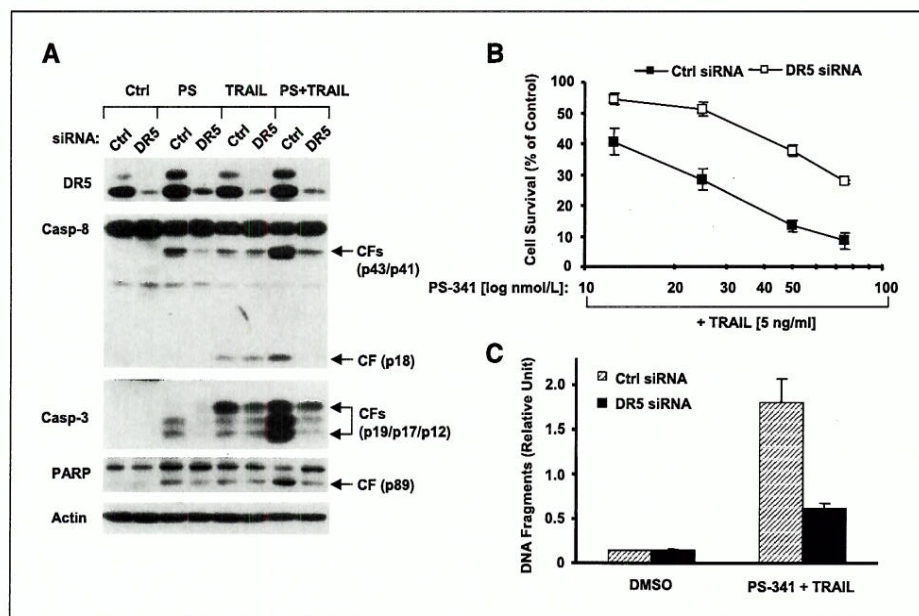


Figure 5. Silencing of DR5 expression attenuates the ability of PS-341 to cooperate with TRAIL to activate caspases (A), decrease cell survival (B), and increase DNA fragmentation (C). H157 cells were cultured in a 24-well plate and on the 2nd day transfected with control or DR5 siRNA. Twenty-four hours after the transfection, cells were reseeded in a 6-well plate (A) or 96-well plates (B and C) and treated with 50 nmol/L PS-341 (PS), 5 ng/mL TRAIL or PS-341, respectively (B), or with the solvent control DMSO or the combination of 50 nmol/L PS-341 and 10 ng/mL TRAIL (C) on the 2nd day after reseeding. After 24-h (A and B) or 12-h (C) treatment, the cells were either harvested for preparation of whole-cell protein lysates and subsequent Western blot analysis (A) or subjected to estimation of cell number by SRB assay (B) or measurement of DNA fragmentation using the Cell Death Detection ELISA^{Plus} kit (C). Points and columns, mean of triplicate (B and C) determinations; bars, SD.

Fig. S3B and C). Collectively, we conclude that PS-341 induces apoptosis in human NSCLC cells independently of TRAIL.

Blockage of FLIP_s elevation sensitizes cells to PS-341 treatment. To determine whether FLIP_s elevation by PS-341 is associated with cell resistance to PS-341, we used c-FLIP siRNA to block PS-341-induced FLIP_s elevation and then examined cell sensitivity to PS-341 treatment. As presented in Fig. 6A, transfection of c-FLIP siRNA not only decreased basal levels of c-FLIP (both FLIP_L and FLIP_S) but also more importantly abrogated PS-341-induced FLIP_s elevation. Subsequently, the cell sensitivity to PS-341 treatment in c-FLIP siRNA-transfected cells was greatly increased in comparison with cells transfected with control siRNA (Fig. 6B). In both H157 and H460 cells, PS-341 induced more apoptosis in c-FLIP siRNA-transfected cells than in control siRNA-transfected cells (Fig. 6C). For example, PS-341 induced ~15% apoptosis in control siRNA-transfected cells but 30% apoptosis in c-FLIP siRNA-transfected cells, whereas transfection of c-FLIP siRNA alone caused only ~10% apoptosis (Fig. 6C). Thus, these results have proved our speculation that FLIP_s elevation protects cells from PS-341-induced apoptosis.

Discussion

Induction of DR4 and/or DR5 and enhancement of TRAIL-induced apoptosis by PS-341 have been shown in certain types of cancer cells, including colon cancer, prostate cancer, bladder cancer, and chronic lymphocytic leukemia cells (37, 38). Moreover, a recent study has shown that the TRAIL/DR4 or DR5 apoptotic pathway mediates proteasome inhibitor (including PS-341)-induced apoptosis in primary chronic lymphocytic leukemia cells (37). In the present study, we have shown for the first time that PS-341 induces apoptosis in human NSCLC cells through a DR5-mediated mechanism because of the following findings: first, PS-341 induced the activation of caspase-8 and other caspases, whereas inhibition of caspase-8 activation diminished PS-341-induced apoptosis, indicating that PS-341 induces a caspase-8-dependent apoptosis; second, PS-341 induced DR5 expression, including cell surface DR5 and enhanced TRAIL-induced apoptosis;

and last, blockage of DR5 up-regulation by siRNA-mediated DR5 silencing abrogated PS-341-induced apoptosis and enhancement of TRAIL-induced apoptosis, indicating that DR5 up-regulation is required for PS-341-induced apoptosis and sensitization to TRAIL-induced apoptosis. In this regard, our results partially agree with the findings by Kabore et al. (37) that PS-341-induced apoptosis in primary chronic lymphocytic leukemia cells involves up-regulation of DR4 and DR5, although we failed to show the role of DR4 in PS-341-induced apoptosis in H157 human NSCLC cells. In primary chronic lymphocytic leukemia cells, TRAIL was induced and is required for PS-341-induced apoptosis because soluble DR4:Fc inhibited PS-341-induced cell death (37). However, we failed to detect TRAIL up-regulation in cells treated with PS-341 and protective effects of soluble DR5:Fc on PS-341-induced cell death in human NSCLC cells, suggesting that PS-341 induces apoptosis independently of TRAIL ligand in human NSCLC cells.

DR5 expression is regulated through p53-dependent and p53-independent mechanisms (2, 39). Although PS-341 was reported to increase p53 expression (20, 40), we found that PS-341 increased DR5 expression in NSCLC cell lines with wild-type p53 (H460) and mutant p53 (H157 and H1792). Thus, PS-341 is likely to up-regulate DR5 expression through a p53-independent mechanism. Some studies have shown that JNK regulates DR5 expression (6, 41, 42). Although PS-341 indeed induced JNK activation in our cell lines as shown previously (20, 21), we found that the JNK inhibitor SP600125 only weakly attenuated PS-341-induced DR5 induction,¹ suggesting that other mechanism(s) beyond JNK may be involved in PS-341-induced DR5 expression in human NSCLC cells. Because PS-341 induces endoplasmic reticulum stress, including up-regulation of CHOP/GADD153 (43, 44), a transcriptional factor known to regulate DR5 expression (27, 45), it remains to be determined whether PS-341 induces a CHOP-dependent up-regulation of DR5.

c-FLIP is regulated by an ubiquitin-proteasome mechanism (46, 47), and certain cancer therapeutic agents stimulate down-regulation of c-FLIP expression through this mechanism (46). PS-341, as a proteasome inhibitor, was surprisingly reported to

¹ Unpublished data.

reduce c-FLIP levels (24), although other studies showed that PS-341 did not alter c-FLIP levels (38) or increased the levels of c-FLIP in the DISC (48). In our study, we clearly showed that PS-341 increased the levels of FLIP_S without altering FLIP_L levels in all of the tested NSCLC cell lines. Moreover, we also showed that other proteasome inhibitors, including MG132 and epoxomicin, exhibited similar effects on modulation of c-FLIP expression as PS-341. Therefore, this is the first study to show that PS-341 and other proteasome inhibitors selectively increase FLIP_S levels, although the underlying mechanism is currently unclear. A recent study has shown that FLIP_S is more prone to ubiquitination and has a considerably shorter half-life in comparison with FLIP_L (47). Therefore, it would be interesting to investigate whether PS-341 increases FLIP_S levels through inhibition of the proteasome. Nevertheless, our results indicate that it is unlikely for PS-341 to enhance TRAIL-induced apoptosis through modulation of c-FLIP in human NSCLC cells.

The basal levels of c-FLIP in H157 and H460 cells, which were less sensitive to PS-341-induced apoptosis, were much higher than in H1792 cells, which were more sensitive to PS-341-induced apoptosis. Moreover, FLIP_S levels were greatly increased in H157 and H460 cells in comparison with those in H1792 cells (Fig. 3). Thus, it seems that the levels of c-FLIP, particularly FLIP_S elevation during PS-341 treatment, may provide a protective mechanism for cells to counteract PS-341-induced apoptosis. Indeed, this notion was supported by our findings that reduction of c-FLIP levels, particularly prevention of PS-341-induced FLIP_S elevation in both H157 and H460 cells, significantly sensitized cells to PS-341-induced apoptosis (Fig. 6).

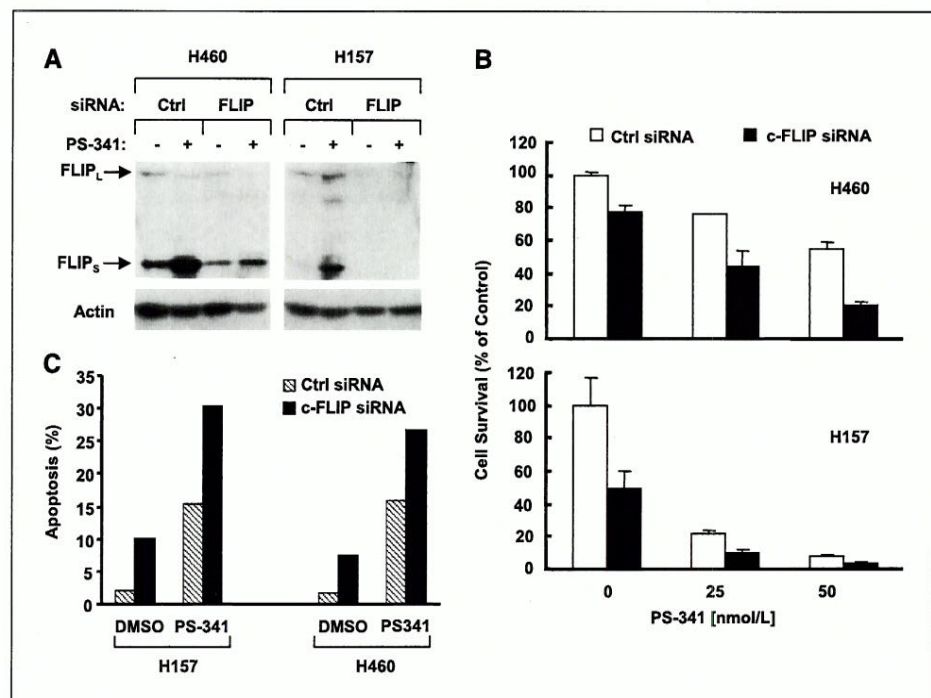
Survivin, Bcl-2, and Bcl-X_L are known to regulate apoptosis or enhance TRAIL-induced apoptosis (13, 35, 36). In our study, we found that PS-341 did not alter the expression of either Bcl-2 or Bcl-X_L in human NSCLC cells, which agree with published results in other types of cancer cells (22, 23). In a similar fashion to FLIP_S modulation, PS-341 also increased the levels of survivin in human NSCLC cells (Fig. 3A). To the best of our knowledge, this is the first study showing

that PS-341 increases survivin expression. Given the antiapoptotic property of survivin, it is likely that survivin up-regulation, like FLIP_S elevation, may counteract the apoptosis-inducing effect of PS-341. It has been shown that the ubiquitin-proteasome regulates survivin degradation (49). Given that other proteasome inhibitors (e.g., MG132 and epoxomicin) other than PS-341 also increased survivin levels (Fig. 3C), it is plausible to speculate that PS-341 may stabilize survivin through inhibition of the proteasome. Studies to evaluate this hypothesis are ongoing.

Our results clearly indicate that PS-341 treatment generates conflicting signals by activating both proapoptotic (e.g., DR5) and antiapoptotic signaling (e.g., c-FLIP and survivin). Despite up-regulation of c-FLIP and survivin, PS-341 indeed induced apoptosis and enhanced TRAIL-induced apoptosis in human NSCLC cells albeit with various degrees. Thus, it seems that PS-341-activated proapoptotic signaling, such as DR5 induction, can override activation of antiapoptotic signaling, such as up-regulation of FLIP_S and survivin caused by PS-341, leading to induction of apoptosis and enhancement of TRAIL-induced apoptosis. Given that prevention of c-FLIP elevation during PS-341 treatment sensitized cells to PS-341-induced apoptosis, it may be possible to enhance the anticancer efficacy of PS-341 via combination with other agents, which decrease c-FLIP and survivin expression.

It is known that TRAIL functions as a DR5 ligand and rapidly induces apoptosis in a wide variety of transformed cells but is not cytotoxic in normal cells *in vitro* and *in vivo* (1, 2). Therefore, TRAIL is considered to be a tumor-selective, apoptosis-inducing cytokine and a promising new candidate for cancer treatment. Unfortunately, certain cancer cell lines and tumors are resistant to TRAIL-mediated cell killing (2). In addition, agonistic anti-DR5 antibodies can also induce DR5 trimerization, which triggers the extrinsic apoptotic pathway, thus having great cancer therapeutic potential (50). In fact, the agonistic anti-DR5 antibody is already being tested in phase I clinical trials. Therefore, PS-341 may be useful in combination with TRAIL or an agonistic anti-DR5

Figure 6. Silencing of c-FLIP sensitizes NSCLC cells to PS-341 treatment. H460 and H157 cells seeded in a 96-well plate or a 24-well plate were transfected with control or c-FLIP siRNA. Twenty-four hours after the transfection, cells were treated with 50 nmol/L PS-341 (in a 24-well plate) for 24 h (A and C) or with the given concentrations of PS-341 for 48 h (B). The cells were then harvested for preparation of whole-cell protein lysates and subsequent Western blot analysis to evaluate the silencing efficiency of c-FLIP (A) or subjected to the SRB assay for estimation of cell survival (B) or sub-G₁ analysis for measurement of apoptosis (C). Columns, mean of triplicate treatments (B); bars, SD.



antibody to achieve an enhanced effect on apoptosis induction or overcome TRAIL resistance in human cancer cells.

In summary, our study has shown that PS-341 induces DR5 expression, which contributes to PS-341-induced apoptosis and enhancement of TRAIL-induced apoptosis in human NSCLC cells despite up-regulation of FLIP_s and survivin. Our findings provide novel insight into the mechanism by which PS-341 induces apoptosis and enhances TRAIL-induced apoptosis in human cancer cells.

References

- Kelley SK, Ashkenazi A. Targeting death receptors in cancer with Apo2L/TRAIL. *Curr Opin Pharmacol* 2004;4:333-9.
- Wang S, El-Deiry WS. TRAIL and apoptosis induction by TNF-family death receptors. *Oncogene* 2003;22:8628-33.
- Sun SY. Chemopreventive agent-induced modulation of death receptors. *Apoptosis* 2005;10:1203-10.
- Liu X, Yue P, Zhou Z, Khuri FR, Sun SY. Death receptor regulation and celecoxib-induced apoptosis in human lung cancer cells. *J Natl Cancer Inst* 2004;96:1769-80.
- Jin F, Liu X, Zhou Z, et al. Activation of nuclear factor- κ B contributes to induction of death receptors and apoptosis by the synthetic retinoid CD437 in DU145 human prostate cancer cells. *Cancer Res* 2005;65:6354-63.
- Zou W, Liu X, Yue P, et al. c-Jun NH2-terminal kinase-mediated up-regulation of death receptor 5 contributes to induction of apoptosis by the novel synthetic triterpenoid methyl-2-cyano-3,12-dioxooleana-1,9-dien-28-oate in human lung cancer cells. *Cancer Res* 2004;64:7570-8.
- Nagane M, Pan G, Weddle JJ, et al. Increased death receptor 5 expression by chemotherapeutic agents in human gliomas causes synergistic cytotoxicity with tumor necrosis factor-related apoptosis-inducing ligand *in vitro* and *in vivo*. *Cancer Res* 2000;60:847-53.
- Gibson SB, Oyer R, Spalding AC, Anderson SM, Johnson GL. Increased expression of death receptors 4 and 5 synergizes the apoptosis response to combined treatment with etoposide and TRAIL. *Mol Cell Biol* 2000;20:205-12.
- Kim H, Kim EH, Eom YW, et al. Sulforaphane sensitizes tumor necrosis factor-related apoptosis-inducing ligand (TRAIL)-resistant hepatoma cells to TRAIL-induced apoptosis through reactive oxygen species-mediated up-regulation of DR5. *Cancer Res* 2006;66:1740-50.
- Wajant H. Targeting the FLICE inhibitory protein (FLIP) in cancer therapy. *Mol Interv* 2003;3:124-7.
- Krueger A, Baumann S, Krammer PH, Kirchhoff S. FLICE-inhibitory proteins: regulators of death receptor-mediated apoptosis. *Mol Cell Biol* 2001;21:8247-54.
- Green DR. Apoptotic pathways: paper wraps stone blunts scissors. *Cell* 2000;102:1-4.
- Altieri DC. Validating survivin as a cancer therapeutic target. *Nat Rev Cancer* 2003;3:46-54.
- Adams J, Kauffman M. Development of the proteasome inhibitor Velcade (bortezomib). *Cancer Invest* 2004;22:304-11.
- Richardson PG, Mitsiades C, Hideshima T, Anderson KC. Bortezomib: proteasome inhibition as an effective anticancer therapy. *Annu Rev Med* 2006;57:33-47.
- Schenkein DP. Preclinical data with bortezomib in lung cancer. *Clin Lung Cancer* 2005;7 Suppl 2:S49-55.
- Voorhees PM, Orlowski RZ. The proteasome and proteasome inhibitors in cancer therapy. *Annu Rev Pharmacol Toxicol* 2006;46:189-213.
- An J, Sun Y, Fisher M, Rettig MB. Maximal apoptosis of renal cell carcinoma by the proteasome inhibitor bortezomib is nuclear factor- κ B dependent. *Mol Cancer Ther* 2004;3:727-36.
- Yin D, Zhou H, Kumagai T, et al. Proteasome inhibitor PS-341 causes cell growth arrest and apoptosis in human glioblastoma multiforme (GBM). *Oncogene* 2005;24:344-54.
- Yang Y, Ikezoe T, Saito T, et al. Proteasome inhibitor PS-341 induces growth arrest and apoptosis of non-small cell lung cancer cells via the JNK/c-Jun/AP-1 signaling. *Cancer Sci* 2004;95:176-80.
- Lauricella M, Emanuele S, D'Anneo A, et al. JNK and AP-1 mediate apoptosis induced by bortezomib in HepG2 cells via FasL/caspase-8 and mitochondria-dependent pathways. *Apoptosis* 2006;11:607-25.
- Nikrad M, Johnson T, Puthalath H, et al. The proteasome inhibitor bortezomib sensitizes cells to killing by death receptor ligand TRAIL via BH3-only proteins Bik and Bim. *Mol Cancer Ther* 2005;4:443-9.
- Zhu H, Zhang L, Dong F, et al. Bik/NBK accumulation correlates with apoptosis-induction by bortezomib (PS-341, Velcade) and other proteasome inhibitors. *Oncogene* 2005;24:4993-9.
- Sayers TJ, Brooks AD, Koh CY, et al. The proteasome inhibitor PS-341 sensitizes neoplastic cells to TRAIL-mediated apoptosis by reducing levels of c-FLIP. *Blood* 2003;102:303-10.
- He Q, Huang Y, Sheikh MS. Proteasome inhibitor MG132 upregulates death receptor 5 and cooperates with Apo2L/TRAIL to induce apoptosis in Bax-proficient and -deficient cells. *Oncogene* 2004;23:2554-8.
- Nencioni A, Wille L, Dal Bello G, et al. Cooperative cytotoxicity of proteasome inhibitors and tumor necrosis factor-related apoptosis-inducing ligand in chemoresistant Bcl-2-overexpressing cells. *Clin Cancer Res* 2005;11:4259-65.
- Yoshida T, Shiraishi T, Nakata S, et al. Proteasome inhibitor MG132 induces death receptor 5 through CCAAT/enhancer-binding protein homologous protein. *Cancer Res* 2005;65:5662-7.
- Sun SY, Kurie JM, Yue P, et al. Differential responses of normal, premalignant, and malignant human bronchial epithelial cells to receptor-selective retinoids. *Clin Cancer Res* 1999;5:431-7.
- Ramirez RD, Sheridan S, Girard L, et al. Immortalization of human bronchial epithelial cells in the absence of viral oncoproteins. *Cancer Res* 2004;64:9027-34.
- Sun SY, Yue P, Dawson MI, et al. Differential effects of synthetic nuclear retinoid receptor-selective retinoids on the growth of human non-small cell lung carcinoma cells. *Cancer Res* 1997;57:4931-9.
- Sun SY, Zhou Z, Wang R, Fu H, Khuri FR. The farnesyltransferase inhibitor Lonafarnib induces growth arrest or apoptosis of human lung cancer cells without downregulation of Akt. *Cancer Biol Ther* 2004;3:1092-8; discussion 9-101.
- Sun SY, Yue P, Hong WK, Lotan R. Induction of Fas expression and augmentation of Fas/Fas ligand-mediated apoptosis by the synthetic retinoid CD437 in human lung cancer cells. *Cancer Res* 2000;60:6537-43.
- Longley DB, Wilson TR, McEwan M, et al. c-FLIP inhibits chemotherapy-induced colorectal cancer cell death. *Oncogene* 2006;25:838-48.
- Sun SY, Yue P, Zhou JY, et al. Overexpression of BCL2 blocks TNF-related apoptosis-inducing ligand (TRAIL)-induced apoptosis in human lung cancer cells. *Biochem Biophys Res Commun* 2001;280:788-97.
- Harada H, Grant S. Apoptosis regulators. *Rev Clin Exp Hematol* 2003;7:117-38.
- Chawla-Sarkar M, Bae SI, Reu FJ, et al. Down-regulation of Bcl-2, FLIP, or IAPs (XIAP and survivin) by siRNAs sensitizes resistant melanoma cells to Apo2L/TRAIL-induced apoptosis. *Cell Death Differ* 2004;11:915-23.
- Kabore AF, Sun J, Hu X, et al. The TRAIL apoptotic pathway mediates proteasome inhibitor induced apoptosis in primary chronic lymphocytic leukemia cells. *Apoptosis* 2006;11:1175-93.
- Johnson TR, Stone K, Nikrad M, et al. The proteasome inhibitor PS-341 overcomes TRAIL resistance in Bax and caspase 9-negative or Bcl-xL over-expressing cells. *Oncogene* 2003;22:4953-63.
- Sheikh MS, Fornace AJ, Jr. Death and decoy receptors and p53-mediated apoptosis. *Leukemia* 2000;14:1509-13.
- Ling YH, Liebes L, Jiang JD, et al. Mechanisms of proteasome inhibitor PS-341-induced G(2)-M-phase arrest and apoptosis in human non-small cell lung cancer cell lines. *Clin Cancer Res* 2003;9:1145-54.
- Higuchi H, Grambihler A, Canbay A, Bronk SF, Gores GJ. Bile acids up-regulate death receptor 5/TRAIL-receptor 2 expression via a c-Jun N-terminal kinase-dependent pathway involving Sp1. *J Biol Chem* 2004;279:51-60.
- Chen D, Chan R, Waxman S, Jing Y. Buthionine sulfoximine enhancement of arsenic trioxide-induced apoptosis in leukemia and lymphoma cells is mediated via activation of c-Jun NH2-terminal kinase and up-regulation of death receptors. *Cancer Res* 2006;66:11416-23.
- Nawrocki ST, Carew JS, Pino MS, et al. Bortezomib sensitizes pancreatic cancer cells to endoplasmic reticulum stress-mediated apoptosis. *Cancer Res* 2005;65:11658-66.
- Fribley A, Zeng Q, Wang CY. Proteasome inhibitor PS-341 induces apoptosis through induction of endoplasmic reticulum stress-reactive oxygen species in head and neck squamous cell carcinoma cells. *Mol Cell Biol* 2004;24:9695-704.
- Yamaguchi H, Wang HG. CHOP is involved in endoplasmic reticulum stress-induced apoptosis by enhancing DR5 expression in human carcinoma cells. *J Biol Chem* 2004;279:45495-502.
- Kim Y, Suh N, Sporn M, Reed JC. An inducible pathway for degradation of FLIP protein sensitizes tumor cells to TRAIL-induced apoptosis. *J Biol Chem* 2002;277:22320-9.
- Poukkula M, Kaunisto A, Hietakangas V, et al. Rapid turnover of c-FLIPshort is determined by its unique C-terminal tail. *J Biol Chem* 2005;280:27345-55.
- Ganten TM, Koschny R, Haas TL, et al. Proteasome inhibition sensitizes hepatocellular carcinoma cells, but not human hepatocytes, to TRAIL. *Hepatology* 2005;42:588-97.
- Zhao J, Tenev T, Martins LM, Downward J, Lemoine NR. The ubiquitin-proteasome pathway regulates survivin degradation in a cell cycle-dependent manner. *J Cell Sci* 2000;113 Pt 23:4363-71.
- Ichikawa K, Liu W, Zhao L, et al. Tumorcidal activity of a novel anti-human DR5 monoclonal antibody without hepatocyte cytotoxicity. *Nat Med* 2001;7:954-60.

Acknowledgments

Received 11/20/2006; revised 2/5/2007; accepted 3/14/2007.

Grant support: The Georgia Cancer Coalition Distinguished Cancer Scholar award (S-Y. Sun) and Department of Defense VITAL grant W81XWH-04-1-0142 (S-Y. Sun for Project 4).

The costs of publication of this article were defrayed in part by the payment of page charges. This article must therefore be hereby marked *advertisement* in accordance with 18 U.S.C. Section 1734 solely to indicate this fact.

We thank Dr. R. Lotan and J.D. Minna for providing immortalized normal bronchial epithelial cell lines.

Implication of the Insulin-like Growth Factor-IR Pathway in the Resistance of Non-small Cell Lung Cancer Cells to Treatment with Gefitinib

Floriana Morgillo,¹ Woo-Young Kim,¹ Edward S. Kim,¹ Fortunato Ciardiello,³ Waun Ki Hong,¹ and Ho-Young Lee^{1,2}

Abstract **Purpose:** Epidermal growth factor receptor (EGFR) tyrosine kinase inhibitors have been found to be effective against lung cancer *in vitro*, but clinical resistance to these agents has developed as their usage has increased. In this study, we determined whether the insulin-like growth factor I (IGF-I) signaling pathway induces resistance of non-small cell lung cancer (NSCLC) cells to the EGFR tyrosine kinase inhibitor gefitinib.

Experimental Design: The effects of gefitinib and cetuximab on NSCLC cells, alone or with an IGF-I receptor (IGF-IR) inhibitor, were assessed using the 3-(4,5-dimethylthiazol-2-yl)-2,5-diphenyltetrazolium bromide assay, the flow cytometry-based terminal nucleotidyl transferase-mediated nick end labeling assay, coimmunoprecipitation, and Western blot analysis. EGFR and IGF-IR expression in NSCLC tissues were examined by Western blot analysis.

Results: Gefitinib inhibited NSCLC cell proliferation by inducing apoptosis when IGF-IR signaling was suppressed. Treatment with gefitinib, but not cetuximab, induced EGFR:IGF-IR heterodimerization and activation of IGF-IR and its downstream signaling mediators, resulting in increased survivin expression in NSCLC cell lines with high levels of IGF-IR expression. Inhibition of IGF-IR activation and knockdown of survivin expression led to increased apoptosis. In contrast, overexpression of survivin protected cells with low IGF-IR expression from gefitinib-induced apoptosis. Most NSCLC tissues with EGFR overexpression had associated high levels of IGF-IR expression.

Conclusions: IGF-IR expression may be useful as a predictive marker for gefitinib treatment of NSCLC. Suppression of IGF-IR signaling pathways may prevent or delay development of gefitinib resistance in patients with NSCLC.

Lung cancer is the leading cause of cancer-related death in both sexes in the United States and throughout the world, and its overall mortality rate has not changed substantially in decades (1). Advances in the understanding of lung tumor biology and oncogenesis have provided several molecular targets for the treatment of non-small cell lung cancer (NSCLC). Of these,

inhibitors of epidermal growth factor receptor (EGFR) tyrosine kinase pathways are the most extensively studied.

EGFR is overexpressed in several solid tumor types, including NSCLC (it has been found in 40-80% of cases; ref. 2). The EGFR signaling pathway activates the phosphoinositide-3-kinase/Akt and mitogen-activated protein kinase (MAPK) pathways, which mediate proliferation, differentiation, and survival in both normal and malignant epithelial cells (3, 4). Activated EGFR also promotes angiogenesis, tumor cell motility, and invasion by regulating the expression and activity of matrix metalloproteinases and by interacting with components of the integrin pathway (5). These findings indicate that EGFR-targeted agents would be effective against cancer.

Small-molecular-weight EGFR tyrosine kinase inhibitors (TKI) and anti-EGFR monoclonal antibodies have been in advanced clinical development (6, 7). Monoclonal antibodies bind to the extracellular domain of EGFR. The EGFR-antibody complex is subsequently internalized, causing decreases in EGFR expression and heterodimerization in a phosphorylation status-independent manner. Treatment with cetuximab, a chimeric human-mouse anti-EGFR monoclonal immunoglobulin G₁ (IgG₁) antibody, has been found to block cell cycle progression by inducing G₁ arrest and to inhibit human cancer xenograft growth in nude mice *in vivo* (8) by inhibiting tumor-induced angiogenesis (9). Treatment with cetuximab has shown therapeutic activities in patients with head and neck

Authors' Affiliations: ¹Department of Thoracic/Head and Neck Medical Oncology, M. D. Anderson Cancer Center, and ²Graduate School of Biomedical Sciences at Houston, The University of Texas, Houston, Texas and ³Dipartimento Medico-Chirurgico di Internistica Clinica e Sperimentale F. Magrassi e A. Lanzara, Seconda Università degli Studi di Napoli, Naples, Italy
Received 8/18/06; revised 1/25/07; accepted 2/9/07.

Grant support: NIH grants R01 CA100816 and CA109520 (H.-Y. Lee), American Cancer Society grant RSG-04-082-01-TBE 01 (H.-Y. Lee), and partly by Department of Defense grants W81XWH-06-1-0303-BATTLE and W81XWH-04-1-0142-01-VITAL (W.K. Hong). W.K. Hong is an American Cancer Society Clinical Research Professor.

The costs of publication of this article were defrayed in part by the payment of page charges. This article must therefore be hereby marked *advertisement* in accordance with 18 U.S.C. Section 1734 solely to indicate this fact.

Requests for reprints: Ho-Young Lee, Department of Thoracic/Head and Neck Medical Oncology, Unit 432, The University of Texas M. D. Anderson Cancer Center, 1515 Holcombe Boulevard, Houston, TX 77030. Phone: 713-792-6363; Fax: 713-792-0430; E-mail: hlee@mdanderson.org.

© 2007 American Association for Cancer Research.

doi:10.1158/1078-0432.CCR-06-2077

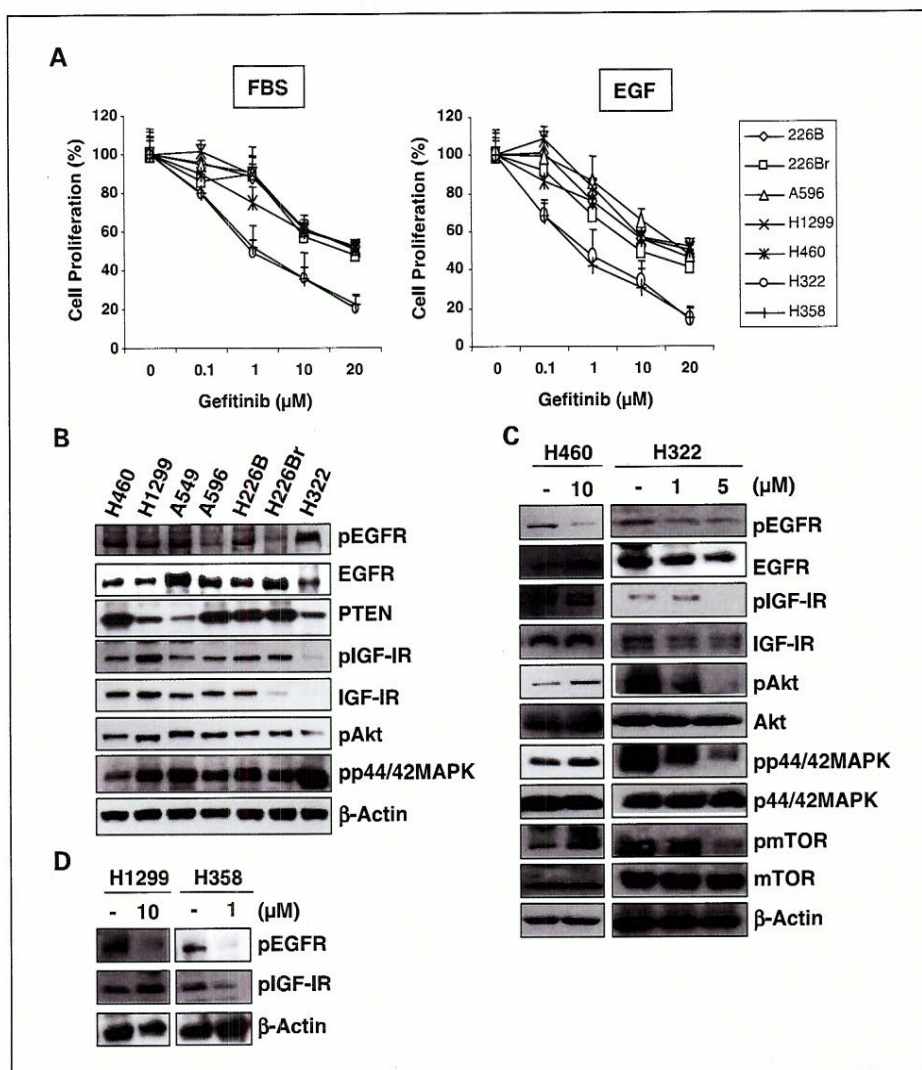


Fig. 1. Stimulation of IGF-IR signaling pathway in gefitinib-resistant NSCLC cell lines. **A**, results of the MTT assay of H460, H1299, A596, H226B, H226Br, H322, and H358 cell lines treated with the indicated concentrations of gefitinib in RPMI 1640 containing 10% FBS or EGF for 3 d. Independent experiments were repeated at least thrice each, and one representative result is shown. Points, mean value of eight identical wells of a single representative experiment; bars, upper 95% CIs. **, $P < 0.01$ and ***, $P < 0.001$ for comparisons between gefitinib-treated and control cells. **B**, basal expression of EGFR, IGF-IR, p44/42 MAPK, Akt, and their phosphorylated forms and PTEN in seven NSCLC cell lines. **C** and **D**, immunoblotting of EGFR, IGF-IR, and their downstream signaling components in H460, H322 (**C**), H1299, and H358 (**D**) cells treated with the indicated concentrations of gefitinib. **B** and **C**, Western blotting on β -actin was included as a loading control.

cancer or colorectal cancer (10, 11). Unlike monoclonal antibodies, TKIs do not affect internalization of the EGF receptor and are often not EGFR specific; thus, they affect the kinase activity of other ErbB family receptors. EGFR TKIs block the ATP pocket of EGFR, thereby inhibiting EGFR phosphorylation and downstream signal transduction (12).

Preclinical studies have shown that the EGFR TKI gefitinib, when used in combination with standard chemotherapeutic agents or radiotherapy, inhibits EGFR activation, causing G_1 arrest and additive-to-synergistic growth inhibition (6). However, negative results from clinical trials (13, 14) have diminished the enthusiasm for gefitinib and indicate that a better understanding is needed of the mechanisms of acquired resistance to this drug. The effectiveness of gefitinib is currently being studied in a population of patients who may have a biomarker that sensitizes their tumors to gefitinib. However, mechanistic studies of gefitinib resistance have not been completed.

Because recent studies have suggested that the insulin-like growth factor I receptor (IGF-IR) pathway is involved in NSCLC cells' resistance to EGFR-targeting agents (15, 16), we studied whether the IGF-IR-mediated signaling pathway influences the NSCLC response to gefitinib and cetuximab. We also sought to

determine the proteins mediating survival of NSCLC cells against gefitinib treatment. In the present studies, we show that treatment with gefitinib but not cetuximab stimulates the IGF-IR pathway and its downstream signaling mediators via the EGFR:IGF-IR heterodimer and induces survivin expression that protects NSCLC cells from apoptosis.

Materials and Methods

Cells and reagents. The human NSCLC cell lines H596, H226B, H226Br, H460, H1299, H358, and H322 were purchased from the American Type Culture Collection and maintained in RPMI 1640 supplemented with 10% fetal bovine serum (FBS; Life Technologies-BRL) in a humidified atmosphere with 5% CO_2 . EGF was purchased from R&D Systems. Gefitinib (AstraZeneca) was prepared as a 10 mmol/L stock solution in DMSO. Cetuximab was obtained from ImClone Systems and prepared as a 20 mmol/L stock solution. AG1024, an IGF-IR TKI, was purchased from Calbiochem-Novabiochem. Adenoviruses, with and without survivin (Ad-survivin and Ad-EV, respectively), were amplified as described previously (17).

Cell proliferation assay. To determine the effects of gefitinib and AG1024 on NSCLC cell proliferation, we plated 3×10^3 cells per well of the indicated NSCLC cell lines in 96-well plates. The next day, cells were

treated with either 0.1% DMSO as a diluent control or with different concentrations of drugs (0.1–10.0 $\mu\text{mol/L}$ in a final DMSO concentration of 0.1%) in RPMI with 10% FBS or EGF (50 ng/mL). Cell medium was replaced with fresh medium containing gefitinib, AG1024, or both everyday for 3 days. At the end of the treatment period, cell proliferation was measured using the 3-(4,5-dimethylthiazol-2-yl)-2,5-diphenyltetrazolium bromide (MTT) assay. The drug concentrations required to inhibit cell growth by 50% were determined by interpolation from the dose-response curves. Eight replicate wells were used for each analysis, and at least three independent experiments were done. The data from replicate wells are presented as the mean numbers of cells remaining, with 95% confidence intervals (CI). To determine the effect of the combined drug treatments, any potentiation was estimated by multiplying the percentage of cells remaining (% growth) for each agent. The classification index was calculated as described previously (18). Supra-additivity was defined as $\% AB / (\% A \times \% B) > 1.0$; additivity was defined as $\% AB / (\% A \times \% B) = 0.9$ –1.0; and subadditivity was defined as $\% AB / (\% A \times \% B) < 0.9$. (In these equations, A and B are the effects of individual agents, and AB is the effect of the combination of the two drugs.)

Cell cycle and apoptosis assays. For cell cycle and apoptosis assays, 2×10^5 NSCLC cells per well were plated in six-well plates. The next day, the cells were treated with various concentrations of gefitinib (5 $\mu\text{mol/L}$), AG1024 (5 $\mu\text{mol/L}$), or both. Both adherent and nonadherent cells were harvested, pooled, and fixed with 1% paraformaldehyde and 70% ethanol. To determine the percentages of cells in the phases of the cell cycle (G_1 , S, and G_2 -M), we stained cells with 50 $\mu\text{g/mL}$ propidium iodide and analyzed them with a flow cytometer (Epics Profile II; Beckman Coulter Inc.) equipped with a 488-nm argon laser. Apoptosis was assessed using a modified flow cytometry-based terminal nucleotidyl transferase-mediated nick end

labeling (TUNEL) assay with an APO-bromodeoxyuridine staining kit (Phoenix Flow Systems) as described previously (19). Data from at least three experiments are presented as means with 95% CIs.

Immunoblotting and coimmunoprecipitation. NSCLC cells were either left uninfected or infected with Ad-EV or Ad-survivin (50 infection-forming units) and then left untreated or treated with gefitinib (1–10 $\mu\text{mol/L}$), AG1024 (5 $\mu\text{mol/L}$), and cetuximab (1–10 $\mu\text{mol/L}$), alone or in combination, in growth medium that was changed daily. For growth factor stimulation, cells were cultured in serum-free medium for 1 day and then incubated with EGF (50 ng/mL). For small interfering RNA (siRNA) transfection, H460 cells in the logarithmic growth phase in six-well plates (5×10^5 cells per well) were transfected with 10 μL of 20 $\mu\text{mol/L}$ survivin siRNA or control scrambled siRNA (Dharmacon) using LipofectAMINE 2000 (Invitrogen) according to the manufacturer's protocol. Cells were incubated for 24 h in growth medium, and gefitinib was added. Cells were harvested after 3 days of incubation.

We did a biochemical analysis of 14 lung tumor and 14 healthy adjacent tissue specimens from patients with NSCLC who had been treated at The University of Texas M.D. Anderson Cancer Center. This study was approved by the M.D. Anderson Cancer Center Institutional Review Board. All tissue specimens were frozen in liquid nitrogen immediately after being resected and rinsed in PBS; they were kept in a -80°C freezer until retrieved for the study. Total protein isolation and Western blot analyses were done as described previously (20).

Immunoprecipitation was done using 3 mg of protein from the total cell lysates and 3 μg of mouse monoclonal anti-EGFR antibody (Santa Cruz Biotechnology), mouse monoclonal anti-IGF-IR antibody ($\alpha\text{IR-3}$; Oncogene Science), or healthy preimmune serum anti-mouse antibody (sc-2025) as the negative control, followed by incubation overnight at 4°C . The immunoprecipitates were resolved by 6% SDS-PAGE and then

Fig. 2. Effects of combined blockade of EGFR and IGF-IR pathways on NSCLC cells. **A**, effects of treatment with 5 $\mu\text{mol/L}$ gefitinib, 5 $\mu\text{mol/L}$ AG1024, or both on the expression of pEGFR and pIGF-IR were determined in H460 cells by Western blot analysis. β -Actin was used as a loading control. **B**, effect of targeting EGFR and IGF-IR on cell proliferation. H460 cells were treated with the indicated concentrations of gefitinib, AG1024, or both in RPMI 1640 containing 10% FBS for 3 d. The results of the MTT assay are shown. Columns, mean value of eight (MTT) identical wells in a single representative experiment; $n = 3$. Bars, upper 95% CIs. ***, $P < 0.001$ for comparisons between cells treated with a single drug or both drugs. **C**, effects of treatment with the indicated concentrations of gefitinib, AG1024, or both on the cell cycle distribution of H460 cells. DNA content was evaluated by propidium iodide uptake, and the percentages of cells in specific phases of the cell cycle were determined using flow cytometry. Columns, mean value of three identical experiments. **, $P < 0.01$; ***, $P < 0.001$. **D**, apoptosis in H460 cells assessed using a modified TUNEL assay. Two independent experiments were done; the data shown are from a single representative experiment.

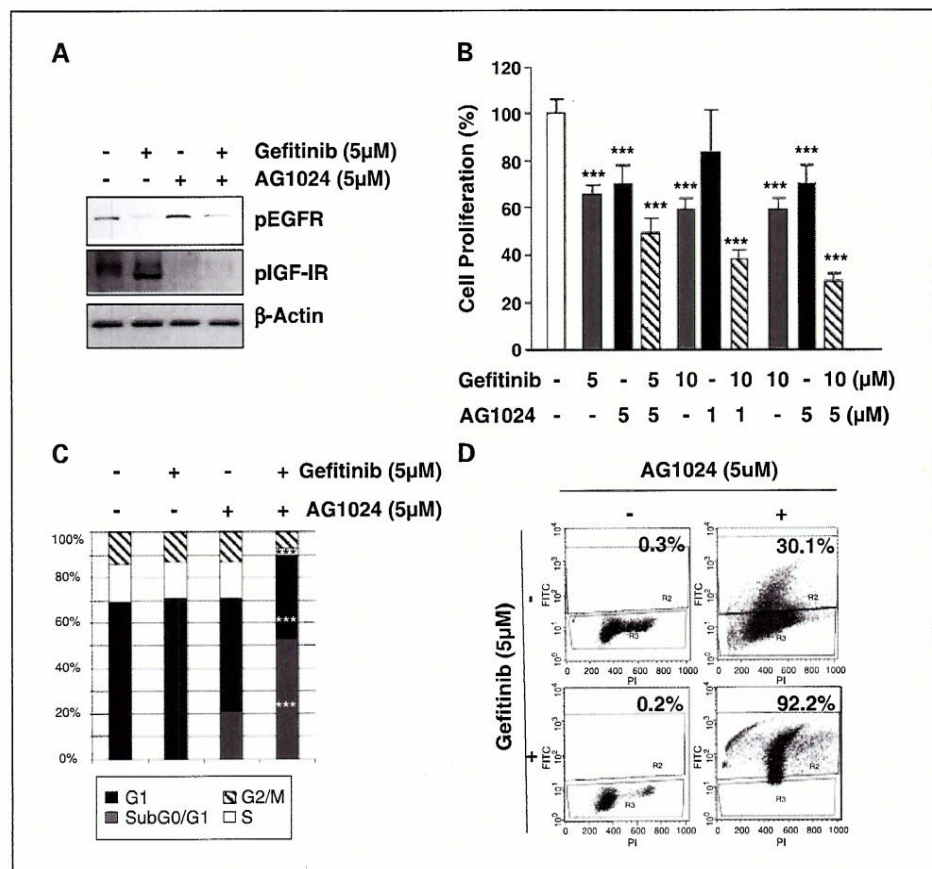


Table 1. Synergistic indices of combination treatment with gefitinib and AG1024

Treatment A				Treatment B				Combination treatment			Index*
Drug	Concentration (μmol/L)	MGI	P value [†]	Drug	Concentration (μmol/L)	MGI	P value [†]	Expected [‡]	Observed [§]	P value [†]	
Gefitinib	1	0.85	5.3E-05	AG1024	1	0.87	0.0299	0.73	0.69	0.000124	1.05
					5	0.70	7.5E-07	0.59	0.57	1.3E-09	1.03
	5	0.65	1.9E-09		1	0.87	0.0299	0.56	0.50	8.3E-08	1.12
					5	0.70	7.5E-07	0.45	0.44	1.9E-10	1.022
	10	0.59	4.3E-10		1	0.87	0.0299	0.51	0.32	1.2E-12	1.59
					5	0.70	7.5E-07	0.41	0.28	9.9E-14	1.46

NOTE: H460 cell proliferation treated with indicated concentrations of gefitinib, AG1024, or their combinations was calculated by the MTT assay. Abbreviation: MGI, mean growth inhibition rate = growth rate of treated group/growth rate of untreated group.

*Calculated by dividing the expected growth inhibition rate by the observed growth inhibition rate. An index more than 1 indicates synergistic effect and <1 indicates less than additive effect.

[†]P value (two-sided) was calculated by *t* test compared with no treatment.

[‡]Growth inhibition rate of treatment A \times growth inhibition rate of treatment B.

[§]Growth inhibition rate of combined treatment on treatments A and B.

analyzed by Western blot using rabbit polyclonal antibodies against human phosphorylated EGFR (pEGFR; Tyr¹⁰⁶⁸), EGFR, and phosphorylated IGF-IR (pIGF-IR and Tyr¹¹³¹/Tyr¹¹⁴⁶; 1:1,000; Cell Signaling Technology); rabbit polyclonal antibodies against human IGF-IR (1:500; Santa Cruz Biotechnology); rabbit polyclonal antibodies against human phosphorylated Akt (pAkt; Ser⁴⁷³; 1:1,000), and Akt (1:1,000) and a mouse monoclonal antibody against human anti-phosphorylated p44/42 MAPK (pp44/42MAPK and Thr²⁰²/Tyr²⁰⁴; 1:500; Cell Signaling Technology); goat polyclonal antibodies against p44/42 MAPK (1:1,000; Cell Signaling Technology); and a rabbit polyclonal anti-poly(ADP-ribose) polymerase antibody (1:1,000; VIC 5; Roche Molecular Biochemicals). Other products used in the Western blot analysis included rabbit polyclonal caspase-3 (1:1,000), rabbit polyclonal antibodies against X inhibitor of apoptosis protein (XIAP; 1:1,000; Cell Signaling Technology), rabbit polyclonal antibodies against mammalian target of rapamycin (mTOR; 1:1,000; Cell Signaling Technology), pmTOR (1:1,000; Cell Signaling Technology), mouse monoclonal survivin (1:1,000; Santa Cruz Biotechnology), goat polyclonal antibody against β -actin (1:4,000; Santa Cruz Biotechnology), and rabbit anti-mouse IgG-horseradish peroxidase conjugate (1:2,000; DakoCytomation).

Statistical analysis. The MTT assay data were analyzed using the Student's *t* test. Eight replicate wells were used for each analysis, and data from replicate wells are presented as mean values with 95% CIs. At least three independent experiments were done to obtain each result, and cell survival among groups was compared using ANOVA for a 2×2 factorial design. The mean values from three experiments with the eight replicates and 95% CIs were calculated using the SAS software (version 8.02; SAS Institute). In all statistical analyses, two-sided *P* values of <0.05 were considered statistically significant.

Results

Stimulation of the IGF-IR signaling pathway in gefitinib-resistant NSCLC cell lines. We determined the effects of gefitinib on cell proliferation in H596, H226B, H226Br, H460, H1299, H358, and H322 cell lines. We treated cells with gefitinib in the presence of 10% FBS or 50 ng/mL EGF. The MTT assay revealed that gefitinib decreased NSCLC cell proliferation in a dose-dependent manner (Fig. 1A). H322 and H358 cells were more sensitive to gefitinib than were the other cell lines [H322 in 10% FBS, 47.5% (95% CI, 41.5-53.5%; *P* < 0.001); H322 in EGF, 46.8% (95% CI, 40.8-52.8%; *P* < 0.01); H358 in 10% FBS, 52.1% (95% CI, 50.0-54.2%; *P* < 0.001); and H358 in EGF, 41.6% (95% CI, 37.3-45.9%; *P* < 0.01) after 72 h]. The gefitinib concentrations required to inhibit H596, H226B, H226Br, H460, and H1299 cell growth by 50.0% were 10 to 20 times higher than were those for H322 and H358 cells.

We next determined the mechanisms responsible for the sensitivity of NSCLC cells to gefitinib. We first measured the basal levels of EGFR and pEGFR in the cell lines. As shown in Fig. 1B, all cell lines except H322 had high levels of EGFR expression. Four of these six cell lines also had high levels of pEGFR expression, indicating that no relationship exists between gefitinib response and EGFR activation. Because of the role of phosphatase and tensin homologue (PTEN) in NSCLC cells' resistance to EGFR TKIs (21), we next determined

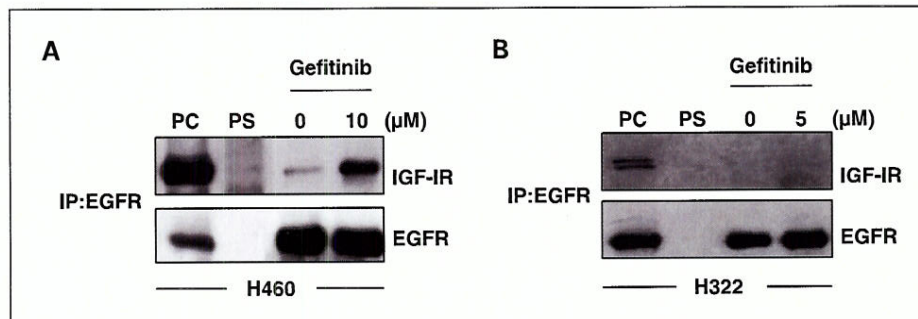
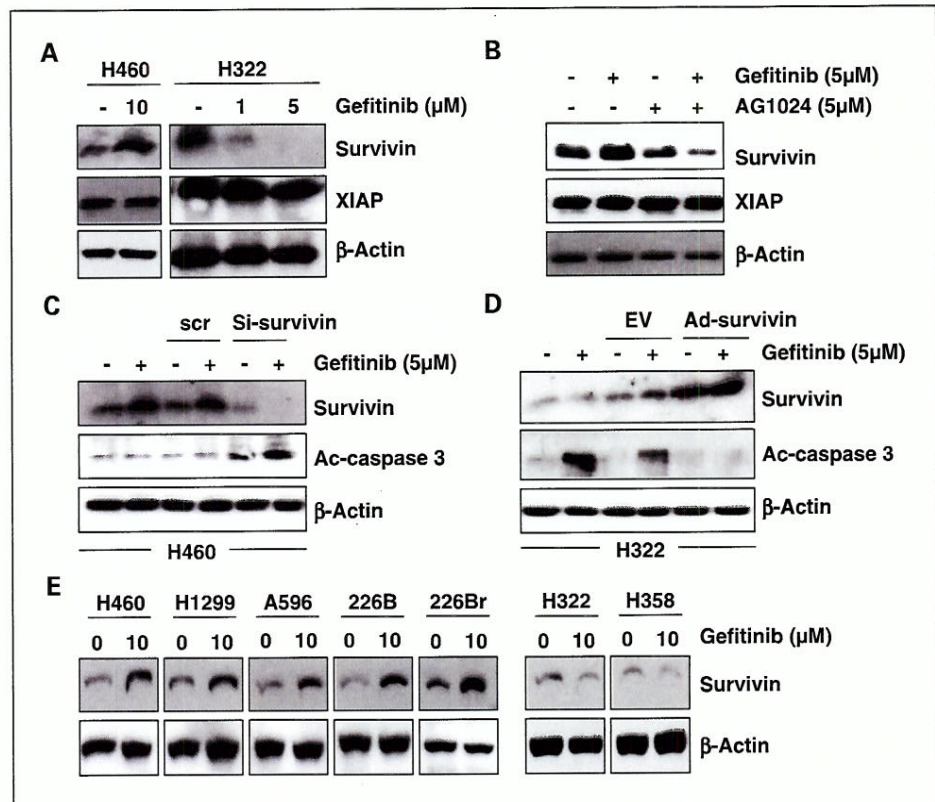


Fig. 3. Effect of gefitinib on EGFR:IGF-IR heterodimerization and activation of IGF-IR signaling pathway. Whole-cell extracts (3 mg) from (A) H460 and (B) H322 cells, left untreated or treated with gefitinib (10 and 5 $\mu\text{mol/L}$, respectively) for 3 d, were immunoprecipitated (IP) with anti-EGFR antibodies. The immunoprecipitates were subjected to Western blot analysis with the indicated antibodies. Input (PC) represents cell lysates (30 μg) that were not subjected to immunoprecipitation. Control immunoprecipitation was done using mouse preimmune serum.

Fig. 4. Role of survivin in the resistance of NSCLC cells to gefitinib. **A**, immunoblotting of survivin and XIAP in H460 and H322 cells treated with the indicated concentrations of gefitinib. **B**, effects of treatment with 5 $\mu\text{mol/L}$ gefitinib, 5 $\mu\text{mol/L}$ AG1024, or both on the expression of survivin and XIAP in H460 cells. **C** and **D**, effect of knockdown of expression or overexpression of survivin on H460 and H322 cells treated with gefitinib. H460 cells were transfected with scrambled (*scr*) or survivin siRNA and left untreated or treated with gefitinib for 48 h. H322 cells were infected with a control virus (Ad-EV or Ad-survivin) and incubated for 3 d in the presence of gefitinib. The protein extracts were subjected to Western blotting for evaluation of survivin and active caspase-3. **E**, Western blot analysis of survivin expression in NSCLC cell lines treated with 10 $\mu\text{mol/L}$ gefitinib. β -Actin was used as a loading control.



the level of PTEN protein expression. PTEN was expressed in all cell lines, suggesting that gefitinib resistance is not caused by a PTEN deficiency. We then determined the expression of IGF-IR, pIGF-IR, Akt, and pAkt and found that most cell lines had high levels of IGF-IR expression, which were associated with high levels of pIGF-IR expression. The levels of pIGF-IR, IGF-IR, and pAkt expression were higher in H460, H1299, A549, H226B, and H226Br cells than in H322 cells, and the levels of pEGFR, EGFR, and pp44/42MAPK expression did not substantially differ among these cell lines. H358 cells also had lower levels of IGF expression than did H460, H1299, A549, H226B, and H226Br cells (data not shown). The two cell lines most sensitive to gefitinib treatment (H322 and H358) had the lowest level of IGF-IR expression, suggesting that IGF-IR is involved in NSCLC cells' sensitivity to gefitinib.

We selected four representative cell lines, two resistant (H1299 and H460) and two sensitive (H322 and H358) to gefitinib, to determine whether IGF-IR and its downstream signaling components confer resistance to gefitinib. We first determined the phosphorylated and unphosphorylated levels of IGF-IR, EGFR, Akt, and mammalian target of rapamycin (mTOR) in H460 and H322 cells after 72 h of treatment with gefitinib. The treatment (10 $\mu\text{mol/L}$ for H460 cells and 1 or 5 $\mu\text{mol/L}$ for H322 cells) resulted in the complete inhibition of pEGFR expression, verifying gefitinib's effects on EGFR tyrosine kinase activity (Fig. 1C). It was surprising that the levels of pIGF-IR, pAkt, pp44/42MAPK, and pmTOR expression increased in H460 cells after treatment with 10 $\mu\text{mol/L}$ gefitinib, the drug concentration that had completely suppressed pEGFR expression. However, these proteins remained suppressed in gefitinib-treated H322 cells. A gefitinib-induced increase in

pIGF-IR expression was observed in H1299 cells that had high levels of IGF-IR expression but not in H358 cells with low levels of IGF-IR expression (Fig. 1D). Taken together, these findings suggest that gefitinib treatment induces activation of the IGF-IR pathway and its downstream signaling components.

Effects of the combined blockade of the EGFR and IGF-IR pathways on the proliferation of NSCLC cells. To determine the roles of the IGF-IR signaling pathway in the development of gefitinib resistance, we evaluated the effects of gefitinib and AG1024, an IGF-IR TKI (22), on the proliferation and apoptosis of H460 cells.

Treatment with gefitinib and AG1024 efficiently blocked the gefitinib-induced increase in pIGF-IR expression in H460 cells (Fig. 2A). We observed more sensitivity to gefitinib when we simultaneously treated H460 cells with gefitinib and AG1024 than with either agent alone (Fig. 2B). In fact, the combined treatment resulted in synergistically enhanced antiproliferative effects on H460 cells [10 $\mu\text{mol/L}$ gefitinib, 59% (95% CI, 55.9–62.1%; $P < 0.001$); 5 $\mu\text{mol/L}$ AG1024, 70.1% (95% CI, 64.7–75.5%; $P < 0.001$); 10 $\mu\text{mol/L}$ gefitinib plus 5 $\mu\text{mol/L}$ AG1024, 28.5% (95% CI, 26–31%; $P < 0.001$; Table 1].

No obvious changes in cell cycle progression were found in H460 cells that had been treated with gefitinib for 3 days; however, a decrease in the G_1 phase population and an increase in the sub G_0/G_1 phase population were found in those treated with AG1024. Combined treatment with gefitinib (5 $\mu\text{mol/L}$) and AG1024 (5 $\mu\text{mol/L}$) for the same duration led to a decrease in the S population, a further decrease in the G_1 population, and an increase in the sub G_0/G_1 population ($P < 0.001$ for all; Fig. 2C). Moreover, TUNEL staining of cells treated with gefitinib and AG1024 showed a marked increase in apoptosis

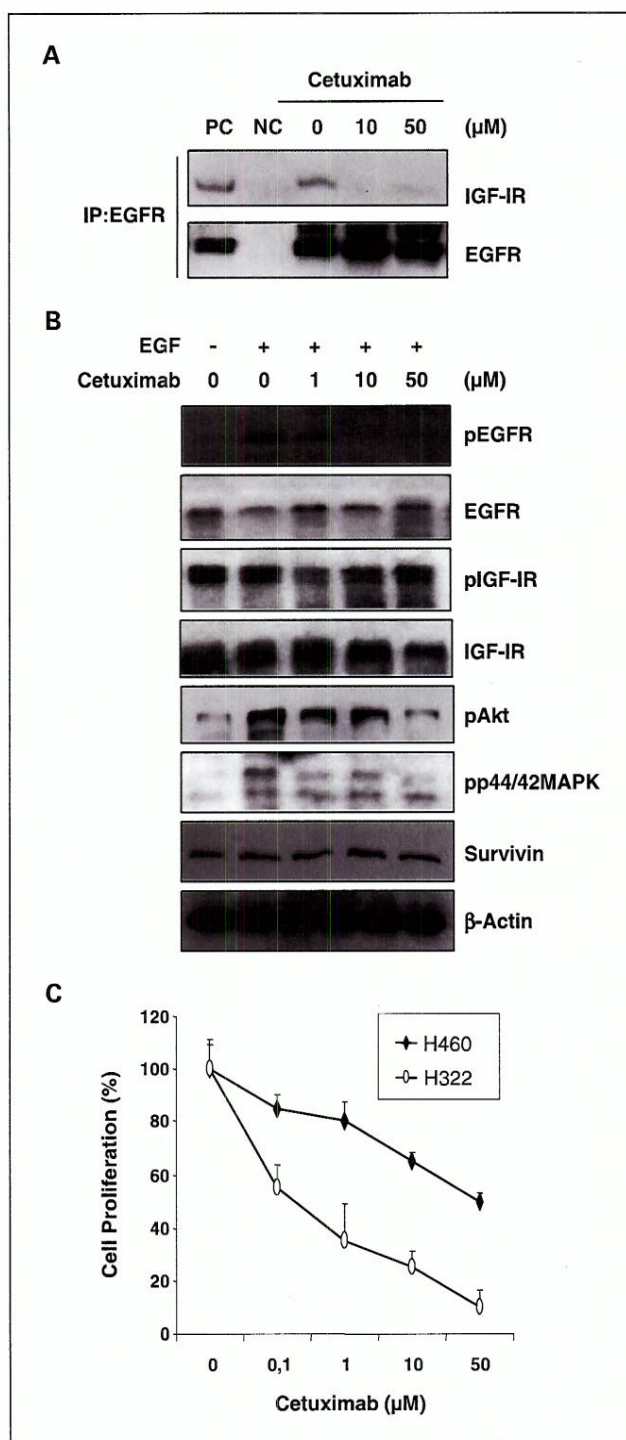


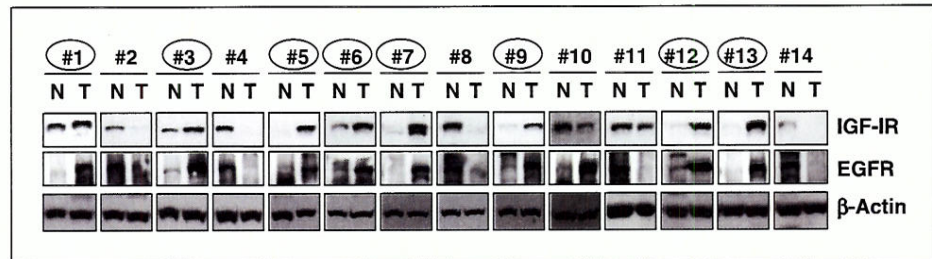
Fig. 5. Effects of cetuximab on EGFR:IGF-IR interaction in NSCLC cells. **A**, effect of cetuximab treatment on EGFR:IGF-IR heterodimerization and activation of the IGF-IR and EGFR signaling pathways. Whole-cell extracts (3 mg) from H460 cells were left untreated or treated with cetuximab (10 and 50 μmol/L) for 3 d. They were then immunoprecipitated with anti-EGFR antibodies, and the immunoprecipitates were subjected to Western blot analysis with the indicated antibodies. Input represents cell lysates (30 μg) that were not subjected to immunoprecipitation. Control immunoprecipitation was done using mouse preimmune serum (PS) as a negative control. **B**, Western blot analysis of survivin, pIGF-IR, IGF-IR, pEGFR, EGFR, pAkt, and pp44/42MAPK expression in H460 cells treated with cetuximab (1, 10, and 50 μmol/L) for 3 d in the absence or presence of EGF (50 ng/mL). **C**, results of the MTT assay of H460 and H322 cell lines after treatment with cetuximab in RPMI 1640 containing 10% FBS for 3 d. Points, mean value of eight identical wells of a single representative experiment; bars, upper 95% CIs.

(Fig. 2D); administration of 5 μmol/L of both gefitinib and AG1024 as single agents induced apoptosis in 0.2% (95% CI, 0.0-2.8%; $P > 0.05$) and 30.1% (95% CI, 14.3-37.6%; $P < 0.05$) of cells, respectively, whereas combined treatment with gefitinib and AG1024 induced apoptosis in more than 90% (95% CI, 64.4-89.8%; $P < 0.001$). These findings suggest that the IGF-IR pathway provides an alternative proliferation or survival mechanism for NSCLC cells in which the EGFR pathway is blocked by gefitinib treatment. Thus, cotargeting the IGF-IR and EGFR pathways may be an effective therapeutic strategy for NSCLC.

Gefitinib induces heterodimerization of IGF-IR and EGFR in H460 cells. EGFR signaling can be modulated by several mechanisms, including heterodimerization with other members of the EGFR family, such as HER-2, and other growth factor receptors, such as IGF-IR (15, 16, 23, 24). We recently observed increased heterodimerization between EGFR and IGF-IR in NSCLC cells after treating them with erlotinib, an EGFR TKI (25). In the current study, we determined the effects of gefitinib on the interaction between EGFR and IGF-IR in H460 and H322 cells. EGFR immunoprecipitates from gefitinib-treated H460 cells showed an obvious increase in IGF-IR binding, whereas control immunoprecipitates that had been treated with preimmune serum had no immunoreactive bands (Fig. 3A). In contrast, both EGFR and control immunoprecipitates from H322 cells lacked immunoreactive bands (Fig. 3B). These results suggest that EGFR and IGF-IR interact through physical contact, and that treatment with gefitinib increases the heterodimerization of EGFR and IGF-IR in H460 cells.

Role of survivin in resistance of NSCLC cells to gefitinib. We next evaluated the signaling mediator that connects gefitinib-induced IGF-IR pathway activation and H460 cell survival. Because inhibitors of apoptosis protein (IAP) such as survivin and XIAP play a role in tumor cells' resistance to chemotherapeutic drugs (26), we determined the effects of gefitinib on the expression of these proteins in H460 and H322 cells. As shown in Fig. 4A, the expression level of survivin but not XIAP markedly increased in H460 cells after treatment with gefitinib. In contrast, no changes were detected in the expression levels of survivin or XIAP in these cells. Moreover, treatment with gefitinib (5 μmol/L) and AG1024 (5 μmol/L) efficiently suppressed the gefitinib-induced increase in survivin expression (Fig. 4B). We then evaluated the influence of survivin on gefitinib-induced apoptosis in NSCLC cells by knockdown of expression or overexpression of survivin. H460 cells transfected with control scrambled or survivin siRNA before treatment with 10 μmol/L gefitinib (a concentration that did not induce apoptosis) had an obvious increase in the rate of apoptosis as determined by a Western blot analysis of an increase in activated caspase-3 expression (Fig. 4C). Furthermore, among H322 cells infected with Ad-survivin, the level of gefitinib-induced apoptosis was substantially reduced (Fig. 4D). These findings suggest that NSCLC cells can escape apoptosis by inducing survivin expression. To determine whether the induction of survivin by gefitinib is related to the resistance of cell lines to the drug, we compared the expression of survivin in a subset of NSCLC cell lines that had been treated with TKI. The five nonsensitive or resistant NSCLC cell lines (H460, H1299, A596, 226B, and 226Br cells) showed an increase in survivin expression after treatment with gefitinib; no increase

Fig. 6. Expression of EGFR and IGF-IR in paired lung tumor and normal tissue specimens from patients with NSCLC. Proteins were extracted from lung tumor and healthy lung tissue and subjected to Western blot analysis to determine the expression of EGFR and IGF-IR. β -Actin was used as a loading control. The samples marked with a circle had increased IGF-IR and EGFR expression.



was found in the two most sensitive NSCLC cell lines (H322 and H358; Fig. 4E). These results suggest that NSCLC cells' resistance to gefitinib can be mediated by survivin induction.

Effects of cetuximab on EGFR:IGF-IR interaction in NSCLC cells. We evaluated the effects of cetuximab on the interaction between IGF-IR and EGFR. EGFR precipitates from cetuximab-treated H460 cells showed no detectable binding to IGF-IR, suggesting that cetuximab suppressed the interaction between EGFR and IGF-IR (Fig. 5A). Moreover, treatment with cetuximab decreased EGF-stimulated pEGFR expression in H460 cells in a dose-dependent manner, without inducing pIGF-IR, pAkt, pp44/42MAPK, or survivin expression (Fig. 5B). A cell proliferation assay showed that H460 cells were more resistant to the antibody than were H358 cells (Fig. 5C). Overall, these findings suggest that heterodimerization between IGF-IR and EGFR, activation of IGF-IR, and induction of survivin expression are at least partly responsible for the induction of acquired resistance to EGFR TKIs, but not to the monoclonal antibody against EGFR in NSCLC cells.

Expression of EGFR and IGF-IR in human lung tissue. Our data suggested that IGF-IR expression has an important role in determining NSCLC cells' sensitivity to EGFR TKIs. Therefore, we determined the levels of EGFR and IGF-IR expression in NSCLC tissue. Nine of the fourteen tumor specimens had higher levels of EGFR expression than did normal tissue specimens from the same patients. Eight of those specimens also had higher levels of IGF-IR expression than those did in normal tissue (Fig. 6).

Discussion

We have previously shown that erlotinib, an EGFR TKI, induces heterodimerization of EGFR/IGF-IR, resulting in the activation of IGF-IR and induction of Akt/mTOR-mediated synthesis of survivin protein, which protects NSCLC cells from the drug-induced apoptosis (25). In the present study, we show that the activation of the IGF-IR via heterodimerization of EGFR/IGF-IR and consequent induction of survivin expression also mediate gefitinib resistance in NSCLC cells, confirming and extending our previous findings (25). Our studies also show that IGF-IR pathway did not affect antiproliferative activities of cetuximab, a monoclonal antibody blocking EGFR. Overall, these findings suggest that heterodimerization between IGF-IR and EGFR, activation of IGF-IR, and induction of survivin expression contribute to the acquired resistance to EGFR TKIs, but not to the monoclonal antibody against EGFR in NSCLC cells.

In clinical trials, the EGFR TKIs, such as erlotinib and gefitinib, were found to be effective in the treatment of patients with NSCLC (27, 28). These agents were approved for NSCLC

treatment after resulting in response rates of 10% and survival advantages in patients previously treated with chemotherapy (29). However, large-scale phase III clinical trials in advanced NSCLC have had contrasting results (13, 14, 29, 30). In the current study, we found that gefitinib treatment did not inhibit NSCLC cell proliferation at doses sufficient to suppress EGFR activation, suggesting that the development of resistance to EGFR TKIs is caused by the activation of alternative cell survival signaling mechanisms.

To develop better anticancer therapeutic strategies using gefitinib, we sought to identify the pathways whereby NSCLC cell trigger alternative survival signaling. PTEN expression and EGFR and Kirsten ras (KRAS) somatic mutation have been involved in the cellular response to EGFR-targeted therapy (31–33). Bianco et al. (34) found that the loss of PTEN expression in the MDA-468 breast cancer cell line contributed to gefitinib resistance. These findings suggest that PTEN-deficient cell lines maintain their Akt activity and survive when EGFR is inactivated. However, deletion of PTEN does not frequently occur in NSCLC cells (31, 35). In fact, all NSCLC cell lines used in our study expressed PTEN, suggesting that gefitinib resistance in NSCLC cells is not caused by a PTEN deficiency. Similarly, the NSCLC cell lines without somatic mutations of EGFR responded to gefitinib, which is consistent with previously reported findings (36, 37). Moreover, in our study, gefitinib showed antiproliferative effects on H358 cells that have somatic mutation in KRAS (38). Together, these findings indicate that expression of PTEN and mutational status of EGFR and KRAS are not entirely responsible for NSCLC cells' resistance to gefitinib.

Our *in vitro* data suggest that the cross-talk between the IGF-IR and EGFR signaling pathways is involved in the development of gefitinib resistance in NSCLC cells. First, we found that the levels of IGF-IR and pIGF-IR expression in NSCLC cells were inversely associated with the antiproliferative effects of gefitinib. Second, gefitinib induced phosphorylation of IGF-IR and its downstream mediators in NSCLC cell lines with high levels of IGF-IR expression. Third, gefitinib induced heterodimerization between IGF-IR and EGFR and survivin expression in the high IGF-IR-expressing H460 cells but not in the low IGF-IR-expressing H322 cells. Finally, gefitinib exhibited apoptotic activity in H460 cells, in which IGF-IR activation was blocked. These NSCLC cell lines have shown a similar response to the erlotinib treatment (25). EGFR and IGF-IR have similar extracellular domain structures (39); therefore, it is plausible that EGFR TKIs induce a direct interaction between EGFR and IGF-IR, leading to the activation of IGF-IR pathways and induction of survivin expression and, thus, maintain NSCLC cell proliferation. Recent reports showing a direct interaction between EGFR and IGF-IR (40, 41) also support our hypothesis.

The induced expression of survivin found in our study seemed to protect H460 cell from apoptosis in the presence of gefitinib: survivin overexpression protected H322 cells from gefitinib-induced apoptosis. In addition, gefitinib induced apoptosis in H460 cells, in which transfection with survivin-specific siRNA silenced survivin expression. Survivin is a member of the IAP family and is associated with both cancer progression and drug resistance (42, 43). Therefore, the resistance and sensitivity of NSCLC cells to gefitinib may be determined, at least in part, by their ability to activate the IGF-IR-mediated pathway and induce survivin expression. Most strikingly, we found no evidence of EGFR and IGF-IR heterodimerization, IGF-IR activation, and induction of survivin expression in H460 cells after cetuximab treatment. These findings suggest that activation of the IGF-IR pathway and the subsequent expression of survivin are at least partly responsible for the sensitivity of NSCLC cells to EGFR TKIs but not to anti-EGFR monoclonal antibodies.

In summary, we showed that the cross-talk between IGF-IR and EGFR has a specific role in inducing gefitinib resistance in NSCLC cells. Gefitinib induced heterodimerization of EGFR and IGF-IR; stimulated IGF-IR and downstream pathways, including phosphoinositide-3-kinase/Akt/mTOR and p44/42 MAPK; and increased survivin expression in NSCLC cell lines. Overexpression of the EGFR family and its ligands have been found in 30% to 80% of NSCLC (30, 44, 45). However, we found no

interaction between EGFR and IGF-IR in NSCLC cells with low levels of IGF-IR expression, suggesting that the basal level of IGF-IR expression is important for initiating the formation of the EGFR:IGF-IR complex. Nine of the fourteen (64%) tumor specimens in our study exhibited higher levels of EGFR expression, and eight of those had related higher IGF-IR expression compared with paired normal tissue. The number of IGF-IRs may determine the response to IGF-I; activated IGF-IRs in sufficient numbers change the mode of IGF's effect from nonmitogenic to mitogenic, resulting in cell cycle progression, translation, and DNA synthesis (46). Overexpression of IGF-IR has been associated with survival of NSCLC patients treated with gefitinib (47). Therefore, our newly identified mechanism of EGFR TKI resistance could provide new therapeutic avenues for NSCLC. Treatment with the anti-EGFR monoclonal antibody cetuximab may be effective once resistance to EGFR TKIs has been established, and the use of combination regimens with EGFR TKIs and IGF-IR inhibitors may be effective at treating NSCLC in patients with high levels of EGFR and IGF-IR expression. However, the results of an *in vitro* study with a limited number of cell lines are not sufficient to generalize the roles of the IGF-IR signaling pathway and survivin expression in gefitinib resistance in NSCLC cells. Further clinical trials are needed to determine whether combined treatment with EGFR TKIs and IGF-IR pathway inhibitors enhances objective responses and survival in patients with NSCLC.

References

- Jemal. American Cancer Society: Cancer facts and figures 2006. Atlanta, GA: American Cancer Society; 2006.
- Mendelsohn J. The epidermal growth factor receptor as a target for cancer therapy. *Endocr Relat Cancer* 2001;8:3-9.
- Brogna J, Clark AS, Ni Y, Dennis PA. Akt/protein kinase B is constitutively active in non-small cell lung cancer cells and promotes cellular survival and resistance to chemotherapy and radiation. *Cancer Res* 2001;61:3986-97.
- Brogna J, Dennis PA. Variable apoptotic response of NSCLC cells to inhibition of the MEK/ERK pathway by small molecules or dominant negative mutants. *Cell Death Differ* 2002;9:933-904.
- Woodburn JR. The epidermal growth factor receptor and its inhibition in cancer therapy. *Pharmacol Ther* 1999;82:241-50.
- Ciardiello F, Bianco R, Damiano V, et al. Antiangiogenic and antitumor activity of anti-epidermal growth factor receptor C225 monoclonal antibody in combination with vascular endothelial growth factor antisense oligonucleotide in human GEO colon cancer cells. *Clin Cancer Res* 2000;6:3739-47.
- Fan Z, Lu Y, Wu X, Mendelsohn J. Antibody-induced epidermal growth factor receptor dimerization mediates inhibition of autocrine proliferation of A431 squamous carcinoma cells. *J Biol Chem* 1994;269:27595-602.
- Goldstein NI, Prewett M, Zuklys K, Rockwell P, Mendelsohn J. Biological efficacy of a chimeric antibody to the epidermal growth factor receptor in a human tumor xenograft model. *Clin Cancer Res* 1995;1:1311-8.
- Ciardiello F, Damiano V, Bianco R, et al. Antitumor activity of combined blockade of epidermal growth factor receptor and protein kinase A. *J Natl Cancer Inst* 1996;88:1770-6.
- Bonner JA, Harari PM, Giral J, et al. Radiotherapy plus cetuximab for squamous-cell carcinoma of the head and neck. *N Engl J Med* 2006;354:567-78.
- Meyerhardt JA, Mayer RJ. Systemic therapy for colorectal cancer. *N Engl J Med* 2005;352:476-87.
- Fry DW, Bridges AJ, Denny WA, et al. Specific, irreversible inactivation of the epidermal growth factor receptor and erbB2, by a new class of tyrosine kinase inhibitor. *Proc Natl Acad Sci U S A* 1998;95:12022-7.
- Giaccone G, Herbst RS, Manegold C, et al. Gefitinib in combination with gemcitabine and cisplatin in advanced non-small-cell lung cancer: a phase III trial—INTACT 1. *J Clin Oncol* 2004;22:777-84.
- Herbst RS, Giaccone G, Schiller JH, et al. Gefitinib in combination with paclitaxel and carboplatin in advanced non-small-cell lung cancer: a phase III trial—INTACT 2. *J Clin Oncol* 2004;22:785-94.
- Jones HE, Goddard L, Gee JM, et al. Insulin-like growth factor-I receptor signalling and acquired resistance to gefitinib (ZD1839; Iressa) in human breast and prostate cancer cells. *Endocr Relat Cancer* 2004;11:793-814.
- Chakravarti A, Loeffler JS, Dyson NJ. Insulin-like growth factor receptor I mediates resistance to anti-epidermal growth factor receptor therapy in primary human glioblastoma cells through continued activation of phosphoinositide 3-kinase signaling. *Cancer Res* 2002;62:200-7.
- Lee CT, Park KH, Adachi Y, et al. Recombinant adenoviruses expressing dominant negative insulin-like growth factor-I receptor demonstrate antitumor effects on lung cancer. *Cancer Gene Ther* 2003;10:57-63.
- Goldstein D, Bushmeyer SM, Witt PL, Jordan VC, Borden EC. Effects of type I and II interferons on cultured human breast cells: interaction with estrogen receptors and with tamoxifen. *Cancer Res* 1989;49:2698-702.
- Chun KH, Kosmeder JW II, Sun S, et al. Effects of deguelin on the phosphatidylinositol 3-kinase/Akt pathway and apoptosis in premalignant human bronchial epithelial cells. *J Natl Cancer Inst* 2003;95:291-302.
- Lee HY, Moon H, Chun KH, et al. Effects of insulin-like growth factor binding protein-3 and farnesyltransferase inhibitor SCH66336 on Akt expression and apoptosis in non-small-cell lung cancer cells. *J Natl Cancer Inst* 2004;96:1536-48.
- Tang JM, He QY, Guo RX, Chang XJ. Phosphorylated Akt overexpression and loss of PTEN expression in non-small cell lung cancer confers poor prognosis. *Lung Cancer* 2006;51:181-91.
- Parrizas M, Gazit A, Levitzki A, Wertheimer E, LeRoith D. Specific inhibition of insulin-like growth factor-1 and insulin receptor tyrosine kinase activity and biological function by typhostins. *Endocrinology* 1997;138:1427-33.
- Balana ME, Labriola L, Salatiello M, et al. Activation of ErbB-2 via a hierarchical interaction between ErbB-2 and type I insulin-like growth factor receptor in mammary tumor cells. *Oncogene* 2001;20:34-47.
- Gilmore AP, Valentini AJ, Wang P, et al. Activation of BAD by therapeutic inhibition of epidermal growth factor receptor and transactivation by insulin-like growth factor receptor. *J Biol Chem* 2002;277:27643-50.
- Morgillo F, Woo JK, Kim ES, Hong WK, Lee HY. Heterodimerization of insulin-like growth factor receptor/epidermal growth factor receptor and induction of survivin expression counteract the antitumor action of erlotinib. *Cancer Res* 2006;66:10100-11.
- Altieri DC. The molecular basis and potential role of survivin in cancer diagnosis and therapy. *Trends Mol Med* 2001;7:542-7.
- Kris MG, Natale RB, Herbst RS, et al. Efficacy of gefitinib, an inhibitor of the epidermal growth factor receptor tyrosine kinase, in symptomatic patients with non-small cell lung cancer: a randomized trial. *JAMA* 2003;290:2149-58.
- Fukuoka M, Yano S, Giaccone G, et al. Multinational randomized phase II trial of gefitinib for previously treated patients with advanced non-small-cell lung cancer (the IDEAL 1 trial) [corrected]. *J Clin Oncol* 2003;21:2237-46.
- Shepherd FA, Rodrigues Pereira J, Ciuleanu T, et al.

- Erlotinib in previously treated non-small-cell lung cancer. *N Engl J Med* 2005;353:123–32.
30. Thatcher N, Chang A, Parikh P, et al. Gefitinib plus best supportive care in previously treated patients with refractory advanced non-small-cell lung cancer: results from a randomised, placebo-controlled, multicentre study (Iressa Survival Evaluation in Lung Cancer). *Lancet* 2005;366:1527–37.
 31. Kohno T, Takahashi M, Manda R, Yokota J. Inactivation of the PTEN/MMAC1/TEP1 gene in human lung cancers. *Genes Chromosomes Cancer* 1998;22:152–6.
 32. Lynch TJ, Bell DW, Sordella R, et al. Activating mutations in the epidermal growth factor receptor underlying responsiveness of non-small-cell lung cancer to gefitinib. *N Engl J Med* 2004;350:2129–39.
 33. Paez JG, Janne PA, Lee JC, et al. EGFR mutations in lung cancer: correlation with clinical response to gefitinib therapy. *Science* 2004;304:1497–500.
 34. Bianco R, Shin I, Ritter CA, et al. Loss of PTEN/MMAC1/TEP in EGF receptor-expressing tumor cells counteracts the antitumor action of EGFR tyrosine kinase inhibitors. *Oncogene* 2003;22:2812–22.
 35. Yokomizo A, Tindall DJ, Drabkin H, et al. PTEN/MMAC1 mutations identified in small cell, but not in non-small cell lung cancers. *Oncogene* 1998;17:475–9.
 36. Amann J, Kalyankrishna S, Massion PP, et al. Aberrant epidermal growth factor receptor signaling and enhanced sensitivity to EGFR inhibitors in lung cancer. *Cancer Res* 2005;65:226–35.
 37. Tracy S, Mukohara T, Hansen M, Meyerson M, Johnson BE, Janne PA. Gefitinib induces apoptosis in the EGFR L858R non-small-cell lung cancer cell line H3255. *Cancer Res* 2004;64:7241–4.
 38. Mitsudomi T, Steinberg SM, Nau MM, et al. p53 gene mutations in non-small-cell lung cancer cell lines and their correlation with the presence of ras mutations and clinical features. *Oncogene* 1992;7:171–80.
 39. Garrett TP, McKern NM, Lou M, et al. Crystal structure of the first three domains of the type-1 insulin-like growth factor receptor. *Nature* 1998;394:395–9.
 40. Gschwind A, Zwick E, Prenzel N, Leserer M, Ullrich A. Cell communication networks: epidermal growth factor receptor transactivation as the paradigm for interreceptor signal transmission. *Oncogene* 2001;20:1594–600.
 41. Roudabush FL, Pierce KL, Maudsley S, Khan KD, Luttrell LM. Transactivation of the EGF receptor mediates IGF-I-stimulated shc phosphorylation and ERK1/2 activation in COS-7 cells. *J Biol Chem* 2000;275:22583–9.
 42. Adida C, Crotty PL, McGrath J, Berrebi D, Diebold J, Altieri DC. Developmentally regulated expression of the novel cancer anti-apoptosis gene survivin in human and mouse differentiation. *Am J Pathol* 1998;152:43–9.
 43. Zhang M, Latham DE, Delaney MA, Chakravarti A. Survivin mediates resistance to antiandrogen therapy in prostate cancer. *Oncogene* 2005;24:2474–82.
 44. Rusch V, Klimstra D, Venkatraman E, Pisters PW, Langenfeld J, Dmitrovsky E. Overexpression of the epidermal growth factor receptor and its ligand transforming growth factor α is frequent in resectable non-small cell lung cancer but does not predict tumor progression. *Clin Cancer Res* 1997;3:515–22.
 45. Fontanini G, De Laurentis M, Vignati S, et al. Evaluation of epidermal growth factor-related growth factors and receptors and of neoangiogenesis in completely resected stage I-IIIa non-small-cell lung cancer: amphiregulin and microvessel count are independent prognostic indicators of survival. *Clin Cancer Res* 1998;4:241–9.
 46. Kurmasheva RT, Houghton PJ. IGF-I mediated survival pathways in normal and malignant cells. *Biochim Biophys Acta* 2006;1766:1–22.
 47. Cappuzzo F, Toschi L, Tallini G, et al. Insulin-like growth factor receptor 1 (IGFR-1) is significantly associated with longer survival in non-small-cell lung cancer patients treated with gefitinib. *Ann Oncol* 2006;17:1120–7.

The Farnesyltransferase Inhibitor R115777 Up-regulates the Expression of Death Receptor 5 and Enhances TRAIL-Induced Apoptosis in Human Lung Cancer Cells

Yuanzheng Qiu,^{1,2} Xiangguo Liu,¹ Wei Zou,¹ Ping Yue,¹ Sagar Lonial,¹ Fadlo R. Khuri,¹ and Shi-Yong Sun¹

¹Department of Hematology and Oncology, Winship Cancer Institute, Emory University School of Medicine, Atlanta, Georgia and

²Department of Otolaryngology-Head and Neck Surgery, Xiang-Ya Hospital, Central South University, Changsha, Hunan, P.R. China

Abstract

Tumor necrosis factor-related apoptosis-inducing ligand (TRAIL) preferentially induces apoptosis in transformed or malignant cells, thus exhibiting potential as a tumor-selective apoptosis-inducing cytokine for cancer treatment. Many studies have shown that the apoptosis-inducing activity of TRAIL can be enhanced by various cancer therapeutic agents. R115777 (tipifarnib) is the first farnesyltransferase inhibitor (FTI) that showed clinical activity in myeloid malignancies. In general, R115777, like other FTIs, exerts relatively weak effects on the induction of apoptosis in cancer cells with undefined mechanism(s). In the current study, we studied its effects on the growth of human lung cancer cells, including induction of apoptosis, and examined potential underlying mechanisms for these effects. We showed that R115777 induced apoptosis in human lung cancer cells, in addition to inducing G₁ or G₂-M arrest. Moreover, we found that R115777 up-regulated the expression of death receptor 5 (DR5), an important death receptor for TRAIL, and exhibited an augmented effect on the induction of apoptosis when combined with recombinant TRAIL. Blockage of DR5 induction by small interfering RNA (siRNA) abrogated the ability of R115777 to enhance TRAIL-induced apoptosis, indicating that R115777 augments TRAIL-induced apoptosis through up-regulation of DR5 expression. Thus, our findings show the efficacy of R115777 in human lung cancer cells and suggest that R115777 may be used clinically in combination with TRAIL for treatment of human lung cancer. [Cancer Res 2007;67(10):4973–80]

Introduction

The tumor necrosis factor-related apoptosis-inducing ligand (TRAIL) receptor death receptor 5 (DR5, also named TRAIL-R2, TRICK2, or Killer/DR5) is one of the death receptors that share a similar, cysteine-rich extracellular domain and additional cytoplasmic death domain (1). DR5 locates at the cell surface, becomes activated or oligomerized (trimerized) upon binding to its ligand TRAIL or overexpression, and then signals apoptosis through caspase-8-mediated rapid activation of caspase cascades (1, 2).

Recently, DR5 has attracted much more attention because its ligand TRAIL preferentially induces apoptosis in transformed or malignant cells, thus demonstrating potential as a tumor-selective apoptosis-inducing cytokine for cancer treatment (3, 4). Certain cancer therapeutic agents induce the expression of DR5 in cancer cells and are thereby able to augment TRAIL-induced apoptosis or initiate apoptosis (5–7).

Farnesyltransferase inhibitors (FTI) are a class of agents that suppress the farnesyltransferase enzyme to prevent certain proteins such as the Ras oncoprotein from undergoing farnesylation (8–10). These agents inhibit proliferation and induce apoptosis in various types of cancer cell lines in culture or suppress the growth of xenografts in nude mice with limited toxicity (8–10). In the clinic, FTIs are well tolerated and have some positive outcomes in certain settings, such as hematologic malignancies and breast cancer, although the response rates to FTIs alone are generally poor. When combined with other therapeutic agents or radiotherapy, FTIs exhibits some encouraging clinical responses (8, 10). Although FTIs were historically developed as anti-Ras agents, it is now generally agreed upon that FTIs exert their antitumor activity independent of their activity on inhibiting Ras farnesylation (8, 9). Otherwise, the mechanisms underlying the antitumor effects of FTIs remain largely undefined.

R115777 is one of the clinically tested FTIs and is the first one to show clinical activity in myeloid malignancies (11). Preclinical studies have shown that this agent inhibited the growth of the majority of tested human cancer cell lines (12), induced apoptosis in certain types of cancer cells (13–15), and suppressed the growth of tumor xenografts in nude mice with an increase in apoptotic index (12, 16). When R115777 was combined with other therapeutic agents, such as taxol and the proteasome inhibitor bortezomib, enhanced effects on growth inhibition or apoptosis induction were observed (17–19). Moreover, R115777 was also effective in inhibiting the growth of chemical-induced lung carcinogenesis in mice (20), suggesting potential activity as a chemopreventive agent. In the clinic, the most promising activity of R115777 has been seen primarily in hematologic malignancies (8, 11). Although R115777 as a single agent exhibited limited clinical activity in solid tumors, when used in combination with other agents such as tamoxifen, it did induce responses in some patients with solid tumors (8).

In an effort to elucidate the molecular mechanisms of FTI-induced growth arrest and apoptosis and to develop mechanism-oriented, FTI-based combination regimens for effective treatment of cancer, we found that R115777 up-regulated DR5 expression, including causing an increase in cell surface DR5 levels. Accordingly, R115777 cooperated with TRAIL to enhance induction of apoptosis in human lung cancer cells. Thus, our findings in this

Note: S.-Y. Sun and F.R. Khuri are Georgia Cancer Coalition Distinguished Cancer Scholars.

Requests for reprints: Shi-Yong Sun, Winship Cancer Institute, Emory University School of Medicine, 1365-C Clifton Road, C3088, Atlanta, GA 30322. Phone: 404-778-2170; Fax: 404-778-5520; E-mail: shi-yong.sun@emoryhealthcare.org.

©2007 American Association for Cancer Research.

doi:10.1158/0008-5472.CAN-06-4044

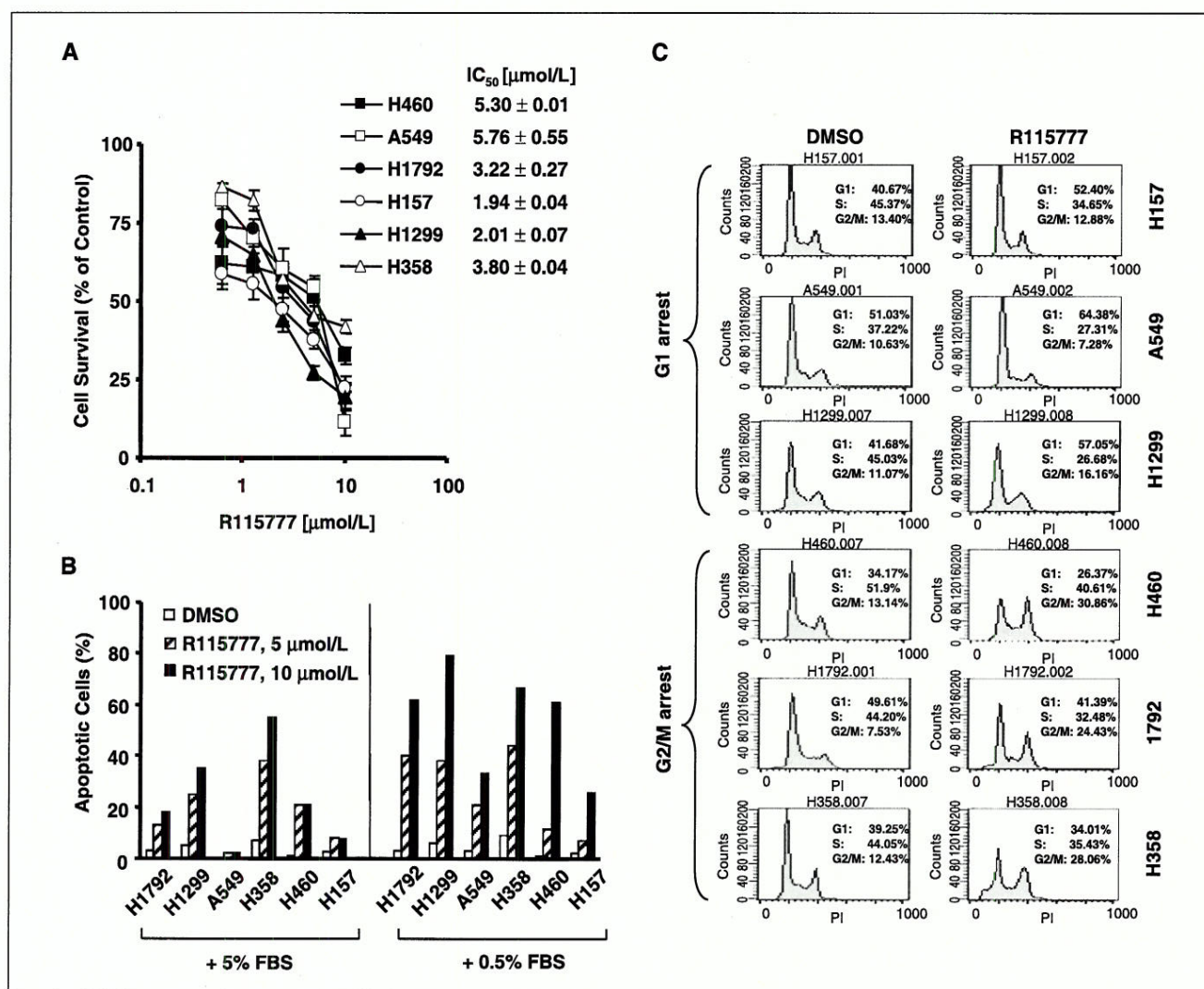


Figure 1. R115777 inhibits cell growth (A) and induces apoptosis (B) and cell cycle arrest (C) in human lung cancer cells. A, the indicated cell lines were seeded in 96-well plates. On the second day, the cells were treated with different concentrations of R115777. After 3 d, the cells were fixed and subjected to estimation of cell number using the sulforhodamine B assay. IC₅₀ refers to the concentration that decreases cell number by 50%; B, the indicated cell lines were treated with 0, 5, and 10 μmol/L of R115777 in medium with either 5% or 0.1% FBS. After 48 h, the cells were harvested for analysis of sub-G₁ population by flow cytometry; C, the indicated cell lines were treated with DMSO or 5 μmol/L of R115777 in medium with 5% FBS. After 48 h, the cells were harvested for analysis of cell cycle distribution by flow cytometry.

study provide a scientific rationale for the combination of R115777 and TRAIL for the treatment of human lung cancer and possibly other types of cancer as well.

Materials and Methods

Reagents. R115777 was provided by Johnson & Johnson Pharmaceutical Research and Development, LLC. It was dissolved in DMSO at a concentration of 10 mmol/L, and aliquots were stored at -80°C. Stock solutions were diluted to the desired final concentrations with growth medium just before use. Soluble recombinant human TRAIL was purchased from PeproTech Inc. Rabbit polyclonal anti-DR5 antibody was purchased from ProSci Inc. Mouse monoclonal anti-caspase-3 was purchased from Imgenex. Rabbit polyclonal anti-caspase-9, anti-caspase-8, and anti-poly(ADP-ribose) polymerase (PARP) antibodies were purchased from Cell Signaling Technology, Inc. Mouse monoclonal anti-RasGAP antibody (B4F8) was purchased from Santa Cruz Biotechnology. Mouse monoclonal anti-HDJ-2 antibody (clone KA2A5.6) was purchased from Lab Vision Corp.

Mouse monoclonal anti-FLICE inhibitory protein (FLIP) antibody (NF6) was purchased from Alexis Biochemicals. Rabbit polyclonal anti-β-actin antibody was purchased from Sigma Chemical Co.

Cell lines and cell cultures. All human lung cancer cell lines used in this study were purchased from the American Type Culture Collection. H157-Lac Z-5 and H157-FLIP₁₋₆, which stably express Lac Z and FLIP₁, respectively, were described previously (21). These cell lines were grown in monolayer culture in RPMI 1640 supplemented with glutamine and 5% fetal bovine serum (FBS) at 37°C in a humidified atmosphere consisting of 5% CO₂ and 95% air.

Western blot analysis. The procedures for preparation of whole-cell protein lysates and Western blot analysis were described previously (22, 23).

Detection of DR5 mRNA expression. DR5 mRNA was detected using reverse transcription-PCR (RT-PCR) described as follows. Total RNA was isolated from cells using TRI Reagent (Sigma Chemical Co.) as instructed by the manufacturer. First-strand cDNA was synthesized from 2 μg of total RNA using iScript cDNA Synthesis Kit (Bio-Rad Laboratories) following the manufacturer's instructions. The given cDNAs were then amplified by PCR

using the following primers: DR5 sense 5'-GACCTAGCTCCCCAGCAGAGAG-3', DR5 antisense 5'-CGGCTGCAACTGTGACTCCTAT-3', β -actin sense, 5'-GAAACTACCTTCAACTCCATC-3', and β -actin antisense 5'-CTAAGCATTTGCGGTGGACGATGGAGGGGCC-5'. The 25- μ L amplification mixture contained 2 μ L of cDNA, 0.5 μ L of deoxynucleotide triphosphate (25 mmol/L each), 1 μ L each of the sense and antisense primers (20 μ mol/L each), 5 μ L of TaqMaster PCR enhancer, 1 μ L of Taq DNA polymerase (5 units/ μ L; Eppendorf), 2.5 μ L 10 \times reaction buffer, and sterile H₂O. PCR was done for 28 cycles. After an initial step at 95°C for 3 min, each cycle consisted of 50 s of denaturation at 94°C, 50 s of annealing at 58°C, and 55 s of extension at 72°C. This was followed by an additional extension step at 72°C for 10 min. The housekeeping gene β -actin was also amplified as an internal reference. PCR products were resolved by electrophoresis on a 2% agarose gel, stained, and directly visualized under UV illumination.

Construction of DR5 reporter plasmids, transient transfection, and luciferase activity assay. The plasmid containing a 5'-flanking region of DR5 gene was kindly provided by Dr. G.S. Wu (Wayne State University School of Medicine, Detroit, MI). We then used this plasmid as a template to amplify different lengths of the 5'-flanking region of the DR5 gene by PCR and then subcloned these fragments, respectively, into pGL3-basic reporter vector (Promega) through *Kpn*I and *Bgl*II restriction sites. In the PCR amplification, the reverse primer 5'-CTTAAGATCTGGCGGTAGGGAACGCTCTTATAGTC-3' was used to make all deletion constructs. The upstream primers used were 5'-CTTAGGTACCTGGCTCGTCTGTTCCTCTACGGCCCC-3' (-3,070), 5'-CTTAGGTACCTCAACTCATTTCCCCCAAGTTTC-3' (-420), and 5'-CTTAGGTACCAACCCAGAAACAAACACAGCCCGGG-3' (-373), respectively. These constructs were then named pGL3-DR5(-3070), pGL3-DR5(-420), and pGL3-DR5(-373), respectively.

For examining the effect of R115777 on DR5 transactivation activity, cells were seeded in 24-well plates and cotransfected with the given reporter plasmid (0.5 μ g per well) and pCH110 plasmid encoding β -galactosidase (β -gal; Pharmacia Biotech; 0.2 μ g per well) using FuGene 6 transfection reagent (3:1 ratio; Roche Molecular Biochemicals) following the manufacturer's protocol. Twenty-four hours later, the cells were treated with R115777. After 12 h, the cells were lysed and subjected to luciferase activity assay using Luciferase Assay System (Promega) in a luminometer. Relative luciferase activity was normalized to β -gal activity, which was measured as described previously (24).

Detection of cell surface DR5. Cell surface DR5 expression was analyzed using flow cytometry as described previously (25). The mean fluorescence intensity (MFI) that represents antigenic density on a per-cell basis was used to represent DR5 expression level. Phycoerythrin-conjugated mouse anti-human DR5 monoclonal antibody (DJR2-4), anti-human DR4 monoclonal antibody (DJR1), and mouse immunoglobulin G₁ (IgG₁) isotype control (MOPC-21/P3) were purchased from eBioscience.

Detection of caspase activation and apoptosis. Caspase activation and their substrate cleavage were detected by Western blot analysis as described above. Apoptosis was detected using an annexin V:phycoerythrin Apoptosis Detection kit purchased from BD Biosciences following the manufacturer's instructions. In addition, sub-G₁ was also measured by flow cytometry as described previously (26) as another indication of apoptosis.

Cell survival assay. Cells were seeded in 96-well cell culture plates and treated on the second day with the indicated agents. At the end of treatment, cell number was estimated by the sulforhodamine B assay as previously described (27). The cell survival was presented as the percentage

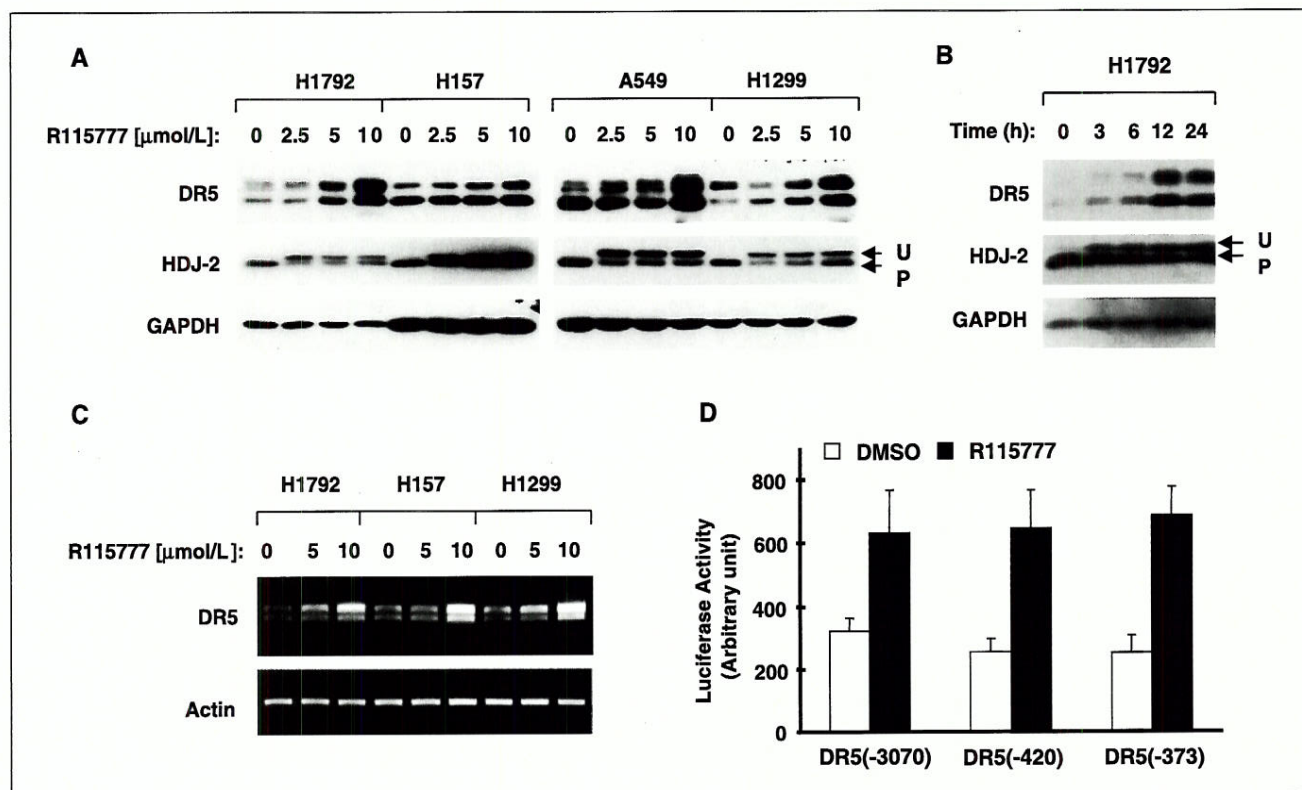


Figure 2. R115777 increases DR5 expression at both protein (A and B) and mRNA (C) levels and transactivates DR5 promoter (D) in human lung cancer cells. A and B, the indicated cell lines were treated with the given concentrations of R115777 for 16 h (A), or H1792 cells were treated with 5 μ mol/L R115777 for the indicated times (B). Whole-cell protein lysates were then prepared from aforementioned treatments for detection of DR5 and HDJ-2 using Western blot analysis. U, unprocessed; P, processed; C, the indicated cell lines were exposed to the given concentrations of R115777 for 12 h. Cellular total RNA was then prepared for detection of DR5 mRNA using RT-PCR. Actin levels were used as an internal control. D, the given reporter constructs with different lengths of the 5'-flanking region of the DR5 gene were cotransfected with pCH110 plasmid into H1792 cells. After 24 h, the cells were treated with DMSO or 10 μ mol/L R115777 for 12 h and then subjected to luciferase assay. Columns, means of triplicate determinations; bars, SD.

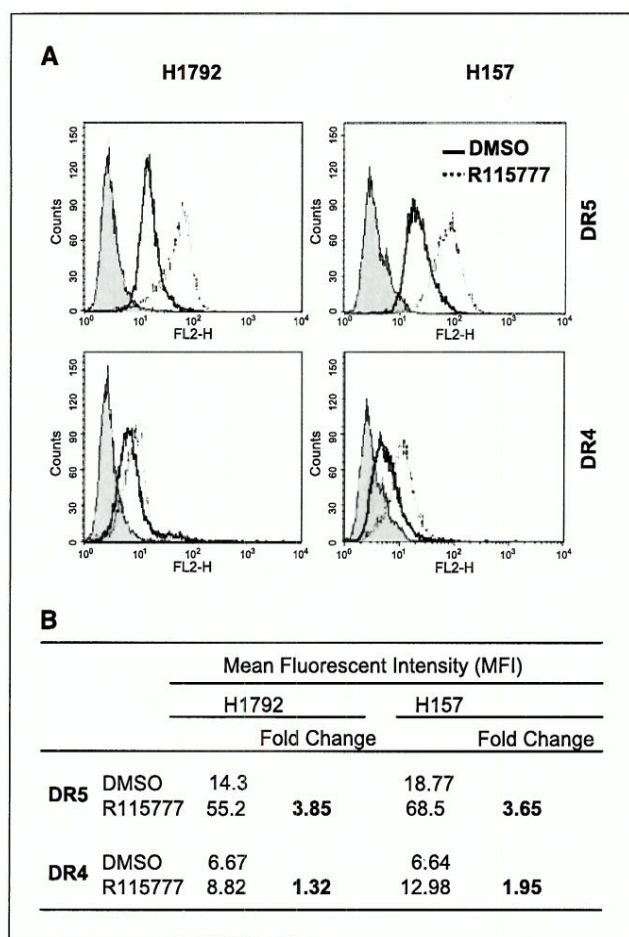


Figure 3. R115777 increases cell surface DR5 distribution. Both H1792 and H157 cell lines were exposed to 10 $\mu\text{mol/L}$ for 16 h. **A**, the cells were then harvested, stained with phycoerythrin-conjugated DR5 or DR4 antibody, and analyzed by flow cytometry. *Filled gray peak*, cells stained with matched phycoerythrin-conjugated IgG isotype. *Open peaks*, cells stained with phycoerythrin-conjugated anti-DR5 or anti-DR4 antibody. **B**, summary of changes in MFIs from cells treated with R115777 as presented in (A).

of control as calculated by using the equation: $A_t/A_c \times 100$, where A_t and A_c represent the absorbance in treated and control cultures, respectively.

Cell cycle analysis. Cells were seeded in 10-cm-diameter cell culture dishes and treated on the second day with DMSO control or R115777. At the end of treatment, cells were trypsinized, and single-cell suspensions were subjected to staining and subsequent analysis of cell cycle by flow cytometry as described previously (28).

Silencing of DR5 expression using small interfering RNA. High-purity control (nonsilencing) and DR5 small interfering RNA (siRNA) oligos were described previously (23) and synthesized from Qiagen. The transfection of siRNA was conducted in a 24-well plate (1 μg per well) using Lipofect-AMINE transfection reagent purchased from Invitrogen following the manufacturer's instruction. Forty-eight hours after the transfection, cells were treated with R115777 alone, TRAIL alone, and their combination. Gene-silencing effect was evaluated by Western blot analysis, and apoptosis was measured with annexin V staining.

Results

R115777 effectively inhibits the growth of human lung cancer cells through induction of apoptosis and growth arrest. The effects of R115777 on the growth of human lung cancer cells have not been systemically evaluated. Therefore, we examined the

effects of R115777 on the growth of a panel of human non-small cell lung cancer cells by different assays. R115777 effectively inhibited the growth of six tested cell lines by measuring cell number, with IC_{50} s ranging from 2 to 6 $\mu\text{mol/L}$ after a 3-day exposure (Fig. 1A). Under normal culture condition (i.e., 5% FBS), R115777 in general was a weak inducer of apoptosis because it induced apoptosis in some cell lines (e.g., H358 and H1299) but not in others (e.g., A549 and H157). However, under low-serum (i.e., 0.1%) culture conditions, the effects of R115777 on apoptosis induction were substantially enhanced in all of the tested cell lines. Under both culture conditions, A549 and H157 were relatively resistant to R115777-induced apoptosis (Fig. 1B). In addition to induction of apoptosis, R115777 induced cell cycle arrest either at the G_1 phase (i.e., H157, A549, and H1299) or at the G_2 -M phase (i.e., H460, H1792, and H358), indicating that R115777 induces growth arrest. Collectively, these results show that R115777 inhibits the growth of human lung cancer cells through the induction of apoptosis and/or growth arrest.

R115777 induces DR5 expression in human lung cancer cells.

To understand the mechanism by which R115777 induces apoptosis, we screened its effects on the expression of certain genes related to apoptosis. Our preliminary results indicate that DR5 is a gene up-regulated in cells exposed to R115777. Therefore, we did detailed experiments to study the effects of R115777 on the expression of DR5 in a panel of human lung cancer cells. We found that R115777 at concentrations ranging from 2.5 to 10 $\mu\text{mol/L}$ increased DR5 protein levels in a concentration-dependent manner. The most dramatic increase in DR5 levels post-R115777 exposure were observed in H1792 cells and H1299 cell lines (Fig. 2A). R115777 induced a weak increase in DR5 levels in H157 cells. Time course analysis indicated that R115777 started to increase DR5 levels at 3 h, which was sustained up to 24 h (Fig. 2B). Under these conditions, the farnesylation of HDJ-2 protein was apparently inhibited (Fig. 2A and B), indicating that R115777 indeed inhibits protein farnesylation in the tested cell lines. Moreover, we determined whether R115777 up-regulated DR5 at the transcriptional level. R115777 increased not only DR5 mRNA levels evaluated by RT-PCR (Fig. 2C), but also the luciferase activity of the cells transfected with reporter plasmids with different lengths of the 5'-flanking region of the DR5 gene ranging from 3,070 to 373 bp upstream of the translation start site (Fig. 2D). These results show that R115777 induces DR5 expression at the transcriptional level.

R115777 induces cell surface DR5 distribution. Because DR5 is a functional protein on the cell surface, we then analyzed cell surface DR5 levels in cells exposed to R115777. As shown in Fig. 3A, both H1792 and H157 cells treated with R115777 exhibited increased fluorescent intensity of DR5 staining in comparison with DMSO-treated cells (i.e., DR5 staining peak shifted to the right). The MFIs in both H1792 and H157 cells were increased close to 4-fold over those in DMSO-treated cells (Fig. 3B). These results clearly indicate that R115777 increases the amounts of DR5 on the cell surface. We also analyzed the effects of R115777 on the distribution of cell surface DR4, a protein with similar functions to DR5, in these cell lines. R115777 increased cell surface DR4 in H157 cells (1.95-fold), but only minimally in H1792 cells (1.32-fold; Fig. 3). Thus, these results indicate that R115777 primarily increases cell surface DR5 in human lung cancer cells.

R115777 cooperates with TRAIL to induce apoptosis in human lung cancer cells. Because R115777 increases cell surface DR5, we hypothesized that R115777 would sensitize cells to TRAIL-induced apoptosis. Therefore, we examined the effects of the

combination of R115777 and TRAIL on cell survival and apoptosis in human lung cancer cells. As presented in Fig. 4A, the combination of R115777 and TRAIL worked better than each single agent in decreasing cell survival. Accordingly, the combination was more potent than each single agent in inducing apoptosis estimated by annexin V staining (Fig. 4B). For example, R115777 at 5 $\mu\text{mol/L}$ and TRAIL at 20 ng/mL alone induced 11.5% and 22.4% of cells to undergo apoptosis, respectively, whereas their combination induced 40% of cells to undergo apoptosis. Thus, it seems that the combination of R115777 and TRAIL synergistically induces apoptosis. Moreover, we examined the effects of R115777 and TRAIL combination on the activation of caspase cascades. R115777 alone at concentrations ranging from 2.5 to 10 $\mu\text{mol/L}$ did not cause cleavage of the tested caspases. TRAIL alone at 20 ng/mL weakly induced cleavage of caspases and caspase-3 substrates, PARP, and RasGAP. However, their combinations exhibited enhanced effects on cleavage of these proteins (Fig. 4C). As the

concentrations of R115777 in the combinations were increased, the cleavage of the caspases and related proteins were more pronounced. Thus, the combination of R115777 and TRAIL augments activation of caspases, further indicating that R115777 cooperates with TRAIL to induce apoptosis.

R115777 enhances TRAIL-induced apoptosis through up-regulation of DR5. To determine whether R115777 enhances TRAIL-induced apoptosis through DR5 up-regulation, we examined the effects of R115777 and TRAIL combination on apoptosis induction in cells where DR5 expression was silenced with DR5 siRNA. In control siRNA-transfected cells, R115777 increased DR5 levels (Fig. 5A, lane 2). In DR5 siRNA-transfected cells, the basal levels of DR5 were reduced (Fig. 5A, lane 5) and not increased further by R115777 (Fig. 5A, lane 6). These results indicate a successful silencing of DR5 expression. By apoptotic assay, we detected up to 70% apoptotic cells in control siRNA-transfected cells, but only 28% apoptotic cells in DR5 siRNA-transfected cells

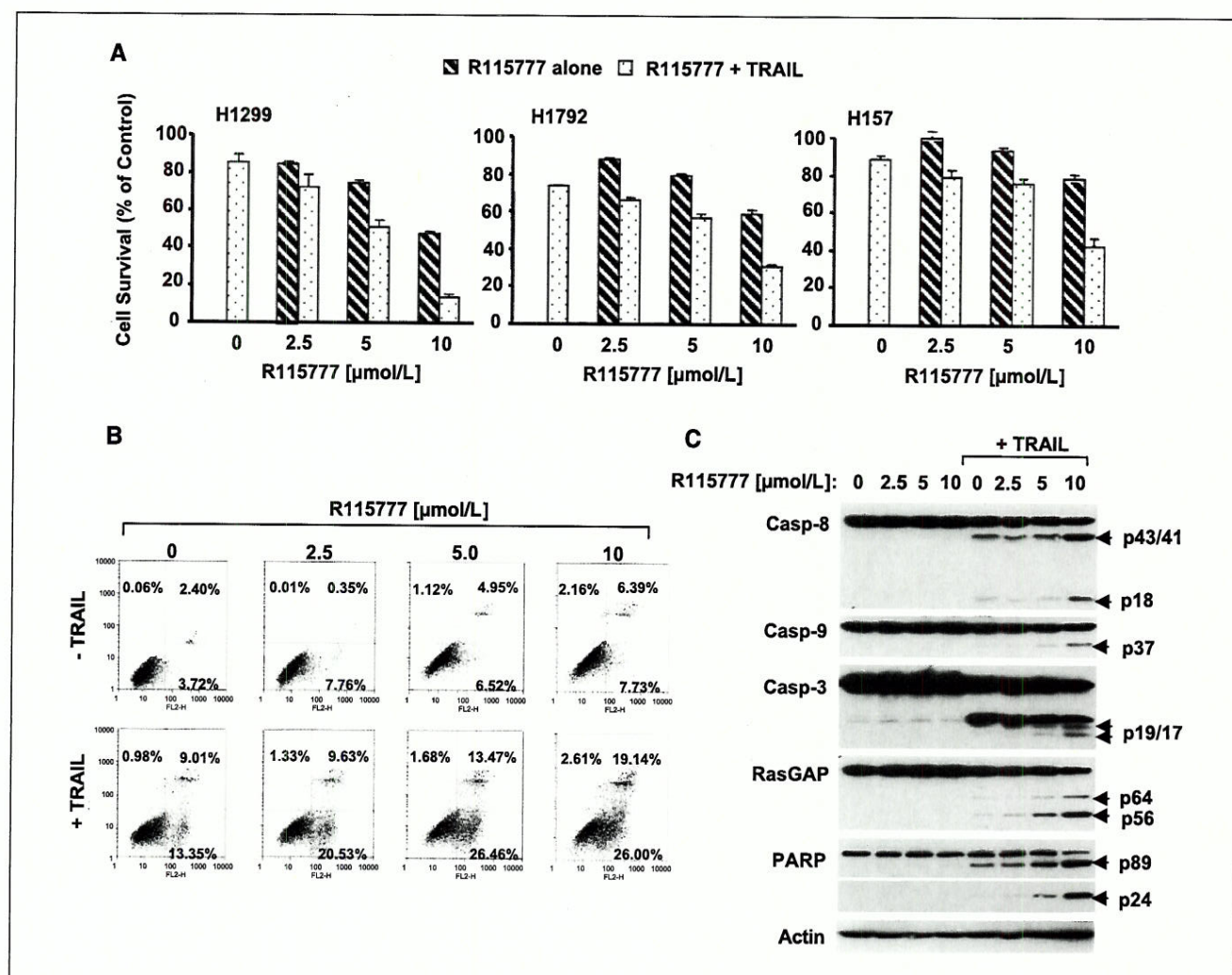


Figure 4. Combination of R115777 and TRAIL exerts augmented effects on decreasing cell survival (A), inducing apoptosis (B), and activating caspases (C). A, the indicated cell lines were treated with the indicated concentrations of R115777 alone, 25 ng/mL TRAIL alone, and their respective combinations as indicated. After 24 h, cell number was estimated using sulforhodamine B assay for calculation of cell survival; B, H157 cells were treated with the indicated concentrations of R115777 alone, 20 ng/mL TRAIL alone, and their respective combinations as indicated. After 24 h, the cells were harvested for measurement of apoptosis using annexin V staining. The percent positive cells in the top right and bottom right quadrants were added to yield the total of apoptotic cells. The cells in the bottom left quadrant were surviving cells; C, H157 cells were treated with the indicated concentrations of R115777 alone, 20 ng/mL TRAIL alone, and their respective combinations for 16 h. The cells were then subjected to preparation of whole-cell protein lysates and subsequent Western blot analysis for detecting cleavage of caspases and their substrates. Casp, caspase.

upon treatment with R115777 and TRAIL combination (Fig. 5B). Collectively, these results clearly indicate that up-regulation of DR5 is a key event that mediates augmentation of apoptosis induced by the combination of R115777 and TRAIL. We noted that more apoptotic cells were detected in control siRNA-transfected H157 cells treated with either TRAIL or the combination of R115777 and TRAIL compared with the result presented in Fig. 4B generated from the same cell line exposed to the similar treatment. In another transfection experiments, we generated identical results from control siRNA-transfected H157 cells treated with the same combination. Therefore, it is possible that the transfected cells are somehow more susceptible than their parental cells to undergo apoptosis upon treatment with TRAIL or the combination of R115777 and TRAIL. Of course, the discrepancy may also be caused by varied activities of different batches of recombinant TRAIL.

R115777 modulates c-FLIP expression in a cell line-dependent manner. c-FLIP including FLIP_L and FLIP_S are key proteins that negatively regulate the extrinsic death receptor-mediated apoptotic pathway by inhibiting caspase-8 activation (29). Some cancer therapeutic agents enhance cell sensitivity to TRAIL-induced apoptosis via down-regulation of c-FLIP expression (30–33). Therefore, we further examined the effects of R115777 on c-FLIP expression in human lung cancer cells. In H1792 cells, R115777 at the given concentrations decreased the levels of both FLIP_L and FLIP_S. However, R115777 slightly increased the levels of both forms of c-FLIP in H157 and A549 cells. We detected neither basal levels of c-FLIP nor clear modulation by R115777 in H1299 cells (Fig. 6A). Thus, it seems that R115777 exerts a cell line-dependent modulation of c-FLIP in human lung cancer cells.

Enforced expression of exogenous c-FLIP protects cells from apoptosis induced by the combination of R115777 and TRAIL. Because the combination of R115777 and TRAIL still augmented apoptosis in the H157 cell line, in which c-FLIP levels were increased, we examined whether enforced expression of exogenous c-FLIP inhibited apoptosis induced by the combination of R115777 and TRAIL. By means of lentiviral infection, we established a stable H157 cell line that expressed high levels of

exogenous FLIP_L (Fig. 6B). In Lac Z (control)-transfected cell line, we detected ~2%, 10%, 14%, and 42% annexin V-positive (apoptotic) cells from cells treated with DMSO, R115777, TRAIL, and the combination of R115777 and TRAIL, respectively. However, annexin V-positive cells were ~2%, 3%, 2%, and 6% in FLIP_L-transfected H157 cells treated with DMSO, R115777, TRAIL, and the combination of R115777 and TRAIL, respectively (Fig. 6C). These results clearly indicate that enforced expression of FLIP_L abolished apoptosis induced by R115777 and TRAIL.

Discussion

The effects of R115777 on the growth including apoptosis and cell cycle distribution of human lung cancer cells have not been fully evaluated in a preclinical setting. In this study, we show that R115777, at a clinically achievable and safe concentration range (2–6 $\mu\text{mol/L}$; refs. 34–37), effectively inhibited the growth of human lung cancer cells, primarily through inducing growth arrest and apoptosis. In general, R115777 was not a potent inducer of apoptosis under normal serum culture condition, although its apoptosis-inducing effects could be substantially enhanced by low-serum culture condition. Moreover, R115777 induced cell cycle arrest either at the G₁ phase or at the G₂-M phase depending on cell lines. All of these phenomena are consistent with those observed from other FTIs (26, 38, 39).

In this study, we show, for the first time, that R115777 induces DR5 expression not only at protein levels but also at mRNA levels. Moreover, R115777 increased transactivation of the DR5 promoter, indicating that R115777 modulates DR5 expression at the transcriptional level. In addition, we showed that R115777 increased amounts of DR5 at the cell surface, indicating that R115777 induces cell surface DR5 distribution. We noted that R115777 exerted only a moderate effect on modulation of DR5 protein levels in H157 cells (Fig. 1A). However, it increased cell surface DR5 in H157 cells as strongly as in H1792 cells (Fig. 3). These results suggest that R115777 induces DR5 redistribution at the cell surface in addition to increasing DR5 expression.

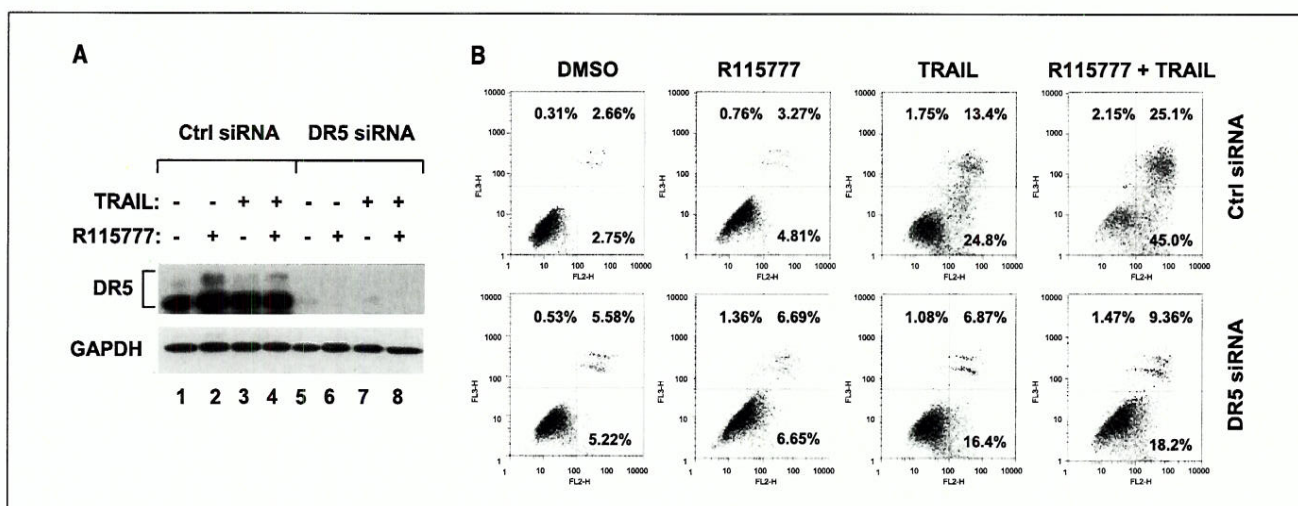


Figure 5. Silencing of DR5 expression by siRNA (A) attenuates apoptosis induced by the combination of R115777 and TRAIL (B). H157 cells were seeded in a 24-well cell culture plate and on the second day transfected with control (Ctrl) or DR5 siRNA. Forty hours later, the cells were treated with 10 $\mu\text{mol/L}$ R115777, 20 ng/mL TRAIL, and their combination. After 15 h, the cells were harvested for preparation of whole-cell protein lysates and subsequent Western blot analysis (A) or for detection of apoptotic cells using annexin V staining (B). In annexin V assay, the percent positive cells in the top right and bottom right quadrants were added to yield the total of apoptotic cells. The cells in the bottom left quadrant were surviving cells.

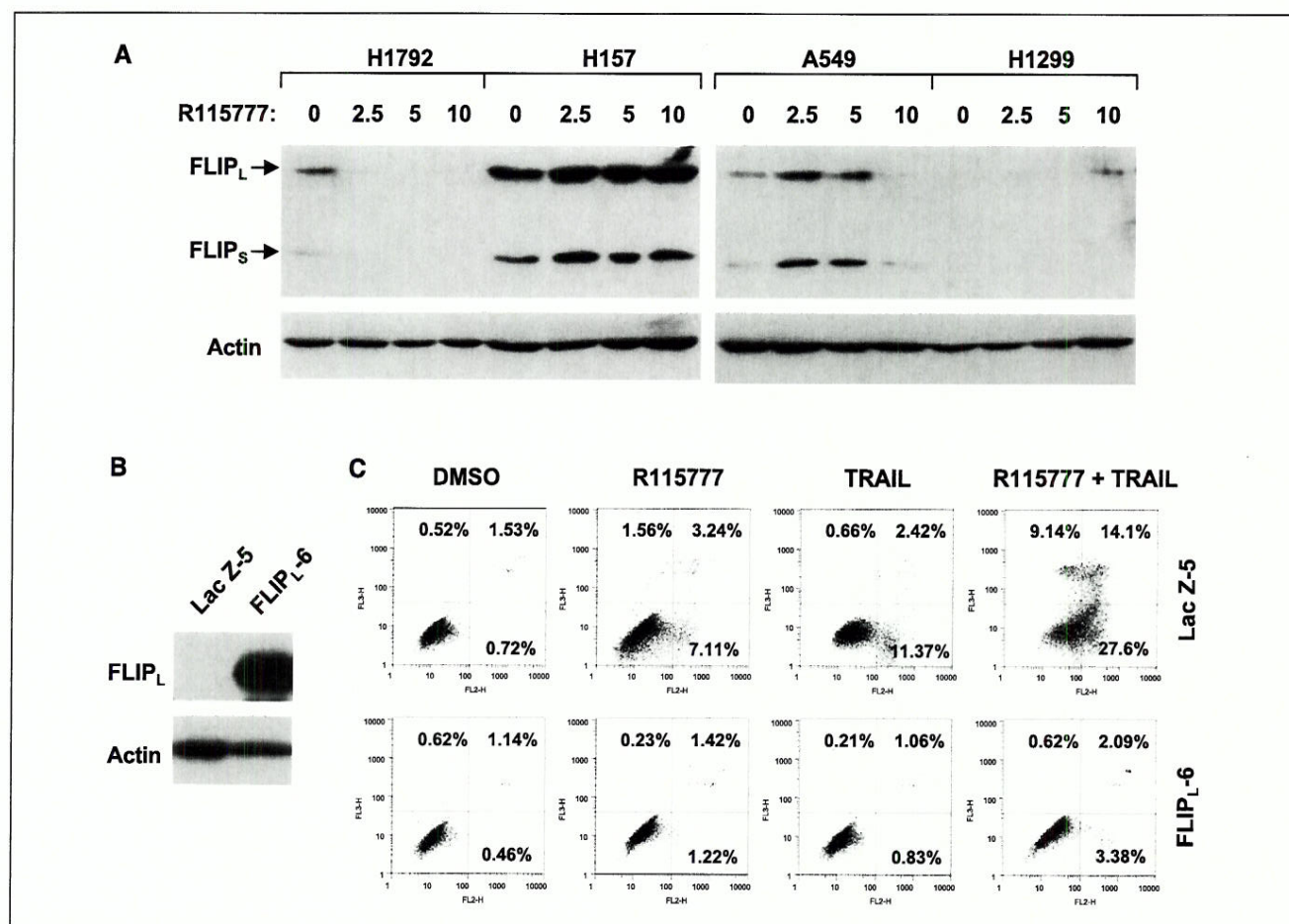


Figure 6. Differential effects of R115777 on c-FLIP levels (A) and protection of enforced c-FLIP expression (B) on apoptosis induced by the combination of R115777 and TRAIL (C). A, the indicated cell lines were treated with the given concentrations of R115777. After 16 h, the cells were subjected to preparation of whole-cell protein lysates and subsequent Western blot analysis. B, whole-cell protein lysates were prepared from H157 cells transfected with Lac Z and FLIP_L, respectively, and then subjected to detection of FLIP_L expression by Western blot analysis. C, H157-Lac Z-5 or H157-FLIP_L-6 cells were treated with DMSO, 10 μmol/L R115777, 5 ng/mL TRAIL, and the combination of R115777 and TRAIL, respectively. After 24 h, the cells were harvested and subjected to detection of apoptotic cells using annexin V staining. The percent positive cells in the top right and bottom right quadrants were added to yield the total of apoptotic cells. The cells in the bottom left quadrant were surviving cells.

In addition to R115777, we found that another FTI called SCH66336 (lonafarnib) also induced DR5 expression and cell surface DR5 distribution.³ Both agents have farnesyltransferase-inhibitory activity; however, they have distinct chemical structures. In our study, R115777 rapidly increased DR5 expression at 3 h posttreatment, which was accompanied by inhibition of HDJ-2 protein farnesylation (Fig. 3B). Therefore, we suggest that DR5 up-regulation by R115777 is associated with its ability to inhibit protein farnesylation. Because R115777 functions like SCH66336 to increase DR5 mRNA as well, it is unlikely that R115777 directly modulates DR5 protein. Rather, it may inhibit the farnesylation of an unknown protein, leading to increased DR5 transcription. Nevertheless, our findings on R115777 as well as SCH66336 warrant further study on the relationship between protein farnesylation and DR5 modulation.

Preliminary results from clinical trials have shown that R115777 exhibits promising efficacy in hematologic malignancies with a favorable toxicity profile (8, 11). R115777, at a clinically achievable and safe concentration range (2–6 μmol/L; refs. 34–37), up-regulated

DR5 expression and induced cell surface DR5 distribution. Accordingly, we showed that the combination of a clinically achievable concentration of R115777 with TRAIL exhibited augmented effects on decreasing cell survival and inducing apoptosis (Fig. 4). Given that TRAIL is considered as a cancer-selective cytokine with cancer therapeutic potential and is being tested in phase I clinical trials, our current finding that R115777 enhances TRAIL-induced apoptosis clearly has translational significance in the clinic.

Some studies have shown that certain cancer therapeutic agents enhance TRAIL-induced apoptosis via down-regulation of c-FLIP expression (30–32, 40). In our study, we found that R115777 induced DR5 expression and cell surface distribution in all of the tested cell lines. However, it modulated c-FLIP expression in a cell line-dependent manner. R115777 even slightly increased c-FLIP levels in some cell lines (e.g., H157), whereas it decreased c-FLIP expression in other cell lines (e.g., H1792). Regardless of the differential modulation of c-FLIP expression, the combination of R115777 and TRAIL exerted augmented effects on decreasing cell survival and inducing apoptosis in these lung cancer cell lines, suggesting that it is unlikely for R115777 to enhance TRAIL-induced apoptosis via modulation of c-FLIP levels in certain cell lines in which c-FLIP levels are not decreased. Through

³ S.Y. Sun, X. Liu, W. Zou, P. Yue, A.I. Marcus, and F.R. Khuri, unpublished data.

silencing DR5 expression and blocking DR5 induction by R115777 using siRNA targeting DR5, our data clearly show that apoptosis induced by the combination of R115777 and TRAIL was substantially attenuated. This result thus indicates that R115777 enhances TRAIL-induced apoptosis primarily via up-regulation of DR5.

Our results show that the combination of R115777 and TRAIL augmented induction of apoptosis in H157 cells, in which c-FLIP levels were actually increased upon R115777 treatment. When FLIP_L expression was enforced to high levels in this cell line, either TRAIL alone or the combination of R115777 and TRAIL failed to induce apoptosis, indicating that FLIP_L overexpression indeed inhibits TRAIL/death receptor-mediated apoptosis. Therefore, we suggest that R115777-induced DR5 expression and cell surface distribution override c-FLIP up-regulation, leading to enhancement of TRAIL-induced apoptosis in cell lines where c-FLIP expression is high or increased by R115777. If this is correct, we assume that cell lines in which c-FLIP levels are reduced upon R115777 treatment (e.g., H1792) will be more susceptible than other cell lines where c-FLIP expression is increased or not altered by R115777 (e.g., H157) to apoptosis induction by the combination of R115777 and TRAIL as shown in Fig. 4A.

Among the tested lung cancer cell lines, A549 and H157 cell lines are the least sensitive to R115777-induced apoptosis even under low-serum culture condition (Fig. 1C). We noted that these two cell lines had relatively higher levels of c-FLIP compared with H1792 and H1299 cells (Fig. 6A), which are sensitive to R115777-induced apoptosis (Fig. 1C). Whether these results suggest that the levels of c-FLIP determine cell sensitivity to R115777-induced apoptosis needs to be investigated in the future.

In summary, we have shown that R115777 increases DR5 expression, induces DR5 distribution at the cell surface, and subsequently enhances TRAIL-induced apoptosis. These findings warrant clinical evaluation of the efficacy of R115777 and TRAIL in the treatment of human lung and other types of cancer in the future.

Acknowledgments

Received 11/1/2006; revised 1/19/2007; accepted 3/2/2007.

Grant support: Georgia Cancer Coalition Distinguished Cancer Scholar award (S.-Y. Sun) and Department of Defense grant W81XWH-04-1-0142-VITAL (S.-Y. Sun for Project 4).

The costs of publication of this article were defrayed in part by the payment of page charges. This article must therefore be hereby marked *advertisement* in accordance with 18 U.S.C. Section 1734 solely to indicate this fact.

References

- Ashkenazi A, Dixit VM. Death receptors: signaling and modulation. *Science* 1998;281:1305-8.
- Wajant H, Gerspach J, Pfizenmaier K. Tumor therapeutics by design: targeting and activation of death receptors. *Cytokine Growth Factor Rev* 2005;16:55-76.
- Almasan A, Ashkenazi A. Apo2L/TRAIL: apoptosis signaling, biology, and potential for cancer therapy. *Cytokine Growth Factor Rev* 2003;14:337-48.
- Kelley SK, Ashkenazi A. Targeting death receptors in cancer with Apo2L/TRAIL. *Curr Opin Pharmacol* 2004;4:333-9.
- Wu GS, Burns TF, McDonald ER III, et al. KILLER/DR5 is a DNA damage-inducible p53-regulated death receptor gene. *Nat Genet* 1997;17:141-3.
- Debatin KM, Krammer PH. Death receptors in chemotherapy and cancer. *Oncogene* 2004;23:2950-66.
- Sheikh MS, Huang Y. Death receptors as targets of cancer therapeutics. *Curr Cancer Drug Targets* 2004;4:97-104.
- Basso AD, Kirschmeier P, Bishop WR. Thematic review series: lipid posttranslational modifications. Farnesyl transferase inhibitors. *J Lipid Res* 2006;47:15-31.
- Sebti SM, Adjei AA. Farnesyltransferase inhibitors. *Semin Oncol* 2004;31:28-39.
- Brunner TB, Hahn SM, Gupta AK, et al. Farnesyltransferase inhibitors: an overview of the results of preclinical and clinical investigations. *Cancer Res* 2003;63:5656-68.
- Jabbour E, Kantarjian H, Cortes J. Clinical activity of farnesyl transferase inhibitors in hematologic malignancies: possible mechanisms of action. *Leuk Lymphoma* 2004;45:2187-95.
- End DW, Smets G, Todd AV, et al. Characterization of the antitumor effects of the selective farnesyl protein transferase inhibitor R115777 *in vivo* and *in vitro*. *Cancer Res* 2001;61:131-7.
- Le Gouill S, Pellat-Deceunynck C, Harousseau JL, et al. Farnesyl transferase inhibitor R115777 induces apoptosis of human myeloma cells. *Leukemia* 2002;16:1664-7.
- Ochiai N, Uchida R, Fuchida S, et al. Effect of farnesyl transferase inhibitor R115777 on the growth of fresh and cloned myeloma cells *in vitro*. *Blood* 2003;102:3349-53.
- Beaupre DM, Cepero E, Obeng EA, Boise LH, Lichtenheld MG. R115777 induces Ras-independent apoptosis of myeloma cells via multiple intrinsic pathways. *Mol Cancer Ther* 2004;3:179-86.
- Kelland LR, Smith V, Valenti M, et al. Preclinical antitumor activity and pharmacodynamic studies with the farnesyl protein transferase inhibitor R115777 in human breast cancer. *Clin Cancer Res* 2001;7:3544-50.
- Yanamandra N, Colaco NM, Parquet NA, et al. Tipifarnib and bortezomib are synergistic and overcome cell adhesion-mediated drug resistance in multiple myeloma and acute myeloid leukemia. *Clin Cancer Res* 2006;12:591-9.
- Zhu K, Gerbino E, Beaupre DM, et al. Farnesyltransferase inhibitor R115777 (Zarnestra, tipifarnib) synergizes with paclitaxel to induce apoptosis and mitotic arrest and to inhibit tumor growth of multiple myeloma cells. *Blood* 2005;105:4759-66.
- Caraglia M, Giuberti G, Marra M, et al. Docetaxel induces p53-dependent apoptosis and synergizes with farnesyl transferase inhibitor R115777 in human epithelial cancer cells. *Front Biosci* 2005;10:2566-75.
- Gunning WT, Kramer PM, Lubet RA, et al. Chemoprevention of benzo(a)pyrene-induced lung tumors in mice by the farnesyltransferase inhibitor R115777. *Clin Cancer Res* 2003;9:1927-30.
- Liu X, Yue P, Schonthal AH, Khuri FR, Sun SY. Cellular FLICE-inhibitory protein down-regulation contributes to celecoxib-induced apoptosis in human lung cancer cells. *Cancer Res* 2006;66:1115-9.
- Sun SY, Yue P, Wu GS, et al. Mechanisms of apoptosis induced by the synthetic retinoid CD437 in human non-small cell lung carcinoma cells. *Oncogene* 1999;18:2357-65.
- Liu X, Yue P, Zhou Z, Khuri FR, Sun SY. Death receptor regulation and celecoxib-induced apoptosis in human lung cancer cells. *J Natl Cancer Inst* 2004;96:1769-80.
- Pfahl M, Tzukerman M, Zhang XK, et al. Nuclear retinoic acid receptors: cloning, analysis, and function. *Methods Enzymol* 1990;189:256-70.
- Sun SY, Yue P, Hong WK, Lotan R. Induction of Fas expression and augmentation of Fas/Fas ligand-mediated apoptosis by the synthetic retinoid CD437 in human lung cancer cells. *Cancer Res* 2000;60:6537-43.
- Sun SY, Zhou Z, Wang R, Fu H, Khuri FR. The farnesyltransferase inhibitor lonafarnib induces growth arrest or apoptosis of human lung cancer cells without down-regulation of Akt. *Cancer Biol Ther* 2004;3:1092-8; discussion 9-101.
- Sun SY, Yue P, Dawson MI, et al. Differential effects of synthetic nuclear retinoid receptor-selective retinoids on the growth of human non-small cell lung carcinoma cells. *Cancer Res* 1997;57:4931-9.
- Sun SY, Yue P, Shroot B, Hong WK, Lotan R. Induction of apoptosis in human non-small cell lung carcinoma cells by the novel synthetic retinoid CD437. *J Cell Physiol* 1997;173:279-84.
- Wajant H. Targeting the FLICE inhibitory protein (FLIP) in cancer therapy. *Mol Interv* 2003;3:124-7.
- Chawla-Sarkar M, Bae SI, Reu FJ, et al. Down-regulation of Bcl-2, FLIP or IAPs (XIAP and survivin) by siRNAs sensitizes resistant melanoma cells to Apo2L/TRAIL-induced apoptosis. *Cell Death Differ* 2004;11:915-23.
- Hyer ML, Croxton R, Krajewska M, et al. Synthetic triterpenoids cooperate with tumor necrosis factor-related apoptosis-inducing ligand to induce apoptosis of breast cancer cells. *Cancer Res* 2005;65:4799-808.
- Kim Y, Suh N, Sporn M, Reed JC. An inducible pathway for degradation of FLIP protein sensitizes tumor cells to TRAIL-induced apoptosis. *J Biol Chem* 2002;277:22320-9.
- Olsson A, Diaz T, Aguilar-Santelises M, et al. Sensitization to TRAIL-induced apoptosis and modulation of FLICE-inhibitory protein in B chronic lymphocytic leukemia by actinomycin D. *Leukemia* 2001;15:1868-77.
- Zujewski J, Horak ID, Bol CJ, et al. Phase I and pharmacokinetic study of farnesyl protein transferase inhibitor R115777 in advanced cancer. *J Clin Oncol* 2000;18:927-41.
- Crul M, de Klerk GJ, Swart M, et al. Phase I clinical and pharmacologic study of chronic oral administration of the farnesyl protein transferase inhibitor R115777 in advanced cancer. *J Clin Oncol* 2002;20:2726-35.
- Karp JE, Lancet JE, Kaufmann SH, et al. Clinical and biologic activity of the farnesyltransferase inhibitor R115777 in adults with refractory and relapsed acute leukemias: a phase 1 clinical-laboratory correlative trial. *Blood* 2001;97:3361-9.
- Widemann BC, Salzer WL, Arceri RJ, et al. Phase I trial and pharmacokinetic study of the farnesyltransferase inhibitor tipifarnib in children with refractory solid tumors or neurofibromatosis type I and plexiform neurofibromas. *J Clin Oncol* 2006;24:507-16.
- Du W, Liu A, Prendergast GC. Activation of the PI3K-AKT pathway masks the proapoptotic effects of farnesyltransferase inhibitors. *Cancer Res* 1999;59:4208-12.
- Jiang K, Coppola D, Crespo NC, et al. The phosphoinositide 3-OH kinase/AKT2 pathway as a critical target for farnesyltransferase inhibitor-induced apoptosis. *Mol Cell Biol* 2000;20:139-48.
- Longley DB, Wilson TR, McEwan M, et al. c-FLIP inhibits chemotherapy-induced colorectal cancer cell death. *Oncogene* 2006;25:838-48.

The Farnesyltransferase Inhibitor Lonafarnib Induces CCAAT/Enhancer-binding Protein Homologous Protein-dependent Expression of Death Receptor 5, Leading to Induction of Apoptosis in Human Cancer Cells^{*[5]}

Received for publication, December 13, 2006, and in revised form, May 8, 2007. Published, JBC Papers in Press, May 9, 2007, DOI 10.1074/jbc.M611438200

Shi-Yong Sun^{1,2}, Xiangguo Liu, Wei Zou, Ping Yue, Adam I. Marcus, and Fadlo R. Khuri¹

From the Department of Hematology and Oncology, Winship Cancer Institute, Emory University School of Medicine, Atlanta, Georgia 30322

Pre-clinical studies have demonstrated that farnesyltransferase inhibitors (FTIs) induce growth arrest or apoptosis in various human cancer cells independently of Ras mutations. However, the underlying mechanism remains unknown. Death receptor 5 (DR5) is a pro-apoptotic protein involved in mediating the extrinsic apoptotic pathway. Its role in FTI-induced apoptosis has not been reported. In this study, we investigated the modulation of DR5 by the FTI lonafarnib and the involvement of DR5 up-regulation in FTI-induced apoptosis. Lonafarnib activated caspase-8 and its downstream caspases, whereas the caspase-8-specific inhibitor benzyloxycarbonyl-Ile-Glu(methoxy)-Thr-Asp(methoxy)-fluoromethyl ketone or small interfering RNA abrogated lonafarnib-induced apoptosis, indicating that lonafarnib induces caspase-8-dependent apoptosis. Lonafarnib up-regulated DR5 expression, increased cell-surface DR5 distribution, and enhanced tumor necrosis factor-related apoptosis-inducing ligand-induced apoptosis. Overexpression of a dominant-negative Fas-associated death domain mutant or silencing of DR5 expression using small interfering RNA attenuated lonafarnib-induced apoptosis. These results indicate a critical role of the DR5-mediated extrinsic apoptotic pathway in lonafarnib-induced apoptosis. By analyzing the DR5 promoter, we found that lonafarnib induced a CCAAT/enhancer-binding protein homologous protein (CHOP)-dependent transactivation of the DR5 promoter. Lonafarnib increased CHOP expression, whereas silencing of CHOP expression abrogated lonafarnib-induced DR5 expression. These results thus indicate that lonafarnib induces CHOP-dependent DR5 up-regulation. We conclude that CHOP-dependent DR5 up-regulation contributes to lonafarnib-induced apoptosis.

Farnesyltransferase inhibitors (FTIs)³ are a class of agents that suppress the farnesyltransferase enzyme to prevent farnesylation of certain proteins such as the Ras oncoprotein (1, 2). These agents inhibit proliferation and induce apoptosis in various cancer cell lines in culture or suppress the growth of xenografts in nude mice with limited toxicity (1, 2). In the clinic, FTIs are well tolerated and have some positive outcomes in certain settings such as hematological malignancies and breast cancer, although the response rates to FTIs alone are generally poor. When combined with other therapeutic agents or radiotherapy, FTIs exhibit some encouraging clinical responses (1, 2).

Lonafarnib (LNF; also called SCH66336 and Sarasar), a non-peptide tricyclic FTI, was one of the first FTIs to undergo clinical testing and to exhibit significant activity (3). *In vitro*, this agent, either alone or in combination with other therapeutic agents, inhibits the growth or induces apoptosis of several types of human cancer cells (4–12). In animal models, LNF demonstrates potent oral activity in a wide array of human tumor xenograft models including tumors of colon, lung, pancreas, prostate, and urinary bladder origin (12). When LNF is combined with other chemotherapeutic agents, enhanced antitumor activity is observed (4, 6). In a phase I trial enrolling individuals with lung or aerodigestive tract cancer, a provocative clinical activity was observed when LNF was combined with paclitaxel (13). In a recent phase II trial, LNF plus paclitaxel achieved significant clinical activity with a favorable safety profile in patients with taxane-refractory/resistant metastatic non-small cell lung cancer (14), and these results were later supported by pre-clinical data in cell lines (15).

There are two major apoptotic pathways: one involves death signals transduced through death receptors (extrinsic apoptotic pathway), and the other relies on mitochondrial signals (intrinsic apoptotic pathway) (16). Both pathways are involved in an ordered activation of a set of caspases, which in turn cleave cellular substrates, leading to apoptosis. The activation of caspase-8 and caspase-9 has been documented to play a central

^{*} This work was supported by a Georgia Cancer Coalition Distinguished Cancer Scholar award (to S.-Y. S.) and by Department of Defense TARGET Grant DAMD 17-02-1-0706 (to F. R. K. for Project 6) and VITAL Grant W81XWH-04-1-0142 (to S.-Y. S. for Project 4). The costs of publication of this article were defrayed in part by the payment of page charges. This article must therefore be hereby marked "advertisement" in accordance with 18 U.S.C. Section 1734 solely to indicate this fact.

^[5] The on-line version of this article (available at <http://www.jbc.org>) contains supplemental Figs. S1–S3.

¹ Georgia Cancer Coalition Distinguished Cancer Scholars.

² To whom correspondence should be addressed: Winship Cancer Inst., Emory University School of Medicine, 1365-C Clifton Rd., C3088, Atlanta, GA 30322. Tel.: 404-778-2170; Fax: 404-778-5520; E-mail: shi-yong.sun@emoryhealthcare.org.

³ The abbreviations used are: FTIs, farnesyltransferase inhibitors; LNF, lonafarnib; TRAIL, tumor necrosis factor-related apoptosis-inducing ligand; DR5, death receptor 5; CHOP, CCAAT/enhancer-binding protein homologous protein; ER, endoplasmic reticulum; OMe, methoxy; RasGAP, Ras GTPase-activating protein; FADDm, Fas-associated death domain mutant; FBS, fetal bovine serum; PE, phycoerythrin; PIPES, 1,4-piperazinediethanesulfonic acid; siRNA, small interfering RNA.

role in mediating apoptosis signaled by death receptors and by mitochondria, respectively; however, caspase-8 can activate the caspase-9-mediated apoptotic pathway by activating or cleaving Bid protein (16).

The tumor necrosis factor-related apoptosis-inducing ligand (TRAIL) receptor, death receptor 5 (DR5; also named Apo2, TRAIL receptor 2, TRICK2, or Killer/DR5), belongs to the tumor necrosis factor receptor gene superfamily, the members of which all share a similar cysteine-rich extracellular domain and an additional cytoplasmic death domain (17). DR5 localizes to the cell surface, becomes activated or oligomerized (trimerized) upon binding to its ligand TRAIL or through overexpression, and then signals an apoptotic response through caspase-8-mediated rapid activation of caspase cascades (17). DR5 has recently attracted more attention because its ligand TRAIL preferentially induces apoptosis in transformed or malignant cells, demonstrating potential as a tumor-selective apoptosis-inducing cytokine for cancer treatment (18, 19). Certain cancer therapeutic agents induce the expression of DR5 in various types of cancer cells and thus are able to augment TRAIL-induced apoptosis or to initiate apoptosis (20).

The CCAAT/enhancer-binding protein homologous protein (CHOP), also known as GADD153 (growth arrest and DNA damage gene 153), is an endoplasmic reticulum (ER) stress-induced transcription factor involved in the regulation of apoptosis, particularly ER stress-associated apoptosis (21). Recent studies have demonstrated that CHOP directly regulates DR5 expression through a CHOP-binding site in the 5'-flanking region of the DR5 gene (22, 23). Certain drugs induce DR5 expression through CHOP-dependent transactivation of the DR5 gene (22–24).

The mechanisms underlying FTI-mediated growth arrest and apoptosis induction are largely undefined (1). Several non-Ras targets such as RhoB and Rab geranylgeranyltransferase have been proposed (25, 26). In addition, Akt inactivation appears to play a role in apoptosis induced by a subset of FTIs (5, 27, 28), although some studies have been unable to demonstrate this role (29–31). However, DR5 has not been suggested to be involved in the biological actions of FTIs. In this study, we reveal, for the first time, a novel mechanism in human cancer cells by which FTIs, particularly LNF, induce apoptosis via the CHOP-dependent up-regulation of DR5 expression and subsequent caspase-8 activation.

EXPERIMENTAL PROCEDURES

Reagents—LNF and its analog SCH66337 were provided by Schering-Plough Research Institute (Kenilworth, NJ). They were dissolved in Me₂SO at a concentration of 10 mM, and aliquots were stored at –80 °C. Stock solutions were diluted to the desired final concentrations with growth medium just before use. Soluble human recombinant TRAIL was purchased from BIOMOL International (Plymouth Meeting, PA). The caspase inhibitors benzyloxycarbonyl-Val-Ala-Asp-fluoromethyl ketone and benzyloxycarbonyl-Ile-Glu(OMe)-Thr-Asp(OMe)-fluoromethyl ketone were purchased from Enzyme System Products (Livermore, CA). Staurosporine and other chemicals were purchased from Sigma. Rabbit polyclonal anti-DR5 antibody was purchased from ProSci Inc. (Poway, CA).

Role of DR5 Up-regulation in FTI-induced Apoptosis

Mouse monoclonal anti-caspase-3 antibody was purchased from Imgenex (San Diego, CA). Rabbit polyclonal anti-caspase-9, anti-caspase-8, and anti-poly(ADP-ribose) polymerase antibodies were purchased from Cell Signaling Technology, Inc. (Beverly, MA). Mouse monoclonal anti-Ras GTPase-activating protein (RasGAP) antibody B4F8 was purchased from Santa Cruz Biotechnology, Inc. (Santa Cruz, CA). Mouse monoclonal anti-HDJ-2 antibody (clone KA2A5.6) was purchased from Lab Vision Corp. (Fremont, CA). Mouse monoclonal anti-BiP/GRP78 antibody was purchased from BD Transduction Laboratories.

Cell Lines and Cell Cultures—All cell lines were purchased from American Type Culture Collection (Manassas, VA). H460 cell lines stably expressing a dominant-negative Fas-associated death domain mutant (FADDm) were described previously (32). These cell lines were grown in monolayer culture in RPMI 1640 medium supplemented with glutamine and 5% fetal bovine serum (FBS) at 37 °C in a humidified atmosphere consisting of 5% CO₂ and 95% air.

Western Blot Analysis—The procedures for preparation of whole cell protein lysates and Western blot analysis were described previously (32, 33).

Detection of DR5 mRNA Expression—DR5 mRNA was detected by reverse transcription-PCR as follows. Total RNA was isolated from cells using TriReagent (Sigma) as instructed by the manufacturer. First-strand cDNA was synthesized from 2 µg of total RNA in a volume of 20 µl containing 1 µl of avian myeloblastosis virus reverse transcriptase, 0.5 µl of dNTP (25 mM each), 0.5 µl of random primer (0.5 µg/µl), 4 µl of 5× reverse transcription buffer, and sterile H₂O, followed by incubation at 42 °C for 60 min and inactivation by heating at 70 °C for 15 min. cDNA was then amplified by PCR using the following primers: DR5, 5'-GACCTAGCTCCCCAGCAGAG-3' (sense) and 5'-CGGCTGCAACTGTGACTCTAT-3' (antisense); and β-actin, 5'-GAACTACCTTCACTCCATC-3' (sense) and 5'-CTAGAAGCATTTCGGTGGACGATGGAGGGGCC-5' (antisense). The 25-µl amplification mixture contained 2 µl of cDNA, 0.5 µl of dNTP (25 mM each), 1 µl each of the sense and antisense primers (20 µM each), 1 µl of Taq DNA polymerase (5 units/µl; Promega, Madison, MI), 2.5 µl of 10× reaction buffer, and sterile H₂O. PCR was performed for 28 cycles. After an initial step at 95 °C for 3 min, each cycle consisted of 50 s of denaturation at 94 °C, 50 s of annealing at 58 °C, and 55 s of extension at 72 °C. This was followed by an additional extension step at 72 °C for 10 min. The housekeeping gene β-actin was also amplified as an internal reference. PCR products were resolved by electrophoresis on a 4% agarose gel, stained, and directly visualized under UV illumination.

Construction of DR5 Reporter Plasmid, Transient Transfection, and Luciferase Activity Assay—The plasmid containing a 5'-flanking region of the DR5 gene was kindly provided by Dr. G. S. Wu (Wayne State University School of Medicine, Detroit, MI). We used this plasmid as a template to amplify a series of deletion fragments of the 5'-flanking region of the DR5 gene ranging from 3070 to 120 bp upstream of the translation start site by PCR and then subcloned these fragments into the pGL3-Basic reporter vector (Promega) through KpnI and

Role of DR5 Up-regulation in FTI-induced Apoptosis

BglII restriction sites. In the PCR amplification, the reverse primer 5'-CTTAAGATCTGGCGGTAGGGAACGCTCTT-ATAGTC-3' was used to make all deletion constructs. The upstream primers used were 5'-CTTAGGTACCTGGCTC-GTCTGTTCTCTACGGCCCC-3' (-3070), 5'-CTTAGG-TACCTCAACTCATTTCCTCCCAAGTTTC-3' (-420), 5'-CTTAGGTACCAACCCAGAAACAAACCACAGCCCGGG-3' (-373), 5'-CTTAGGTACCTTATTTATTGTCACCAACCTGTGG-3' (-240), and 5'-CTTAGGTACCGACGCGG-CCGGAGAACCCC-3' (-120). These constructs were named pGL3-DR5(-3070), pGL3-DR5(-420), pGL3-DR5(-373), pGL3-DR5(-240), and pGL3-DR5(-120), respectively. The reporter constructs containing a 552-bp 5'-flanking region of the DR5 gene with a wild-type or mutated CHOP-binding site, an NF- κ B-binding site, or an Elk-binding site were generously provided by Dr. H.-G. Wang (University of South Florida College of Medicine, Tampa, FL) (22). In this study, we also used the pGL3-Promoter luciferase vector (pGL3-SV40-Luc; Promega), which contains an SV40 promoter, as a control. A pCH110 plasmid encoding β -galactosidase (GE Healthcare) was used in the cotransfection for normalization. These plasmids were purified with a Qiafilter plasmid maxi kit (Qiagen Inc.).

To examine the effect of LNF on DR5 transactivation activity, cells were seeded in 24-well plates and cotransfected with the given reporter plasmid (0.5 μ g/well) and the pCH110 plasmid (0.2 μ g/well) using FuGENE 6 transfection reagent (3:1 ratio; Roche Applied Science) following the manufacturer's protocol. Twenty-four hours later, the cells were treated with LNF. After 12 h, the cells were lysed and subjected to luciferase activity assay using a luciferase assay system (Promega) in a luminometer. Relative luciferase activity was normalized to β -galactosidase activity, which was measured as described previously (34).

Detection of Cell-surface DR5—In this study, cell-surface DR5 expression was analyzed by both flow cytometry and immunofluorescent staining. The procedure for direct antibody staining and subsequent flow cytometric analysis of cell-surface protein was described previously (35). The mean fluorescent intensity that represents antigenic density on a per cell basis was used to represent DR5 expression levels. Phycoerythrin (PE)-conjugated mouse monoclonal anti-human DR5 (clone DJR2-4), anti-human DR4 (clone DJR1), anti-human decoy receptor 1 (clone DJR3), anti-human decoy receptor 2 (clone DJR4-1), and anti-human Fas (clone DX2) antibodies and PE-conjugated mouse IgG1 isotype control (MOPC21/P3) were purchased from eBioscience (San Diego, CA). For immunofluorescent staining, cells were plated overnight on coverslips in 24-well plates and treated with different concentrations of LNF. Cells were then fixed in 68 mM PIPES, 25 mM HEPES, 15 mM EGTA, and 3 mM MgCl₂ with 3.7% formaldehyde, 0.05% glutaraldehyde, and 0.5% Triton X-100 for 10 min; washed three times with phosphate-buffered saline; and then blocked for 15 min with 10% normal goat serum. Next, cells were incubated with PE-conjugated mouse monoclonal anti-DR5 antibody (clone DJR2-4) diluted 1:15 in 5% normal goat serum for 1 h at room temperature. After the cells were washed three times, coverslips were removed from wells, inverted, and placed on slides. Images were acquired using a \times 63 Zeiss Plan-Apoc-

hromat oil lens (numerical aperture = 1.4) mounted on a Zeiss LMS 510 confocal laser scanning microscope.

Detection of Apoptosis—The amounts of cytoplasmic histone-associated DNA fragments (mono- and oligonucleosomes) formed during apoptosis were measured using a Cell Death Detection ELISA^{plus} kit (Roche Applied Science) according to the manufacturer's instructions. Caspase activation and substrate cleavage were detected by Western blot analysis as described above. In addition, we also counted floating cells in the medium as another indicator of apoptotic cell death. Because the albumin in the serum attenuates the FTI effect in culture (31), we performed these experiments in 0.1% serum-containing medium to increase induction of apoptosis.

Cell Survival Assay—Cells were seeded in 96-well cell culture plates and treated on the 2nd day with the indicated agents. At the end of treatment, the cell number was estimated by the sulforhodamine B assay as described previously (36).

Small Interfering RNA (siRNA)-mediated Gene Silencing—High purity control (non-silencing) siRNA oligonucleotides that target sequence 5'-AATTCTCCGAACGTGTCACGT-3' was purchased from Qiagen Inc. Caspase-8, DR5, and CHOP siRNA duplexes that target sequences 5'-AACTACCAGAAA-GGTATACCT-3', 5'-AAGACCCCTGTGCTCGTTGTC-3' (32, 37), and 5'-AAGAACCAGCAGAGGUCACAA-3' (22), respectively, were synthesized by Qiagen Inc. The additional DR5 siRNA-2, which targets sequence 5'-AAGTTGCAGCCG-TAGTCTTGA-3' (22), was also synthesized by Qiagen Inc. Transfection of siRNA was performed as described previously (32). Gene silencing effects and caspase activation were evaluated by Western blot analysis, whereas DNA fragmentation was measured using the Cell Death Detection ELISA^{plus} kit as described above.

Statistical Analysis—Cell survival and apoptosis (*i.e.* DNA fragmentation) between two groups were analyzed with two-sided unpaired Student's *t* tests when the variances were equal or with Welch's corrected *t* test when the variances were not equal using GraphPad InStat Version 3 software. The assumption for use of the *t* tests was calculated and suggested by the same software. All means \pm S.D. from triplicate or quadruplicate samples were calculated with Microsoft Excel Version 5.0 software. In all statistical analyses, results were considered to be statistically significant at *p* < 0.05.

RESULTS

LNF Induces Caspase-8-dependent Apoptosis—Our previous study has shown that LNF induces apoptosis, particularly in low serum culture medium (31). Here, we examined further the effects of LNF on caspase activation and its involvement in LNF-induced apoptosis in human lung cancer cells. In both H157 and H1792 human lung cancer cell lines, LNF decreased the levels of the proforms of caspase-8, -9, and -3; increased the levels of their cleaved forms; and induced cleavage of poly(ADP-ribose) polymerase and RasGAP, both of which are caspase-3 substrates (38), in a concentration-dependent manner (Fig. 1A). These results indicate that LNF activates both caspase-8- and caspase-9-mediated activation of caspase cascades. Because caspase-8 activation is a critical event in the extrinsic apoptotic signaling pathway, we tested

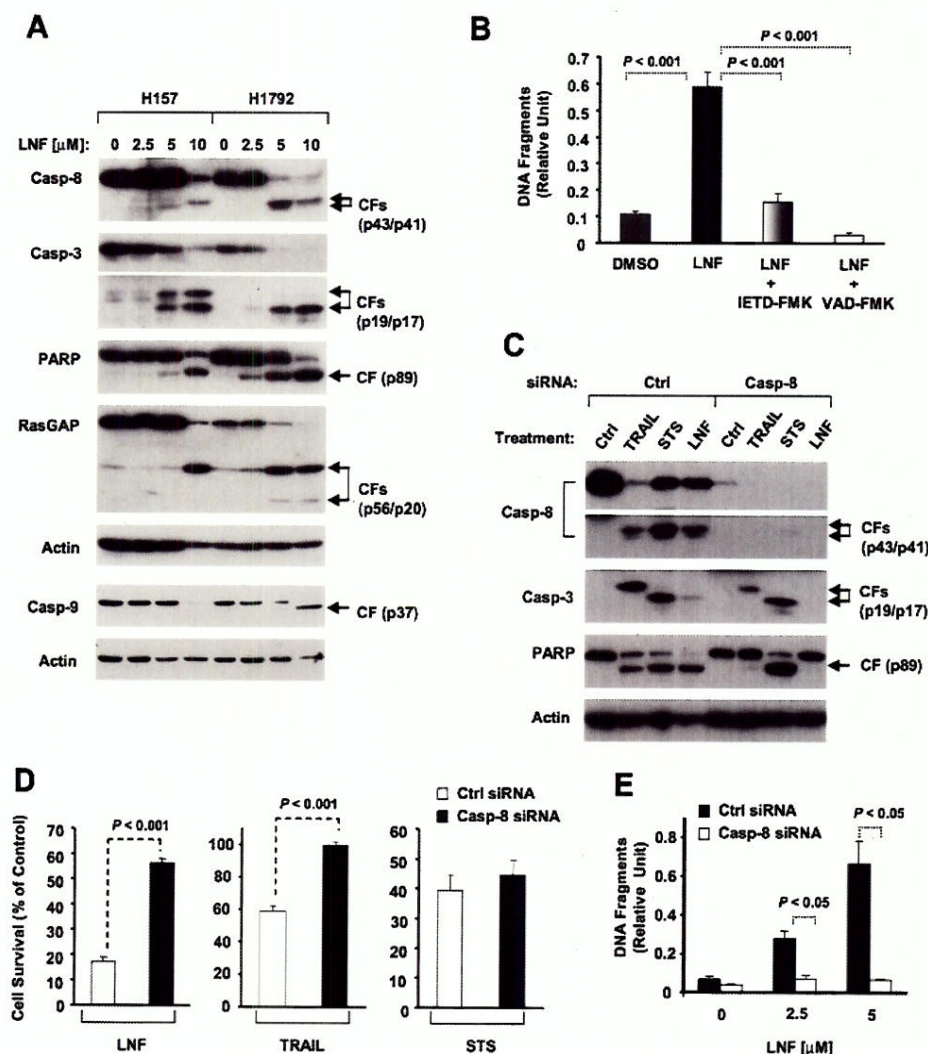


FIGURE 1. LNF induces caspase-8-mediated apoptosis. A, LNF induces caspase activation. The indicated lung cancer cell lines were treated with the indicated concentrations of LNF in 0.1% FBS for 24 h. Whole cell protein lysates were then prepared from these cell lines and subjected to detection of cleavage of caspase (Casp)-8, caspase-9, caspase-3, RasGAP, and poly(ADP-ribose) polymerase (PARP) by Western blot analysis. Actin expression was used as a loading control. CFs, cleaved forms. B, suppression of LNF-induced DNA fragmentation by caspase inhibitors. H1792 cells were pretreated with 50 μ M caspase inhibitors as indicated and then cotreated with the given caspase inhibitor and 5 μ M LNF in 0.1% FBS. After 24 h, the cells were subjected to estimation of DNA fragmentation using the Cell Death Detection ELISA^{plus} kit. Data are the means \pm S.D. of three identical wells. DMSO, Me₂SO; IETD-FMK, benzoyloxycarbonyl-Ile-Glu(OMe)-Thr-Asp(OMe)-fluoromethyl ketone; VAD-FMK, benzoyloxycarbonyl-Val-Ala-Asp-fluoromethyl ketone. C and D, silencing of caspase-8 expression (C) decreases cell sensitivity to LNF-induced cell death (D) and inhibits LNF-induced caspase activation (C). H1792 cells were seeded in a 24-well cell culture plate and transfected with control (Ctrl) or caspase-8 siRNA. After 48 h, the cells were treated with the Me₂SO control (Ctrl), 7.5 μ M LNF, 40 ng/ml TRAIL, or 0.5 μ M staurosporine (STS) in 0.1% fetal calf serum for 24 h. The cells were then subjected to preparation of whole cell protein lysates and subsequent Western blot analysis (C). In addition, cells were also seeded in 96-well plates and treated with the solvent control, 7.5 μ M LNF, 80 ng/ml TRAIL, or 0.25 μ M staurosporine. After 24 h, the cell numbers were estimated using the sulforhodamine B assay (D). Data are the means \pm S.D. of four identical wells. E, silencing of caspase-8 expression abrogates LNF-induced DNA fragmentation. H1792 cells were seeded in a 24-well cell culture plate and transfected twice with control or caspase-8 siRNA in a 48-h interval. Forty hours later after the second transfection, the cells were treated with the indicated concentrations of LNF in 0.1% FBS for 24 h and then subjected to evaluation of DNA fragmentation using the Cell Death Detection ELISA^{plus} kit. Data are the means \pm S.D. of three identical wells.

whether caspase-8 activation is required for LNF-induced apoptosis. LNF significantly increased the amount of DNA fragments ($p < 0.001$), but in the presence of the pan-caspase inhibitor benzoyloxycarbonyl-Val-Ala-Asp-fluoromethyl ketone or the caspase-8 inhibitor benzoyloxycarbonyl-Ile-Glu(OMe)-Thr-Asp(OMe)-fluoromethyl ketone, LNF failed to increase the levels of DNA fragments ($p < 0.001$) (Fig. 1B),

siRNA-transfected cells (Fig. 1C).

LNF Induces DR5 Expression—Because caspase-8 activation is an essential step in the extrinsic death receptor-mediated apoptotic pathway, we next tested whether LNF affects the expression of death receptors. By Western blot analysis, we found that LNF increased DR5 expression in a time- and concentration-dependent manner (Fig. 2, A and B). Specifically,

indicating that LNF-induced apoptosis is caspase-dependent, particularly caspase-8-dependent. To further demonstrate the importance of caspase-8 activation in LNF-induced apoptosis, we silenced the expression of caspase-8 and then examined its impact on LNF-induced apoptosis. As shown in Fig. 1C, caspase-8 levels were dramatically decreased in H1792 cells transfected with the caspase-8 siRNA in comparison with caspase-8 levels in those cells transfected with the control siRNA. By measuring cell survival, we found that LNF caused significantly less cell death in caspase-8 siRNA-transfected cells than in control siRNA-transfected cells (Fig. 1D). Accordingly, we detected cleaved forms of caspase-8, caspase-3, and poly(ADP-ribose) polymerase (Fig. 1C) and increased amounts of DNA fragments (Fig. 1E) in control siRNA-transfected cells but not in caspase-8 siRNA-transfected cells after exposure to LNF. These results clearly indicate that silencing of caspase-8 expression inhibits LNF-induced apoptosis, further supporting the essential role of caspase-8 activation in LNF-induced apoptosis. Used as control treatments, TRAIL, a cytokine known to trigger the extrinsic apoptotic pathway, failed to decrease cell survival (Fig. 1D) and exhibited attenuated effects on the cleavage of caspase-8, caspase-3, and poly(ADP-ribose) polymerase (Fig. 1C) in caspase-8 siRNA-transfected cells, whereas staurosporine, a small molecule known to induce apoptosis through the mitochondrial apoptotic pathway, was equally active in inducing cell death (Fig. 1D) and cleavage of caspase-3 and poly(ADP-ribose) polymerase in both control and caspase-8 siRNA-transfected cells, although caspase-8 cleavage was inhibited in caspase-8

Role of DR5 Up-regulation in FTI-induced Apoptosis

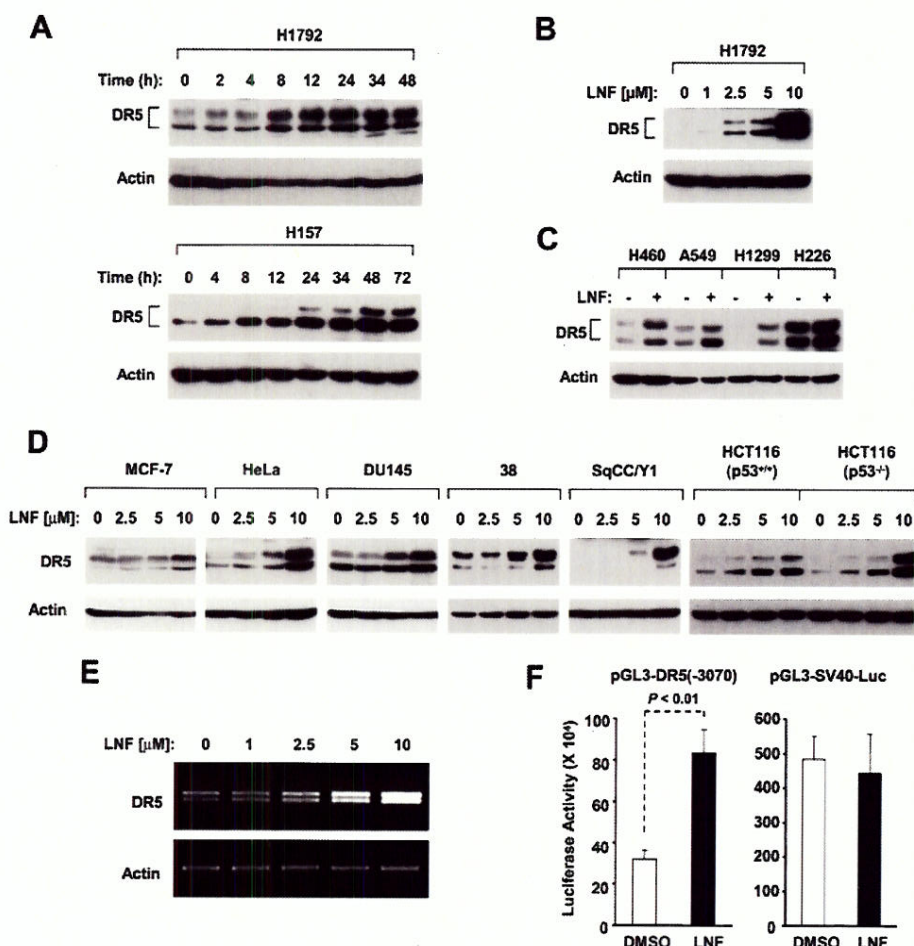


FIGURE 2. LNF increases DR5 expression at both the protein (A–D) and mRNA (E and F) levels in human cancer cells. A, the indicated cell lines were treated with 5 μ M LNF for the indicated times. B, H1792 cells were treated with the indicated concentrations of LNF for 24 h. C, the indicated human lung cancer cell lines were treated with 5 μ M LNF for 16 h. D, the indicated cell lines were treated with the given concentrations of LNF for 16 h. Whole cell protein lysates were then prepared from the aforementioned treatments for detection of DR5 expression by Western blot analysis. E, H1792 cells were exposed to the indicated concentrations of LNF for 8 h. Cellular total RNA was then prepared for detection of DR5 mRNA by reverse transcription-PCR. Actin levels were used as an internal control. F, H1792 cells were transiently transfected with pGL3-DR5(–3070) or pGL3-SV40-Luc for 24 h and then treated with Me₂SO (DMSO) or 10 μ M LNF for an additional 12 h. The cells were subjected to a luciferase assay. Data are the means \pm S.D. of three identical determinants.

LNF-induced DR5 expression occurred at 8 h, reached a peak at 24 h (H1792 cells) or 48 h (H157 cells), and was sustained up to 48 h (H1792 cells) or 72 h (H157 cells) post-LNF treatment (Fig. 2A). The highest levels of DR5 expression were observed with 10 μ M LNF; however, 2.5 μ M LNF was sufficient to increase DR5 expression relative to untreated cells (Fig. 2B). Therefore, it appears that, at clinically achievable and tolerable concentrations (2–5 μ M) (39, 40), LNF induces rapid but sustained up-regulation of DR5 expression. Moreover, we found that LNF also increased DR5 expression in other human lung cancer cell lines, as shown in Fig. 2C, as well as in other types of cancer cell lines, including breast (MCF-7), cervical (HeLa), prostate (DU145), head and neck (38 and SqCC/Y1), and colon (HCT116) (Fig. 2D). We also compared the effects of LNF on DR5 induction in HCT116(p53^{+/+}) and HCT116(p53^{-/-}) cell lines and found that LNF up-regulated DR5 expression in both cell lines (Fig. 2D). These findings indicate that DR5 induction by LNF commonly occurs in human cancer cells. We noted that LNF also increased DR4 expression; however, it did not occur in

all tested cell lines (data not shown). Thus, we focused our subsequent studies on DR5 induction.

To determine whether DR5 induction by LNF occurs at the transcriptional level, we detected DR5 mRNA levels in cells exposed to different concentrations of LNF using reverse transcription-PCR. As shown in Fig. 2E, LNF at concentrations ranging from 2.5 to 10 μ M increased DR5 mRNA levels in a concentration-dependent manner. Moreover, we examined the effect of LNF on DR5 promoter activity and observed that LNF significantly increased luciferase activity in cells transfected with a luciferase reporter plasmid carrying a DR5 5'-flanking region (*i.e.* pGL3-DR5(–3070)), but not in cells transfected with a reporter plasmid driven by the SV40 promoter (*i.e.* pGL3-SV40-Luc) (Fig. 2F), indicating that LNF enhances DR5 transactivation. Collectively, these results clearly show that LNF up-regulates DR5 expression at the transcriptional level.

LNF Increases Cell-surface DR5 Levels—It is known that DR5 functions as a cell-surface protein (17). Thus, we were interested in determining whether LNF increases cell-surface DR5 levels. In this study, we treated cells with LNF, stained the cells with PE-conjugated anti-DR5 antibody, and analyzed PE-positive cells by flow cytometry and confocal

microscopy. By flow cytometry, we detected a dramatic increase in fluorescent intensity in both H1792 and H157 cells treated with LNF compared with cells exposed to the Me₂SO control (Fig. 3A). The mean fluorescent intensities were 22.82, 60.01, and 142.71 in H1792 cells treated with the Me₂SO control, 5 μ M LNF, and 10 μ M LNF, respectively, and 29.44, 67.70, and 109.96 in H157 cells, respectively. By confocal microscopy, we observed low levels of cytoplasmic DR5 protein in control cells without cell-surface staining of DR5. After treatment with LNF, we observed clear DR5 staining on the cell surface, particularly at 5 and 10 μ M (Fig. 3B), indicating that LNF induces cell-surface localization of DR5. Collectively, these data clearly demonstrate that LNF increases cell-surface DR5 levels.

In addition, we determined whether LNF alters the levels of other death or TRAIL receptors. H1792 cells expressed cell-surface DR4 and Fas, but very low levels of decoy receptors 1 and 2. Upon treatment with either 5 or 10 μ M LNF, the levels of these surface receptors were not further increased (supplemental Fig. S1). Thus, it is clear that LNF does not affect the levels of

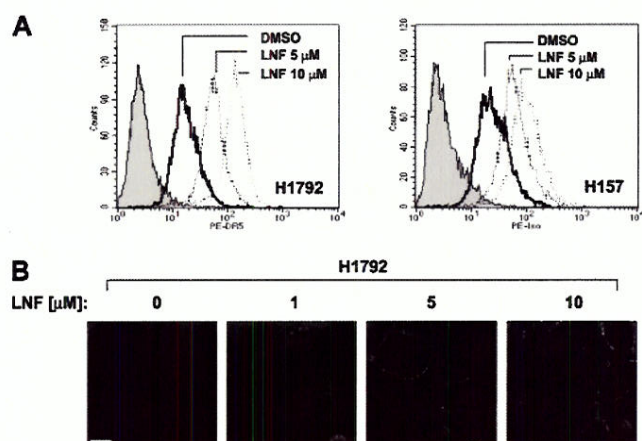


FIGURE 3. LNF increases cell-surface DR5 levels. A, H1792 and H157 cell lines were exposed to the indicated concentrations of LNF for 24 h. The cells were then harvested, stained with PE-conjugated DR5 antibody, and analyzed by flow cytometry. The shaded peak represents cells stained with a matched PE-conjugated IgG isotype control (PE-iso). The open peaks were cells stained with PE-conjugated anti-DR5 antibody. DMSO, Me₂SO. B, H1792 cells were treated with the indicated concentrations of LNF for 16 h and then stained with PE-conjugated DR5 antibody. DR5 expression was visualized under a confocal microscope.

other death or TRAIL receptors at the cell surface. Collectively, these data further suggest the importance of DR5 up-regulation in LNF-induced apoptosis.

LNF Induces DR5 Expression through a CHOP-dependent Mechanism—To determine how FTIs increase DR5 expression at the transcriptional level, we examined the effects of LNF on the transactivation of reporter constructs with different lengths of DR5 5'-flanking regions (Fig. 4A) to identify the region responsible for LNF-mediated DR5 transactivation. In this transient transfection and luciferase assay, LNF failed to increase the luciferase activity of pGL3-DR5(-240) and pGL3-DR5(-120) while significantly increasing the luciferase activity of pGL3-DR5(-373), pGL3-DR5(-420), and pGL3-DR5(-3070) (Fig. 4A), indicating that the region between -240 and -373 contains essential element(s) responsible for LNF-induced DR5 transactivation. We identified a CHOP-binding site in this region, which has been demonstrated to be responsible for DR5 up-regulation by several cancer therapeutic agents (22–24). Thus, we further compared the effects of LNF on the transactivation of reporter constructs carrying wild-type and mutated CHOP-binding sites. We also included constructs carrying mutated NF- κ B- and Elk-binding sites as controls (Fig. 4B). As shown in Fig. 4B, LNF increased the luciferase activity of the constructs carrying the wild-type DR5 promoter region or the DR5 promoter region with a mutated NF- κ B- or Elk-binding site. However, LNF failed to increase the luciferase activity of the construct carrying the DR5 promoter region with a mutated CHOP-binding site. These results clearly indicate that the CHOP-binding site in the DR5 promoter region is required for LNF-mediated DR5 transactivation.

We next examined whether LNF actually modulates the expression of CHOP. By Western blot analysis, we detected a time-dependent DR5 induction accompanied by CHOP up-regulation in cells exposed to LNF, both of which occurred at 3 h and were sustained up to 24 h post-LNF treatment (Fig.

Role of DR5 Up-regulation in FTI-induced Apoptosis

4C). The cleavage of caspase-8, caspase-3, and poly(ADP-ribose) polymerase was detected at 12 h after LNF treatment (Fig. 4C). Thus, the up-regulation of both CHOP and DR5 appears to be an early event that occurs before induction of apoptosis. By blocking LNF-induced CHOP expression using CHOP siRNA, we detected that DR5 induction by LNF was also accordingly diminished (Fig. 4D), indicating that LNF-induced DR5 up-regulation is secondary to CHOP induction. We conclude that LNF induces CHOP-dependent DR5 expression.

Given that CHOP is an ER stress-associated protein (21), we further examined whether LNF alters the expression levels of BiP/GRP78, another key protein marker of ER stress (21). As shown in Fig. 4C, under the same conditions used to test CHOP and DR5, LNF did not alter the levels of BiP/GRP78 from 3 to 16 h post-treatment. At 24 h, LNF only slightly increased the BiP/GRP78 levels. Together, these data clearly show that LNF increases the levels of CHOP, but not BiP/GRP78.

Induction of DR5 Contributes to LNF-induced Apoptosis—It is well known that DR5 activation (e.g. ligation with TRAIL) recruits and activates caspase-8 via the adaptor molecule FADD, leading to induction of apoptosis (18, 19). One common strategy to disrupt death receptor-induced apoptosis is to use a dominant-negative FADDm, which prevents death receptors from recruiting caspase-8 (41). To determine whether DR5 up-regulation contributes to LNF-induced apoptosis, we compared the effects of LNF on apoptosis induction in vector-transfected H460 cells (H460/V1) and FADDm-transfected cells (H460/Fm6 and H460/Fm16). These cell lines were equally sensitive to staurosporine in terms of decreasing cell survival. However, both H460/Fm6 and H460/Fm16 cell lines were significantly less sensitive to TRAIL in comparison with H460/V1 cells (Fig. 5A). LNF effectively increased the number of floating (dead) cells (Fig. 5B) and the levels of DNA fragments (Fig. 5C) in H460/V1 cells. However, these effects were significantly diminished in H460 cells expressing FADDm (i.e. H460/Fm6 and H460/Fm16; $p < 0.05$), indicating that FADDm overexpression abrogates the ability of LNF to induce apoptotic cell death, suggesting that the death receptor-mediated extrinsic apoptotic pathway is critical for LNF-induced apoptosis.

To further decipher the role of DR5 in LNF-induced apoptosis, we knocked down DR5 gene expression using siRNA and then examined its impact on LNF-induced apoptosis. In both H1792 and H157 cells, DR5 siRNA transfection dramatically decreased the basal levels of DR5 expression and, more important, abolished LNF-induced DR5 expression as detected by Western blot analysis (Fig. 5D). Furthermore, in cells transfected with DR5 siRNA, LNF-induced DNA fragmentation was significantly suppressed compared with cells transfected with control siRNA (Fig. 5E). To avoid possible off-target effects of siRNA, we also used a second DR5 siRNA (i.e. DR5 siRNA-2) that targets a different sequence of the DR5 gene to reproduce the aforementioned results. Similarly, blockage of DR5 induction by silencing DR5 using DR5 siRNA-2 significantly inhibited LNF-induced DNA fragmentation (supplemental Fig. S2). Collectively, these results further support the critical role of the DR5-mediated extrinsic apoptotic pathway in LNF-induced apoptosis.

Role of DR5 Up-regulation in FTI-induced Apoptosis

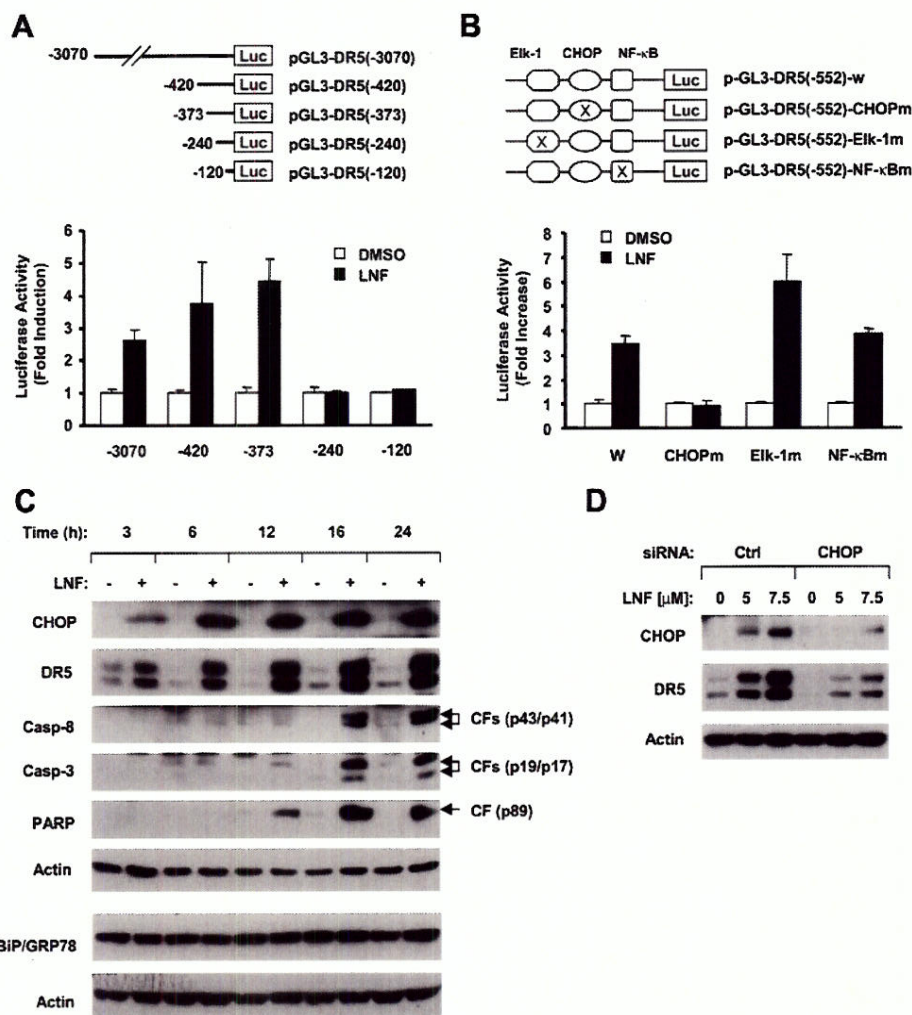


FIGURE 4. LNF up-regulates DR5 expression through a CHOP-dependent mechanism. *A*, identification of the region in the DR5 5'-flanking region that is responsible for LNF-induced DR5 transactivation. The given reporter constructs with different lengths of the 5'-flanking region of the DR5 gene were cotransfected with the pCH110 plasmid into H1792 cells. After 24 h, the cells were treated with Me₂SO (DMSO) or 10 μM LNF for 12 h and then subjected to luciferase (Luc) assay. Each bar represents the mean ± S.D. of triplicate determinations. *B*, the CHOP-binding site is required for LNF-induced DR5 transactivation. The given reporter constructs with and without different mutated (m) binding sites were cotransfected with the pCH110 plasmid into H1792 cells. After 24 h, the cells were treated with Me₂SO or 10 μM LNF for 12 h and then subjected to luciferase assay. Each bar represents the mean ± S.D. of triplicate determinations. *W*, wild-type. *C*, effects of LNF on the expression of CHOP, DR5, and BiP/GRP78 and cleavage of caspase (Casp)-8, caspase-3, and poly(ADP-ribose) polymerase (PARP). H1792 cells were treated with Me₂SO or 5 μM LNF in 0.1% FBS for the indicated times and then subjected to preparation of whole cell protein lysates and subsequent Western blot analysis. *CFs*, cleaved fragments. *D*, blockage of CHOP induction inhibits LNF-induced DR5 up-regulation. H1792 cells were transfected with control (Ctrl) or CHOP siRNA. After 48 h, the cells were treated with the indicated concentrations of LNF for 12 h and then subjected to preparation of whole cell protein lysates and subsequent Western blot analysis.

Combination of LNF and TRAIL Enhances Induction of Apoptosis—Because LNF increases cell-surface DR5 expression, we speculated that LNF would cooperate with exogenous TRAIL to augment induction of apoptosis if the induced DR5 is functional. Thus, we examined the effect of the combination of LNF with exogenous human recombinant TRAIL on apoptosis in two human lung cancer cell lines. As shown in Fig. 6A, 5 μM LNF alone did not apparently induce cleavage of caspase-8, caspase-3, poly(ADP-ribose) polymerase, and RasGAP, whereas TRAIL at the tested doses, particularly 10 and 20 ng/ml, caused only weak cleavage of the caspases and their substrates. Notably, the combination of LNF and TRAIL induced

obvious cleavage of not only caspase-8, but also caspase-3 and its substrate poly(ADP-ribose) polymerase, as indicated by the dramatic decreases in their proforms (uncleaved forms) and/or increase in the cleaved bands. LNF alone did not affect RasGAP levels, and TRAIL alone at 20 and 30 ng/ml caused only weak cleavage of RasGAP. However, the combination of LNF with TRAIL, even at 10 ng/ml TRAIL, induced cleavage of RasGAP (Fig. 6A). Therefore, it appears that LNF cooperates with TRAIL to enhance activation of caspase-8 and its downstream caspase-3.

In addition, both LNF alone (1–5 μM) and TRAIL alone (25 ng/ml) did not increase or only slightly increased the amount of DNA fragments; however, the combination of the two agents induced a striking increase in DNA fragment levels, which were apparently greater than the sums of the levels caused by each single agent alone in both cell lines (Fig. 5B). For example, in H1792 cells, LNF at 5 μM increased DNA fragmentation by <0.2 arbitrary units, whereas TRAIL at 25 ng/ml increased DNA fragmentation by ~0.3 arbitrary units. However, the combination of these two agents increased DNA fragmentation by ~1.4 arbitrary units. Therefore, it appears that LNF synergizes with TRAIL to induce apoptosis in human cancer cells.

DISCUSSION

Although FTIs were historically developed as anti-Ras agents, it is now generally agreed that FTIs exert their antitumor activity independently of their inhibition of Ras farnesylation (1, 2, 25). In this study, we have demonstrated that induction of DR5 and its mediated activation of the extrinsic apoptotic pathway play critical roles in LNF-induced apoptosis in human lung cancer cells due to the following findings. First, LNF activated caspase-8, which is required for LNF-induced apoptosis because inhibition of caspase-8 activation by either a caspase-8 inhibitor or siRNA-mediated caspase-8 silencing abolished LNF-induced apoptosis. Second, overexpression of FADDm abrogated LNF-induced caspase activation and apoptotic cell death, suggesting that the activation of the extrinsic apoptotic pathway is critical for LNF-induced apoptosis. Finally,

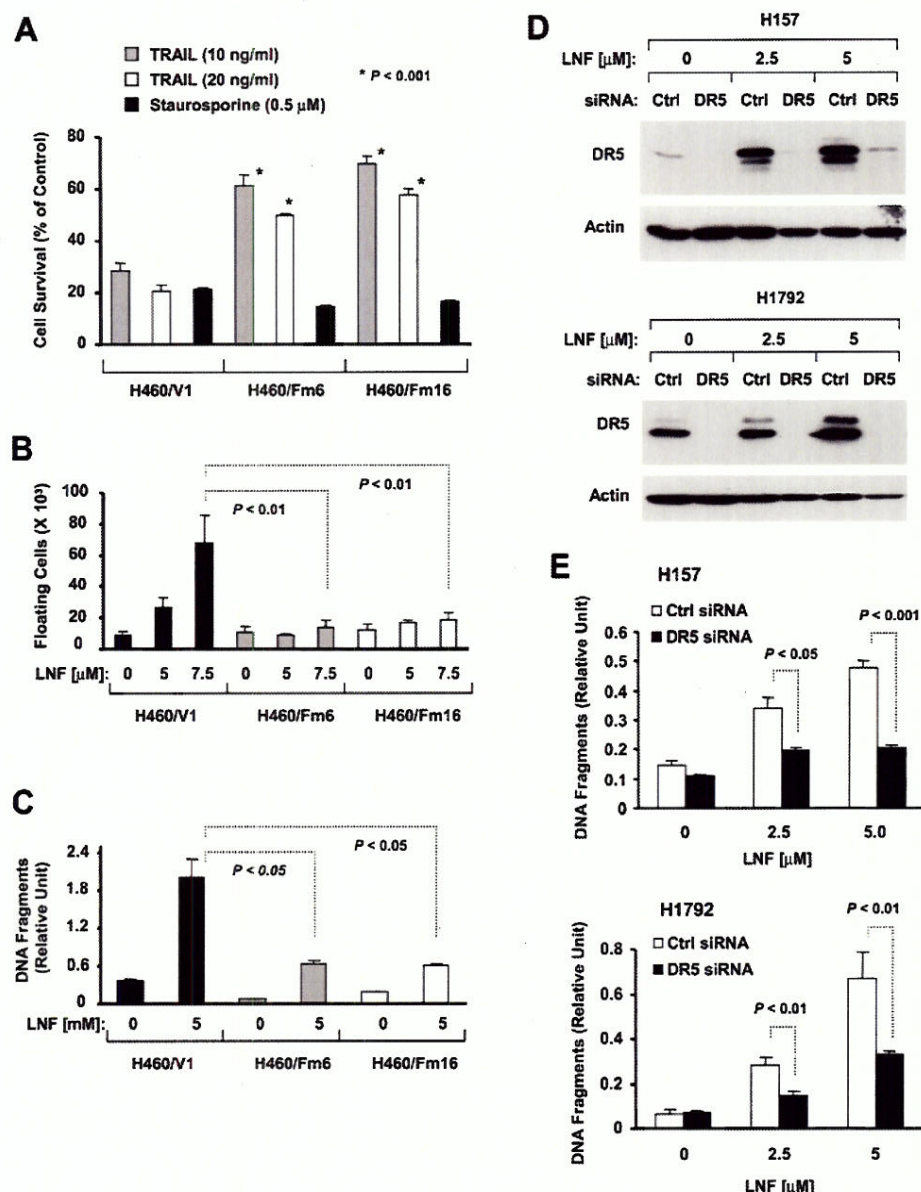


FIGURE 5. Overexpression of a dominant-negative FADDm (A–C) or silencing of DR5 expression by siRNA (D and E) protects cells from LNF-induced apoptosis. A, overexpression of FADDm protects cells from death induced by TRAIL, but not by staurosporine. The indicated cell lines were treated with the given concentrations of TRAIL or staurosporine for 24 h. The cells were then subjected to measurement of cell survival by the sulforhodamine B assay. Data are the means \pm S.D. of four identical treatments. B and C, overexpression of FADDm protects cells from LNF-induced apoptosis. The indicated cell lines were exposed to the given concentrations of LNF in 0.1% FBS for 24 h. The cells were then subjected to detection of floating or dead cells in the medium by direct cell counting (B) and evaluation of DNA fragmentation using the Cell Death Detection ELISA^{plus} kit (C). D, the indicated cell lines were seeded in a 24-well cell culture plate and transfected twice on the 2nd day with control (Ctrl) or DR5 siRNA in a 48-h interval. Forty hours later after the second transfection, cells were treated with the indicated concentrations of LNF in 0.1% FBS. After 24 h, DR5 expression was assessed by Western blot analysis. E, the indicated cell lines were transfected with control or DR5 siRNA as aforementioned and then treated with the indicated concentrations of LNF in 0.1% FBS. After 24 h, cells were subjected to estimation of DNA fragmentation using the Cell Death Detection ELISA^{plus} kit. Data in C and E are the means \pm S.D. of three identical wells.

LNF primarily induced DR5 expression (including an increase in cell-surface DR5), whereas DR5 silencing using DR5 siRNA attenuated LNF-induced caspase activation and apoptosis, indicating that DR5 induction contributes to LNF-induced apoptosis. Thus, our study is the first to demonstrate that an FTI induces DR5-mediated, caspase-8-dependent apoptosis in human cancer cells.

DR5 expression is regulated through p53-dependent and -independent mechanisms (42, 43). In our study, most of the cell lines used for examining DR5 up-regulation, including H1792, H157, H1299, H226, DU145, HeLa, and SqCC/Y1, have mutant or deleted p53 (44–47). Because LNF still increased DR5 expression in these cell lines (Fig. 2), we conclude that LNF induces DR5 expression independently of p53. This is further supported by our observation that LNF up-regulated DR5 expression with equal potency in both HCT116 and p53 knock-out HCT116 cell lines (Fig. 2). Currently, it is known that DR5 can be regulated in a p53-independent manner (43, 48), but the underlying mechanisms remain largely unclear.

CHOP has been demonstrated recently to regulate DR5 expression through the CHOP-binding site in the DR5 gene (22, 23), revealing a novel p53-independent regulation of DR5 expression. In our study, LNF appeared to increase DR5 expression at the transcriptional level because it increased DR5 mRNA levels and the activity of the DR5 promoter (Fig. 2). The deletion and mutation analyses of the DR5 5'-flanking region revealed that the region containing the CHOP-binding site is essential for LNF-mediated DR5 transactivation (Fig. 4). Indeed, LNF induced a time-dependent CHOP expression accompanied by the up-regulation of DR5 expression. Blockage of LNF-mediated CHOP induction by the CHOP siRNA accordingly inhibited DR5 up-regulation (Fig. 4). We conclude that LNF induces DR5 expression through a CHOP-dependent mechanism.

It is known that CHOP is an ER stress-regulated protein (21). It was reported that another FTI called R115777 induces ER stress in myeloma cells because it increased the levels of both CHOP and particularly BiP/GRP78 after a prolonged treatment (*i.e.* 72 h) (49). In our system, LNF at a concentration that induces DR5 expression (*e.g.* 5 μM) increased the levels of CHOP, but not BiP/GRP78 (Fig. 4), arguing that LNF induces ER stress in our system. Nonetheless, whether

Role of DR5 Up-regulation in FTI-induced Apoptosis

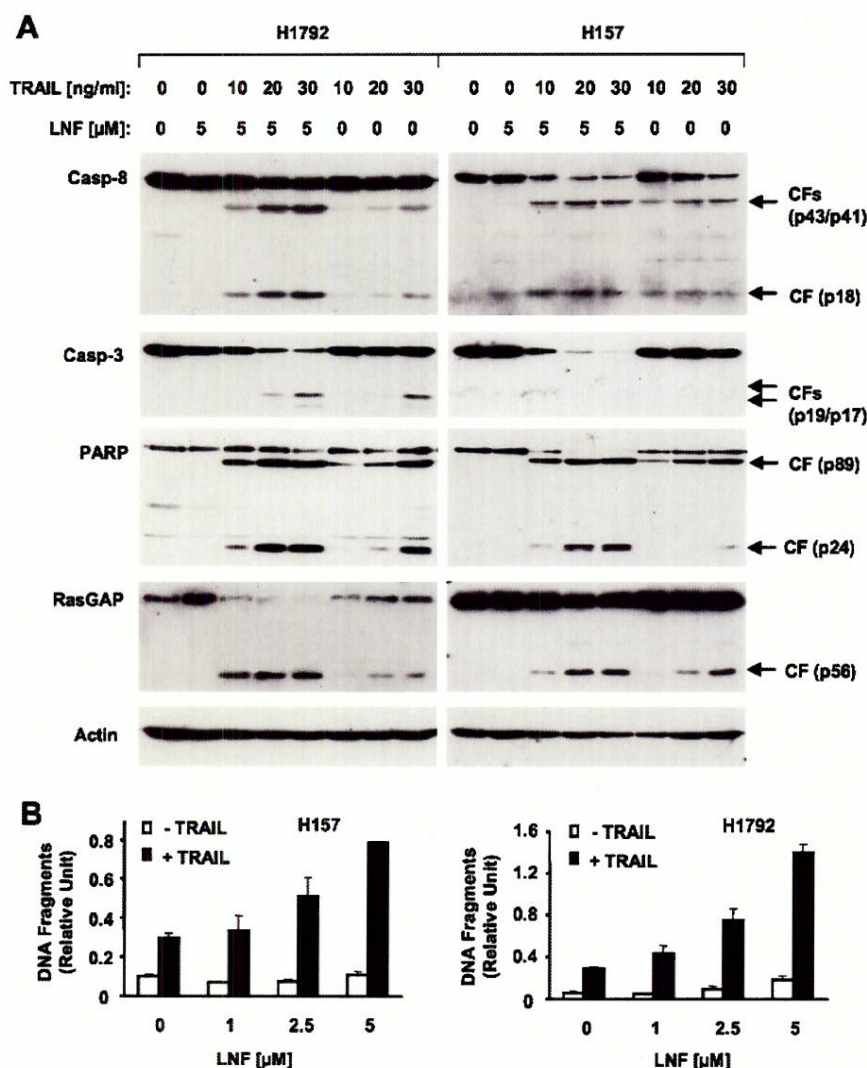


FIGURE 6. Combination of LNF and TRAIL augments caspase activation (A) and DNA fragmentation (B). A, the indicated cell lines were treated with LNF alone, TRAIL alone, and their combinations as indicated. After 14 h, whole cell protein lysates were prepared from both detached and attached cells and subjected to Western blot analysis to detect cleavage of caspases and their substrates. *Casp*, caspase; *PARP*, poly(ADP-ribose) polymerase; *CFs*, cleaved forms. B, the indicated cell lines were seeded in a 96-well plate and treated on the 2nd day with the indicated concentrations of LNF alone, TRAIL at 25 ng/ml alone, and their combinations. After 24 h, cells were subjected to measurement of DNA fragments using the Cell Death Detection ELISA^{plus} kit. Data are the means \pm S.D. of three identical wells.

CHOP elevation by LNF is due to ER stress or other mechanisms needs to be studied further.

In addition to LNF, R115777 also increased DR5 expression.⁴ The LNF analog SCH66337, which was much weaker than LNF in inhibiting protein farnesylation, also showed weaker activity than LNF in inducing DR5 expression and enhancing TRAIL-induced apoptosis (supplemental Fig. S3). Therefore, future studies should address whether there is a relationship between inhibition of protein farnesylation and induction of CHOP and DR5.

Although R115777 was reported to induce apoptosis in the presence of a caspase-8 inhibitor in myeloma cells (49), this FTI did enhance death receptor-induced apoptosis mediated by Fas ligand or TRAIL in myeloma cells (50) and lung cancer cells.⁴

⁴ Y. Qiu, X. Liu, P. Yue, F. R. Khuri, and S.-Y. Sun, unpublished data.

These findings are in agreement with our current finding that LNF enhances TRAIL-induced apoptosis in human lung cancer cells. In our study, we have clearly shown that LNF induces caspase-8-dependent apoptosis through both pharmacological (inhibitor) and molecular (siRNA) approaches (Fig. 1). Because both LNF and R115777 induced DR5 expression in myeloma cells,⁴ further studies are needed to address whether the death receptor-mediated apoptotic pathway is also involved in FTI-induced apoptosis in myeloma cells as well as in other types of cancer cells.

Our findings that FTIs increase DR5 expression and enhance TRAIL-induced apoptosis have clinically meaningful implications. It is known that TRAIL functions as the DR5 ligand and rapidly induces apoptosis in a wide variety of transformed cells, but is not cytotoxic in normal cells *in vitro* and *in vivo* (18, 19). Therefore, TRAIL is considered to be a tumor-selective, apoptosis-inducing cytokine and a promising new candidate for cancer treatment. In addition, agonistic anti-DR5 antibodies can also induce DR5 trimerization, which triggers the extrinsic apoptotic pathway, thus having great cancer therapeutic potential (51). In fact, the agonistic anti-DR5 antibody is already being tested in phase I clinical trials. Therefore, LNF, as well as other FTIs that increase cell-surface DR5 expression, can be used in combination with TRAIL or an

agonistic anti-DR5 antibody to achieve an enhanced effect on apoptosis induction in human cancer cells. In summary, our study has demonstrated, for the first time, that an FTI (e.g. LNF) induces CHOP-dependent DR5 expression at a clinically achievable concentration range, contributing to FTI-induced apoptosis.

Acknowledgments—We are grateful to Zhongmei Zhou for excellent technical support. We thank Drs. G. S. Wu and H.-G. Wang for providing some plasmids.

REFERENCES

- Sebti, S. M. (2005) *Cancer Cell* 7, 297–300
- Brunner, T. B., Hahn, S. M., Gupta, A. K., Muschel, R. J., McKenna, W. G., and Bernhard, E. J. (2003) *Cancer Res.* 63, 5656–5668
- Adjei, A. A., Erlichman, C., Davis, J. N., Cutler, D. L., Sloan, J. A., Marks,

- R. S., Hanson, L. J., Svingen, P. A., Atherton, P., Bishop, W. R., Kirschmeier, P., and Kaufmann, S. H. (2000) *Cancer Res.* **60**, 1871–1877
4. Adjei, A. A., Davis, J. N., Bruzek, L. M., Erlichman, C., and Kaufmann, S. H. (2001) *Clin. Cancer Res.* **7**, 1438–1445
5. Chun, K. H., Lee, H. Y., Hassan, K., Khuri, F., Hong, W. K., and Lotan, R. (2003) *Cancer Res.* **63**, 4796–4800
6. Smalley, K. S., and Eisen, T. G. (2003) *Int. J. Cancer* **105**, 165–175
7. Nakajima, A., Tauchi, T., Sumi, M., Bishop, W. R., and Ohyashiki, K. (2003) *Mol. Cancer Ther.* **2**, 219–224
8. Hoover, R. R., Mahon, F. X., Melo, J. V., and Daley, G. Q. (2002) *Blood* **100**, 1068–1071
9. Feldkamp, M. M., Lau, N., Roncari, L., and Guha, A. (2001) *Cancer Res.* **61**, 4425–4431
10. Reichert, A., Heisterkamp, N., Daley, G. Q., and Groffen, J. (2001) *Blood* **97**, 1399–1403
11. Shi, B., Yaremko, B., Hajian, G., Terracina, G., Bishop, W. R., Liu, M., and Nielsen, L. L. (2000) *Cancer Chemother. Pharmacol.* **46**, 387–393
12. Liu, M., Bryant, M. S., Chen, J., Lee, S., Yaremko, B., Lipari, P., Malkowski, M., Ferrari, E., Nielsen, L., Prioli, N., Dell, J., Sinha, D., Syed, J., Korfmacher, W. A., Nomeir, A. A., Lin, C. C., Wang, L., Taveras, A. G., Doll, R. J., Njoroge, F. G., Mallams, A. K., Remiszewski, S., Catino, J. J., Girijavallabhan, V. M., Kirschmeier, P., and Bishop, W. R. (1998) *Cancer Res.* **58**, 4947–4956
13. Khuri, F. R., Glisson, B. S., Kim, E. S., Statkevich, P., Thall, P. F., Meyers, M. L., Herbst, R. S., Munden, R. F., Tendler, C., Zhu, Y., Bangert, S., Thompson, E., Lu, C., Wang, X. M., Shin, D. M., Kies, M. S., Papadimitrakopoulou, V., Fossella, F. V., Kirschmeier, P., Bishop, W. R., and Hong, W. K. (2004) *Clin. Cancer Res.* **10**, 2968–2976
14. Kim, E. S., Kies, M. S., Fossella, F. V., Glisson, B. S., Zaknoen, S., Statkevich, P., Munden, R. F., Summey, C., Pisters, K. M., Papadimitrakopoulou, V., Tighiouart, M., Rogatko, A., and Khuri, F. R. (2005) *Cancer* **104**, 561–569
15. Marcus, A. I., O'Brate, A. M., Buey, R. M., Zhou, J., Thomas, S., Khuri, F. R., Andreu, J. M., Diaz, F., and Giannakakou, P. (2006) *Cancer Res.* **66**, 8838–8846
16. Green, D. R. (2000) *Cell* **102**, 1–4
17. Ashkenazi, A., and Dixit, V. M. (1998) *Science* **281**, 1305–1308
18. Wang, S., and El-Deiry, W. S. (2003) *Oncogene* **22**, 8628–8633
19. Almasan, A., and Ashkenazi, A. (2003) *Cytokine Growth Factor Rev.* **14**, 337–348
20. Debatin, K. M., and Krammer, P. H. (2004) *Oncogene* **23**, 2950–2966
21. Oyadomari, S., and Mori, M. (2004) *Cell Death Differ.* **11**, 381–389
22. Yamaguchi, H., and Wang, H.-G. (2004) *J. Biol. Chem.* **279**, 45495–45502
23. Yoshida, T., Shiraishi, T., Nakata, S., Horinaka, M., Wakada, M., Mizutani, Y., Miki, T., and Sakai, T. (2005) *Cancer Res.* **65**, 5662–5667
24. Abdelrahim, M., Newman, K., Vanderlaag, K., Samudio, I., and Safe, S. (2006) *Carcinogenesis* **27**, 717–728
25. Lebowitz, P. F., and Prendergast, G. C. (1998) *Oncogene* **17**, 1439–1445
26. Lackner, M. R., Kindt, R. M., Carroll, P. M., Brown, K., Cancilla, M. R., Chen, C., de Silva, H., Franke, Y., Guan, B., Heuer, T., Hung, T., Keegan, K., Lee, J. M., Manne, V., O'Brien, C., Parry, D., Perez-Villar, J. J., Reddy, R. K., Xiao, H., Zhan, H., Cockett, M., Plowman, G., Fitzgerald, K., Costa, M., and Ross-Macdonald, P. (2005) *Cancer Cell* **7**, 325–336
27. Du, W., Liu, A., and Prendergast, G. C. (1999) *Cancer Res.* **59**, 4208–4212
28. Jiang, K., Coppola, D., Crespo, N. C., Nicosia, S. V., Hamilton, A. D., Sebt, S. M., and Cheng, J. Q. (2000) *Mol. Cell. Biol.* **20**, 139–148
29. Edamatsu, H., Gau, C. L., Nemoto, T., Guo, L., and Tamanoi, F. (2000) *Oncogene* **19**, 3059–3068
30. Marzo, I., Perez-Galan, P., Giraldo, P., Lopez-Royuela, N., Gomez-Benito, M., Larrad, L., Laserra, P., Rubio-Felix, D., Anel, A., and Naval, J. (2004) *Leukemia (Basingstoke)* **18**, 1599–1604
31. Sun, S.-Y., Zhou, Z., Wang, R., Fu, H., and Khuri, F. R. (2004) *Cancer Biol. Ther.* **3**, 1092–1098; Discussion 1099–1101
32. Liu, X., Yue, P., Zhou, Z., Khuri, F. R., and Sun, S.-Y. (2004) *J. Natl. Cancer Inst.* **96**, 1769–1780
33. Sun, S.-Y., Yue, P., Wu, G. S., El-Deiry, W. S., Shroot, B., Hong, W. K., and Lotan, R. (1999) *Oncogene* **18**, 2357–2365
34. Pfahl, M., Tzukerman, M., Zhang, X. K., Lehmann, J. M., Hermann, T., Wills, K. N., and Graupner, G. (1990) *Methods Enzymol.* **189**, 256–270
35. Sun, S.-Y., Yue, P., Hong, W. K., and Lotan, R. (2000) *Cancer Res.* **60**, 6537–6543
36. Sun, S.-Y., Yue, P., Dawson, M. I., Shroot, B., Michel, S., Lamph, W. W., Heyman, R. A., Teng, M., Chandraratna, R. A., Shudo, K., Hong, W. K., and Lotan, R. (1997) *Cancer Res.* **57**, 4931–4939
37. Zou, W., Liu, X., Yue, P., Zhou, Z., Sporn, M. B., Lotan, R., Khuri, F. R., and Sun, S.-Y. (2004) *Cancer Res.* **64**, 7570–7578
38. Wen, L. P., Madani, K., Martin, G. A., and Rosen, G. D. (1998) *Cell Death Differ.* **5**, 729–734
39. Awada, A., Eskens, F. A., Piccart, M., Cutler, D. L., van der Gaast, A., Bleiberg, H., Wanders, J., Faber, M. N., Statkevich, P., Fumoleau, P., and Verweij, J. (2002) *Eur. J. Cancer* **38**, 2272–2278
40. Sharma, S., Kemeny, N., Kelsen, D. P., Ilson, D., O'Reilly, E., Zaknoen, S., Baum, C., Statkevich, P., Hollywood, E., Zhu, Y., and Saltz, L. B. (2002) *Ann. Oncol.* **13**, 1067–1071
41. Chinnaiyan, A. M., O'Rourke, K., Tewari, M., and Dixit, V. M. (1995) *Cell* **81**, 505–512
42. Wu, G. S., Burns, T. F., McDonald, E. R., III, Jiang, W., Meng, R., Krantz, I. D., Kao, G., Gan, D. D., Zhou, J. Y., Muschel, R., Hamilton, S. R., Spinner, N. B., Markowitz, S., Wu, G., and El-Deiry, W. S. (1997) *Nat. Genet.* **17**, 141–143
43. Sheikh, M. S., Burns, T. F., Huang, Y., Wu, G. S., Amundson, S., Brooks, K. S., Fornace, A. J., Jr., and El-Deiry, W. S. (1998) *Cancer Res.* **58**, 1593–1598
44. Mitsudomi, T., Steinberg, S. M., Nau, M. M., Carbone, D., D'Amico, D., Bodner, S., Oie, H. K., Linnoila, R. I., Mulshine, J. L., Minna, J. D., and Gazdar, A. F. (1992) *Oncogene* **7**, 171–180
45. Sun, S.-Y., Yue, P., Mao, L., Dawson, M. I., Shroot, B., Lamph, W. W., Heyman, R. A., Chandraratna, R. A., Shudo, K., Hong, W. K., and Lotan, R. (2000) *Clin. Cancer Res.* **6**, 1563–1573
46. Sun, S.-Y., Yue, P., and Lotan, R. (2000) *Oncogene* **19**, 4513–4522
47. Bohnke, A., Westphal, F., Schmidt, A., El-Awady, R. A., and Dahm-Daphi, J. (2004) *Int. J. Radiat. Biol.* **80**, 53–63
48. Meng, R. D., and El-Deiry, W. S. (2001) *Exp. Cell Res.* **262**, 154–169
49. Beaupre, D. M., Cepero, E., Obeng, E. A., Boise, L. H., and Lichtenheld, M. G. (2004) *Mol. Cancer Ther.* **3**, 179–186
50. Beaupre, D. M., McCafferty-Grad, J., Bahlis, N. J., Boise, L. H., and Lichtenheld, M. G. (2003) *Leuk. Lymphoma* **44**, 2123–2134
51. Ichikawa, K., Liu, W., Zhao, L., Wang, Z., Liu, D., Ohtsuka, T., Zhang, H., Mountz, J. D., Koopman, W. J., Kimberly, R. P., and Zhou, T. (2001) *Nat. Med.* **7**, 954–960

Inhibition of Stat3 activation and tumor growth suppression of non-small cell lung cancer by G-quartet oligonucleotides

PRIYA WEERASINGHE¹, GABRIELA E. GARCIA¹, QIQING ZHU¹,
PING YUAN³, LILI FENG¹, LI MAO³ and NAIJIE JING^{1,2}

¹Department of Medicine, and ²Dan Duncan Cancer Center, Baylor College of Medicine; ³Department of Thoracic/Head and Neck Medical Oncology, The University of Texas MD Anderson Cancer Center, Houston, TX, USA

Received February 20, 2007; Accepted April 12, 2007

Abstract. Lung cancer is the leading cause of cancer mortality in the United States. Despite advances made over the past decades, the overall survival of patients with lung cancer remains dismal. Here we report novel G-quartet oligodeoxynucleotides (GQ-ODN) that were designed to selectively target signal transducer and activator of transcription 3 (Stat3), in the treatment of human non-small cell lung cancer (NSCLC). The objective of this study was to evaluate the effects of two novel GQ-ODN STAT3 inhibitors, T40214 and T40231, on NSCLC bearing nude mice. NSCLC bearing nude mice were assigned to 5 groups, which were treated by vehicle, control ODN, T40214, T40231, and Paclitaxel, respectively. Tumors were measured, isolated and analyzed using Western blotting, immuno-histochemistry, RPA and TUNEL. Results show that GQ-ODN T40214 and T40231 significantly suppress the growth of NSCLC tumors in nude mice by selectively inhibiting the activation of Stat3 and its downstream proteins Bcl-2, Bcl-x_L, Mcl-1, survivin, VEGF, Cyclin D1 and c-myc; thereby, promoting apoptosis and reducing angiogenesis and cell proliferation. These findings validate Stat3 as an important molecular target for NSCLC therapy and demonstrate the efficacy of GQ-ODN in inhibiting Stat3 phosphorylation.

Introduction

Lung cancer is one of the most prevalent cancers and a leading cause of cancer mortality worldwide. In the United States, approximately 170,000 people are diagnosed with lung cancer each year (1,2); approximately 85% of those diagnosed die of the disease. The number of lung cancer deaths exceeds those due to breast, prostate, and colon cancers combined (3). Lung cancer has two major subtypes

based on histology, i.e. small cell lung cancer (SCLC) and non-small cell lung cancer (NSCLC) which account for 85% of all lung cancers. More than 60% of all NSCLC patients have advanced or metastatic tumors at the time of diagnosis and are not suitable for surgery (3). Despite advances made in treating the disease over the past two decades, the overall survival of patients with NSCLC remains extremely poor (4). Therefore, innovative treatment approaches that employ new agents targeting novel molecules are urgently needed. In this regard, Stat3, a critical mediator of oncogenic signaling that is highly activated in a wide variety of human tumors (5), may hold promise.

Signal transducer and activator of transcription (STAT) proteins were discovered as latent cytoplasmic transcription factors (6). Seven known mammalian STAT proteins (i.e., Stat1, 2, 3, 4, 5a, 5b, and 6) are involved in immune response, inflammation, proliferation, differentiation, development, cell survival, and apoptosis (5). These proteins contain several domains: a tetramerization domain, a coil-coil domain, a DNA-binding domain, a linker domain, an Src-homology 2 (SH2) domain, a critical tyrosine residing near the C-terminal end, and a C-terminal transactivation domain (7,8). STAT proteins are activated in response to the binding of a number of ligands, including cytokines (e.g., IL-6) and growth factors (e.g., EGF), to their cognate cell surface receptors, and are recruited to specific phosphotyrosine residues within receptor complexes through their SH2 domains; they subsequently become phosphorylated on the tyrosine residue within their C-terminus and dimerize through reciprocal interactions between the SH2 domain of one monomer and the phosphorylated tyrosine of the other. The activated dimers translocate to the nucleus, where they bind to DNA-response elements in the promoters of target genes and activate specific gene expression programs (9).

Stat3 has been identified as an important target for cancer therapy, since it participates in oncogenesis through the upregulation of genes encoding apoptosis inhibitors (Bcl-x_L, Mcl-1, and survivin), cell-cycle regulators (cyclin D1 and c-myc), and inducers of angiogenesis (VEGF) (9). Mounting evidence has shown that Stat3 is also constitutively activated in many human cancers, including 82% of prostate cancers, 70% of breast cancers, over 90% of head and neck cancers, and more than 50% of lung cancers (10-13). These findings provide a strong rationale for targeting Stat3 to treat human cancers.

Correspondence to: Dr Naijie Jing, Department of Medicine, Baylor College of Medicine, Houston, TX 77030, USA
E-mail: njing@bcm.tmc.edu

Key words: G-quartet oligonucleotides, signal transducer and activator of transcription 3, non-small cell lung cancer, apoptosis, angiogenesis

Recently, we laid the groundwork to develop G-quartet oligodeoxynucleotide (GQ-ODN), which forms G-quartet helical DNA structures, as a potent inhibitor of Stat3 activation. In our preliminary studies, we have: i) demonstrated that GQ-ODN selectively inhibits Stat3 activation in cancer cells; ii) developed a novel delivery system for GQ-ODN, to increase drug activity in cells and *in vivo*; and iii) shown that GQ-ODN T40214 and T40231 significantly suppress tumor growth and greatly increase the survival of nude mice with tumors in which Stat3 is activated (14-16). This report is a part of our systematic *in vivo* examination, which aims to determine whether Stat3 as an oncogenic signaling molecule will have the same influence on tumor progression in different human cancers and whether GQ-ODN will have a similar effect on suppressing tumor growth in different xenografted models under the same conditions. Here we have demonstrated that: i) as a critical oncogenic signaling pathway, Stat3 strongly influences the progression of NSCLC *in vivo*; and ii) targeting the Stat3 molecule with GQ-ODN constitutes a novel and potent therapeutic treatment for NSCLC. We also provide experimental evidence for the proposed mechanism, that a tyrosine-phosphorylated STAT dimer is quickly dephosphorylated when the STAT dimer is dissociated from DNA in cells (17,18). Based on the results, we suggest that GQ-ODN is a novel and promising class of anti-cancer drug in the treatment of metastatic tumors.

Materials and methods

Materials. The following polyclonal antibodies were obtained from Santa Cruz Biotechnology, Inc. (Santa Cruz, CA): anti-Stat3; anti-Stat1; anti-Cyclin D1 against amino acids 1-295, which represents full-length cyclin D1 of human origin; anti-VEGF; anti-Bcl-x_L; and anti-Bcl-2. Phospho-specific antibodies, p-Stat1 and p-Stat3, were purchased from Cell Signaling Technology (Beverly, MA). Goat anti-rabbit horseradish peroxidase (HRP) conjugate was purchased from Bio-Rad Laboratories (Hercules, CA), goat anti-mouse HRP conjugate was purchased from BD Transduction Laboratories (Lexington, KY). Penicillin, streptomycin, RPMI-1640 medium, fetal bovine serum (FBS), and 0.4% trypan blue vital stain were obtained from Invitrogen Corporation/Life Technologies, Inc. (Grand Island, NY). Oligonucleotides were synthesized by The Midland Certified Reagent Company, Inc. (Midland, TX), dissolved in Polyethylenimine (PEI) (Aldrich Chemical, WI) as a 1 $\mu\text{g}/\mu\text{l}$ stock solution, and stored at room temperature (RT).

Cell lines and cell culture. The cell lines used in our studies included: A549 (human non-small cell lung carcinoma); H292 (human lung epithelial cell carcinoma); and H359, H596, H1792, and H1299 cells, which were purchased from ATCC (Manassas, VA). These cell lines were cultured in DMEM medium supplemented with 10% FBS, 100 units/ml penicillin, and 100 $\mu\text{g}/\text{ml}$ streptomycin.

Western blot analysis. To determine the effect of GQ-ODN on Stat3 phosphorylation, cytoplasmic extracts were prepared, as previously described (14), from murine tumor tissue or A549 lung cancer cells that had been pretreated with GQ-ODN.

Lung tumor cells (1 million cells per well in 6-well plates) were first pre-treated with IL-6 (25 ng/ml) or EGF (25 ng/ml) for 30 min. Cells were then washed in serum-free medium and incubated with various concentrations (1.4-142 μM) of GQ-ODN/PEI complexes for 24 h. Cells were lysed with cell lysis buffer and 30 μg of whole cell protein was resolved on 10% SDS-PAGE gel, transferred to a nitrocellulose membrane, blocked with 5% nonfat milk, and probed with specific antibody against Stat3 and tyrosine-phosphorylated Stat3 (p-Stat3). Xenografted tumors were harvested at the end of treatment, diced into small pieces, and sonicated on ice for 2 min. Tumor tissue (100 mg) was lysed in 300 μl of lysis buffer containing protease and phosphatase inhibitors. Tumor tissue protein (50 μg) was resolved on SDS-PAGE and probed by specific antibodies, as previously described. The bands were quantitated using a Personal Densitometer Scanner (version 1.30) and ImageQuant software (version 3.3) (GE Healthcare/Amersham Biosciences).

Animal/xenograft model. Athymic nude mice (Balb-nu/nu, 4 weeks old, weighing approximately 20 g) were obtained from Charles River Laboratories, Inc. (Wilmington, MA); 2.5 million A549 NSCLC cells in 200 μl of PBS were then injected subcutaneously into the right flank of each mouse. After the NSCLC tumors were established (50-150 mm³), the nude mice were randomly assigned to 5 groups of 5 (or 4): Group 1, was treated with PEI (2.5 mg/kg) (vehicle) alone; Group 2 was treated with paclitaxel (a conventional chemotherapeutic agent) at 10 mg/kg; Group 3 was treated with GQ-ODN T40214/PEI (10 mg/kg/+2.5 mg/kg); and Group 4 was treated with GQ-ODN T40231/PEI (10 mg/kg/+2.5 mg/kg) and Group 5 was treated with ns-ODN/PEI (10 mg/kg/+2.5 mg/kg) (control ODN). PEI and ODNs were administered every other day and paclitaxel was injected intraperitoneally (IP) every 4 days. Weight and tumor size were measured every other day. Tumor size was calculated by using the function $[a \times (0.5^b)^2]$, where *a* equals the length and *b* equals the width of tumors.

RNase protection assay (RPA). RPA was performed, as previously described (19,20). Briefly, for each sample prepared from NSCLC tumor tissue, five micrograms of total RNA were used in the RNase protection assay. Probes specific to survivin, *c-myc*, and Mcl-1 mouse genes were prepared. Mouse Angio-1, Apo-2, and CYC-1 multi-probes were obtained from BD Biosciences/Pharmingen (San Diego, CA). An RNase protection assay was performed using a kit (Torrey Pines Biolabs, Inc.; Houston, TX), in accordance with the manufacturer's instructions. The ³²P[UTP] (3000 Ci/mmol, ICN)-labeled antisense RNA probes were synthesized using mCK5 multi-probes (BD Biosciences/Pharmingen) as templates, through an *in vitro* transcription system (Promega Corporation; Madison, WI). Antisense RNA probes were hybridized with the RNA samples at 90°C for 25 min. Unhybridized single-stranded RNA was digested by ribonuclease A/T1 (Sigma-Aldrich; St. Louis, MO) for 30 min. Double-stranded RNA was precipitated by stop solution at -80°C for 15-30 min, and centrifuged at maximum speed for 30 min. The samples were resolved by 6% sequencing gel. Subsequently, the gels were dried and exposed to X-ray film.

A. Control ODN: TGCCGGATCAAGAGCTACCA
 G-quartet ODNs: T40214: GGGCGGGCGGGCGGGG
 T40231: GGTGGGTGGGTGGG

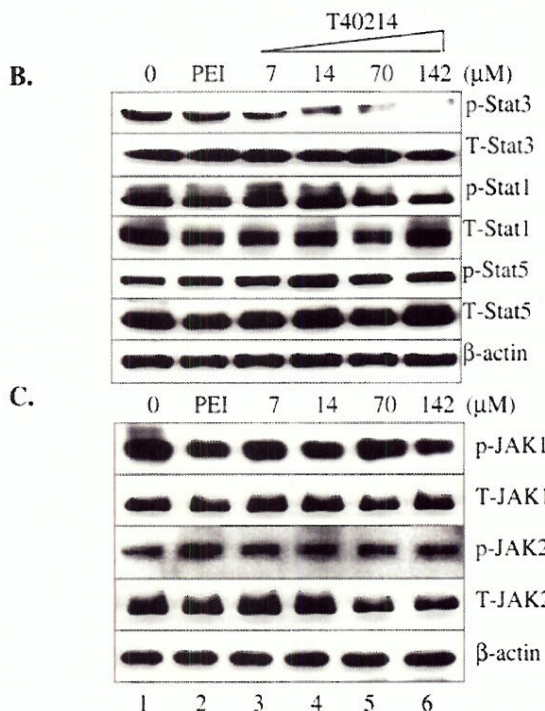
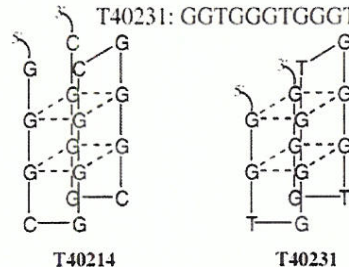


Figure 1. (A) The structures of GQ-ODN T40214 and T40231. (B) Western blot analysis shows the inhibition of Stat3 phosphorylation by GQ-ODNs T40214 and T40231 in NSCLC cells (A549). Comparing with the control band (lane 1), T40214 significantly inhibited the expression of p-Stat3 in NSCLC cells (A549) ($IC_{50} = 5.4 \mu M$). p-Stat3 and T-Stat3, phosphorylated Stat3 and total Stat3, respectively. PEI did not inhibit p-Stat3 (lane 2), and GQ-ODN T40214 did not inhibit p-Stat1 and p-Stat5 in A549 cells. (C) T40214 did not inhibit the expression of p-JAK1 and p-JAK2 in A549 cells. β actin served as the internal control.

Hematoxylin and eosin staining. Xenografted tumors were harvested from athymic mice treated with vehicle alone (PEI), GQ-ODN T40214, GQ-ODN T40231, and paclitaxel, fixed (with 10% formaldehyde in paraffin), sectioned (5- μm tissue sections) and stained with hematoxylin and eosin (H&E).

Terminal deoxyribonucleotidyl transferase-mediated dUTP nick end labeling (TUNEL) analysis. Tissue sections (5 μm) were mounted on siliconized glass slides, air dried, and heated at 45°C overnight. After deparaffinization and rehydration, the sections were digested with proteinase K (120 $\mu g/ml$) for 20 min at room temperature. Following quenching of the endogenous peroxidase activity, the sections were washed in PBS, and subsequently incubated with equilibration buffer

for 10 min at room temperature. Sections were boiled and 50 μl of a mix containing terminal deoxynucleotidyl transferase, reaction buffer containing dATP, and digoxigenin-11-dUTP was then added. The sections were covered with a plastic coverslip, washed in stop/wash buffer for 10 min at room temperature, and subsequently washed in PBS. The sections were then incubated with anti-digoxigenin peroxidase for 30 min at room temperature and washed in PBS. Color development was accomplished through immersion of the slides in 3'3' diaminobenzidine/0.1% H_2O_2 for 3-7 min. Sections were counterstained with ethyl green, washed in butanol, cleared in xylol and mounted with permount.

Results

Inhibition of Stat3 activation by GQ-ODN. Recently, we have developed GQ-ODNs as a new class of Stat3 inhibitors. We have previously reported that the leading compounds, T40214 and T40231, selectively inhibit Stat3 activity ($IC_{50} = 5 \mu M$) in the cells of prostate, breast and head and neck cancers (14,16). Here we employed Western blotting to ascertain if GQ-ODN inhibits Stat3 phosphorylation in NSCLC cells. The sequences and structures of GQODN T40214 and T40231 have been previously delineated (Fig. 1A) (14). PEI (poly-ethylenimine) was used as vehicle for intracellular delivery of ODN at the ODN/PEI ratio of 4:1. β -actin was used as the loading control. When compared to the tyrosine-phosphorylated Stat3 (p-Stat3) band in lane 1, lane 2 shows that PEI alone has no inhibitory effect on p-Stat3 in NSCLC cells. The p-Stat3 was significantly reduced when the concentration of T40214 increased (lanes 3 to 6). The IC_{50} of p-Stat3 dephosphorylation for T40214 was $\sim 5.4 \mu M$. Along with p-Stat3, we also detected tyrosine-phosphorylated Stat1 (p-Stat1) and Stat5 (p-Stat5) in NSCLC cells under similar experimental conditions. Importantly, we found that GQ-ODN T40214 does not inhibit the activation of p-Stat1 nor p-Stat5 in NSCLC cells, showing that GQ-ODN T40214 selectively inhibits p-Stat3 activation (Fig. 1B). Furthermore, tyrosine-phosphorylated JAK1 (p-JAK1) and JAK2 (p-JAK2) were also detected in NSCLC cells; and were not found to be inhibited by GQ-ODN T40214. This further reinforces the specificity of GQ-ODN to the selective inhibition of Stat3 protein (Fig. 1C).

GQ-ODN suppressed the growth of NSCLC tumors. Assessing the effectiveness of a drug in animal models is an important step toward establishing its potential clinical utility. To this end, we utilized nude mice xenografts as animal models of *in vivo* drug testing in order to evaluate the anti-cancer potential of GQ-ODN. First, nude mice were injected subcutaneously with NSCLC cells (e.g., A549) in which Stat3 is constitutively active. After tumors were established (vol. 50~150 mm^3), treatment of nude mice with NSCLC (A549) tumors was performed by intraperitoneal (IP) injection. The nude mice were randomly assigned to 5 groups (4 or 5 mice in each group): Group 1 was treated with PEI alone (2.5 mg/kg); Group 2 was treated with paclitaxel (a clinical drug) (10 mg/kg); Groups 3 and 4 were treated with T40231/PEI and T40214/PEI (10 mg/kg/+2.5 mg/kg), respectively; and Group 5 was treated by ns-ODN/PEI (10 mg/kg/+2.5 mg/kg). PEI and ODNs were administered every two days; paclitaxel was

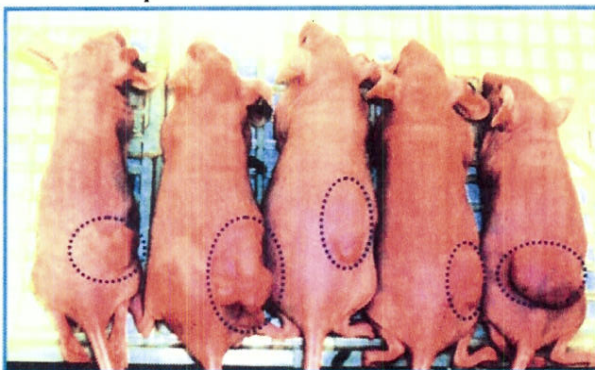
A. Beginning of placebo-treatment



Beginning of T40214-treatment



B. After placebo-treatment



After T40214-treatment

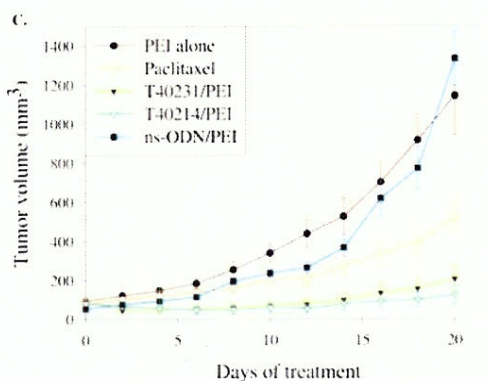
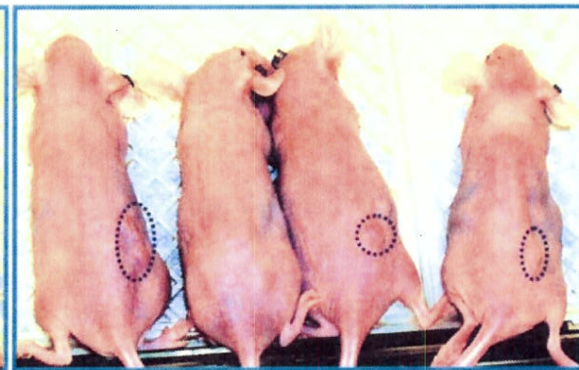


Figure 2. The photographs show nude mice with NSCLC tumors treated by PEI alone (left panels) and by GQ-ODN T40214/PEI (right panels) over a period of 21 days, (A) at the beginning of treatment and (B) at the end of treatment. (C) Tumor volumes versus days of drug treatment for the five groups of mice: i) treated by PEI alone; ii) treated by paclitaxel; iii) treated by T40231/PEI; iv) treated by T40214/PEI; and v) treated by ns-ODN/PEI.

injected every four days, to ensure safety of the mice from toxicity. Results demonstrate that, over the 21-day treatment period, i) the mean size of NSCLC tumors in the PEI- and ns-ODN-treated mice increased from 93 to 1144 mm³ and from 53 to 1334 mm³, respectively; ii) the mean size of NSCLC tumors in the paclitaxel-treated mice increased from 88 to 519 mm³; and iii) the mean size of NSCLC tumors in the mice treated with T40231 and T40214 only increased from 89 to 204 mm³ and from 83 to 123 mm³, respectively (Fig. 2). Significant differences in tumor growth were observed between PEI-treated mice and T40214-treated ($p=0.002$) or T40231-treated mice ($p=0.004$) and between the mice treated by ns-ODN (a control ODN) and by T40214 ($p=0.019$) or by T40231 ($p=0.028$) as well.

Targets of GQODN. To determine the targets of GQ-ODN and possible mechanism of GQ-ODN suppressing tumor growth, we performed immunoblotting assays on tumor tissue, as described in Materials and methods. Results demonstrate the expression of p-Stat3 and its regulated proteins in NSCLC tumors (Fig. 3A). An equal amount of protein from each tumor sample was loaded, and the intensities of the bands from mice treated with T40214/PEI (lane 2), T40231/PEI (lane 3) or paclitaxel (lane 4), were compared with that from the PEI-treated mice (lane 1). We found that GQ-ODN T40214 and T40231 totally blocked expression of phosphorylated Stat3 (p-Stat3) and its downstream proteins (i.e., Bcl-2, Bcl-x_L, Mcl-1, survivin, VEGF, Cyclin D1, and c-myc) in NSCLC tumors. However, paclitaxel did not inhibit p-Stat3, and only

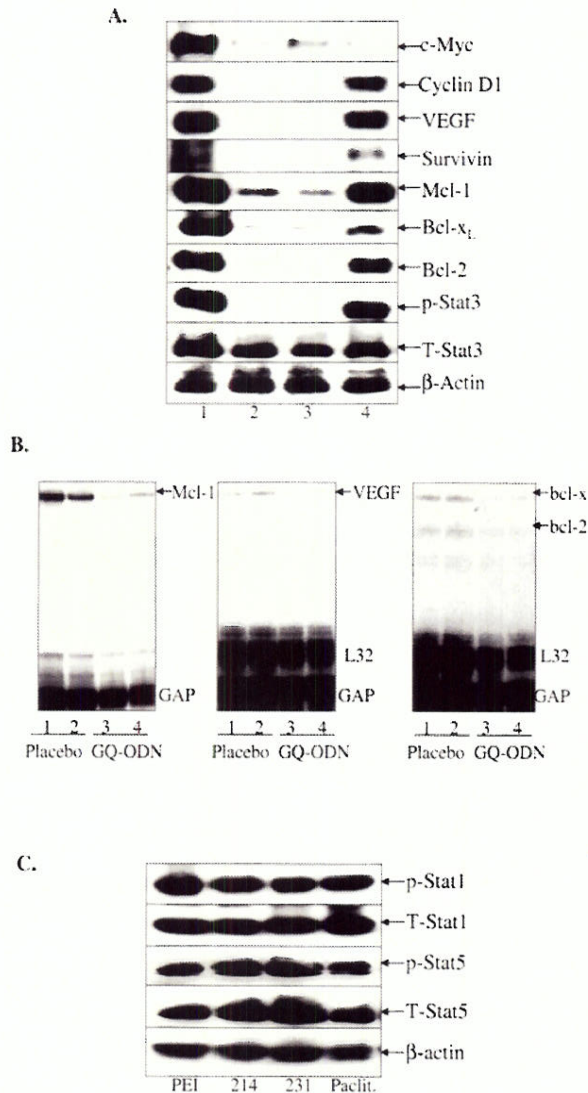


Figure 3. (A) Western blots obtained from NSCLC tumors demonstrate the expression of total Stat3 (T-Stat3), phosphorylated Stat3 (p-Stat3), and its downregulated proteins, including Bcl-2, Bcl-x_L, Mcl-1, survivin, VEGF, Cyclin D1 and c-myc. Lane 1, tumor treated by PEI alone; lane 2, tumor treated by T40214/PEI; lane 3, tumor treated by T40231/PEI; and lane 4, tumor treated by paclitaxel. β actin serves as the internal control. (B) RPA results were obtained from tumors of two PEI-treated mice (lanes 1 and 2) and two T40214-treated mice (lanes 3 and 4). The mRNA levels of the Stat3-regulated genes in T40214-treated tumors were much less than in the PEI-treated control tumors, showing that Stat3-regulated transcription of candidate genes, i.e. Mcl-1 (left), VEGF (middle), survivin (middle), Bcl-x_L, and Bcl-2 (right), was inhibited by GQ-ODNs. L32 and GAPDH represent internal controls. (C) GQ-ODN T40214 did not inhibit p-Stat1 and p-Stat5 activation *in vivo*. (C) The proteins of Stat1 and Stat5 were obtained from the same tumor samples and under the same experimental conditions as Stat3. Comparing with proteins of total Stat1 (T-Stat1) and Stat5 (T-Stat5), T40214 and T40231 did not inhibit p-Stat1 and p-Stat5 in NSCLC tumors.

partially blocked expression of Bcl-x_L, Bcl-2, survivin, and c-myc in NSCLC tumors.

To determine whether the Stat3-regulated proteins (e.g., Bcl-2, Bcl-x_L, Mcl-1, VEGF, and others) are inhibited by blocking Stat3 DNA transcription or directly by GQ-ODN, an RNase protection assay (RPA) was employed to test the

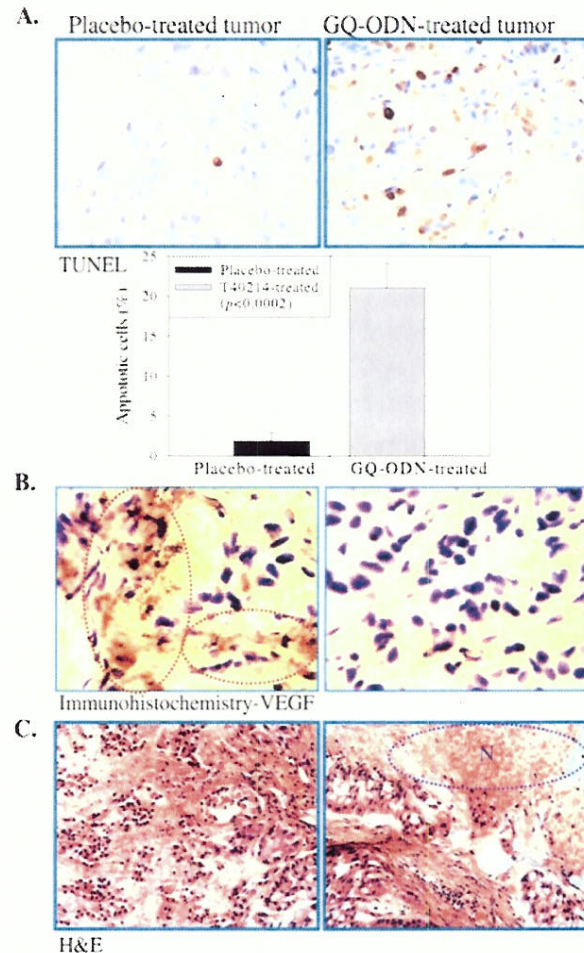


Figure 4. (A) Apoptosis of cells induced by GQ-ODN T40214 in NSCLC tumors. TUNEL-stained slides demonstrate an absence of TUNEL-positive cells (i.e., no cells are stained dark brown) in placebo-treated tumors (top left panel), whereas GQ-ODN-treated tumors (top right panel) exhibited a high number of TUNEL-positive tumor cells (photographs x400 magnification). The ratio of apoptotic cells to total cells increased 10-fold from placebo-treated tumor (1.9%) to T40214-treated tumor (21%). (B) Immunohistochemistry data show that VEGF, which appears brown in the images, was highly expressed in the tissue of NSCLC tumors treated by PEI (the circled areas); however, tumors treated by GQ-ODN T40214 showed no evidence of VEGF (photographs x400 magnification). (C) H&E images show that in PEI-treated tumors (left), all NSCLC cells were intact. In contrast, in GQ-ODN-treated tumors (right) most NSCLC cells shrank, partially resulting in necrosis (the circled area) (photographs x100 magnification).

mRNA of the Stat3-regulated genes in NSCLC tumors. The results, obtained from the tumors of two PEI-treated mice (lanes 1 and 2) and two T40214/PEI-treated mice (lanes 3 and 4), clearly show that the level of mRNA of Mcl-1, VEGF, bcl-x, and bcl-2 in T40214/PEI-treated tumors were much lower than those in the PEI-treated tumors (Fig. 3B). The mRNAs of L32 and GAP were equally loaded as controls. The RPA data provide solid evidence that GQ-ODNs inhibit the activation of Bcl-2, Bcl-x_L, Mcl-1, survivin, VEGF, Cyclin D1, and c-myc in NSCLC tumors through the disruption of Stat3 transcription.

Independent of Stat3, Stat1 and Stat5 are also active in human cancers, including NSCLC; and therefore the selective

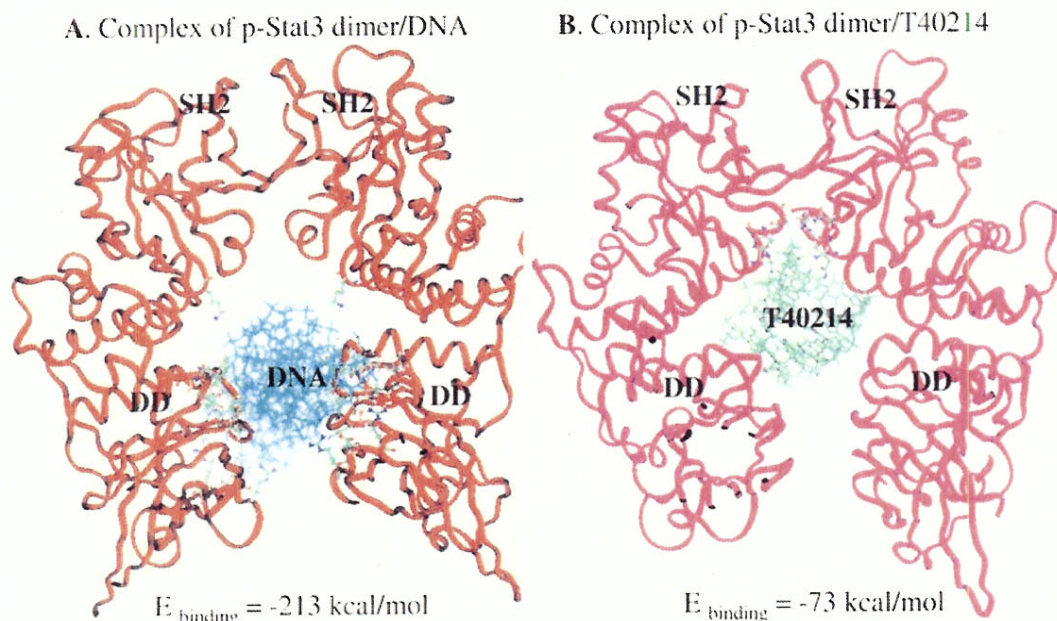


Figure 5. The complexes of p-Stat3 dimer with DNA and of p-Stat3 dimer with T40214 are demonstrated in A and B, respectively. The binding energies between Stat3 dimer and DNA and between Stat3 dimer and T40214 were calculated as -231 kcal/mol and -73 kcal/mol, respectively. (A) 30 H-bonds are formed between p-Stat3 dimer and DNA in the residues of M331 to V432 of DNA binding domains (7), and (B) seven H-bonds are formed between p-Stat3 dimer and T40214 in the residues of Q643 to N647 of SH2 domains. The residues in Stat3 forming H-bonds with DNA or T40214 are shown in stick and ball types. DD denotes DNA binding domain and SH2 denotes SH2 domain.

targeting of Stat3 becomes a key factor in the development of a potent Stat3 inhibitor. Using Western blot analysis we have shown that GQ-ODN T40214 and T40231 do not target Stat1 and Stat5. A comparison of the bands was made between T-Stat1 (total Stat1) and p-Stat1 and between T-Stat5 (total Stat5) and p-Stat5 of each tumor treated with PEI, T40214, T40231 and paclitaxel, respectively. Results demonstrate an absence of inhibition of Stat1 and Stat5 activation in GQ-ODN T40214- and T40231-treated NSCLC tumors (Fig. 3C). These results from tumor tissues are consistent with that obtained from NSCLC cells.

Tumor apoptosis and angiogenesis. We set out to determine if suppression of tumor-growth by GQ-ODN T40214 and T40231 was associated with an increase in apoptosis and reduction in angiogenesis in tumors. The TUNEL assay based on labeling the apoptotic cells with cleaved DNA fragments at the single cell level was performed to quantify apoptosis in tumors and light microscopy was used for data analysis. The apoptotic tumor cells were stained dark brown via TUNEL-positive staining, and the normal tumor cells remained unstained. Results show significant apoptosis in NSCLC tumors treated by GQ-ODN T40214 (Fig. 4A, right panel), when compared with NSCLC tumors treated by PEI alone (Fig. 4A, left panel). The analyses of the TUNEL-positive cells among total cells indicated that the percentage of apoptotic cells in PEI-treated tumors was 1.9% while that in T40214-treated tumors increased to 21.1% ($p < 0.0002$, Wilcoxin rank sum test) (Fig. 4A, bottom panel).

VEGF staining was performed using immunohistochemistry with peroxidase-labeled secondary antibodies; negative controls (first incubation step, without primary antibody) were also

included. When no staining was observed, the result was considered negative, whereas, moderate staining in the majority of the cells was considered positive. Slides were incubated with a mouse anti-VEGF monoclonal antibody. VEGF was highly expressed in the tissue of NSCLC tumors treated by PEI alone (the cycled areas) (Fig. 4B, left panel); however, VEGF was not observed in the tumors treated by GQ-ODN (Fig. 4B, right panel). These observations are consistent with the Western blotting results, which indicate that the expression of VEGF was totally blocked in GQ-ODN-treated tumors, but not in PEI-treated tumors. Microscopy with H&E staining clearly showed GQ-ODN-treatment to cause tumor cell shrinkage with chromatin condensation and partial necrosis (Fig. 4C, right panel); in contrast, PEI-treatment did not result in such changes in tumors (Fig. 4C, left panel).

Discussion

Although chemotherapy provides a clinically significant benefit for patients with advanced NSCLC, the improvement of survival for these patients is only modest (21); thus, there is a need to search for novel therapeutics. Haura *et al* showed that p-Stat3 was highly expressed in 54% of NSCLC primary tumors, suggesting that Stat3 is a promising molecular target for lung cancer (22). Our results show that when GQ-ODN was incubated with NSCLC cells for 24 h, T40214 selectively inhibited Stat3 phosphorylation. Moreover, GQ-ODN T40214 did not inhibit the activation of JAK kinases, the upstream proteins of STAT. In addition, our results in cell and tumor clearly show that GQ-ODN selectively inhibits the activation of Stat3, but not Stat1 and Stat5, both *in vitro* and *in vivo*. The selective inhibition of Stat3 activation for GQ-ODN *in vivo*

is considered beneficial to prospective clinical studies with regard to GQ-ODN since this selective targeting of Stat3 becomes a key factor in the development of a potent Stat3 inhibitor. Independent of Stat3, Stat1 and Stat5 are also active in many human cancers (5). Stat5-induced cell survival promotion has a potent oncogenic role similar to Stat3 (21). Stat1, which acts in a pro-apoptotic and anti-proliferative manner, seems to be a tumor suppressor whose functions totally differ from those of Stat3 (22,23).

In our previous studies (14,16), we demonstrated that GQ-ODN predominantly interacts with the p-Stat3 dimer in the range of amino acid residues 638 to 652, within the SH2 domains. The selective inhibition of p-Stat3 activity by GQ-ODN is based upon a few critical residues that form a local structure different from that of p-Stat1 dimer. In the p-Stat3 dimer, the paired residues of Q643 and N646 repel one another to form a channel conformation, in which GQ-ODN is held by seven H-bonds. However, the corresponding paired-residues of Stat1 dimer, K637 and S640, lock the dimer together; thereby, blocking the interaction of GQ-ODN with Stat1. Destabilizing the complex between p-Stat3 dimer and DNA is a critical step for the dephosphorylation of p-Stat3 by GQ-ODN. GQ-ODN T40214 promotes p-Stat3 dephosphorylation by blocking DNA binding to p-Stat3 dimer and forming an unstable complex between GQ-ODN T40214 and p-Stat3 dimer (3D model shown in Fig. 5). This unstable complex will dephosphorylate faster than the DNA complex. Computational energy calculation supported this hypothesis. The binding energy for the complexes DNA/p-Stat3 dimer and GQ-ODN T40214/p-Stat3 dimer are -213 kcal/mol and -73 kcal/mol, respectively. This selective inhibition of Stat3 phosphorylation observed in GQ-ODN-treated tumors (Fig. 3) is one of the greatest advantages of GQ-ODN as an anti-cancer drug.

We have demonstrated that T40214 and its analog T40231 totally blocked p-Stat3 and its downstream target proteins, including anti-apoptotic proteins: Bcl-2, Bcl-x_L, Mcl-1, and survivin; inducer of angiogenesis, VEGF; and the proteins for cell proliferation: Cyclin D1, and c-myc in tumor tissue (Fig. 3A). Additionally, we also have demonstrated that GQ-ODN also blocks the transcription of Stat3-regulated genes: Bcl-2, Bcl-x_L, Mcl-1, survivin, and VEGF in tumor tissue (Fig. 3B). To our knowledge, this is the first report to provide *in vivo* evidence of the relationship between Stat3 and its regulated genes and proteins, although it has been observed in cell culture previously (5). The inhibition of Stat3 protein induced a tremendous increase in apoptosis (Fig. 4A) and a concomitant decrease in angiogenesis (Fig. 4B) and cell proliferation in tumors, all of which strongly deter tumor growth. Consequently, the inhibition of Stat3 activation, which significantly promotes apoptosis and reduces angiogenesis and cell proliferation, strongly suppressed tumor growth.

Molecules of JAK/STAT signaling pathways, in particular Stat3, have been validated to be potential targets for cancer therapy and much effort has been made to develop novel anticancer drugs targeting Stat3 (24-49). Our systematic *in vivo* analysis (14,16) has shown that GQ-ODN as an anti-cancer agent selectively targeted Stat3 and significantly suppressed the tumor growth of a variety of tumors in nude mouse xenografts: prostate cancer ($p=0.001$); breast cancer ($p=0.001$); head and neck squamous cell carcinoma (HNSCC) ($p<0.001$);

and NSCLC ($p=0.002$). This demonstrates that GQ-ODN has the capacity to be a potent Stat3 inhibitor, and represents a novel and promising class of anti-cancer drug in the treatment of metastatic human tumors.

Acknowledgments

The authors wish to thank Maryann Mastrangelo for assisting in immuno-histochemistry and Judy Young for assisting in the revision of the manuscript. This study was in part supported by R01 CA104035, SPORE CA97007, SPORE CA58204 (to NJ) and DOD W81XWH-04-1-0142 (to LM).

References

1. Stewart BW and Kleihues P: Lung Cancer. World Cancer Report. IARC Press, Lyon, France, 2003.
2. Greenlee RT, Murray T, Bolden S and Wingo PA: Cancer statistics, 2000. CA Cancer J Clin 50: 7-33, 2000.
3. Cohen V and Khuri FR: Chemoprevention of lung cancer: current status and future prospects. Cancer Metastasis Rev 21: 349-362, 2002.
4. Ginsberg RJ, Goldberg M and Waters PF: Surgery in non-small cell lung cancer. In: Thoracic Oncology. Roth JA RJ, Weisenburger TH (eds). 2nd edition. W.B. Saunders Company, Philadelphia, PA, pp124-126, 1995.
5. Yu H and Jove R: The STATs of cancer - new molecular targets come of age. Nat Rev Cancer 4: 97-105, 2004.
6. Darnell JE Jr: STATs and gene regulation. Science 277: 1630-1635, 1997.
7. Becker S, Groner B and Muller CW: Three-dimensional structure of the Stat3beta homodimer bound to DNA. Nature 394: 145-151, 1998.
8. Chen X, Vinkemeier U, Zhao Y, Jeruzalmi D, Darnell JE Jr and Kuriyan J: Crystal structure of a tyrosine phosphorylated STAT-1 dimer bound to DNA. Cell 93: 827-839, 1998.
9. Buettner R, Mora LB and Jove R: Activated STAT signaling in human tumors provides novel molecular targets for therapeutic intervention. Clin Cancer Res 8: 945-954, 2002.
10. Mora LB, Buettner R, Seigne J, Diaz J, Ahmad N, Garcia R, Bowman T, Falcone R, Fairclough R, Cantor A, Muro-Cacho C, Livingston S, Karras J, Pow-Sang J and Jove R: Constitutive activation of Stat3 in human prostate tumors and cell lines: direct inhibition of Stat3 signaling induces apoptosis of prostate cancer cells. Cancer Res 62: 6659-6666, 2002.
11. Dolled-Filhart M, Camp RL, Kowalski DP, Smith BL and Rimm DL: Tissue microarray analysis of signal transducers and activators of transcription 3 (Stat3) and phospho-Stat3 (Tyr705) in node-negative breast cancer shows nuclear localization is associated with a better prognosis. Clin Cancer Res 9: 594-600, 2003.
12. Nagpal JK, Mishra R and Das BR: Activation of Stat-3 as one of the early events in tobacco chewing-mediated oral carcinogenesis. Cancer 94: 2393-2400, 2002.
13. Song L, Turkson J, Karras JG, Jove R and Haura EB: Activation of Stat3 by receptor tyrosine kinases and cytokines regulates survival in human non-small cell carcinoma cells. Oncogene 22: 4150-4165, 2003.
14. Jing N, Li Y, Xiong W, Sha W, Jing L and Tweardy DJ: G-quartet oligonucleotides: a new class of signal transducer and activator of transcription 3 inhibitors that suppresses growth of prostate and breast tumors through induction of apoptosis. Cancer Res 64: 6603-6609, 2004.
15. Jing N, Sha W, Li Y, Xiong W and Tweardy DJ: Rational drug design of G-quartet DNA as anti-cancer agents. Curr Pharm Des 11: 2841-2854, 2005.
16. Jing N, Zhu Q, Yuan P, Li Y, Mao L and Tweardy DJ: Targeting signal transducer and activator of transcription 3 with G-quartet oligonucleotides: a potential novel therapy for head and neck cancer. Mol Cancer Ther 5: 279-286, 2006.
17. Zhong M, Henriksen MA, Takeuchi K, Schaefer O, Liu B, ten Hoeve J, Ren Z, Mao X, Chen X, Shuai K and Darnell JE Jr: Implications of an antiparallel dimeric structure of nonphosphorylated STAT1 for the activation-inactivation cycle. Proc Natl Acad Sci USA 102: 3966-3971, 2005.

18. Darnell JE: Validating Stat3 in cancer therapy. *Nat Med* 11: 595-596, 2005.
19. Feng L, Garcia GE, Yang Y, Xia Y, Gabbai FB, Peterson OW, Abraham JA, Blantz RC and Wilson CB: Heparin-binding EGF-like growth factor contributes to reduced glomerular filtration rate during glomerulonephritis in rats. *J Clin Invest* 105: 341-350, 2000.
20. Chen S, Bacon KB, Li L, Garcia GE, Xia Y, Lo D, Thompson DA, Siani MA, Yamamoto T, Harrison JK and Feng L: *In vivo* inhibition of CC and CX3C chemokine-induced leukocyte infiltration and attenuation of glomerulonephritis in Wistar-Kyoto (WKY) rats by vMIP-II. *J Exp Med* 188: 193-198, 1998.
21. Debierre-Grockiego F: Anti-apoptotic role of STAT5 in haematopoietic cells and in the pathogenesis of malignancies. *Apoptosis* 9: 717-728, 2004.
22. Reck M and Gatzemeier U: Chemotherapy in stage-IV NSCLC. *Lung Cancer* 45 (suppl 2): S217-S222, 2004.
23. O'Shea JJ, Gadina M and Schreiber RD: Cytokine signaling in 2002: new surprises in the Jak/Stat pathway. *Cell* 109 (suppl): S121-S131, 2002.
24. Turkson J, Ryan D, Kim JS, Zhang Y, Chen Z, Haura E, Laudano A, Sebt SM, Hamilton AD and Jove R: Phosphotyrosyl peptides block Stat3-mediated DNA binding activity, gene regulation, and cell transformation. *J Biol Chem* 276: 45443-45455, 2001.
25. Stahl N, Farruggella TJ, Boulton TG, Zhong Z, Darnell JE Jr and Yancopoulos GD: Choice of STATs and other substrates specified by modular tyrosine-based motifs in cytokine receptors. *Science* 267: 1349-1353, 1995.
26. Shao H, Cheng HY, Cook RG and Twardy DJ: Identification and characterization of signal transducer and activator of transcription 3 recruitment sites within the epidermal growth factor receptor. *Cancer Res* 63: 3923-3930, 2003.
27. Wiederkehr-Adam M, Ernst P, Muller K, Bieck E, Gombert FO, Ottl J, Graff P, Grossmuller F and Heim MH: Characterization of phosphopeptide motifs specific for the Src homology 2 domains of signal transducer and activator of transcription 1 (STAT1) and STAT3. *J Biol Chem* 278: 16117-16128, 2003.
28. Coleman DR, Ren Z, Mandal PK, Cameron AG, Dyer GA, Muranjan S, Campbell M, Chen X and McMurray JS: Investigation of the binding determinants of phosphopeptides targeted to the SRC homology 2 domain of the signal transducer and activator of transcription 3. Development of a high-affinity peptide inhibitor. *J Med Chem* 48: 6661-6670, 2005.
29. Grandis JR, Drenning SD, Zeng Q, Watkins SC, Melhem MF, Endo S, Johnson DE, Huang L, He Y and Kim JD: Constitutive activation of Stat3 signaling abrogates apoptosis in squamous cell carcinogenesis *in vivo*. *Proc Natl Acad Sci USA* 97: 4227-4232, 2000.
30. Niu G, Shain KH, Huang M, Ravi R, Bedi A, Dalton WS, Jove R and Yu H: Overexpression of a dominant-negative signal transducer and activator of transcription 3 variant in tumor cells leads to production of soluble factors that induce apoptosis and cell cycle arrest. *Cancer Res* 61: 3276-3280, 2001.
31. Epling-Burnette PK, Liu JH, Catlett-Falcone R, Turkson J, Oshiro M, Kothapalli R, Li Y, Wang JM, Yang-Yen HF, Karras J, Jove R and Loughran TP Jr: Inhibition of STAT3 signaling leads to apoptosis of leukemic large granular lymphocytes and decreased Mcl-1 expression. *J Clin Invest* 107: 351-362, 2001.
32. Leong PL, Andrews GA, Johnson DE, Dyer KF, Xi S, Mai JC, Robbins PD, Gadiparthi S, Burke NA, Watkins SF and Grandis JR: Targeted inhibition of Stat3 with a decoy oligonucleotide abrogates head and neck cancer cell growth. *Proc Natl Acad Sci USA* 100: 4138-4143, 2003.
33. Meydan N, Grunberger T, Dadi H, Shahar M, Arpaia E, Lapidot Z, Leeder JS, Freedman M, Cohen A, Gazit A, Levitzki A and Roifman CM: Inhibition of acute lymphoblastic leukaemia by a Jak-2 inhibitor. *Nature* 379: 645-648, 1996.
34. Faderl S, Ferrajoli A, Harris D, Van Q, Priebe W and Estrov Z: WP-1034, a novel JAK-STAT inhibitor, with proapoptotic and antileukemic activity in acute myeloid leukemia (AML). *Anticancer Res* 25: 1841-1850, 2005.
35. Blaskovich MA, Sun J, Cantor A, Turkson J, Jove R and Sebt SM: Discovery of JSI-124 (cucurbitacin I), a selective Janus kinase/signal transducer and activator of transcription 3 signaling pathway inhibitor with potent antitumor activity against human and murine cancer cells in mice. *Cancer Res* 63: 1270-1279, 2003.
36. Rajasingh J, Raikwar HP, Muthian G and Johnson C: Curcumin induces growth-arrest and apoptosis in association with the inhibition of constitutively active JAK-STAT pathway in T cell leukemia. *Biochem Biophys Res Commun* 340: 359-368, 2006.
37. Shi X, Franko B, Frantz C, Amin HM and Lai R: JSI-124 (cucurbitacin I) inhibits Janus kinase-3/signal transducer and activator of transcription-3 signalling, downregulates nucleophosmin-anaplastic lymphoma kinase (ALK), and induces apoptosis in ALK-positive anaplastic large cell lymphoma cells. *Br J Haematol* 135: 26-32, 2006.
38. Song L, Morris M, Bagui T, Lee FY, Jove R and Haura EB: Dasatinib (BMS-354825) selectively induces apoptosis in lung cancer cells dependent on epidermal growth factor receptor signaling for survival. *Cancer Res* 66: 5542-5548, 2006.
39. Lee YK, Isham CR, Kaufman SH and Bible KC: Flavopiridol disrupts STAT3/DNA interactions, attenuates STAT3-directed transcription, and combines with the Jak kinase inhibitor AG490 to achieve cytotoxic synergy. *Mol Cancer Ther* 5: 138-148, 2006.
40. Chakravarti N, Myers JN and Aggarwal BB: Targeting constitutive and interleukin-6-inducible signal transducers and activators of transcription 3 pathway in head and neck squamous cell carcinoma cells by curcumin (diferuloylmethane). *Int J Cancer* 119: 1268-1275, 2006.
41. Cuevas P, Diaz-Gonzalez D, Sanchez I, Lozano RM, Gimenez-Gallego G and Dujovny M: Dobesilate inhibits the activation of signal transducer and activator of transcription 3, and the expression of cyclin D1 and bcl-XL in glioma cells. *Neurol Res* 28: 127-130, 2006.
42. Kotha A, Sekharam M, Cilenti L, Siddiquee K, Khaled A, Zervos AS, Carter B, Turkson J and Jove R: Resveratrol inhibits Src and Stat3 signaling and induces the apoptosis of malignant cells containing activated Stat3 protein. *Mol Cancer Ther* 5: 621-629, 2006.
43. Amit-Vazina M, Shishodia S, Harris D, Van Q, Wang M, Weber D, Alexanian R, Talpaz M, Aggarwal BB and Estrov Z: Atiprimod blocks STAT3 phosphorylation and induces apoptosis in multiple myeloma cells. *Br J Cancer* 93: 70-80, 2005.
44. Nam S, Buettner R, Turkson J, Kim D, Cheng JQ, Muchlbeyer S, Hippe F, Vatter S, Merz KH, Eisenbrand G and Jove R: Indirubin derivatives inhibit Stat3 signaling and induce apoptosis in human cancer cells. *Proc Natl Acad Sci USA* 102: 5998-6003, 2005.
45. Venkatasubbarao K, Choudary A and Freeman JW: Farnesyl transferase inhibitor (R115777)-induced inhibition of STAT3(Tyr705) phosphorylation in human pancreatic cancer cell lines require extracellular signal-regulated kinases. *Cancer Res* 65: 2861-2871, 2005.
46. Sun J, Blaskovich MA, Jove R, Livingston SK, Coppola D and Sebt SM: Cucurbitacin Q: a selective STAT3 activation inhibitor with potent antitumor activity. *Oncogene* 24: 3236-3245, 2005.
47. Turkson J, Zhang S, Palmer J, Kay H, Stanko J, Mora LB, Sebt S, Yu H and Jove R: Inhibition of constitutive signal transducer and activator of transcription 3 activation by novel platinum complexes with potent antitumor activity. *Mol Cancer Ther* 3: 1533-1542, 2004.
48. Barton BE, Murphy TF, Shu P, Huang HF, Meyenhofer M and Barton A: Novel single-stranded oligonucleotides that inhibit signal transducer and activator of transcription 3 induce apoptosis *in vitro* and *in vivo* in prostate cancer cell lines. *Mol Cancer Ther* 3: 1183-1191, 2004.
49. Bharti AC, Donato N and Aggarwal BB: Curcumin (diferuloylmethane) inhibits constitutive and IL-6-inducible STAT3 phosphorylation in human multiple myeloma cells. *J Immunol* 171: 3863-3871, 2003.

Characterizing the cancer genome in lung adenocarcinoma

Barbara A. Weir^{1,2*}, Michele S. Woo^{1*}, Gad Getz^{2*}, Sven Perner^{3,4}, Li Ding⁵, Rameen Beroukhi^{1,2}, William M. Lin^{1,2}, Michael A. Province⁶, Aldi Kraja⁶, Laura A. Johnson³, Kinjal Shah^{1,2}, Mitsuo Sato⁸, Roman K. Thomas^{1,2,9,10}, Justine A. Barletta³, Ingrid B. Borecki⁶, Stephen Broderick^{11,12}, Andrew C. Chang¹⁴, Derek Y. Chiang^{1,2}, Lucian R. Chirieac^{3,16}, Jeonghee Cho¹, Yoshitaka Fujii¹⁸, Adi F. Gazdar⁸, Thomas Giordano¹⁵, Heidi Greulich^{1,2}, Megan Hanna^{1,2}, Bruce E. Johnson¹, Mark G. Kris¹¹, Alex Lash¹¹, Ling Lin⁵, Neal Lindeman^{3,16}, Elaine R. Mardis⁵, John D. McPherson¹⁹, John D. Minna⁸, Margaret B. Morgan¹⁹, Mark Nadel^{1,2}, Mark B. Orringer¹⁴, John R. Osborne⁵, Brad Ozenberger²⁰, Alex H. Ramos^{1,2}, James Robinson², Jack A. Roth²¹, Valerie Rusch¹¹, Hidefumi Sasaki¹⁸, Frances Shepherd²⁵, Carrie Sougnez², Margaret R. Spitz²², Ming-Sound Tsao²⁵, David Twomey², Roel G. W. Verhaak², George M. Weinstock¹⁹, David A. Wheeler¹⁹, Wendy Winckler^{1,2}, Akihiko Yoshizawa¹¹, Soyoung Yu¹, Maureen F. Zakowski¹¹, Qunyu Zhang⁶, David G. Beer¹⁴, Ignacio I. Wistuba^{23,24}, Mark A. Watson⁷, Levi A. Garraway^{1,2}, Marc Ladanyi^{11,12}, William D. Travis¹¹, William Pao^{11,12}, Mark A. Rubin^{2,3}, Stacey B. Gabriel², Richard A. Gibbs¹⁹, Harold E. Varmus¹³, Richard K. Wilson⁵, Eric S. Lander^{2,17,26} & Matthew Meyerson^{1,2,16}

Somatic alterations in cellular DNA underlie almost all human cancers¹. The prospect of targeted therapies² and the development of high-resolution, genome-wide approaches^{3–8} are now spurring systematic efforts to characterize cancer genomes. Here we report a large-scale project to characterize copy-number alterations in primary lung adenocarcinomas. By analysis of a large collection of tumours ($n = 371$) using dense single nucleotide polymorphism arrays, we identify a total of 57 significantly recurrent events. We find that 26 of 39 autosomal chromosome arms show consistent large-scale copy-number gain or loss, of which only a handful have been linked to a specific gene. We also identify 31 recurrent focal events, including 24 amplifications and 7 homozygous deletions. Only six of these focal events are currently associated with known mutations in lung carcinomas. The most common event, amplification of chromosome 14q13.3, is found in ~12% of samples. On the basis of genomic and functional analyses, we identify *NKX2-1* (NK2 homeobox 1, also called *TTF1*), which lies in the minimal 14q13.3 amplification interval and encodes a lineage-specific transcription factor, as a novel candidate proto-oncogene involved in a significant fraction of lung adenocarcinomas. More generally, our results indicate that many of the genes that are involved in lung adenocarcinoma remain to be discovered.

A collection of 528 snap-frozen lung adenocarcinoma resection specimens, with at least 70% estimated tumour content, was selected by a panel of thoracic pathologists (Supplementary Table 1); samples were anonymized to protect patient privacy. Tumour and normal

DNAs were hybridized to Affymetrix 250K Sty single nucleotide polymorphism (SNP) arrays. Genomic copy number for each of over 238,000 probe sets was determined by calculating the intensity ratio between the tumour DNA and the average of a set of normal DNAs^{9,10}. Segmented copy numbers for each tumour were inferred with the GLAD (gain and loss analysis of DNA) algorithm¹¹ and normalized to a median of two copies. Each copy number profile was then subjected to quality control, resulting in 371 high-quality samples used for further analysis, of which 242 had matched normal samples (Methods).

To identify regions of copy-number alteration, we applied GISTIC (genomic identification of significant targets in cancer)¹², a statistical method that calculates a score that is based on both the amplitude and frequency of copy-number changes at each position in the genome, using permutation testing to determine significance (Methods).

GISTIC identified 26 large-scale events and 31 focal events, reported below. Although the overall pattern is broadly consistent with the literature on lung cancer^{8,13–15}, our sample size and resolution provide more power to accurately identify and localize both large-scale and focal chromosomal alterations. With respect to large-scale events, no single previous study has identified more than 5 of the gains or 11 of the losses^{13,14} (Supplementary Table 2). With respect to focal events, three recent studies^{8,14,15} report a total of ~200 events, including 23 of the 31 recurrent focal events observed in our study. The overlap among these three studies is limited to only four events (amplification of *EGFR*, *CCNE1*, *MDM2* and 8p11, all seen

¹Department of Medical Oncology and Center for Cancer Genome Discovery, Dana-Farber Cancer Institute, Boston, Massachusetts 02115, USA. ²Cancer Program, Genetic Analysis Platform, and Genome Biology Program, Broad Institute of Harvard and MIT, Cambridge, Massachusetts 02142, USA. ³Department of Pathology, Brigham and Women's Hospital, Boston, Massachusetts 02115, USA. ⁴Institute of Pathology, University of Ulm, Ulm 89081, Germany. ⁵Genome Sequencing Center, ⁶Division of Statistical Genomics and ⁷Department of Pathology and Immunology, Washington University in Saint Louis, Saint Louis, Missouri 63130, USA. ⁸University of Texas Southwestern Medical Center, Dallas, Texas 75390, USA. ⁹Max Planck Institute for Neurological Research with Klaus-Joachim Zülch Laboratories of the Max-Planck Society and the Medical Faculty of the University of Cologne, Cologne 50931, Germany. ¹⁰Center for Integrated Oncology and Department I for Internal Medicine, University of Cologne, Cologne 50931, Germany. ¹¹Departments of Medicine, Surgery, Pathology, and Computational Biology. ¹²Human Oncology and Pathogenesis Program. ¹³Cancer Biology and Genetics Program, Memorial Sloan-Kettering Cancer Center, New York, New York 10065, USA. ¹⁴Section of Thoracic Surgery, Department of Surgery and ¹⁵Department of Pathology, University of Michigan, Ann Arbor, Michigan 48109, USA. ¹⁶Department of Pathology and ¹⁷Department of Systems Biology, Harvard Medical School, Boston, Massachusetts 02115, USA. ¹⁸Department of Surgery, Nagoya City University Medical School, Nagoya 467-8602, Japan. ¹⁹Human Genome Sequencing Center, Baylor College of Medicine, Houston, Texas 77030, USA. ²⁰National Human Genome Research Institute, National Institutes of Health, Bethesda, Maryland 20892, USA. ²¹Department of Thoracic and Cardiovascular Surgery, ²²Department of Epidemiology, ²³Department of Pathology and ²⁴Department of Thoracic/Head and Neck Medical Oncology, The University of Texas M.D. Anderson Cancer Center, Houston, Texas 77030, USA. ²⁵University Health Network and Princess Margaret Hospital, Toronto M5G 2C4, Canada. ²⁶Department of Biology, Massachusetts Institute of Technology, Cambridge, Massachusetts 02142, USA.

*These authors contributed equally to this work.

here; Supplementary Table 3 and Supplementary Results). A genome-wide view of segmented copy number reveals that most chromosomal arms undergo either amplification or deletion across a large proportion of the samples (Fig. 1a). The distinctive pattern of amplification and loss is also apparent when the median copy number for each chromosome arm is plotted (Supplementary Fig. 1 and Supplementary Table 4). In total, GISTIC identifies 26 large segments (at least half of a chromosome arm), 10 with significant gains and 16 with significant losses (Fig. 1b and Supplementary Table 5).

Visual inspection reveals that similar chromosomal patterns of copy number loss and gain across the genome are found in almost all samples, but that the samples show substantial differences in the amplitude of copy-number variation (Fig. 1a). When the samples are

partitioned into tertiles on the basis of overall variation in copy-number amplitude, each shows similar regions of amplification and loss across the genome. The attenuation seen in many samples is consistent with admixture with euploid non-tumour DNA, which we estimate at 50%, 65% and 78% respectively in the three tertiles (Supplementary Results and Supplementary Fig. 2). The significant non-tumour admixture in these tumour samples also makes it difficult to assess genome-wide loss of heterozygosity (LOH). Because normal DNA admixture limits sensitivity, we report LOH only in the top tertile; we see both LOH associated with copy-number loss and copy-neutral LOH (chromosomes 17p and 19p) (Supplementary Results, Supplementary Figs 3 and 4, and Supplementary Table 6).

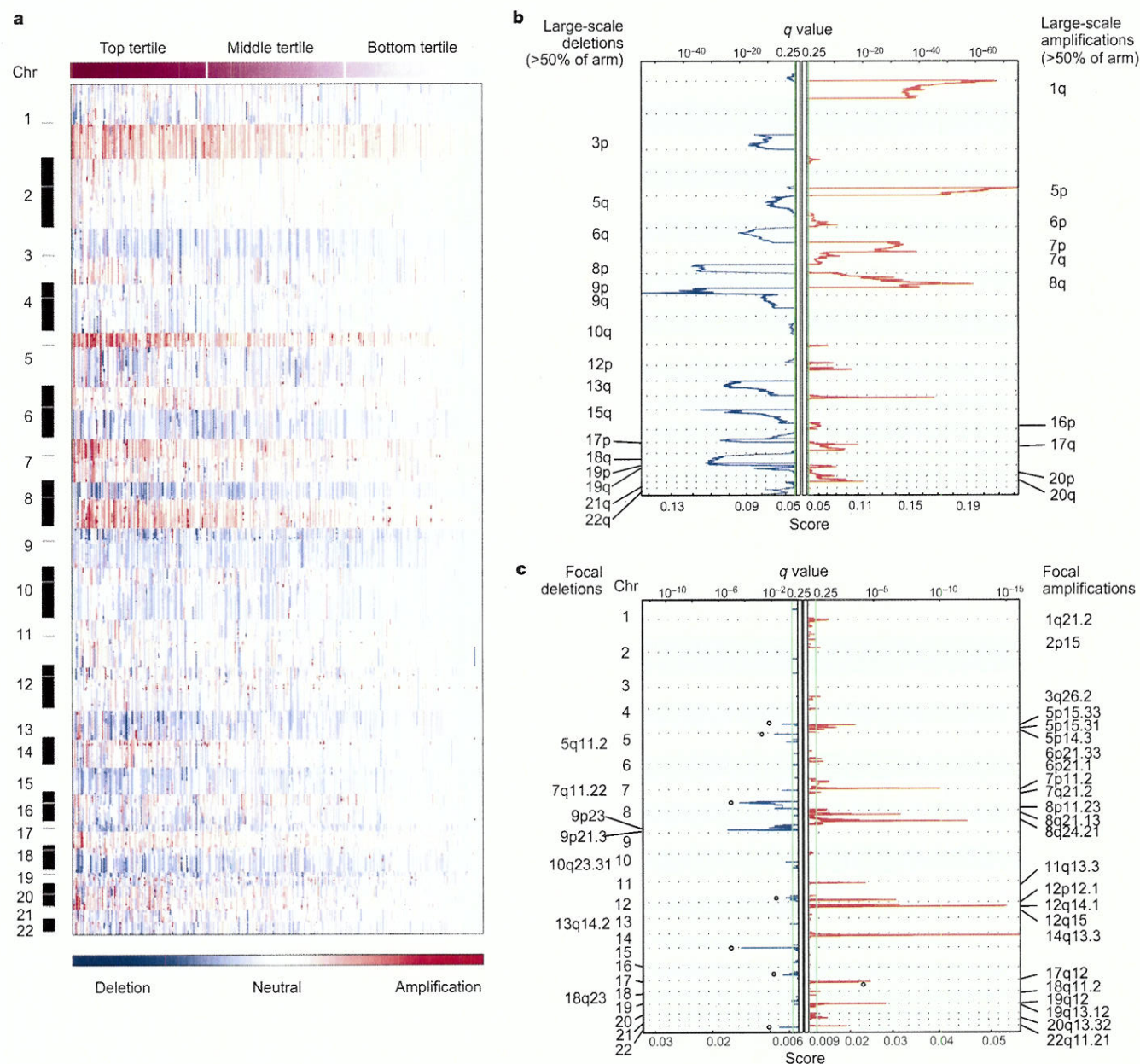


Figure 1 | Large-scale genomic events in lung adenocarcinoma.

a, Smoothed copy number data for 371 lung adenocarcinoma samples (columns; ordered by degree of interchromosomal variation and divided into top, middle and bottom tertiles) is shown by genomic location (rows). The colour scale ranges from blue (deletion) through white (neutral; two copies in diploid specimens) to red (amplification). **b**, **c**, False-discovery rates (q values; green line is 0.25 cut-off for significance) and scores for each

alteration (x axis) are plotted at each genome position (y axis); dotted lines indicate the centromeres. Amplifications (red lines) and deletions (blue lines) are shown for large-scale events (**b**; $\geq 50\%$ of a chromosome arm; copy number threshold = 2.14 and 1.87) and focal events (**c**; copy number threshold = 3.6 and 1.2). Open circles label known or presumed germline copy-number polymorphisms.

The most common genomic alteration in lung adenocarcinoma is copy-number gain of chromosome 5p, which is found in 60% of total samples and over 80% of the top tertile (Supplementary Table 5). Another 15 large-scale events are seen in at least 33% of all samples and over 40% of the top tertile. Together, the regions of common copy-number gain (~650 megabases (Mb)) and copy-number loss (~1,010 Mb) comprise more than half of the human genome (Supplementary Results and Supplementary Table 5). Despite their high frequency, few of these large-scale events have been clearly related to functional effects on specific genes. Loss of a chromosome arm is likely to act by uncovering an inactivated tumour suppressor gene, yet such mutations have been well-established in lung adenocarcinoma in only three of the sixteen deleted chromosome arms (*CDKN2A* on 9p, *TP53* on 17p and *STK11* on 19p)^{16–18}. We tested for correlations between the large-scale lesions and clinical parameters, but none was significant after correction for multiple hypothesis testing (Supplementary Results and Supplementary Table 7).

Focal deletions may help pinpoint tumour suppressor genes, particularly on chromosome arms that show frequent copy-number loss. At a threshold set to detect homozygous deletions in the presence of stromal contamination, GISTIC analysis identified seven focal candidate regions (Fig. 1c and Supplementary Table 8). The most significant focal deletions, detected in 3% of all samples and 6.5% of the top tertile, encompass *CDKN2A/CDKN2B*, two well-documented tumour suppressor genes on chromosome 9p21 (Fig. 1c, Table 1 and Supplementary Table 8). The protein products of *CDKN2A* and *CDKN2B* inhibit two cyclin-dependent kinases, Cdk4 and Cdk6, the genes of which both reside in frequently amplified regions (see below). Two other deleted regions also encompass known tumour suppressor genes, *PTEN* and *RBI* (Supplementary Table 8).

Three additional deletion regions each localize to a single gene. Deletions of the 5' untranslated region of *PTPRD*, encoding a tyrosine phosphatase, occur in 4% of the top tertile. Although *PTPRD* deletions have been reported in lung adenocarcinoma cell lines^{8,19,20}, this is the first observation in primary human lung adenocarcinomas. Homozygous deletions of *PDE4D* occur in 1.6% of the top tertile and typically remove several hundred kilobases and affect multiple exons (Supplementary Fig. 5). These deletions may be significant for lung

biology because *PDE4D* encodes the major phosphodiesterase responsible for degrading cyclic AMP in airway epithelial cells²¹. Another single-gene deletion occurs within *AUTS2*, a gene of unknown function in chromosome 7q11.22 (Table 1 and Supplementary Table 8). We cannot exclude the possibility that some recurrent copy-number losses are due to genomic fragility unrelated to carcinogenesis; the presence of point mutations would provide additional support for a role in cancer.

We therefore sequenced all exons of *AUTS2*, *PDE4D* and *PTPRD*, as each of these genes showed single-gene deletions but no mutations have been reported in primary tumours. Although we did not detect somatic mutations in *AUTS2* or *PDE4D*, we identified validated somatic *PTPRD* mutations in 11 of 188 samples sequenced. Notably, three of the mutations encode predicted inactivating changes in the tyrosine phosphatase domain (Supplementary Table 9 and Supplementary Fig. 6). These results implicate *PTPRD* as a probable cancer-associated gene, although further studies are needed to establish a causative role in cancer via gain or loss of function.

We focused above on homozygous deletions, but note that this approach will miss important genes. Notably, the *TP53* locus is known to be mutated in ~50% of lung adenocarcinomas but shows no homozygous deletions in our data.

We next focused on focal amplification events, for which it may be easier to pinpoint target genes. At a threshold designed to identify high-copy amplification, the GISTIC analysis identified 24 recurrent genomic segments with maximum copy number ranging from about 4- to 16-fold (Fig. 1c, Table 1 and Supplementary Table 10). The amplification events are seen in 1–7% of all samples (1–12% in the top tertile). Each of these events is seen in at least two samples and all but eight are seen in at least five samples. In the 13 most significant amplifications ($q < 0.01$), the regions can be localized to relatively small genomic segments containing 15 or fewer genes. Although 14 of the 24 regions of recurrent amplification contain a known proto-oncogene (Supplementary Table 10), only three of these genes (*EGFR*, *KRAS* and *ERBB2*) have been previously reported to be mutated in lung adenocarcinoma (Supplementary Results). The remaining 11 genes are clear targets for re-sequencing in lung tumours.

Table 1 | Top focal regions of amplification and deletion

Cytoband*	q value	Peak region (Mb)*	Max/Min inferred copy no.	Number of genes*†	Known proto-oncogene/ tumour suppressor gene in region*‡	New candidate(s)
Amplifications						
14q13.3	2.26×10^{-29}	35.61–36.09	13.7	2	–	NKX2-1, MBIP
12q15	1.78×10^{-15}	67.48–68.02	9.7	3	MDM2	–
8q24.21	9.06×10^{-13}	129.18–129.34	10.3	0	MYC§	–
7p11.2	9.97×10^{-11}	54.65–55.52	8.7	3	EGFR	–
8q21.13	1.13×10^{-7}	80.66–82.55	10.4	8	–	–
12q14.1	1.29×10^{-7}	56.23–56.54	10.4	15	CDK4	–
12p12.1	2.83×10^{-7}	24.99–25.78	10.4	6	KRAS	–
19q12	1.60×10^{-6}	34.79–35.42	6.7	5	CCNE1	–
17q12	2.34×10^{-5}	34.80–35.18	16.1	12	ERBB2	–
11q13.3	5.17×10^{-5}	68.52–69.36	6.5	9	CCND1	–
5p15.33	0.000279	0.75–1.62	4.2	10	TERT	–
22q11.21	0.001461	19.06–20.13	6.6	15	–	–
5p15.31	0.007472	8.88–10.51	5.6	7	–	–
1q21.2	0.028766	143.48–149.41	4.6	86	ARNT	–
20q13.32	0.0445	55.52–56.30	4.4	6	–	–
5p14.3	0.064673	19.72–23.09	3.8	2	–	–
6p21.1	0.078061	43.76–44.12	7.7	2	–	VEGFA
Deletions						
9p21.3	3.35×10^{-13}	21.80–22.19	0.7	3	CDKN2A/ CDKN2B	–
9p23	0.001149	9.41–10.40	0.4	1	–	PTPRD
5q11.2	0.005202	58.40–59.06	0.6	1	–	PDE4D
7q11.22	0.025552	69.50–69.62	0.7	1	–	AUTS2
10q23.31	0.065006	89.67–89.95	0.5	1	PTEN	–

* Based on hg17 human genome assembly.

† RefSeq genes only.

‡ Known tumour suppressor genes and proto-oncogenes defined as found in either COSMIC³², CGP Census³¹ or other evidence; if there is more than one known proto-oncogene in the region, only one is listed (priority for listing is, in order: known lung adenocarcinoma mutation; known lung cancer mutation; other known mutation (by COSMIC frequency); listing in CGP Census).

§ MYC is near, but not within, the peak region.

|| Single gene deletions previously seen, this study provides new mutations as well.

Our data localize the amplification peak on chromosome 5p to the telomerase catalytic subunit gene, *TERT*. Although broad amplification of chromosome 5p has been described in non-small-cell lung cancer (NSCLC)^{13,22,23}, the target of 5p amplification has not been determined. In our data set, eight tumours with amplicons in chromosome 5p15 delineate a region containing ten genes, including *TERT* (Table 1 and Supplementary Table 10), suggesting that *TERT* may be the target of the amplification and thereby contributes to cellular immortalization.

Chromosome 6p21.1 shows focal amplification in four samples in a region containing two genes, one of which (*VEGFA*) encodes vascular endothelial growth factor (Table 1 and Supplementary Table 10). This amplification suggests a possible mechanism for increased angiogenesis and for the reported response to angiogenic inhibitors such as the anti-VEGF antibody bevacizumab in lung adenocarcinoma^{24,25}. Similarly, amplification of regions including several cell cycle genes such as *CDK4*, *CDK6* and *CCND1* suggests an important role for these genes (Table 1 and Supplementary Table 10).

Notably, the most common focal amplification does not include any known proto-oncogenes: chromosome 14q13.3 is amplified in 6% of the samples overall and 12% of the samples in the top tertile (Fig. 1c, Table 1 and Supplementary Table 10; $q < 10^{-28}$). Although previous studies have reported amplification of 14q13 in lung cancer cell lines¹⁴ and the region is mentioned in studies of primary lung tumours^{8,15}, the target gene in this region had not been identified. With our large sample size, we are able to narrow the critical region to a 480-kilobase interval containing only two known genes, *MBIP* and *NKX2-1* (Fig. 2a, b, Table 1 and Supplementary Table 10). Data for a single tumour with a small region of high-level amplification, comprising *MBIP* and *NKX2-1*, exclude the neighbouring gene, *NKX2-8* (Fig. 2c).

We confirmed the amplification of the region by fluorescence *in situ* hybridization (FISH) and quantitative polymerase chain reaction (qPCR; data not shown). FISH analysis was performed with a bacterial artificial chromosome (BAC) probe containing *NKX2-1* and *NKX2-8* (Fig. 2c) on an independent set of 330 lung adenocarcinoma samples from tissue microarrays. High-level amplification of the chromosome 14q13.3 region was seen in 12% (40 out of 330) of these lung tumours. The FISH studies revealed amplification up to an estimated 100-fold (Fig. 2d and Supplementary Fig. 7); the lower amplification estimated on the SNP arrays (up to 14-fold) probably reflects signal saturation, stromal admixture and tumour heterogeneity. No significant difference in patient survival after surgical resection and long-term follow-up was observed between tumours with amplified or non-amplified *NKX2-1* (Supplementary Fig. 8 and Supplementary Table 11). Exon-based sequencing in 384 lung adenocarcinoma DNA samples showed no somatic mutations in either *NKX2-1* or *MBIP* (Supplementary Results), indicating that any oncogenic function might be exerted by the wild-type gene.

We used RNA interference (RNAi) to test the roles of both *MBIP* and *NKX2-1* with respect to cell survival and oncogenic properties. Expression of two different short hairpin RNAs (shRNAs) targeting *NKX2-1* significantly reduced the levels of *NKX2-1* protein in NCI-H2009 cells (Fig. 3a) and NCI-H661 cells (data not shown)—NSCLC lines that carry 14q amplifications¹⁴. No *NKX2-1* protein was detected in A549 cells that lack 14q amplification (Fig. 3a).

RNAi-mediated inhibition of *NKX2-1* expression substantially decreased the ability of NCI-H2009 cells to grow in an anchorage-independent manner as measured by colony formation in soft agar (Fig. 3b), which may be due, in part, to a loss of cell viability. NCI-H661 cell viability was also impaired by *NKX2-1* RNAi (Supplementary Fig. 9). *NKX2-1* knockdown leads to a decrease in colony formation in lung adenocarcinoma lines (NCI-H1975 and HCC1171) that lack chromosome 14q13 amplification but express *NKX2-1* (Supplementary Fig. 10), but has no effect on either soft agar colony formation or cell viability in A549 cells, which express little or no *NKX2-1* protein (Fig. 3a, c). In contrast to the results for *NKX2-1*,

RNAi-based *MBIP* knockdown neither decreased colony formation in NCI-H2009 cells (Fig. 3d, e) or in NCI-H661 cells (Supplementary Fig. 11a, b), nor reduced cell viability (Supplementary Fig. 11c, d). It thus seems that *NKX2-1*, but not *MBIP*, is essential for the survival and tumorigenic properties of lung adenocarcinoma cell lines that express *NKX2-1*.

Systematic understanding of the molecular basis of a particular type of cancer will require at least three steps: comprehensive characterization of recurrent genomic aberrations (including copy-number changes, nucleotide sequence changes, chromosomal rearrangements and epigenetic alterations); elucidation of their biological role in cancer pathogenesis; and evaluation of their utility for diagnostics, prognostics and therapeutics. This study represents a step towards comprehensive genomic characterization of one of the

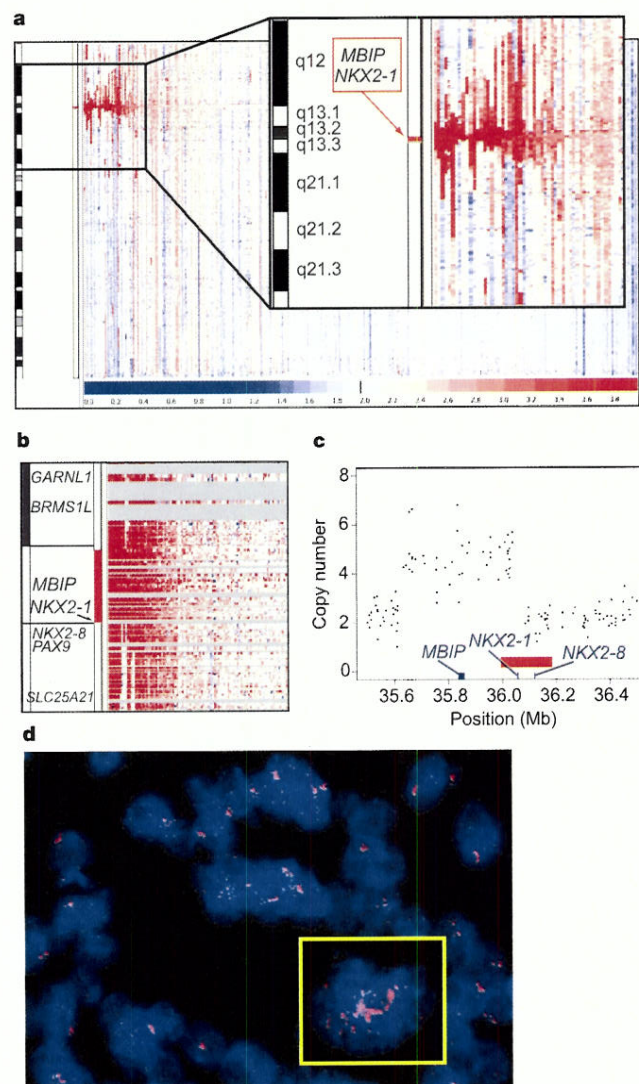


Figure 2 | High-prevalence amplification of the *MBIP/NKX2-1* locus on chromosome 14q. **a**, Copy number on chromosome 14q is shown for 371 lung adenocarcinomas (columns; ordered by amplification) from centromere (top) to telomere (bottom). Colour scale as in Fig. 1. **b**, Magnified view of the amplified region from **a**; grey bars represent the absence of SNPs on the array. **c**, Raw copy number data (y axis) for one sample defining the minimally amplified region are plotted according to chromosome 14 position (x axis; scale in megabases). Genomic positions of *MBIP*, *NKX2-1*, *NKX2-8* and the BAC used for FISH (red bar) are shown along the x axis. **d**, FISH for *NKX2-1* (red) and a chromosome 14 reference probe (green) on a lung adenocarcinoma specimen with high-level amplification of the *NKX2-1* probe. Nuclei are stained with 4,6-diamidino-2-phenylindole (DAPI; blue). The yellow box shows a single nucleus.

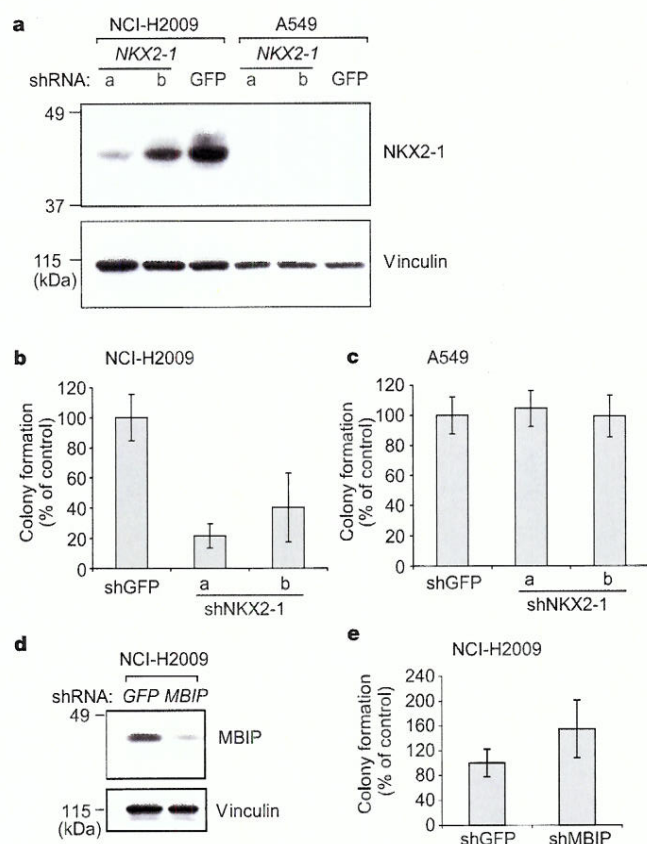


Figure 3 | *NKX2-1* RNAi leads to reduced anchorage-independent growth and viability of NCI-H2009 cells but not A549 cells. **a**, Anti-*NKX2-1* and control anti-vinculin immunoblots of lysates from NCI-H2009 and A549 cells expressing shRNA against *NKX2-1* (shNKX2-1a and shNKX2-1b) or GFP (shGFP) as control. **b**, Soft agar colony formation by NCI-H2009 cells is shown relative to the shGFP control as a mean percentage (\pm standard deviation in triplicate samples; $P = 5.8 \times 10^{-6}$ when comparing shGFP to shNKX2-1a and $P = 5.1 \times 10^{-4}$ when comparing shGFP to shNKX2-1b). **c**, Colony formation assays as in **b** for A549 cells ($P > 0.5$). **d**, Anti-MBIP and anti-vinculin immunoblots of lysates from shRNA-expressing NCI-H2009 cells. **e**, Colony formation of shMBIP NCI-H2009 cells relative to that of control shGFP cells ($P = 0.0344$).

most common cancers, lung adenocarcinoma. We define two main types of recurrent events in this disease: frequent, large-scale events and rare, focal events. Further efforts to identify the target genes of the frequent, large-scale events will probably involve systematic screens to produce orthogonal data sets (mutational, epigenetic, expression and loss-of-function phenotypes).

Strikingly, the single most common focal event in lung adenocarcinoma (amplification of 14q13.3) was not previously associated with a specific gene. We show here that the target gene is *NKX2-1*, a transcription factor that has an essential role in the formation of type II pneumocytes, the cell type that lines the alveoli of the lung^{26,27}. *Nkx2-1* knockout mice fail to develop normal type II pneumocytes or alveoli and die of respiratory insufficiency at birth²⁸, which highlights the importance of *NKX2-1* in lung development. *NKX2-1* shows hallmarks of a novel lineage-survival oncogene, similar to the *MITF* gene in melanoma⁷. The lineage-restricted amplification of such genes contrasts with the more ubiquitous amplifications seen for genes in cell cycle (for example, *CDK4*, *CDK6*, *CCND1*, *CCNE1*) and signal transduction (for example, *EGFR*, *ERBB2*, *KRAS*) pathways.

More generally, our results, together with other recent studies²⁹, illustrate the power of systematic copy-number analysis with SNP arrays. They make clear that many important cancer-related genes remain to be discovered and can be revealed by systematic genomic study.

METHODS SUMMARY

DNA specimens were labelled and hybridized to the Affymetrix 250K Sty I array to obtain signal intensities and genotype calls. Loci identified by GISTIC analysis were further characterized by sequencing, genotype validation, tissue microarray FISH and functional studies. RNAi was performed by stable expression of shRNA lentiviral vectors targeting *NKX2-1*, *MBIP* or *GFP* in lung cancer cell lines, which were then used in soft agar and cell proliferation assays. Raw data and related files are available at <http://www.broad.mit.edu/tsp>.

Full Methods and any associated references are available in the online version of the paper at www.nature.com/nature.

Received 12 April; accepted 10 October 2007.

Published online 4 November 2007.

- Weir, B., Zhao, X. & Meyerson, M. Somatic alterations in the human cancer genome. *Cancer Cell* **6**, 433–438 (2004).
- Sawyers, C. Targeted cancer therapy. *Nature* **432**, 294–297 (2004).
- Pinkel, D. et al. High resolution analysis of DNA copy number variation using comparative genomic hybridization to microarrays. *Nature Genet.* **20**, 207–211 (1998).
- Pollack, J. R. et al. Genome-wide analysis of DNA copy-number changes using cDNA microarrays. *Nature Genet.* **23**, 41–46 (1999).
- Bignell, G. R. et al. High-resolution analysis of DNA copy number using oligonucleotide microarrays. *Genome Res.* **14**, 287–295 (2004).
- Zhao, X. et al. An integrated view of copy number and allelic alterations in the cancer genome using single nucleotide polymorphism arrays. *Cancer Res.* **64**, 3060–3071 (2004).
- Garraway, L. A. et al. Integrative genomic analyses identify *MITF* as a lineage survival oncogene amplified in malignant melanoma. *Nature* **436**, 117–122 (2005).
- Zhao, X. et al. Homozygous deletions and chromosome amplifications in human lung carcinomas revealed by single nucleotide polymorphism array analysis. *Cancer Res.* **65**, 5561–5570 (2005).
- Li, C. & Wong, W. H. Model-based analysis of oligonucleotide arrays: expression index computation and outlier detection. *Proc. Natl Acad. Sci. USA* **98**, 31–36 (2001).
- Li, C. & Wong, W. H. Model-based analysis of oligonucleotide arrays: model validation, design issues and standard error application. *Genome Biol.* **2**, RESEARCH0032 (2001).
- Hu, P., Stransky, N., Thiery, J. P., Radvanyi, F. & Barillot, E. Analysis of array CGH data: from signal ratio to gain and loss of DNA regions. *Bioinformatics* **20**, 3413–3422 (2004).
- Beroukhi, R. et al. Assessing the significance of chromosomal aberrations in cancer: Methodology and application to glioma. *Proc. Natl Acad. Sci. USA*. (in the press).
- Balsara, B. R. & Testa, J. R. Chromosomal imbalances in human lung cancer. *Oncogene* **21**, 6877–6883 (2002).
- Garnis, C. et al. High resolution analysis of non-small cell lung cancer cell lines by whole genome tiling path array CGH. *Int. J. Cancer* **118**, 1556–1564 (2006).
- Tonon, G. et al. High-resolution genomic profiles of human lung cancer. *Proc. Natl Acad. Sci. USA* **102**, 9625–9630 (2005).
- Hayashi, N., Sugimoto, Y., Tsuchiya, E., Ogawa, M. & Nakamura, Y. Somatic mutations of the *MTS* (multiple tumor suppressor) 1/*CDK4* (cyclin-dependent kinase-4 inhibitor) gene in human primary non-small cell lung carcinomas. *Biochem. Biophys. Res. Commun.* **202**, 1426–1430 (1994).
- Sanchez-Cespedes, M. et al. Inactivation of *LKB1/STK11* is a common event in adenocarcinomas of the lung. *Cancer Res.* **62**, 3659–3662 (2002).
- Takahashi, T. et al. p53: a frequent target for genetic abnormalities in lung cancer. *Science* **246**, 491–494 (1989).
- Sato, M. et al. Identification of chromosome arm 9p as the most frequent target of homozygous deletions in lung cancer. *Genes Chromosomes Cancer* **44**, 405–414 (2005).
- Cox, C. et al. A survey of homozygous deletions in human cancer genomes. *Proc. Natl Acad. Sci. USA* **102**, 4542–4547 (2005).
- Barnes, A. P. et al. Phosphodiesterase 4D forms a cAMP diffusion barrier at the apical membrane of the airway epithelium. *J. Biol. Chem.* **280**, 7997–8003 (2005).
- Zhu, C. Q. et al. Amplification of telomerase (*hTERT*) gene is a poor prognostic marker in non-small-cell lung cancer. *Br. J. Cancer* **94**, 1452–1459 (2006).
- Zhang, A. et al. Frequent amplification of the telomerase reverse transcriptase gene in human tumors. *Cancer Res.* **60**, 6230–6235 (2000).
- Johnson, D. H. et al. Randomized phase II trial comparing bevacizumab plus carboplatin and paclitaxel with carboplatin and paclitaxel alone in previously untreated locally advanced or metastatic non-small-cell lung cancer. *J. Clin. Oncol.* **22**, 2184–2191 (2004).
- Sandler, A. et al. Paclitaxel-carboplatin alone or with bevacizumab for non-small-cell lung cancer. *N. Engl. J. Med.* **355**, 2542–2550 (2006).
- Bingle, C. D. Thyroid transcription factor-1. *Int. J. Biochem. Cell Biol.* **29**, 1471–1473 (1997).
- Ikeda, K. et al. Gene structure and expression of human thyroid transcription factor-1 in respiratory epithelial cells. *J. Biol. Chem.* **270**, 8108–8114 (1995).

28. Yuan, B. *et al.* Inhibition of distal lung morphogenesis in *Nkx2.1*^{-/-} embryos. *Dev. Dyn.* **217**, 180–190 (2000).
29. Mullighan, C. G. *et al.* Genome-wide analysis of genetic alterations in acute lymphoblastic leukaemia. *Nature* **446**, 758–764 (2007).
30. Bamford, S. *et al.* The COSMIC (Catalogue of Somatic Mutations in Cancer) database and website. *Br. J. Cancer* **91**, 355–358 (2004).
31. Futreal, P. A. *et al.* A census of human cancer genes. *Nature Rev. Cancer* **4**, 177–183 (2004).

Supplementary Information is linked to the online version of the paper at www.nature.com/nature.

Acknowledgements This work was supported by grants from the US National Cancer Institute (B.A.W., M.S.W., M.R.S., M.M., I.I.W., A.F.G., J.A.R., M.S., J.D.M.), the US National Human Genome Research Institute (R.A.G., R.K.W., E.S.L.), the Canadian Cancer Society/National Cancer Institute (M.S.T.), the American Lung Association (M.M.), Joan's Legacy Foundation (M.M.), the American Cancer Society (M.M.), the International Association for the Study of Lung Cancer (R.K.T.), the US Department of Defense (R.B., I.I.W., J.D.M.) and the Carmel Hill Fund (W.P., M.G.K., H.E.V.).

Author Information Reprints and permissions information is available at www.nature.com/reprints. Correspondence and requests for materials should be addressed to M.M. (matthew_meyerson@dfci.harvard.edu).

METHODS

Primary lung specimens. A total of 575 DNA specimens were obtained from primary lung tumours (all of them with the original diagnosis of lung adenocarcinoma, 528 of which were confirmed to be lung adenocarcinomas), 439 matched normal samples and 53 additional normal specimens. These DNAs were labelled and hybridized to SNP arrays (see below) without previous whole-genome amplification. Each of the selected tumour samples was determined to have greater than 70% tumour percentage by pathology review.

Of the 575 selected tumours, 384 anonymous lung tumour and matched normal DNAs for the Tumour Sequencing Project (TSP) were collected from five sites: Memorial-Sloan Kettering Cancer Center (102 tumours and paired normal samples), University of Michigan (101 tumours and paired normal samples), MD Anderson Cancer Center (29 tumours and paired normal samples), Washington University (84 tumours and paired normal samples) and Dana-Farber Cancer Institute/The Broad Institute (68 tumours and paired normal samples). Additional anonymous lung adenocarcinoma samples or DNAs were collected from the Brigham and Women's Hospital tissue bank (19 tumours and 18 paired normal samples), H. Sasaki at the Nagoya City University Medical School (112 tumours and 37 paired normal samples) and from the University Health Network in Toronto (60 tumour samples). In addition to the matched normal samples, 53 unmatched normal tissue or blood samples were used for SNP array normalization purposes (sources include J. Llovet, S. Pomeroy, S. Singer, the Genomics Collaborative, Inc., Massachusetts General Hospital and R. Beroukhi). All tumour samples were surgically dissected and frozen at -80°C until use.

SNP array experiments. For each sample, SNPs were genotyped with the Sty I chip of the 500K Human Mapping Array set (Affymetrix Inc.). Array experiments were performed according to manufacturer's directions. In brief, for each sample, 250 ng of genomic DNA was digested with the StyI restriction enzyme (New England Biolabs). The digested DNA was then ligated to an adaptor with T4 ligase (New England Biolabs) and PCR-amplified using an Applied Biosystems 9700 Thermal Cycler I and Titanium Taq (Clontech) to achieve a size range of 200–1,100 bp. Amplified DNA was then pooled, concentrated and put through a clean-up set. The product was then fragmented using DNaseI (Affymetrix Inc.) and subsequently labelled, denatured and hybridized to arrays. Hybridized arrays were scanned using the GeneChip Scanner 3000 7G (Affymetrix Inc.). Batches of 96 samples were processed as a single plate using a Biomek FX robot with dual 96 and span-8 heads (Beckman Coulter) and a GeneChip Fluidics Station FS450 (Affymetrix Inc.). Samples and plates were tracked using ABGene 2D barcode rack and single tube readers (ABGene). Tumour and paired normal sample (where applicable) were always placed in adjacent wells on the same plate to minimize experimental differences. Raw data (.CEL and .txt files) are available at <http://www.broad.mit.edu/tsp>.

Primary SNP array data analysis. SNP arrays were processed as a plate of 96 samples using the GenePattern software package³², with modules based on dChipSNP algorithms^{9,10}. GenePattern modules are available at <http://www.broad.mit.edu/cancer/software/genepattern/>. Intensity (.CEL) files were normalized and modelled using the PM-MM difference modelling method⁹ with the SNPfileCreator module. Array normalization, similar to quantile normalization, was performed³³; 6,000 matching quantiles from the probe density distributions of two arrays were used to fit a running median normalization curve for normalization of each array to a common baseline array¹⁰.

Array quality control analysis. Further analysis was performed on arrays that met certain quality control criteria. As a first step, non-adenocarcinoma samples ($n = 47$) from the TSP set of 384 tumours were removed from further analysis (leaving 528 adenocarcinomas). Technical failure criteria (removing 33 tumours) included a requirement for correct tumour/normal matching, genotyping call rates (% of SNPs that a genotype call can be inferred for) greater than 85% and a score measuring copy-number variation between neighbouring SNPs of less than 0.5. The measure of local SNP copy number variation is calculated by the formula: $\text{variation score} = \text{mean}[(\log(RC_i) - \log(RC_{i+1}))^2 + (\log(RC_i) - \log(RC_{i-1}))^2]$, where RC_i is the raw copy number at SNP i and the mean is taken over all SNPs. Criteria also included a requirement that after taking the log2 ratio and performing segmentation by GLAD¹¹, the number of times the smoothed copy number crossed ± 0.1 on the log scale in the genome of tumour samples was < 100 (removing 73 tumours). The same test was used to exclude normal samples, with the number of times the smoothed copy number crossed ± 0.1 decreased to < 45 (removing 50 normal samples). A histogram quality control step, as part of the GISTIC procedure, then removed tumours ($n = 51$) with high degrees of non-tumour DNA contamination by looking for samples with only one peak of copy number across its whole genome. This histogram quality control step also removed normals ($n = 20$) with tumour DNA contamination by looking for samples with greater than one peak of copy number across its whole genome.

GISTIC analysis. GISTIC analysis¹² was performed on arrays that met certain quality control criteria. Raw intensity value files from the GenePattern SNPfileCreator module were used as input into the GISTIC algorithm. In brief, batch correction, data normalization, copy-number determination using either the paired normal sample or the average of the five closest normal samples and copy number segmentation was performed. Data-set-specific copy number polymorphisms were identified by running GISTIC on the set of normal samples alone; the regions identified from this analysis were then also removed from the subsequent analysis of tumours. GISTIC then assigns G^{AMP} and G^{DEL} scores to each locus, respectively representing the frequency of amplifications (deletions) seen at that locus, multiplied by the average increase (decrease) in the log2 ratio in the amplified (deleted) samples. The score (G) is based on the average amplitude (a) of the lesion type (amplification or deletion) and its frequency (f) in the data set according to the formula: $G_{\text{lesion type}} = f_{\text{lesion type}} a_{\text{lesion type}}$. The significance of each score is determined by comparison to similar scores obtained after permuting the data within each sample. The resulting q -value is an upper bound for the expected fraction of false positives among all regions with a particular q -value or less. GISTIC also implements a peel-off step, which identifies additional secondary peaks within a region.

GISTIC analysis was performed essentially the same as is described in a future publication¹², with the following exceptions. Copy number determination was performed for each tumour using its matched normal sample when available and of good quality ($n = 242$). For all others, the average of the five closest normal samples was used ($n = 129$). Copy number segmentation was performed using the GLAD algorithm with parameter $d = 10$. GLAD segments less than eight SNPs in length were also removed.

Regions identified by GISTIC were also compared to known copy-number polymorphisms³⁴ and were manually reviewed for the presence of the alteration in the paired normal sample. Focal deletion regions with events that occurred in tumour samples that did not have paired normal samples were considered presumed polymorphisms and also removed from the list. Secondary peaks and known and presumed germline copy number polymorphisms are listed in Supplementary Tables 12 and 13.

GISTIC analysis of large-scale regions. Significant broad regions of amplification and deletion were identified by applying GISTIC with the default thresholds of 2.14/1.87 (log2 ratio of ± 0.1). Regions identified by GISTIC that were greater than 50% of a chromosome arm were considered large-scale. Region frequencies were calculated by determining the number of samples that had a median log2 ratio greater/less than the threshold (± 0.1), for those SNPs within the region.

GISTIC analysis of focal regions. Significant focal regions of amplification and deletion were identified by applying GISTIC with a threshold of 3.6/1.2 (log2 ratio of 0.848/−0.737).

Data visualization. Normalized raw copy number from GISTIC analysis was used as input for visualization in the GenePattern SNPviewer (<http://www.broad.mit.edu/cancer/software/genepattern/>)³². Mapping information for SNP, RefGene and cytoband locations are based on Affymetrix annotations and the hg17 build of the human genome sequence from the University of California, Santa Cruz (<http://genome.ucsc.edu>).

Chromosome arm analysis. After segmentation by GLAD, the median of each chromosome arm for each sample was calculated. Amplification or deletion of an arm across the data set was tested for significance by a two-sided binomial test, after removing log2 copy number ratios between ± 0.1 . P values were false-discovery rate (FDR) corrected to give a FDR q value; significance is set to a q value of 0.01. The standard deviation of the median copy number of significant arms was then used to sort samples into three groups. Higher standard deviation implies higher interchromosomal variation, which correlates with less stromal contamination. Frequencies were then calculated for the total set and for only the top one-third least stromally contaminated samples to give a better idea of true frequencies in the context of attenuated signal owing to stromal contamination.

Comparison between tertiles. A similar chromosome arm analysis was performed independently on the three sample groups, separated according to the standard deviations of their median arm log2 copy number ratios. Amplification or deletion of an arm across the data set was tested for significance by a two-sided binomial test, after removing values between ± 0.0125 . P values were FDR corrected to give a FDR q value, significance is set to a q value of 0.01.

Estimation of stromal contamination. To attempt to estimate stromal contamination, we calculated the allele-specific copy numbers by taking all informative SNPs in each of the 237 tumours that have a paired normal (removing five bad pairs) and dividing the allele-specific signal from the tumour by that of the normal. Then for each SNP we found M , the minimum between the copy numbers of the A and B alleles. In regions in which one allele has zero copies (for example, one copy loss in diploid cells) M represents the stromal contamination level (as the stroma has one copy of each allele). We calculated the median value

of *M* across each of the chromosome arms and then estimated the stromal contamination by taking their minimum.

LOH analysis. Inferred LOH calls using an HMM algorithm for 242 tumour/normal sample pairs were generated using dChipSNP³⁵. Default parameters were used, except the genotyping error rate was set to 0.2. Five bad-quality sample pairs were removed before visualization and GISTIC analysis. GISTIC analysis of LOH calls and copy loss for 237 samples were performed as described¹².

Correlation analysis. Associations were tested between each large-scale alteration identified by GISTIC and certain clinical parameters. A Fisher's exact test was used to determine association of large-scale copy-number lesions with the binary clinical parameters (gender and smoking status). A chi-squared test was used to determine whether each large-scale copy number alteration was independent of each non-binary clinical parameter (age range, differentiation, tumour stage or patient's reported ancestry). *P* values were FDR corrected to give a FDR *q* value, significance is set to a *q* value of 0.05.

Correlation of clinical features and NKX2-1 amplification. The analysis included 123 consecutive patients with lung adenocarcinoma treated at Brigham and Women's Hospital between January 1997 and December 1999. Fifty-two of these cases had a FISH amplification status that was not assessable (6 cases showed no tumour on the tissue cores and 46 cases had insufficient hybridization). Of the remaining 71 cases, 10 cases had NKX2-1 amplification, 1 had a NKX2-1 deletion, and 60 cases showed no NKX2-1 alteration. All cases for which the NKX2-1 amplification status was not assessable and the one case that showed a NKX2-1 deletion were excluded, bringing the final number of cases included in the analysis to 70.

All cases were histologically confirmed as lung adenocarcinomas. For cases that showed a pure solid growth pattern, mucicarmine and immunohistochemical stains were performed to confirm that the tumour was an adenocarcinoma. Well-differentiated tumours were defined as tumours with a purely bronchioloalveolar growth pattern or mixed tumours with an acinar component with cytologic atypia equivalent to that seen with bronchioloalveolar carcinoma. Poorly differentiated tumours were defined as tumours that showed any amount of solid growth. All other tumours were classified as moderately differentiated. Patient demographics, smoking status, tumour location, type of surgical resection, tumour stage (according to the 6th edition of the American Joint Committee on Cancer system for lung carcinoma) and nodal status were recorded.

Overall survival of patients with NKX2-1 amplification. We excluded from the survival analysis three cases with NKX2-1 amplification and 11 cases that had no NKX2-1 alterations. Exclusion criteria included: cancer was a recurrence; patients received neoadjuvant treatment; patients died within the first 30 days after surgery; and patients had another cancer diagnosed in the 5 years before the diagnosis of lung adenocarcinoma. Survival was plotted by Kaplan–Meier method using the date of resection and date of death or last follow-up.

Sequencing. NKX2-1, MBIP and AUTS2 were sequenced in all 384 TSP lung adenocarcinomas. Primers were designed in an automated fashion using Primer 3 (ref. 36) and characterized by amplification in genomic DNA from three Coriell cell lines. Primers that show an agarose gel band for at least two of the three DNAs were then used for production PCR. Passing primers were arrayed into 384-well PCR plates along with samples and PCR master mix. A total of 5 ng of whole-genome-amplified sample DNA was PCR amplified over 35 cycles in Thermo-Hybrid units, followed by a SAP/Exo clean-up step. NKX2-1 PCR reactions for sequencing contained an addition of 5% DMSO. The resulting purified template is then diluted and transferred to new plates for the sequencing reaction. After cycling (also performed on Thermo-Hybrid), the plates are cleaned up with an ethanol precipitation, re-hydrated and detected on an ABI 3730xl DNA analyser (Applied Biosystems). Output from the detectors is transferred back to the directed sequencing platform's informatics pipeline. SNPs and/or mutations are then identified using three mutation-detecting algorithms in parallel: PolyPhred³⁷ and PolyDHAN (D. Richter *et al.*, manuscript in preparation), which are bundled into the in-house software package SNP Compare, and the commercially available Mutation Surveyor (SoftGenetics, LLC.). Candidates were filtered to remove silent variants, intronic variants (with the exception of potential splice site mutations) and validated SNPs registered in dbSNP or confirmed as SNPs in our previous experiments.

Mutation validation by genotyping. Homogeneous mass extension (hME) genotyping for validation of sequencing candidates was performed in 96-well plates with up to 7-plex reactions. PCR was performed with final concentrations of 0.83 mM dNTPs, 1.56× of 10× buffer, 3.38 mM MgCl₂, 0.03 U μl⁻¹ HotStar Taq (Qiagen), 0.10 μM PCR primers. Thermocycling was performed at 92 °C for 15 min, followed by 45 cycles of 92 °C for 20 s, 56 °C for 30 s and 72 °C for 1 min, with an additional extension at 72 °C for 3 min. Shrimp alkaline phosphatase (SAP) clean-up was performed using a master mix made up of 0.5× buffer and SAP. Reactions were performed at 34 °C for 20 min, 85 °C for 5 min

and then held at 4 °C. After the SAP clean-up, hME reaction was performed using thermosequase and final concentrations of 0.06 mM sequenom termination mix (specific to the pool being used), and 0.64 μM extension primer. Reactions were cycled at 94 °C for 2 min, followed by 55 cycles of 94 °C for 5 s, 52 °C for 5 s and 72 °C for 5 s. Samples were then put through a resin clean-up step, then the purified primer extension reaction was loaded onto a matrix pad (3-hydroxypropionic acid) of a SpectroCHIP (Sequenom) and detected by a Bruker Biflex III MALDI-TOF mass spectrometer (SpectroREADER, Sequenom).

PTPRD mutation discovery and validation. The *PTPRD* gene was sequenced in 188 lung adenocarcinoma samples. Sequence traces (reads) were aligned to human reference sequence using cross-match. PolyPhred³⁷ and PolyScan were used to predict SNPs and insertions/deletions. Identified SNPs were validated using the Illumina Goldengate assay. ENST00000356435 is the transcript used for annotating the mutations. Both synonymous and non-synonymous candidates were identified, but only non-synonymous mutations were validated.

Tissue microarray FISH (TMA-FISH). A Biotin-14-dCTP-labelled BAC clone RP11-1083E2 (conjugated to produce a red signal) was used for the NKX2-1 probe and a Digoxin-dUTP labelled BAC clone RP11-7218 (conjugated to produce a green signal) was used for the reference probe. Tissue hybridization, washing and colour detection were performed as described previously^{7,38}. NKX2-1 amplification by FISH was assessed using a total of 935 samples (represented by 2,818 tissue microarray cores).

The BAC clones were obtained from the BACPAC Resource Center, Children's Hospital Oakland Research Institute (CHORI, Oakland, California, USA). Before tissue analysis, the integrity and purity of all probes were verified by hybridization to metaphase spreads of normal peripheral lymphocytes. The samples were analysed under a ×60 oil immersion objective using an Olympus BX-51 fluorescence microscope equipped with appropriate filters, a CCD (charge-coupled device) camera and the CytoVision FISH imaging and capturing software (Applied Imaging). Semi-quantitative evaluation of the tests was independently performed by two evaluators (S.P. and L.A.J.); at least 100 nuclei for each case were analysed when possible. Cases with significant differences between the two independent evaluations were referred by a third person (M.A.R.). The statistical analysis was performed using SPSS 13.0 for Windows (SPSS Inc.) with a significance level of 0.05.

Cell lines and cell culture conditions. NCI-H2009 (ref. 39), NCI-H661 (ref. 40), NCI-H1975 (ref. 39) and HCC1171 (ref. 8) have been previously described. A549 cells were purchased from American Type Culture Collection. NSCLC cells were maintained in RPMI growth media consisting of RPMI 1640 plus 2 mM L-glutamine (Mediatech) supplemented with 10% fetal bovine serum (Gemini Bio-Products), 1 mM sodium pyruvate, and penicillin/streptomycin (Mediatech).

RNAi knockdown. shRNA vectors targeted against NKX2-1, MBIP and GFP were provided by TRC (The RNAi Consortium). The sequences targeted by the NKX2-1 shRNAs are as follows: shNKX2-1a (TRCN0000020449), 5'-CGCTTGTAATACCAGGATT-3', and shNKX2-1b (TRCN0000020453), 5'-TCCGTTCTCAGTGTCTGACAT-3'. The sequences targeted by the MBIP shRNA and GFP shRNA are 5'-CCACCGGAAGAGATTATT-3' (TRCN0000003069) and 5'-GCAAGCTGACCTGAAGTTCAT-3', respectively. Lentiviruses were made by transfection of 293T packaging cells with a three plasmid system^{41,42}. Target cells were incubated with lentiviruses for 4.5 h in the presence of 8 μg ml⁻¹ polybrene. After the incubation, the lentiviruses were removed and cells were fed fresh medium. Two days after infection, puromycin (0.75 μg ml⁻¹ for NCI-H1975, 1.0 μg ml⁻¹ for NCI-H661, 1.5 μg ml⁻¹ for NCI-H2009, 1.0 μg ml⁻¹ for NCI-H661 and 2.0 μg ml⁻¹ for A549 and HCC1171) was added. Cells were grown in the presence of puromycin for 3 days or until all of the non-infected cells died. Twenty-five micrograms of total cell lysates prepared from the puro-selected cell lines was analysed by western blotting using anti-NKX2-1 polyclonal antibody (Santa Cruz Biotechnology), anti-MBIP polyclonal antibody (Proteintech Group, Inc.) and anti-vinculin monoclonal antibody (Sigma).

Soft agar anchorage-independent growth assay. NCI-H2009 (1 × 10⁴), NCI-H661 (2.5 × 10⁴), A549 (3.3 × 10³), NCI-H1975 (5 × 10⁴) or HCC1171 (1 × 10⁴) cells expressing shRNAs targeting NKX2-1, MBIP or GFP were suspended in a top layer of RPMI growth media and 0.4% Noble agar (Invitrogen) and plated on a bottom layer of growth media and 0.5% Noble agar in 35-mm wells. Soft agar colonies were counted 3–4 weeks after plating. The data are derived from two independent experiments unless otherwise noted and are graphed as the percentage of colonies formed relative to the shGFP control cells (set to 100%) ± 1 standard deviation of the triplicate samples. *P* values between shGFP and shNKX2-1 or shMBIP samples were calculated using a *t*-test.

Cell proliferation assays. NCI-H2009 (500 cells per well), A549 (400 cells per well) and NCI-H661 (600 cells per well) cells expressing shRNAs targeting NKX2-1, MBIP or GFP were seeded in 6 wells in a 96-well plate. Cell viability

was determined at 24-h time points for a total of 4 days using the WST-1-based colorimetric assay (Roche Applied Science). The percentage of cell viability is plotted for each cell line ± 1 standard deviation of the reading from six wells, relative to day 0 readings. Experiments were performed two or more times and a representative experiment is shown.

32. Reich, M. *et al.* GenePattern 2.0. *Nature Genet.* **38**, 500–501 (2006).
33. Bolstad, B. M., Irizarry, R. A., Astrand, M. & Speed, T. P. A comparison of normalization methods for high-density oligonucleotide array data based on variance and bias. *Bioinformatics* **19**, 185–193 (2003).
34. Iafrate, A. J. *et al.* Detection of large-scale variation in the human genome. *Nature Genet.* **36**, 949–951 (2004).
35. Lin, M. *et al.* dChipSNP: significance curve and clustering of SNP-array-based loss-of-heterozygosity data. *Bioinformatics* **20**, 1233–1240 (2004).
36. Rozen, S. & Skaletsky, H. Primer3 on the WWW for general users and for biologist programmers. *Methods Mol. Biol.* **132**, 365–386 (2000).
37. Nickerson, D. A., Tobe, V. O. & Taylor, S. L. PolyPhred: automating the detection and genotyping of single nucleotide substitutions using fluorescence-based resequencing. *Nucleic Acids Res.* **25**, 2745–2751 (1997).
38. Rubin, M. A. *et al.* Overexpression, amplification, and androgen regulation of TPD52 in prostate cancer. *Cancer Res.* **64**, 3814–3822 (2004).
39. Phelps, R. M. *et al.* NCI-Navy Medical Oncology Branch cell line data base. *J. Cell. Biochem., Suppl.* **24**, 32–91 (1996).
40. Banks-Schlegel, S. P., Gazdar, A. F. & Harris, C. C. Intermediate filament and cross-linked envelope expression in human lung tumor cell lines. *Cancer Res.* **45**, 1187–1197 (1985).
41. Naldini, L. *et al.* *In vivo* gene delivery and stable transduction of nondividing cells by a lentiviral vector. *Science* **272**, 263–267 (1996).
42. Zufferey, R., Nagy, D., Mandel, R. J., Naldini, L. & Trono, D. Multiply attenuated lentiviral vector achieves efficient gene delivery *in vivo*. *Nature Biotechnol.* **15**, 871–875 (1997).

Genetics of Preneoplasia: Lessons from Lung Cancer

Ignacio I. Wistuba*

Departments of Pathology and Thoracic/Head and Neck Medical Oncology, The University of Texas M. D. Anderson Cancer Center, Houston, Texas 77030, USA

Abstract: From biological, histopathologic, and clinical perspectives, lung cancer is a highly complex neoplasm probably having multiple preneoplastic pathways. The sequence of histopathologic changes in the bronchial mucosa that precedes the development of squamous carcinomas of the lung has been identified. For the other major forms of lung cancer, however, such sequences have been poorly documented. This review summarizes the current knowledge regarding the molecular and histopathologic pathogenesis of lung cancer and discusses the complexity of identifying novel molecular mechanisms involved in the development of the lung premalignant disease, and their relevance to the development of new strategies for early detection and chemoprevention. Although our current knowledge of the molecular pathogenesis of lung cancer is still meager, work over the last decade has taught several important lessons about the molecular pathogenesis of this tumor, including the following: a) Better characterization of the high-risk population is needed. b) There are several histopathologic and molecular pathways associated with the development of the major types of non-small cell lung cancer. c) Although there is a field effect phenomenon for lung preneoplastic lesions, recent data suggest that there are at least two distinct lung airway compartments (central and peripheral) for lung cancer pathogenesis. d) Inflammation may play an important role in lung cancer development and could be an important component of the field effect phenomenon. e) For lung adenocarcinoma, at least two pathways (smoking-related and nonsmoking-related) have been identified. f) Finally, the identification of deregulated molecular signaling pathways in lung cancer preneoplasias may provide a rationale for designing novel strategies for early detection and targeted chemoprevention of lung cancer.

Keywords: Preneoplasias, field effect, lung cancer risk, inflammation, smoking, NF- κ B, EGFR, KRAS.

INTRODUCTION

Lung cancer is the leading cause of cancer deaths in the United States and worldwide [1,2]. This high mortality is attributed to diagnosis at advanced stages, when the options for treatment are mostly palliative. Thus, to reduce the mortality of lung cancer, new approaches must be developed to prevent, diagnose, and treat premalignant lesions, shifting the paradigm to consider premalignancy as the disease and lung cancer as the endpoint. However, the identification of the early molecular and histopathologic pathogenesis of lung cancer represents an enormous challenge.

From biological, histopathologic, and clinical perspectives, lung cancer is a highly complex neoplasm [1], probably having multiple preneoplastic pathways. Lung cancer consists of several histological types, including small cell lung carcinoma (SCLC, 25% of cases) and the non-small cell lung carcinoma (NSCLC, 75%) types of squamous cell carcinoma, adenocarcinoma (including the non-invasive type of bronchioloalveolar carcinoma) and large cell carcinoma [3]. Lung cancers may arise from the major bronchi (central tumors) or from the small

bronchi, bronchioles, or alveoli (peripheral tumors) of the distant airway of the lung. Squamous cell carcinomas and SCLCs usually arise centrally, whereas adenocarcinomas and large cell carcinomas usually arise peripherally [3]. The population of normal respiratory epithelial cells varies along different compartments of the respiratory tree, and the specific respiratory epithelial cell type from which each lung cancer type develops has not been established with certainty.

The sequence of histopathologic changes in the bronchial mucosa that precedes the development of squamous carcinomas of the lung has been identified (Fig. 1) [4]. For the other major forms of lung cancer, however, such sequences have been poorly documented [5]. Although many molecular abnormalities have been described in clinically evident lung cancers [1], relatively little is known about the molecular events preceding the development of lung carcinomas and the underlying molecular basis of lung carcinogenesis. Although several studies have provided relevant information regarding the molecular characterization of the premalignant changes involved in the pathogenesis of lung cancer, especially for squamous cell carcinoma [6], that information has proven insufficient to identify with certainty the molecular pathogenetic pathways or molecular markers useful for risk assessment, targeted chemoprevention or treatment, and early detection of lung premalignant

*Address correspondence to this author at the Department of Pathology – Unit 85, M. D. Anderson Cancer Center, 1515 Holcombe Blvd., Houston, TX 77030-4009, USA; Tel: 713-563-9184; Fax: 713-563-1848; E-mail: iiwistuba@mdanderson.org

lesions. Attempts to better define the pathogenesis of lung premalignancy have been thwarted by the relative invisibility of the cellular lesions and their random distribution throughout the respiratory airway field, and new methodologies, including computed tomography (CT) imaging [7] and fluorescence bronchoscopy [8], has been introduced to better identify and visualize lung premalignant lesions. Because examination of the sputum and bronchoscopy specimens examines the central airways, whereas spiral CT detects mainly peripheral tumors, different approaches are required to detect tumors in different compartments of the lung.

This review summarizes the current knowledge regarding the molecular and histopathologic pathogenesis of lung cancer and discusses the complexity of identifying novel molecular mechanisms involved in the development of the lung premalignant disease, and their relevance to the development of new strategies for early detection and chemoprevention. Although our current knowledge of the molecular pathogenesis of lung cancer is still meager, work over the last decade has taught several important lessons about the molecular pathogenesis of this tumor, including the following: a) Better characterization of the high-risk population

is needed. b) There are several histopathologic and molecular pathways associated with the development of the major types of NSCLC. c) Although there is a field effect phenomenon for lung preneoplastic lesions, recent data suggest that there are at least two distinct lung airway compartments (central and peripheral) for lung cancer pathogenesis. d) Inflammation may play an important role in lung cancer development and could be an important component of the field effect phenomenon. e) For lung adenocarcinoma, at least two pathways (smoking-related and nonsmoking-related) have been identified. f) Finally, the identification of deregulated molecular signaling pathways in lung cancer preneoplasias may provide a rationale for designing novel strategies for early detection and targeted chemoprevention of lung cancer.

HIGH-RISK POPULATION

In lung cancer, there is a consensus that the high-risk population targeted for early detection and chemoprevention efforts has been identified: heavy smokers and patients who have survived a cancer of the upper aerodigestive tract [2,9-13]. Evidence for the relationship between lung cancer and smoking is

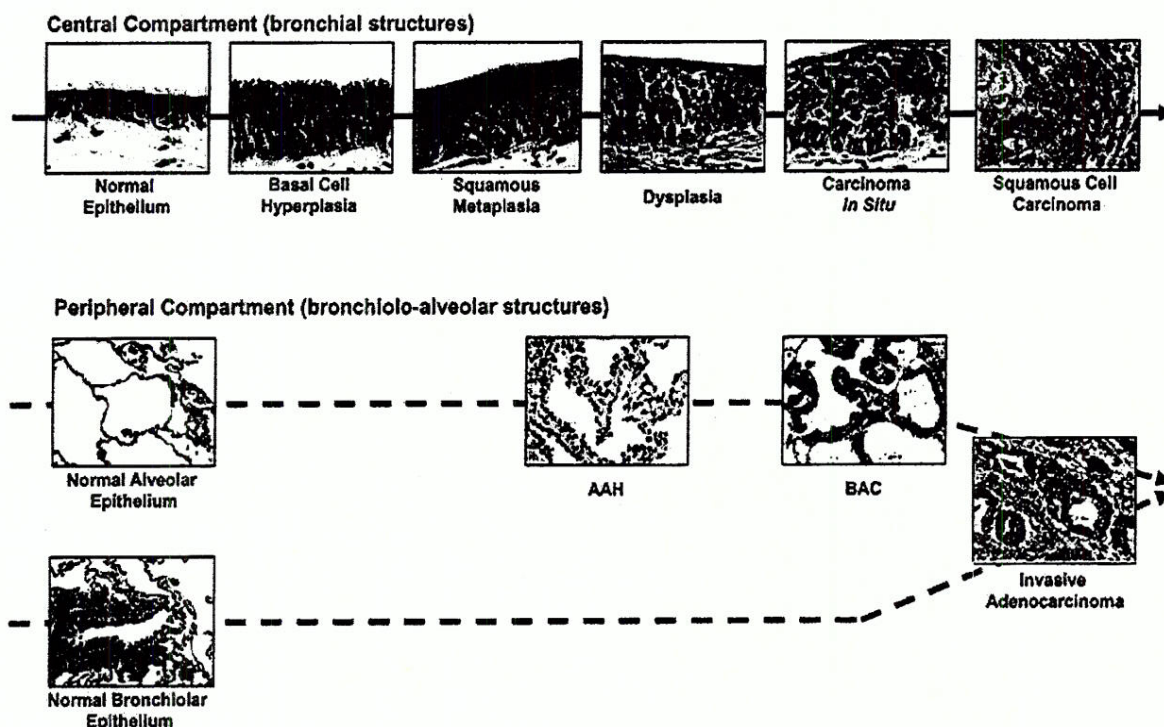


Fig. (1). Summary of the histopathologic changes during the pathogenesis of squamous cell carcinoma and adenocarcinoma of the lung. At least two types of epithelial cells (alveolar and bronchiolar/bronchial) have been suggested as precursor of lung adenocarcinoma. (AAH = atypical adenomatous hyperplasia; BAC = bronchioloalveolar carcinoma).

clear. The risk of lung cancer increases with the number of cigarettes smoked, the years of smoking, an earlier age of onset of smoking, the degree of inhalation, the tar and nicotine content of the cigarettes smoked, and the use of unfiltered cigarettes [2,9-13]. However, based on the fact that only 11% of smokers develop lung cancer, better criteria are needed for the identification of the subset of smokers that will develop lung cancer.

Lung premalignant lesions of the central airway are frequent in smokers and rare in never-smokers [4-6]. Precisely how much smoking is necessary to develop lung premalignant changes is unknown, but there is consensus that the frequency and severity of those lesions increases with increasing tobacco exposure [13]. In the effort to characterize better the population of smokers at higher risk to develop lung cancer, research has been focused on, among other characteristics, sex, lung function abnormalities, and duration of cessation of smoking. However, the data available are somehow controversial. Although there is evidence that at every level of exposure to cigarette smoke, the risk of lung cancer (especially SCLC and adenocarcinoma) is 1.2-fold to 1.7-fold higher in women than in men [14], a study of central bronchial premalignant lesions using fluorescent bronchoscopy indicated that men had a higher prevalence of high-grade squamous premalignant lesions [13]. In addition to smoking, the presence of chronic obstructive pulmonary disease (COPD) with different levels of airway obstruction is a strong indicator for the subsequent development of lung cancer, with a 1.3-fold to 4.9-fold increased risk [15]. The risk of lung cancer increases in proportion to the degree of airway obstruction, indicating that smokers with ventilatory obstruction are at greater risk for lung cancer than are smokers without obstruction [16]. Notably, although smoking causes most cases of COPD, only 15% of smokers develop COPD. Although a high proportion (~67%) of smokers with COPD demonstrate cytological atypia compatible with mild or worse dysplastic changes [17], approximately 50% of smokers demonstrating histologically documented squamous premalignant lesions by fluorescence bronchoscopy examination do not have airway obstruction consistent with COPD [13]. It has been established that in terms of reduced risk of lung cancer mortality, smoking cessation is beneficial at any age, with much greater benefits accruing to those quitting at younger ages [10]. Although the risk decreases proportionately with the number of years after quitting [18], for men the risk was still significantly elevated even 10 years after smoking cessation [12]. This phenomenon correlates with the finding that the prevalence of high-grade premalignant lesions is not reduced significantly for more than 10 years after cessation of smoking [13]. Consequently, former smokers make up a large proportion (~50%) of lung cancer patients in the United States [11].

Despite intense epidemiological and clinical research, the subset of smokers with a greater risk of

developing lung cancer has not been identified with certainty, and novel approaches to identify the best population to be targeted for early detection and chemoprevention strategies should be devised. Those novel approaches could be based on the detection of lung cancer precursors using histopathologic, imaging, or molecular methodologies. For these purposes, a better understanding of the biology and molecular pathology of the early pathogenesis of lung cancer, including premalignancy, is needed.

HISTOPATHOLOGIC AND MOLECULAR PATHWAYS FOR LUNG CANCER DEVELOPMENT

Most of the molecular and histopathologic changes in the respiratory epithelium associated with lung cancer pathogenesis have been related to smoking [6]. However, the recent discovery of frequent *EGFR* gene mutations in lung cancer and adjacent normal epithelium in never-smokers or light smokers suggests the presence of at least two distinct pathways for the molecular pathogenesis of lung cancer, smoking- and nonsmoking-related [19,20]. Because a relatively small subset of smokers develops lung cancer, attention has been focused on the identification of specific molecular and histopathologic pathways that can predict lung cancer development in high risk-populations. One of those key pathways, currently under intense investigation, is the activation of inflammation-related pathways. We will focus this review on the discussion of the major molecular and histopathologic pathways at different compartments of the lung airway that have been identified in the pathogenesis of the major types of lung cancer. A summary of our current understanding of the molecular pathways involved in the pathogenesis of lung cancer is shown in Fig. (2).

INFLAMMATION AND LUNG CANCER

Accumulating evidence suggests that tumor progression is governed not only by genetic changes intrinsic to cancer cells but also by epigenetic and environmental factors. Chronic inflammation has been hypothesized as one of the most important epigenetic and environmental factors contributing to epithelial cancer development and tumor progression [21]. A chronic inflammatory process enhances cell proliferation, cell survival, and cell migration in epithelial cells, as well as angiogenesis in the adjacent stroma, thereby promoting epithelial tumor development [21]. In the last decades, inflammation and related pathways have been suggested to play an important role in the pathogenesis of lung cancer, particularly in smoking-damaged respiratory epithelium [22,23]. However, the mechanisms involved are not well understood.

The specific cellular and molecular pathways that link such inflammatory responses to malignant transformation vary depending on the

microorganism, target organ, and tumor subtype [21,23]. However, despite these differences, several common features exist. A microbial presence in or near epithelia provides a stimulus for recruitment and activation of inflammatory cells (macrophages, neutrophils, and lymphocytes) from the blood stream [21]. Cytokines, chemokines, and free radicals initiate and perpetuate inflammatory responses. This process leads to the release of free radicals that contribute to the malignant transformation of epithelial cells by peroxidizing lipids and inducing genetic mutations [21]. Such damage to epithelial cells stimulates apoptotic cell death and reactive epithelial hyperproliferation that promotes further mutation. In epithelial sites, the nature of the inflammatory response is governed initially by the dominant type of T helper lymphocyte cells recruited to the epithelium in response to inflammation [24]. Moreover, inflammation-related carcinogenesis results from the stimulation of angiogenesis and from

inflammatory cells and mediators that act directly on epithelial cells and indirectly on stromal cells and extracellular matrix components [21].

The association between chronic inflammatory conditions of the lung and cancer has been studied extensively [23]. As stated above, several studies have found that smokers with COPD have an increased risk of lung cancer compared with smokers without COPD [23]. In persons with COPD, at the level of the alveoli, inflammation leads to protease release and oxidative inactivation of antiproteases by inflammatory cells, contributing to degradation of the extracellular matrix [25,26]. At the level of the conducting airways, there is metaplasia of the airway epithelium to a mucus-secreting phenotype, thickening of the airway wall from the increased deposition of matrix molecules and the proliferation of mesenchymal cells, and narrowing from fibrosis [25,26]. These changes are also present in the

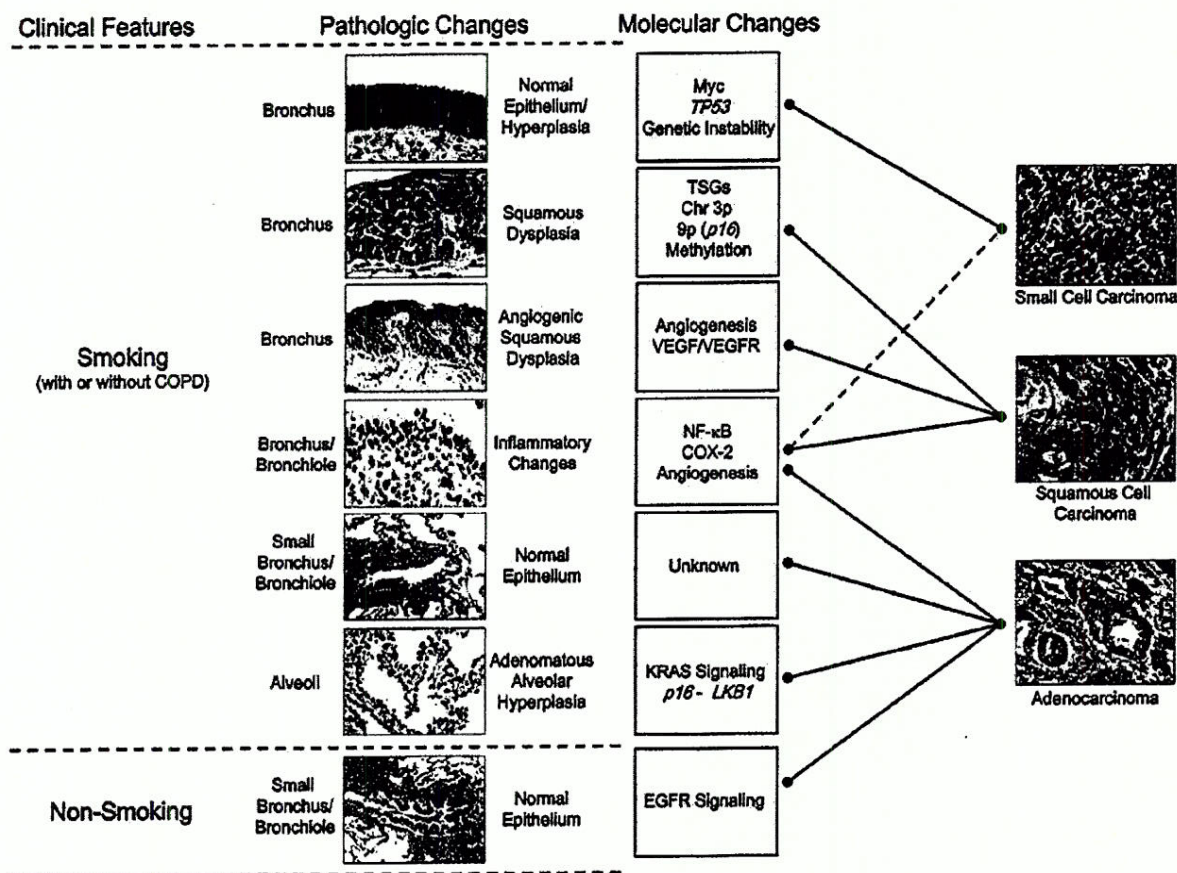


Fig. (2). Schema showing the association between histopathologic and molecular pathways known to be involved in the pathogenesis of lung carcinomas. At least, two pathways, smoking and nonsmoking-associated, are involved. The smoking pathway includes several distinct mechanisms, including inactivation of tumor suppressor genes (TSG), inflammation, angiogenesis and activation of several signaling pathways. However, currently the pathologic and molecular mechanisms responsible of lung adenocarcinoma pathogenesis are mostly unknown. The smoking pathway includes smokers with and without chronic obstructive pulmonary disease (COPD).

lungs of smokers without COPD, but they are not as severe [27]. COPD patients with 40 or more pack-years of smoking history have demonstrated a high prevalence of premalignant dysplasia (24% severe and carcinoma *in situ*) detectable through sputum cytology [28].

A number of lines of evidence suggest that chronic inflammation contributes to the process of lung carcinogenesis through activation of a number of molecular pathways, including the nuclear factor kappa B (NF- κ B) [22,23]. In NSCLC cell lines, it has been demonstrated that tobacco components stimulate NF- κ B-dependent survival [29], and the cyclooxygenase (COX)-2 inhibitor celecoxib suppresses NF- κ B activation induced by various carcinogens [30]. To date, however, the activation of NF- κ B has not been studied comprehensively in lung cancer tumors and lung preneoplastic lesion tissues. Recently, Tichelaar *et al.* [31], reported findings of increased nuclear NF- κ B expression in a limited number of squamous moderate and severe dysplasias obtained from smokers without cancer compared with normal epithelium specimens. NF- κ B has recently been identified as a molecular link between chronic inflammation and cancer [32,33], suggesting that NF- κ B exerts its oncogenic effects in both the tumor and the microenvironment, promoting the survival of premalignant epithelial cells [34]. NF- κ B has been shown to suppress apoptosis and induce expression of proto-oncogenes such as c-myc and cyclin D1, which directly stimulate cell proliferation [35]. In addition, NF- κ B regulates the expression of various molecules important in tumorigenesis, such as matrix metalloproteinases, COX-2, inducible nitric oxide synthase, chemokines, and inflammatory cytokines, all of which promote tumor cell invasion and angiogenesis [36].

The eicosanoid pathway, specifically COX-2, is involved in the pathogenesis of lung cancer. COX-2, an intermediate early response gene induced by growth factors, oncogenes, carcinogens, and tumor-promoter phorbol esters [37], has been shown to be overexpressed in lung adenocarcinoma and squamous cell carcinoma [38]. Cyclooxygenase catalyzes the synthesis of prostaglandins from arachidonic acid, and both arachidonic acid and eicosanoids are potent inflammatory and growth agents. Both preclinical and clinical trials of the effect of celecoxib on lung cancer prevention have shown a marked reduction in prostaglandin E₂ production [39]. COX-2 immunohistochemical expression has shown to be highly expressed in bronchial squamous dysplasias, especially those having high-grade histology (severe dysplasia and carcinoma *in situ*) [40]. Recent findings suggest that the COX-2 inhibitor celecoxib may modulate the proliferation indices and apoptotic balance in the bronchial tissue of active smokers [41].

However, it is currently unknown whether NF- κ B or COX-2 activity itself plays a causal role in the initiation event leading to lung cancer or whether it

may participate in tumor promotion and progression. Clearly, despite recent advances, the role of inflammation in lung cancer pathogenesis still remains an open question.

FIELD DEFECT PHENOMENON

Current information suggests that lung premalignant lesions are frequently extensive and multifocal throughout the respiratory epithelium, indicating a field effect [42]. In this phenomenon, called field cancerization, much of the respiratory epithelium has been mutagenized, presumably from exposure to tobacco-related carcinogens [43]. Several studies performed in the respiratory epithelium of lung cancer patients and smokers have demonstrated that multiple molecularly altered foci of bronchial epithelium are present throughout the airway [44-46]. A detailed analysis of premalignant and malignant epithelium from patients with squamous cell carcinoma indicated that multiple, sequentially occurring allele-specific chromosomal deletions (loss of heterozygosity [LOH]) commence in widely dispersed, apparently clonally independent foci, early in the multistage pathogenesis of squamous cell carcinoma of the lung [44,45]. These observations were extended to former and current smokers [47,48], whose bronchial epithelia demonstrate multiple foci of genetic changes, similar to those found in lung cancers, that may persist for many years after smoking cessation [47]. One of the most intriguing findings regarding the molecular field effect in lung cancer patients and smokers is the high frequency of multiple foci of histologically normal and mildly abnormal (hyperplasia and squamous metaplasia) epithelia exhibiting molecular abnormalities [44,45,47-49]. Because at least some degree of inflammation and inflammatory-related damage is almost invariably present in the central and peripheral airway of smokers [26,50], and because these changes precede the development of lung cancer, the field cancerization phenomenon can be explained both by a direct effect of smoking carcinogens on the epithelial cell and by the initiation of inflammatory response in the epithelial mucosa that may perpetuate the epithelial genetic damage. However, as discussed below, some evidence suggests that there are two distinct lung airways compartments (central and peripheral) for lung cancer pathogenesis (Fig. 3). This concept is supported by the findings of low frequency of molecular abnormalities detected in the centrally located bronchial respiratory epithelium in patients with peripheral lung adenocarcinomas, compared with specimens from patients with squamous cell carcinomas and SCLC [46] indicating the presence of two compartments in the lung with different degrees of smoking-related genetic damage. Recently, the *EGFR* mutation detected in the normal airway of non-smokers has shown to be a "localized" field effect phenomenon affecting the peripheral airway (see below) [20].

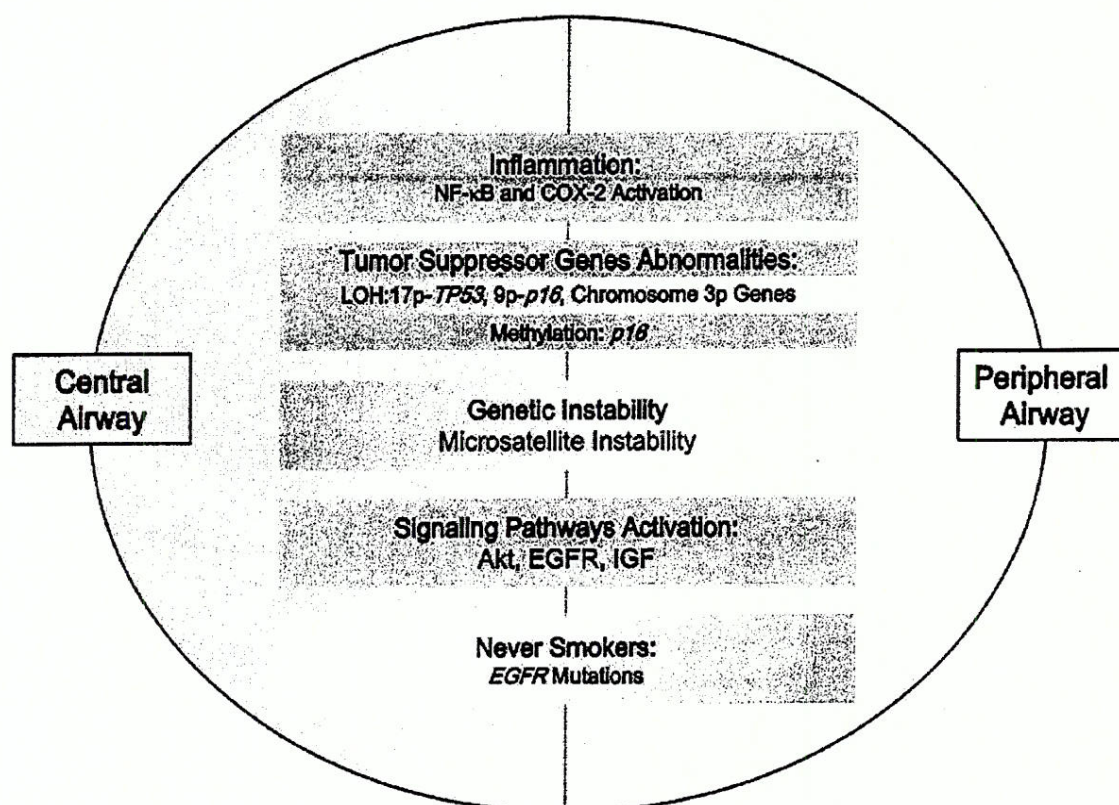


Fig. (3). The field effect phenomenon is called field cancerization, by which much of the respiratory epithelium has been mutagenized, presumably from exposure to tobacco-related carcinogenesis. However, localized field effect has been also detected for *EGFR* mutations in never smokers. While some molecular changes (i.e., inflammation and some signaling pathways activation) have been detected throughout the lung airway and including both compartments (central and peripheral airway), others have been more frequently altered in either central (i.e., loss of heterozygosity, LOH, and genetic instability) or peripheral (i.e., *EGFR* mutations) airway.

MOLECULAR ABNORMALITIES IN THE PATHOGENESIS OF LUNG CANCER

Multiple genetic changes have been found in clinically evident lung cancers in several studies, and these changes have involved known and putative tumor-suppressor genes as well as several dominant oncogenes [1]. Lung cancers arise after a series of molecular changes that commence in histologically normal epithelium and demonstrate a specific sequence [6,44]. There is a preferred order of these allele loss changes, with 3p allele loss (several 3p sites) followed by 9p (*p16*^{INK4a} locus) as the earliest changes occurring in histologically normal epithelium [44,45,51]. Telomerase activation has been also implicated as an early event in lung cancer pathogenesis [52,53]. Telomerase shortening is an early genetic abnormality in bronchial carcinogenesis, preceding telomerase expression and p53/Rb inactivation, and predominates in high-grade squamous preinvasive lesions [54]. Precise microscopic-based microdissection of epithelial tissue followed by allelotyping of smoking-damaged lung from lung cancer patients or from current or former smokers without lung cancer has found multiple

lesions containing clonal abnormalities of allele loss, occurring in both histologically normal as well as mildly abnormal (hyperplasia and squamous metaplasia) and preneoplastic (dysplasia) respiratory epithelium [49]. Although those changes are found in the lungs of current and former smokers without lung cancer, they are almost never found in life-time never-smokers [47,48]. Interestingly, those clonal changes persist for decades after smoking cessation [47].

Similar evidence exists for multiple promoter methylation changes in smoking-damaged lung epithelium and sputum specimens [55,56]. Recent results for methylation analyses of several genes, including *RAR β -2*, *H-cadherin*, *APC*, *p16*^{INK4a}, and *RASFF1A*, indicate that abnormal gene methylation is relatively frequent (one or more genes in 48%) in oropharyngeal and bronchial epithelial cells in heavy smokers with evidence of sputum atypia [56]. Methylation in one or more of three genes tested (*p16*^{INK4a}, *GSTP1*, and *DAPK*) has been demonstrated in bronchial brush specimens in about one third of smokers [57]. Results from another study indicated that aberrant promoter hypermethylation of

the *p16^{INK4a}* gene occurs frequently in the bronchial epithelium of lung cancer patients and smokers without cancer and persists after smoking cessation [58,59]. Aberrant promoter methylation of *p16^{INK4a}* was seen in at least one bronchial epithelial site from 44% of lung cancer patients and cancer-free smokers. A recent nested case-control study [60] of incident lung cancer cases from an extremely high-risk cohort for evaluating promoter methylation of 14 genes in sputum showed that the prevalence for methylation of gene promoters increased as the time to lung cancer diagnosis decreased. Six (*p16^{INK4a}*, *MGMT*, *DAPK*, *RASSF1A*, *PAX5 β* , and *GATA5*) of 14 genes were associated with a >50% increased risk of lung cancer. In addition, in the same study, the concomitant methylation of three or more of these six genes was associated with a 6.5-fold increased risk and a sensitivity and specificity of 64%.

Considerable attention has been given to the identification of the 3p genes involved in lung cancer pathogenesis, including *RAR β* at 3p24, *FHIT* at 3p14.2, *RASSF1A*, *BLU*, *FUS1*, and *SEMA3B* located at 3p21.3, and potentially *ROBO1* at 3p12 [45,55,61]. Their expression is frequently lost in lung cancer, usually by promoter methylation [62]. However, specific roles of the genes undergoing activation or inactivation and the order of cumulative molecular changes that lead to the development of each lung tumor histologic type remain to be elucidated.

Profiling studies using high-throughput technologies for the identification of molecular signatures associated with the development and progression of lung cancer precursor lesions are extremely difficult to perform, because usually such lesions are small and need histological confirmation by tissue fixation and histopathologic processing. Although some profiling studies have been performed using *in vitro* cultured human normal bronchial epithelial cells [63,64], recently a specific pattern of protein expression using proteomic methodology of the airway epithelium that accurately classified bronchial and alveolar tissue with normal histology from preinvasive bronchial lesions and from invasive lung cancer was reported [63]. Although these findings need to be further validated, this represents a first step toward a new proteomic characterization of the human model of lung cancer development.

PRENEOPLASTIC LESIONS AT THE CENTRAL LUNG AIRWAY

Squamous Metaplasia and Dysplasia

Mucosal changes in the large airways that may precede or accompany invasive squamous cell carcinoma include hyperplasia, squamous metaplasia, squamous dysplasia, and carcinoma *in situ* [4,5,65]. Dysplastic squamous lesions are considered true preneoplastic lesions and may be of various degrees (i.e., mild, moderate, and severe);

however, these lesions represent a continuum of cytologic and histologic atypical changes that may show some overlapping features between categories. These lesions are often not detected by conventional white light bronchoscopy or gross examination. However, the use of fluorescent bronchoscopy greatly increases the sensitivity for detection of squamous dysplastic and carcinoma *in situ* lesions [66-68]. Little is known about the rate and risks of progression of squamous dysplasia to carcinoma *in situ* and ultimately to invasive squamous cell carcinoma.

There are no squamous cells in the normal airways. The progenitor or stem cells for the squamous metaplastic epithelium for the proximal airway are not known, but it is presumed that the basal cells represent a relatively quiescent zone that is the precursor of preneoplastic epithelium. In fact, squamous metaplasia is usually preceded and accompanied by basal cell hyperplasia. It is of interest that these cells express significant levels of *Egfr* protein and increased proliferative activity as measured by Ki-67 staining [69,70].

The current working model of the sequential molecular abnormalities in the pathogenesis of squamous cell lung carcinoma indicates the following: (a) Genetic abnormalities commence in histologically normal epithelium and increase with increasing severity of histologic changes [44]. (b) Mutations follow a sequence, with progressive allelic losses at multiple 3p (3p21, 3p14, 3p22-24, and 3p12) chromosome sites and 9p21 (*p16^{INK4a}*) as the earliest detected changes. Later changes include 8p21-23, 13q14 (*RB*), and 17p13 (*TP53*) [44,45,51]. *p16^{INK4a}* methylation has been also detected at an early stage of squamous preinvasive lesions with a frequency that increases during histopathologic progression (24% in squamous metaplasia and 50% in carcinoma *in situ*) [58]. (c) Molecular changes in the respiratory epithelium are extensive and multifocal throughout the bronchial tree of smokers and lung cancer patients, indicating a field effect or field cancerization [44,45,47,48]. (d) Multiple clonal and subclonal patches of molecular abnormalities not much larger in size than the average bronchial biopsy obtained by fluorescent bronchoscopy (estimated to be approximately 40,000 to 360,000 cells) can be detected in the normal and slightly abnormal bronchial epithelium of patients with lung cancer [49]. Despite encouraging results from isolated studies [60], most of these findings have not been useful for the development of successful strategies for lung cancer risk assessment, early detection, or chemoprevention.

Angiogenic Squamous Dysplasia

Interestingly, in a subset of squamous metaplastic and dysplastic changes, the basal membrane becomes thickened and there is vascular budding in the subepithelial tissues that results in papillary protrusions of the epithelium, lesions that Keith *et al.*

termed angiogenic squamous dysplasia (ASD) [71]. ASD lesions are more frequently detected by using fluorescent bronchoscopy than by using white-light conventional bronchoscopy [69]. In the bronchial biopsies of these lesions, microvessel density is elevated compared with normal mucosa but not compared with other forms of hyperplasia or dysplasia. ASD thus represents a qualitatively distinct form of angiogenesis in which there is architectural rearrangement of the capillary microvasculature. Genetic analysis of surface epithelium in a subset of lesions found a LOH at chromosome 3p in 53% of lesions, and compared with normal epithelium, proliferative activity was markedly elevated in ASD lesions. ASD was found in approximately 19% of high-risk smokers without carcinoma who underwent fluorescence bronchoscopy [68] and was not present in biopsy specimens from 16 normal nonsmoker control subjects [71]. The presence of this lesion in high-risk smokers suggests that aberrant patterns of microvascularization may occur at an early stage of bronchial carcinogenesis. The finding of vascular endothelial growth factor (VEGF) isoforms and VEGF receptors (VEGFR) by semiquantitative reverse transcriptase-PCR, confirmed by immunohistochemistry in bronchial squamous dysplastic epithelia compared with normal bronchial epithelia [72], supports the notion that angiogenesis develops early in lung carcinogenesis and that these abnormalities provide a rationale for the development of targeted antiangiogenic chemoprevention strategies.

PRENEOPLASTIC LESIONS AT THE PERIPHERAL LUNG AIRWAY

Despite the evidence that atypical adenomatous hyperplasia (AAH) is a precursor lesion for peripheral lung adenocarcinomas [5,73], there is consensus that the pathogenesis of many adenocarcinomas is still unknown. AAH is a discrete parenchymal lesion arising in the alveoli close to terminal and respiratory bronchioles, and AAH may be single or multiple. These lesions maintain an alveolar structure lined by rounded, cuboidal, or low columnar cells. The postulated progression of AAH to adenocarcinoma especially the bronchioloalveolar (BAC) subtype, is supported by morphometric, cytofluorometric, and molecular studies [65,73]. AAH is most frequently detected in lung from patients bearing lung cancers (9-20%), especially adenocarcinomas (up to 40%) compared with squamous cell carcinomas (11%) [65,74-77]. In contrast, autopsy studies have reported AAH in approximately 3% of persons without cancer [78]. It is extremely difficult to know the progression rate of AAH to lung adenocarcinoma, and it is also currently almost impossible to determine whether AAH may regress. Because they are air-filled structures, they may appear as ground glass opacities on CT scans. However, the location, size, and relative invisibility of AAH by most imaging methods make longitudinal

studies of AAH even more difficult than studies of centrally located squamous preneoplastic lesions. Another type of lung peripheral lesion, termed bronchiolization of the alveoli [79,80], which is characterized by replacement of the alveolar epithelium by columnar bronchiolar-type epithelium with and without cytological atypia and which may exhibit molecular abnormalities such as chromosomal abnormalities by comparative genome hybridization (CGH) [79], has been also associated with the pathogenesis of lung adenocarcinoma.

Several molecular changes frequently present in lung adenocarcinomas are also present in AAH lesions, and they are further evidence that AAH may represent true preneoplastic lesions [73,81]. The most important finding is the presence of KRAS (codon 12) mutations, which are also relatively frequent alterations in lung adenocarcinomas, in up to 39% of AAH [73]. Other molecular alterations detected in AAH are overexpression of cyclin D1 (~70%), p53 (ranging from 10% to 58%), survivin (48%), and Her-2/neu (7%) proteins [73,82,83]. Some AAH lesions have demonstrated LOH in chromosomes 3p (18%), 9p (*p16^{INK4a}*, 13%), 9q (53%), 17q, and 17p (*TP53*, 6%), changes that are frequently detected in lung adenocarcinomas [84,85]. A study of lung adenocarcinoma with synchronous multiple AAH showed frequent LOH of tuberous sclerosis complex (TSC)-associated regions (*TSC1* at 9q, 53%, and *TSC2* at 16p, 6%), suggesting that these are candidate loci for a tumor-suppressor gene in a subset of adenocarcinomas of the lung [85]. Activation of telomerase, expressed by expression of human telomerase RNA component (*hTERC*) and telomerase reverse transcriptase (*hTERT*) mRNA, has been detected in 27% to 78% of AAH lesions, depending on their atypia level [86]. Recently, it has been shown that loss of *LKB1*, a serine/threonine kinase that functions as a tumor-suppressor gene, is frequent in lung adenocarcinomas (25%) and in AAH with severe cytological atypia (21%), while it is rare in mild atypical AAH lesions (5%), suggesting that *LKB1* inactivation may play a role in the AAH progression to malignancy [87].

Several mouse models have been developed to better study various oncogenic molecular signaling pathways and the sequence of molecular events involved in the pathogenesis of peripheral lung tumors and to test novel chemopreventive agents [88]. The *K-RAS* oncogenic mouse model is characterized by the development of the peripheral alveolar type of proliferations, including AAH, adenoma, and adenocarcinoma [88]. Using this mouse model, several important findings that need to be further validated in human tissues have been reported. Kim *et al.* [89] identified the potential stem cell population (expressing Clara cells-specific protein and surfactant protein-C, termed bronchioalveolar stem cell, BASC) that maintains the bronchiolar Clara cells and alveolar cells of the distal respiratory epithelium and which could be considered the

precursors of lung *K-RAS* neoplastic lesions in mice. Wislez *et al.* [90] provided evidence that the expansion of lung adenocarcinoma precursors induced by oncogenic *K-RAS* requires mammalian target of rapamycin (mTOR)-dependent signaling and, most importantly, that inflammation-related host factors, including factors derived from macrophages, play a critical role in adenocarcinoma progression in mice. Recent findings reported by Collado *et al.* [91] suggest that *K-RAS* oncogene-induced senescence may help restrict tumor progression of lung peripheral lesions in mice. They discovered that a substantial number of cells in mouse premalignant alveolar-type lesions undergo oncogene-induced senescence, but the cells that escape senescence by loss of oncogene-induced senescence effectors, such as p16^{INK4a} or p53, progress to malignancy. Thus, senescence is a defining feature of premalignant lung lesions but not invasive tumors.

NONSMOKING-RELATED PATHWAYS

Although most lung cancers are smoking-related tumors, a subset of NSCLCs arises in never-smokers. Adenocarcinoma histology is the tumor type most frequently detected in never-smokers. Recently, somatic mutations of *EGFR* and *HER-2/NEU*, tyrosine kinase (TK) members of the ErbB family, have been reported in a subset of lung adenocarcinoma patients having never-smoker or light-smoker status, female sex, and East Asian ethnicity [92-99]. The *EGFR* mutations are clinically relevant because most of them have been associated with sensitivity of lung adenocarcinoma to small-molecule TK inhibitors (gefitinib and erlotinib) [92-94,100]. More than 80% of the mutations detected in *EGFR* are in-frame deletions in exon 19 and a single missense mutation in exon 21 (L858R) [92-98]. It has been proposed that lung cancer cells with mutant *EGFR* might become physiologically dependent on the continued activity of the gene for the maintenance of their malignant phenotype, leading to accelerated development of lung adenocarcinoma [19]. Recent studies have demonstrated that tumor cell high *EGFR* copy number, identified by the fluorescent *in situ* hybridization (FISH) technique, may also be a predictor for response to *EGFR* TK inhibitors [101-103] and be involved in the pathogenesis of lung adenocarcinoma.

To better understand the pathogenesis of *EGFR* mutant lung adenocarcinomas, we investigated the presence of *EGFR* mutations in the normal bronchial and bronchiolar epithelium adjacent to mutant tumors. We detected *EGFR* mutations in normal-appearing peripheral respiratory epithelium in nine (44%) of 21 adenocarcinoma patients, but not in patients without mutations in the tumors [20]. Our finding of more frequent *EGFR* mutations in normal epithelium within the tumor (43%) than in adjacent sites (24%) suggests a localized field effect phenomenon, probably affecting preferentially the

peripheral lung airway compartment, for this abnormality in the respiratory epithelium of the lung. Although the cell type having those mutations is unknown, we have hypothesized that stem or progenitor cells of the bronchial and bronchiolar epithelium are the cell type bearing such mutations. The finding of relatively infrequent *EGFR* mutations in AAH lesions (three out of 40 examined) [104,105] and the finding of no mutation [98] or a relatively low frequency of mutation in true BACs of the lung support the concept that genetic abnormalities of *EGFR* are not relevant in the pathogenesis of alveolar-type lung neoplasia. Our recent unpublished data suggest that *EGFR* mutation precedes increased copy number of the gene in the pathogenesis of lung adenocarcinoma. Thus, two different molecular pathways have been identified in the pathogenesis of lung adenocarcinoma, a smoking-associated activation of *KRAS* signaling and a nonsmoking-associated activation of *EGFR* signaling, the latter detected in histologically normal bronchial and bronchiolar epithelium.

SIGNALING PATHWAY ACTIVATION IN LUNG CANCER PRENEOPLASTIC LESIONS

The recent developments in molecular biology have increased our knowledge of critical biological pathways that are deregulated in lung cancer cells, and they have provided a rationale for the development of targeted therapy in human tumors, including lung cancer [106]. Activation of tyrosine kinases, particularly receptor tyrosine kinases, is increasingly recognized as a common cause for deregulation of these pathways, and inhibiting tyrosine kinases has proven to be an effective strategy for a number of malignancies, including lung cancer [107]. Thus, the possible activation of signaling pathways early in the pathogenesis of lung cancer has created an opportunity for the design of targeted chemoprevention strategies [108,109]. Of interest, most important signaling pathways that are being targeted in lung cancer have been shown to be also deregulated in lung cancer preneoplastic lesions, mostly in the squamous cell carcinoma pathway, including (among others) the inflammation-related polyunsaturated fatty acid metabolic pathways [110], retinoic acid signaling [109], and pathways involving Ras [73,90,111,112], *EGFR* [20,113], phosphoinositide 3-kinase (PI3K)/Akt [114-116], insulin-like growth (IGF) factor axis [117], VEGF/VEGFR [72], and mTOR [90].

PERSPECTIVE

During the last decade, encouraged by the development of methodologies such as laser microdissection for the isolation of cells from small histologic lesions, combined with techniques to perform genomic studies from minute amounts of DNA, RNA, and protein, several groups have made substantial progress in discovering the molecular and

genetic abnormalities of lung cancer precursor lesions, including those evolving to centrally located squamous cell carcinoma and peripheral adenocarcinoma. However, it seems that the enthusiasm has somehow substantially decreased, for in the last few years little progress has been made. The recent development of a panel of human normal bronchial epithelial cells immortalized with telomerase and Cdk4-mediated *p16^{INK4a}* bypass, which can be modified with a combination of oncogene activation and tumor-suppressor gene knockdowns for *in vitro* discovery work [118], coupled with the development of more relevant lung cancer animal models [119] and new high-throughput genomic [120] and proteomic [63,121] profiling techniques that can be applied to small amounts of microdissected tissues, may stimulate the scientific community to perform innovative investigations in the fields of molecular and pathologic research to understand the molecular malignant potential of respiratory epithelium even before histologic changes occur. Currently, two major National Cancer Institute programs, Specialized Programs of Research Excellence and the Early Detection Research Network, are concentrating on a search for new biomarkers in lung cancer. All these efforts may help us to better characterize the malignant potential of lung cancer preneoplastic lesions and to understand the field cancerization compartmental (central versus periphery) phenomenon in lung cancer pathogenesis.

ACKNOWLEDGEMENT

Supported by grant Department of Defense W81XWH-04-1-0142.

ABBREVIATIONS

SCLC	= small cell lung carcinoma
NSCLC	= non-small cell lung carcinoma
CT	= computed tomography
COPD	= chronic obstructive pulmonary disease
EGFR	= epidermal growth factor receptor
COX-2	= cyclooxygenase-2
NF- κ B	= nuclear factor kappa B
LOH	= loss of heterozygosity
ASD	= angiogenic squamous dysplasia
AAH	= atypical adenomatous hyperplasia

REFERENCES

- [1] Minna, J.D. and Gazdar, A. (2002) *Cancer Cell*, **1**, 49-52.
- [2] Jemal, A., Murray, T., Ward, E., Samuels, A., Tiwari, R.C., Ghafoor, A., Feuer, E.J. and Thun, M.J. (2005) *C.A. Cancer J. Clin.*, **55**, 10-30.
- [3] Travis, W.D., Brambilla, E., Muller-Hermelink, H.K. and Harris, C.C. (2004). *Pathology and Genetics: Tumours of the Lung, Pleura, Thymus and Heart: World Health Organization Classification of Tumours*. Pathology & Genetics. Travis Wd, Brambilla E, Muller-Hermelink Hk and Harris Cc (eds). International Agency for Research on Cancer (IARC): Lyon, pp. 9-124.
- [4] Franklin, W., Wistuba, I., Geisinger, K., Lam, S., Hirsch, F., Muller, K.M., Sozzi, G., Brambilla, E. and Gazdar, A. (2004). *Pathology and Genetics. Tumors of the Lung, Pleura, Thymus and Heart: World Health Organization Classification of Tumours*. Travis W, Brambilla E, Muller-Hermelink Hk and Harris Cc (eds). International Agency for Research on Cancer (IARC): Lyon, pp. 68-72.
- [5] Colby, T.V., Wistuba, I.I. and Gazdar, A. (1998) *Adv. Anat. Pathol.*, **5**, 205-215.
- [6] Wistuba, I.I., Mao, L. and Gazdar, A.F. (2002) *Oncogene*, **21**, 7298-7306.
- [7] Mulshine, J.L. (2005) *Oncol. (Williston Park)*, **19**, 1724-1730; discussion 1730-1721.
- [8] Lam, S., MacAulay, C., leRiche, J.C. and Palicic, B. (2000) *Cancer*, **89**, 2468-2473.
- [9] Lubin, J.H. and Blot, W.J. (1993) *J. Natl. Cancer Inst.*, **85**, 422-423.
- [10] Halpern, M.T., Gillespie, B.W. and Warner, K.E. (1993) *J. Natl. Cancer Inst.*, **85**, 457-464.
- [11] Tong, L., Spitz, M.R., Fueger, J.J. and Amos, C.A. (1996) *Cancer*, **78**, 1004-1010.
- [12] Risch, H.A., Howe, G.R., Jain, M., Burch, J.D., Holowaty, E.J. and Miller, A.B. (1993) *Am. J. Epidemiol.*, **138**, 281-293.
- [13] Lam, S., leRiche, J.C., Zheng, Y., Coldman, A., MacAulay, C., Hawk, E., Kelloff, G. and Gazdar, A.F. (1999) *J. Natl. Cancer Inst.*, **91**, 691-696.
- [14] Zang, E.A. and Wynder, E.L. (1996) *J. Natl. Cancer Inst.*, **88**, 183-192.
- [15] O'Byrne, P.M. and Postma, D.S. (1999) *Am. J. Respir. Crit. Care Med.*, **159**, S41-63.
- [16] Tockman, M.S., Anthonisen, N.R., Wright, E.C. and Donithan, M.G. (1987) *Ann. Intern. Med.*, **106**, 512-518.
- [17] Prindiville, S.A., Byers, T., Hirsch, F.R., Franklin, W.A., Miller, Y.E., Vu, K.O., Wolf, H.J., Baron, A.E., Shroyer, K.R., Zeng, C., Kennedy, T.C. and Bunn, P.A. (2003) *Cancer Epidemiol. Biomarkers Prev.*, **12**, 987-993.
- [18] Garfinkel, L. and Stellman, S.D. (1988) *Cancer Res.*, **48**, 6951-6955.
- [19] Gazdar, A.F., Shigematsu, H., Herz, J. and Minna, J.D. (2004) *Trends Mol. Med.*, **10**, 481-486.
- [20] Tang, X., Shigematsu, H., Bekele, B.N., Roth, J.A., Minna, J.D., Hong, W.K., Gazdar, A.F. and Wistuba, I.I. (2005) *Cancer Res.*, **65**, 7568-7572.
- [21] Coussens, L.M. and Werb, Z. (2002) *Nature*, **420**, 860-867.
- [22] Ballaz, S. and Mulshine, J.L. (2003) *Clin. Lung Cancer*, **5**, 46-62.
- [23] Anderson, G.P. and Bozinovski, S. (2003) *Trends Pharmacol. Sci.*, **24**, 71-76.
- [24] Suzuki, H., Graziano, D.F., McKolanis, J. and Finn, O.J. (2005) *Clin. Cancer Res.*, **11**, 1521-1526.
- [25] Hogg, J.C. (2004) *Lancet*, **364**, 709-721.
- [26] Barnes, P.J. (2000) *N. Engl. J. Med.*, **343**, 269-280.
- [27] Hida, T., Kozaki, K., Muramatsu, H., Masuda, A., Shimizu, S., Mitsudomi, T., Sugiura, T., Ogawa, M. and Takahashi, T. (2000) *Clin. Cancer Res.*, **6**, 2006-2011.
- [28] Kennedy, T.C., Proudfoot, S.P., Franklin, W.A., Merrick, T.A., Saccomanno, G., Corkill, M.E., Mumma, D.L., Sirgi, K.E., Miller, Y.E., Archer, P.G. and Prochazka, A. (1996) *Cancer Res.*, **56**, 4673-4678.
- [29] Tsurutani, J., Castillo, S.S., Brognard, J., Granville, C.A., Zhang, C., Gills, J.J., Sayyah, J. and Dennis, P.A. (2005) *Carcinogenesis*, **26**, 1182-1195.
- [30] Shishodia, S., Koul, D. and Aggarwal, B.B. (2004) *J. Immunol.*, **173**, 2011-2022.
- [31] Tichelaar, J.W., Zhang, Y., leRiche, J.C., Biddinger, P.W., Lam, S. and Anderson, M.W. (2005) *BMC Cancer*, **5**, 155.
- [32] Aggarwal, B.B. (2004) *Cancer Cell*, **6**, 203-208.
- [33] Karin, M. and Greten, F.R. (2005) *Nat. Rev. Immunol.*, **5**, 749-759.
- [34] Pikarsky, E., Porat, R.M., Stein, I., Abramovitch, R., Amit, S., Kasem, S., Galkovich-Pyest, E., Urieli-Shoval, S., Galun, E. and Ben-Neriah, Y. (2004) *Nature*, **431**, 461-466.
- [35] Kumar, A., Takada, Y., Boriek, A.M. and Aggarwal, B.B. (2004) *J. Mol. Med.*, **82**, 434-448.

- [36] Shishodia, S. and Aggarwal, B.B. (2004) *Biochem. Pharmacol.*, **68**, 1071-1080.
- [37] Dannenberg, A.J., Altorki, N.K., Boyle, J.O., Dang, C., Howe, L.R., Weksler, B.B. and Subbaramaiah, K. (2001) *Lancet Oncol.*, **2**, 544-551.
- [38] Hasturk, S., Kemp, B., Kalapurakal, S.K., Kurie, J.M., Hong, W.K. and Lee, J.S. (2002) *Cancer*, **94**, 1023-1031.
- [39] Mao, J.T., Cui, X., Reckamp, K., Liu, M., Krysan, K., Dalwadi, H., Sharma, S., Hazra, S., Strieter, R., Gardner, B. and Dubinett, S.M. (2005) *Clin. Lung Cancer*, **7**, 30-39.
- [40] Mascaux, C., Martin, B., Verdebout, J.M., Ninane, V. and Sculier, J.P. (2005) *Eur. Respir. J.*, **26**, 198-203.
- [41] Mao, J.T., Fishbein, M.C., Adams, B., Roth, M.D., Goodglick, L., Hong, L., Burdick, M., Strieter, E.R., Holmes, C., Tashkin, D.P. and Dubinett, S.M. (2006) *Clin. Cancer Res.*, **12**, 314-320.
- [42] Auerbach, O., Stout, A.P., Hammond, E.C. and Garfinkel, L. (1961) *N. Engl. J. Med.*, **265**, 253-267.
- [43] Slaughter, D.P., Southwick, H.W. and Smejkal, W. (1954) *Cancer*, **6**, 963-968.
- [44] Wistuba, I.I., Behrens, C., Milchgrub, S., Bryant, D., Hung, J., Minna, J.D. and Gazdar, A.F. (1999) *Oncogene*, **18**, 643-650.
- [45] Wistuba, I.I., Behrens, C., Virmani, A.K., Mele, G., Milchgrub, S., Girard, L., Fondon, J.W., Garner, H.R., McKay, B., Latif, F., Lerman, M.I., Lam, S., Gazdar, A.F. and Minna, J.D. (2000) *Cancer Res.*, **60**, 1949-1960.
- [46] Wistuba, I.I., Berry, J., Behrens, C., Maitra, A., Shivapurkar, N., Milchgrub, S., Mackay, B., Minna, J.D. and Gazdar, A.F. (2000) *Clin. Cancer Res.*, **6**, 2604-2610.
- [47] Wistuba, I.I., Lam, S., Behrens, C., Virmani, A.K., Fong, K.M., LeRiche, J., Samet, J.M., Srivastava, S., Minna, J.D. and Gazdar, A.F. (1997) *J. Natl. Cancer Inst.*, **89**, 1366-1373.
- [48] Mao, J., Lee, J.S., Kurie, J.M., Fan, Y.H., Lippman, S.M., Lee, J.J., Ro, J.Y., Broxson, A., Yu, R., Morice, R.C., Kemp, B.L., Khuri, F.R., Walsh, G.L., Hittelman, W.N. and Hong, W.K. (1997) *J. Natl. Cancer Inst.*, **89**, 857-862.
- [49] Park, I.W., Wistuba, I.I., Maitra, A., Milchgrub, S., Virmani, A.K., Minna, J.D. and Gazdar, A.F. (1999) *J. Natl. Cancer Inst.*, **91**, 1863-1868.
- [50] Sin, D.D., Man, S.F., McWilliams, A. and Lam, S. (2006) *Am. J. Respir. Crit. Care Med.*, **173**, 535-539.
- [51] Wistuba, I.I., Behrens, C., Virmani, A.K., Milchgrub, S., Syed, S., Lam, S., Mackay, B., Minna, J.D. and Gazdar, A.F. (1999) *Cancer Res.*, **59**, 1973-1979.
- [52] Yashima, K., Milchgrub, S., Gollahon, L.S., Maitra, A., Saboorian, M.H., Shay, J.W. and Gazdar, A.F. (1998) *Clin. Cancer Res.*, **4**, 229-234.
- [53] Miyazu, Y.M., Miyazawa, T., Hiyama, K., Kurimoto, N., Iwamoto, Y., Matsuura, H., Kanoh, K., Kohno, N., Nishiyama, M. and Hiyama, E. (2005) *Cancer Res.*, **65**, 9623-9627.
- [54] Lantuejoul, S., Soria, J.C., Morat, L., Lorimier, P., Moro-Sibilot, D., Sabatier, L., Brambilla, C. and Brambilla, E. (2005) *Clin. Cancer Res.*, **11**, 2074-2082.
- [55] Zochbauer-Muller, S., Fong, K.M., Maitra, A., Lam, S., Geradts, J., Ashfaq, R., Virmani, A.K., Milchgrub, S., Gazdar, A.F. and Minn, J.D. (2001) *Cancer Res.*, **61**, 3581-3585.
- [56] Zochbauer-Muller, S., Lam, S., Toyooka, S., Virmani, A.K., Toyooka, K.O., Seidl, S., Minna, J.D. and Gazdar, A.F. (2003) *Int. J. Cancer*, **107**, 612-616.
- [57] Soria, J.C., Rodriguez, M., Liu, D.D., Lee, J.J., Hong, W.K. and Mao, L. (2002) *Cancer Res.*, **62**, 351-355.
- [58] Belinsky, S.A., Nikula, K.J., Palmisano, W.A., Michels, R., Saccomanno, G., Gabrielson, E., Baylin, S.B. and Herman, J.G. (1998) *Proc. Natl. Acad. Sci. USA*, **95**, 11891-11896.
- [59] Belinsky, S.A., Palmisano, W.A., Gilliland, F.D., Crooks, L.A., Divine, K.K., Winters, S.A., Grimes, M.J., Harms, H.J., Tellez, C.S., Smith, T.M., Moots, P.P., Lechner, J.F., Stidley, C.A. and Crowell, R.E. (2002) *Cancer Res.*, **62**, 2370-2377.
- [60] Belinsky, S.A., Liechty, K.C., Gentry, F.D., Wolf, H.J., Rogers, J., Vu, K., Haney, J., Kennedy, T.C., Hirsch, F.R., Miller, Y., Franklin, W.A., Herman, J.G., Baylin, S.B., Bunn, P.A. and Byers, T. (2006) *Cancer Res.*, **66**, 3338-3344.
- [61] Lerman, M.I. and Minna, J.D. (2000) *Cancer Res.*, **60**, 6116-6133.
- [62] Zabarovsky, E.R., Lerman, M.I. and Minna, J.D. (2002) *Oncogene*, **21**, 6915-6935.
- [63] Rahman, S.M., Shyr, Y., Yildiz, P.B., Gonzalez, A.L., Li, H., Zhang, X., Chaurand, P., Yanagisawa, K., Slovis, B.S., Miller, R.F., Ninan, M., Miller, Y.E., Franklin, W.A., Caprioli, R.M., Carbone, D.P. and Massion, P.P. (2005) *Am. J. Respir. Crit. Care Med.*, **172**, 1556-1562.
- [64] Jorgensen, E.D., Dozmorov, I., Frank, M.B., Centola, M. and Albino, A.P. (2004) *Cell Cycle*, **3**, 1154-1168.
- [65] Kerr, K.M. (2001) *J. Clin. Pathol.*, **54**, 257-271.
- [66] Lam, S., Kennedy, T., Unger, M., Miller, Y.E., Gelmont, D., Rusch, V., Gipe, B., Howard, D., LeRiche, J.C., Coldman, A. and Gazdar, A.F. (1998) *Chest*, **113**, 696-702.
- [67] Kennedy, T.C., Lam, S. and Hirsch, F.R. (2001) *Oncologist*, **6**, 257-262.
- [68] Hirsch, F.R., Prindiville, S.A., Miller, Y.E., Franklin, W.A., Dempsey, E.C., Murphy, J.R., Bunn, P.A., Jr. and Kennedy, T.C. (2001) *J. Natl. Cancer Inst.*, **93**, 1385-1391.
- [69] Hirsch, F.R., Franklin, W.A., Gazdar, A.F. and Bunn, P.A., Jr. (2001) *Clin. Cancer Res.*, **7**, 5-22.
- [70] Lee, J.J., Liu, D., Lee, J.S., Kurie, J.M., Khuri, F.R., Ibarguen, H., Morice, R.C., Walsh, G., Ro, J.Y., Broxson, A., Hong, W.K. and Hittelman, W.N. (2001) *J. Natl. Cancer Inst.*, **93**, 1081-1088.
- [71] Keith, R.L., Miller, Y.E., Gemmill, R.M., Drabkin, H.A., Dempsey, E.C., Kennedy, T.C., Prindiville, S. and Franklin, W.A. (2000) *Clin. Cancer Res.*, **6**, 1616-1625.
- [72] Merrick, D.T., Haney, J., Petrunich, S., Sugita, M., Miller, Y.E., Keith, R.L., Kennedy, T.C. and Franklin, W.A. (2005) *Lung Cancer*, **48**, 31-45.
- [73] Westra, W.H. (2000) *Respir. Med.*, **1**, 163-169.
- [74] Weng, S.Y., Tsuchiya, E., Kasuga, T. and Sugano, H. (1992) *Virchows Arch. A. Pathol. Anat. Histopathol.*, **420**, 463-471.
- [75] Nakanishi, K. (1990) *Arch. Pathol. Lab. Med.*, **114**, 363-368.
- [76] Chapman, A.D. and Kerr, K.M. (2000) *Br. J. Cancer*, **83**, 632-636.
- [77] Koga, T., Hashimoto, S., Sugio, K., Yonemitsu, Y., Nakashima, Y., Yoshino, I., Matsuo, Y., Mojtahedzadeh, S., Sugimachi, K. and Sueishi, K. (2002) *Am. J. Clin. Pathol.*, **117**, 464-70.
- [78] Yokose, T., Doi, M., Tanno, K., Yamazaki, K. and Ochiai, A. (2001) *Lung Cancer*, **33**, 155-161.
- [79] Jensen-Taubman, S.M., Steinberg, S.M. and Linnoila, R.I. (1998) *Int. J. Cancer*, **75**, 489-496.
- [80] Ullmann, R., Bongiovanni, M., Halbwed, I., Petzmann, S., Gogg-Kammerer, M., Sapino, A., Papotti, M., Bussolati, G. and Popper, H.H. (2003) *Virchows Arch.*, **442**, 429-436.
- [81] Kitamura, H., Kameda, Y., Ito, T. and Hayashi, H. (1999) *Am. J. Clin. Pathol.*, **111**, 610-622.
- [82] Tominaga, M., Sueoka, N., Irie, K., Iwanaga, K., Tokunaga, O., Hayashi, S.I., Nakachi, K. and Sueoka, E. (2003) *Lung Cancer*, **40**, 45-53.
- [83] Nakanishi, K., Kawai, T., Kumaki, F., Hiroi, S., Mukai, M. and Ikeda, E. (2003) *Am. J. Clin. Pathol.*, **120**, 712-719.
- [84] Kitaguchi, S., Takeshima, Y., Nishisaka, T. and Inai, K. (1998) *Hiroshima. J. Med. Sci.*, **47**, 17-25.
- [85] Takamochi, K., Ogura, T., Suzuki, K., Kawasaki, H., Kurashima, Y., Yokose, T., Ochiai, A., Nagai, K., Nishiwaki, Y. and Esumi, H. (2001) *Am. J. Pathol.*, **159**, 1941-1948.
- [86] Nakanishi, K., Kawai, T., Kumaki, F., Hiroi, S., Mukai, M. and Ikeda, E. (2002) *Hum. Pathol.*, **33**, 697-702.
- [87] Ghaffar, H., Sahin, F., Sanchez-Cespedes, M., Su, G.H., Zahurak, M., Sidransky, D. and Westra, W.H. (2003) *Clin. Cancer Res.*, **9**, 2998-3003.
- [88] Nikitin, A.Y., Alcaraz, A., Anver, M.R., Bronson, R.T., Cardiff, R.D., Dixon, D., Fraire, A.E., Gabrielson, E.W., Gunning, W.T., Haines, D.C., Kaufman, M.H., Linnoila, R.I., Maronpot, R.R., Rabson, A.S., Reddick, R.L., Rehm, S., Rozengurt, N., Schuller, H.M., Schmidt, E.N., Travis, W.D., Ward, J.M. and Jacks, T. (2004) *Cancer Res.*, **64**, 2307-2316.
- [89] Kim, C.F., Jackson, E.L., Woolfenden, A.E., Lawrence, S., Babar, I., Vogel, S., Crowley, D., Bronson, R.T. and Jacks, T. (2005) *Cell*, **121**, 823-835.
- [90] Wislez, M., Spencer, M.L., Izzo, J.G., Juroskie, D.M., Balhara, K., Cody, D.D., Price, R.E., Hittelman, W.N., Wistuba, I.I. and Kurie, J.M. (2005) *Cancer Res.*, **65**, 3226-3235.
- [91] Collado, M., Gil, J., Efeyan, A., Guerra, C., Schuhmacher, A.J., Barradas, M., Benguria, A., Zaballos, A., Flores, J.M., Barbacid, M., Beach, D. and Serrano, M. (2005) *Nature*, **436**, 642.
- [92] Paez, J.G., Janne, P.A., Lee, J.C., Tracy, S., Greulich, H., Gabriel, S., Herman, P., Kaye, F.J., Lindeman, N., Boggon, T.J., Naoki, K., Sasaki, H., Fujii, Y., Eck, M.J., Sellers, W.R.,

- Johnson, B.E. and Meyerson, M. (2004) *Science*, **304**, 1497-1500.
- [93] Lynch, T.J., Bell, D.W., Sordella, R., Gurubhagavatula, S., Okimoto, R.A., Brannigan, B.W., Harris, P.L., Haserlat, S.M., Supko, J.G., Haluska, F.G., Louis, D.N., Christiani, D.C., Settleman, J. and Haber, D.A. (2004) *N. Engl. J. Med.*, **350**, 2129-2139.
- [94] Pao, W., Miller, V., Zakowski, M., Doherty, J., Politi, K., Sarkaria, I., Singh, B., Heelan, R., Rusch, V., Fulton, L., Mardis, E., Kupfer, D., Wilson, R., Kris, M. and Varmus, H. (2004) *Proc. Natl. Acad. Sci. USA*, **101**, 13306-13311.
- [95] Huang, S.F., Liu, H.P., Li, L.H., Ku, Y.C., Fu, Y.N., Tsai, H.Y., Chen, Y.T., Lin, Y.F., Chang, W.C., Kuo, H.P., Wu, Y.C., Chen, Y.R. and Tsai, S.F. (2004) *Clin. Cancer Res.*, **10**, 8195-8203.
- [96] Kosaka, T., Yatabe, Y., Endoh, H., Kuwano, H., Takahashi, T. and Mitsudomi, T. (2004) *Cancer Res.*, **64**, 8919-8923.
- [97] Tokumo, M., Toyooka, S., Kiura K., Shigematsu, H., Tomii, K., Aoe, M., Ichimura, K., Tsuda, T., Yano, M., Tsukuda, K., Tabata, M., Ueoka, H., Tanimoto, M., Date, H., Gazdar, A.F. and Shimizu, N. (2005) *Clin. Cancer Res.*, **11**, 1167-1173.
- [98] Shigematsu, H., Lin, L., Takahashi, T., Nomura, M., Suzuki, M., Wistuba, I., Fong, K.M., Lee, H., Toyooka, S., Shimizu, N., Fujisawa, T., Feng, Z., Roth, J.A., Herz, J., Minna, J.D. and Gazdar, A.F. (2005) *J. Natl. Cancer Inst.*, **97**, 339-346.
- [99] Shigematsu, H., Takahashi, T., Nomura, M., Majumdar, K., Suzuki, M., Lee, H., Wistuba, I., Fong, K.M., Toyooka, S., Shimizu, N., Fujisawa, T., Minna, J.D. and Gazdar, A.F. (2005) *Cancer Res.*, **65**, 1642-1646.
- [100] Amann, J., Kalyankrishna, S., Massion, P.P., Ohm, J.E., Girard, L., Shigematsu, H., Peyton, M., Juroske, D., Huang, Y., Stuart Salmon, J., Kim, Y.H., Pollack, J.R., Yanagisawa, K., Gazdar, A., Minna, J.D., Kurie, J.M. and Carbone, D.P. (2005) *Cancer Res.*, **65**, 226-235.
- [101] Cappuzzo, F., Hirsch, F.R., Rossi, E., Bartolini, S., Ceresoli, G.L., Bemis, L., Haney, J., Witta, S., Danenberg, K., Domenichini, I., Ludovini, V., Magrini, E., Gregorc, V., Doglioni, C., Sidoni, A., Tonato, M., Franklin, W.A., Crino, L., Bunn, P.A., Jr. and Varella-Garcia, M. (2005) *J. Natl. Cancer Inst.*, **97**, 643-655.
- [102] Hirsch, F.R., Varella-Garcia, M., McCoy, J., West, H., Xavier, A.C., Gumerlock, P., Bunn, P.A., Jr., Franklin, W.A., Crowley, J. and Gandara, D.R. (2005) *J. Clin. Oncol.*, **23**, 6838-6845.
- [103] Tsao, M.S., Sakurada, A., Cutz, J.C., Zhu, C.Q., Kamel-Reid, S., Squire, J., Lorimer, I., Zhang, T., Liu, N., Daneshmand, M., Marrano, P., da Cunha Santos, G., Lagarde, A., Richardson, F., Seymour, L., Whitehead, M., Ding, K., Pater, J. and Shepherd, F.A. (2005) *N. Engl. J. Med.*, **353**, 133-144.
- [104] Yatabe, Y., Kosaka, T., Takahashi, T. and Mitsudomi, T. (2005) *Am. J. Surg. Pathol.*, **29**, 633-639.
- [105] Yoshida, Y., Shibata, T., Kokubu, A., Tsuta, K., Matsuno, Y., Kanai, Y., Asamura, H., Tsuchiya, R. and Hirohashi, S. (2005) *Lung Cancer*, **50**, 1-8.
- [106] Massarelli, E. and Herbst, R.S. (2006) *Semin. Oncol.*, **33**, S9-16.
- [107] Santarpia, M., Altavilla, G., Salazar, F., Taron, M. and Rosell, R. (2006) *Clin. Transl. Oncol.*, **8**, 71-76.
- [108] Abbruzzese, J.L. and Lippman, S.M. (2004) *Cancer Cell*, **6**, 321-326.
- [109] Khuri, F.R. and Cohen, V. (2004) *Clin. Cancer Res.*, **10**, 4249s-4253s.
- [110] Hirsch, F.R. and Lippman, S.M. (2005) *J. Clin. Oncol.*, **23**, 3186-3197.
- [111] Westra, W.H., Baas, I.O., Hruban, R.H., Askin, F.B., Wilson, K., Offerhaus, G.J. and Slebos, R.J. (1996) *Cancer Res.*, **56**, 2224-2228.
- [112] Wislez, M., Fujimoto, N., Izzo, J.G., Hanna, A.E., Cody, D.D., Langley, R.R., Tang, H., Burdick, M.D., Sato, M., Minna, J.D., Mao, L., Wistuba, I., Strieter, R.M. and Kurie, J.M. (2006) *Cancer Res.*, **66**, 4198-4207.
- [113] Merrick, D.T., Kittelson, J., Winterhalter, R., Kotantoulas, G., Ingeberg, S., Keith, R.L., Kennedy, T.C., Miller, Y.E., Franklin, W.A. and Hirsch, F.R. (2006) *Clin. Cancer Res.*, **12**, 2281-2288.
- [114] Tsao, A.S., McDonnell, T., Lam, S., Putnam, J.B., Bekele, N., Hong, W.K. and Kurie, J.M. (2003) *Cancer Epidemiol. Biomarkers Prev.*, **12**, 660-664.
- [115] Balsara, B.R., Pei, J., Mitsuuchi, Y., Page, R., Klein-Szanto, A., Wang, H., Unger, M. and Testa, J.R. (2004) *Carcinogenesis*, **25**, 2053-2059.
- [116] Lee, H.Y., Oh, S.H., Woo, J.K., Kim, W.Y., Van Pelt, C.S., Price, R.E., Cody, D., Tran, H., Pezzuto, J.M., Moriarty, R.M. and Hong, W.K. (2005) *J. Natl. Cancer Inst.*, **97**, 1695-1699.
- [117] Lee, H.Y., Moon, H., Chun, K.H., Chang, Y.S., Hassan, K., Ji, L., Lotan, R., Khuri, F.R. and Hong, W.K. (2004) *J. Natl. Cancer Inst.*, **96**, 1536-1548.
- [118] Sato, M., Vaughan, M.B., Girard, L., Peyton, M., Lee, W., Shames, D.S., Ramirez, R.D., Sunaga, N., Gazdar, A.F., Shay, J.W. and Minna, J.D. (2006) *Cancer Res.*, **66**, 2116-2128.
- [119] Kwak, I., Tsai, S.Y. and DeMayo, F.J. (2004) *Annu. Rev. Physiol.*, **66**, 647-663.
- [120] Kobayashi, K., Nishioka, M., Kohno, T., Nakamoto, M., Maeshima, A., Aoyagi, K., Sasaki, H., Takenoshita, S., Sugimura, H. and Yokota, J. (2004) *Oncogene*, **23**, 3089-3096.
- [121] Yanagisawa, K., Shyr, Y., Xu, B.J., Massion, P.P., Larsen, P.H., White, B.C., Roberts, J.R., Edgerton, M., Gonzalez, A., Nadaf, S., Moore, J.H., Caprioli, R.M. and Carbone, D.P. (2003) *Lancet*, **362**, 433-439.

Research Paper

c-FLIP Downregulation Contributes to Apoptosis Induction by the Novel Synthetic Triterpenoid methyl-2-cyano-3, 12-dioxooleana-1, 9-dien-28-oate (CDDO-Me) in Human Lung Cancer Cells

Wei Zou^{1,†}

Shuzhen Chen^{1,†}

Xiangguo Liu¹

Ping Yue¹

Michael B. Sporn²

Fadlo R. Khuri¹

Shi-Yong Sun^{1,*}

¹Winship Cancer Institute, Emory University School of Medicine, Atlanta, Georgia USA

[†]These authors contributed equally to this work.

*Correspondence to: Shi-Yong Sun; Winship Cancer Institute; Emory University School of Medicine; 1365-C Clifton Road NE C3088; Atlanta, Georgia 30322 USA; Tel.: 404.778.2170; Fax: 404.778.5520; Email: shi-yong.sun@emory-healthcare.org

Original manuscript submitted: 04/26/07

Revised manuscript submitted: 07/19/07

Manuscript accepted: 07/19/07

This manuscript has been published online, prior to printing for Cancer Biology & Therapy, Volume 6, Issue 10. Definitive page numbers have not been assigned. The current citation is: Cancer Biol Ther 2007; 6(10):

<http://www.landesbioscience.com/journals/cbt/article/4763>

Once the issue is complete and page numbers have been assigned, the citation will change accordingly.

KEY WORDS

c-FLIP, CDDO-Me, degradation, JNK, apoptosis, lung cancer

ACKNOWLEDGEMENTS

This study is supported by Georgia Cancer Coalition Distinguished Cancer Scholar award (to S-Y S.) and Department of Defense VITAL grant W81XWH-04-1-0142 (to S-Y Sun for Project 4). FR Khuri and S-Y Sun are Georgia Cancer Coalition Distinguished Cancer Scholars. We are thankful to H. A. Elrod in our lab for editing the manuscript.

ABSTRACT

The novel synthetic triterpenoid methyl-2-cyano-3, 12-dioxooleana-1, 9-dien-28-oate (CDDO-Me) induces apoptosis of cancer cells, enhances tumor necrosis factor-related apoptosis-inducing ligand (TRAIL)-induced apoptosis, and exhibits potent anticancer activity in animal models with a favorable pharmacokinetic profile. Thus, CDDO-Me is being tested in Phase I clinical trials. In an effort to understand the mechanism by which CDDO-Me induces apoptosis, particularly in human lung cancer cells, we previously demonstrated that CDDO-Me induces apoptosis involving c-Jun N-terminal kinase (JNK)-dependent upregulation of death receptor 5 (DR5) expression. In the current work, we determined the modulatory effects of CDDO-Me on the levels of c-FLIP, a major inhibitor of death receptor-mediated caspase-8 activation, and its impact on CDDO-Me-induced apoptosis and enhancement of TRAIL-induced apoptosis in human lung cancer cells. CDDO-Me rapidly and potently decreased c-FLIP levels including both long (FLIP_L) and short (FLIP_S) forms of c-FLIP in multiple human lung cancer cell lines. The presence of the proteasome inhibitor MG132, but not the JNK inhibitor SP600125, prevented CDDO-Me-induced c-FLIP reduction. Moreover, CDDO-Me increased ubiquitination of c-FLIP. Thus, CDDO-Me induces ubiquitin/proteasome-dependent c-FLIP degradation independently of JNK activation. Importantly, overexpression of c-FLIP (e.g., FLIP_L) protected cells not only from CDDO-Me-induced apoptosis, but also from induction of apoptosis by the combination of CDDO-Me and TRAIL. Accordingly, silencing of c-FLIP with c-FLIP siRNA sensitized cancer cells to CDDO-Me. Collectively, these results indicate that c-FLIP downregulation contributes to CDDO-Me-initiated apoptosis and also to enhancement of TRAIL-induced apoptosis by CDDO-Me.

INTRODUCTION

The novel synthetic triterpenoid methyl-2-cyano-3, 12-dioxooleana-1, 9-dien-28-oate (CDDO-Me) has been documented to be a potent inducer of apoptosis in several types of human cancer cell lines, including lung cancer cells.¹⁻⁵ Thus, CDDO-Me holds promise as a cancer chemopreventive and therapeutic agent. It is well known that there are two major apoptotic pathways: the intrinsic mitochondria-mediated pathway and the extrinsic death receptor-induced pathway, and cross-talk between these pathways is mediated by the truncation of the proapoptotic protein Bid.⁶ We and others have demonstrated that CDDO-Me activates both apoptotic pathways.^{1,2,7} However, the detailed molecular mechanisms by which CDDO-Me induces apoptosis have not been fully elucidated although it appears to be associated with inhibition of NFκB,^{5,8} activation of c-Jun N-terminal kinase (JNK) and p38,^{4,7,9,10} generation of reactive oxygen species⁴ and induction of death receptor 5 (DR5).^{7,9} In addition, CDDO-Me enhances induction of apoptosis by the death receptor ligand tumor necrosis factor (TNF) or TNF-related apoptosis-inducing ligand (TRAIL).^{5,7,11}

The cellular FLICE-inhibitory protein (c-FLIP) is a key regulatory protein that inhibits activation of the death receptor-mediated extrinsic apoptotic pathway,^{12,13} primarily through binding to Fas-associated death domain (FADD) and caspase-8 at the death-inducing signaling complex, preventing caspase-8 activation.¹⁴ c-FLIP has multiple splice variants, and two main forms have been well characterized: c-FLIP short form (c-FLIP_S), which is 26 kDa in size and contains two death effector domains, and c-FLIP long form (c-FLIP_L), which is 55 kDa in size and contains an inactive caspase-like domain

in addition to the two death effector domains.^{12,13} It has been documented that the levels of c-FLIP including both FLIP_L and FLIP_S are regulated by ubiquitin/proteasome-mediated degradation.¹⁵⁻¹⁷ A recent study has shown that JNK activation contributes to ubiquitin/proteasome-mediated degradation of FLIP_L during TNF-induced apoptosis.¹⁷

It has been documented that elevated c-FLIP expression protects cells from death receptor-mediated apoptosis in various cell types, whereas downregulation of c-FLIP by chemicals or siRNA sensitizes cells to death receptor-mediated apoptosis.^{12,13} Moreover, overexpression of c-FLIP also protects cells from apoptosis induced by certain cancer therapeutic agents such as etoposide and cisplatin.¹⁸⁻²⁰ A previous study has shown that CDDO-Me-induced apoptosis and enhancement of TRAIL-induced apoptosis in human leukemia cells correlates with CDDO-Me's ability to downregulate c-FLIP levels in human leukemia cells.¹¹ However, direct evidence for participation of c-FLIP in mediating CDDO-Me-induced apoptosis in human cancer cells has not been shown. Here we demonstrate that CDDO-Me facilitates ubiquitin/proteasome-mediated degradation of c-FLIP in a JNK-independent manner, which is associated with induction of apoptosis in human non-small cell lung cancer (NSCLC) cells. The current study complements our previous finding that CDDO-Me induces apoptosis involving DR5 induction in human NSCLC cells.^{7,9}

MATERIALS AND METHODS

Reagents. CDDO-Me, which was (described previously, Ref. 21) was dissolved in dimethyl sulfoxide (DMSO) at a concentration of 10 mM, and aliquots were stored at -80°C. Stock solutions were diluted to the desired final concentrations with growth medium just before use. The soluble recombinant human TRAIL was purchased from PeproTech, Inc. (Rocky Hill, NJ). The specific JNK inhibitor SP600125 was purchased from Biomol (Plymouth Meeting, PA). The proteasome inhibitor MG132 was purchased from Sigma Chemical Co. (St. Louis, MO). Rabbit polyclonal anti-DR5 antibody was purchased from ProSci Inc (Poway, CA). Mouse monoclonal anti-FLIP antibody (NF6) was purchased from Alexis Biochemicals (San Diego, CA). Mouse monoclonal anti-caspase-3 was purchased from Imgenex (San Diego, CA). Rabbit polyclonal anti-caspase-8, anti-caspase-9, and anti-PARP antibodies were purchased from Cell Signaling Technology, Inc. (Beverly, MA). Rabbit polyclonal anti-β-actin antibody was purchased from Sigma Chemical Co.

Cell lines and cell culture. The human NSCLC cell lines used in this study were purchased from the American Type Culture Collection (Manassas, VA). The stable transfectants A549-Lac Z-2, A549-Lac Z-9, A549-FLIP_L-2 and A549-FLIP_L-4 were described previously (ref. 22). The stable transfectants H157-FLIP_L-5 and H157-FLIP_L-21 that express ectopic FLIP_L and H157-FLIP_L-16 transfectant that were infected with lentiviral FLIP_L but did not express FLIP_L were established (as described previously Ref. 23). Both H157-lac Z-5²³ and H157-FLIP_L-16 transfectants were used as control cell lines. These cell lines were cultured in RPMI 1640 containing 5% fetal bovine serum at 37°C in a humidified atmosphere of 5% CO₂ and 95% air.

Cell survival assay. Cells were seeded in 96-well cell culture plates and treated next day with the agents indicated. The viable cell number was estimated using the sulforhodamine B (SRB) assay (as previously described in ref. 24).

Detection of apoptosis. Apoptosis was evaluated by Annexin V staining using Annexin V-PE apoptosis detection kit purchased from BD Biosciences (San Jose, CA) following the manufacturer's instructions or by measuring sub-G₁ populations using flow cytometry (as described previously Ref. 25). We also detected caspase activation by Western blotting (as described below) as an additional indicator of apoptosis.

Western blot analysis. Whole-cell protein lysates were prepared and analyzed by Western blotting (as described previously Ref. 26, 27).

Immunoprecipitation for detection of ubiquitinated c-FLIP. H157-FLIP_L-21 cells, which stably express FLIP_L, were transfected with HA-ubiquitin plasmid using the FuGENE 6 transfection reagent (Roche Diagnostics Corp., Indianapolis, IN) following the manufacturer's instruction. After 24 h, the cells were treated with CDDO-Me or MG132 plus CDDO-Me for 4 h and then were lysed for immunoprecipitation of Flag-FLIP_L using Flag M2 monoclonal antibody (Sigma chemicals) (as previously described Ref. 28) followed by the detection of ubiquitinated FLIP_L with Western blotting using anti-HA antibody (Abgent; San Diego, CA).

Small interfering siRNAs (siRNA)-mediated silencing of c-FLIP. Silencing of c-FLIP was achieved by transfecting non-silencing control or c-FLIP siRNA using RNAifect transfection reagent (Qiagen, Valencia, CA) following the manufacturer's instructions. The control and c-FLIP siRNAs were described previously (refs. 27 and 29).

RESULTS

CDDO-Me decreases the levels of c-FLIP in human NSCLC cells. To determine whether CDDO-Me modulates the levels of c-FLIP, we detected c-FLIP alterations in two representative NSCLC cell lines, H157 and A549, which undergo CDDO-Me induced apoptosis.¹ After exposure to CDDO-Me for different times, the levels of c-FLIP including both FLIP_L and FLIP_S were decreased in a time-dependent manner starting at 3 h post treatment with CDDO-Me in the both cell lines (Fig. 1A). Reduction of c-FLIP was accompanied with increased levels of cleaved caspase-8 and PARP. We previously have shown that H157 cells were more sensitive than A549 cells to CDDO-Me-induced apoptosis.¹ Accordingly, reduction of c-FLIP levels were more pronounced and rapid in H157 compared to A549 cells, in which cleavage of caspase-8 and PARP were detected at relatively late time points (e.g., 9 h) post treatment (Fig. 1A). These results indicate that c-FLIP downregulation is an early event before the onset of apoptosis. In addition to H157 and A549 cell lines, CDDO-Me also decreased c-FLIP levels in other NSCLC cell lines (i.e., H460, H522 and H1944) in a concentration-dependent manner accompanied with increased cleavage of caspase-8 (Fig. 1B), indicating that CDDO-Me-induced c-FLIP downregulation commonly occurs in NSCLC cells.

CDDO-Me downregulates c-FLIP through enhancement of ubiquitin/proteasome-mediated degradation. To get insight into the mechanism underlying CDDO-Me-induced c-FLIP downregulation, we determined whether CDDO-Me facilitated c-FLIP degradation through a ubiquitin/proteasome-mediated mechanism because c-FLIP proteins are known to be regulated by ubiquitin/proteasome-mediated degradation.¹⁵⁻¹⁷ To this end, we found that CDDO-Me-induced downregulation of c-FLIP was abolished by the

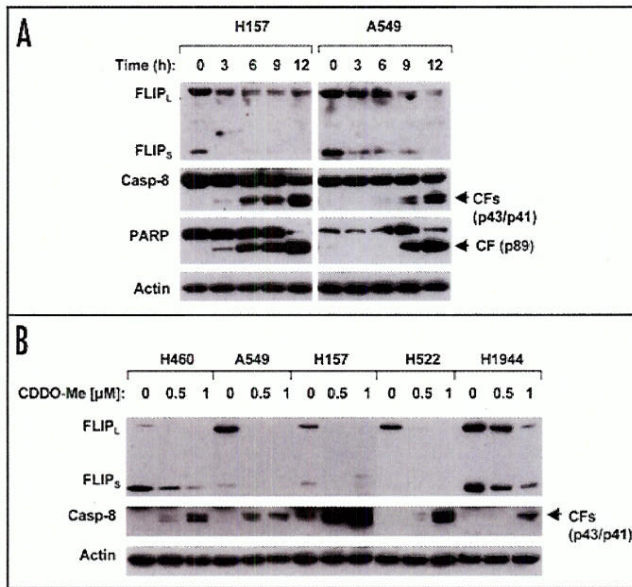


Figure 1. CDDO-Me downregulates c-FLIP levels in time- (A) and dose- (B) dependent manners in human NSCLC cells. The indicated cell lines were treated with 1 μ M CDDO-Me for the times as indicated (A) or with the given doses of CDDO-Me for 8 h (B). The cells were then harvested for preparation of whole-cell protein lysates and subsequent Western blot analysis.

presence of the proteasome inhibitor MG132 (Fig. 2A), suggesting that CDDO-Me-induced c-FLIP reduction is indeed proteasome-dependent. By immunoprecipitation/Western blotting, we detected the highest levels of ubiquitinated FLIP_L in cells treated with CDDO-Me plus MG132 compared to cells exposed to CDDO-Me alone or MG132 alone (Fig. 2B), indicating that DMC increases c-FLIP ubiquitination. Taken together, we conclude that CDDO-Me facilitates ubiquitin/proteasome-mediated c-FLIP degradation, leading to downregulation of c-FLIP in human NSCLC cells.

CDDO-Me downregulates c-FLIP levels independently of JNK activation. Recently, JNK has been demonstrated to be responsible for tumor necrosis factor-induced, ubiquitin/proteasome-mediated FLIP_L degradation.¹⁷ Our previous study has shown that CDDO-Me activates JNK, which contributes for CDDO-Me-induced DR5 expression and apoptosis in human NSCLC cells.⁷ Thus, we next asked whether JNK activation is responsible for c-FLIP downregulation by CDDO-Me. To this end, we examined the effects of CDDO-Me on c-FLIP reduction in the presence of the JNK-specific inhibitor SP600125³⁰ in H157 cells. SP600125 at the concentrations of 5–30 μ M, as expected, inhibited CDDO-Me-induced increase of p-c-Jun in a dose-dependent fashion. Accordingly, CDDO-induced DR5 upregulation and PARP cleavage were inhibited in the presence of SP600125 (Fig. 3), thus confirming our previous finding that CDDO-Me induces JNK-dependent DR5 expression in human NSCLC cells.⁷ However, under such a condition, SP600125 failed to prevent FLIP_L from downregulation by CDDO-Me (Fig. 3), indicating that CDDO-Me induces JNK-independent downregulation of degradation of c-FLIP in human NSCLC cells.

c-FLIP downregulation contributes to CDDO-Me-induced apoptosis. Given that CDDO-Me induces apoptosis of human NSCLC cells involving DR5 upregulation,⁷ we speculated that c-FLIP downregulation would further sensitize NSCLC cells to undergo extrinsic death receptor-mediated apoptosis and hence

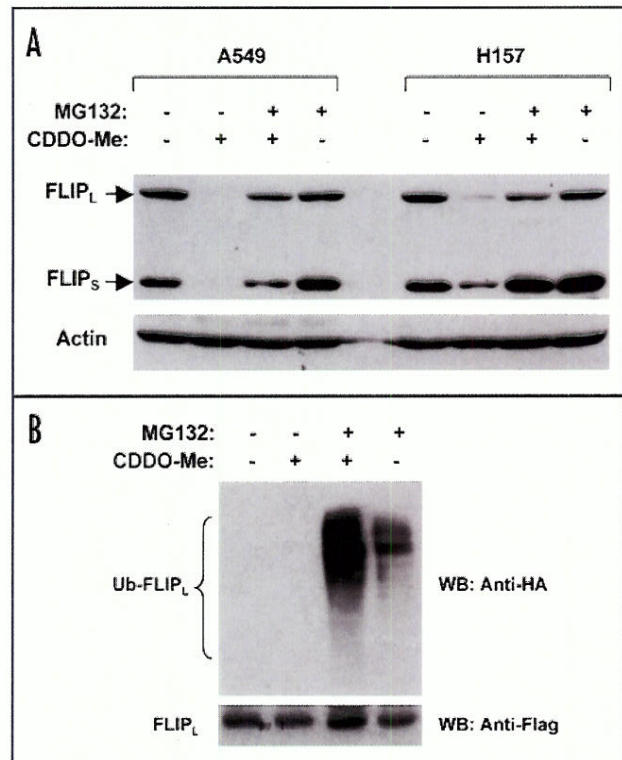


Figure 2. The proteasome inhibitor MG132 prevents CDDO-Me-induced c-FLIP downregulation (A) and detection of CDDO-Me-induced increase of ubiquitinated c-FLIP (B). A, The given cell lines were pretreated with 20 μ M MG132 for 30 minutes and then co-treated with 1 μ M CDDO-Me for another 4 h. The cells were then harvested for preparation of whole-cell protein lysates and subsequent Western blot analysis. B, H157-FLIP_L-21 cells which stably express ectopic flag-FLIP_L were transfected with HA-ubiquitin plasmid using FuGENE 6 transfection reagent for 24 h. The cells were then pretreated with 20 μ M MG132 for 30 minutes and then co-treated with 1 μ M CDDO-Me for 4 h. Whole-cell protein lysates were then prepared for immunoprecipitation using anti-Flag antibody followed by Western blotting (WB) using anti-HA antibody for detection of ubiquitinated FLIP_L (Ub-FLIP_L) and anti-Flag antibody for detection of ectopic FLIP_L.

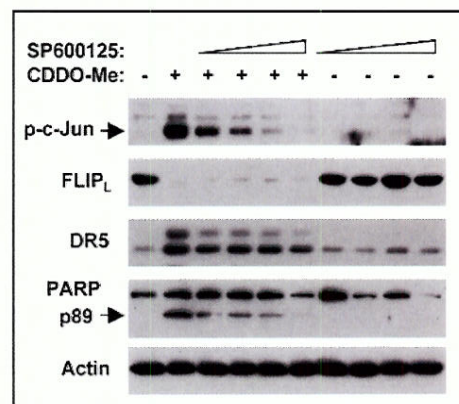


Figure 3. Effects of the JNK inhibitor SP600125 on CDDO-Me-induced c-Jun phosphorylation, c-FLIP downregulation, DR5 induction and PARP cleavage. H157 cells were pretreated with increased concentrations of SP600125 (5, 10, 20 and 30 μ M) for 30 min and then co-treated with 0.5 μ M CDDO-Me. After another 8 h, the cells were subjected to preparation of whole-cell protein lysates for detection of the indicated proteins by Western blot analysis.

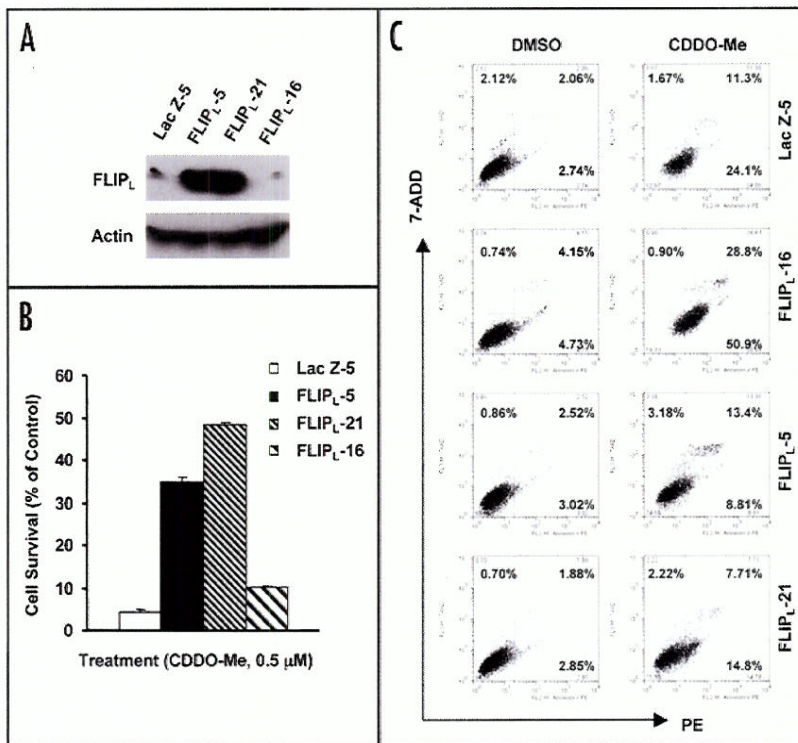


Figure 4. Enforced expression of ectopic FLIP_L (A) confers resistance to CDDO-Me-induced decrease in cell survival (B) and apoptosis (C) in H157 cells. The indicated H157 transfectants that express or do not express ectopic FLIP_L (A) were treated with 0.5 μM CDDO-Me for 24 h. The cell survival was evaluated by the SRB assay (B) and apoptosis was measured by Annexin V staining (C). Data in (B) are means of four replicate determinations. Bars, ± SDs. In the Annexin V assay, the percent positive cells in the upper right and lower right quadrants were added to yield the total of apoptotic cells.

contribute to CDDO-Me-induced apoptosis. To test this hypothesis, we used a lentiviral expression system to enforce c-FLIP overexpression (e.g., FLIP_L) in NSCLC cells and then analyzed its impact on CDDO-Me's ability to induce apoptosis. Taking advantage of

apoptosis using Annexin V staining, we detected less apoptotic cells in H157-FLIP_L-5 (22%) and H157-FLIP_L-21 (23%) cell lines compared to H157-Lac Z-5 (35%) and H157-FLIP_L-16 (80%) control cell lines when exposed to CDDO-Me, indicating that enforced overexpression of ectopic FLIP_L attenuates CDDO-Me's ability to induce apoptosis.

Moreover, we also compared the effects of CDDO-Me on decreasing cell survival and inducing apoptosis in A549 cell lines that stably express ectopic FLIP_L (i.e., A549-FLIP_L-2 and A549-FLIP_L-4) and control Lac Z (i.e., A549-Lac Z-2 and A549-Lac Z-9), respectively (Fig. 5C). As shown in Figure 5A, CDDO-Me was less effective in decreasing cell survival in A549-FLIP_L-2 and A549-FLIP_L-4 cell lines (by approximately less than 50% on average) than in A549-Lac Z-2 and A549-Lac Z-9 cell lines (by approximately 70% on average). In agreement, we detected

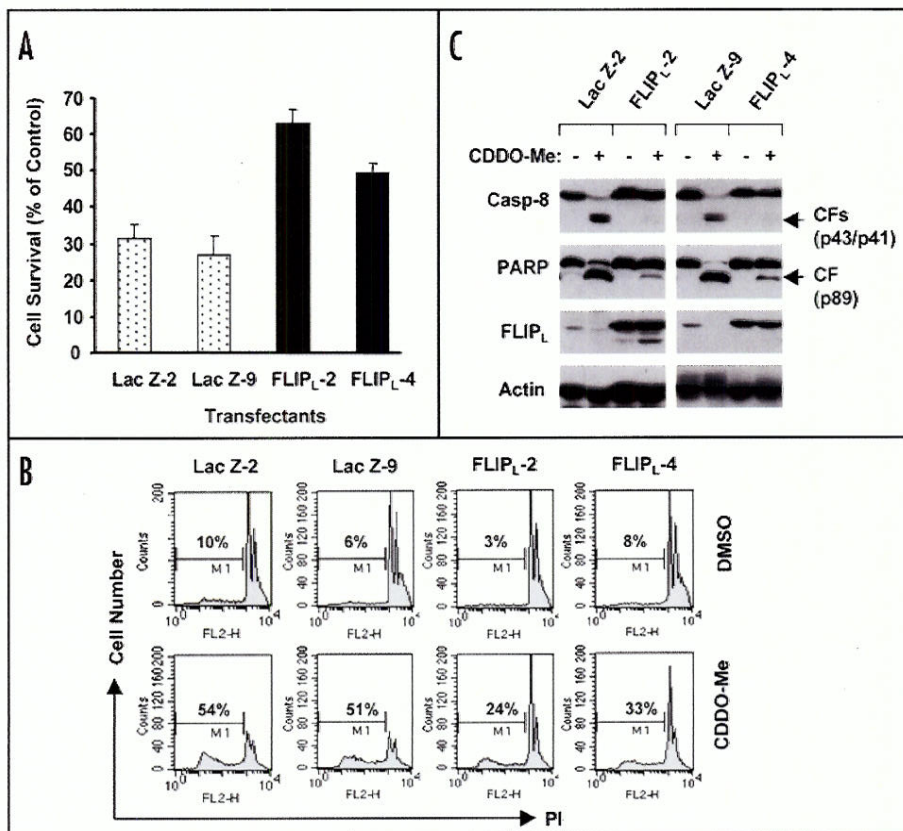


Figure 5. Enforced expression of ectopic FLIP_L confers resistance to CDDO-Me-induced decrease in cell survival (A) and apoptosis (B and C) in A549 cells. The indicated A549 transfectants that express or do not express ectopic FLIP_L (C) were treated with 0.5 μM CDDO-Me for 24 h. Cell survival was evaluated by the SRB assay (A) and apoptosis was measured by flow cytometry for sub-G₁ cells (B) and by Western blotting for cleavage of caspase-8 and PARP (C). Data in A are means of four replicate determinations. Bars, ± SDs. CF, cleaved form.

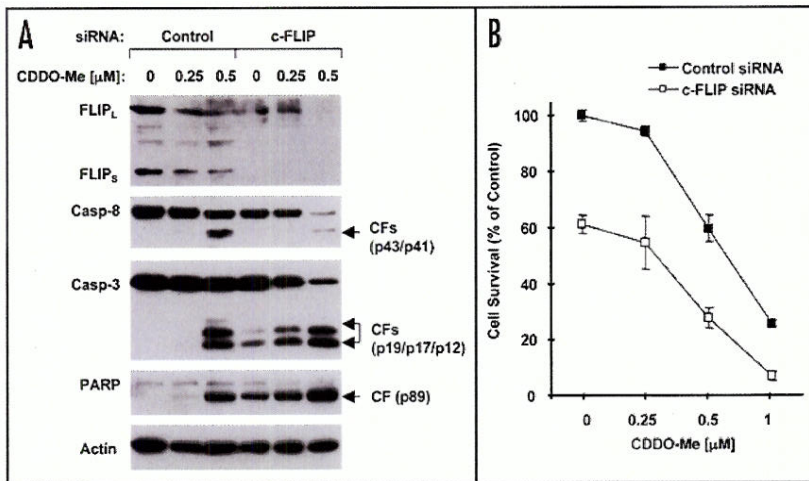


Figure 6. siRNA-mediated reduction of endogenous levels of c-FLIP sensitizes cancer cells to CDDO-Me-induced apoptosis. H1944 cells plated in a 24-well plate (A) or a 96-well (B) plate were transfected with control or c-FLIP siRNA. Twenty-four hour later, the cells were exposed to the indicated concentration of CDDO-Me. After 12 h, the cells were subjected to preparation of whole-cell protein lysates and subsequent detection of the indicated proteins using Western blot analysis (A) or to estimation of cell survival by SRB assay (B). Data in B are means of four replicate determinations. Bars, \pm SDs. CF, cleaved form.

less apoptotic cells in A549-FLIP_L-2 (24%) and A549-FLIP_L-4 (33%) cells than in A549-Lac Z-2 (54%) and A549-Lac Z-9 (51%) cells (Fig. 5B). Correspondingly, the cleavage of caspase-8 and PARP was substantially inhibited in A549 cell lines expressing ectopic FLIP_L compared to the Lac Z-transfected control cell lines, evidenced by no reduction of uncleaved forms of caspase-8 and PARP and less amounts of cleaved caspase-8 and PARP (Fig. 5C). Thus these results further show that overexpression of ectopic FLIP_L confers cell resistance to CDDO-Me-induced apoptosis.

To complement our above findings, we further silenced the expression of endogenous c-FLIP and then examined its impact on cell sensitivity to CDDO-Me. Here we chose the H1944 cell line because it has high levels of c-FLIP, which were only weakly reduced by CDDO-Me (Fig. 1B). As presented in Figure 6, transfection of

c-FLIP siRNA substantially reduced the levels of both FLIP_L and FLIP_S compared to transfection of control siRNA. Transfection of c-FLIP siRNA alone increased cleavage of caspase-3 and PARP (Fig. 6A) and decreased cell survival (by approximately 40%) (Fig. 6B). CDDO-Me treatment induced more cleavage of caspase-8, caspase-3 and PARP, as evidenced by reduced levels of pro-forms of the proteins and increased levels of cleaved forms (Fig. 6A) and more cell death (Fig. 6B) in c-FLIP siRNA-transfected cells than in control siRNA-transfected cells, indicating that downregulation of endogenous c-FLIP levels sensitizes cancer cells to CDDO-Me-induced apoptotic cell death. Taken together, we conclude that downregulation of c-FLIP plays a critical role in CDDO-Me-induced apoptosis in human NSCLC cells.

Downregulation of c-FLIP contributes to cooperative induction of apoptosis by CDDO-Me and TRAIL combination. Our previous work has demonstrated that CDDO-Me cooperates with TRAIL to augment induction of apoptosis in human NSCLC cells.⁷ Given that c-FLIP is a key negative regulator of the TRAIL/

death receptor-mediated apoptosis, it was plausible to hypothesize that c-FLIP downregulation might contribute to augmented induction of apoptosis by the combination of CDDO-Me and TRAIL. To test this speculation, we compared induction of apoptosis by the combination of CDDO-Me and TRAIL in A549 transfectants aforementioned that express or do not express ectopic FLIP_L. The combinations of

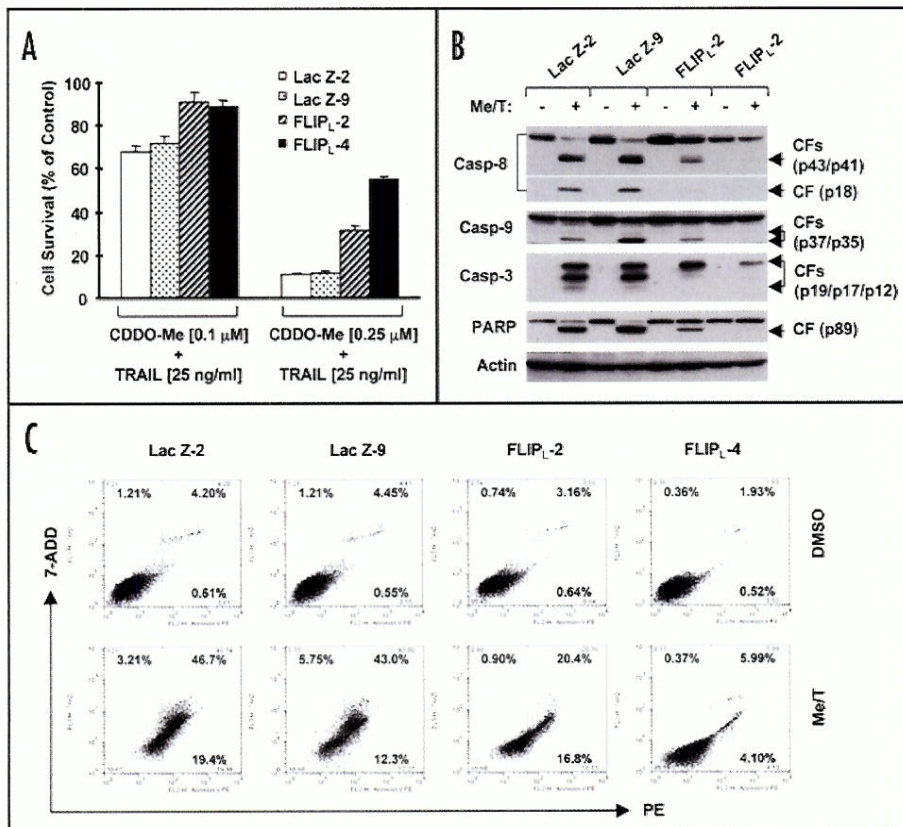


Figure 7. Enforced expression of ectopic FLIP_L decreases cell sensitivity to CDDO-Me/TRAIL combination-induced decrease in cell survival (A) and apoptosis (B and C). The indicated A549 transfectants that express or do not express ectopic FLIP_L were treated with the combinations of the given doses of CDDO-Me and TRAIL (A) or the combination of 0.25 μ M CDDO-Me and 25 ng/ml TRAIL (B and C) for 24 h. Cell survival was evaluated by the SRB assay (A) and apoptosis was measured by Western blotting for cleavage of the given caspases and PARP (B) and by Annexin V staining for Annexin V positive cells (C) and. Data in (A) are means of four replicate determinations. Bars, \pm SDs. In the Annexin V assay, the percent positive cells in the upper right and lower right quadrants were added to yield the total of apoptotic cells. CF, cleaved form; Me/T, CDDO-Me plus TRAIL.

CDDO-Me and TRAIL at the tested low doses were more effective in decreasing cell survival in A549-Lac Z-2 and A549-Lac Z-9 cells than in A549-FLIP_L-2 and A549-FLIP_L-4 (Fig. 7A). This combination potentially caused cleavage of caspase-8, caspase-9, caspase-3 and PARP evidenced in both A549-Lac Z-2 and A549-Lac Z-9 cell lines as the pro-forms of the proteins were strikingly decreased and strong cleaved bands were detected by Western blot analysis; these effects were drastically attenuated in A549-FLIP_L-2 and A549-FLIP_L-4 cells (Fig. 7B). Accordingly, the combination of CDDO-Me and TRAIL induced more apoptotic cells (i.e., annexin V positive cells) in A549-Lac Z-2 (67%) and A549-Lac Z-9 (55%) cells than in A549-FLIP_L-2 (37%) and A549-FLIP_L-4 (10%) cells (Fig. 7C). Collectively, these results show that enforced expression of ectopic FLIP_L protects cells from CDDO-Me/TRAIL-induced apoptosis, indicating that c-FLIP downregulation is also involved in mediating the cooperative induction of apoptosis by the combination of CDDO-Me and TRAIL.

DISCUSSION

We previously have shown that CDDO-Me induces DR5 upregulation, which contributes to CDDO-Me induced apoptosis and enhancement of TRAIL-induced apoptosis in human NSCLC cells.^{7,9} In the present study, we further show that, in addition to DR5 induction, CDDO-Me rapidly and potentially downregulates c-FLIP levels in the multiple tested human NSCLC cell lines. Downregulation of c-FLIP appears to participate in CDDO-Me-induced apoptosis and enhancement of TRAIL-induced apoptosis because enforced expression of ectopic c-FLIP (i.e., FLIP_L) protected human NSCLC cells from apoptosis induced by either CDDO-Me alone or by the combination of CDDO-Me and TRAIL, whereas reduction of endogenous levels of c-FLIP sensitizes cancer cells to CDDO-Me-induced apoptosis. Given the critical role of c-FLIP in negatively regulating the extrinsic apoptotic pathway, the current results complement our previous findings⁷ to further indicate that CDDO-Me induces apoptosis involving activation of the extrinsic apoptotic pathway. It is possible that CDDO-Me induces DR5 expression, resulting in triggering of apoptosis, whereas downregulation of c-FLIP lowers the cell threshold to undergo extrinsic pathway-mediated apoptosis, amplifying CDDO-Me-induced apoptosis. To the best of our knowledge, this is the first direct evidence for the involvement of c-FLIP downregulation in CDDO-Me-induced apoptosis in human cancer cells. We also believe that DR5 induction and c-FLIP downregulation are two key events responsible for CDDO-Me-mediated enhancement of TRAIL-induced apoptosis in human NSCLC cells.

It is known that c-FLIP is subjected to ubiquitin/proteasome-dependent degradation.¹⁵⁻¹⁷ In this study, the presence of proteasome inhibitor MG132 prevented c-FLIP (both FLIP_L and FLIP_S) from CDDO-Me-induced downregulation. Moreover, increased levels of ubiquitinated c-FLIP (i.e., FLIP_L) were detected in cells co-treated with MG132 and CDDO-Me by immunoprecipitation-Western blotting (Fig. 2). Thus, these results collectively indicate that CDDO-Me decreases c-FLIP levels through facilitating ubiquitin/proteasome-dependent degradation of c-FLIP. This is in agreement with the finding that the CDDO-Me's analogue CDDO induces ubiquitin/proteasome-mediated degradation of c-FLIP in other cancer cell lines.¹⁵

A recent study has shown that JNK activation is involved in regulating ubiquitin/proteasome-dependent degradation of FLIP_L.¹⁷

In our study, we found that the JNK inhibitor SP600125 at concentrations (5–30 μ M) that inhibited JNK activation (e.g., c-Jun phosphorylation) did not prevent FLIP_L from CDDO-Me-induced downregulation. Under the same condition, CDDO-Me-induced DR5 expression and PARP cleavage were indeed inhibited (Fig. 3), confirming our previous demonstration that CDDO-Me induces apoptosis involving JNK-dependent DR5 upregulation in human NSCLC cells.^{7,9} Thus, we conclude that CDDO-Me induces ubiquitin/proteasome-mediated degradation of c-FLIP independently of JNK activation. Since c-FLIP downregulation also contributes to CDDO-Me-induced apoptosis, we believe that CDDO-Me induces apoptosis through both JNK-dependent (e.g., DR5 upregulation) and -independent (e.g., c-FLIP degradation) mechanisms.

In summary, the present study has demonstrated that CDDO-Me downregulates c-FLIP levels in human NSCLC cells through JNK-independent ubiquitin/proteasome-mediated degradation of c-FLIP. Importantly, c-FLIP downregulation contributes to CDDO-Me-induced apoptosis and enhancement of TRAIL-induced apoptosis. Thus, the current finding together with our previous finding on the involvement of JNK-dependent DR5 induction in CDDO-Me-induced apoptosis provide compelling evidence for the involvement of the activation of the extrinsic apoptotic pathway in CDDO-Me-induced apoptosis in human NSCLC cells.

References

- Kim KB, Lotan R, Yue P, Sporn MB, Suh N, Gribble GW, Honda T, Wu GS, Hong WK, Sun SY. Identification of a novel synthetic triterpenoid, methyl-2-cyano-3,12-dioxooleana-1,9-dien-28-oate, that potently induces caspase-mediated apoptosis in human lung cancer cells. *Mol Cancer Ther* 2002; 1:177-84.
- Konopleva M, Tsao T, Ruvalo P, Stouf I, Estrov Z, Leysath CE, Zhao S, Harris D, Chang S, Jackson CE, Munsell M, Suh N, Gribble G, Honda T, May WS, Sporn MB, Andreeff M. Novel triterpenoid CDDO-Me is a potent inducer of apoptosis and differentiation in acute myelogenous leukemia. *Blood* 2002; 99:326-35.
- Chintharlapalli S, Papineni S, Konopleva M, Andreeff M, Samudio I, Safe S. 2-Cyano-3,12-dioxooleana-1,9-dien-28-oic acid and related compounds inhibit growth of colon cancer cells through peroxisome proliferator-activated receptor gamma-dependent and -independent pathways. *Mol Pharmacol* 2005; 68:119-28.
- Ikeda T, Sporn M, Honda T, Gribble GW, Kufe D. The novel triterpenoid CDDO and its derivatives induce apoptosis by disruption of intracellular redox balance. *Cancer Res* 2003; 63:5551-8.
- Shishodia S, Sethi G, Konopleva M, Andreeff M, Aggarwal BB. A synthetic triterpenoid, CDDO-Me, inhibits I κ B kinase and enhances apoptosis induced by TNF and chemotherapeutic agents through down-regulation of expression of nuclear factor κ B-regulated gene products in human leukemic cells. *Clin Cancer Res* 2006; 12:1828-38.
- Hengartner MO. The biochemistry of apoptosis. *Nature* 2000; 407:770-6.
- Zou W, Liu X, Yue P, Zhou Z, Sporn MB, Lotan R, Khuri FR, Sun SY. c-Jun NH2-terminal kinase-mediated up-regulation of death receptor 5 contributes to induction of apoptosis by the novel synthetic triterpenoid methyl-2-cyano-3,12-dioxooleana-1,9-dien-28-oate in human lung cancer cells. *Cancer Res* 2004; 64:7570-8.
- Ahmad R, Raina D, Meyer C, Kharbanda S, Kufe D. Triterpenoid CDDO-Me blocks the NF- κ B pathway by direct inhibition of IKK β on Cys-179. *J Biol Chem* 2006; 281:35764-9.
- Yue P, Zhou Z, Khuri FR, Sun SY. Depletion of intracellular glutathione contributes to JNK-mediated death receptor 5 upregulation and apoptosis induction by the novel synthetic triterpenoid methyl-2-cyano-3, 12-dioxooleana-1, 9-dien-28-oate (CDDO-Me). *Cancer Biol Ther* 2006; 5:492-7.
- Konopleva M, Contractor R, Kurinna SM, Chen W, Andreeff M, Ruvalo P. The novel triterpenoid CDDO-Me suppresses MAPK pathways and promotes p38 activation in acute myeloid leukemia cells. *Leukemia* 2005; 19:1350-4.
- Suh WS, Kim YS, Schimmer AD, Kitada S, Minden M, Andreeff M, Suh N, Sporn M, Reed JC. Synthetic triterpenoids activate a pathway for apoptosis in AML cells involving downregulation of FLIP and sensitization to TRAIL. *Leukemia* 2003; 17:2122-9.
- Wajant H. Targeting the FLICE inhibitory protein (FLIP) in cancer therapy. *Mol Interv* 2003; 3:124-7.
- Kataoka T. The caspase-8 modulator c-FLIP. *Crit Rev Immunol* 2005; 25:31-58.
- Irmeler M, Thome M, Hahne M, Schneider P, Hofmann K, Steiner V, Bodmer JL, Schroter M, Burns K, Mattmann C, Rimoldi D, French LE, Tschopp J. Inhibition of death receptor signals by cellular FLIP. *Nature* 1997; 388:190-5.
- Kim Y, Suh N, Sporn M, Reed JC. An inducible pathway for degradation of FLIP protein sensitizes tumor cells to TRAIL-induced apoptosis. *J Biol Chem* 2002; 277:22320-9.

16. Poukkula M, Kaunisto A, Hietakangas V, Denessiouk K, Katajamäki T, Johnson MS, Sistonen L, Eriksson JE. Rapid turnover of c-FLIPshort is determined by its unique C-terminal tail. *J Biol Chem* 2005; 280:27345-55.
17. Chang L, Kamata H, Solinas G, Luo JL, Maeda S, Venuprasad K, Liu YC, Karin M. The E3 ubiquitin ligase itch couples JNK activation to TNF α -induced cell death by inducing c-FLIP(L) turnover. *Cell* 2006; 124:601-13.
18. Kamarajan P, Sun NK, Chao CC. Up-regulation of FLIP in cisplatin-selected HeLa cells causes cross-resistance to CD95/Fas death signalling. *Biochem J* 2003; 376:253-60.
19. Longley DB, Wilson TR, McFwan M, Allen WL, McDermott U, Galligan L, Johnston PG. c-FLIP inhibits chemotherapy-induced colorectal cancer cell death. *Oncogene* 2006; 25:838-48.
20. Abedini MR, Qiu Q, Yan X, Tsang BK. Possible role of FLICE-like inhibitory protein (FLIP) in chemoresistant ovarian cancer cells in vitro. *Oncogene* 2004; 23:6997-7004.
21. Honda T, Rounds BV, Bore L, Favaloro Jr FG, Gribble GW, Suh N, Wang Y, Spor MB. Novel synthetic oleanane triterpenoids: A series of highly active inhibitors of nitric oxide production in mouse macrophages. *Bioorg Med Chem Lett* 1999; 9:3429-34.
22. Zou W, Liu X, Yue P, Khuri FR, Sun SY. PPAR γ ligands enhance TRAIL-induced apoptosis through DR5 upregulation and c-FLIP downregulation in human lung cancer cells. *Cancer Biol Ther* 2007; 6:99-106.
23. Liu X, Yue P, Schonthal AH, Khuri FR, Sun SY. Cellular FLICE-inhibitory protein down-regulation contributes to celecoxib-induced apoptosis in human lung cancer cells. *Cancer Res* 2006; 66:11115-9.
24. Sun SY, Yue P, Dawson MI, Shroot B, Michel S, Lamph WW, Heyman RA, Teng M, Chandraratna RA, Shudo K, Hong WK, Lotan R. Differential effects of synthetic nuclear retinoid receptor-selective retinoids on the growth of human non-small cell lung carcinoma cells. *Cancer Res* 1997; 57:4931-9.
25. Sun SY, Yue P, Shroot B, Hong WK, Lotan R. Induction of apoptosis in human non-small cell lung carcinoma cells by the novel synthetic retinoid CD437. *J Cell Physiol* 1997; 173:279-84.
26. Sun SY, Yue P, Wu GS, El-Deiry WS, Shroot B, Hong WK, Lotan R. Mechanisms of apoptosis induced by the synthetic retinoid CD437 in human non-small cell lung carcinoma cells. *Oncogene* 1999; 18:2357-65.
27. Liu X, Yue P, Zhou Z, Khuri FR, Sun SY. Death receptor regulation and celecoxib-induced apoptosis in human lung cancer cells. *J Natl Cancer Inst* 2004; 96:1769-80.
28. Chen C, Sun X, Ran Q, Wilkinson KD, Murphy TJ, Simons JW, Dong JT. Ubiquitin-proteasome degradation of KLF5 transcription factor in cancer and untransformed epithelial cells. *Oncogene* 2005; 24:3319-27.
29. Elrod HA, Lin YD, Yue P, Wang X, Lonial S, Khuri FR, Sun SY. The alkylphospholipid perifosine induces apoptosis of human lung cancer cells requiring inhibition of Akt and activation of the extrinsic apoptotic pathway. *Mol Cancer Ther* 2007; 6:2029-38.
30. Bennett BL, Sasaki DT, Murray BW, O'Leary EC, Sakata ST, Xu W, Leisten JC, Motiwala A, Pierce S, Satoh Y, Bhagwat SS, Manning AM, Anderson DW. SP600125, an anthranylazolonone inhibitor of Jun N-terminal kinase. *Proc Natl Acad Sci USA* 2001; 98:13681-6.

Research Paper

PPAR γ Ligands Enhance TRAIL-induced Apoptosis through DR5 Upregulation and c-FLIP Downregulation in Human Lung Cancer Cells

Wei Zou

Xiangguo Liu

Ping Yue

Fadlo R. Khuri

Shi-Yong Sun*

Department of Hematology and Oncology; Winship Cancer Institute; Emory University School of Medicine; Atlanta, Georgia USA

*Correspondence to: Shi-Yong Sun; Winship Cancer Institute, Emory University School of Medicine; 1365-C Clifton Road, C3088; Atlanta, Georgia 30322 USA; Tel.: 404.778.2170; Fax: 404.778.5520; Email: shi-yong.sun@emoryhealthcare.org

Original manuscript submitted: 10/06/06

Manuscript accepted: 10/29/06

Previously published online as a *Cancer Biology & Therapy* E-publication: <http://www.landesbioscience.com/journals/cb/abstract.php?id=3555>

KEY WORDS

PPAR γ ligands, death receptor 5, c-FLIP, TRAIL, apoptosis, lung cancer cells

ACKNOWLEDGEMENTS

We thank Dr. Jürg Tschopp (University of Lausanne, Switzerland) for c-FLIP cDNAs. S-Y. Sun and F. Khuri are Georgia Cancer Coalition Distinguished Cancer Scholars. This work is supported in part by the Georgia Cancer Coalition Distinguished Cancer Scholar award (to S-Y. Sun) and Department of Defense VITAL grant W81XWH-04-1-0142 (to S-Y. Sun for Project 4).

ABSTRACT

Peroxisome proliferator-activated receptor γ (PPAR γ) ligands are potential chemopreventive agents. Many studies have shown that PPAR γ ligands induce apoptosis in various types of cancer cells including lung cancer cells. Some PPAR γ ligands have been shown to downregulate c-FLIP expression and thus enhance tumor necrosis factor-related apoptosis-inducing ligand (TRAIL)-induced apoptosis in some cancer cell lines. In the current study, we further show that PPAR γ ligands induced the expression of death receptor 5 (DR5) and increased DR5 distribution at the cell surface in addition to reducing c-FLIP levels in human lung cancer cells. These agents cooperated with TRAIL to enhance induction of apoptosis in human lung cancer cells. Both overexpression of c-FLIP and knockdown of DR5 abrogated PPAR γ ligand's ability to enhance TRAIL-induced apoptosis. Thus, it appears that not only c-FLIP downregulation but also DR5 upregulation contribute to PPAR γ ligand-mediated enhancement of TRAIL-induced apoptosis in human lung cancer cells. Both the PPAR γ antagonist GW9662 and silencing PPAR γ expression failed to diminish PPAR γ ligand-induced DR5 upregulation or c-FLIP downregulation, indicating that PPAR γ ligands modulate the expression of DR5 and c-FLIP through a PPAR γ -independent mechanism. Collectively, we conclude that PPAR γ ligands exert PPAR γ -independent effects on inducing DR5 expression and downregulating c-FLIP levels, leading to enhancement of TRAIL-induced apoptosis.

INTRODUCTION

Tumor necrosis factor-related apoptosis-inducing (TRAIL) is a soluble protein that induces apoptosis upon binding to death receptor 4 (DR4, also named TRAIL-R1) or death receptor 5 (DR5, also named TRAIL-R2, TRICK2, or Killer/DR5). TRAIL preferentially induces apoptosis in transformed or malignant cells, demonstrating potential as a tumor-selective apoptosis-inducing cytokine for cancer treatment.^{1,2} Importantly, many small molecules including traditional chemotherapeutic agents are able to augment TRAIL-induced apoptosis in multiple types of cancer cells including lung cancer cells. Thus, TRAIL shows a strong potential as a cancer therapeutic agent and is being tested in phase I clinical trials.

There are several key components that modulate TRAIL-induced apoptosis. One such component is death receptor 5, which is one of the apoptotic death receptors that compose of a cysteine-rich extracellular domain and cytoplasmic death domain.³ DR5 locates at the cell surface, becomes activated or oligomerized (trimerized) upon binding to its ligand TRAIL, and then signals apoptosis through caspase-8-mediated rapid activation of caspase cascades.^{3,4} Another important protein involved in TRAIL signaling is cellular FLICE-inhibitory protein (c-FLIP; also called Casper/I-FLICE/FLAME-1/CASH/CLARP/MRIT), which is the major negative regulator of TRAIL/death receptor-induced apoptosis.^{5,6} c-FLIP binds to Fas-associated death domain (FADD) and caspase-8 at the death-inducing signaling complex (DISC), and thereby inhibits death receptor-mediated apoptosis.⁷ c-FLIP has multiple splice variants, and two main forms have been well characterized: c-FLIP short form (c-FLIP_s) and c-FLIP long form (c-FLIP_l).^{5,6} It has been well documented that elevated c-FLIP expression protects cells from death receptor-mediated apoptosis in various cell types, whereas downregulation of c-FLIP by chemicals or siRNA sensitizes cells to death receptor-mediated apoptosis.^{5,6} Both DR5 and c-FLIP are subjected to modulation by certain cancer therapeutic agents. Generally speaking, agents that either upregulate DR5 expression and/or downregulate c-FLIP levels often exhibit activity in enhancing TRAIL induced apoptosis.⁸

Peroxisome proliferator-activated receptor γ (PPAR γ) ligands are potential cancer chemopreventive and therapeutic agents.^{9,10} Many preclinical studies have shown that PPAR γ ligands induces growth arrest and apoptosis in various types of cancer cells including lung cancer cells in vitro and inhibit tumor growth and carcinogenesis in animal models.^{9,11,12} Moreover, these agents can be combined with other agents to exhibit enhanced anticancer activity.^{13,14} Some PPAR γ ligands have been shown to downregulate c-FLIP expression and thus enhance TRAIL-induced apoptosis in certain types of cancer cell lines.^{15,16} In contrast to c-FLIP, the studies on the modulation of PPAR γ ligands on DR5 expression have generated conflicting results. The PPAR γ agonists 15-deoxy- $\Delta^{12,14}$ -prostaglandin J₂ (15d-PGJ₂) and troglitazone, but not pioglitazone and rosiglitazone, were shown to induce DR5 expression.^{16,17} However, 15d-PGJ₂ was not shown to have such an effect in a different study.¹⁵ Moreover, it is not clear whether DR5 upregulation is involved in enhancement of TRAIL-induced apoptosis by PPAR γ ligands.

In the current study, we investigated the modulatory effects of synthetic PPAR γ ligands on the TRAIL/death receptor-mediated apoptotic pathway in human lung cancer cells. In addition to downregulation of c-FLIP, we, for the first time, demonstrate that PPAR γ ligands also induce DR5 expression in various lung cancer cell lines. Like c-FLIP downregulation, DR5 upregulation also contributes to enhancement of TRAIL-induced apoptosis by PPAR γ ligands.

MATERIALS AND METHODS

Reagents. Troglitazone, pioglitazone and rosiglitazone were purchased from LKT Laboratories Inc (St. Paul, MN). Ciglitazone and GW1929 were purchased from Tocris (Ellisville, MO). WY14363 was purchased from Biomol (Plymouth Meeting, PA). CDDO was provided by Dr. M. B. Sporn (Dartmouth Medical School, Hanover, NH). These agents were dissolved in dimethyl sulfoxide (DMSO) at a concentration of 10 mM or 100 mM, and aliquots were stored at -80°C. Stock solutions were diluted to the desired final concentrations with growth medium just before use. Soluble recombinant human TRAIL was purchased from PeproTech Inc (Rocky Hill, NJ). Rabbit polyclonal anti-DR5 antibody was purchased from ProSci Inc (Poway, CA). Mouse monoclonal anti-caspase-3 was purchased from Imgenex (San Diego, CA). Rabbit polyclonal anti-caspase-9, anti-caspase-8, and anti-PARP antibodies were purchased from Cell Signaling Technology, Inc. (Beverly, MA). Mouse monoclonal anti-FLIP antibody (NF6) was purchased from Alexis Biochemicals (San Diego, CA). Rabbit polyclonal anti- β -actin antibody was purchased from Sigma Chemical Co. (St. Louis, MO).

Cell lines and cell cultures. All lung cancer cell lines used in this study were purchased from the American Type Culture Collection (Manassas, VA). These cell lines were grown in monolayer culture in RPMI 1640 medium supplemented with glutamine and 5% fetal bovine serum (FBS) at 37°C in a humidified atmosphere consisting of 5% CO₂ and 95% air.

Establishment of stable cell lines that overexpress c-FLIP_L or c-FLIP_S. c-FLIP_L and c-FLIP_S coding regions were amplified by PCR using plasmids containing full length cDNAs of FLIP_L and FLIP_S, respectively, which were provided by Dr. J. Tschopp (University of Lausanne, Switzerland).⁷ The amplified fragments were then ligated into the pT-easy vector (Promega, Madison WI) following the manufacturer's protocol as pT-easy-FLIP_L and pT-easy-FLIP_S, respectively, using the primers: c-FLIP_L sense, 5'-GACTAGTGCCGCCACCATGGATTACAAAGACGATGACG-3', and FLIP_L antisense, 5'-CGG-

CCCCITATGTGTAGGAGAGGATAAGTTTC-3'. c-FLIP_S sense, 5'-GACTAGTGCCGCCACCATGTCTGCTGAAGTCATCCATCAGG-3' and c-FLIP_S antisense, 5'-CGGGCCCTCACATGGACAATTTCCAAG-3'. Both pLenti-DcR1 (a lentiviral vector harboring the DcR1 gene, which was constructed using the pLenti6/V5 Directional TOPO Cloning kit purchased from Invitrogen) and pT-easy-FLIP_L or pT-easy-FLIP_S were cut with *SpeI* and *ApaI* restriction enzymes. The released fragment containing c-FLIP_L or c-FLIP_S gene was then cloned into the digested pLenti6/V5 vector and the resultant constructs were named pLenti-Flag-FLIP_L and pLenti-FLIP_S, respectively. In this study, we used pLenti-LacZ as a vector control, which was included in the pLenti6/V5 Directional TOPO Cloning kit. Lentiviral production and titer determination were done following the manufacturer's instruction. To establish stable cell lines, A549 cells were infected with the lentiviruses at ten of multiplicity of infection (MOI) with 10 μ g/mL polybrene. After a two-week selection using 50 μ g/mL blasticidin post infection, the survival clones were picked up and screened for c-FLIP expression by Western blotting using c-FLIP antibody. The clones with the highest levels of c-FLIP expression were used in the experiment.

Cell survival assay. Cells were seeded in 96-well cell culture plates and treated on the second day with the indicated agents. At the end of treatment, cell number was estimated by the sulforhodamine B (SRB) assay as previously described.¹⁸ The cell survival was presented as percentage of control as calculated by using the equation: $At/Ac \times 100$, where *At* and *Ac* represent the absorbance in treated and control cultures, respectively.

Western blot analysis. The procedures for preparation of whole-cell protein lysates and Western blot analysis were the same as described previously.^{19,20}

Detection of cell surface DR5. In this study, cell surface DR5 expression was analyzed using flow cytometry. The procedure for direct antibody staining and subsequent flow cytometric analysis of cell surface protein was described previously.²¹ The mean fluorescence intensity (MFI) that represents antigenic density on a per cell basis was used to represent DR5 expression level. Phycoerythrin (PE)-conjugated mouse anti-human DR5 monoclonal antibody (DJR2-4) and PE mouse IgG1 isotype control (MOPC-21/P3) were purchased from eBioscience (San Diego, CA).

Detection of caspase activation and apoptosis. Caspase activation and their substrate cleavage were detected by Western blot analysis as described above. Apoptosis was detected by estimating sub-G₁ population as described previously.²² In addition, the amounts of cytoplasmic histone-associated DNA fragments (mononucleosome and oligonucleosomes) formed during apoptosis were also measured using a Cell Death Detection ELISA^{plus} kit (Roche Molecular Biochemicals, Indianapolis, IN) according to the manufacturer's instructions.

Silencing of DR5 expression using small interfering RNA (siRNA). High purity control (nonsilencing) and DR5 siRNA oligos were described previously²⁰ and synthesized from Qiagen (Valencia, CA). The transfection of siRNA was conducted in a 24-well plate (1 μ g/well) using RNAiFectTM transfect reagent purchased from Qiagen following the manufacturer's instruction. Forty-eight hours after the transfection, cells were treated with a PPAR γ ligand alone, TRAIL alone and their combination. Gene silencing effect was evaluated by Western blot analysis and apoptosis was measured as described above.

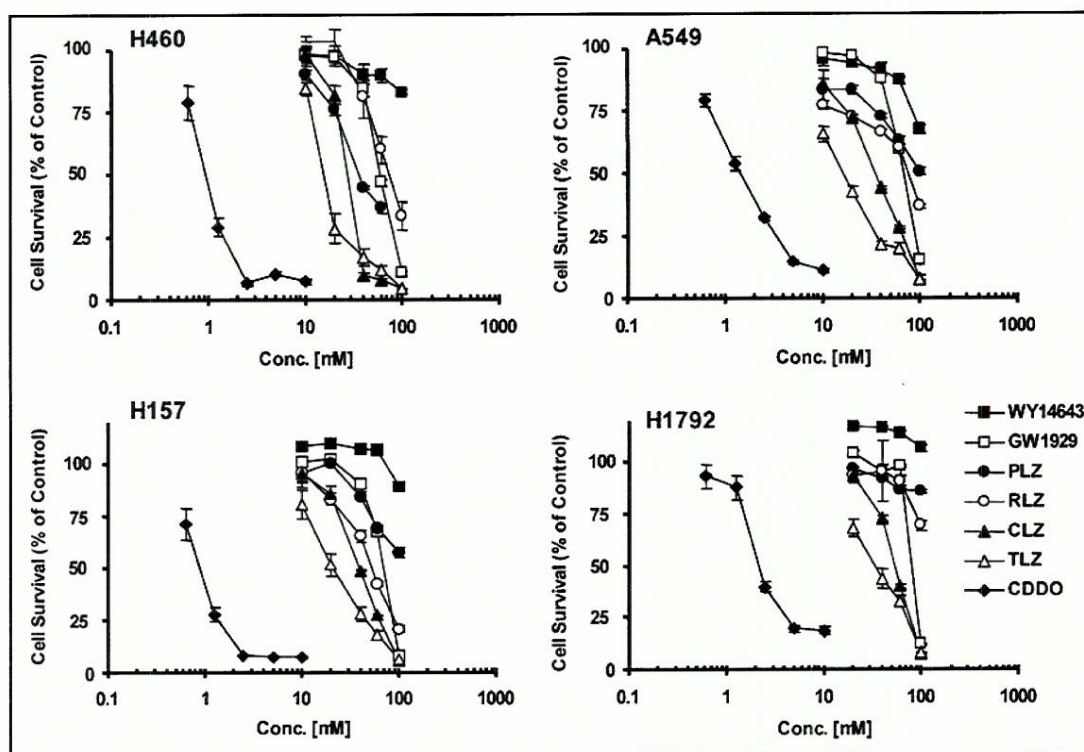


Figure 1. Effects of various PPAR γ ligands on the growth of human lung cancer cells. The indicated cell lines were seeded in 96-well cell culture plates. On the second day, the cells were treated with different concentrations ranging from 0.5 to 100 μ M of the given PPAR γ ligands and WY14643 which is a PPAR α ligand. After three days, the cells were fixed and subjected to estimation of cell number using the sulforhodamine B (SRB) assay. Each data value is a mean \pm SD of four replicates. PLZ, pioglitazone; RLZ, rosiglitazone; CLZ, ciglitazone; TLZ, troglitazone

RESULTS

PPAR γ ligands inhibit the growth of human lung cancer cells. To determine the concentration ranges or potencies of individual PPAR γ ligands that effectively inhibit the growth of human lung cancer cells, we treated four lung cancer cell lines with several PPAR γ ligands for three days and then evaluated their effects on the growth of the given cell lines. As presented in Figure 1, WY14643, a PPAR α ligand, even at a concentration of 100 μ M had minimal effects on decreasing the survival of four lung cancer cell lines tested, whereas all PPAR γ ligands at the tested concentrations ranges effectively decreased cell survival at least in one of the tested cell lines albeit with various degrees. Among these ligands, CDDO stood out to be the most potent with IC_{50} s of 0.5–2 μ M. Pioglitazone and rosiglitazone showed the weakest activity in decreasing the survival of the lung cancer cell lines with IC_{50} s ranging from 40 μ M to > 100 μ M. Ciglitazone, troglitazone and GW1929 were in between with IC_{50} s ranging from 15 μ M to 100 μ M. Therefore, we chose to use ciglitazone, troglitazone and GW1929 in our following experiments.

PPAR γ ligands cooperate with TRAIL to induce apoptosis in human lung cancer cells. To determine whether the combination of a PPAR γ ligand with TRAIL exhibits enhanced effects on induction of apoptosis in human lung cancer cells as observed in other types of cancer cell lines, we first examined the effects of PPAR γ ligands on the survival of human lung cancer cells in the presence of TRAIL. As presented in Figure 2A, the addition of low doses of TRAIL, which itself minimally decreased cell survival (no more than 20%), greatly enhanced the effects of either of the tested PPAR γ ligands (i.e., troglitazone, ciglitazone and GW1929) in the lung cancer cell

lines tested. For example, troglitazone alone at 50 μ M and TRAIL alone at 20 ng/ml decreased the survival of A549 cells by approximately 20%, whereas their combination decreased cell survival by >75%. Thus, it appears that the combination of a PPAR γ ligand with TRAIL exhibits enhanced effects on decreasing the survival of lung cancer cells.

Following the cell survival study, we analyzed apoptosis in cells exposed to the combination of a PPAR γ ligand and TRAIL. The single agent of the given PPAR γ ligands or TRAIL at the concentrations tested caused minimal apoptosis (<15%). However, the combination of TRAIL with either PPAR γ ligand tested induced apoptosis in >40% of cells (Fig. 1B). In agreement, we detected minimal cleaved forms of caspase-8, caspase-9, caspase-3 and PARP from cells treated with TRAIL or the PPAR γ ligands tested alone under the tested conditions by Western blot analysis. However, we easily detected the cleaved forms from cells exposed to the respective combinations of TRAIL with PPAR γ ligands (Fig. 2C). Collectively, these results clearly show that PPAR γ ligands cooperate with TRAIL to enhance induction of apoptosis in human lung cancer cells.

PPAR γ ligands induces DR5 expression in addition to down-regulation of c-FLIP expression. It has been documented that some PPAR γ ligands decrease c-FLIP expression, which contributes to enhancement of TRAIL-induced apoptosis by PPAR γ ligands in certain types of cancer cells.¹⁵ Thus, we examined effects of PPAR γ ligands on c-FLIP expression in human lung cancer cells. The three PPAR γ ligands troglitazone, ciglitazone and GW1929 decreased the levels of both FLIP_L and FLIP_S in a dose-dependent manner in A549 cells (Fig. 3A). The downregulation of c-FLIP occurred after 6 h treatment with the given ligands (Fig. 3B), indicating that

c-FLIP downregulation is an early event induced by PPAR γ ligands. Downregulation of c-FLIP expression by PPAR γ ligands occurred not only in A549 cells as described, but also in other lung cancer cells (e.g., H157, H460, and H1792) as presented in (Fig. 3C). Therefore, it appears that downregulation of c-FLIP by PPAR γ ligands commonly occurs in human lung cancer cells.

DR5 is also a key protein involved in TRAIL-mediated apoptosis and is susceptible to modulation by certain small molecules. Therefore, we were interested in determining whether PPAR γ ligands modulate DR5 expression. To this end, we treated A549 cells with different concentrations of troglitazone, ciglitazone or GW1929 for 12 h and then detected DR5 expression in these cells by Western blot analysis. Similar to modulation of c-FLIP expression, all three ligands increased DR5 expression in a concentration-dependent manner. These ligands even at 25 μ M were able to upregulate DR5 expression (Fig. 3A). Similar to c-FLIP downregulation, DR5 expression was increased after 6 h exposure to the ligands (Fig. 3B), indicating that DR5 upregulation is also an early event induced by PPAR γ ligands. These ligands increased DR5 expression in other lung cancer cell lines as well (Fig. 3C), indicating that induction of DR5 by PPAR γ ligands is also a common event in lung cancer cells. Because DR5 is a cell surface protein, we further analyzed DR5 distribution on the cell surface in cells treated with different PPAR γ ligands. As presented in Figure 3D, these ligands increased the mean fluorescent intensity (MFI) of DR5 staining in both H1792 and A549 cells, indicating that PPAR γ ligands increase cell surface DR5 levels in addition to upregulating the total levels of DR5.

Small interfering RNA (siRNA)-mediated silencing of DR5 expression confers resistance to induction of apoptosis by the combination of a PPAR γ ligand and TRAIL. To determine whether DR5 upregulation contributes to cooperative induction of apoptosis by the combination of a PPAR γ ligand and TRAIL, we used DR5 siRNA to silence DR5 expression and then examined its impact on the apoptosis-inducing effect of the combination. The result in Figure 4A demonstrates the successful silencing the expression of DR5. The combination of troglitazone and TRAIL

was much more potent than each single agent in decreasing the levels of uncleaved forms of caspase-8 and caspase-3 or increasing the levels of cleaved form of caspase-9 and PARP (Fig. 4B) and in increasing DNA fragment levels (Fig. 4C) in control siRNA-transfected A549 cells. These effects were all diminished in the cells transfected with DR5 siRNA (Fig. 4B and C). Thus, these results demonstrate that DR5 upregulation contributes to enhanced induction of apoptosis by the combination of a PPAR γ ligand and TRAIL.

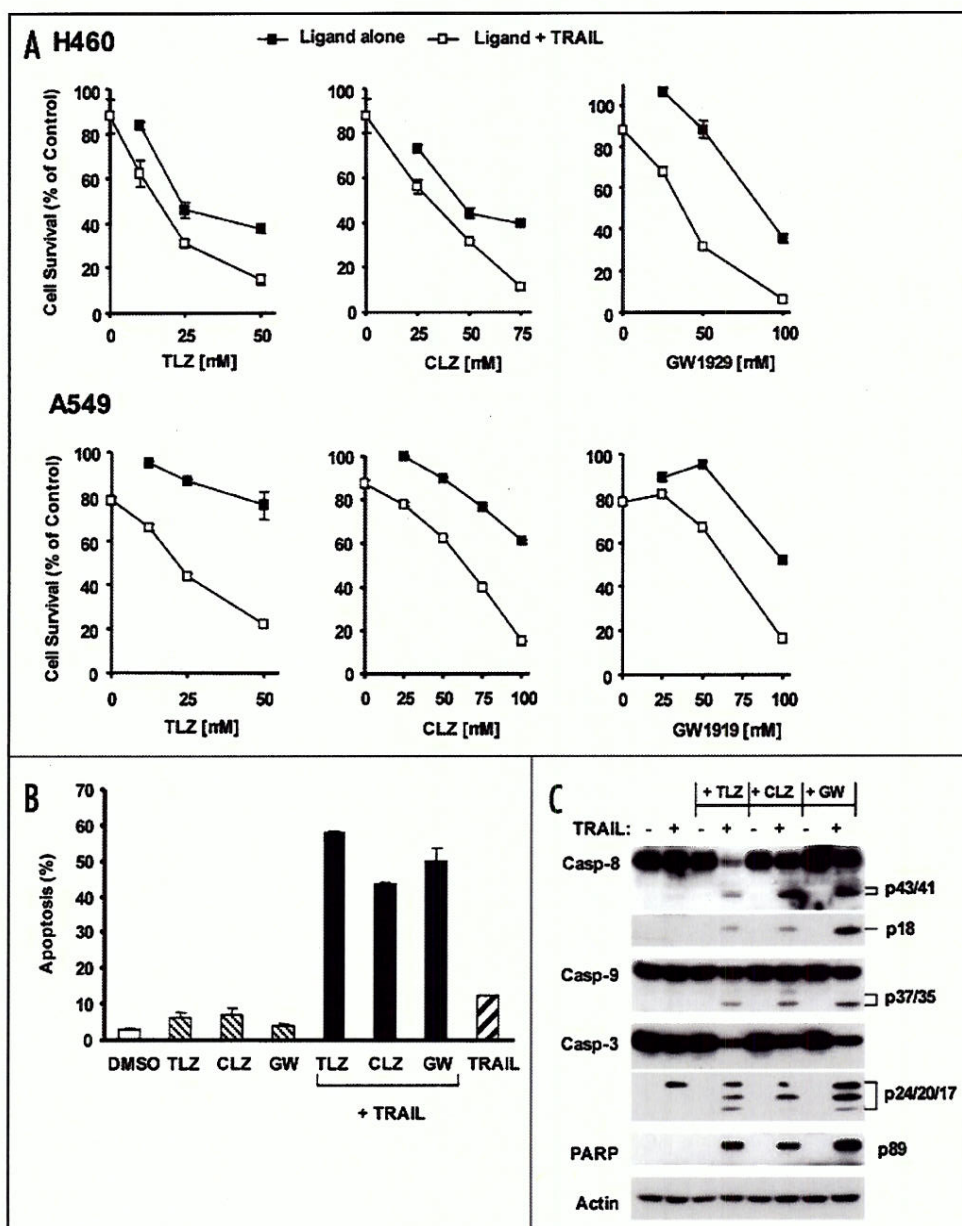


Figure 2. Effects of PPAR γ ligands in combination with TRAIL on cell survival (B) and apoptosis (B and C) in human lung cancer cells. (A) H460 and A549 cell lines were seeded in 96-well plates. On the second day, the cells were treated with the indicated concentrations of troglitazone (TLZ), ciglitazone (CLZ), or GW1929 alone, 20 ng/ml TRAIL alone, and the combination of TRAIL with the respective PPAR γ ligand. After 24 h, the cells were fixed and subjected to estimation of cell number using the SRB assay. Each data value is a mean \pm SD of four replicates. (B and C) A549 cells were treated with 50 μ M of the indicated PPAR γ ligands alone, 20 ng/ml TRAIL alone and their respective combinations. After 24 h (B) or 12 h (C), the cells were harvested for detection of apoptosis by analyzing sub-G₁ population using flow cytometry (B) or for detection of activation of the indicated caspases using Western blot analysis (C). Each column in (B) is the mean \pm SD of duplicate determinations. Casp, caspase.

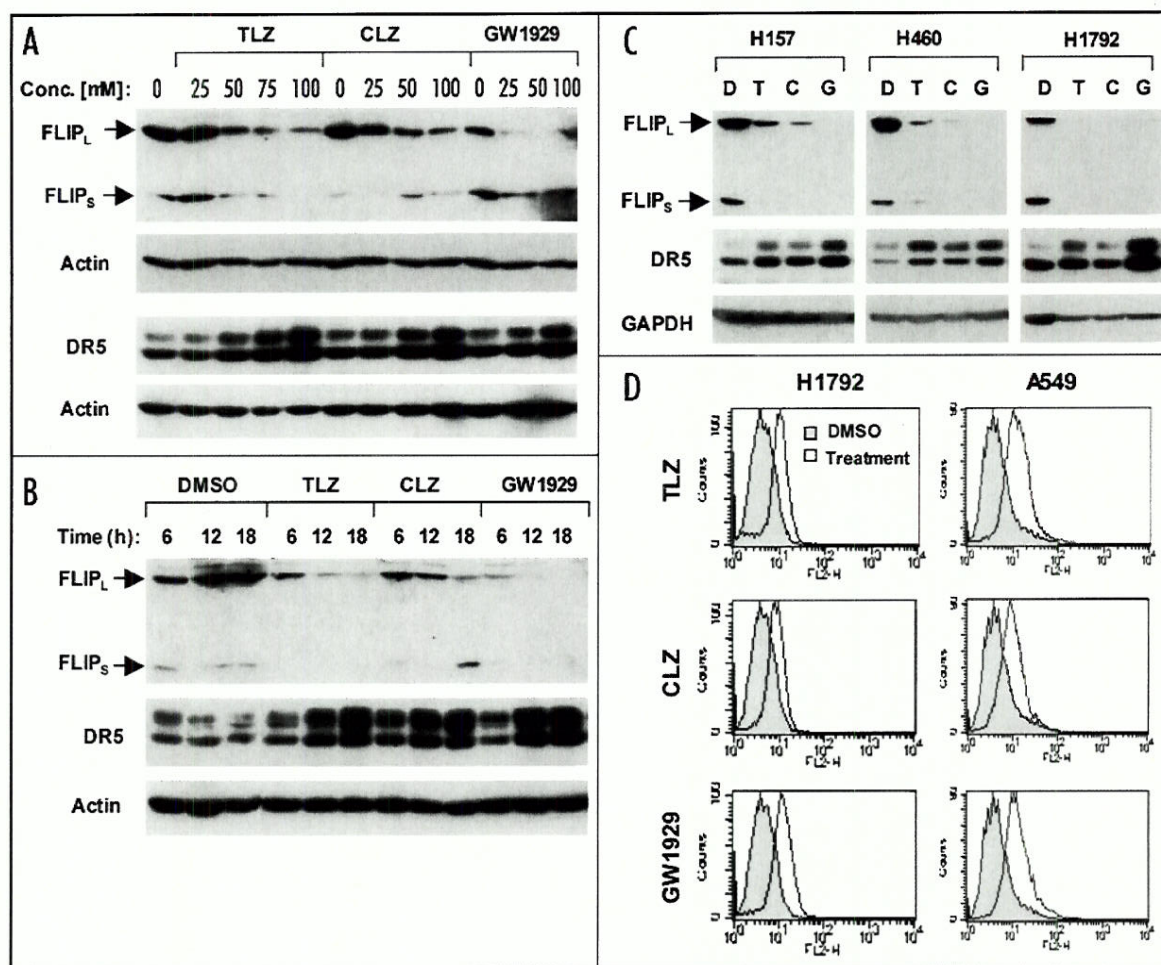


Figure 3. PPAR γ ligands increase DR5 expression in addition to downregulation of c-FLIP expression (A–C) and increase cell surface DR5 (D) in human lung cancer cells. (A and B) A549 cells were treated with the indicated concentrations of troglitazone (TLZ), ciglitazone (CLZ) or GW1929 for 12 h (A) or 50 μ M of the agents for the indicated times (B). Whole-cell protein lysates were then prepared from aforementioned treatments for detection of DR5, c-FLIP and actin using Western blot analysis. (C) The indicated lung cancer cell lines were treated with DMSO (D), 50 μ M of troglitazone (T), ciglitazone (C) or GW1929 (G) for 12 h and then subjected to preparation of whole-cell protein lysates and subsequent Western blot analysis for the indicated proteins. (D) Both H1792 and A549 cell lines were exposed to 50 μ M of the indicated PPAR γ ligands for 12 h. The cells were then harvested, stained with PE-conjugated DR5 antibody, and analyzed by flow cytometry.

Enforced c-FLIP overexpression protects cells from induction of apoptosis by the combination of a PPAR γ ligand and TRAIL. To determine the involvement of c-FLIP downregulation in enhancement of TRAIL-induced apoptosis by PPAR γ ligands, we established A549 stable cell lines that overexpress Lac Z (serves as a control), FLIP_L or FLIP_S as presented in Figure 5A. In agreement with aforementioned results, the combination of troglitazone and TRAIL exhibited enhanced induction of apoptosis compared to each single agent in Lac Z-2 and Lac Z-9 cell lines. This effect was inhibited in all cell lines expressing either FLIP_L or FLIP_S, particularly in cell lines expressing FLIP_L (Fig. 5A). Consistently, apoptosis induced by TRAIL alone was also inhibited in c-FLIP-overexpressing cell lines (Fig. 5A). Results in (Fig. 5B) shows representative expression levels of FLIP_L (i.e., FLIP_L-2) and FLIP_S (FLIP_S-8) in the given cell lines. In agreement with induction of apoptosis, the combination of troglitazone and TRAIL strongly induced cleavage of both caspase-8 and PARP in Lac Z-2 cells, but only minimally in FLIP_S-8 cells and in FLIP_L-2 cells (Fig. 5B). Collectively, these results clearly show that overexpression of c-FLIP protects cells from induction of apoptosis by the combination of TRAIL with a PPAR γ ligand. In another

words, downregulation of c-FLIP contributes to enhanced induction of apoptosis by the combination of a PPAR γ ligand and TRAIL.

PPAR γ ligands modulate the expression of DR5 and c-FLIP independently of PPAR γ . To determine whether PPAR γ plays a role in mediating the modulation of DR5 or c-FLIP expression by PPAR γ ligands, we compared the effects of troglitazone on the expression of DR5 and c-FLIP in the absence and presence of the PPAR γ antagonist GW9662. As presented in Figure 6A, the presence of GW9662 at 50 μ M and the maximal tolerated dose of 75 μ M failed to impair the ability of troglitazone to induce DR5 or downregulate c-FLIP expression in both A549 and H1792 cells. Moreover, we silenced the expression of PPAR γ and then examined its impact on PPAR γ ligand-induced DR5 upregulation and c-FLIP downregulation. As shown in Figure 6B, transfection of PPAR γ siRNA into A549 cells substantially decreased the levels of PPAR γ . However, both troglitazone and GW1929 induced DR5 expression and decreased c-FLIP levels in both control siRNA- and PPAR γ siRNA transfected cells with comparable degrees, indicating that silencing of PPAR γ expression does not affect the effects of PPAR γ ligands on modulation of DR5 and c-FLIP. Taken together, we conclude that PPAR γ

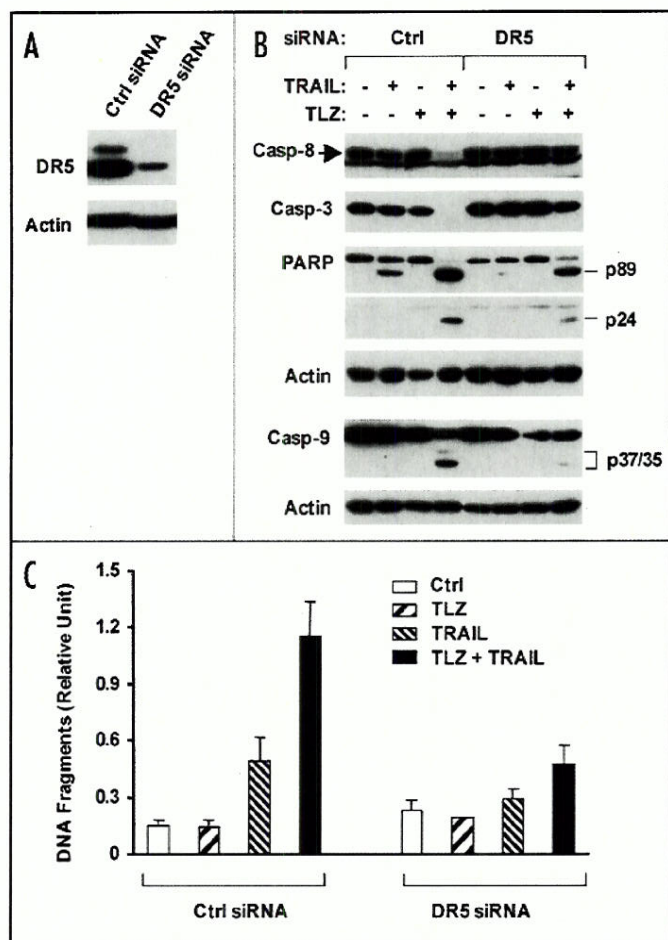


Figure 4. Silencing of DR5 expression by DR5 siRNA (A) attenuates caspase activation (B) and apoptosis (C) induced by the combination of troglitazone (TLZ) and TRAIL. A549 cells were seeded in a 24-well cell culture plate and on the second day transfected with control (Ctrl) or DR5 siRNA. Forty hours later, the cells were treated with 50 μ M TLZ, 20 ng/ml TRAIL and their combination. After 12 h (A and B) or 24 h (C), the cells were harvested for preparation of whole-cell protein lysates and subsequent Western blot analysis (A and B) or for detection of DNA fragmentation using an ELISA kit. Each column (C) represents the mean \pm SD of triplicate determinations.

ligands modulate the expression of DR5 and c-FLIP independently of PPAR γ .

DISCUSSION

Enhancement of TRAIL-induced apoptosis by PPAR γ ligands has been documented in certain types of cancer cell lines including glioma, neuroblastoma, breast, ovarian, prostate and colon cancer cells *in vitro*^{15,16,23,24} and in breast cancer *in vivo*.²⁴ Our current study confirms and extends this finding in human lung cancer cells. PPAR γ ligands alone in general have weak apoptosis-inducing activity as demonstrated in our study (Fig. 1). However, the presence of a low dose of TRAIL can result in enhanced or synergistic induction of apoptosis in various types of cancer cells by previous studies^{15,16,23,24} and our current finding. Given that some PPAR γ ligands are marketed drugs for treatment of type II diabetes, these findings warrant the clinical testing of the combination of a PPAR γ ligand with TRAIL as an effective cancer therapeutic regimen.

Downregulation of c-FLIP, survivin and cyclin D3 or induction of p21^{waf1/cip1} has been documented to account for the mechanisms by

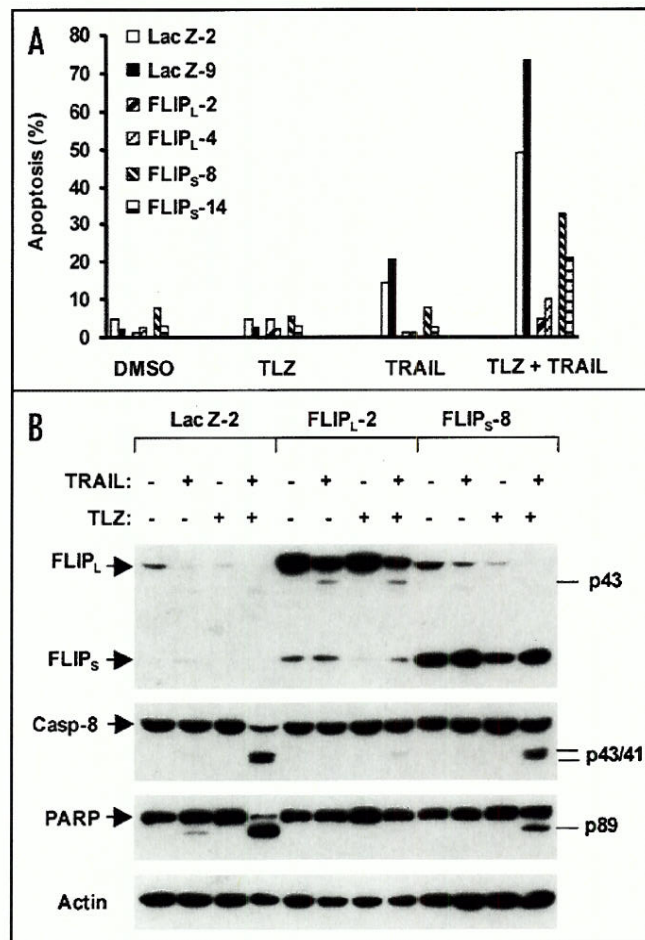


Figure 5. Enforced c-FLIP expression protects cells from induction of apoptosis (A) and caspase activation (B) by the combination of troglitazone (TLZ) and TRAIL. The indicated A549 cell lines expressing lac Z (control), FLIP_L or FLIP_S were treated with DMSO, 50 μ M TLZ alone, 10 ng/ml TRAIL alone and the combination of TLZ and TRAIL, respectively. After 24 h (A) or 12 h (B), the cells were harvested and subjected to detection of apoptotic cells by analyzing sub-G₁ population using flow cytometry (A) or detection of caspase activation using Western blot analysis (B).

which PPAR γ ligands enhance TRAIL-induced apoptosis.^{15,16,23,24} Among these mechanisms, downregulation of c-FLIP by PPAR γ ligands and its role in sensitizing cancer cells to TRAIL-induced apoptosis were extensively studied.^{15,16} In agreement with these findings, we also found that PPAR γ ligands such as troglitazone, ciglitazone and GW1929 decreased the levels of both FLIP_L and FLIP_S in human lung cancer cells (Fig. 3). Moreover, we demonstrate that downregulation of c-FLIP contributes to enhancement of TRAIL-induced apoptosis by PPAR γ ligands because enforced expression of exogenous c-FLIP (either FLIP_L or FLIP_S) inhibited induction of apoptosis by the combination of TRAIL with troglitazone (Fig. 5). Taken together, it appears that c-FLIP downregulation is an important mechanism accounting for PPAR γ ligand-mediated enhancement of TRAIL-induced apoptosis in human cancer cells.

By far, the few reports on the modulation of DR5 expression by PPAR γ ligands have conflicting results.¹⁵⁻¹⁷ Moreover, the involvement of DR5 modulation in PPAR γ ligand-mediated enhancement of TRAIL-induced apoptosis in cancer cells has not been addressed. In this study, we clearly show that several PPAR γ ligands including troglitazone, ciglitazone and GW1929 induced DR5 expression

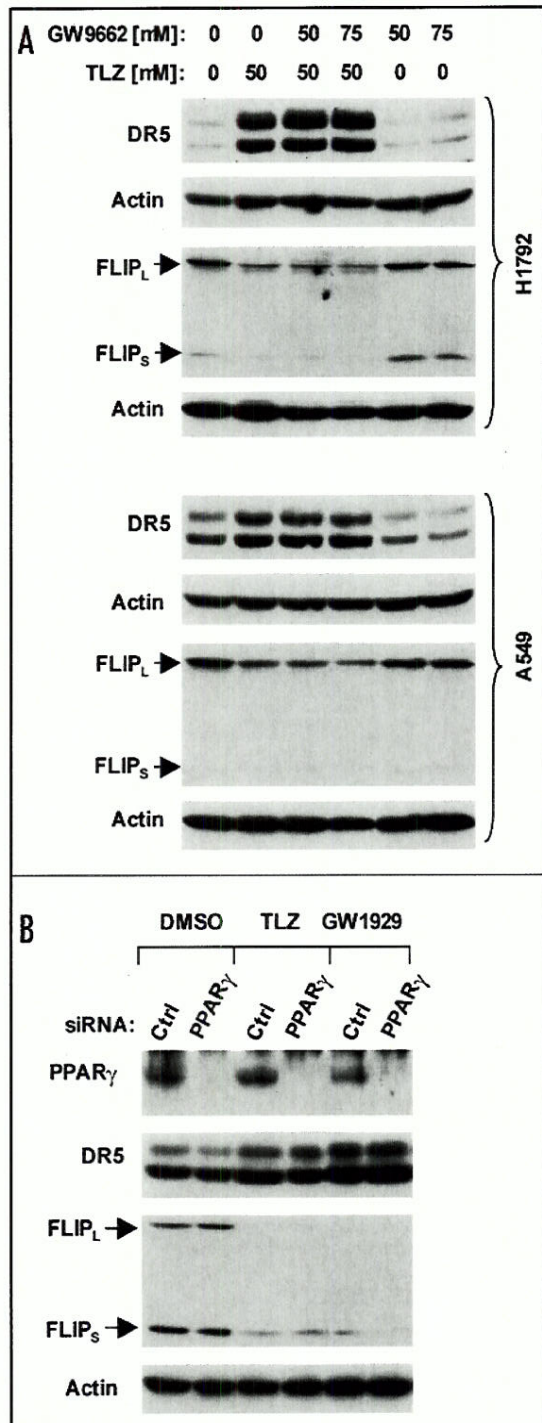


Figure 6. Effects of the PPAR γ antagonist GW9662 (A) and the silencing of PPAR γ expression (B) on PPAR γ ligand-induced modulation of DR5 and c-FLIP expression. A, The indicated cell lines were pretreated with the given doses of GW9662 and then cotreated with 50 μ M troglitazone (TLZ). After 12 h, the cells were subjected to preparation of whole-cell protein lysates and subsequent Western blot analysis. B, A549 cells were transfected with control (Ctrl) or PPAR γ siRNA. After 48 h, the cells were treated with DMSO control, 50 μ M TLZ or GW1929. Twelve hours later, the cells were harvested for preparation of whole-cell protein lysates and subsequent Western blot analysis.

while downregulating c-FLIP levels in multiple human lung cancer cell lines (Fig. 3), indicating that both DR5 upregulation and c-FLIP reduction are concurrent events in cells exposed to PPAR γ ligands. By siRNA-mediated silencing of DR5 expression, we found that the enhanced induction of apoptosis including caspase activation and DNA fragmentation by the combination of troglitazone and TRAIL was substantially attenuated. Thus, we conclude that DR5 upregulation also contributes to cooperative induction of apoptosis by the combination of a PPAR γ ligand and TRAIL. This should be the first demonstration for the involvement of DR5 upregulation in sensitization of cancer cells to TRAIL-induced apoptosis by PPAR γ ligands.

The downregulation of c-FLIP by PPAR γ ligands was documented to be independent of PPAR γ ,¹⁵ as was the induction of DR5 by 15d-PGJ₂.¹⁷ In our study, the presence of a PPAR γ antagonist or siRNA-mediated silencing of PPAR γ expression failed to inhibit the modulation of either DR5 or c-FLIP expression by PPAR γ ligands (Fig. 6). Thus, we conclude that PPAR γ ligands induce DR5 and downregulate c-FLIP expression independently of PPAR γ in human lung cancer cells.

In summary, we demonstrate that PPAR γ ligands enhance TRAIL-induced apoptosis in human lung cancer cells. In addition to downregulation of c-FLIP, PPAR γ ligands also upregulate DR5 expression, both of which contribute to PPAR γ ligand-mediated enhancement of TRAIL-induced apoptosis. Thus, our findings extend our understanding on the mechanisms by which PPAR γ ligands sensitize cancer cells to TRAIL-induced apoptosis.

References

- Almasan A, Ashkenazi A. Apo2L/TRAIL: Apoptosis signaling, biology, and potential for cancer therapy. *Cytokine Growth Factor Rev* 2003; 14:337-48.
- Kelley SK, Ashkenazi A. Targeting death receptors in cancer with Apo2L/TRAIL. *Curr Opin Pharmacol* 2004; 4:333-9.
- Ashkenazi A, Dixit VM. Death receptors: Signaling and modulation. *Science* 1998; 281:1305-8.
- Wajant H, Gerspach J, Pfizenmaier K. Tumor therapeutics by design: Targeting and activation of death receptors. *Cytokine Growth Factor Rev* 2005; 16:55-76.
- Wajant H. Targeting the FLICE Inhibitory Protein (FLIP) in cancer therapy. *Mol Interv* 2003; 3:124-7.
- Kataoka T. The caspase-8 modulator c-FLIP. *Crit Rev Immunol* 2005; 25:31-58.
- Irmeler M, Thome M, Hahne M, Schneider P, Hofmann K, Steiner V, Bodmer JL, Schroter M, Burns K, Mattmann C, Rimoldi D, French LE, Tschopp J. Inhibition of death receptor signals by cellular FLIP. *Nature* 1997; 388:190-5.
- Sun SY. Chemopreventive agent-induced modulation of death receptors. *Apoptosis* 2005; 10:1203-10.
- Sporn MB, Suh N, Mangelsdorf DJ. Prospects for prevention and treatment of cancer with selective PPAR γ modulators (SPARMs). *Trends Mol Med* 2001; 7:395-400.
- Rumi MA, Ishihara S, Kazumori H, Kadowaki Y, Kinoshita Y. Can PPAR gamma ligands be used in cancer therapy? *Curr Med Chem Anticancer Agents* 2004; 4:465-77.
- Koeffler HP. Peroxisome proliferator-activated receptor gamma and cancers. *Clin Cancer Res* 2003; 9:1-9.
- Li MY, Lee TW, Yim AP, Chen GG. Function of PPAR γ and its ligands in lung cancer. *Crit Rev Clin Lab Sci* 2006; 43:183-202.
- Chang TH, Szabo E. Enhanced growth inhibition by combination differentiation therapy with ligands of peroxisome proliferator-activated receptor-gamma and inhibitors of histone deacetylase in adenocarcinoma of the lung. *Clin Cancer Res* 2002; 8:1206-12.
- Avis I, Martinez A, Tauler J, Zudaire E, Mayburd A, Abu-Ghazaleh R, Ondrey F, Mulshine JL. Inhibitors of the arachidonic acid pathway and peroxisome proliferator-activated receptor ligands have superadditive effects on lung cancer growth inhibition. *Cancer Res* 2005; 65:4181-90.
- Kim Y, Suh N, Sporn M, Reed JC. An inducible pathway for degradation of FLIP protein sensitizes tumor cells to TRAIL-induced apoptosis. *J Biol Chem* 2002; 277:22320-9.
- Schultze K, Bock B, Eckert A, Oevermann L, Ramacher D, Wiestler O, Roth W. Troglitazone sensitizes tumor cells to TRAIL-induced apoptosis via down-regulation of FLIP and Survivin. *Apoptosis* 2006.
- Nakata S, Yoshida T, Shiraishi T, Horinaka M, Kouhara J, Wakada M, Sakai T. 15-Deoxy-Delta12,14-prostaglandin J(2) induces death receptor 5 expression through mRNA stabilization independently of PPAR γ and potentiates TRAIL-induced apoptosis. *Mol Cancer Ther* 2006; 5:1827-35.

18. Sun SY, Yue P, Dawson MI, Shroot B, Michel S, Lamph WW, Heyman RA, Teng M, Chandraratna RA, Shudo K, Hong WK, Lotan R. Differential effects of synthetic nuclear retinoid receptor-selective retinoids on the growth of human nonsmall cell lung carcinoma cells. *Cancer Res* 1997; 57:4931-9.
19. Sun SY, Yue P, Wu GS, El-Deiry WS, Shroot B, Hong WK, Lotan R. Mechanisms of apoptosis induced by the synthetic retinoid CD437 in human nonsmall cell lung carcinoma cells. *Oncogene* 1999; 18:2357-65.
20. Liu X, Yue P, Zhou Z, Khuri FR, Sun SY. Death receptor regulation and celecoxib-induced apoptosis in human lung cancer cells. *J Natl Cancer Inst* 2004; 96:1769-80.
21. Sun SY, Yue P, Hong WK, Lotan R. Induction of Fas expression and augmentation of Fas/Fas ligand-mediated apoptosis by the synthetic retinoid CD437 in human lung cancer cells. *Cancer Res* 2000; 60:6537-43.
22. Sun SY, Yue P, Shroot B, Hong WK, Lotan R. Induction of apoptosis in human nonsmall cell lung carcinoma cells by the novel synthetic retinoid CD437. *J Cell Physiol* 1997; 173:279-84.
23. Goke R, Goke A, Goke B, El-Deiry WS, Chen Y. Pioglitazone inhibits growth of carcinoid cells and promotes TRAIL-induced apoptosis by induction of p21waf1/cip1. *Digestion* 2001; 64:75-80.
24. Lu M, Kwan T, Yu C, Chen F, Freedman B, Schafer JM, Lee EJ, Jameson JL, Jordan VC, Cryns VL. Peroxisome proliferator-activated receptor gamma agonists promote TRAIL-induced apoptosis by reducing survivin levels via cyclin D3 repression and cell cycle arrest. *J Biol Chem* 2005; 280:6742-51.

2007 AACR Annual Meeting

April 14-18, 2007

Los Angeles, CA

 [Print this Page for Your Records](#)[Close Window](#)

Abstract Number: 2956

Presentation Title: Identification of biomarkers for human lung carcinogenesis by analysis of transcriptomes of cell lines representing different stages of lung carcinogenesis

Presentation Start/End Time: Monday, Apr 16, 2007, 1:00 PM - 5:00 PM

Location: Exhibit Hall, Los Angeles Convention Center

Poster Section: 17

Poster Board Number: 9

Author Block: Ludovic Lacroix, Eiji Tahara, Carmen Behrens, Humam N. Kadara, Dafna Lotan, Ignacio I. Wistuba, Reuben Lotan. UT M.D. Anderson Cancer Ctr., Houston, TX

Detection of tumors at early stages of lung carcinogenesis appears to be an efficient approach to reduce lung cancer morbidity and mortality because patients diagnosed with early stage lung cancer exhibit better prognosis than those diagnosed with advanced cancers. Identification of biomarkers in premalignant lung lesions is challenging due to limited availability of adequate biopsy samples. Therefore, we hypothesized that certain genes that are expressed differentially among cultured cells representing different stages of lung cancer progression can serve as biomarkers for early detection and targets for clinical intervention. As an *in vitro* human lung carcinogenesis model, we used normal (NHBE), immortalized (BEAS-2B and 1799), transformed (1198), and tumorigenic (1170-I) human bronchial epithelial (HBE) cells. The transcriptome of these cells was analyzed using the Affymetrix U133A GeneChip®. Subsequent bioinformatic analysis allowed us to identify 346 up-regulated genes and 466 down-regulated genes that displayed expression level variation from NHBE and normal small airway epithelial cells (SAEC) to the tumorigenic cell line (1170-I). Functional pathway analysis of the gene array data revealed modulation of expression of many genes involved in cell cycle, DNA regulation, cell adhesion, and enzymatic pathways. Several genes, mainly related to cell cycle (e.g., G2/M) or DNA replication, have previously been related to chromosomal instability and to cancer prognosis, and other genes such as PCNA and MCM2 have also been reported to be up-regulated in preneoplastic tissues consistent with our findings. The differential expression of putative biomarkers (UBE2C, MCM2, MCM6, BIRC5, FEN-1, TPX2, SFN, S100A8 and S100A4) was confirmed at the mRNA and protein levels in the premalignant cell line model as well as in cell lines derived from human lung cancers by quantitative real-time PCR and Western blotting, respectively. We also analyzed the expression levels of those genes, using quantitative real time-PCR, in 41 non-small cell lung carcinomas (NSCLC) and their non-tumoral counterparts. Furthermore, the expression levels of ubiquitin-conjugating enzyme E2C (UBE2C), mini-chromosome maintenance 2 (MCM2), Flap Endonuclease-1 (FEN-1), and S100 calcium binding protein A4 (S100A4) were assessed by immunohistochemistry in several normal, preneoplastic, and neoplastic human lung tissues. Although many of the potential biomarkers have to be validated in a larger collection of human lung cancer and premalignant lesions, our findings demonstrate that this *in vitro* human lung carcinogenesis model is a useful system for discovering potential early and late biomarkers of lung carcinogenesis and putative targets for chemoprevention. Supported in part by Department of Defense grant DAMD W81XWH-04-1-0142.

2007 AACR Annual Meeting

April 14-18, 2007

Los Angeles, CA

2007 AACR Annual Meeting**April 14-18, 2007****Los Angeles, CA** **Print this Page for Your Records****Close Window**

Abstract Number: 2869

Presentation Title: **Caveolin-1 gene methylation is a field effect phenomenon in lung cancer patients**

Presentation Start/End Time: Monday, Apr 16, 2007, 1:00 PM - 5:00 PM

Location: Exhibit Hall, Los Angeles Convention Center

Poster Section: 14

Poster Board Number: 8

Author Block: *Ximing Tang, Natalie C. Ozburn, Ignacio I. Wistuba.* UT M.D. Anderson Cancer Ctr., Houston, TX

Caveolin-1 (Cav-1), an essential structural constituent of caveolae that plays an important role in cellular process such as transport and signaling, has been implicated in the development of several cancers, including lung. Reduction and absence of Cav-1 expression has been reported in almost all small cell lung cancers (SCLC) and a subset of non-small cell lung cancers (NSCLC), mostly due to gene promoter methylation. Although several studies have provided information on the molecular characterization of NSCLC premalignant changes, they have been poorly documented for SCLCs. For lung cancer, molecular changes commence in histologically normal epithelium as field effect phenomenon. To better understand the role of *CAV1* gene in the early pathogenesis of lung cancers we investigated gene methylation and protein immunohistochemical (IHC) expression in the lung respiratory field by examining histologically normal respiratory epithelia adjacent to lung tumors. We studied formalin-fixed surgically resected tumor specimens from 100 lung cancers, including 40 SCLCs and 60 NSCLCs (48 adenocarcinomas, AC; 12 squamous cell carcinomas, SCC). For *CAV1* methylation analysis we extracted DNA from 202 precisely microdissected tissue sites, including 101 tumoral and 101 normal epithelial sites (79 small bronchi and 22 bronchioles). Among normal epithelial sites, 30 were located inside tumors (INE), 60 closed to tumors (<1mm, ONE), and 11 were distant to tumors (DNE). The DNA was undergone methylation specific polymerase chain reaction for assessing *CAV1* methylation and the results were confirmed by sequencing. Cav-1 protein IHC expression was studied in the same tumoral and epithelial sites examined for methylation. A high level of *CAV1* methylation rate was detected in tumors, being more frequent in SCLC (100%) compared to AC (49%) and SCC (50%). NSCLCs, but not SCLCs, demonstrated heterogeneity in *CAV1* methylation in all the 6 cases in which multiple tumor sites were examined. *CAV1* methylation was also frequently detected in histologically normal respiratory epithelia adjacent to lung tumors, without differences in methylation frequency by lung tumor histology (SCLC 64%, AC 69% and SCC 63%), and type (bronchi 65% and bronchioles 66%) and location (INE 67%, ONE 66% and DNE 64%) of respiratory structures examined. Gene methylation was highly correlated with protein expression in tumor (90%) and normal epithelium (95%) tissue sites. Our findings indicate that *CAV1* methylation is a frequent molecular abnormality in lung tumors, especially SCLC. The finding of high frequency of Cav-1 abnormalities in normal bronchial and bronchiolar epithelia adjacent to lung cancers suggests that *CAV1* may be involved in the early pathogenesis of lung cancer as field effect phenomenon (Supported by grant VITAL W81XWH-04-1-0142).

2007 AACR Annual Meeting**April 14-18, 2007****Los Angeles, CA**